The Dissertation Committee for Feng Pan Certifies that this is the approved version of the following dissertation:

DEVELOPMENT AND APPLICATION OF A COUPLED GEOMECHANICS MODEL FOR A PARALLEL COMPOSITIONAL RESERVOIR SIMULATOR

Committee:

Kamy Sepehrnoori, Supervisor

Steven L. Bryant

Lee Chin

Mojdeh Delshad

Eric P. Fahrenthold

DEVELOPMENT AND APPLICATION OF A COUPLED GEOMECHANICS MODEL FOR A PARALLEL COMPOSITIONAL RESERVOIR SIMULATOR

by

Feng Pan, B.S.; M.Sc.

Dissertation

Presented to the Faculty of the Graduate School of

The University of Texas at Austin

in Partial Fulfillment

of the Requirements

for the Degree of

Doctor of Philosophy

The University of Texas at Austin

December 2009

Dedication

To my parents, Zhenyou Pan and Lizhen Guan, who brought me into this world;

To my wife, Haiwen Zhao, who is accompanying me in enjoying the splendid life;

To my son, Eric (Yushi) Pan, who makes me proud as a father;

To my sister, Wei Pan, who is always encouraging me to realize my ideals;

To my friends who are sharing the happiness and lessons of life.

Acknowledgements

"It takes a teacher to transmit wisdom, impart knowledge, and resolve doubts," said Han Yu, a famous Chinese poet during the Tang dynasty. During my PhD study at The University of Texas at Austin, my supervisor Professor Kamy Sepehrnoori has helped me in so many different ways over the years. He has always encouraged me to explore research frontiers and provided me with insight into problems in both Petroleum Engineering and Computational Mathematics. No words can fully express my thanks to him. Everything I have learned from him is a most valuable treasure and will benefit me in the future.

Special thanks go to Dr. Lee Chin, who has been a collaborator of my PhD research. He spent a lot of time discussing problems with me and resolving my doubts. My conversations with him will guide my professional career as it progresses.

I am also in debt to the other members of my committee: Dr. Steven L. Bryant, Dr. Mojdeh Delshad, and Dr. Eric P. Fahrenthold. They have always been warmhearted and willing to help me during these years. Thanks for their time and comments.

I am grateful to the members of our GPAS group, Dr. Choongyong Han, Dr. Fracisco Marcondes, Dr. Abdoljalil Varavei, and Dr. Farhad Tarahhom. Special thanks to Tim Guinn and Roger Terzian for their computer assistance, Cheryl Kruzie for her constant assistance, Mary Pettengill for her library guidance, and Anais Langston as well for her review of my dissertation.

A deep gratitude goes to my Chinese friends in the Department of Petroleum and Geosystems Engineering.

The most driving force for me is the love, patience, understanding, and encouragement from my family: my parents, Zhenyou Pan and Lizhen Guan; my wife, Haiwen Zhao; my son, Eric (Yushi) Pan; and my sister, Wei Pan. I would like to express my deepest gratitude to you all.

DEVELOPMENT AND APPLICATION OF A COUPLED GEOMECHANICS MODEL FOR A PARALLEL COMPOSITIONAL RESERVOIR SIMULATOR

Publication No._____

Feng Pan, Ph.D.

The University of Texas at Austin, 2009

Supervisor: Kamy Sepehrnoori

For a stress-sensitive or stress-dependent reservoir, the interactions between its seepage field and *in situ* stress field are complex and affect hydrocarbon recovery. A coupled geomechanics and fluid-flow model can capture these relations between the fluid and solid, thereby presenting more precise history matchings and predictions for better well planning and reservoir management decisions. A traditional reservoir simulator cannot adequately or fully represent the ongoing coupled fluid-solid interactions during the production because of using the simplified update-formulation for porosity and the static absolute permeability during simulations. Many researchers have studied multiphase fluid-flow models coupled with geomechanics models during the past fifteen years. The purpose of this research is to develop a coupled geomechanics and compositional model and apply it to problems in the oil recovery processes. An equation of state compositional simulator called the General Purpose Adaptive Simulator (GPAS) is developed at The University of Texas at Austin and uses finite difference /

finite control volume methods for the solution of its governing partial differential equations (PDEs). GPAS was coupled with a geomechanics model developed in this research, which uses a finite element method for discretization of the associated PDEs. Both the iteratively coupled solution procedure and the fully coupled solution procedure were implemented to couple the geomechanics and reservoir simulation modules in this work. Parallelization, testing, and verification for the coupled model were performed on parallel clusters of high-performance workstations. MPI was used for the data exchange in the iteratively coupled procedure. Different constitutive models were coded into GPAS to describe complicated behaviors of linear or nonlinear deformation in the geomechanics model. In addition, the geomechanics module was coupled with the dual porosity model in GPAS to simulate naturally fractured reservoirs. The developed coupled reservoir and geomechanics simulator was verified using analytical solutions. Various reservoir simulation case studies were carried out using the coupled geomechanics and GPAS modules.

Table of Contents

List of Tables

List of Figures

1 Introduction

1.1 RESERVOIR SIMULATION COUPLED WITH GEOMECHANICS

It is well known in the field of Petroleum Engineering that for a stress-sensitive or stress-dependent reservoir, interactions between its seepage field and *in situ* stress field are complex and affect hydrocarbon recovery both negatively and positively. A coupled geomechanics and fluid-flow model can capture these relations between the fluid-flow and the solid deformation and thereby present more accurate history matchings and predictions for better well planning and reservoir management decisions. In addition, the coupled model can predict the subsidence on the surface of the reservoirs. A traditional reservoir simulator cannot adequately or fully represent the ongoing coupled fluid-solid interactions during the production. Many researchers have studied the multiphase fluid-flow models coupled with geomechanics models within the past decade.

The purpose of this project is to develop a coupled geomechanics and compositional model and apply it to problems in the oil recovery processes. An equation of state compositional simulator called General Purpose Adaptive Simulator (GPAS), which is developed at The University of Texas at Austin and uses a finite difference or finite control volume methods for the solution of its mathematical model (a set of partial differential equations, PDEs), is coupled with a geomechanics model, which is developed in this research and utilizes a finite element method for discretization of its associated mathematical model (PDEs). Both the iteratively coupled solution procedure and the fully coupled solution procedure, which adopt a two-way communications with coupling parameters between the two physical models, are implemented to solve the coupled PDEs in this work.

1.2 RESEARCH MOTIVATION

As oil and / or gas is produced in a reservoir, the fluid pressure decreases; the lower pressure increases the effective stress of the overburden sediments; and there is an ongoing compaction of the porous media; finally, the subsidence happens on the surface as described in Figure 1-1.

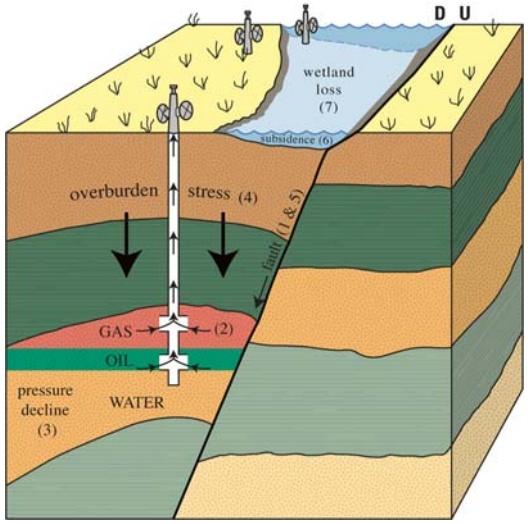

Figure 1-1: Interactions between solid and fluid during petroleum production (after http://coastal.er.usgs.gov).

The above process affects the hydrocarbon recovery positively as well as negatively. For example, the compaction of the porous volume which is considered as a hydrocarbon driver is beneficial to the production; but it is also negative because reservoir subsidence can lead to sand production, pipe crashes, wellbore casing damage, and even well failure (2002; Chin et al. 2003).

However, using the pore compressibility and pressure dependent porosity formula, a traditional reservoir simulator cannot adequately or fully model the ongoing coupled fluid-solid interactions. For instance, the Mandel-Cryer effect (Schiffmann 1960; Schiffmann et al. 1969) or the Noordbergum effect (Verruijt 1969; Kim and Parizek 1977; Gutierrez and Lewis 2002) occurring during the production cannot be

predicted by traditional reservoir simulators and the associated simulations can sometimes produce erroneous results (Settari and Mourits 1994; Gutierrez and Lewis 1998). Hence, we have to couple the geomechanics model with the reservoir simulator to correct the deviations and enhance the capability of history matchings and predictions.

1.2.1 The Origin of the Coupling Geomechanics and Fluid-flow Modeling: Subsidence

Due to subsidence on the surface of reservoirs, petroleum engineers give much importance to geomechanics phenomena during hydrocarbon production. Specifically, the subsidence of the seabed overlying the offshore reservoir largely affects the safe operations. Its related problem is called "*consolidation*" in terms of soil mechanics discipline.

1.2.1.1 Consolidation/Compaction, Subsidence/Settlement

With the fluid dissipation through a deformable/consolidating media, the pore pressure decreases and the volume of the solid decreases as well. This process is called *consolidation*/*compaction* and results in settlement or subsidence on the surface. In soil mechanics, compaction also refers to the method of densification with mechanical equipment, for example, a roller (Lambe and Whitman 1979). The mathematical theory studying the above process of the dissipation of pore pressures and the related deformation of soil is called *consolidation theory* (Terzaghi 1936). With the consolidation/compaction within the deformable media, the settlement or subsidence happen on the surface. The consolidation theory in soil mechanics is the basis of studying the coupled geomechanics and fluid-flow in petroleum industry.

1.2.1.2 Effects of Geomechanics on Petroleum Industry

It is similar to the soil consolidation that the consolidation within reservoirs because of the extraction of oil, gas, and water from a reservoir in the hydrocarbon

recovery results in the large surface subsidence. This subsidence could possibly damage the facilities of oil production on the surface. The above consolidation process will be accompanying the hydrocarbon production.

The first reservoir subsidence record dated in the 1910s is from the Goose Creek field, Texas, USA (Fjaer et al. 1992). Then, in the 1920s, a similar deformation behavior was observed at the Bolivar oil field in Venezuela. A big subsidence, almost 9 feet, happened at Wilmington field in Long Beach, California, since the production in 1937; specifically, from the 1940s and 1950s, and there were up to 29 feet subsided in the center of an elliptical bowl.

Table 1-1: Some oil fields with subsidence

Name of Oil Field	Location
Venice field	Venice, Italy
Latrobe Valley field	Victoria, Australia
Wairakei Geothermal field	Wairakei, New Zealand
Valhall field	North Sea, Norway
Ekofisk field	North Sea, Norway
Bolivar Coast field	Lake Maracaibo, Venezuela
Wilmington field	Long Beach, California, USA
South Belridge field	Kern Country, California, USA

Table 1-1 lists the main reservoirs undergoing subsidence. When we perform history matchings and predictions for this kind of reservoirs, accurate results cannot be obtained using traditional reservoir simulators (Settari and Mourits 1994; Gutierrez and Lewis 1998). Other practical problems related to these reservoirs are sand production,

pipe crashes, wellbore casing damage, well failure, etc. In other words, the interactions between solid and fluid in a same reservoir result in compaction within reservoirs and further affect the production activities.

On the other hand, in the hydrocarbon production process, there is an extra equilibrium evolved in, a stress equilibrium. This equilibrium is ignored or simplified by the traditional reservoir simulators; hence, complicated compactions including the solid compressibility and rearrangements of grains of porous media inside the reservoirs cannot be described accurately using the traditional treatment. A coupled geomechanics and reservoir simulation is needed to model and predict the above compaction process.

1.2.2 Approximation of the Pore Compressibility

Two elements, fluid (water, oil, and gas) and solid (porous rock), reside in a same reservoir. The porous media serving as a skeleton may contain oil, gas, and water in its pores. There are many relations between its associated seepage field (i.e. pore compressibility, permeability, and porosity etc.) and *in situ* stress field (i.e. rock stress, strain, and displacement). Reservoir subsidence is caused by depletion of underground fluid during production from stress-sensitive or stress-dependent reservoirs, such as highly compactable reservoirs, low-permeability reservoirs, chalk reservoirs, unconsolidated (soft or oil) sands, a cyclic steam recovery of heavy oil, among others. Hence, the subsidence has motivated reservoir engineers to investigate the interactions between the fluid and the deformable solid within the recent decades.

The fluid compressibility and the pore volume compressibility (Gutierrez and Lewis 2002) can be defined as,

$$c_{fluid} \equiv \frac{1}{\rho}\left(\frac{\partial \rho}{\partial p}\right)_T, \tag{1-1}$$

$$c_p \equiv \frac{1}{\phi}\left(\frac{\partial \phi}{\partial p}\right)_T, \tag{1-2}$$

where c_p is the pore compressibility at the pore pressure p and the constant reservoir temperature T.

Equation (1-2) can be approximated as follows:

$$c_p \equiv \frac{1}{\phi}\left(\frac{\partial \phi}{\partial p}\right)_T \approx \frac{1}{\phi_0}\left(\frac{\phi - \phi_0}{p - p_0}\right)_T \Rightarrow c_p\left(p - p_0\right) = \frac{\phi}{\phi_0} - 1, \tag{1-3}$$

or, using another approach gives:

$$c_p \equiv \frac{1}{\phi}\left(\frac{\partial \phi}{\partial p}\right)_T \Rightarrow \int_{p_0}^{p} c_p dp = \int_{\phi_0}^{\phi} \frac{1}{\phi} d\phi \Rightarrow c_p\left(p - p_0\right) = \ln\frac{\phi}{\phi_0}, \tag{1-4}$$

$$e^{c_p(p-p_0)} = \frac{\phi}{\phi_0} \Rightarrow \phi = \phi_0 e^{c_p(p-p_0)} \approx \phi_0\left[1 + c_p\left(p - p_0\right)\right]. \tag{1-5}$$

Namely,

$$\phi = \phi_0\left[1 + c_p\left(p - p_0\right)\right], \tag{1-6}$$

where the porosity ϕ_0 is at the reference pressure p_0, and ϕ denotes the porosity used in the reservoir simulator in this paper, is named "reservoir porosity." The above equation is used in the traditional reservoir simulators (Aziz and Settari 1979). Aziz and Settari call this pore volume compressibility as the rock compressibility (c_R). In other words, the pore volume compressibility c_p, the rock compressibility c_R, or the formation compressibility c_f all refer to the same thing, the variation of the pore volume with the pore pressure p. Also, the above parameters are interchangeable.

Thus far, the above derivation is rigorous. However, the evaluation of the pore volume compressibility c_p is not resolved yet. Because the porosity in the traditional reservoir simulators is based on the fixed bulk volume for each block cell, we prefer to call this porosity is the "reservoir porosity." While for the coupled geomechanics and

fluid-flow model, c_p is not only dependent on the change of the pore volume but also the change of the bulk volume during the production.

A traditional reservoir simulator, which essentially models a multiphase multi-component fluid-flow behavior in the porous media, assumes (Settari and Mourits 1994) a constant bulk volume ($\Delta x_i \cdot \Delta y_j \cdot \Delta z_k = \text{constant}$ for the grid block (i, j, k) during the simulation). This assumption says the reservoir rock is rigid or nondeformable and then results the approximation of the pore volume compressibility using

$$c_f = c_p \approx \frac{1}{V_p}\left(\frac{\partial V_p}{\partial p}\right)_{T,V_b}. \tag{1-7}$$

The accumulation term of the mass conservation equation of the fluid is given by:

$$\frac{\partial(\rho\phi)}{\partial t} = \frac{\partial(\rho\phi)}{\partial p}\frac{\partial p}{\partial t} = \left[\phi\frac{\partial \rho}{\partial p} + \rho\frac{\partial \phi}{\partial p}\right]\frac{\partial p}{\partial t} = (\rho\phi)\left[\frac{1}{\rho}\frac{\partial \rho}{\partial p} + \frac{1}{\phi}\frac{\partial \phi}{\partial p}\right]\frac{\partial p}{\partial t}. \tag{1-8}$$

Substituting of Equations (1-1) and (1-2) into Equation (1-8) gives

$$\frac{\partial(\rho\phi)}{\partial t} = (\rho\phi)\left[c_{fluid} + c_p\right]\frac{\partial p}{\partial t}, \tag{1-9}$$

where

$$c_p \equiv \frac{1}{\phi}\frac{\partial \phi}{\partial p} = \frac{V_b}{V_p}\frac{\partial}{\partial p}\left(\frac{V_p}{V_b}\right) = \frac{V_b}{V_p}\left(\frac{\frac{\partial V_p}{\partial p}V_b - V_p\frac{\partial V_b}{\partial p}}{V_b^2}\right) = \frac{1}{V_p}\frac{\partial V_p}{\partial p} - \frac{1}{V_b}\frac{\partial V_b}{\partial p}. \tag{1-10}$$

When the bulk volume is constant, the last term of the right hand side in the above equation (called the bulk compressibility, Ahmed 2006),

$$c_B \equiv \frac{1}{V_b}\frac{\partial V_b}{\partial p}, \tag{1-11}$$

disappears and the pore volume compressibility c_p are simplified to c_p[1],

$$c_p \equiv c_p^{[1]} - c_B \approx c_p^{[1]} = \frac{1}{V_p}\left(\frac{\partial V_p}{\partial p}\right)_{T,V_b}. \tag{1-12}$$

Equation (1-12) or the alternative definition of the pore volume compressibility c_p can be found in the books of Walsh and Lake (2003) and Ahmed (2006). This approximation of Equation (1-12) for Equation (1-10) makes an assumption neglecting the deformation and movements of porous media. The following identity is also true (Chen et al. 1995):

$$\nabla \cdot \vec{v}_s = \frac{1}{V_b}\frac{dV_b}{dt} \approx \frac{1}{V_b}\frac{\partial V_b}{\partial t} = \frac{1}{V_b}\frac{\partial V_b}{\partial p}\frac{\partial p}{\partial t} = c_B \frac{\partial p}{\partial t}. \tag{1-13}$$

In conclusion, the treatment in a traditional reservoir simulator ignores the deformation of porous media and uses the approximation $c_p^{[1]}$ to the pore volume compressibility c_p as the follows,

$$c_p = c_p^{[1]} + c_B \approx c_p^{[1]}, \tag{1-14}$$

and relates the porosity, the pore-volume compressibility, and the variation of pressure as the follows:

$$\phi = \phi_0\left[1 + c_f\left(p - p_0\right)\right], \tag{1-15}$$

where the porosity ϕ_0 is at the reference pressure p_0, and ϕ denotes the porosity (named "reservoir porosity") used in the reservoir simulator in this paper.

Equations (1-14) and (1-15), in fact, are one simplification of the complex skeleton behavior because the rock's displacement, stress, and strain in geomechanics models are not of primary interest in the traditional reservoir simulation. Hence for most cases, static parameters (ϕ and $\vec{\vec{K}}$) are used in the simulators (only inputted at the beginning of a simulation, and no changes are considered during the whole simulation procedure). When the initial pressure and porosity are known, porosity ϕ during production linearly varies with the change of reservoir pressure with a constant slope,

c_f. However, in reality the coupled fluid-solid interactions are ongoing over the production, and the "rock compressibility" cannot adequately or fully represent the changes (deformations) of the petrophysical parameters. This is because of stress changes and failures of the solid due to the geomechanics effect, which are nonlinear deformations; for example, nonlinear elastics, Elasto-plastic, and Elasto-viscoplastic (Lewis and Schrefler 1998). In addition, the rock behavior is strongly affected by the load history. The load history is very complicated and has a large effect on hydrocarbon recovery. By ignoring or simplifying such interactions, there will be deviations, even errors, from the reality of underground status (Settari and Mourits 1994; Gutierrez and Lewis 1998), especially for stress-sensitive reservoirs. The simulation results cannot be compatible with the actual production data, and the predictions have also little reliability. Therefore, we can only capture the relations between the fluid and solid using a coupled geomechanics and fluid-flow models. By doing so, we can obtain more precise history matchings and predictions for better well planning and reservoir management decisions.

1.2.3 Effective Stress Law

The Geomechanics is an issue for the petroleum industry because the porous rocks are subject to a high overburden stress, the weight of overlaying rocks. As shown in Figure 1-2, this stress is the so-called total stress (σ); the total stress is taken by the solids and fluids of porous rocks. The part carried by fluid (p) is called pore pressure or reservoir pressure; the part carried by solid (σ') is called the effective stress (Terzaghi 1936; Biot 1941).

Traditionally, we assume that the total overburden stress is constant and known, and if we also know pore pressure from traditional reservoir simulations, the effective stress can be calculated. Changes in the effective stress may induce changes of the rock properties, for example, porosity and permeability.

We also mentioned that for stress-sensitive reservoirs, the geomechanics effects must be considered during simulation process. Firstly, how to decide if a reservoir is stress-sensitive or not?

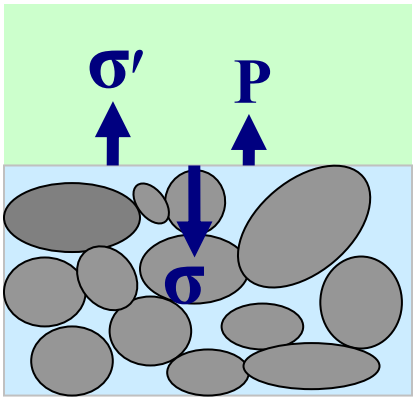

Figure 1-2: The effective stress law.

1.2.4 Definition of Stress-sensitive reservoirs

Thus far, no formal definition of stress-sensitive or stress-dependent reservoirs has been given.

In general, all reservoirs are stress-sensitive. But in this research, we prefer to use the definition of stress-sensitive reservoirs given by Chin et al. (Chin et al. 1998a; Chin et al. 1998b), that "Reservoir rocks with fluid-flow characteristics (permeability) that are highly sensitive to effective stress changes and/or if they are of weak mechanical strength, giving rise to large rock deformation, are considered to be stress-sensitive." Another equivalent statement is that for a reservoir, the changes of reservoir properties, porosity, permeability, etc. are due to the change of effective stress or pore pressure;

furthermore, the changes are large enough to affect production or to pose risks to completed wells.

In addition, for a deep, thin formation layer, it is reasonable to consider total stress as approximately constant then the effective stress becomes a function of pressure only; As a result, porosity and permeability are functions of pressure only. This is the traditional treatment in conventional reservoir simulators without considering the interactions between fluid-flow and stress-strain analysis.

The drive mechanism for all reservoirs is partly compaction. As fluid is produced, effective stress is raised; the fluid pressure drawn down increases effective stress by the same amount. In general, reservoirs that are under lower initial effective stress will be more susceptible to compaction strain. A reservoir that has a high component of water drive will draw down less and thus compact less.

Coupled geomechanics simulators are very useful tools for evaluating and analyzing oil and gas production from stress-sensitive fields.

1.2.5 Application Status

This section reviews existing coupled geomechanics reservoir simulators. Considering the geomechanics effects, the coupled reservoir simulations have been performed by oil companies, oil service companies, and universities.

To the best of our knowledge, Chevron and Shell do not release their in-house reservoir simulators integrated with the geomechanics and related publications. The researchers from ConocoPhillips published many papers related to the application in the North Sea reservoirs (Chin and Boade 1990; Sulak et al. 1991; Sulak 1991; Chin et al. 1998b; Chin et al. 2002; Chin et al. 2003).

Compared with the above oil companies, oil service companies did the research more extensively. The Schlumberger company (2002) added geomechanics module to

its ECLIPSE reservoir simulators, including implementations in their compositional, thermal, and blackoil models. They use a fully coupled procedure based on staggered grid mesh for geomechanics models. The constitutive model is a linear elastic formula. CMG (Computer Modeling Group 2006) released a geomechanics module for STARS , which can be used to solve the following problems: (1) Plastic deformation, (2) Shear dilatancy, (3) Compaction drive in cyclic injection/production strategies, (4) Injection induced fracturing, (5) Near-well formation failure, and (6) Sand co-production. CMG uses an iteratively coupled procedure taking porosity and permeability as coupling parameters.

Many universities are also involved in this research and have made substantial progresses. The University of Texas at Austin (Gai 2004) coupled geomechanics model with the black oil reservoir model using an iteratively coupled solution procedure. Stanford University (Wan 2002) also developed a coupled geomechanics and black oil reservoir simulator using a fully coupled solution procedure. Alberta University (Li 2006) studied geomechanics effects for fractured reservoirs and proposed an stress-related permeability model.

1.3 RESEARCH OBJECTIVES

The ultimate goal of this research is to develop a parallel geomechanics module to be coupled with a parallel compositional reservoir simulator called General Purpose Adaptive Simulator (GPAS) developed by the Center for Petroleum and Geosystems Engineering, at The University of Texas at Austin. A brief description of GPAS will be presented in Section 1.4.1. The objectives that will be achieved in this research are stated below:

1. Development and implementation of a geomechanics model using finite element method

2. Iteratively and/or fully coupled the geomechanics model and GPAS
3. Parallelization of the coupled geomechanics model and compositional simulator for execution on parallel computers
4. Testing and verification of the coupled model
5. Application of the coupled model to realistic problems as time allows

1.4 RESEARCH METHODOLOGY

Our work in this research will concentrate on development and implementation of a parallel coupled geomechanics and compositional simulator. MPI will be used to perform the data exchange in the iteratively coupled procedure. We will investigate development of our code for application on parallel clusters of high-performance workstations. We will also implement appropriate constitutive models for reservoir rocks of complicated deformation behaviors for the geomechanics model.

1.4.1 Previous Work: GPAS

GPAS will be used for modeling fluid-flow in the reservoir in conjunction with the geomechanics model that will be developed in this research.

1.4.2 Key Tasks and Technologies

In order to successfully achieve the research objectives listed in the Section 1.3, the following tasks need to be completed:

1. Thorough literature review of coupled geomechanics-reservoir models. In order to fully understand and grasp the latest developments of the geomechanics model coupled with fluid-flow, a more exhaustive literature review will be performed and will be included in the final dissertation. Due to development of geomechanical modeling for saturated soil mechanics in

civil engineering, which is closely related to reservoir with rock formation, we will follow the new development in material constitutive models.

2. Development of the coupled mathematical model. A coupled geomechanics and reservoir model will be formulated in Chapter 2.
3. Development and verification of the geomechanics model. The governing equations for the geomechanics model in conjunction with a linear elastic or a nonlinear plastic material equation will be discretized using a finite element method.
4. Parallelization of the geomechanics model for execution on massively parallel computers. The source code developed in Tasks 3 and 4 will be fully parallelized using Domain Decomposition Method (DDM) based on MPI parallel platform.
5. Iteratively or / and fully coupled the geomechanics model with GPAS;
6. Verification of the coupled model. The developed reservoir and geomechanics models will be verified using analytical solutions and published results.
7. Application of the coupled models for realistic problems will be carried out as time allows.

1.4.3 Outline of Research Steps

On the basis of GPAS, we will execute the research with the following steps.

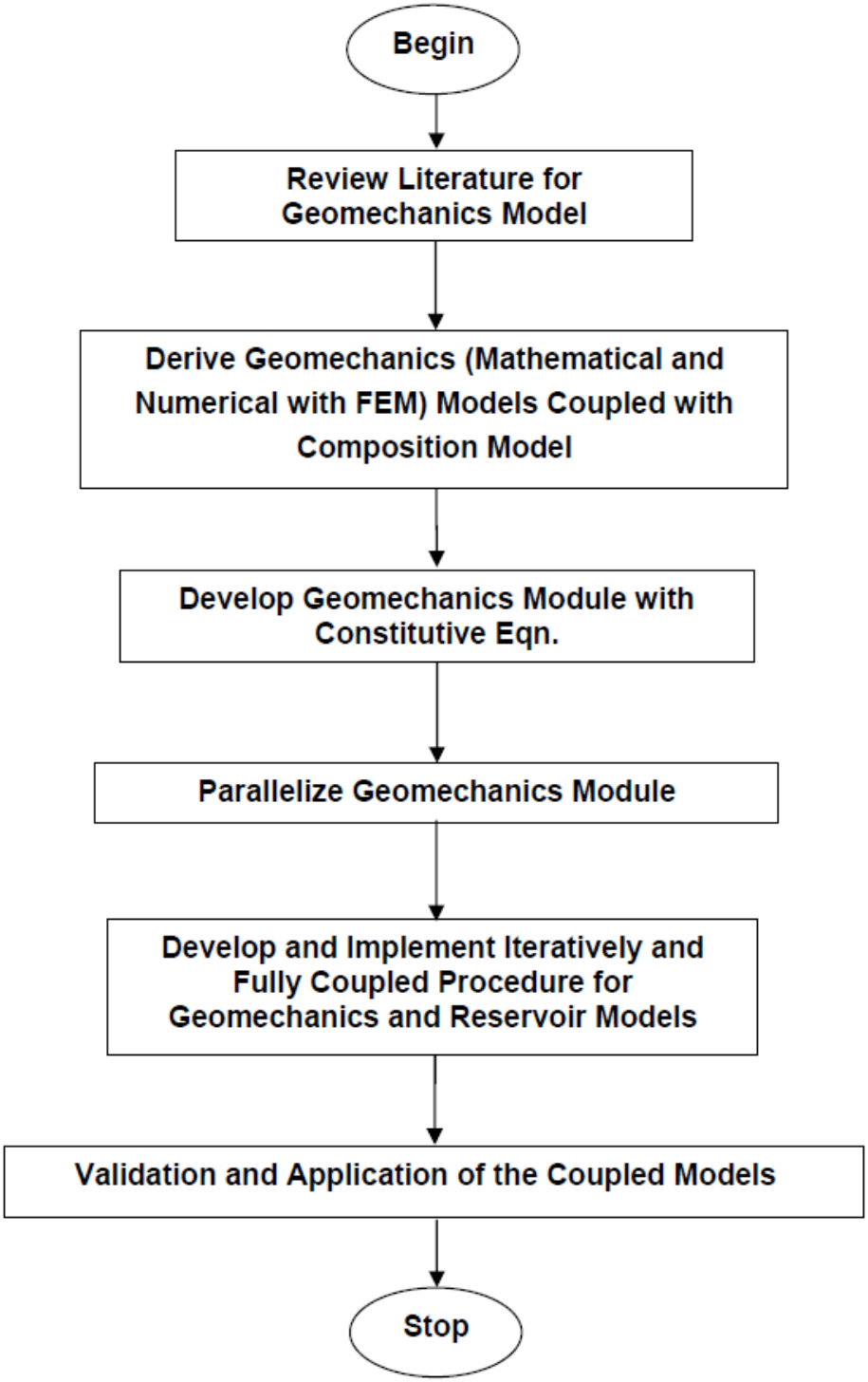

Figure 1-3: A flow chart for tasks involved in the research.

1.5 OUTLINE OF THE DISSERTATION

The arrangement of the dissertation proceeds in a logical order as the PhD project research evolved. The coupling modeling is an inter-discipline problem, which includes the knowledge on soil mechanics, hydraulic mechanics, material mechanics, numerical and computational mathematics (including the finite element method, the finite / control volume method or the finite difference method), reservoir engineering, etc. However, we try to cover the necessary parts for the theory, numerical treatments, and programming and executions of the code. One of the ultimate objectives is to present a clear and complete solution to the reservoir simulation coupled with geomechanics. The outline of the dissertation is as follows.

Chapter 2 gives a short review on the compositional reservoir simulators, geomechanics modeling, and the coupled simulations. The intention is to introduce the basic theory of the coupled geomechanics and reservoir simulation, including the mathematical models, numerical models, solution procedures, and the selection of coupling parameters.

Chapter 3 derives in detail the mathematical model of the coupled geomechanics and compositional simulation. The governing equations are obtained, describing the multiphase, multicomponent fluid-flow in a deformable permeable media. This derivation uses the Eulerian (or spatial) description in a fixed coordinate. The different approximations for the above coupled governing equations are introduced and discussed; meanwhile, the mass balance equation of a single phase fluid-flow is studied as a special case. The content of this chapter, as a fundamental of this research, is crucial for us to solve problems and achieve expected results.

Chapter 4 discusses the discretization of the coupled mathematical model derived in Chapter 3. Specifically, the Finite Element Method (FEM) is used to obtain the numerical model of geomechanics formulation. The Virtual Work Principle (VWP), Gauss numerical integration, among others, are covered in Chapter 4 as well.

Chapter 5 is devoted to the constitutive models of geomechanics, which refer to the relationship between the stresses and stains. The linear elasticity and nonlinear plasticity constitutive models are discussed in this chapter. For the nonlinear plasticity of the solid behavior, the classical failure criteria are used to decide whether the material is ongoing a plastic deformation or not. These failure criteria comprise Von Mises, Mohr-Coulomb, Tresca, and Drucker-Prager models. The nonlinearity is limited to the material nonlinearity, rather than the geometrical nonlinearity based on large strains or displacements.

Chapter 6 focuses on the solution procedures for the coupled geomechanics and fluid-flow model as discussed in Chapters 3 and 4. Two solution procedures are investigated in detail; one is called the fully coupled solution procedure and the other is the iteratively coupled solution procedure. Traditional fully coupled solution procedures are programmed using the same numerical technique for the solid and fluid fields which is impossible to reuse the existing simulators in each field. A novel implementation of the fully coupled geomechanics and compositional reservoir simulator is proposed, which is based on the Schur complement. From the mathematical point of view, the advantage of this solution procedure is that it has an assured convergence and high accuracy compared to the iteratively coupled solution procedure. The iteratively coupling of the geomechanics and compositional reservoir simulators can be implemented using different approaches, which are described and studied in detail; furthermore, the convergence of this procedure is discussed and explained. In addition,

the dual porosity module in GPAS is also integrated with the geomechanical module. The Mohr-Coulomb constitutive model is implemented to describe the nonlinear deformation behaviors of rocks. A series of test problems is presented to verify and apply our program in this chapter.

Chapter 7 gives a short comparison between the iteratively coupled and fully coupled solution procedures.

Chapter 8 is devoted to parallelization of the coupled codes for solving large-scale problems. The element by element idea is adopted to parallelize the geomechanics finite element codes. This parallelization approach is general framework to parallel any finite element codes. Case study is included as well.

Chapter 9 provides a summary, conclusions, and recommendations for future research.

2 Review of Relevant Literature

It has been more than several decades since researchers realized the importance of geomechanics for oil and gas production in stress-sensitive reservoirs. Though initially a subsidence phenomenon from the depletion of underground fluid (water, oil, and gas) attracted the reservoir engineers' attention, well-bore stability, sand production, and pipe crash have all been proven related to the deformable porous rock mechanics in the stress-sensitive reservoirs. For such particular reservoirs, in some cases, simulation results using traditional reservoir models cannot be consistent with associated recorded production data. Then the engineers find that using a geomechanics model coupled with a traditional reservoir simulator usually can correct the deviations.

This chapter provides a summary of relevant work with respect to the mathematical governing equations of the coupled seepage and *in situ* fields. The objective is to provide some background and introduction to topics covered in the rest of the work as well as to provide references to sources where some of these topics are covered in more detail.

Background materials based on our literature review are organized in the following sections: 1) the governing equations of the compositional model used in GPAS, a geomechanics model, and a compositional mathematical model coupled with geomechanics; 2) current four coupling methods (decoupled, explicitly coupled, iteratively coupled, and fully coupled method) for solving the geomechanics and multiphase multi-component fluid-flow equations are reviewed; 3) dynamic coupling reservoir parameters' models, namely volume and flow properties coupling models (porosity, compressibility and permeability) and because different computational

domains and grid-partitionings are used for the seepage and *in-situ* stress fields, a coupling interface must be investigated for mapping the coupling properties from one grid mesh to another; 4) numerical models and relevant solvers; 5) some issues regarding a parallel framework used in this research.

2.1 COUPLED GOVERNING EQUATIONS OF TWO FIELDS

In this section, the formulation for a compositional mathematical model and a geomechanics mathematical model are described. Subsequently, a description of a coupled geomechanics and compositional mathematical model is presented.

2.1.1 Compositional Model

The compositional model of the isothermal reservoir used in GPAS, which is described by Wang, et al. (1997; 1999), can be described by the following partial differential equations. It is assumed that there are n_c hydrocarbon components and n_p phases including aqueous phase, and neglecting mass fluxes (dispersion and mutual solubility) between the water phase and the other phases. All the assumptions will be listed in Section 3.1 in detail.

Hydrocarbon Component Mass Balance

$$V_b \frac{\partial(\phi N_i)}{\partial t} + V_b \nabla \cdot \sum_{j=1}^{n_p} \left(\xi_j x_{ij} \vec{v}_j \right) - q_i = 0, \qquad i = 1,2,..,n_c+1, \tag{2-1}$$

where the moles of component i per unit pore volume $N_i = \sum_{j=1}^{n_p} \left(S_j x_{ij} \xi_j \right)$, S_j, x_{ij}, ξ_j represent the saturation of fluid phase j, the mole fraction of component i in fluid phase j, and the molar density of fluid phase j, respectively; $\vec{v}_j$ is the macroscopic Darcy velocity for fluid phase j; ϕ is the reservoir porosity; q_i is the molar injection (positive) or production (negative) rate for component i; V_b is the bulk volume of a grid block. For the grid block which is not a well block, q_i is set to zero.

Equality of Component Fugacities (Phase-Equilibrium Equations)

$$f_i^{oil} - f_i^{gas} = 0, \qquad i = 1,2,..,n_c, \tag{2-2}$$

where f_i^{α} is the fugacity of component i in phase α, $\alpha = oil, gas$.

Volume Constraint

$$\sum_{j=1}^{3}\left(\frac{N_j}{\xi_j}\right) = 1.0, \tag{2-3}$$

where j can be 1, 2, and 3, which represents water, oil, and gas phases, respectively.

The PDE system, Equations (2-1)-(2-3), is the mathematical model of the multi-phase and multi-compositional reservoir simulator GPAS, and its primary unknowns (totally $2n_c + 2$) are chosen as

$$p = p_w,\ N_w, N_1,..., N_{n_c};\ \ln K_1,...,\ \ln K_{n_c}. \tag{2-4}$$

2.1.2 Geomechanical Model

Chin, et al. (Chin et al. 1998a; Chin et al. 1998b; Chin et al. 2002) described the following geomechanics mathematical model, Equations (2-5)-(2-9), based on a linear momentum equation and the effective stress law (Terzaghi 1936; Biot 1941). The following formulations mainly adopted from their work.

Stress Equilibrium Equation (Balance of Linear Momentum and Effective Stress Law)

$$\nabla \cdot \bar{\bar{\sigma}} + \rho \vec{b} = \nabla \cdot \left(\bar{\bar{\sigma}}'^{s} - \alpha p \bar{\bar{\delta}}\right) + \rho \vec{b} = \vec{0}, \tag{2-5}$$

where $\bar{\bar{\sigma}}$ is the total stress tensor; $\rho = \left(1-\phi^*\right)\rho_s + \phi^* \rho_f$ is the total mass density; ϕ^* is the true porosity; $\vec{b}$ is the body force per unit mass; ρ_s, ρ_f is the solid and fluid density, respectively; $\bar{\bar{\sigma}}'^{s}$ is the solid effective stress tensor; α is the Biot-Willis coefficient describing the form of fluid-solid coupling; p is the pore fluid pressure which can be defined as the average pore fluid pressure (Lewis and Pao 2002); and $\bar{\bar{\delta}}$ is

the Kronecker delta tensor.

The effective stress law,

$$\bar{\bar{\sigma}} = \bar{\bar{\sigma}}'^{s} - \alpha p \bar{\bar{\delta}}, \tag{2-6}$$

or in an incremental form,

$$\Delta\bar{\bar{\sigma}} = \Delta\bar{\bar{\sigma}}'^{s} - \alpha \Delta p \bar{\bar{\delta}}, \tag{2-7}$$

is used in Equation (2-5), where $\Delta(\cdot)$ represents the change between two consecutive time-steps or iterations. We follow the *sign convention* of positive stresses in tension, negative stresses in compress or compaction and always positive fluid pressure in both tension and compression. For clearity, two examples are listed as follows:

Table 2-1: Examples of the effective stress law to show the sign convention

	One-dimensional cases (a constant total stress in z direction, $\alpha = 1$)
Example 1	$t = 0:\ \sigma = -6000\ psi\ (compression),\ \ p = 6000\ psi;$ so $\sigma = \sigma'^{s} - p \Rightarrow -6000 = \sigma'^{s} - 6000 \Rightarrow \sigma'^{s} = 0\ psi.$
Example 2	$t = t_0:\ \sigma = -6000\ psi\ (compression),\ \ p = 5000\ psi;$ so $\sigma = \sigma'^{s} - p \Rightarrow -6000 = \sigma'^{s} - 5000 \Rightarrow \sigma'^{s} = -1000\ psi;$ or $\Delta\sigma = \Delta\sigma'^{s} - \Delta p \Rightarrow 0 = \Delta\sigma'^{s} - (5000 - 6000) \Rightarrow \Delta\sigma'^{s} = -1000\ psi;$ $\Delta\sigma'^{s} = \left(\sigma'^{s}\right)_{t_0} - \left(\sigma'^{s}\right)_{0} = \left(\sigma'^{s}\right)_{t_0} - 0 = -1000\ psi \Rightarrow \left(\sigma'^{s}\right)_{t_0} = -1000\ psi.$

The effective stress law, as will be clear later in Chapter 3, is basic in the description of soil mechanics.

Material Constitutive Equations

A general formulation of the constitutive equations is given by

$$\bar{\bar{\sigma}}'^{s} = \bar{\bar{f}}\left(\bar{\bar{\varepsilon}}, \bar{\bar{K}}\right), \tag{2-8}$$

where $\bar{\bar{\sigma}}'^{s}$ is the effective stress tensor; $\bar{\bar{f}}(*)$ is the tensor function; the solid strain tensor $\bar{\bar{\varepsilon}} = \int \dot{\bar{\bar{\varepsilon}}} dt$, $\dot{\bar{\bar{\varepsilon}}}$ is the solid strain rate tensor; and $\bar{\bar{K}}$ is the set of history dependent tensorial quantities.

Strain-Displacement Relation

When assuming incompressible solid grain (ρ_s is a constant) and small strain in a time increment, the solid strain tensor is

$$\bar{\bar{\varepsilon}} = \nabla \vec{u}_{()} \equiv \left(\nabla \vec{u} + (\nabla \vec{u})^T \right) / 2, \tag{2-9}$$

where $\nabla u_{()}$ is the symmetric part of the solid displacement gradient, and $\vec{u} = (u_x, u_y, u_z)$ is the displacement of the solid.

For the mathematical model of geomechanics, Equations (2-5)-(2-9), the unknowns are the displacement vector $\vec{u}$, the effective stress tensor $\bar{\bar{\sigma}}'^{s}$, and the strain tensor $\bar{\bar{\varepsilon}}$. Substitution of Equations (2-8)-(2-9) into Equation (2-5), we first obtain $\vec{u}$ and then calculate $\bar{\bar{\varepsilon}}$ and $\bar{\bar{\sigma}}'^{s}$ from Equations (2-9) and (2-8) in turn.

2.1.3 Coupled Geomechanical and Compositional Model

Many researchers presented coupled fluid-solid mathematical models (Lacy 1986; Lewis and Sukirman 1993; Chen et al. 1995; Gutierrez and Lewis 1998; Lewis and Schrefler 1998; Chin et al. 1998a; Chin et al. 1998b; Lewis and Pao 2002; Wan 2002; Gutierrez and Lewis 2002; Gai 2004). We present a compositional model under a deforming environment coupled with the geomechanics model. Note that the compositional model presented by Equations (2-1)-(2-4) used in GPAS is a simplified version of the compositional model coupled with a geomechanics model presented in this section.

We make the following modifications for the fluid mass conservation equations,

1. The *true porosity* ϕ^* is used, other than the *reservoir porosity* ϕ;

2. The *absolute* macroscopic *superficial* fluid phase velocity $\left(\phi^* S_j \vec{v}_{ij}^*\right)$ *with respect to a fixed coordinate system* is used, other than the *relative* macroscopic Darcy *(superficial)* fluid phase velocity $\vec{v}_j$ *with respect to a moving solid matrix*.

Then, the multiphase multi-component compositional model coupled with the geomechanics model can be obtained as follows:

Stress Equilibrium Equations

$$\vec{E}\left(p,\ N_w, N_1,\ ...,\ N_{n_c},\ \ln K_1,\ ...,\ \ln K_{n_c};\ \vec{u}\right) \equiv \nabla \cdot \left(\bar{\bar{\sigma}}'^{s} - \alpha p \bar{\bar{\delta}}\right) + \rho \vec{b} = \vec{0}. \tag{2-10}$$

Mass Conservation Equations for Fluid-flow

$$F_i\left(p,\ N_w, N_1,\ ...,\ N_{n_c},\ \ln K_1,\ ...,\ \ln K_{n_c};\ \vec{u}\right) \equiv$$

$$V_b \frac{D}{Dt}\left(\phi^* N_i\right) - V_b \vec{\nabla} \cdot \left\{ \sum_{j=1}^{n_p} \left[\left(\xi_j x_{ij}\right) \frac{\bar{\bar{K}} k_{rj}}{\mu_j} \left(\nabla P_j - \gamma_j \nabla D\right) \right] \right\} + V_b \phi^* N_i \frac{D\varepsilon_v}{Dt} - q_i = 0, \tag{2-11}$$

$$i = 1, .., n_c + 1;$$

or

$$F_i\left(p,\ N_w, N_1,\ ...,\ N_{n_c},\ \ln K_1,\ ...,\ \ln K_{n_c};\ \vec{u}\right) \equiv$$

$$V_b \frac{D\left[\left(1+\varepsilon_v\right)\phi^* N_i\right]}{Dt} - V_b \nabla \cdot \sum_{j=1}^{n_p} \left[\xi_j x_{ij} \frac{\bar{\bar{K}} k_{rj}}{\mu_j} \left(\nabla P_j - \gamma_j \nabla D\right) \right] - V_b \varepsilon_v \frac{D\left(\phi^* N_i\right)}{Dt} - q_i = 0, \tag{2-12}$$

$$i = 1, 2, ..., n_c + 1.$$

Equality of Component Fugacities

$$G_i\left(p,\ N_w, N_1,\ ...,\ N_{n_c},\ \ln K_1,\ ...,\ \ln K_{n_c};\ \vec{u}\right) \equiv f_i^{oil} - f_i^{gas} = 0, \qquad i = 1, 2, .., n_c. \tag{2-13}$$

Volume Constraint

$$H\left(p,\ N_w, N_1,\ ...,\ N_{n_c},\ \ln K_1,\ ...,\ \ln K_{n_c};\ \vec{u}\right) \equiv \sum_{j=1}^{3} \left(\frac{N_j}{\xi_j} \right) - 1.0 = 0. \tag{2-14}$$

The primary unknowns of Equations (2-10)-(2-14) are chosen as

$$P = P_w,\ N_w, N_1,\ ...,\ N_{n_c},\ \ln K_1,\ ...,\ \ln K_{n_c}, \vec{u}. \tag{2-15}$$

where the displacement vector $\vec{u} = \left(u_x, u_y, u_z\right)$. Here the total number of the "primary unknowns" is $2\left(n_c + 1\right) + 3 = 2n_c + 5$. The "secondary unknowns" are the saturations $S_j \ \left(j = w; 1,..., n_p\right)$, the mole fraction x_{ij} of component i in phase j, the effective stress tensor $\bar{\bar{\sigma}}'^{s}$, the strain tensor $\bar{\bar{\varepsilon}}$, etc. that can be determined using the values of the primary unknowns.

Equation (2-11) or (2-12) is derived in detail in Chapter 3. Note that Equation (2-11) or (2-12) reduces to Equation (2-1) when we ignore the solid velocity. Please also pay attention to two kinds of porosities in this research, the symbol ϕ denotes "reservoir porosity", while ϕ^* is true porosity calculated from the geomechanics model. The relationship between the reservoir porosity and the true porosity is given by Chin et al. (2002) as follows

$$\begin{cases} \phi^* = 1 - \left(1 - \phi_0\right) e^{-\varepsilon_v}, \\ \phi = \left(\dfrac{1 - \phi_0}{1 - \phi^*}\right) \phi^*. \end{cases} \tag{2-16}$$

or

$$\begin{cases} \phi^* = 1 - \left(1 - \phi_0\right) e^{-\varepsilon_v}, \\ \phi = \left(\dfrac{1 - \phi_0}{1 - \phi^*}\right) \phi^* = \left(\dfrac{1 - \phi_0}{\left(1 - \phi_0\right) e^{-\varepsilon_v}}\right) \left[1 - \left(1 - \phi_0\right) e^{-\varepsilon_v}\right] = e^{\varepsilon_v} - \left(1 - \phi_0\right). \end{cases} \tag{2-17}$$

2.2 SOLUTION PROCEDURES OF COUPLING METHODS

In fact, in this case methods of coupling mean solution procedures to the coupled multiphase multi-component model and geomechanics mathematical model, Equations (2-10)-(2-14). There are two kinds of coupling methods, the partially coupling (the stress equations, (2-10), and flow equations, (2-11)-(2-14), are solved separately for

each time increment or each Newton iteration) and fully coupling (two equations, (2-10)-(2-14), are solved simultaneously, like a pure one problem). Settari and Walters (1999) also classified different solutions into four kinds on the basis of the coupling degree: *decoupled, explicitly coupled, iteratively coupled, and fully coupled methods*.

Decoupled Method (Chin and Boade 1990; Fredrich et al. 1998; Settari and Walters 1999) The method is a one-way coupling / pseudo coupling in which two simulators essentially separately solve the individual equations over the same or different total time interval.

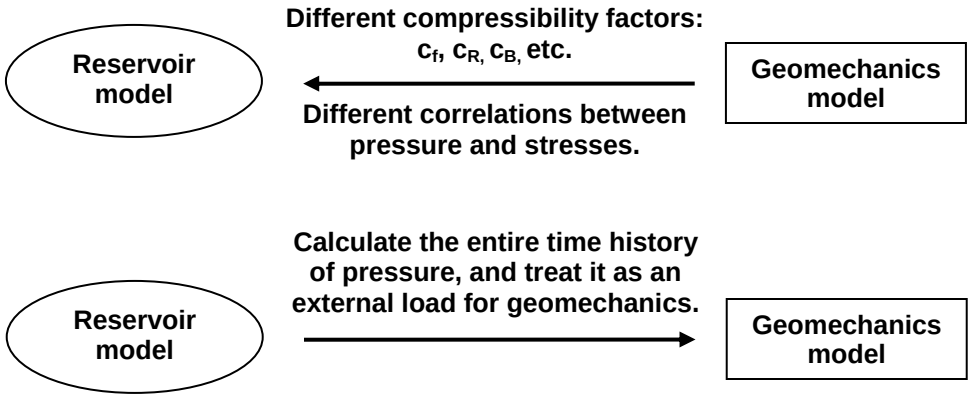

Figure 2-1: The decoupled method of geomechanics and reservoir models.

As shown in Figure 2-1, on the one hand, for a reservoir model, using compressibility factors, the same treatment as a traditional reservoir simulator, simulate the deformation behaviors of solids during hydrocarbon production; another option based on the correlations between pressure and stresses from the field data or lab work to approximate the stresses or displacements in the geomechanics model. In other words, the characteristic is that geomechanics model is not solved during the simulation. On the other hand, a reservoir simulator can firstly perform and output the entire history of

pressure; and then transfer the pressure to geomechanics as an external load for the geomechanics modeling. If the time intervals are different between the two models, the pressure must be interpolated firstly and then is transferred to geomechanics model.

Explicitly Coupled Method This method is asynchronous respect to the time-step or period (several time-steps) for reservoir simulation and geomechanical simulation so that there is one lag for coupled terms between two coupled models. Settari and Walters (1999) gave one time-step lag algorithm and also pointed out that the method solves the problems as rigorously as a fully coupled (simultaneous) solution if iterated to full convergence. Also, another explicitly coupled methods called a loose (staggered-in-time) coupling algorithm was presented by some researchers (Sulak et al. 1991; Koutsabeloulis and Hope 1998; Minkoff et al. 1999; Daim et al. 2002; Minkoff et al. 2003).

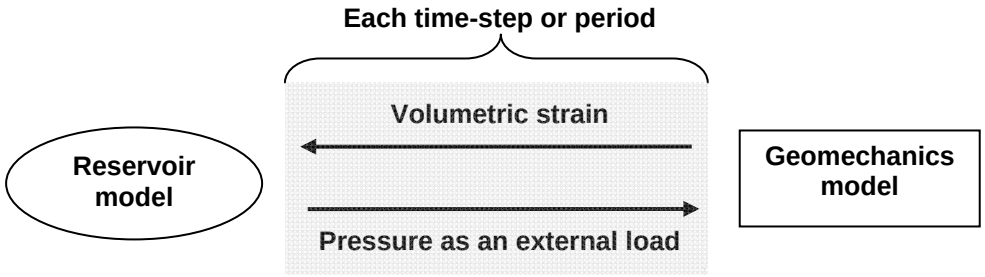

Figure 2-2: The explicit method of geomechanics and reservoir models.

Iteratively Coupled Method We rewrite the coupled Equations (2-10)-(2-14) in Section 2.1.3:

$$F_{fluid}\left(\vec{X}_f;\ \vec{u}\right)=0, \tag{2-18}$$

$$F_{solid}\left(\vec{X}_f;\ \vec{u}\right)=0, \tag{2-19}$$

where $\vec{X}_f=\left(p,\ N_w, N_1, ..., N_{n_c}, \ln K_1, ..., \ln K_{n_c}\right)$ is the unknown-vector of the compositional model, $\vec{u}=\left(u_x, u_y, u_z\right)$ is the displacement of the geomechanics model,

$F_{fluid} = \left(F_1,...,F_{n_c+1};G_1,...,G_{n_c};H\right)^{\mathrm{T}}$ is the nonlinear differential operator vector from the compositional model, $F_1,...,F_{n_c+1}$, $G_1,...,G_{n_c},H$ are defined by Equation (2-11) or (2-12), (2-13) and (2-14) in Section 2.1.3, $F_{solid} = \vec{E} = \left(E_x,\ E_y,\ E_z\right)^{\mathrm{T}}$ is the nonlinear differential operator vector from the geomechanics model, and $\vec{E}$ are defined by Equation (2-10) in Section 2.1.3.

Consider the following solution procedure:

$$\tilde{F}_{fluid}\left(\vec{X}_{f,k+1}^{n+1};\ \vec{u}_k^{n+1}\right) = 0, \tag{2-20}$$

where $\tilde{F}_{fluid}$ is a nonlinear function arising from its associated nonlinear iteration scheme of the F_{fluid} in the reservoir simulator. $\vec{u}_k^{n+1}$ is the k^{th} displacement of the approximate value to the $(n+1)^{th}$ time-step or period reservoir variables, such that $\lim_{k\to\infty}\vec{u}_k^{n+1} = \vec{u}^{n+1}$ and $\vec{u}_0^{n+1} = \vec{u}^{n}$. The unknown is the reservoir variables $\vec{X}_{f,k+1}^{n+1}$, the $(k+1)^{th}$ approximate value to the $(n+1)^{th}$ time-step or period, such that: $\lim_{k\to\infty}\vec{X}_{f,k}^{n+1} = \vec{X}_{f}^{n+1}$ and $\vec{X}_{f,0}^{n+1} = \vec{X}_{f}^{n}$, k is the number of nonlinear iteration.

$$F_{solid}\left(\vec{X}_{f,k+1}^{n+1};\ \vec{u}_{k+1}^{n+1}\right) = 0, \tag{2-21}$$

where $\vec{X}_{f,k+1}^{n+1}$ is the $(k+1)^{th}$ approximate value to the $(n+1)^{th}$ time-step or period reservoir variables just obtained from the nonlinear solver iteration of the reservoir model, and the unknown is $\vec{u}_{k+1}^{n+1}$, the displacement of the $(k+1)^{th}$ approximate value to the $(n+1)^{th}$ time-step or period variables. Equations (2-20) and (2-21) gives the *Gauss-Seidel method* for the nonlinear equations.

The above procedure is called *the iteratively coupled method*. Settari and Mourits (1994) firstly described this method. The coupling is implemented on the basis of the nonlinear iteration, not the time-step or period, of the reservoir simulation. And its outer loop is the nonlinear iteration at one time-step of the reservoir simulation embedded with the geomechanics model (see Figure 2-3).

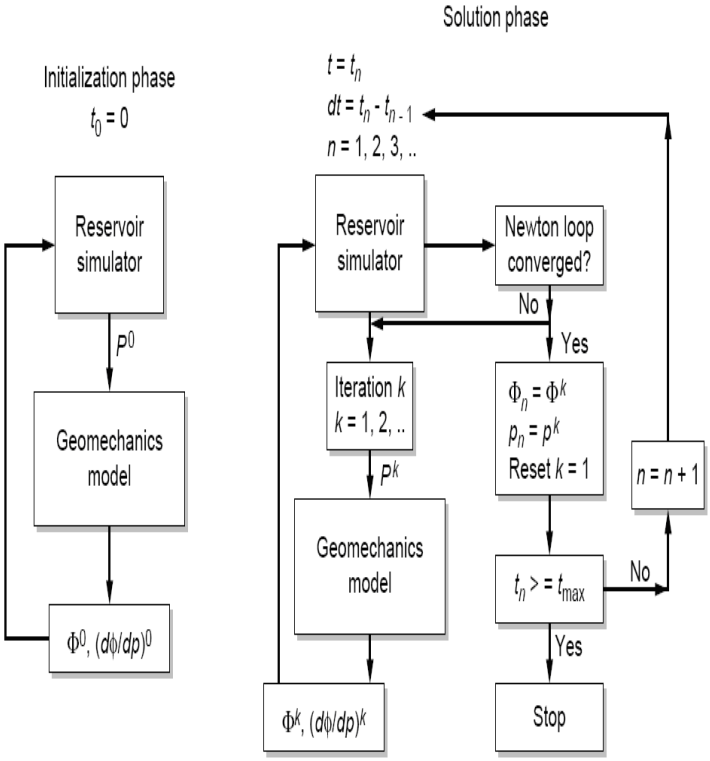

Figure 2-3: Flow Chart of Iteratively coupled Analysis (after Chin et al. 2002).

Another choice of the outer loop is based on the nonlinear iteration at one time-step of the geomechanics simulation with the embedded reservoir model (see Figure 2-4). Hence, there is one issue to decide which model's nonlinear solver is the main control iteration. The porosity and permeability needed by the reservoir simulator are not from some compressibility factors, but directly from the geomechanical model. The iteratively coupled method appears to be the most preferable method for field-scale simulation. Much work has been studied by numerous researchers for this method in the past years: fractured reservoirs model coupled with geomechanics (Ji et al. 2004; Bagheri and Settari 2005), interface functions between fluid-flow and rock stress variables (Tran et al. 2004; Tran et al. 2005), parallel realization (Thomas et al. 2002; Gai

et al. 2003; Gai 2004), application to weaker rock formations with complex constitutive behavior, and oil recovery caused by reservoir compaction (Chin and Thomas 1999; Chin et al. 2002).

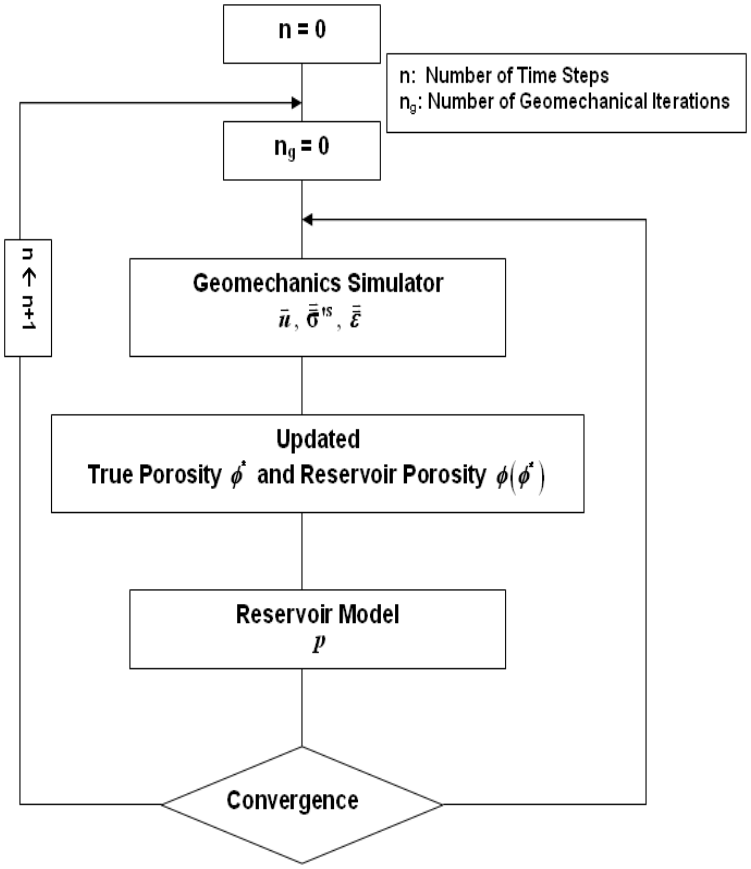

Figure 2-4: Flow Chart for Iteratively Coupling (after Tran et al. 2004).

Fully Coupled Method When simultaneously solving the coupled model with the same or different (mixed) discretization method, the solution is called the fully coupled method (Fredrich et al. 1998; Gutierrez and Lewis 1998; Koutsabeloulis and Hope 1998; Lewis and Schrefler 1998; Osorio et al. 1998; Chin et al. 1998a; Chin et al. 1998b; Chin et al. 2000; Settari 2000; Stone et al. 2000; Lewis and Pao 2002). The fully coupled method is completely synchronous respect to time-steps, periods, or nonlinear iterations of the

coupled geomechanical and reservoir modeling procedure, because the variables of the reservoir and geomechanics models are obtained simultaneously from solving one linear system at each nonlinear-iteration. Previously, the fully coupled method was considered less flexible than the iteratively coupled method because it cannot reuse the existing simulators in each field. However, Pan et al. (2009) proposed a new solution procedure for a fully coupled geomechanics and compositional modeling process. The novel solution procedure uses the Schur complement technique to solve the associated fully coupled Jacobian system. The proposed approach has the following features: (1) it has similar convergence properties as the fully implicit method, (2) combined with Krylov subspace iterative solvers, it can deal with symmetric and nonsymmetric problems, and (3) it can be easily parallelized to solve large-scale reservoir simulation problems.

2.3 COUPLING PARAMETERS

As many researchers (Settari and Mourits 1994; Settari and Mourits 1995; Settari 2000; Thomas et al. 2002) presented the coupling parameters between reservoir flow and rock (or soil) mechanics. There are main two kinds of coupling parameters: one is a volume coupling related to porosity, ϕ; and the other is a flow properties coupling related to permeability, $\bar{\bar{K}}$.

Let us analyze the coupled terms in the coupled mass conservation Equation (2-11) or (2-12). On the one hand, for the reservoir model, a true porosity (ϕ^*), a true permeability ($\bar{\bar{K}}$), and a volumetric strain (ε_v) appear; however, a true porosity (ϕ^*) and a true permeability ($\bar{\bar{K}}$) are all the function of the volumetric strain (ε_v), which is calculated from the geomechanics model. On the other hand, the (average) pressure (p) appears in Equation (2-10), which is calculated from the reservoir model.

Therefore, we can conclude that the coupling parameters between reservoir model and geomechanics model are the (average) pressure (p) and the volumetric strain (ε_v).

The (average) pressure (p) can be directly used in the geomechanics model; however, the usage of the volumetric strain (ε_v) in the reservoir model is complicated by the different formulations among the true porosity (ϕ^*), the true permeability ($\bar{\bar{K}}$),and the volumetric strain (ε_v).

2.3.1 Volume Coupling

The volume coupling refers to the reservoir porosity, ϕ, which is a function of not only the pressure from the reservoir model, but also the unknowns calculated from the geomechanics model. The reservoir porosity, ϕ, acts as the coupling interface (its implementation will be discussed in the next section) in coupled models.

2.3.2 Flow Properties Coupling

The flow properties coupling means that permeability, $\bar{\bar{K}}$, is a function of macroscopic variables (such as fluid pressure, porosity, mean normal stress, shear stress and strain etc.) while it is considered a constant tensor in the traditional reservoir simulators. Many studies (Chin et al. 1998a; Chin et al. 1998b) have shown that such "stress-dependent permeability" in a stress-sensitive reservoir has significant impacts on deformation process (geomechanics models) and fluid production (reservoir models).

The permeability relation with the volumetric strain ε_v, $\frac{k}{k_0} = \frac{1}{1+\varepsilon_v}\left(1+\frac{\varepsilon_v}{\phi_0}\right)$, is deduced by Ran and Li (1997) based on the Kozeny Equation (Peters 2004) $k = \frac{\phi}{k_z S_p^{\,2}}$ (k is a component of an isotropic permeability, k_z is the Kozeny constant, and S_p is the special surface area). Chin et al. (1998a; 1998b) performed studies to show the significant influences of a fully coupled model in a well-test analysis. They tested five

different permeability functions (Table 2-2). There are two procedures for implementing the stress-dependent permeability (Settari and Mourits 1995): implicit coupling (which updates the permeability at every iteration step each time-step) and explicitly coupling (which updates at the beginning of each time-step).

Table 2-2: Normalized Functions for Variable Permeability (after Chin et al. 1998a; Chin et al. 1998b)

State Variable	Normalized Permeability Functions
Fluid Pressure	$k/k_i = a + (1-a)(p/p_i)^n$
Porosity	$k/k_i = (\phi^*/\phi_i^*)^n$
Mean Normal Stress	$k/k_i = \left\{ ln\left[1+(\sigma^*/\sigma_n)^2\right] / ln\left[1+(\sigma^*/\sigma_{n,0})^2\right] \right\}^m$
Shear Stress	$k/k_i = 1-(1-a)(\tau/b)^n$
Axial Strain	$k/k_i = 1-(1-a)(\varepsilon_z/c)^n$

2.4 NUMERICAL MODELS AND SOLVERS

A finite element method is used to discretize the geomechanics model (Chin et al. 1998a; Chin et al. 1998b; Chin et al. 2002). The 8-node quadrilateral element and the 20-node hexahedron element shown in Figure 2-5 and Figure 2-6 are implemented for the two dimensional and three dimensional problems, respectively. Chapter 4 and Chapter 6 will discuss the finite element method and its implementation in detail.

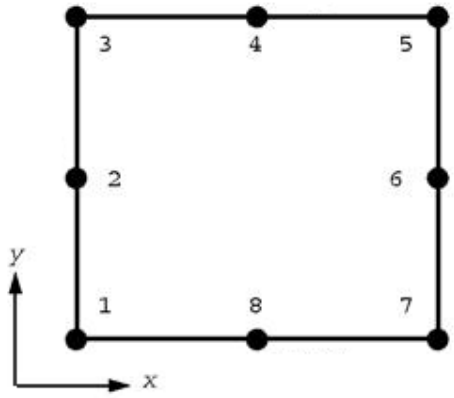

Figure 2-5: Local node numbering for the 8-node quadrilateral element.

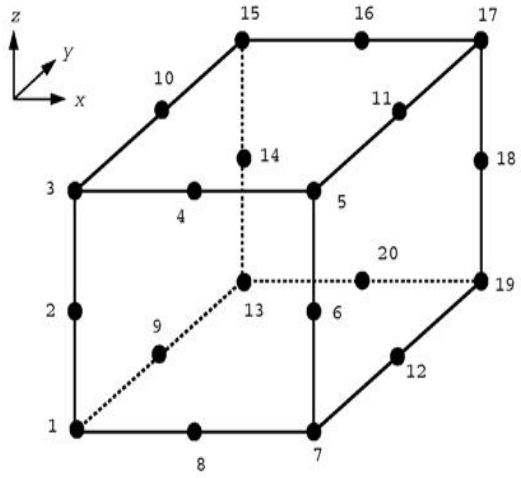

Figure 2-6: Local node numbering for the 20-node hexahedron element.

The coupled geomechanics and multi-component models can capture the interactions between the solid skeleton and fluid-flow. However the large run-time and large-scale computations from the discretized nonlinear systems are key issues for its application to the full-field studies. Hence, let us discuss the parallel realization for the coupled problems.

2.5 A PARALLEL FRAMEWORK

The research and development of an open (for research and modeling), high-efficient (in load balance, I/O, communication) parallel framework is significant for reservoir simulations nowadays. The framework supports the reservoir simulator to have a friendly research-interface, flexibly update new technologies, extend to multi-physical models (including thermal model, geomechanical model, geochemistry, solid transport), and use powerful parallel computing systems, etc. The modern reservoir simulator is not a single program code, but a complex, integrated software of multi-subjects. With the support of a friendly research-interface, the member of the group can only focus on his/her own specialty module under one consistent framework. For example, though the simulator is parallel, most developers do not consider this point and simply write the codes as for the sequential machines. A full-field fine simulation makes the parallel framework necessary for using multi-processors. Researchers from universities and companies in the oil industry have been paying attention to development of frameworks for parallel processing for many years. A simulator, called GPAS (General Purpose Adaptive Simulator) using a fully implicit method with corner point grid option, has been developed by the reservoir simulation group of The Center for Petroleum and Geosystems Engineering (CPGE) in The University of Texas at Austin (Wang et al. 1997; Wang et al. 1999). GPAS has a parallel framework; a developer abides by several rules to write his/her code under the framework. Consequently, the new developed code can be executed in parallel in conjunction with the framework. Namely, parallel interface and language is totally transparent to the developer. However, this framework is only working for the finite difference or control volume methods used in the GPAS. Hence, for the finite element method is used in geomechanics model, a similar parallel framework has to be developed for the

parallelization of the geomechanics code. In this work, we accomplish the parallel finite element framework as discussed in Chapter 8.

2.6 COMPOSITIONAL RESERVOIR SIMULATIONS AND GPAS

Though more than 75% of reservoir simulation is solved by a black-oil simulator, the other fluid types - volatile oil, condensate gas, wet gas and dry gas - still need a compositional simulator to determine oil and gas in place, to predict oil and gas reserves, to decide the approach for the enhanced oil recovery, and to make a reasonable production plan. Moreover, the fluid properties of black oils can be considered either functions of pressure only or functions of pressure and solution gas/oil ratio. However, for the gas condensates or volatile oils, their properties not only depend on pressure but also on the composition, which means the flash calculation based on an equation of state (EOS) is needed to calculate the compositions in each fluid phase during the production (Mattax and Dalton 1990). In addition, the miscible gas or carbon dioxide flooding and the chemical flooding also require the usage of compositional simulators. In order to capture the interactions between fluids and solids for this kind of reservoirs, a coupled geomechanics and compositional reservoir simulator has to be used.

2.7 SUMMARY

This Chapter was devoted to summarize the fundamentals of the coupled geomechanics and multiphase multicomponent reservoir simulation, which covers the mathematical model, the numerical mode, four kinds of solution procedures, and the coupling parameters exchanging between two models. The parallel framework and the necessity for using compositional simulators were also presented. We just presented an overview of the topics considered in this research. The technical details will be discussed in the following chapters.

3 Derivation of the Mathematical Model

The traditional reservoir simulators neglect the movements of the solid phase, which refers to the porous media or the skeleton in this research, during the hydrocarbon production. Therefore, the solid phase is treated as a stationary phase (Lake 1989). Yet, in this research, the porous medium is deforming in time during fluid-flows. In Chapter 2, we already reviewed the coupled model for simulating the solid deformations and fluid-flows and associated approaches.

The objective of this chapter is to derive the governing equations describing the multiphase, multicomponent fluid-flow in a deformable permeable media in detail. The derivation uses the Eulerian (or spatial) description in a fix coordinate, rather than the Lagrangian (or material) description (Spencer 1980). These governing equations will be used in our simulator to represent the fluid-flow and solid deformation behaviors in a porous medium. The derivation in this chapter combines the methodologies of Lake (1989) and Verruijt (1995). The derivation is consistent with that of other researchers: for example, the single phase flow (Verruijt 1995; Chin et al. 1998b; Smith and Griffiths 2004), the black oil model (Gai 2004), and the compositional model (Rutqvist et al. 2001; Wan 2002). After the derivation, different approximate formulations are discussed to solve the same mass balance equations based on the different assumptions (Wan 2002; Gai 2004). The difference between the coupled geomechanics and fluid-flow model and the traditional fluid-flow model is pointed out as well.

When the velocity of solid phase is assumed to be zero, the mass balance equations are the same as the one) used in GPAS (Wang et al. 1997; Wang et al. 1999.

3.1 ASSUMPTIONS

Before deriving the coupled field equations in Section 2.1, the following assumptions are introduced:

For the geomechanics model:

[G1] The small strain theory (Infinitesimal strain theory),

$$\|\vec{u}\| \le 1 \text{ and } \|\nabla \vec{u}\| \le 1, \tag{3-1}$$

is assumed, which means the displacements and the displacement gradients are small compared to unity.

[G2] The solid particles are incompressible, which means the deformation of reservoir results from the rearrangement of incompressible solid particles. Consequently, the density of solid is constant although the medium as a whole undergoes deformations which are changing the rock properties, e.g., porosity and permeability. Another explanation for this assumption is "because the compressibility of soil structure far exceeds the compressibility of both the water and the soil solids" (Terzaghi et al. 1996). Das (1998) summarized that the causes of the compression are a) deformation of soil particles, b) relocations of soil particles, and c) expulsion of water or air from the void space. In this research, b) and c) will be considered.

[G3] The solid velocity is negligibly small, which means that the material derivative is the same as the partial derivative or the Eulerian derivative and that Darcy's law is valid for the fluid-flow.

For the compositional model:

[C1] The reservoir is isothermal.

[C2] Darcy's law is valid to describe the multiphase flow in the porous media.

[C3] There are no chemical reactions in the reservoir.

[C4] There is only the water component in the aqueous phase.

[C5] The diffusive-dispersive between the water phase and the other phases is neglected, which means there are no mass fluxes (dispersion and mutual solubility) between the water phase and the other phases.

[C6] The oleic phases are in instantaneous equilibrium.

[C7] Water is slightly compressible and its viscosity is constant.

[C8] The injectors and producers are treated as source and sink terms, respectively.

[C9] There are no hydrocarbon and water components in the solid phase at any time.

3.2 THEORIES

Besides the assumptions listed in Section 3.1, we also need to clarify some definitions or terms.

3.2.1 Representative Elementary Volume (REV)

From the point of macroscopic view, the continuum mechanics means that a point within a medium is equivalent to a representative elementary volume (REV), over which an average is performed (Bear 1972). Using Euler's approach, a REV is a finite volume fixed in space. The "fixed in space" means that the shape and position of this REV remain unchangeable. All the properties associated REVs should be with respect to a fixed coordinate system (Euler coordinate system). For example, the velocity in a REV should be relative to the fixed frame of reference.

To summarize, the REV based on the Eulerian describes what is ongoing at specific points (forming a surface) within a medium as different particles pass through them (the surface) as time proceeds.

3.2.2 Velocity in Darcy's Law

Note that Darcy's law describes the fluid-flow behaviors with respect to the solid matrix (Biot 1956; Bear 1972) which may be moving or static. Hence, the velocity in REV is different from the one in Darcy's law, and there is a reference velocity, the solid velocity, between them.

3.3 GOVERNING EQUATIONS OF FLUID-FLOW IN DEFORMABLE POROUS MEDIA

Using the REV approach, the following derivation yields the mass conservation of Eulerian form in deformable porous media. "Deformable" means that the porosity of media is changeable with time and the solid skeleton has a velocity.

The multiphase compositional model used in GPAS, which is described by Wang, et al. (1997; 1999), can be described by the following partial differential equations, in which it is assumed that there are n_c hydrocarbon components and n_p phases including the aqueous phase.

Hydrocarbon Component Mass Balance

$$V_b \frac{\partial(\phi N_i)}{\partial t} + V_b \vec{\nabla} \cdot \sum_{j=1}^{n_p} \left(\xi_j x_{ij} \vec{v}_j \right) - q_i = 0, \qquad i = 1,2,..,n_c + 1, \tag{3-2}$$

where the moles of component i per unit pore volume $N_i = \sum_{j=1}^{n_p} \left(S_j x_{ij} \xi_j \right)$, $\vec{v}_j$ is the (relative) macroscopic Darcy (superficial) velocity for fluid phase j, ϕ is the *reservoir porosity*, and q_i is the molar injection (positive) or production (negative) rate for component i. Equation (3-2) assumes that the solid skeleton is stationary. If the

bulk volume V_b is divided by both sides and source term q_i is neglected, Equation (3-2) is simplified to

$$\frac{\partial(\phi N_i)}{\partial t} + \vec{\nabla} \cdot \sum_{j=1}^{n_p} \left(\xi_j x_{ij} \vec{v}_j \right) = 0, \qquad i = 1, 2, .., n_c + 1, \tag{3-3}$$

which is easier to be compared with other mass balance equations later.

The details of how to derive Equations (3-2) are presented by Lake (1989). This part extends Equation (3-2) to consider the solid is deforming during fluids are flowing through permeable media. Besides adapting the same procedure used by Lake, the extension also follows the approach in Verruijt (1995). In other words, there are mainly two modifications for the mass conversation equations:

1. The *true porosity* (ϕ^*) is used, other than the *reservoir porosity* (ϕ);
2. The *absolute* macroscopic *superficial* fluid phase velocity $\left(\phi^* S_j \vec{v}_{ij}^* \right)$ *with respect to a fixed coordinate system* is used, other than the *relative* macroscopic Darcy *(superficial)* fluid phase velocity $\vec{v}_j$ *with respect to a moving solid matrix*.

In traditional treatment, because the solid deformation velocity is zero, the absolute macroscopic superficial fluid phase velocity is the same as the relative macroscopic Darcy (superficial) fluid phase velocity.

Consider that there are n_p flowing phases (including aqueous phase), n_c components (excluding water) in the reservoir fluids. Firstly, the following relationships can be defined,

$$\xi_j = \sum_{i=1}^{n_c} \xi_{ij}, \tag{3-4}$$

$$x_{ij} = \frac{\xi_{ij}}{\xi_j}, \tag{3-5}$$

$$\vec{v}_j^* = \frac{1}{\xi_j}\sum_{i=1}^{n_c}\left(\xi_{ij}\cdot\vec{v}_{ij}^*\right) = \sum_{i=1}^{n_c}\left(x_{ij}\cdot\vec{v}_{ij}^*\right), \tag{3-6}$$

$$N_i = \sum_{j=1}^{n_p}\left(\xi_j S_j x_{ij}\right), \tag{3-7}$$

where ξ_{ij}, ξ_j, and x_{ij} are the molar density of component i in phase j, the molar density of phase j, and the molar fraction of component i in phase j, respectively. $\vec{v}_{ij}^*$ and $\vec{v}_j^*$ are the absolute macroscopic interstitial velocities with respect to a fixed coordinate system which are different from the relative macroscopic Darcy (superficial) velocity $\vec{v}_j$ respect to a moving solid matrix. N_i is the moles of component i per pore volume. Moreover, Equation (3-6) shows that the momentum per unit pore volume of the phase j is equal to the sum of momenta of the individual specials (Bear 1972).

Hence, the mass balance equation for the component i in the phase j can be obtained

$$\frac{\partial}{\partial t}\left[\left(\phi^* S_j\right)\left(\xi_j x_{ij}\right)\right] + \vec{\nabla}\cdot\left[\left(\xi_j x_{ij}\right)\left(\phi^* S_j \vec{v}_{ij}^*\right)\right] = \dot{R}_{ij} \qquad i = 1,...,n_c+1;\ j = 1,...,n_p, \tag{3-8}$$

where $\dot{R}_{ij}$ is the mass rate of production in units of mole of the component i in the phase j per bulk volume-time. In fact, the last equation is the same as the equation (4.3.1) on page 77 of Bear's book (1972),

$$\frac{\partial \rho_\alpha}{\partial t} + div\left(\rho_\alpha \vec{V}_\alpha\right) = I_\alpha, \tag{3-9}$$

where $\rho_{\alpha=ij} = \left(\phi^* S_j\right)\left(\xi_j x_{ij}\right)$ is the molar mass of component i in phase j per pore volume, namely, the molar density based on the pore volume; $\vec{V}_{\alpha=ij} = \vec{v}_{ij}^*$ is the absolute macroscopic interstitial velocities (with respect to a fixed coordinate system) of the

component i in phase j; $I_{\alpha=ij} = \dot{R}_{ij}$ is the mass production rate within the unit pore volume.

The diffusive-dispersive mass flux of component i in the phase j is

$$\vec{J}_{ij} = \left(\xi_j x_{ij}\right)\left(\phi^* S_j \vec{\tilde{v}}_{ij}^*\right), \tag{3-10}$$

where $\vec{\tilde{v}}_{ij}^*$ is the macroscopic diffusive-dispersive velocity, such that

$$\vec{\tilde{v}}_{ij}^* = \vec{v}_{ij}^* - \vec{v}_j^* \tag{3-11}$$

Inserting Equation (3-11) into Equation (3-8) arrives at

$$\frac{\partial}{\partial t}\left[\phi^*\left(\xi_j S_j x_{ij}\right)\right] + \vec{\nabla}\cdot\left[\left(\xi_j x_{ij}\right)\left(\phi^* S_j\left(\vec{\tilde{v}}_{ij}^* + \vec{v}_j^*\right)\right)\right] = \dot{R}_{ij},$$

$$\frac{\partial}{\partial t}\left[\phi^*\left(\xi_j S_j x_{ij}\right)\right] + \vec{\nabla}\cdot\left[\left(\xi_j x_{ij}\right)\left(\phi^* S_j \vec{v}_j^*\right)\right] + \vec{\nabla}\cdot\left[\left(\xi_j x_{ij}\right)\left(\phi^* S_j \vec{\tilde{v}}_{ij}^*\right)\right] = \dot{R}_{ij}.$$

Using Equation (3-10), we have

$$\frac{\partial}{\partial t}\left[\phi^*\left(\xi_j S_j x_{ij}\right)\right] + \vec{\nabla}\cdot\left[\left(\xi_j x_{ij}\right)\left(\phi^* S_j \vec{v}_j^*\right)\right] + \vec{\nabla}\cdot\vec{J}_{ij} = \dot{R}_{ij} \qquad i = 1,...,n_c+1;\ j = 1,...,n_p. \tag{3-12}$$

To sum Equations (3-12) over the n_p phases gives the continuity or conservation of total mass for the component i:

$$\frac{\partial}{\partial t}\sum_{j=1}^{n_p}\left[\phi^*\left(\xi_j S_j x_{ij}\right)\right] + \sum_{j=1}^{n_p}\left\{\vec{\nabla}\cdot\left[\left(\xi_j x_{ij}\right)\left(\phi^* S_j \vec{v}_j^*\right)\right]\right\} + \sum_{j=1}^{n_p}\left(\vec{\nabla}\cdot\vec{J}_{ij}\right) = \sum_{j=1}^{n_p}\left(\dot{R}_{ij}\right) \qquad i = 1,...,n_c+1. \tag{3-13}$$

When there are no chemical reactions, the right hand side of Equation (3-13) $\sum_{j=1}^{n_p}\left(\dot{R}_{ij}\right) = 0$ (for any component i). Finally, discarding the dispersion term, the governing equations of traditional isothermal reservoir simulation model become

$$\frac{\partial}{\partial t}\sum_{j=1}^{n_p}\left[\phi^*\left(\xi_j S_j x_{ij}\right)\right] + \sum_{j=1}^{n_p}\left\{\vec{\nabla}\cdot\left[\left(\xi_j x_{ij}\right)\left(\phi^* S_j \vec{v}_j^*\right)\right]\right\} = 0,\ \ i = 1,...,n_c. \tag{3-14}$$

For measuring the fluid-flow rate into or out of the porous media, the interstitial velocity for the phase j with respect to the solid phase

$$\vec{v}_j^* = \vec{v}_s + \vec{v}_{js}^*. \tag{3-15}$$

Substituting Equation (3-15) into Equations (3-14) gives

$$\frac{\partial}{\partial t}\sum_{j=1}^{n_p}\left[\phi^*\left(\xi_j S_j x_{ij}\right)\right] + \sum_{j=1}^{n_p}\left\{\vec{\nabla}\cdot\left[\left(\xi_j x_{ij}\right)\left(\phi^* S_j\left(\vec{v}_s + \vec{v}_{js}^*\right)\right)\right]\right\} = 0,\ \ i = 1,...,n_c. \tag{3-16}$$

Considering the true porosity ϕ^* is changing with time, and using the formula

$$\vec{\nabla}\cdot\left(\alpha\vec{u}\right) = \vec{u}\cdot\vec{\nabla}\alpha + \alpha\vec{\nabla}\cdot\vec{u}, \tag{3-17}$$

can rewrite Equation (3-16) as

$$\begin{aligned}\phi^*\frac{\partial}{\partial t}\left[\sum_{j=1}^{n_p}\left(\xi_j S_j x_{ij}\right)\right] + \frac{\partial\phi^*}{\partial t}\sum_{j=1}^{n_p}\left(\xi_j S_j x_{ij}\right) + \sum_{j=1}^{n_p}\left\{\vec{\nabla}\cdot\left[\left(\xi_j x_{ij}\right)\left(\phi^* S_j\vec{v}_{js}^*\right)\right]\right\} \\ + \sum_{j=1}^{n_p}\left\{\vec{\nabla}\cdot\left[\left(\xi_j S_j x_{ij}\right)\left(\phi^*\vec{v}_s\right)\right]\right\} = 0,\end{aligned} \tag{3-18}$$

$$\begin{aligned}\phi^*\frac{\partial}{\partial t}\left[\sum_{j=1}^{n_p}\left(\xi_j S_j x_{ij}\right)\right] + \underbrace{\frac{\partial\phi^*}{\partial t}\sum_{j=1}^{n_p}\left(\xi_j S_j x_{ij}\right)}_{A} + \sum_{j=1}^{n_p}\left\{\vec{\nabla}\cdot\left[\left(\xi_j x_{ij}\right)\left(\phi^* S_j\vec{v}_{js}^*\right)\right]\right\} \\ + \underbrace{\sum_{j=1}^{n_p}\left(\xi_j S_j x_{ij}\right)\vec{\nabla}\cdot\left(\phi^*\vec{v}_s\right)}_{B} + \left(\phi^*\vec{v}_s\right)\cdot\sum_{j=1}^{n_p}\left[\nabla\left(\xi_j S_j x_{ij}\right)\right] = 0.\end{aligned} \tag{3-19}$$

Combination of terms A and B in Equation (3-19) gives

$$\begin{aligned}\phi^*\frac{\partial}{\partial t}\left[\sum_{j=1}^{n_p}\left(\xi_j S_j x_{ij}\right)\right] + \sum_{j=1}^{n_p}\left\{\vec{\nabla}\cdot\left[\left(\xi_j x_{ij}\right)\left(\phi^* S_j\vec{v}_{js}^*\right)\right]\right\} + \left(\phi^*\vec{v}_s\right)\cdot\sum_{j=1}^{n_p}\left[\nabla\left(\xi_j S_j x_{ij}\right)\right] \\ + \sum_{j=1}^{n_p}\left(\xi_j S_j x_{ij}\right)\left[\frac{\partial\phi^*}{\partial t} + \vec{\nabla}\cdot\left(\phi^*\vec{v}_s\right)\right] = 0.\end{aligned} \tag{3-20}$$

From the mass balance equation of solid phase and using Assumption [G2], the following identity is true:

$$\frac{\partial\phi^*}{\partial t} + \vec{\nabla}\cdot\left(\phi^*\vec{v}_s\right) = \vec{\nabla}\cdot\vec{v}_s. \tag{3-21}$$

Hence, Equation (3-20) can be simplified to

$$\phi^* \frac{\partial}{\partial t}\left[\sum_{j=1}^{n_p}\left(\xi_j S_j x_{ij}\right)\right] + \sum_{j=1}^{n_p}\left\{\vec{\nabla}\cdot\left[\left(\xi_j x_{ij}\right)\left(\phi^* S_j \vec{v}_{js}^*\right)\right]\right\} + \left(\phi^* \vec{v}_s\right)\cdot\sum_{j=1}^{n_p}\left[\nabla\left(\xi_j S_j x_{ij}\right)\right] + \sum_{j=1}^{n_p}\left(\xi_j S_j x_{ij}\right)\left(\vec{\nabla}\cdot\vec{v}_s\right) = 0. \quad (3\text{-}22)$$

Note that the derivative of the true porosity respect to time is eliminated using the mass reservation of the solid phase. Using Equation (3-7), the above equation can be rewritten as

$$\phi^* \frac{\partial N_i}{\partial t} + \sum_{j=1}^{n_p}\left\{\vec{\nabla}\cdot\left[\left(\xi_j x_{ij}\right)\left(\phi^* S_j \vec{v}_{js}^*\right)\right]\right\} + \left(\phi^* \vec{v}_s\right)\cdot\nabla N_i + N_i\left(\vec{\nabla}\cdot\vec{v}_s\right) = 0. \quad (3\text{-}23)$$

In addition, using the definition of the material derivative,

$$\frac{D}{Dt}(*) \equiv \frac{\partial}{\partial t}(*) + \vec{v}^s\cdot\nabla(*), \quad (3\text{-}24)$$

to combine the 1st and 3rd terms of the above equation, the Equation (3-22) can be rearranged to be

$$\phi^* \frac{D}{Dt}\left(N_i\right) + \sum_{j=1}^{n_p}\left\{\vec{\nabla}\cdot\left[\left(\xi_j x_{ij}\right)\left(\phi^* S_j \vec{v}_{js}^*\right)\right]\right\} + N_i\left(\vec{\nabla}\cdot\vec{v}_s\right) = 0. \quad (3\text{-}25)$$

When the macroscopic Darcy velocity $\vec{\tilde{v}}_{js}$ with respect to the solid matrix,

$$\phi^* S_j \vec{v}_{js}^* = \vec{\tilde{v}}_{js}, \quad (3\text{-}26)$$

is used, Equation (3-23) can be rewritten as

$$\phi^* \frac{\partial N_i}{\partial t} + \sum_{j=1}^{n_p}\left\{\vec{\nabla}\cdot\left[\left(\xi_j x_{ij}\right)\vec{\tilde{v}}_{js}\right]\right\} + \left(\phi^* \vec{v}_s\right)\cdot\vec{\nabla} N_i + N_i\left(\vec{\nabla}\cdot\vec{v}_s\right) = 0, \quad i = 1,...,n_c+1, \quad (3\text{-}27)$$

$$\phi^* \frac{D}{Dt}\left(N_i\right) + \sum_{j=1}^{n_p}\left\{\vec{\nabla}\cdot\left[\left(\xi_j x_{ij}\right)\vec{\tilde{v}}_{js}\right]\right\} + N_i\left(\vec{\nabla}\cdot\vec{v}_s\right) = 0, \quad i = 1,...,n_c+1. \quad (3\text{-}28)$$

Equation (3-27) or (3-28) is the mass balance equations for each component *i* considering the solid deformations. From this equation, we can find that the differences

between Equations (3-27) and the traditional multiphase and multicomponent governing equations are the following:

(1) the true porosity ϕ^*, which is changing with time, is used;

(2) the *absolute* macroscopic *superficial* fluid phase velocity $\left(\phi^* S_j \vec{v}_{ij}^*\right)$ *with respect to a fixed coordinate system* is used for each component i in each phase j;

(3) the final equation for each component i has two extra terms, which are related the solid velocity $\vec{v}_s$.

In addition, $\left(\vec{\nabla}\cdot\vec{v}_s\right)$ can be expressed in term of skeleton volumetric strain ε_v:

$$\vec{\nabla}\cdot\vec{v}_s = \vec{\nabla}\cdot\frac{D\vec{u}_s}{Dt} = \frac{D\left(\vec{\nabla}\cdot\vec{u}_s\right)}{Dt} = \frac{D\varepsilon_v}{Dt}, \tag{3-29}$$

where $\vec{u}_s$ are the displacements of solid.

The above equation can be inserted into Equations (3-27) and (3-28), we arrive at

$$\phi^*\frac{\partial N_i}{\partial t} + \sum_{j=1}^{n_p}\left\{\vec{\nabla}\cdot\left[\left(\xi_j x_{ij}\right)\vec{\vec{v}}_{js}\right]\right\} + \left(\phi^*\vec{v}_s\right)\cdot\vec{\nabla}N_i + N_i\frac{D\varepsilon_v}{Dt} = 0, \qquad i = 1,...,n_c+1, \tag{3-30}$$

$$\phi^*\frac{D}{Dt}\left(N_i\right) + \sum_{j=1}^{n_p}\left\{\vec{\nabla}\cdot\left[\left(\xi_j x_{ij}\right)\vec{\vec{v}}_{js}\right]\right\} + N_i\frac{D\varepsilon_v}{Dt} = 0, \qquad i = 1,...,n_c+1. \tag{3-31}$$

For the mass balance equation of solid,

$$\frac{\partial}{\partial t}\left[\left(1-\phi^*\right)\rho_s\right] + \vec{\nabla}\cdot\left[\left(1-\phi^*\right)\rho_s\vec{v}_s\right] = 0, \tag{3-32}$$

we can derive the following identities,

$$\frac{\partial}{\partial t}\left[\left(1-\phi^*\right)\right] + \vec{\nabla}\cdot\left[\left(1-\phi^*\right)\vec{v}_s\right] = 0, \ \left(\text{assumption }[\text{G2}]\right). \tag{3-33}$$

Applying Equation (3-17) gives

$$\frac{\partial\left(1-\phi^*\right)}{\partial t}+\left(1-\phi^*\right)\vec{\nabla}\cdot\vec{v}_s+\vec{v}_s\cdot\vec{\nabla}\left(1-\phi^*\right)=0. \tag{3-34}$$

In term of the material derivative, Equation (3-24), and Equation (3-29), we obtain

$$\frac{D\left(1-\phi^*\right)}{Dt}+\left(1-\phi^*\right)\frac{D\varepsilon_v}{Dt}=0. \tag{3-35}$$

Inserting Equation (3-35) into Equation (3-31) gives

$$\phi^*\frac{D}{Dt}\left(N_i\right)+\sum_{j=1}^{n_p}\left\{\vec{\nabla}\cdot\left[\left(\xi_j x_{ij}\right)\vec{\tilde{v}}_{js}\right]\right\}+N_i\left[-\frac{1}{\left(1-\phi^*\right)}\frac{D\left(1-\phi^*\right)}{Dt}\right]=0,$$

$$\phi^*\frac{D}{Dt}\left(N_i\right)+N_i\frac{D}{Dt}\left(\phi^*\right)-N_i\frac{D}{Dt}\left(\phi^*\right)+\sum_{j=1}^{n_p}\left\{\vec{\nabla}\cdot\left[\left(\xi_j x_{ij}\right)\vec{\tilde{v}}_{js}\right]\right\}+N_i\left[\frac{1}{\left(1-\phi^*\right)}\frac{D\phi^*}{Dt}\right]=0,$$

$$\frac{D}{Dt}\left(\phi^* N_i\right)+\sum_{j=1}^{n_p}\left\{\vec{\nabla}\cdot\left[\left(\xi_j x_{ij}\right)\vec{\tilde{v}}_{js}\right]\right\}+N_i\left[\frac{1}{\left(1-\phi^*\right)}-1\right]\frac{D\phi^*}{Dt}=0,$$

$$\frac{D}{Dt}\left(\phi^* N_i\right)+\sum_{j=1}^{n_p}\left\{\vec{\nabla}\cdot\left[\left(\xi_j x_{ij}\right)\vec{\tilde{v}}_{js}\right]\right\}+N_i\left[\frac{\phi^*}{\left(1-\phi^*\right)}\right]\frac{D\phi^*}{Dt}=0,$$

$$\frac{D}{Dt}\left(\phi^* N_i\right)+\sum_{j=1}^{n_p}\left\{\vec{\nabla}\cdot\left[\left(\xi_j x_{ij}\right)\vec{\tilde{v}}_{js}\right]\right\}+N_i\left[\frac{-\phi^*}{\left(1-\phi^*\right)}\right]\frac{D\left(1-\phi^*\right)}{Dt}=0,$$

Finally, we obtain

$$\frac{D}{Dt}\left(\phi^* N_i\right)+\vec{\nabla}\cdot\left\{\sum_{j=1}^{n_p}\left[\left(\xi_j x_{ij}\right)\vec{\tilde{v}}_{js}\right]\right\}+\phi^* N_i\frac{D\varepsilon_v}{Dt}=0, \qquad i=1,..,n_c+1. \tag{3-36}$$

Comparison Equation (3-3) with Equation (3-36) gives the differences of mass balance equations between nondeformable and deformable medium as follows:

(1) the true porosity, ϕ^*, and reservoir porosity, ϕ;

(2) an additional term from the deformation of solid matrix, $\left(\phi^* N_i\frac{D\varepsilon_v}{Dt}\right)$, in Equation (3-36).

In short, the above differences results from the interactions between the solid deformation and fluid-flow.

Now, we have concluded the mass balance equations (MBEs) (Equations (3-31) or (3-36)):

$$\phi^* \frac{D}{Dt}\left(N_i\right) + \sum_{j=1}^{n_p}\left\{\vec{\nabla}\cdot\left[\left(\xi_j x_{ij}\right)\vec{\tilde{v}}_{js}\right]\right\} + N_i \frac{D\varepsilon_v}{Dt} = 0, \qquad i = 1,...,n_c+1, \tag{3-37}$$

or

$$\frac{D}{Dt}\left(\phi^* N_i\right) + \vec{\nabla}\cdot\left\{\sum_{j=1}^{n_p}\left[\left(\xi_j x_{ij}\right)\vec{\tilde{v}}_{js}\right]\right\} + \phi^* N_i \frac{D\varepsilon_v}{Dt} = 0, \quad i = 1,..,n_c+1. \tag{3-38}$$

The above equations are equivalent each other.

3.4 THE APPROXIMATIONS OF MBES

This section will discuss the different approximations of Equations (3-37) or (3-38) for the later numerical implementations. One approximation (as described below as Approximation 1) is used by Chin et al. (1998b) , Rutqvist et al. (2001), Wan (2002); another approximation (as described below as Approximation 2) is used by Chin et al. (2002) and Gai (2004). However, based on assumption [G3], they all replace the material derivatives with the partial derivatives or the Eulerian derivatives in Equations (3-37) or (3-38).

Approximation 1:

Based on Assumption [G3], the following is true,

$$\frac{D}{Dt}(*) \equiv \frac{\partial}{\partial t}(*) + \vec{v}^s \cdot \nabla(*) \approx \frac{\partial}{\partial t}(*). \tag{3-39}$$

Hence, Equation (3-37) is reduced to

$$\phi^* \frac{\partial N_i}{\partial t} + \sum_{j=1}^{n_p}\left\{\vec{\nabla}\cdot\left[\left(\xi_j x_{ij}\right)\vec{\tilde{v}}_{js}\right]\right\} + N_i \frac{\partial \varepsilon_v}{\partial t} = 0, \qquad i = 1,...,n_c+1, \tag{3-40}$$

which discards the terms

$$\text{Error1} \equiv \phi^* \vec{v}^s \cdot \nabla\left(N_i\right) + N_i \vec{v}^s \cdot \nabla\left(\varepsilon_v\right). \tag{3-41}$$

Approximation 2:

For Equation (3-38), firstly, the following rearrangement should be done,

$$\frac{D}{Dt}\left(\phi^* N_i\right) + \vec{\nabla} \cdot \left\{ \sum_{j=1}^{n_p} \left[\left(\xi_j x_{ij}\right) \vec{\tilde{v}}_{js} \right] \right\} + \phi^* N_i \frac{D\varepsilon_v}{Dt} = 0,$$

$$\frac{D}{Dt}\left(\phi^* N_i\right) + \vec{\nabla} \cdot \left\{ \sum_{j=1}^{n_p} \left[\left(\xi_j x_{ij}\right) \vec{\tilde{v}}_{js} \right] \right\} + \phi^* N_i \frac{D\varepsilon_v}{Dt} + \varepsilon_v \frac{D\left(\phi^* N_i\right)}{Dt} - \varepsilon_v \frac{D\left(\phi^* N_i\right)}{Dt} = 0,$$

$$\frac{D}{Dt}\left(\phi^* N_i\right) + \vec{\nabla} \cdot \left\{ \sum_{j=1}^{n_p} \left[\left(\xi_j x_{ij}\right) \vec{\tilde{v}}_{js} \right] \right\} + \frac{D\left(\phi^* N_i \varepsilon_v\right)}{Dt} - \varepsilon_v \frac{D\left(\phi^* N_i\right)}{Dt} = 0,$$

$$\frac{D}{Dt}\left[\phi^* N_i \left(1+\varepsilon_v\right)\right] + \vec{\nabla} \cdot \left\{ \sum_{j=1}^{n_p} \left[\left(\xi_j x_{ij}\right) \vec{\tilde{v}}_{js} \right] \right\} - \varepsilon_v \frac{D\left(\phi^* N_i\right)}{Dt} = 0. \tag{3-42}$$

Since $\left|\varepsilon_v\right| \ll 1$ for the small strain theory,

$$\frac{D}{Dt}\left(\phi^* N_i\right) \gg \varepsilon_v \frac{D\left(\phi^* N_i\right)}{Dt}. \tag{3-43}$$

After the last term is neglected, Equation (3-42) is reduced to

$$\frac{D}{Dt}\left[\phi^* N_i \left(1+\varepsilon_v\right)\right] + \vec{\nabla} \cdot \left\{ \sum_{j=1}^{n_p} \left[\left(\xi_j x_{ij}\right) \vec{\tilde{v}}_{js} \right] \right\} = 0. \tag{3-44}$$

Using (3-39) for the above equation yields

$$\frac{\partial}{\partial t}\left[\phi^* \left(1+\varepsilon_v\right) N_i\right] + \vec{\nabla} \cdot \left\{ \sum_{j=1}^{n_p} \left[\left(\xi_j x_{ij}\right) \vec{\tilde{v}}_{js} \right] \right\} = 0. \tag{3-45}$$

When the reservoir porosity in the coupled geomechanics and fluid-flow model, which is different from the reservoir porosity in the traditional reservoir simulators defined in Equation (1-15), is defined as

$$\phi \equiv \left(1+\varepsilon_v\right)\phi^*; \tag{3-46}$$

hence, Equation (3-45) can be also rewritten as

$$\frac{\partial}{\partial t}\left(\phi N_i\right)+\vec{\nabla}\cdot\left\{\sum_{j=1}^{n_p}\left[\left(\xi_j x_{ij}\right)\vec{v}_{js}\right]\right\}=0. \tag{3-47}$$

which has a similar form to Equation (3-3).

From Equation (3-38) through Equation (3-45), the discarded terms are

$$\text{Error2}\equiv\vec{v}^{\,s}\cdot\nabla\left[\phi^*\left(1+\varepsilon_v\right)N_i\right]-\varepsilon_v\frac{D\left(\phi^* N_i\right)}{Dt}. \tag{3-48}$$

Comparison of Approximations 1 and 2

Equations (3-40) and (3-45) are different, because they drop off different terms, Equations (3-41) and (3-48), respectively.

From Equations (3-35) and (3-39), we can determine

$$\left.\begin{aligned}&\frac{D\left(1-\phi^*\right)}{Dt}+\left(1-\phi^*\right)\frac{D\varepsilon_v}{Dt}=0\\&\frac{D(*)}{Dt}\approx\frac{\partial(*)}{\partial t}\end{aligned}\right\}\Rightarrow\vec{v}_s\cdot\vec{\nabla}\left(1-\phi^*\right)+\left(1-\phi^*\right)\vec{v}_s\cdot\vec{\nabla}\varepsilon_v\approx 0. \tag{3-49}$$

Using (3-49), after simple algebraic derivations,

$$\text{Error1}=\phi^*\vec{v}^{\,s}\cdot\vec{\nabla}\left(N_i\right)+N_i\vec{v}^{\,s}\cdot\vec{\nabla}\left(\varepsilon_v\right)\approx\phi^*\vec{v}^{\,s}\cdot\vec{\nabla}\left(N_i\right)+N_i\left[-\frac{1}{\left(1-\phi^*\right)}\right]\vec{v}_s\cdot\vec{\nabla}\left(1-\phi^*\right)$$

$$=\phi^*\vec{v}^{\,s}\cdot\vec{\nabla}\left(N_i\right)+N_i\left[-\frac{\left(1-\phi^*\right)+\phi^*}{\left(1-\phi^*\right)}\right]\vec{v}_s\cdot\vec{\nabla}\left(1-\phi^*\right)$$

$$=\phi^*\vec{v}^{\,s}\cdot\vec{\nabla}\left(N_i\right)+N_i\left[-1-\frac{\phi^*}{\left(1-\phi^*\right)}\right]\vec{v}_s\cdot\vec{\nabla}\left(1-\phi^*\right)$$

$$=\phi^*\vec{v}^{\,s}\cdot\vec{\nabla}\left(N_i\right)-N_i\vec{v}_s\cdot\vec{\nabla}\left(1-\phi^*\right)-\frac{\phi^*}{\left(1-\phi^*\right)}N_i\vec{v}_s\cdot\vec{\nabla}\left(1-\phi^*\right)$$

$$=\vec{v}^{\,s}\cdot\vec{\nabla}\left(\phi^* N_i\right)-\frac{\phi^*}{\left(1-\phi^*\right)}N_i\vec{v}_s\cdot\vec{\nabla}\left(1-\phi^*\right)$$

$$=\vec{v}^{\,s}\cdot\vec{\nabla}\left(\phi^* N_i\right)+\phi^* N_i\left[-\frac{1}{\left(1-\phi^*\right)}\right]\vec{v}_s\cdot\vec{\nabla}\left(1-\phi^*\right)$$

$$
\begin{aligned}
&\approx \vec{v}^{s}\cdot\vec{\nabla}\left(\phi^{*}N_i\right)+\vec{v}^{s}\cdot\left(\phi^{*}N_i\right)\vec{\nabla}\left(\varepsilon_v\right)\\
&=\vec{v}^{s}\cdot\vec{\nabla}\left(\phi^{*}N_i\right)+\vec{v}^{s}\cdot\left[\left(\phi^{*}N_i\right)\vec{\nabla}\left(\varepsilon_v\right)+\varepsilon_v\vec{\nabla}\left(\phi^{*}N_i\right)-\varepsilon_v\vec{\nabla}\left(\phi^{*}N_i\right)\right]\\
&=\vec{v}^{s}\cdot\vec{\nabla}\left(\phi^{*}N_i\right)+\vec{v}^{s}\cdot\left[\vec{\nabla}\left(\phi^{*}N_i\varepsilon_v\right)-\varepsilon_v\vec{\nabla}\left(\phi^{*}N_i\right)\right]\\
&=\vec{v}^{s}\cdot\vec{\nabla}\left[\left(1+\varepsilon_v\right)\phi^{*}N_i\right]-\varepsilon_v\vec{v}^{s}\cdot\vec{\nabla}\left(\phi^{*}N_i\right)\\
&=\vec{v}^{s}\cdot\vec{\nabla}\left[\left(1+\varepsilon_v\right)\phi^{*}N_i\right]-\varepsilon_v\left\{\vec{v}^{s}\cdot\vec{\nabla}\left(\phi^{*}N_i\right)+\frac{\partial\left(\phi^{*}N_i\right)}{\partial t}-\frac{\partial\left(\phi^{*}N_i\right)}{\partial t}\right\}\\
&=\vec{v}^{s}\cdot\vec{\nabla}\left[\left(1+\varepsilon_v\right)\phi^{*}N_i\right]-\varepsilon_v\left\{\frac{D\left(\phi^{*}N_i\right)}{Dt}-\frac{\partial\left(\phi^{*}N_i\right)}{\partial t}\right\}\\
&=\text{Error2}+\varepsilon_v\frac{\partial\left(\phi^{*}N_i\right)}{\partial t}.
\end{aligned}
$$

In other words, we know the difference between *Approximation 1* and *2* is the term, $\varepsilon_v\dfrac{\partial\left(\phi^{*}N_i\right)}{\partial t}$; however, using assumption [G3], $\varepsilon_v\dfrac{\partial\left(\phi^{*}N_i\right)}{\partial t}\approx\varepsilon_v\dfrac{D\left(\phi^{*}N_i\right)}{Dt}$, which is neglected because of Equation (3-43). So we can conclude that Error1 equals Error2, which means Approximations 1 and 2 are the same with an additional assumption (3-43). During coding the simulator, Equations (3-40) or (3-45) can be used, but in this research, we use Equation (3-40) without the additional assumption (3-43).

3.5 DECOUPLING OF FLUID-FLOW EQUATIONS USING THE EQUIVALENT ROCK COMPRESSIBILITY

In Equations (3-37), (3-38), (3-40), or (3-47), there are all the coupling terms $\dfrac{D\varepsilon_v}{Dt}$ or $\dfrac{\partial\left(\phi N_i\right)}{\partial t}=\dfrac{\partial\left[\phi^{*}\left(1+\varepsilon_v\right)N_i\right]}{\partial t}$ which are contributed by the geomechanics to the fluid-flow. In this section, a decoupling approach will be discussed. The objective is to transfer this coupling term related to geomechanics parameters to the term related to fluid-flow and static geomechanics parameters equivalently. The above transition or decoupling is crucial to the convergence of the iteratively coupled solution procedure which will be discussed in Section 6.2.5.

Table 3-1: The coefficient of consolidation

Dimension (n)	**Terzaghi-Rendulic pseudo consolidation theory**	**Biot true consolidation theory**	**Coefficient of consolidation** ($\frac{\partial \varepsilon_v}{\partial p} = m_{v,n}, n = 1,2,3$)
1	$\frac{\partial \varepsilon_v}{\partial t} = \frac{(1-2v)(1+v)}{E(1-v)}\left(-\frac{\partial p}{\partial t}\right),$ $\frac{\partial \theta_1}{\partial t} = 0.$	$\frac{\partial \varepsilon_v}{\partial t} = \frac{(1-2v)(1+v)}{E(1-v)}\left(\frac{\partial \theta_1}{\partial t} - \frac{\partial p}{\partial t}\right).$	$\frac{(1-2v)(1+v)}{E(1-v)}$
2	$\frac{\partial \varepsilon_v}{\partial t} = \frac{2(1-2v)(1+v)}{E}\left(-\frac{\partial p}{\partial t}\right),$ $\frac{\partial \theta_2}{\partial t} = 0.$	$\frac{\partial \varepsilon_v}{\partial t} = \frac{(1-2v)(1+v)}{E}\frac{\partial \theta_2}{\partial t} - \frac{2(1-2v)(1+v)}{E}\frac{\partial p}{\partial t}.$	$\frac{2(1-2v)(1+v)}{E}$
3	$\frac{\partial \varepsilon_v}{\partial t} = \frac{3(1-2v)}{E}\left(-\frac{\partial p}{\partial t}\right),$ $\frac{\partial \theta_3}{\partial t} = 0.$	$\frac{\partial \varepsilon_v}{\partial t} = \frac{(1-2v)}{E}\frac{\partial \theta_3}{\partial t} - \frac{3(1-2v)}{E}\frac{\partial p}{\partial t}.$	$\frac{3(1-2v)}{E}$

In Table 3-1, the second column and the forth column shows the relationships of Terzaghi-Rendulic pseudo consolidation theory and the coefficients of consolidation for one, two and three dimensional cases. Using the above relationships, the coupling terms in the fluid-flow equations can be decoupled from the geomechanics parameters. The derivation of Table 3-1 and the associated implementation will be discussed in detail in Section 6.2.5.

3.6 SPECIAL CASE: SINGLE PHASE FLOW THROUGH POROUS MEDIA

If there is only one flowing phase and one component in this phase, the following equations are true:

$$\begin{cases} n_p = 1, \\ n_c = 1, \\ S_j = 1, \\ x_{ij} = 1, \\ \xi_j = \rho_f, \\ N_i = \sum_{j=1}^{1} \left(\xi_j \cdot 1 \cdot 1 \right) = \xi_j = \rho_f. \end{cases} \tag{3-50}$$

Hence, Equation (3-40) changes to a special form:

$$\phi^* \frac{\partial N_i}{\partial t} + \sum_{j=1}^{n_p} \left\{ \vec{\nabla} \cdot \left[\left(\xi_j x_{ij} \right) \vec{\bar{v}}_{js} \right] \right\} + N_i \frac{\partial \varepsilon_v}{\partial t} = 0, \qquad i = 1, ..., n_c + 1; \tag{3-51}$$

$$\phi^* \frac{\partial \rho_f}{\partial t} + \vec{\nabla} \cdot \left(\rho_f \vec{\bar{v}}_{fs} \right) + \rho_f \frac{\partial \varepsilon_v}{\partial t} = 0, \tag{3-52}$$

or (from Equation (3-30))

$$\phi^* \frac{\partial \rho_f}{\partial t} + \vec{\nabla} \cdot \left(\rho_f \vec{\bar{v}}_{fs} \right) + \left(\phi^* \vec{v}_s \right) \cdot \vec{\nabla} \rho_f + \rho_f \left(\vec{\nabla} \cdot \vec{v}_s \right) = 0. \tag{3-53}$$

With the assumption of impressible homogeneous fluid phase, the density ρ_f is a constant, which is independent of $x, y, z,$ and t. Equations (3-52) and (3-53) all can be simplified further

$$\vec{\nabla}\cdot\vec{\tilde{v}}_{ps}+\frac{\partial\varepsilon_v}{\partial t}=0, \tag{3-54}$$

or,

$$\vec{\nabla}\cdot\vec{\tilde{v}}_{ps}+\vec{\nabla}\cdot\vec{v}_s=0. \tag{3-55}$$

Using Darcy's law

$$\vec{\tilde{v}}_{fs}=-\frac{\vec{\tilde{k}}}{\mu_f}\left(\vec{\nabla}p-\rho_f\vec{g}\right), \tag{3-56}$$

and neglecting the gravity, Equation (3-55) is specified as

$$-\vec{\nabla}\cdot\left[\frac{\vec{\tilde{k}}}{\mu_f}\vec{\nabla}p\right]+\frac{\partial\varepsilon_v}{\partial t}=0. \tag{3-57}$$

Finally, Equation (3-57) is identical with the equation in Smith and Griffiths (2004) under the following assumptions:

(1) the single phase is incompressible and homogeneous: namely, the density of the fluid phase is constant;

(2) the gravity is neglected.

3.7 THE COMPLETE MATHEMATICAL MODEL

When we consider the source term q_i and substitute Darcy's law

$$\vec{\tilde{v}}_{js}=-\frac{\vec{\tilde{K}}k_{rj}}{\mu_j}\left(\nabla P_j-\gamma_j\nabla D\right), \tag{3-58}$$

into Equations (3-40) or (3-45), the final version of the mass balance equations arrive at

$$V_b\frac{D}{Dt}\left(\phi^* N_i\right)-V_b\vec{\nabla}\cdot\left\{\sum_{j=1}^{n_p}\left[\left(\xi_j x_{ij}\right)\frac{\vec{\tilde{K}}k_{rj}}{\mu_j}\left(\nabla P_j-\gamma_j\nabla D\right)\right]\right\}+V_b\phi^* N_i\frac{D\varepsilon_v}{Dt}-q_i=0, \tag{3-59}$$

$$i=1,..,n_c+1,$$

or

$$V_b \frac{D\left[\left(1+\varepsilon_v\right)\phi^* N_i\right]}{Dt} - V_b \nabla \cdot \sum_{j=1}^{n_p}\left[\xi_j x_{ij} \frac{\bar{\bar{K}} k_{rj}}{\mu_j}\left(\nabla P_j - \gamma_j \nabla D\right)\right] - V_b \varepsilon_v \frac{D\left(\phi^* N_i\right)}{Dt} - q_i = 0, \qquad (3\text{-}60)$$

$$i = 1, 2, ..., n_c + 1,$$

or

$$\frac{D}{Dt}\left(\phi N_i\right) + \vec{\nabla} \cdot \left\{\sum_{j=1}^{n_p}\left[\left(\xi_j x_{ij}\right)\vec{\tilde{v}}_{js}\right]\right\} = 0, \qquad (3\text{-}61)$$

where the reservoir porosity, $\phi \equiv \left(1+\varepsilon_v\right)\phi^*$, in the coupled geomechanics and fluid-flow model. Of course, the material derivatives, $\frac{D}{Dt}(*) \equiv \frac{\partial}{\partial t}(*) + \vec{v}^s \cdot \nabla(*) \approx \frac{\partial}{\partial t}(*)$, can be approximated using the partial derivative or the Eulerian derivatives for all the above equations.

3.8 SUMMARY

Using the Eulerian approach, a complete set of mass conservation equations is derived to describe a multiphase multicomponent fluid-flow in the deformable permeable media. The mass conservation equations used in the traditional compositional reservoir simulators can be considered as a specific case when the movement of solid phase is ignored.

4 Discretization of the Coupled Model

The mathematical model of the physical process representing fluid-flow and solid deformation in stress-sensitive reservoirs is presented in Chapter 3, which is a set of partial differential equations (the governing equations) coupling the variables of the compositional model and the geomechanical model. In general, the coupled model is strongly nonlinear; hence a numerical rather than analytical solution is applied to solve the equations. In this work, we use the finite difference method (FDM) and the finite element method (FEM) to discretize the compositional governing equations and the geomechanical governing equations in the space domain respectively, while we use the finite difference method to discretize the compositional governing equations and the geomechanical governing equations in the temporal domain. In this chapter, we first review the discretization of the governing equations of the compositional model considering the geomechanics effect using FDM in the two solution domain of space and time and then derive the numerical model of the geomechanics including the fluid-flow effect using FEM in the space domain.

4.1 DISCRETIZATION OF THE COMPOSITIONAL MODEL

Let us recall the mass balance equation for fluid-flow, Equations (2-11) or (2-12), in Chapter 2.

$$F_i\left(p,\ N_w, N_1,\ ...,\ N_{n_c},\ \ln K_1,\ ...,\ \ln K_{n_c};\ \vec{u}\right) \equiv$$

$$V_b \frac{D}{Dt}\left(\phi^* N_i\right) - V_b \vec{\nabla} \cdot \left\{ \sum_{j=1}^{n_p} \left[\left(\xi_j x_{ij}\right) \frac{\vec{\vec{K}} k_{rj}}{\mu_j} \left(\nabla P_j - \gamma_j \nabla D\right) \right] \right\} + V_b \phi^* N_i \frac{D\varepsilon_v}{Dt} - q_i = 0, \qquad (2\text{-}11)$$

$$i = 1, .., n_c + 1;$$

or

$$F_i\left(p,\ N_w, N_1,\ ...,\ N_{n_c},\ \ln K_1,\ ...,\ \ln K_{n_c};\ \vec{u}\right) \equiv$$

$$V_b \frac{D\left[\left(1+\varepsilon_v\right)\phi^* N_i\right]}{Dt} - V_b \nabla \cdot \sum_{j=1}^{n_p}\left[\xi_j x_{ij} \frac{\bar{\bar{K}} k_{rj}}{\mu_j}\left(\nabla P_j - \gamma_j \nabla D\right)\right] - V_b \varepsilon_v \frac{D\left(\phi^* N_i\right)}{Dt} - q_i = 0, \qquad (2\text{-}12)$$

$$i = 1, 2, ..., n_c + 1.$$

Based on Assumption [G3] in Chapter 3, the following is true,

$$\frac{D}{Dt}(*) \equiv \frac{\partial}{\partial t}(*) + \vec{v}^s \cdot \nabla(*) \approx \frac{\partial}{\partial t}(*). \qquad (3\text{-}39)$$

Hence, Equations (2-11) or (2-12) can be approximate as follows:

$$F_i\left(p,\ N_w, N_1,\ ...,\ N_{n_c},\ \ln K_1,\ ...,\ \ln K_{n_c};\ \vec{u}\right) \approx$$

$$V_b \frac{\partial}{\partial t}\left(\phi^* N_i\right) - V_b \vec{\nabla} \cdot \left\{\sum_{j=1}^{n_p}\left[\left(\xi_j x_{ij}\right)\frac{\bar{\bar{K}} k_{rj}}{\mu_j}\left(\nabla P_j - \gamma_j \nabla D\right)\right]\right\} + V_b \phi^* N_i \frac{\partial \varepsilon_v}{\partial t} - q_i = 0, \qquad (4\text{-}1)$$

$$i = 1, .., n_c + 1,$$

or

$$F_i\left(p,\ N_w, N_1,\ ...,\ N_{n_c},\ \ln K_1,\ ...,\ \ln K_{n_c};\ \vec{u}\right) \approx$$

$$V_b \frac{\partial\left[\left(1+\varepsilon_v\right)\phi^* N_i\right]}{\partial t} - V_b \nabla \cdot \sum_{j=1}^{n_p}\left[\xi_j x_{ij} \frac{\bar{\bar{K}} k_{rj}}{\mu_j}\left(\nabla P_j - \gamma_j \nabla D\right)\right] - V_b \varepsilon_v \frac{\partial\left(\phi^* N_i\right)}{\partial t} - q_i = 0, \qquad (4\text{-}2)$$

$$i = 1, 2, ..., n_c + 1,$$

where the true porosity ϕ^* is computed using the volumetric strain ε_v and the initial porosity ϕ_0,

$$\phi^* = 1 - \left(1 - \phi_0\right) e^{-\varepsilon_v}; \qquad (4\text{-}3)$$

and

$$\phi \equiv \left(1 + \varepsilon_v\right)\phi^*, \qquad (4\text{-}4)$$

is called the reservoir porosity in the coupled geomechanics and fluid-flow model, which is different from the reservoir porosity in the traditional reservoir simulators defined in Equation (1-15).

In this section, we show the discretization process of Equation (4-1) using the finite difference method. Of course, a similar process can be used for Equation (4-2), as well.

There are four terms in the left hand side of Equation (4-1). Because the second (convection) and fourth (source) terms are the same as the one in the traditional compositional model used in GPAS, we focus only on the discretizations of the first and third accumulation terms in the temporal domain. For simplicity in the following derivation, the symbol C denotes the finite difference term after discretization in space for Equation (4-1). Furthermore, the discretization in time space can be done as follows:

For the first accumulation term, using the backward-difference (Smith 1985) for $\frac{\partial}{\partial t}(\cdot)$ gives

$$\left[V_b \frac{\partial}{\partial t}\left(\phi^* N_i\right)\right]^{n+1} \approx \left(V_b\right)^{n+1} \frac{\left(\phi^* N_i\right)^{n+1} - \left(\phi^* N_i\right)^n}{\Delta t}, \tag{4-5}$$

where $\Delta t = t^{n+1} - t^n$, $\left(\cdot\right)^n$ or $\left[\cdot\right]^n$ mean a variable valued at the n$^{\text{th}}$ time-step level.

For the third accumulation term,

$$\left[V_b \phi^* N_i \frac{\partial \varepsilon_v}{\partial t}\right]^{n+1} \approx \left(V_b \phi^* N_i\right)^{n+1} \frac{\left(\varepsilon_v\right)^{n+1} - \left(\varepsilon_v\right)^n}{\Delta t}. \tag{4-6}$$

After that, we arrive at

$$F_i \approx \tilde{F}_i\left(\vec{Y}\right) \equiv C + \left(V_b\right)^{n+1} \frac{\left(\phi^* N_i\right)^{n+1} - \left(\phi^* N_i\right)^n}{\Delta t} + \left(V_b \phi^* N_i\right)^{n+1} \frac{\left(\varepsilon_v\right)^{n+1} - \left(\varepsilon_v\right)^n}{\Delta t} = 0, \quad i = 1,..,n_c+1, \tag{4-7}$$

or

$$\vec{\tilde{F}}\left(\vec{Y}\right) \equiv \left\{\tilde{F}_1\left(\vec{Y}\right), \cdots, \tilde{F}_{n_c+1}\left(\vec{Y}\right)\right\}^T = \vec{0}, \tag{4-8}$$

where $\tilde{F}_i$ is a nonlinear function arising from its associated discretization scheme of the F_i in the both space and time domains, $\vec{\tilde{F}}$ is the vector function of $\tilde{F}_i\ (i = 1,..,n_c+1;)$, and the unknown vector is

$$\begin{aligned} \vec{Y} = &\left\{\left(p,\ N_w, N_1,\ ...,\ N_{n_c},\ \ln K_1,\ ...,\ \ln K_{n_c};\ \vec{u}\right)_1,\right. \\ &\cdots, \\ &\left.\left(p,\ N_w, N_1,\ ...,\ N_{n_c},\ \ln K_1,\ ...,\ \ln K_{n_c};\ \vec{u}\right)_{n_c+1}\right\}^T. \end{aligned} \tag{4-9}$$

Now, we consider the nonlinear solution process to Equation (4-7) using the classical Newton method. $\vec{Y}^{n+1,k}$ is the k^{th} iteration solution of the approximate value to the $(n+1)^{th}$ time-step, such that

$$\lim_{k\to\infty} \vec{Y}^{n+1,k} = \vec{Y}^{n+1}; \tag{4-10}$$

Assume that $\vec{Y}^{n+1,k}$ is known and $\vec{Y}^{n+1,k+1}$ is to be calculated

$$\vec{\tilde{F}}\left(\vec{Y}^{n+1,k+1}\right) \approx \vec{\tilde{F}}\left(\vec{Y}^{n+1,k}\right) + \vec{\tilde{F}}'\left(\vec{Y}^{n+1,k}\right)\left(\vec{Y}^{n+1,k+1} - \vec{Y}^{n+1,k}\right) = \vec{\tilde{F}}\left(\vec{Y}^{n+1,k}\right) + \vec{\tilde{F}}'\left(\vec{Y}^{n+1,k}\right)\Delta\vec{Y}^{n+1,k} = \vec{0}, \tag{4-11}$$

or

$$\vec{\tilde{F}}\left(\vec{Y}^{n+1,k+1}\right) \approx \vec{\tilde{F}}\left(\vec{Y}^{n+1,k}\right) + \vec{\tilde{F}}'\left(\vec{Y}^{n+1,k}\right)\Delta\vec{Y}^{n+1,k} = \vec{0}, \tag{4-12}$$

where

$$\Delta\vec{Y}^{n+1,k} = \left(\vec{Y}^{n+1,k+1} - \vec{Y}^{n+1,k}\right). \tag{4-13}$$

In short, rewriting Equations (4-12) and (4-13) gives the classical Newton iteration process for Equaiton (4-7):

$$\begin{aligned} \Delta\vec{Y}^{n+1,k} &= \left[\vec{\tilde{F}}'\left(\vec{Y}^{n+1,k}\right)\right]^{-1}\left[-\vec{\tilde{F}}\left(\vec{Y}^{n+1,k}\right)\right], \\ \vec{Y}^{n+1,k+1} &= \vec{Y}^{n+1,k} + \Delta\vec{Y}^{n+1,k}, \end{aligned} \tag{4-14}$$

where $\vec{Y}^{n+1,0} = \vec{Y}^{n}$. Now, let us evaluate the contributions from the last two accumulation terms in Equaiton (4-7) to the residual ($\vec{R}$ or R_i, $i = 1,...,2n_c + 5$) and the Jacobian matrix (J), respectively:

$$\vec{R}\left(\vec{Y}^{n+1,k}\right) \equiv \vec{\tilde{F}}\left(\vec{Y}^{n+1,k}\right), \tag{4-15}$$

$$J\left(\vec{Y}^{n+1,k}\right) \equiv \vec{\tilde{F}}'\left(\vec{Y}^{n+1,k}\right). \tag{4-16}$$

4.1.1 Residuals of Accumulation Terms

From Equations (4-7) and (4-15), the residual can be computed as follows:

$$R_i = \tilde{F}_i\left(\vec{Y}^{n+1,k}\right) \equiv C + \left(V_b\right)^{n+1,k} \frac{\left(\phi^* N_i\right)^{n+1,k} - \left(\phi^* N_i\right)^{n}}{\Delta t} + \left(V_b \phi^* N_i\right)^{n+1,k} \frac{\left(\varepsilon_v\right)^{n+1,k} - \left(\varepsilon_v\right)^{n}}{\Delta t}, \tag{4-17}$$

$$i = 1,..,n_c + 1;$$

where $\left(\cdot\right)^{n}$ is already known from the previous time-step.

4.1.2 Derivatives of Accumulation Terms

In this section, we prefer to denote the Jacobian matrix, J as a two by two matrix,

$$\begin{bmatrix} \mathrm{A}_{11}^{\mathrm{GEOM}} & \mathrm{A}_{12}^{\mathrm{GEOM}\leftarrow\mathrm{GPAS}} \\ \mathrm{A}_{21}^{\mathrm{GPAS}\leftarrow\mathrm{GEOM}} & \mathrm{A}_{22}^{\mathrm{GPAS}} \end{bmatrix} \begin{bmatrix} \mathrm{x}_1^{\mathrm{GEOM}} \\ \mathrm{x}_2^{\mathrm{GPAS}} \end{bmatrix} = \begin{bmatrix} \mathrm{b}_1^{\mathrm{GEOM}} \\ \mathrm{b}_2^{\mathrm{GPAS}} \end{bmatrix}, \tag{4-18}$$

where $\mathrm{A}_{11}, \mathrm{A}_{12}, \mathrm{x}_1,$ and b_1 are matrices and vectors from the geomechanics model (with a superscript GEOM), while $\mathrm{A}_{21}, \mathrm{A}_{22}, \mathrm{x}_2,$ and b_2 are matrices and vectors from the fluid-flow model (with a superscript GPAS). A_{12} and A_{21} are the coupling matrices contributed from the coupling of fluid-flow (GEOM←GPAS) and models geomechanics (GPAS←GEOM). The dimensions of x_1 and x_2 are $\mathrm{s1}$ and $\mathrm{f1}$, respectively. Here, for notational convenience in the following discussions, we neglect all the superscripts, GEOM, GPAS, GEOM←GPAS, and GPAS←GEOM.

The coupling (sub)matrices in the Jacobian matrix are not formed in this approach. What we need is the products of the coupling (sub)matrix and the one certain vector.

$$\left[\tilde{F}_i\left(\vec{Y}\right)\right]' = \left[C + \left(V_b\right)^{n+1}\frac{\left(\phi^* N_i\right)^{n+1} - \left(\phi^* N_i\right)^n}{\Delta t} + \left(V_b\phi^* N_i\right)^{n+1}\frac{\left(\varepsilon_v\right)^{n+1} - \left(\varepsilon_v\right)^n}{\Delta t}\right]', \quad (4\text{-}19)$$

$$i = 1,..,n_c + 1;$$

$$\left[\tilde{F}_i\left(\vec{Y}\right)\right]'$$

$$= \left[C + \left(V_b\right)^{n+1}\frac{\left(\phi^* N_i\right)^{n+1} - \left(\phi^* N_i\right)^n}{\Delta t} + \left(V_b\phi^* N_i\right)^{n+1}\frac{\left(\varepsilon_v\right)^{n+1} - \left(\varepsilon_v\right)^n}{\Delta t}\right]'$$

$$= \left[C + \frac{\left(V_b\phi^* N_i\right)^{n+1} - \left(V_b\right)^{n+1}\left(\phi^* N_i\right)^n}{\Delta t} + \left(V_b\phi^* N_i\right)^{n+1}\frac{\left(\varepsilon_v\right)^{n+1} - \left(\varepsilon_v\right)^n}{\Delta t}\right]'$$

$$\approx \left[C + \frac{\overbrace{\left(V_b\right)^0}^{\text{constant}}\left(\phi^* N_i\right)^{n+1,k} - \overbrace{\left(V_b\right)^0\left(\phi^* N_i\right)^n}^{\text{constant}}}{\Delta t} + \overbrace{\left(V_b\right)^0}^{\text{constant}}\left(\phi^* N_i\right)^{n+1,k}\frac{\left(\varepsilon_v\right)^{n+1,k} - \left(\varepsilon_v\right)^n}{\Delta t}\right]'$$

$$= \left[C + \frac{\left(V_b\right)^0\left(\phi^* N_i\right)^{n+1,k}}{\Delta t} + \frac{\left(\varepsilon_v\right)^{n+1,k} - \left(\varepsilon_v\right)^n}{\Delta t}\left(V_b\right)^0\left(\phi^* N_i\right)^{n+1,k}\right]'$$

$$= \left[C + \left[1 + \left(\left(\varepsilon_v\right)^{n+1,k} - \left(\varepsilon_v\right)^n\right)\right]\frac{\left(V_b\right)^0}{\Delta t}\left(\phi^* N_i\right)^{n+1}\right]' \quad (4\text{-}20)$$

$$= C' + \frac{\left[1 + \left(\left(\varepsilon_v\right)^{n+1,k} - \left(\varepsilon_v\right)^n\right)\right]\left(V_b\right)^0}{\Delta t}\left\{\frac{\partial}{\partial p}\left(\phi^* N_i\right)^{n+1} + \frac{\partial}{\partial N_i}\left(\phi^* N_i\right)^{n+1}\right\}.$$

The above equation is used to update the Jacobian matrix at each Newton iteration.

4.2 DISCRETIZATION OF THE GEOMECHANICS MODEL

In this section, the matrix system of geomechanics model using FEM is derived. The starting point is the differential equations of the stress equilibrium that were described in Chapter 3. Here, we derived the three dimensional (3D) problems.

A three dimensional deformable solid body ($\boldsymbol{\Omega}$), as shown in Figure 4-1, is subjected to two types of *external loads*, either *body forces* or *surface forces*. Body forces are $\mathbf{b}\left[\mathrm{N/m^3}\right]$ (for example, gravity and pore pressure in porous media); surface forces are the prescribed tractions $\bar{\mathbf{t}}\left[\mathrm{N/m^2}\right]$ on boundary $\boldsymbol{\Gamma}_{\boldsymbol{\sigma}}$.

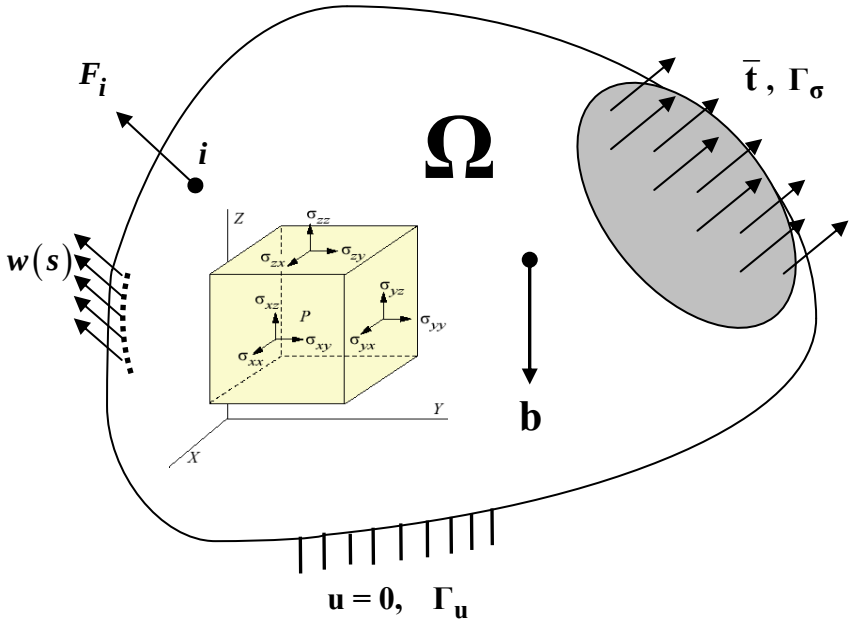

Figure 4-1: A three-dimensional deformable body.

According to the geometric size of the contacts between two bodies, surface forces $\bar{\mathbf{t}}$ can be approximated to the following types:

(1) *Concentrated forces*: if the contact area is so small compared with the total surface area of the body that the surface force ($\boldsymbol{F_i}$) can be approximate as a force applied to one point $\boldsymbol{i}$ of the body;

(2) *Linear distributed loads*: if the contact area ($\boldsymbol{s}$) is very narrow, the surface forces $\bar{\mathbf{t}}$ can be idealized as a series of forces along the curve $\boldsymbol{s}$.

Before deriving the virtual work principle for the deformable system ($\boldsymbol{\Omega}$), strain energy (Hibbeler 2004) as a kind of internal work should be introduced first. When loads are applied to a solid body and result in the deformations, the external work done by the external loads will be converted into the internal work done by the stresses inside the body. This is called *strain energy*, which is caused by the stresses and is stored in the body.

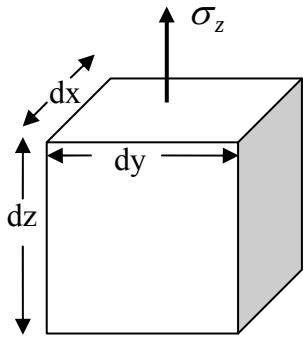

Figure 4-2: A three-dimensional element.

Figure 4-2 shows that one three-dimensional element ($\mathrm{dx}\cdot\mathrm{dy}\cdot\mathrm{dz}$) is subject to a normal stress σ_z. The force from the normal stress on the top is $F_z = \sigma_z \mathrm{dxdy}$. Assuming F_z is constant during the displacement ($\varepsilon_z \mathrm{dz}$), the work done by F_z is

$$F_z\left(\varepsilon_z dz\right) = \sigma_z dxdy\varepsilon_z dz = \sigma_z\varepsilon_z dxdydz = \sigma_z\varepsilon_z dV. \tag{4-21}$$

In general, the strain energy is

$$\int_{\Omega} \left(\varepsilon_z\right)^T \sigma_z d\Omega. \tag{4-22}$$

4.2.1 The General Form of VWP

Zienkiewicz (1972) stated that the external and internal work done by different forces, loads, stresses during a virtual displacement are equal to each other. Namely, the work done during the virtual displacement is zero. This is the so-called the virtual work principle.

4.2.1.1 Voigt Notation

In Figure 4-1, stresses $\boldsymbol{\sigma}$ and the associated strains $\boldsymbol{\varepsilon}$ are all second-order tensors of nine components,

$$\boldsymbol{\sigma} = \begin{bmatrix} \sigma_{xx} & \tau_{xy} & \tau_{xz} \\ \tau_{xy} & \sigma_{yy} & \tau_{yz} \\ \tau_{xz} & \tau_{yz} & \sigma_{zz} \end{bmatrix}, \tag{4-23}$$

$$\boldsymbol{\varepsilon} = \begin{bmatrix} \varepsilon_{xx} & \gamma_{xy} & \gamma_{xz} \\ \tau_{xy} & \varepsilon_{yy} & \gamma_{yz} \\ \gamma_{xz} & \gamma_{yz} & \varepsilon_{zz} \end{bmatrix}. \tag{4-24}$$

Using Voigt kinematics rule, the above tensorial formats can be deducted to the vectors or matrix forms with six components. Hence, we can use the vectors $\vec{\boldsymbol{\sigma}}$ and $\vec{\boldsymbol{\varepsilon}}$ to denote the stress and strain tensors $\boldsymbol{\sigma}$ and $\boldsymbol{\varepsilon}$, respectively. The displacement $\vec{\mathbf{u}}$, the body forces $\vec{\mathbf{b}}$, and the surface forces $\vec{\mathbf{t}}$ are all vectors which have the same number of components as $\vec{\mathbf{u}}$ for the follow expressions to be valid.

In Figure 4-1, for an arbitrary point (x, y, z) in $\boldsymbol{\Omega}$, its displacement, strain, and stress are

$$\vec{\mathbf{u}}_{(x,y,z)} = \left[u, v, w\right]^T_{(x,y,z)}, \tag{4-25}$$

$$\vec{\boldsymbol{\varepsilon}}_{(x,y,z)} = \left[\varepsilon_x, \varepsilon_y, \varepsilon_z, \gamma_{xy}, \gamma_{yz}, \gamma_{zx}\right]^T_{(x,y,z)}, \tag{4-26}$$

$$\vec{\boldsymbol{\sigma}}_{(x,y,z)} = \left[\sigma_x, \sigma_y, \sigma_z, \tau_{xy}, \tau_{yz}, \tau_{zx}\right]^T_{(x,y,z)}, \tag{4-27}$$

respectively. Because the pore-pressure p only effects the three normal stresses ($\sigma_x, \sigma_y, \sigma_z$), the pore-pressure vector $\vec{\mathbf{p}}$ is

$$\vec{\mathbf{p}}_{(x,y,z)} = p_{(x,y,z)} \cdot \vec{\mathbf{m}}^T, \tag{4-28}$$

where

$$\vec{\mathbf{m}}^T = \left(1,1,1,0,0,0\right)^T. \tag{4-29}$$

4.2.1.2 Derivation of the General Form of VWP

The internal forces are the stresses $\boldsymbol{\sigma}$ or $\vec{\boldsymbol{\sigma}}$ induced by external loads; the external forces are the body forces $\vec{\mathbf{b}}$ and the surface forces $\vec{\mathbf{t}}$. Hence during the virtual and compatible displacement-strain changes $\delta\mathbf{u}$ and $\delta\boldsymbol{\varepsilon}$, such that

$$\delta\vec{\boldsymbol{\varepsilon}} = \left[\mathbf{B}\right]\delta\vec{\mathbf{u}}, \tag{4-30}$$

the external work done by the body forces $\vec{\mathbf{b}}$ and the surface forces $\vec{\mathbf{t}}$,

$$\int_{\Omega} \delta\vec{\mathbf{u}}^T \mathbf{b}\, d\Omega + \int_{\Gamma_\sigma} \delta\vec{\mathbf{u}}^T \vec{\mathbf{t}}\, d\Gamma, \tag{4-31}$$

and the internal work done by the stresses $\vec{\boldsymbol{\sigma}}$,

$$\int_{\Omega} \delta\vec{\boldsymbol{\varepsilon}}^T \vec{\boldsymbol{\sigma}}\, d\Omega, \tag{4-32}$$

have to be equal, namely, the sum of virtual work must be zero. From Equations (4-31) and (4-32), we have

$$\int_{\Omega} \delta\vec{\boldsymbol{\varepsilon}}^T \vec{\boldsymbol{\sigma}}\, d\Omega = \int_{\Omega} \delta\vec{\mathbf{u}}^T \vec{\mathbf{b}}\, d\Omega + \int_{\Gamma_\sigma} \delta\vec{\mathbf{u}}^T \vec{\mathbf{t}}\, d\Gamma. \tag{4-33}$$

Rewriting Equation (4-33), then the virtual work of this system is:

$$\int_{\Omega} \delta\vec{\boldsymbol{\varepsilon}}^T \vec{\boldsymbol{\sigma}}\, d\Omega - \int_{\Omega} \delta\vec{\mathbf{u}}^T \vec{\mathbf{b}}\, d\Omega - \int_{\Gamma_\sigma} \delta\vec{\mathbf{u}}^T \vec{\mathbf{t}}\, d\Gamma = 0, \tag{4-34}$$

where $\vec{\mathbf{u}}$ is the displacement vectors which satisfies prescribed displacement on boundary $\mathbf{\Gamma_u}$, $\vec{\boldsymbol{\varepsilon}}$ the strains, $\vec{\boldsymbol{\sigma}}$ the stresses.

The dimensional analysis of Equation (4-34) shows that all the terms of the virtual work principle are consistent in unit, $[\mathrm{N}\cdot\mathrm{m}]$.

$$\int_{\Omega}\delta\vec{\boldsymbol{\varepsilon}}^{T}[1]\vec{\boldsymbol{\sigma}}\left[\frac{\mathrm{N}}{\mathrm{m}^2}\right]d\Omega\left[\mathrm{m}^3\right]-\int_{\Omega}\delta\vec{\mathbf{u}}^{T}[\mathrm{m}]\vec{\mathbf{b}}\left[\frac{\mathrm{N}}{\mathrm{m}^3}\right]d\Omega\left[\mathrm{m}^3\right]-\int_{\Gamma_\sigma}\delta\vec{\mathbf{u}}^{T}[\mathrm{m}]\vec{\mathbf{t}}\left[\frac{\mathrm{N}}{\mathrm{m}^2}\right]d\Gamma\left[\mathrm{m}^2\right]=0. \quad (4\text{-}35)$$

It is important to note that Equation (4-34) is a general form of the virtual work principle without any assumptions. In next section, the virtual work principle will apply to deformable porous media, together with the effective stress law (Terzaghi 1936; Biot 1941).

4.2.2 Terzaghi Application of VWP to Deformable Porous Media

Terzaghi (1936) and Biot (1941) proposed the effective stress law as follows:

$$\vec{\boldsymbol{\sigma}}=\vec{\boldsymbol{\sigma}}'+\vec{\mathbf{p}}, \quad (4\text{-}36)$$

where the vector $\vec{\boldsymbol{\sigma}}$ denotes the total stresses, $\vec{\boldsymbol{\sigma}}'$ the effective stresses, and $\vec{\mathbf{p}}$ the pore-pressures (or excessive pressures) of fluids.

For a deformable porous body, as shown in Figure 4-1 and Figure 4-2, in the absence of body forces $\vec{\mathbf{b}}$ in Equation (4-34), substituting Equation (4-36) into Equation (4-34) results in the virtual work principle for this case is

$$\int_{\Omega}\delta\vec{\boldsymbol{\varepsilon}}^{T}\vec{\boldsymbol{\sigma}}'\,d\Omega+\int_{\Omega}\delta\vec{\boldsymbol{\varepsilon}}^{T}\vec{\mathbf{p}}\,d\Omega-\int_{\Gamma_\sigma}\delta\vec{\mathbf{u}}^{T}\vec{\mathbf{t}}\,d\Gamma=0. \quad (4\text{-}37)$$

From Equation (4-37), the pore-pressure $\vec{\mathbf{p}}$ is considered as a body forces ($-\vec{\mathbf{p}}$) applied to the porous media.

4.2.3 The Finite Element Discretization

Because the incremental form is valid for nonlinear deformation analysis, we directly write the incremental form of the effective stress law (Equation (4-36)) and the virtual work principle (Equation (4-37))

$$\Delta\vec{\boldsymbol{\sigma}} = \Delta\vec{\boldsymbol{\sigma}}' + \Delta\vec{\mathbf{p}}, \tag{4-38}$$

$$\int_{\Omega} \delta\vec{\boldsymbol{\varepsilon}}^{T} \Delta\vec{\boldsymbol{\sigma}}' \, d\Omega + \int_{\Omega} \delta\vec{\boldsymbol{\varepsilon}}^{T} \Delta\vec{\mathbf{p}} \, d\Omega - \int_{\Gamma_{\sigma}} \delta\vec{\mathbf{u}}^{T} \Delta\vec{\mathbf{t}} \, d\Gamma = 0, \tag{4-39}$$

where Δ denotes the changes of two consecutive time-steps.

4.2.3.1 Displacements Function

The displacement is selected as the primary unknown in Equation (4-39). Moreover, the displacement can be approximated using the shape functions of the element.

$$\bar{\mathbf{u}}_{(x,y,z)} \approx \begin{bmatrix} \mathrm{N}_1 & 0 & 0 & \mathrm{N}_2 & 0 & 0 & \mathrm{N}_3 & 0 & 0 & \cdots \\ 0 & \mathrm{N}_1 & 0 & 0 & \mathrm{N}_2 & 0 & 0 & \mathrm{N}_3 & 0 & \cdots \\ 0 & 0 & \mathrm{N}_1 & 0 & 0 & \mathrm{N}_2 & 0 & 0 & \mathrm{N}_3 & \cdots \end{bmatrix}_{(x,y,z)} \begin{Bmatrix} u_1 \\ v_1 \\ w_1 \\ u_2 \\ v_2 \\ w_2 \\ u_3 \\ v_3 \\ w_3 \\ \vdots \end{Bmatrix} \equiv \left[\mathbf{N}\right]_{(x,y,z)} \left\{\mathbf{u}\right\}. \tag{4-40}$$

4.2.3.2 Strains and Displacements

The relationship between stains and displacements is as follows:

$$\vec{\boldsymbol{\varepsilon}}_{(x,y,z)} = \begin{bmatrix} \frac{\partial}{\partial x} & 0 & 0 \\ 0 & \frac{\partial}{\partial y} & 0 \\ 0 & 0 & \frac{\partial}{\partial z} \\ \frac{\partial}{\partial y} & \frac{\partial}{\partial x} & 0 \\ 0 & \frac{\partial}{\partial z} & \frac{\partial}{\partial y} \\ \frac{\partial}{\partial z} & 0 & \frac{\partial}{\partial x} \end{bmatrix} \vec{\mathbf{u}}_{(x,y,z)} = \begin{bmatrix} \frac{\partial}{\partial x} & 0 & 0 \\ 0 & \frac{\partial}{\partial y} & 0 \\ 0 & 0 & \frac{\partial}{\partial z} \\ \frac{\partial}{\partial y} & \frac{\partial}{\partial x} & 0 \\ 0 & \frac{\partial}{\partial z} & \frac{\partial}{\partial y} \\ \frac{\partial}{\partial z} & 0 & \frac{\partial}{\partial x} \end{bmatrix} \begin{bmatrix} u \\ v \\ w \end{bmatrix}_{(x,y,z)} \approx \begin{bmatrix} \frac{\partial}{\partial x} & 0 & 0 \\ 0 & \frac{\partial}{\partial y} & 0 \\ 0 & 0 & \frac{\partial}{\partial z} \\ \frac{\partial}{\partial y} & \frac{\partial}{\partial x} & 0 \\ 0 & \frac{\partial}{\partial z} & \frac{\partial}{\partial y} \\ \frac{\partial}{\partial z} & 0 & \frac{\partial}{\partial x} \end{bmatrix} \left[\mathbf{N}\right]_{(x,y,z)} \left\{\mathbf{u}\right\},$$

$$= \begin{bmatrix} \frac{\partial}{\partial x} & 0 & 0 \\ 0 & \frac{\partial}{\partial y} & 0 \\ 0 & 0 & \frac{\partial}{\partial z} \\ \frac{\partial}{\partial y} & \frac{\partial}{\partial x} & 0 \\ 0 & \frac{\partial}{\partial z} & \frac{\partial}{\partial y} \\ \frac{\partial}{\partial z} & 0 & \frac{\partial}{\partial x} \end{bmatrix} \begin{bmatrix} \mathrm{N}_1 & 0 & 0 & \mathrm{N}_2 & 0 & 0 & \mathrm{N}_3 & 0 & 0 & \cdots \\ 0 & \mathrm{N}_1 & 0 & 0 & \mathrm{N}_2 & 0 & 0 & \mathrm{N}_3 & 0 & \cdots \\ 0 & 0 & \mathrm{N}_1 & 0 & 0 & \mathrm{N}_2 & 0 & 0 & \mathrm{N}_3 & \cdots \end{bmatrix}_{(x,y,z)} \left\{\mathbf{u}\right\},$$

$$= \left[\mathbf{B_1} \quad \mathbf{B_2} \quad \mathbf{B_3} \quad \cdots\right]_{(x,y,z)} \left\{\mathbf{u}\right\},$$

$$
\begin{aligned}
&= \begin{bmatrix}
\frac{\partial N_1}{\partial x} & 0 & 0 & \frac{\partial N_2}{\partial x} & 0 & 0 & \frac{\partial N_3}{\partial x} & 0 & 0 & \cdots \\
0 & \frac{\partial N_1}{\partial y} & 0 & 0 & \frac{\partial N_2}{\partial y} & 0 & 0 & \frac{\partial N_3}{\partial y} & 0 & \cdots \\
0 & 0 & \frac{\partial N_1}{\partial z} & 0 & 0 & \frac{\partial N_2}{\partial z} & 0 & 0 & \frac{\partial N_3}{\partial z} & \cdots \\
\frac{\partial N_1}{\partial y} & \frac{\partial N_1}{\partial x} & 0 & \frac{\partial N_2}{\partial y} & \frac{\partial N_2}{\partial x} & 0 & \frac{\partial N_3}{\partial y} & \frac{\partial N_3}{\partial x} & 0 & \cdots \\
0 & \frac{\partial N_1}{\partial z} & \frac{\partial N_1}{\partial y} & 0 & \frac{\partial N_2}{\partial z} & \frac{\partial N_2}{\partial y} & 0 & \frac{\partial N_3}{\partial z} & \frac{\partial N_3}{\partial y} & \cdots \\
\frac{\partial N_1}{\partial z} & 0 & \frac{\partial N_1}{\partial x} & \frac{\partial N_2}{\partial z} & 0 & \frac{\partial N_2}{\partial x} & \frac{\partial N_3}{\partial z} & 0 & \frac{\partial N_3}{\partial x} & \cdots
\end{bmatrix}_{(x,y,z)} \begin{Bmatrix} u_1 \\ v_1 \\ w_1 \\ u_2 \\ v_2 \\ w_2 \\ u_3 \\ v_3 \\ w_3 \\ \vdots \end{Bmatrix}, \\
&= \left[\mathbf{B}\right]_{(x,y,z)} \left\{\mathbf{u}\right\} = \left\{\boldsymbol{\varepsilon}\right\},
\end{aligned}
\tag{4-41}
$$

where

$$
\mathbf{B}_i = \begin{bmatrix}
\frac{\partial N_i}{\partial x} & 0 & 0 \\
0 & \frac{\partial N_i}{\partial y} & 0 \\
0 & 0 & \frac{\partial N_i}{\partial z} \\
\frac{\partial N_i}{\partial y} & \frac{\partial N_i}{\partial x} & 0 \\
0 & \frac{\partial N_i}{\partial z} & \frac{\partial N_i}{\partial y} \\
\frac{\partial N_i}{\partial z} & 0 & \frac{\partial N_i}{\partial x}
\end{bmatrix}. \tag{4-42}
$$

4.2.3.3 Stresses and Strains

The relationship between stresses and strains is as follows:

$$\left.\begin{aligned}\bar{\boldsymbol{\sigma}}_{(x,y,z)} &= \begin{bmatrix}\sigma_x\\ \sigma_y\\ \sigma_z\\ \tau_{xy}\\ \tau_{yz}\\ \tau_{zx}\end{bmatrix}_{(x,y,z)}, \\ &= [\mathbf{D}]\{(\bar{\boldsymbol{\varepsilon}} - \bar{\boldsymbol{\varepsilon}}_0)\}_{(x,y,z)} + \{\bar{\boldsymbol{\sigma}}_0\}_{(x,y,z)} = [\mathbf{D}][\mathbf{B}]_{(x,y,z)}\{\mathbf{u}\} - [\mathbf{D}]\{\bar{\boldsymbol{\varepsilon}}_0\}_{(x,y,z)} + \{\bar{\boldsymbol{\sigma}}_0\}_{(x,y,z)}.\end{aligned}\right\} \quad (4\text{-}43)$$

4.2.3.4 Procedure of FEM Discretization

From Equations (4-40) and (4-41), the following relationships are true:

$$\bar{\mathbf{u}}_{(x,y,z)} \approx [\mathbf{N}]_{(x,y,z)}\{\mathbf{u}\}, \quad (4\text{-}44)$$

$$\Delta\bar{\mathbf{u}}_{(x,y,z)} \approx [\mathbf{N}]_{(x,y,z)}\{\Delta\mathbf{u}\}, \quad (4\text{-}45)$$

$$\delta\bar{\mathbf{u}}_{(x,y,z)} \approx [\mathbf{N}]_{(x,y,z)}\{\delta\mathbf{u}\}, \quad (4\text{-}46)$$

$$[\mathbf{B}]_{(x,y,z)}\{\mathbf{u}\} = \{\boldsymbol{\varepsilon}\}_{(x,y,z)}, \quad (4\text{-}47)$$

$$[\mathbf{B}]_{(x,y,z)}\{\Delta\mathbf{u}\} = \{\Delta\boldsymbol{\varepsilon}\}_{(x,y,z)}, \quad (4\text{-}48)$$

$$[\mathbf{B}]_{(x,y,z)}\{\delta\mathbf{u}\} = \{\delta\boldsymbol{\varepsilon}\}_{(x,y,z)}, \quad (4\text{-}49)$$

$$\Delta\bar{\boldsymbol{\sigma}}'_{(x,y,z)} \approx [\mathbf{D}][\mathbf{B}]_{(x,y,z)}\{\Delta\mathbf{u}\}, \quad (4\text{-}50)$$

$$\Delta\bar{\mathbf{t}} \approx \begin{Bmatrix}\Delta t_1\\ \Delta t_2\\ \Delta t_3\\ \vdots\end{Bmatrix} = \{\Delta\mathbf{t}\} \qquad (\text{a "distributed loads" approximation}), \quad (4\text{-}51)$$

$$\int_{\Gamma_\sigma} \delta\bar{\mathbf{u}}^T \Delta\bar{\mathbf{t}}\, d\Gamma \approx \{\delta\mathbf{u}\}^T [\mathbf{N}]^T_{(x,y,z)} \{\Delta\mathbf{t}\} \quad (\text{Numerical Integration}). \tag{4-52}$$

Substitution Equation (4-49) into the virtual work principle, Equation (4-39), gives

$$\left.\begin{aligned}
&\int_\Omega \delta\bar{\boldsymbol{\varepsilon}}^T \Delta\bar{\boldsymbol{\sigma}}'\, \boldsymbol{d}\Omega + \int_\Omega \delta\bar{\mathbf{u}}^T \Delta\bar{\mathbf{p}}\, \boldsymbol{d}\Omega - \int_{\Gamma_\sigma} \delta\bar{\mathbf{u}}^T \Delta\bar{\mathbf{t}}\, \boldsymbol{d}\Gamma = 0, \\
&\int_\Omega \left([\mathbf{B}]_{(x,y,z)} \{\delta\mathbf{u}\}\right)^T \Delta\boldsymbol{\sigma}'\, \boldsymbol{d}\Omega + \int_\Omega \left([\mathbf{N}]_{(x,y,z)} \{\delta\mathbf{u}\}\right)^T \Delta\mathbf{p}\, \boldsymbol{d}\Omega - \int_{\Gamma_\sigma} \left([\mathbf{N}]_{(x,y,z)} \{\delta\mathbf{u}\}\right)^T \Delta\bar{\mathbf{t}}\, \boldsymbol{d}\Gamma = 0, \\
&\int_\Omega \{\delta\mathbf{u}\}^T [\mathbf{B}]^T_{(x,y,z)} \Delta\boldsymbol{\sigma}'\, \boldsymbol{d}\Omega + \int_\Omega \{\delta\mathbf{u}\}^T [\mathbf{N}]^T_{(x,y,z)} \Delta\mathbf{p}\, \boldsymbol{d}\Omega - \int_{\Gamma_\sigma} \{\delta\mathbf{u}\}^T [\mathbf{N}]^T_{(x,y,z)} \Delta\bar{\mathbf{t}}\, \boldsymbol{d}\Gamma = 0.
\end{aligned}\right\} \tag{4-53}$$

Note that $\{\delta\mathbf{u}\}^T$ is the displacements at nodes, which are independent of x, y, and z; therefore, the above equation can be rewritten as

$$\{\delta\mathbf{u}\}^T \left(\int_\Omega [\mathbf{B}]^T_{(x,y,z)} \Delta\boldsymbol{\sigma}'\, \boldsymbol{d}\Omega + \int_\Omega [\mathbf{N}]^T_{(x,y,z)} \Delta\mathbf{p}\, \boldsymbol{d}\Omega - \int_{\Gamma_\sigma} [\mathbf{N}]^T_{(x,y,z)} \Delta\bar{\mathbf{t}}\, \boldsymbol{d}\Gamma \right) = 0. \tag{4-54}$$

Furthermore, because of the arbitrariness of $\{\delta\mathbf{u}\}^T$, Equation (4-54) is equivalent to

$$\int_\Omega [\mathbf{B}]^T_{(x,y,z)} \Delta\boldsymbol{\sigma}'\, \boldsymbol{d}\Omega + \int_\Omega [\mathbf{N}]^T_{(x,y,z)} \Delta\mathbf{p}\, \boldsymbol{d}\Omega - \int_{\Gamma_\sigma} [\mathbf{N}]^T_{(x,y,z)} \Delta\bar{\mathbf{t}}\, \boldsymbol{d}\Gamma = 0. \tag{4-55}$$

Assume the pore-pressure can be approximated using a set of shape functions,

$$\left(\tilde{N}_1 \quad \tilde{N}_2 \quad \tilde{N}_3 \quad \cdots\right), \tag{4-56}$$

which is different from the one of displacement field. In addition, the pore-pressure at an arbitrary point (x, y, z) can be expressed as

$$p_{(x,y,z)} \approx \left[\tilde{N}_1 \quad \tilde{N}_2 \quad \tilde{N}_3 \quad \cdots\right]_{(x,y,z)} \begin{Bmatrix} p_1 \\ p_2 \\ p_3 \\ \vdots \end{Bmatrix} \equiv \left[\tilde{\mathbf{N}}\right]_{(x,y,z)} \{\mathbf{p}\}, \tag{4-57}$$

$$\Delta\mathbf{p}_{(x,y,z)} = \Delta p_{(x,y,z)} \cdot \bar{\mathbf{m}} \approx \left[\tilde{\mathbf{N}}\right]_{(x,y,z)} \{\Delta\mathbf{p}\} \cdot \bar{\mathbf{m}} \equiv \{\Delta p\}_{(x,y,z)} \cdot \bar{\mathbf{m}}. \tag{4-58}$$

Substitution of Equations (4-50), (4-51), and (4-58) into Equation (4-55) gives

$$\int_{\Omega}\left[\mathbf{B}\right]^{T}_{(x,y,z)}\Delta\boldsymbol{\sigma}'_{(x,y,z)}\,\boldsymbol{d}\Omega+\int_{\Omega}\left[\mathbf{B}\right]^{T}_{(x,y,z)}\Delta\mathbf{p}_{(x,y,z)}\,\boldsymbol{d}\Omega-\int_{\Gamma_{\sigma}}\left[\mathbf{N}\right]^{T}_{(x,y,z)}\Delta\vec{\mathbf{t}}\,\boldsymbol{d}\Gamma=0,$$

$$\int_{\Omega}\left[\mathbf{B}\right]^{T}_{(x,y,z)}\left(\left[\mathbf{D}\right]\left[\mathbf{B}\right]_{(x,y,z)}\left\{\Delta\mathbf{u}\right\}\right)\boldsymbol{d}\Omega+\int_{\Omega}\left[\mathbf{B}\right]^{T}_{(x,y,z)}\left(\left[\tilde{\mathbf{N}}\right]_{(x,y,z)}\left\{\Delta\boldsymbol{p}\right\}\vec{\mathbf{m}}\right)\boldsymbol{d}\Omega-\int_{\Gamma_{\sigma}}\left[\mathbf{N}\right]^{T}_{(x,y,z)}\Delta\vec{\mathbf{t}}\,\boldsymbol{d}\Gamma=0.$$

Because of the product $\left(\left[\tilde{\mathbf{N}}\right]_{(x,y,z)}\left\{\Delta\boldsymbol{p}\right\}\right)$ is a scale, the following operation is true,

$$\left(\left[\tilde{\mathbf{N}}\right]_{(x,y,z)}\left\{\Delta\boldsymbol{p}\right\}\vec{\mathbf{m}}\right)=\vec{\mathbf{m}}\left(\left[\tilde{\mathbf{N}}\right]_{(x,y,z)}\left\{\Delta\boldsymbol{p}\right\}\right),\tag{4-59}$$

so,

$$\left(\int_{\Omega}\left[\mathbf{B}\right]^{T}_{(x,y,z)}\left[\mathbf{D}\right]\left[\mathbf{B}\right]_{(x,y,z)}\boldsymbol{d}\Omega\right)\left\{\Delta\mathbf{u}\right\}+\left(\int_{\Omega}\left[\mathbf{B}\right]^{T}_{(x,y,z)}\vec{\mathbf{m}}\left[\tilde{\mathbf{N}}\right]_{(x,y,z)}\boldsymbol{d}\Omega\right)\left\{\Delta\boldsymbol{p}\right\}-\int_{\Gamma_{\sigma}}\left[\mathbf{N}\right]^{T}_{(x,y,z)}\Delta\vec{\mathbf{t}}\,\boldsymbol{d}\Gamma=0.$$

Namely, the discretization form of Equation (4-39), the Biot consolidation model, is

$$\left(\int_{\Omega}\left[\mathbf{B}\right]^{T}_{(x,y,z)}\left[\mathbf{D}\right]\left[\mathbf{B}\right]_{(x,y,z)}\boldsymbol{d}\Omega\right)\left\{\Delta\mathbf{u}\right\}+\left(\int_{\Omega}\left[\mathbf{B}\right]^{T}_{(x,y,z)}\vec{\mathbf{m}}\left[\tilde{\mathbf{N}}\right]_{(x,y,z)}\boldsymbol{d}\Omega\right)\left\{\Delta\boldsymbol{p}\right\}=\int_{\Gamma_{\sigma}}\left[\mathbf{N}\right]^{T}_{(x,y,z)}\Delta\vec{\mathbf{t}}\,\boldsymbol{d}\Gamma.\tag{4-60}$$

Now, a dimensional analysis can be performed for Equation (4-60) as well,

$$\begin{aligned}&\left(\int_{\Omega}\left[\mathbf{B}\right]^{T}_{(x,y,z)}\left[\frac{1}{\mathrm{m}}\right]\left[\mathbf{D}\right]\left[\frac{\mathrm{N}}{\mathrm{m}^{2}}\right]\left[\mathbf{B}\right]_{(x,y,z)}\left[\frac{1}{\mathrm{m}}\right]\boldsymbol{d}\Omega\left[\mathrm{m}^{3}\right]\right)\left\{\Delta\mathbf{u}\right\}\left[\mathrm{m}\right]\\&+\left(\int_{\Omega}\left[\mathbf{B}\right]^{T}_{(x,y,z)}\left[\frac{1}{\mathrm{m}}\right]\vec{\mathbf{m}}\left[1\right]\left[\tilde{\mathbf{N}}\right]_{(x,y,z)}\left[1\right]\boldsymbol{d}\Omega\left[\mathrm{m}^{3}\right]\right)\left\{\Delta\boldsymbol{p}\right\}\left[\frac{\mathrm{N}}{\mathrm{m}^{2}}\right]\\&=\int_{\Gamma_{\sigma}}\left[\mathbf{N}\right]^{T}_{(x,y,z)}\left[1\right]\Delta\vec{\mathbf{t}}\left[\frac{\mathrm{N}}{\mathrm{m}^{2}}\right]\boldsymbol{d}\Gamma\left[\mathrm{m}^{2}\right].\end{aligned}\tag{4-61}$$

It is clear that the unit in Equation (4-61) is $\left[\mathrm{N}\right]$, the force unit, which is consistent with the statement, "Virtual work as the 'weak form' of equilibrium equations for analysis of solids or fluids (Zienkiewicz and Taylor 2000)." Namely, the equilibrium equations (the

balance of forces) of a three-dimensional continuum body (Zienkiewicz and Taylor 2000) ,

$$\begin{Bmatrix} A_1 \\ A_2 \\ A_3 \end{Bmatrix} = \begin{Bmatrix} \dfrac{\partial \sigma_x}{\partial x} + \dfrac{\partial \tau_{xy}}{\partial y} + \dfrac{\partial \tau_{xz}}{\partial z} \\ \dfrac{\partial \tau_{xy}}{\partial x} + \dfrac{\partial \sigma_y}{\partial y} + \dfrac{\partial \tau_{yz}}{\partial z} \\ \dfrac{\partial \tau_{xz}}{\partial x} + \dfrac{\partial \tau_{yz}}{\partial y} + \dfrac{\partial \sigma_z}{\partial z} \end{Bmatrix} + \begin{Bmatrix} b_x \\ b_y \\ b_z \end{Bmatrix} = \begin{Bmatrix} 0 \\ 0 \\ 0 \end{Bmatrix}, \tag{4-62}$$

or Equation (4-62) can be written using the tensor and vector formats as

$$\vec{\mathbf{A}} = \nabla \cdot \vec{\vec{\boldsymbol{\sigma}}} + \vec{\mathbf{b}} = \vec{\mathbf{0}}. \tag{4-63}$$

For an any virtual displacement $\delta\vec{\mathbf{u}} = \left[\delta u, \delta v, \delta w\right]^T$, the integral statement of Equation (4-62),

$$\int_{\Omega} \delta\vec{\mathbf{u}}^T \vec{\mathbf{A}}\left(\vec{\mathbf{u}}\right) d\Omega = \int_{\Omega} \left[\delta u \cdot \left(\frac{\partial \sigma_x}{\partial x} + \frac{\partial \tau_{xy}}{\partial y} + \frac{\partial \tau_{xz}}{\partial z} + b_x \right) + \delta v \cdot A_2 + \delta w \cdot A_3 \right] d\Omega = 0. \tag{4-64}$$

After considerable algebra and using Green's formulae, Equations (4-34) (the virtual work principle) can be obtained again. In other words, the same equation can be gotten either from the conservation of energy or the balance of forces.

Note that the right hand side of Equation (4-60),

$$\int_{\Gamma_\sigma} \left[\mathbf{N}\right]^T_{(x,y,z)} \Delta\vec{\mathbf{t}}\, \boldsymbol{d}\Gamma. \tag{4-65}$$

and when a distributed approximation (Equation (4-52)) is used for it, Equation (4-53) can be revised and the subtraction of Equations from (4-54)–(4-59), and finally a more useful alternative form of Equation (4-60) can be obtained

$$\left(\int_{\Omega} \left[\mathbf{B}\right]^T_{(x,y,z)} \left[\mathbf{D}\right] \left[\mathbf{B}\right]_{(x,y,z)} \boldsymbol{d}\Omega \right) \left\{\Delta\mathbf{u}\right\} + \left(\int_{\Omega} \left[\mathbf{B}\right]^T_{(x,y,z)} \vec{\mathbf{m}} \left[\tilde{\mathbf{N}}\right]_{(x,y,z)} \boldsymbol{d}\Omega \right) \left\{\Delta\boldsymbol{p}\right\} = \left[\mathbf{N}\right]^T_{(x,y,z)} \left\{\Delta\mathbf{t}\right\}. \tag{4-66}$$

4.3 SUMMARY

The numerical model of the physical process representing fluid-flow and solid deformation in stress-sensitive reservoirs is derived in this chapter. For the space domain, a finite difference method (FDM) is used to discretize the compositional governing equations, while a finite difference method (FEM) to discretize the geomechanical governing equations. However, both models are discretized using the finite difference method in the temporal domain. Now, a set of nonlinear algebraic equations is formed and ready to be solved in the following chapter.

5 Constitutive Relationships for the Geomechanics Model

The constitutive relationships are used to describe deformation behaviors of the material on the macroscopic dimensional level during loading. There are two tasks for the study material behaviors; one is to decide when to start the plastic nonreversible deformation using yield or failure criteria, another is to figure out the plastically flow behaviors. This chapter presents several yield criteria to check the beginning of plasticity, especially the Mohr Coulomb criteria.

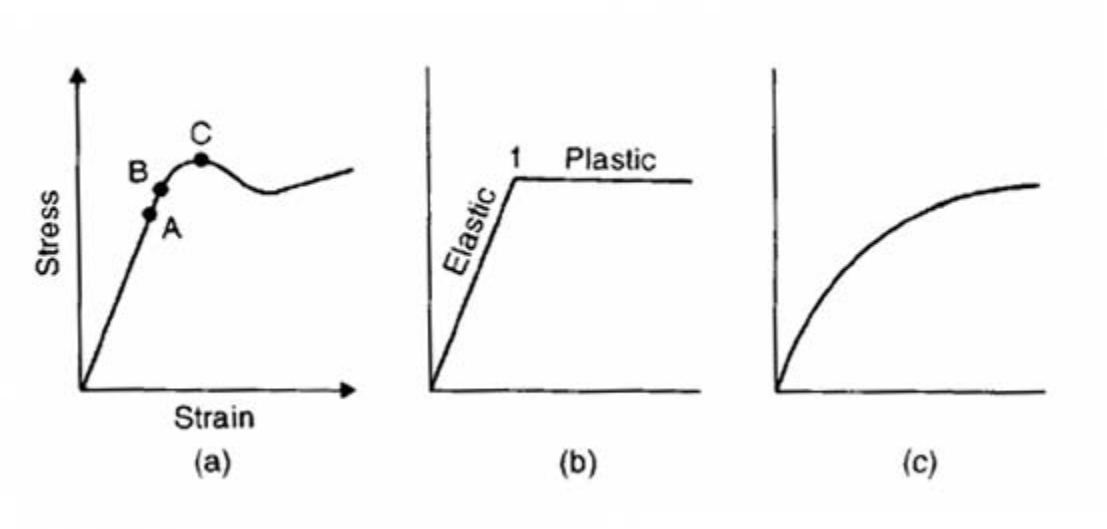

Figure 5-1: A stress-strain relationship (after Smith and Smith 1998).

From Figure 5-1(a), it is seen that there is a linear proportional part until point B (elastic limit), which is the linear elastic region and is reversible if removing the load. After the point B, the material is going to the plastic region till to point C (yield point, which is corresponding to the yield stress), which is nonlinear behaviors and irreversible if unloading. At this stage, there is a continuing strain though the load does not increase. Figure 5-1(a) displays lab experimental results. For simulation convenience,

the results of Figure 5-1(a) are usually approximated as shown in Figure 5-1(b) (an ideal elastic-plastic material). Point 1 in Figure 5-1(b) represents the elastic limit, at which the plastic deformation occurs. A practical stress-strain curve is shown as Figure 5-1(c), which demonstrates that soil behavior during loading is never linear even though for the elastic region. If a continuing load is applied to the material after yield point, it will cause the material to fracture or eventually collapse.

5.1 STRESS INVARIANTS

A yield or failure criterion is a function of the stresses and some solid material parameters. When the yield or failure criterion is plotted in the principal stress space, a surface appears to separate the elasticity and the plasticity states. Within the yield surface, the deformation is elastic; otherwise, the deformation is plastic, which is irrecoverable. A point, $\left[\sigma_x,\sigma_y,\sigma_z,\tau_{xy},\tau_{yz},\tau_{zx}\right]$, in the Cartesian stress space can be equivalently expressed to the related point, $\left[\sigma_1,\sigma_2,\sigma_3\right]$, in the orthogonal, principal stress space. In addition, from the physical point view, for isotropic material, a yield or failure criterion is independent of the orientation of the coordinate system. Hence, a summary regarding the stress invariants is followed firstly, and then the failure criteria will be easily expressed using these stress invariants.

In this dissertation, the following three invariants are used to express the failure or yield functions as shown in Table 5-1:

Table 5-1: Stress invariants

Invariants	Definitions
Mean stress	$\sigma_m = I_1 / 3,$ where $I_1 = (\sigma_1 + \sigma_2 + \sigma_3)$, and $\sigma_1, \sigma_2,$ and σ_3 are the principal stresses.
Deviator stress	$\bar{\sigma} = \sqrt{3J_2},$ where $J_2 = \left[(\sigma_1 - \sigma_2)^2 + (\sigma_2 - \sigma_3)^2 + (\sigma_3 - \sigma_1)^2 \right] / 6.$
Lode angle	$\theta = \frac{1}{3}\sin^{-1}\left(\frac{-3\sqrt{3}}{2} \frac{J_3}{J_2^{3/2}} \right),$ where, $\lvert\theta\rvert \le \pi / 6,$ and $J_3 = \left[(2\sigma_1 - \sigma_2 - \sigma_3) \cdot (2\sigma_2 - \sigma_3 - \sigma_1) \cdot (2\sigma_3 - \sigma_1 - \sigma_2) \right] / 27.$

5.2 FAILURE CRITERIA

The four kinds of classical failure functions - the Mohr Coulomb criterion (1773), the Tresca criterion (1864), the Von Mises criterion (1913), and the Drucker-Prager criterion (1952) - will be described in the later sections. These formulations are mainly from the work of Nayak and Zienkiewicz (1971) and Smith and Griffiths (2004). The following figures are after http://www.pisa.ab.ca/program/model/plastic/plastic.htm.

5.2.1 Mohr Coulomb Criterion

The Mohr Coulomb yield criterion is defined as follows:

$$F_{MC} = \sigma_m \sin\phi + \bar{\sigma}\left(\frac{\cos\theta}{\sqrt{3}} - \frac{\sin\theta\sin\phi}{3}\right) - c\cos\phi, \tag{5-1}$$

where ϕ is the friction angle and c is the cohesion of the material. Both ϕ and c are the material constants determined by experiments. Equation (5-1) shows that the Mohr Coulomb failure criterion is dependent of all the three stress invariants $(\sigma_m, \bar{\sigma}, \theta)$. Also, this criterion considers the effect of the shear stresses on the yield. In the principal stress space, this criterion describes an irregular hexagonal cone as shown in Figure 5-2. In a special case, when $\phi = 0^o$ (frictionless material), the Mohr Coulomb criterion reduces to the Tresca criterion.

5.2.2 Tresca Criterion

The Tresca failure function can be expressed as

$$F_T = \frac{\bar{\sigma}}{\sqrt{3}}\cos\theta - \frac{\sqrt{3}}{2}c_u, \tag{5-2}$$

where c_u is the undrained "cohesion" or shear strength of the soil.

The Tresca yield surface in the principal stress space is shown as in Figure 5-3, which is an infinitely long regular hexagonal cylinder.

5.2.3 Drucker-Prager Criterion

Another two-invariant yield criterion is so-called the Drucker-Prager criterion. It depends on the two invariants $(\sigma_m, \bar{\sigma})$ and can be defined as

$$F_{DP} = \sqrt{3}\alpha\sigma_m + \bar{\sigma} - \sqrt{3}k', \tag{5-3}$$

where $\alpha = (6\sin\phi)/\left[\sqrt{3}(3 \pm \sin\phi)\right]$, and $k' = (6c\cos\phi)/\left[\sqrt{3}(3 \pm \sin\phi)\right]$; "+" indicates to match the inner apices of the Mohr Coulomb hexagon surface, and "-" indicates to match the outer apices of the Mohr Coulomb hexagon surface, as shown in Figure 5-6.

5.2.4 Von Mises Criterion

Similarly to the Tresca failure, an alternative one-invariant is the Von Mises criterion, which is related to the second stress invariant of the deviator stress,

$$F_{VM} = \bar{\sigma} - \sqrt{3}c_u. \tag{5-4}$$

Its yield surface is a cylinder along the space diagonal as shown in Figure 5-5. The criterion gives the equal weighting to all the three principle stresses.

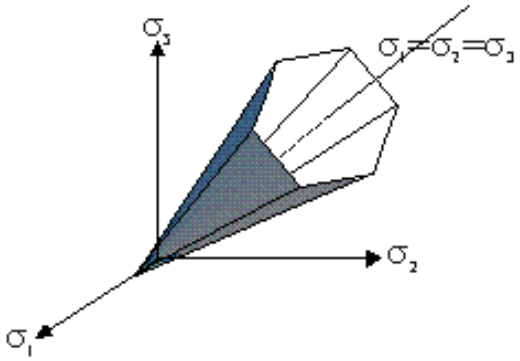

Figure 5-2: The Mohr-Coulomb yield surface in the principal stress space.

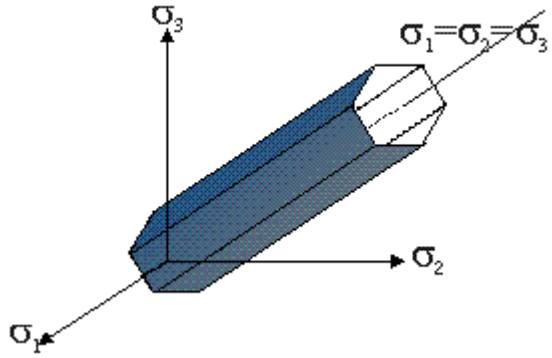

Figure 5-3: The Tresca yield surface in the principal stress space.

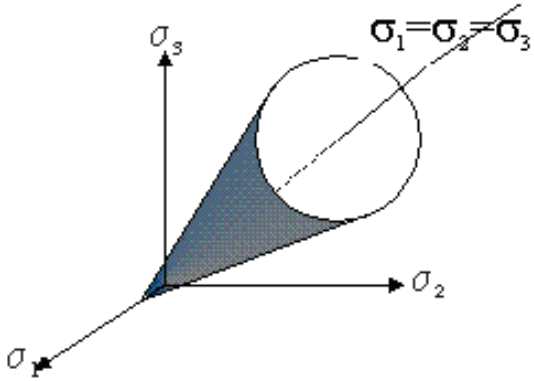

Figure 5-4: The Drucker-Prager yield surface in the principal stress space.

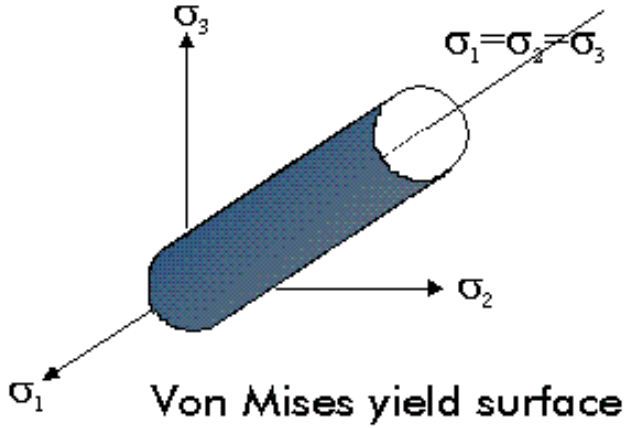

Figure 5-5: The Von Mises yield surface in the principal stress space

5.3 THE ASSOCIATED FLOW RULE

In this project, only the associated flow rule is considered in the geomechanics model, which means that the plastic potential function Q is equal to the yield function F.

In addition, when the viscoplasticity method is used to solve the nonlinear systems from the elastic-plastic models, the derivatives of the plastic potential function Q with respect to stress invariants have to be calculated as shown in Table 5-2.

Table 5-2: Derivatives of plastic potential functions

Constitutive relationships	$\frac{\partial Q}{\partial \sigma_m}$	$\frac{\partial Q}{\partial J_2}$	$\frac{\partial Q}{\partial J_3}$
Tresca	0	$\frac{\sqrt{3}}{2\bar{\sigma}}\cos\theta\left(1+\tan\theta\tan 3\theta\right)$	$\frac{3\sqrt{3}}{2\bar{\sigma}^2}\frac{\sin\theta}{\cos 3\theta}$
Mohr Coulomb	$\sin\psi$	$\frac{\sqrt{3}}{2\bar{\sigma}}\cos\theta\left[\begin{matrix}\left(1+\tan\theta\tan 3\theta\right)+\\ \sin\phi\left(\tan 3\theta-\tan\theta\right)/\sqrt{3}\end{matrix}\right]$	$\frac{3}{2\bar{\sigma}^2}\frac{\left(\sqrt{3}\sin\theta+\cos\theta\sin\phi\right)}{\cos 3\theta}$
Drucker-Prager	$3\sqrt{3}\alpha(\psi)$	$\frac{3}{2\bar{\sigma}}$	0
Von Mises	0	$\frac{3}{2\bar{\sigma}}$	0

5.4 SUMMARY

In the above four classical yield or failure criteria, the Mohr Coulomb has been used extensively to model the deformation behaviors of the geomechanical material.

For comparison, all the above four yield surfaces have been projected to the π-plane which is normal to the space diagonal in the principal stress space, as shown in Figure 5-6.

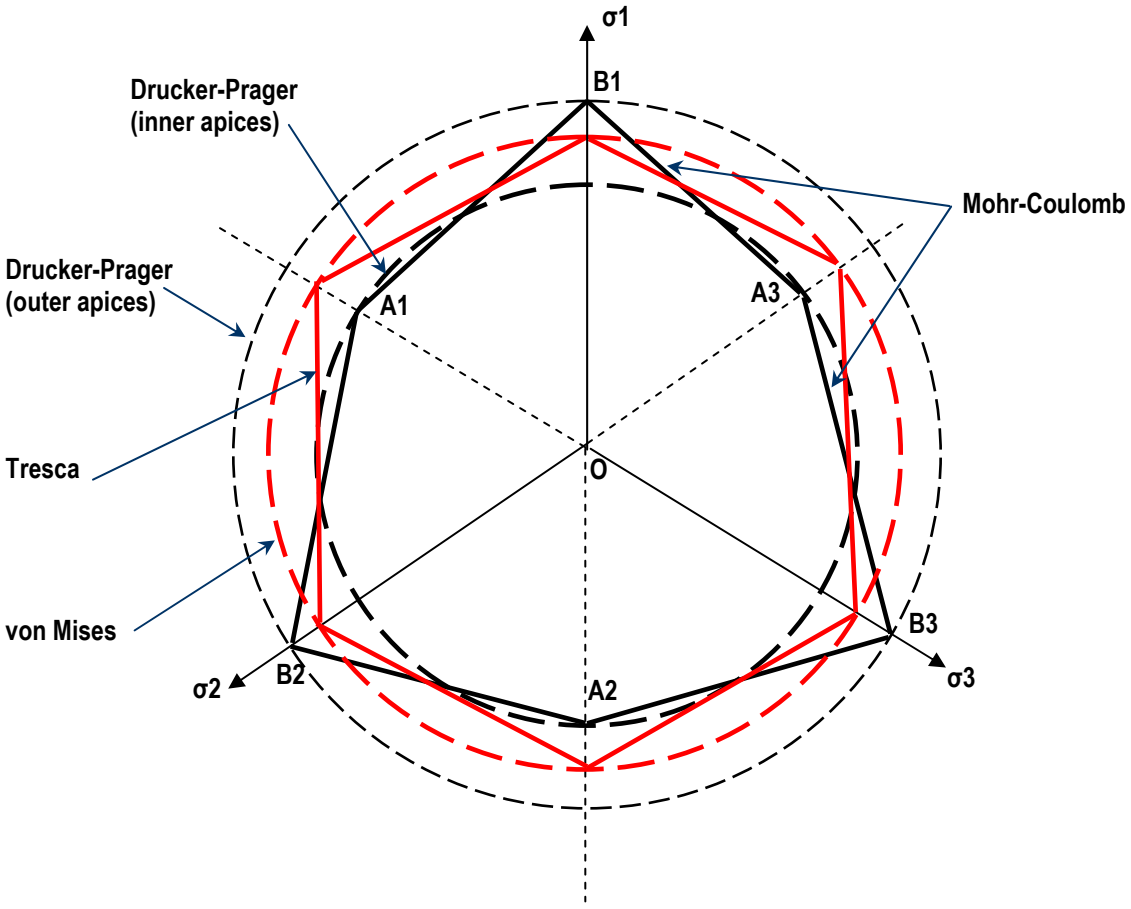

Figure 5-6: Yield surfaces in the π-plane for the Mohr-Coulomb criterion, the Tresca criterion, the Von Mises criterion, and the Drucker-Prager criterion.

6 Solution Procedures for the Coupled Model

The previous chapters mainly presented the mathematical and numerical models, which in terms of mathematics discipline are called the partial differential equations (PDEs), the finite difference equations (FDEs), and the finite element equations (FEEs) respectively. This chapter will focus on how to solve FDEs and FEEs effectively and efficiently. Two kinds of solution procedure are going to be investigated: an iteratively coupled solution procedure and a fully coupled solution procedure, for each of which there are different implementations. These two solution procedures and related implementations will be described and compared in detail, not only theoretically, but also numerically. Furthermore, the code will be verified by the means of analytical solutions or published results; at the same time, some problems will be modeled using our reservoir simulator, GPAS, coupled with geomechanics.

6.1 FULLY COUPLED SOLUTION PROCEDURE

In general, the coupled model, Equations (2-10) through (2-14) can be solved using the fully coupled solution procedure which utilizes the same numerical scheme to discretize both the solid deformation model and the fluid-flow model. However, the traditional stress-analysis packages utilize FEM, while the conventional reservoir simulators adopt FDM. Namely, two different kinds of numerical methods are used in the individual existing software. One of the disadvantages of the fully coupled solution procedure is that a new code has to be developed, which means that the existing software package in each field cannot be reused. Some researchers have developed fully coupled codes that uses the same discretization scheme (i.e. FEM) to solve the coupled geomechanics reservoir engineering problems (Fredrich et al. 1998; Gutierrez and Lewis

1998; Koutsabeloulis and Hope 1998; Lewis and Schrefler 1998; Osorio et al. 1998; Chin et al. 1998b; Chin et al. 2000; Lewis and Pao 2002).

However, Pan et al. (2009) proposed a new solution procedure for a fully coupled geomechanics and compositional modeling process, which overcomes the above drawback. The novel solution procedure uses the Schur complement technique to solve the associated fully coupled Jacobian system. The proposed approach has the following features:

1. it has similar convergence properties as the fully implicit method;
2. it combines with Krylov subspace iterative solvers with the capability of dealing with symmetric and nonsymmetric problems;
3. it can be easily parallelized to solve large-scale reservoir simulation problems.

6.1.1 Introduction

The coupled model, Equations (2-10) through (2-14) will be solved using the Schur complement approach together with preconditioned Krylov subspace iterative method. The idea follows that the partitioned procedure proposed by Prevost (1997), which solved the discretized linear system resulted from the coupled model using the finite element method. The system is a symmetric positive definite (SPD) system using the preconditioned conjugate gradient (PCG) method without assembling the coupling matrices and the related Schur complement matrix and obtained the two sets of unknowns in the coupled field synchronously.

Zyvoloski et al. (1979) also discussed the similar reduced degree of freedom algorithm using the preconditioned Schur complement. They pointed out that in the coupled physical processes describing the fluid-flow through the porous media, often one process is dominant. For example, in the heat and fluid-flow process, the pressure

change is more rapid than the temperature. This analysis helps to create a computationally efficient scheme to calculate the associated Schur complement by neglecting the off-diagonal derivatives with respect to the temperature. Three coupled physical processes were discussed by them as well.

In this dissertation, Prevost's partitioned procedure is modified and extended further:

1. A mixed discretization scheme is utilized for the two coupled field, which is the finite difference / finite volume discretization method for the fluid-flow field and the finite element for the solid deformation field.
2. A BiCGstab(*l*) linear solver is integrated within the partition procedure which can deal with nonsymmetric systems.
3. The global Jacobian / stiffness matrices are not formed using the element by element in the finite element method for the geomechanics model.
4. For improving the efficiency of computations, the unknown vector related to the Schur complement system should converge firstly and then another unknown vector is solved.

6.1.2 Schur Complement

After discretization of Equations (2-10) through (2-14) in space and time, the following (mixed) linear fully coupled system is obtained

$$\begin{bmatrix} A_{11}^{GEOM} & A_{12}^{GEOM \leftarrow GPAS} \\ A_{21}^{GPAS \leftarrow GEOM} & A_{22}^{GPAS} \end{bmatrix} \begin{bmatrix} x_1^{GEOM} \\ x_2^{GPAS} \end{bmatrix} = \begin{bmatrix} b_1^{GEOM} \\ b_2^{GPAS} \end{bmatrix}, \tag{6-1}$$

where $A_{11}, A_{12}, x_1,$ and b_1 are matrices and vectors from the geomechanics model, while $A_{21}, A_{22}, x_2,$ and b_2 are matrices and vectors from the fluid-flow model. A_{12} and A_{21} are the coupling matrices contributed from the coupling of geomechanics and fluid-flow models. The dimensions of x_1 and x_2 are sl and fl, respectively.

Here, for simplicity of the following discussions, we neglect the superscripts, GEOM, GPAS, GEOM←GPAS, and GPAS←GEOM.

For the sake of simplicity, the following uses the notations of Prevost (1997). Let the coupled geomechanics and fluid-flow linear Jacobian system be

$$\begin{bmatrix} A_{11} & A_{12} \\ A_{21} & A_{22} \end{bmatrix} \begin{bmatrix} x_1 \\ x_2 \end{bmatrix} = \begin{bmatrix} b_1 \\ b_2 \end{bmatrix}, \tag{6-2}$$

where A_{11}, A_{12}, x_1 and b_1 are from the discretization of the geomechanics model, while A_{22}, A_{21}, x_2 and b_2 are from the discretization of the fluid-flow model; A_{12} and A_{21} are from the discretizations of the coupling terms. Please note that the same discretization scheme is not limited in two models.

When a block Gaussian elimination method (Saad 2000) is utilized to Equation (6-2), the Schur complement associated with the x_2 variable can be formed as follow:

$$\tilde{S}x_2 = \tilde{b}_2, \tag{6-3}$$

with

$$\tilde{S} = A_{22} - A_{21}A_{11}^{-1}A_{12}, \tag{6-4}$$

$$\tilde{b}_2 = b_2 - A_{21}A_{11}^{-1}b_1. \tag{6-5}$$

And if the unknown vector x_2 is solved by any linear iterative method, x_2 can be back-substituted to the first equation:

$$A_{11}x_1 + A_{12}x_2 = b_1, \tag{6-6}$$

so, the unknown vector x_1 can be obtained as

$$x_1 = A_{11}^{-1}\left(b_1 - A_{12}x_2\right). \tag{6-7}$$

In other words, the coupled system Equations (6-2) can be naturally decoupled using the following four steps without loss of accuracy.

Block Gaussian elimination method (Saad 2000)

(1) Calculate the Schur complement matrix $\tilde{\mathrm{S}}$, Equation (6-4);

(2) Calculate the right hand side $\tilde{\mathrm{b}}_2$, Equation (6-5);

(3) Solve the Schur complement system, Equation (6-3), for x_2;

(4) Back-substitute x_2 into Equation (6-7) for x_1.

We note here that in block Gaussian elimination method the Schur complement matrix $\tilde{\mathrm{S}}$ is not formed explicitly when a Krylov subspace iterative method is used to solve for the x_2 variable. The reason is that only the matrix-vector product and vector-dot-product are needed for the iteration processes.

6.1.3 Prevost's Partition Procedure Using the Schur Complement

Firstly, we recast the original iteratively partitioned procedure given in Prevost (1997). The following expresses the procedure step by step:

(1) select PCG as a linear solver: a projection iterative method, which is the basis of the partition procedure;

(2) calculate the product of the Schur complement matrix $\tilde{\mathrm{S}}$ and a vector without explicitly forming the matrix; for example, for an arbitrary vector p_2, the product of $\tilde{\mathrm{S}}\mathrm{p}_2$ can be computed using the following two steps:

   a) compute the vector $\mathrm{p}_1 = -A_{11}^{-1}A_{12}\mathrm{p}_2$;

   b) compute the product $\tilde{\mathrm{S}}\mathrm{p}_2 = A_{21}p_1 + A_{22}p_2$;

(3) from Step (2), if

$$x_2^{k+1} = x_2^k + \Delta x_2^k; \tag{6-8}$$

then

$$x_1^{k+1} = x_1^k + \left(-A_{11}^{-1}A_{12}\Delta x_2^k\right); \tag{6-9}$$

namely, the partition procedure generates two series of approximation

solution, x_1^k and x_2^k $(k = 0,1,2,...)$ simultaneously.

(4) calculate the coupling terms $A_{12}x_2$ and $A_{21}x_1$ without assembling the matrixes A_{12} and A_{21};

a) use the finite difference to approximate the above matrix-vector product because of the Jacobian matrix properties;

$$A_{12}p_2 = -\lim_{\varepsilon \to 0}\left[\frac{r_1(x_1, x_2 + \varepsilon p_2) - r_1(x_1, x_2)}{\varepsilon}\right]; \quad (6\text{-}10)$$

$$A_{21}p_1 = -\lim_{\varepsilon \to 0}\left[\frac{r_2(x_1 + \varepsilon p_1, x_2) - r_2(x_1, x_2)}{\varepsilon}\right]; \quad (6\text{-}11)$$

b) the verification of Equations (6-10) and (6-11) is based on that the linear system (6-2) is a Jacobian one.

6.1.4 A Generalization of Prevost's Partition Procedure

In general, for coupled geomechanics and reservoir simulation problems, the SPD property of the Schur complement matrix will not be preserved during numerical processes. An extension, that a nonsymmetric linear solver replaces the one (PCG) to SPD systems is necessary to apply this partition procedure to more general coupled problems. Hence, the extension is as follows: (1) to expand the iterative partitioned conjugate gradient procedure to cover general coupled systems and their associated Schur complements; (2) to use the Krylov subspace iterative methods (BiCGstab(*l*), GMRES, etc.) to solve the associated Schur complement and at the same time to partition the coupled system. In this research, we implemented the combination of the Schur complement and BiCGstab(*l*) (Sleijpen and Fokkema 1993) to solve the coupled geomechanics and fluid-flow problems.

6.1.4.1 Krylov Subspace Iterative Linear Solvers

Besides the classical iterative methods for the linear system, for example, the Jacobian or Gauss-Seidel iterative methods at present, the most popular iterative methods are called the Krylov subspace methods, which construct the approximation solution series from the Krylov subspace for solving a general linear system. GMRES, BiCG, BiCGstab, BiCGstab(*l*), and so on, all belong to this kind of methods. Saad (2000) gives a complete discussion regarding the Krylov subspace iterative methods and also releases several linear solver packages at his website (www.cs.umn.edu/~saad).

6.1.4.2 Schur-Complement-Vector Product

It is well-known that the main operation of the Krylov subspace iterative methods is matrix-vector products. How to effectively and efficiently calculate this operation is the key point of this novel partition solution. Now, we examine the computations in detail.

For an arbitrary vector y with the same number of components as each row vector of the Schur complement $\tilde{S}$, their product $\tilde{S}y$ is complemented as following:

$$\tilde{S}y = \left(A_{22} - A_{21}A_{11}^{-1}A_{12}\right)y = A_{22}y - A_{21}A_{11}^{-1}A_{12}y. \tag{6-12}$$

The above product can be calculated from a four-step process:

1. Compute $y1 \equiv A_{22}y$ by reusing the existing solver of GPAS.
2. Compute $y2 \equiv A_{12}y$ using the element-by-element procedure without forming the global coupling matrix.
3. Compute $y3 \equiv A_{11}^{-1}y2$ using the element-by-element procedure without forming the global stiffness matrix.

4. Compute $y4 \equiv A_{21}y3$ using the approximation of the directional derivatives without forming the coupling matrix;

$$y4 \equiv A_{21}y3 = -\lim_{\varepsilon \to 0}\left[\frac{b_2\left(x_1^{n+1,k} + \varepsilon y3,\, x_2^{n+1,k}\right) - b_2\left(x_1^{n+1,k},\, x_2^{n+1,k}\right)}{\varepsilon}\right]. \tag{6-13}$$

Finally, Equation (6-12) can be rewritten as

$$\tilde{S}y = \left(A_{22} - A_{21}A_{11}^{-1}A_{12}\right)y = y1 - y4. \tag{6-14}$$

For the solid model, the global stiffness matrices are not formed using the element by element strategy during the above computation process. This is one improvement of Prevost partition solution procedure.

6.1.4.3 BiCGstab(l) Solver

For solid-fluid coupling simulations, when the material behavior is not elastic, the responding linear system is not symmetric. Hence, Krylov subspace iterative methods can be used to solve these nonsymmetrical systems. The BiCGstab(*l*) (Sleijpen and Fokkema 1993), one of Krylov subspace iterative methods, is implemented in this part. Two cases, without or with a diagonal preconditioner, are examined. The following presents the BiCGstab(*l*) without preconditioners (after Sleijpen and Fokkema 1993).

$k = -l$,
choose x_0, $\tilde{r}_0$,
compute $\mathbf{r}_0 = b - Ax_0$,
take $\mathbf{u}_{-1} = 0$, $\mathbf{x}_0 = x_0$, $\rho_0 = 1$, $\alpha = 0$, $\omega = 1$.

repeat until $\|\mathbf{r}_{k+l}\|$ is small enough

$k = k + l$,
Put $\hat{u}_0 = \mathbf{u}_{k-1}$, $\hat{r}_0 = \mathbf{r}_k$ and $\hat{x}_0 = \mathbf{x}_k$.
$\rho_0 = -\omega\rho_0$

For $j = 0, \ldots, l-1$ (Bi-CG part)
$\rho_1 = (\hat{r}_j, \tilde{r}_0)$, $\beta = \beta_{k+j} = \alpha\frac{\rho_1}{\rho_0}$, $\rho_0 = \rho_1$
For $i = 0, \ldots, j$
$\hat{u}_i = \hat{r}_i - \beta\hat{u}_i$
end
$\hat{u}_{j+1} = A\hat{u}_j$
$\gamma = (\hat{u}_{j+1}, \tilde{r}_0)$, $\alpha = \alpha_{k+j} = \frac{\rho_1}{\gamma}$
For $i = 0, \ldots, j$
$\hat{r}_i = \hat{r}_i - \alpha\hat{u}_{i+1}$
end
$\hat{r}_{j+1} = A\hat{r}_j$, $\hat{x}_0 = \hat{x}_0 + \alpha\hat{u}_0$
end

For $j = 1, \ldots, l$ (mod.G–S) (MR part)
For $i = 1, \ldots, j-1$
$\tau_{ij} = \frac{1}{\sigma_i}(\hat{r}_j, \hat{r}_i)$
$\hat{r}_j = \hat{r}_j - \tau_{ij}\hat{r}_i$
end
$\sigma_j = (\hat{r}_j, \hat{r}_j)$, $\gamma'_j = \frac{1}{\sigma_j}(\hat{r}_0, \hat{r}_j)$
end

$\gamma_l = \gamma'_l$, $\omega = \gamma_l$
For $j = l-1, \ldots, 1$ $(\vec{\gamma} = T^{-1}\vec{\gamma}')$
$\gamma_j = \gamma'_j - \sum_{i=j+1}^{l} \tau_{ji}\gamma_i$
end
For $j = 1, \ldots, l-1$ $(\vec{\gamma}'' = TS\vec{\gamma})$
$\gamma''_j = \gamma_{j+1} + \sum_{i=j+1}^{l-1} \tau_{ji}\gamma_{i+1}$
end

$\hat{x}_0 = \hat{x}_0 + \gamma_1\hat{r}_0$, $\hat{r}_0 = \hat{r}_0 - \gamma'_l\hat{r}_l$, $\hat{u}_0 = \hat{u}_0 - \gamma_l\hat{u}_l$ (update)
For $j = 1, \ldots, l-1$
$\hat{u}_0 = \hat{u}_0 - \gamma_j\hat{u}_j$ BLAS2 or BLAS3
$\hat{x}_0 = \hat{x}_0 + \gamma''_j\hat{r}_j$ _GEMV _GEMM
$\hat{r}_0 = \hat{r}_0 - \gamma'_j\hat{r}_j$
end

Put $\mathbf{u}_{k+l-1} = \hat{u}_0$, $\mathbf{r}_{k+l} = \hat{r}_0$ and $\mathbf{x}_{k+l} = \hat{x}_0$.

When BiCGstab(l) is used to solve Equation (6-3), the following correspondence is used, $A \sim \tilde{S}, x \sim x_2, b \sim \tilde{b}_2$. The matrix-vector products needed can be calculated as described in Section 6.1.4.2.

6.1.4.4 The Flowchart of the Fully Coupe Solution Procedure

A flowchart that explains the fully coupled procedure using the Schur complement is shown in Figure 6-1. Considering the calculation from n time-step to n+1 time-step, both reservoir and geomechanics models set the approximation solution at n time-step as the initial guess of n+1 time-step to start Newton iteration (j = 0,1,2,…).

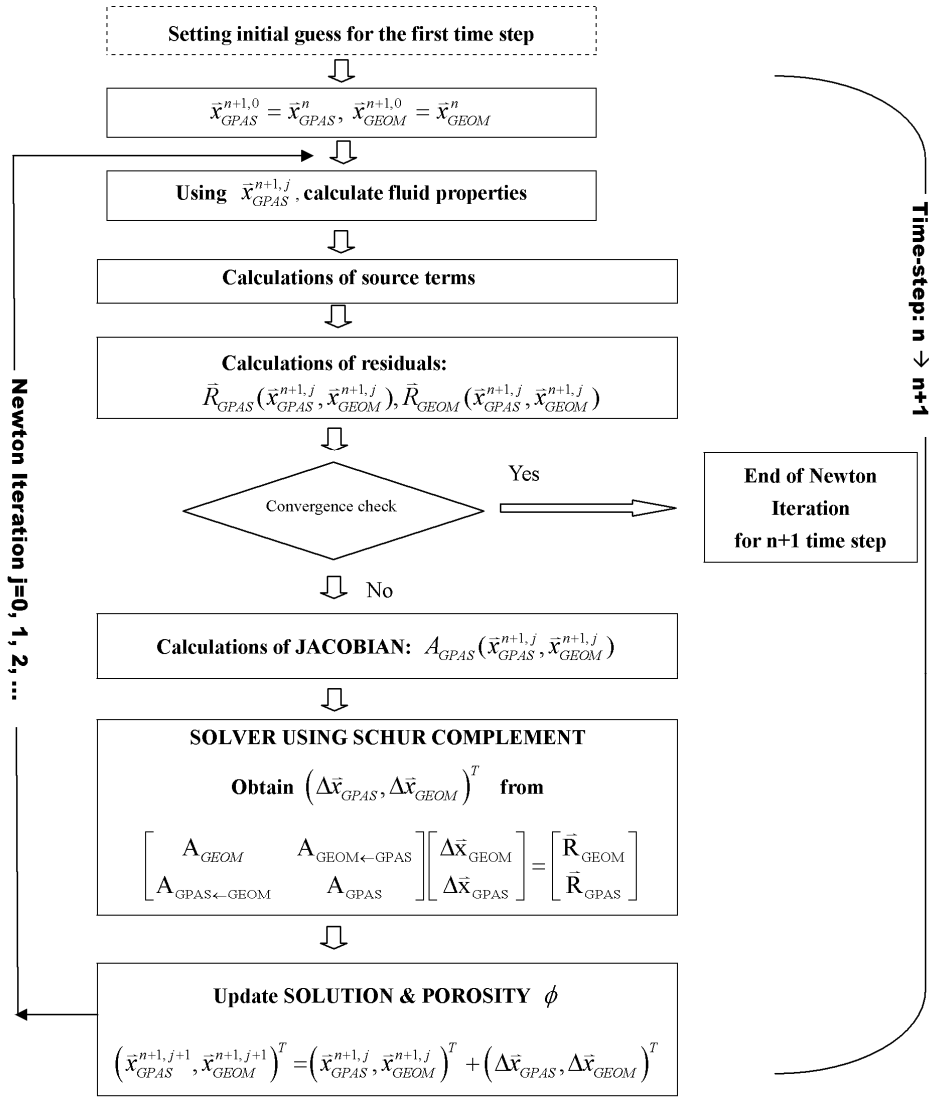

Figure 6-1: Flow chart of time-step loop of GPAS coupled with Geomechanics module using Schur complement.

Based on the known quantities, we first need to calculate the residuals for both models using the latest solution at Newton iteration j and do the convergence check. If the convergence criterion is satisfied, go to n+1 time-step; otherwise, the associated Jacobian matrices of GPAS and the geomechanics model are formed. Note that for geomechanics model, its Jacobian matrix is formed element by element without generating the global Jacobian matrix. Then, a Schur complement system will be created and solved for the change of primary unknowns given in Equation (2-15) by using the techniques discussed in the previous sections. Finally, updates for Newton approximation and porosity are performed in order to calculate the residuals at the next Newton iteration.

6.1.5 Reusing Existing Solvers through Reverse Communication

Before wrapping up the discussion regarding the implement the fully coupled solution procedure, the following observation has to be pointed out:

Recast Equation (6-12) as

$$\tilde{\mathrm{S}}\mathrm{y} = \left(\mathrm{A}_{22} - \mathrm{A}_{21}\mathrm{A}_{11}^{-1}\mathrm{A}_{12}\right)\mathrm{y} = \mathrm{A}_{22}\mathrm{y} - \mathrm{A}_{21}\mathrm{A}_{11}^{-1}\mathrm{A}_{12}\mathrm{y}. \tag{6-15}$$

In BiCGstab(*l*) or any other Krylov subspace solvers, the Schur-complement-vector product, Equation (6-12) or Equation (6-15), is one of the main operations. As we mentioned before, $\tilde{\mathrm{S}}\mathrm{y}$ will be evaluated implicitly without forming the Schur-complement matrix $\tilde{\mathrm{S}}$. However, the inverse of A_{11} is needed during iterations. In fact, similar to the iteratively coupled solution procedure, the existing linear solver (A_{11}) for the solid deformation model can be reused through the reverse communication approach, which isolates the solver (A_{11}) from the solvers (A_{22} and $\tilde{\mathrm{S}}$). In addition, $\mathrm{A}_{22}\mathrm{y}$ can be evaluated using the existing subroutines in the fluid-flow module. This mechanism makes the fully coupled solution procedure substantially simple and portable.

In other words, Equation (6-12) or Equation (6-15) can be computed using the existing solvers with the minimum modifications and without passing the matrix structures to the routine, which sets up the Schur complement system, as shown in Figure 6-2. Another advantage of the reverse communication is that the solvers in individual modules, even the preconditioners, can be updated easily and flexibly in the future, if necessary.

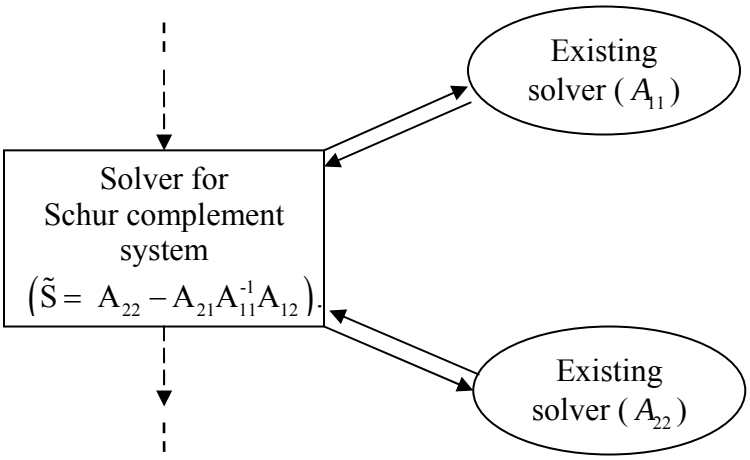

Figure 6-2: Reverse communication in the fully coupled solution procedure.

6.1.6 Case Studies

In the case studies section, unless specified otherwise, a constant overburden is assumed on the surface for the geomechanics model. The user manual including input data is attached in Appendix A.

6.1.6.1 Verification of Poro-Elastic Code

Several cases will be modeled using the coupled Geomechanics and GPAS simulator in this section. These cases consider a fully saturated single-phase, incompressible, homogeneous fluid-flow with flow (drained) or no-flow (undrained)

boundary conditions. The results will be compared with analytical solutions. One-dimensional and two-dimensional cases of consolidations will be used to verify the codes of poro-elastic and poro-elastoplastic modules. Furthermore, a set of nonlinear constitutive relationship will be investigated in the following sections.

6.1.6.1.1 One-Dimensional Consolidation Case

The first case for the verification is the one-dimensional consolidation problem with a linear time-dependent load on the top surface. The problem studies the compressions of soil or rock with an imposed surface loading along the infinite lateral surface. Schiffmann (1960) gave the analytical solution to this problem with a homogeneous fluid-flowing through a constant permeability porous media as shown in Figure 6-3.

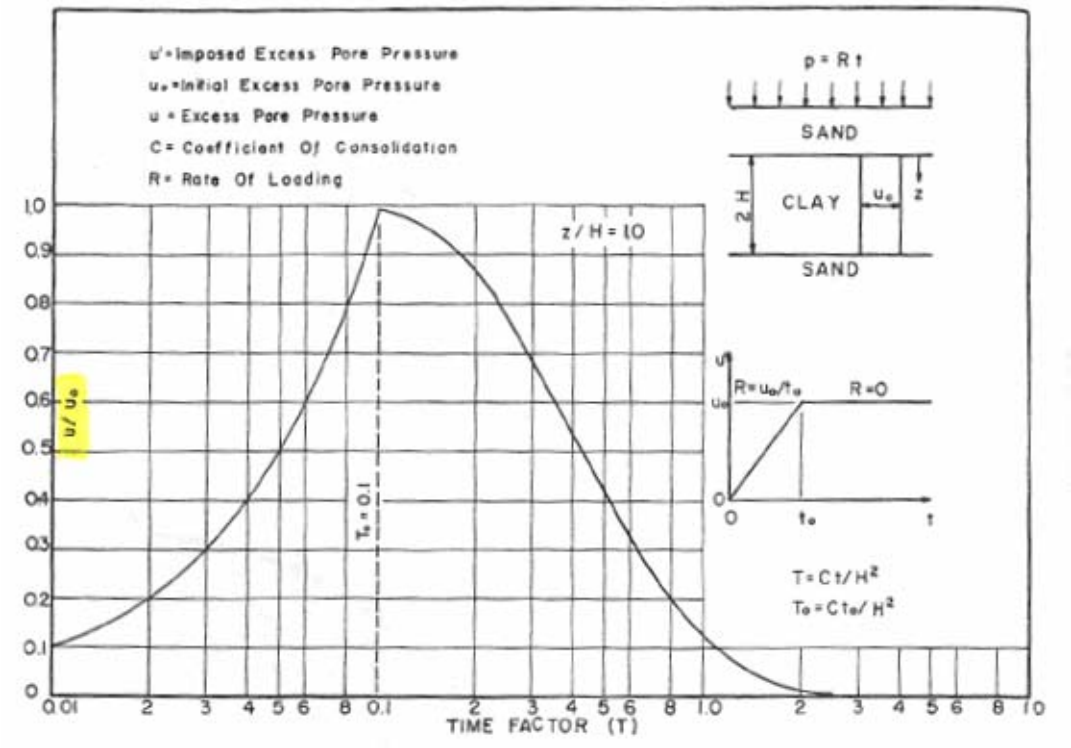

Figure 6-3: One-dimensional consolidation problem with a linear time-dependent loading and its analytical solution (after Schiffmann 1960) for Case 6.1.6.1.1.

In this case, the specific parameters are described in Table 6-1. A one-dimensional reservoir with the length (0.82 ft), width (0.82 ft) and thickness (3.28 ft) is used in this simulation example. The total number of gridblocks or element is four to simulate the fluid-flow and solid deformation along the z direction. The porosity is 0.20. An incompressible rock and fluid are assumed in this problem to maximize the compaction effects in the reservoir during the two field interactions. The standard viscosity and density are inputted into the simulator. The reservoir has a 2000 psi initial pressure everywhere. A producer with a constant BHP (2000 psi) is located on the surface to mimic the flow boundary condition for the simulator.

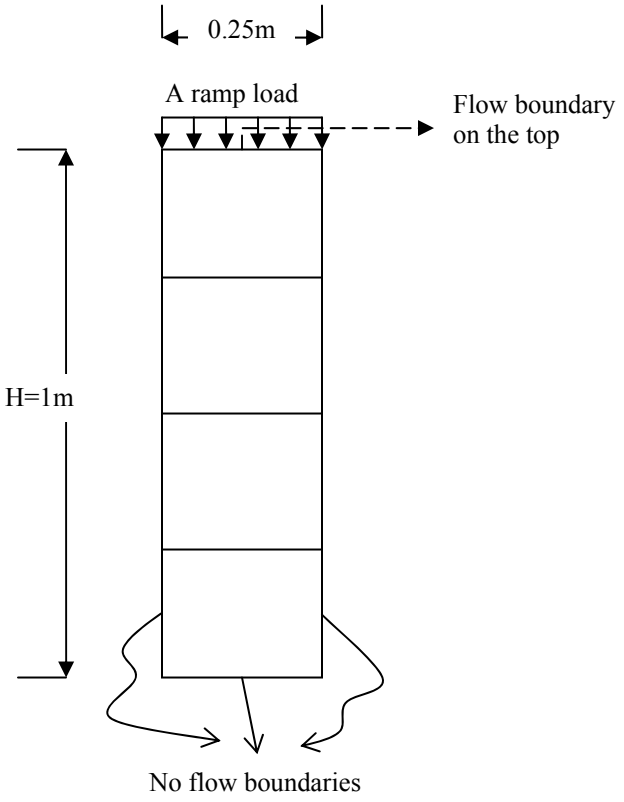

Figure 6-4: The finite element mesh and boundary conditions for one-dimensional consolidation problem with a time-dependent loading for Case 6.1.6.1.1.

Because of the symmetry of the problem (Figure 6-3), only one half of the domain was considered in the simulation as shown in Figure 6-4. A four element mesh is used to discretize the reservoir. Each element has 8-node displacements and 4-node pore pressures; hence, for this case, there are 20 unknowns at most for each element. Young's modulus and Poisson's ratio for the reservoir skeleton is selected as unity and zero, respectively. A dimensionless time (T) is defined as Equation (6-16)

$$T = \frac{Ct}{H^2}, \tag{6-16}$$

where T is the dimensionless time, t is the simulation time, C is the so-called coefficient of consolidation, and H is the maximum length of drainage path. C is defined as the follows:

$$C = \frac{k_c}{m_v \gamma}, \tag{6-17}$$

where the k_c is the coefficient of permeability, which has the relationship with the absolute permeability of the reservoir (k), the viscosity (μ), and the unit weight of fluid (γ) as

$$k_c = k\frac{\gamma_w}{\mu}. \tag{6-18}$$

And m_v is defined as

$$m_v = \frac{(1+v)(1-2v)}{E(1-v)}. \tag{6-19}$$

From Table 6-1, a two-unit system is used in the simulator, which means that the oilfield unit is for the fluid-flow and the SI unit for the geomechanics.

The excess pressure profiles at the z=H with the dimensionless time T is plotted and compared with the analytical solution of Schiffmann (1960). A very good match is obtained as seen in Figure 6-5.

Table 6-1: Summary of input data for one-dimensional consolidation problem with a time-dependent loading for Case 6.1.6.1.1

	Parameter	Value
Reservoir model	Length (ft) x Width (ft) x Thickness (ft)	0.82 x 0.82 x 3.28
	Number of gridblocks	1 x 1 x 4
	Gridblock size (ft^3)	0.82 x 0.82 x 0.82
	Porosity	0.2
	Rock compressibility (psi^{-1})	0
	Fluid compressibility (psi^{-1})	0
	Initial water saturation	1.0
	Water viscosity (cp)	1
	Water density (lb/ft^3)	62.343
	Initial pressure (psi)	2000
	Producer (BHP)	2000
Geomechanics model	Number of elements	1 x 4
	Element type	8-node quadrilateral
	Element size (m^2)	0.25 x 0.25
	Young's modulus (kPa)	1
	Poisson's ratio	0
	Time-dependent load (kPa/s)	0 0 0.1 1.0 3.0 1.0

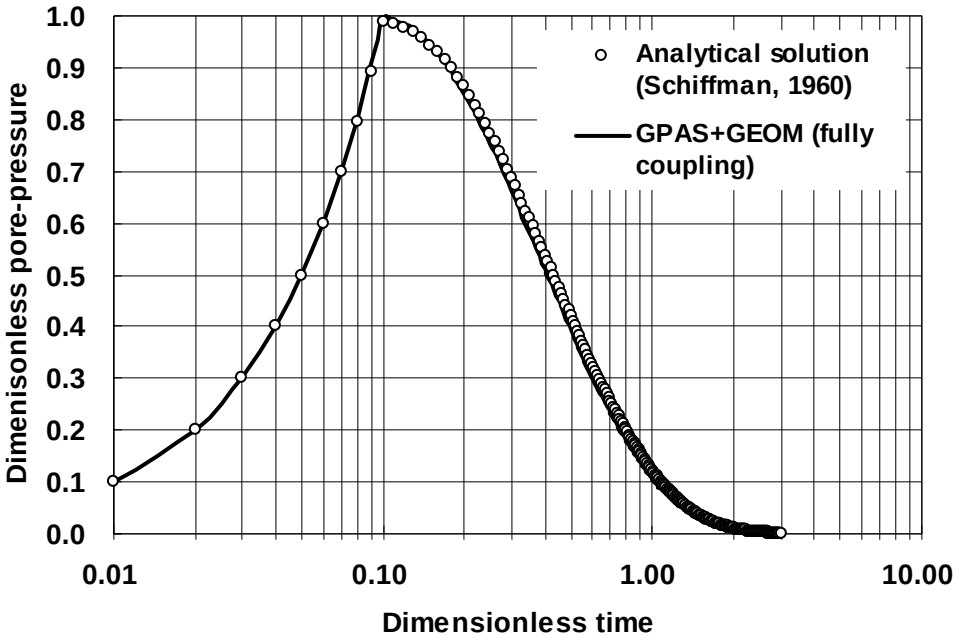

Figure 6-5: Comparison of the fully coupled geomechanics and GPAS with the analytical solution from Schiffmann (1960) for Case 6.1.6.1.1.

6.1.6.1.2 Two-Dimensional Consolidation Case

In this section, a two-dimensional plane-strain consolidation of a half-plane loaded by a strip uniform load, as shown in Figure 6-6, is solved to show the Mandel-Cryer effect during the early stage of the settlement process.

This problem has been studied and discussed by several researchers (McNamee and Gibson 1960a; McNamee and Gibson 1960b; Schiffmann et al. 1969). Its mathematical description is given in the following:

$$\begin{cases} \nabla^2 u_x - (2\eta - 1)\dfrac{\partial \varepsilon_v}{\partial x} - \dfrac{E}{2(1+\nu)}\dfrac{\partial p_w}{\partial x} = 0, \\ \nabla^2 u_z - (2\eta - 1)\dfrac{\partial \varepsilon_v}{\partial z} - \dfrac{E}{2(1+\nu)}\dfrac{\partial p_w}{\partial z} = 0, \end{cases} \tag{6-20}$$

where the elastic constant $\eta = (1-v)/(1-2v)$, and u_x and u_z are the displacements, and p_w is the pore pressure.

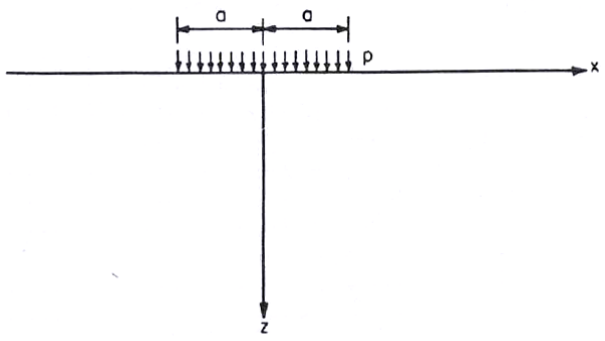

Figure 6-6: A two-dimensional plane-strain consolidation of a half-plane loaded by a strip (2a) uniform load (p) (after Schiffmann et al. 1969) for Case 6.1.6.1.2.

The boundary conditions are

$$\begin{cases} \sigma_{zz} = p, \text{ for } z = 0, |x| \le a, \\ \sigma_{zz} = 0, \text{ for } z = 0, |x| > a, \\ \sigma_{xz} = 0, \text{ for } z = 0, |x| < \infty, \\ p_w = 0, \text{ for } z = 0, |x| < \infty. \end{cases} \tag{6-21}$$

and the initial conditions are

$$\begin{cases} \sigma_{zz} = p \text{ , for } t = 0, |x| \le a, \\ \varepsilon_v = 0, \text{ for } t = 0, |x| < \infty. \end{cases} \tag{6-22}$$

They plotted the analytical solution and also pointed out the difference of the pseudo consolidation theory (the Terzaghi-Rendulic consolidation theory, Lambe and Whitman 1979) and the Biot consolidation theory (Biot 1941): the pseudo consolidation theory cannot predict the Mandel-Cryer effect at the early time of consolidation, while the Biot consolidation theory can capture this effect. The reason is that the pseudo consolidation theory assumes a time-independent total stresses during consolidation,

while the Biot consolidation theory makes allowance for the total stress changes during consolidation. In fact, the Mandel-Cryer effect was confirmed experimentally by some researchers. From the physical interpretation of the Mandel-Cryer effect, the Biot consolidation theory keeps the compatibility of strain between the free drained surface and the interior elements, while the pseudo consolidation theory takes no account of strain compatibility within the solid mass.

Because of the symmetry of the domain, a half domain is considered during the numerical simulation (Figure 6-7). The approximation of the half-plane is a rectangular of the dimension 6a x 9a with appropriate boundary conditions employed as noted in Figure 6-7. The domain is partitioned into a 12 x 1 x 13 grid mesh. During simulation, the uniform load intensity q was applied in a very short time (less than the size of the initial time-step). The input data is summarized in Table 6-2. A non-uniform grid mesh is utilized in this simulation. The loading region has a fine grid mesh. Similarly to the analysis of Case 6.1.6.1.1, a dimensionless time is selected to relate the certain parameters.

The pore pressure profile beneath the center of the loaded strip (x/a = 0, z) is given in Figure 6-8 at the dimensionless time T = 0.1. It can be found that the numerical solution (the solid line) from the fully coupled geomechanics and GPAS has an excellent match in the lower depths beneath the loaded area, while overpredicts at greater depths close to the fixed base. Because the original problem as shown in Figure 6-6 is an infinite half plane and the associated analytical solution (Schiffmann et al. 1969) is also derived for the infinite half plane. In the numerical grid, a finite lateral and base boundaries are used to approximate the original domain, which results in the discrepancy. However, the interest region is close to the surface which the simulation can give a good prediction as shown in Figure 6-8. A fully coupled finite element code (Smith and

Griffiths 2004) was also ran to solve this problem as shown in the dashed line in Figure 6-8. A similar discrepancy appeared at the locations close to the fixed base.

In Figure 6-9, one specific point, (x = 0, z = 2), within the domain is selected to analyze the variation of pore pressure with the dimensionless time T. A good agreement is obtained between the simulation results and the closed form solution (Schiffmann et al. 1969). In addition, the Mandel-Cryer effect is presented in the curves of both the analytical solution (scattered points) and simulation results (solid and dashed lines) of the fully coupled geomechanics and GPAS and the fully coupled finite element code (Smith and Griffiths 2004).

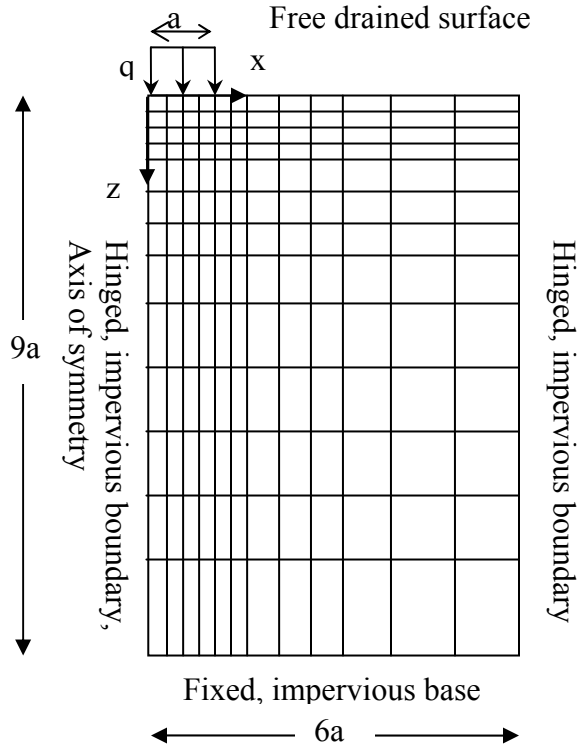

Figure 6-7: The grid mesh for a two-dimensional plane-strain consolidation of a half-plane loaded by a strip uniform load for Case 6.1.6.1.2.

Table 6-2: Summary of input data for a two-dimensional plane-strain consolidation of a half-plane loaded by a strip uniform load for Case 6.1.6.1.2

	Parameter	Value
Reservoir model	Length (ft) x Width (ft) x Thickness (ft)	19.68 x 0.82 x 29.52
	Number of gridblocks	12 x 1 x 13
	Gridblock size (ft)	
	DX	0.82 0.82 0.82 0.82 0.82 0.82 1.64 1.64 2.46 2.46 3.28 3.28
	DY	0.82
	DZ	0.82 0.82 0.82 0.82 1.23 1.23 1.64 1.64 2.46 2.46 3.28 4.1 8.2
	Porosity	0.2
	Rock compressibility (psi^{-1})	0
	Fluid compressibility (psi^{-1})	0
	Initial water saturation	1.0
	Water viscosity (cp)	1
	Water density (lb/ft^3)	62.343
	Initial pressure (psi)	2000
	Producer (BHP)	2000
Geomechanics model	Number of elements	12 x 1 x 13
	Element type	8-node quadrilateral
	Young's modulus (kPa)	1
	Poisson's ratio	0
	Load (q) at t =0	1 kPa
	a	1 m

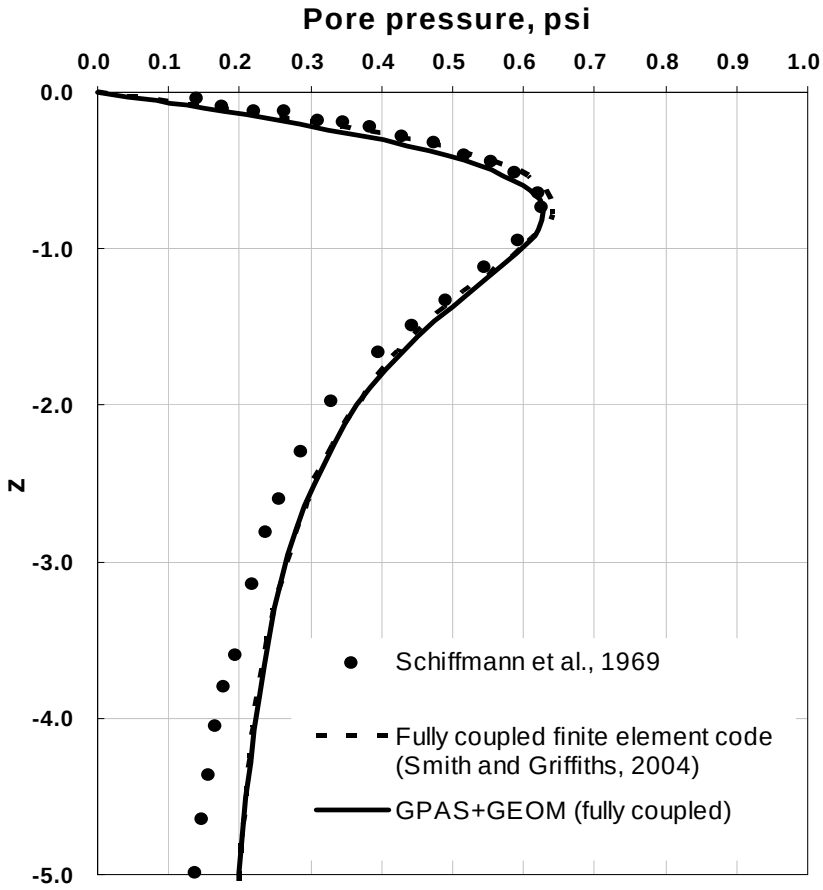

Figure 6-8: Comparison of the pore pressure profile with the analytical solution (after Schiffmann et al. 1969): beneath the center of the loaded area for Case 6.1.6.1.2.

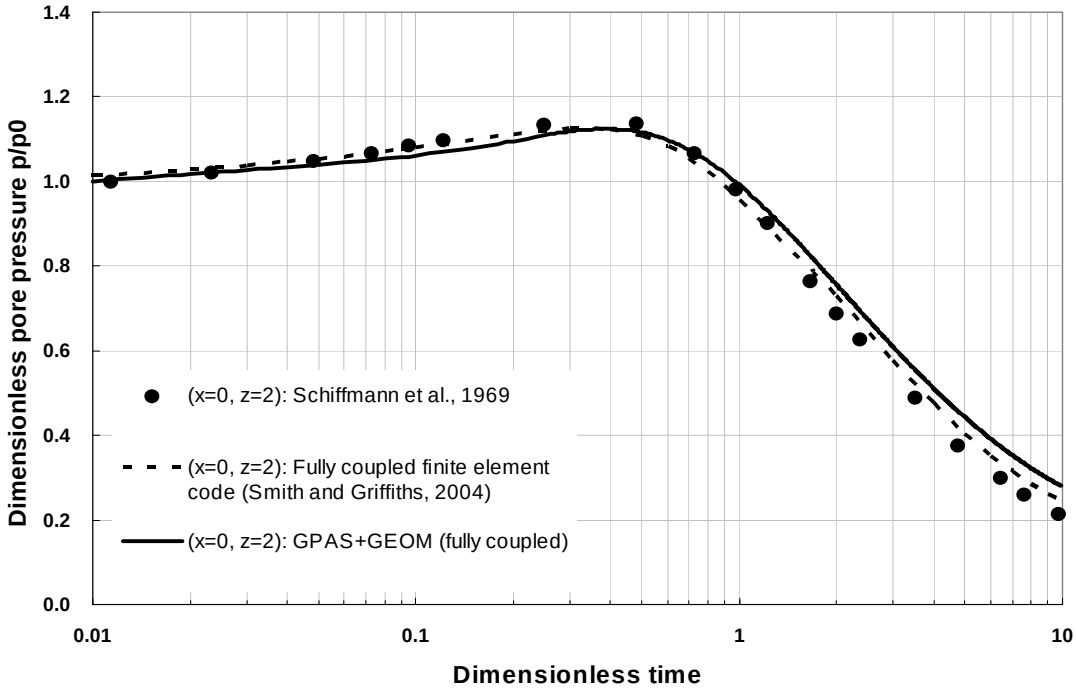

Figure 6-9: Comparison of the variation of pore pressure and time with the analytical solution (after Schiffmann et al. 1969); The Mandel-Cryer effect is predicted by the numerical solutions at (x=0, z=2) for Case 6.1.6.1.2.

For this problem, the drainage rate decreases with increasing depth. It has been pointed out by Schiffmann et al. (1969) that the peak of the effect would advance in time with increasing depth. In Figure 6-10, the two specific points, (x/a=0, z/a=0.75) and (x/a=0, z/a=2), within the domain are selected to analyze the variation of pore pressure with the dimensionless time T. The simulation results, as seen in Figure 6-10 and Figure 6-11, confirmed the above comment. A very good agreement is reached between the simulation results of the fully coupled geomechanics and GPAS and the fully coupled finite element code (Smith and Griffiths 2004). Different numerical schemes are used in the two codes, that is, a mixed finite volume and finite element discretization is utilized for GPAS, and a finite element method is used for the solid and fluid models in Smith

and Griffiths (2004). Hence, there is a little discrepancy in the plot. In addition, the Mandel-Cryer effect is presented in the curves of both simulation results. At the early time, the Skepton effect (an increased pore pressure because of the load) is detected and the Mandel-Cryer effect is predicted later.

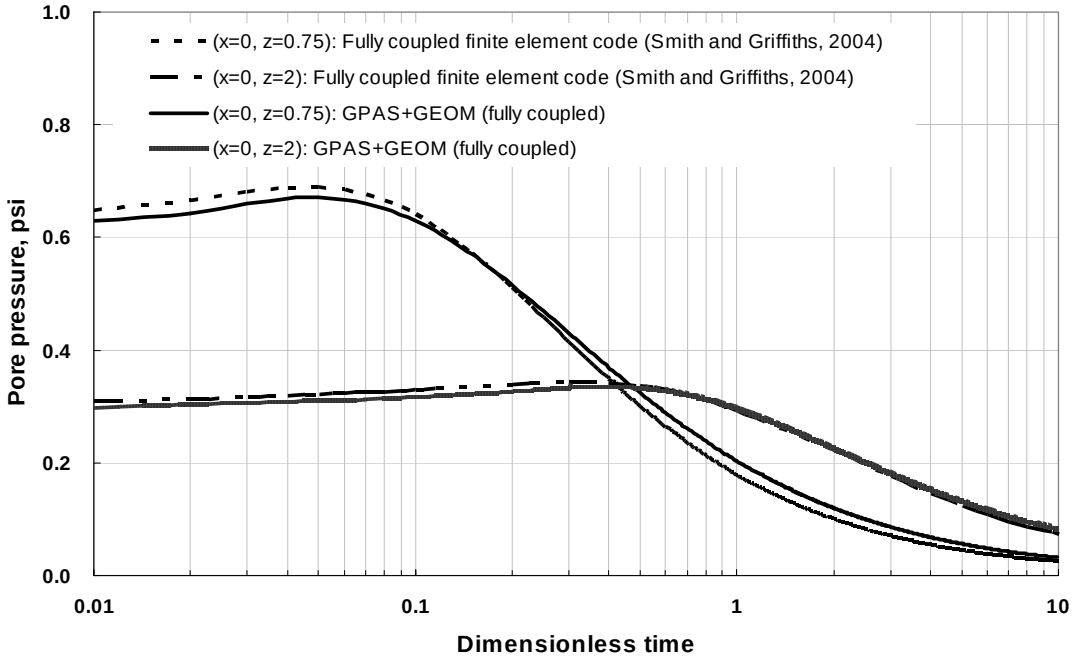

Figure 6-10: The Mandel-Cryer effects are predicted by the numerical solutions at (x=0, z=0.75) and (x=0, z=2) for Case 6.1.6.1.2.

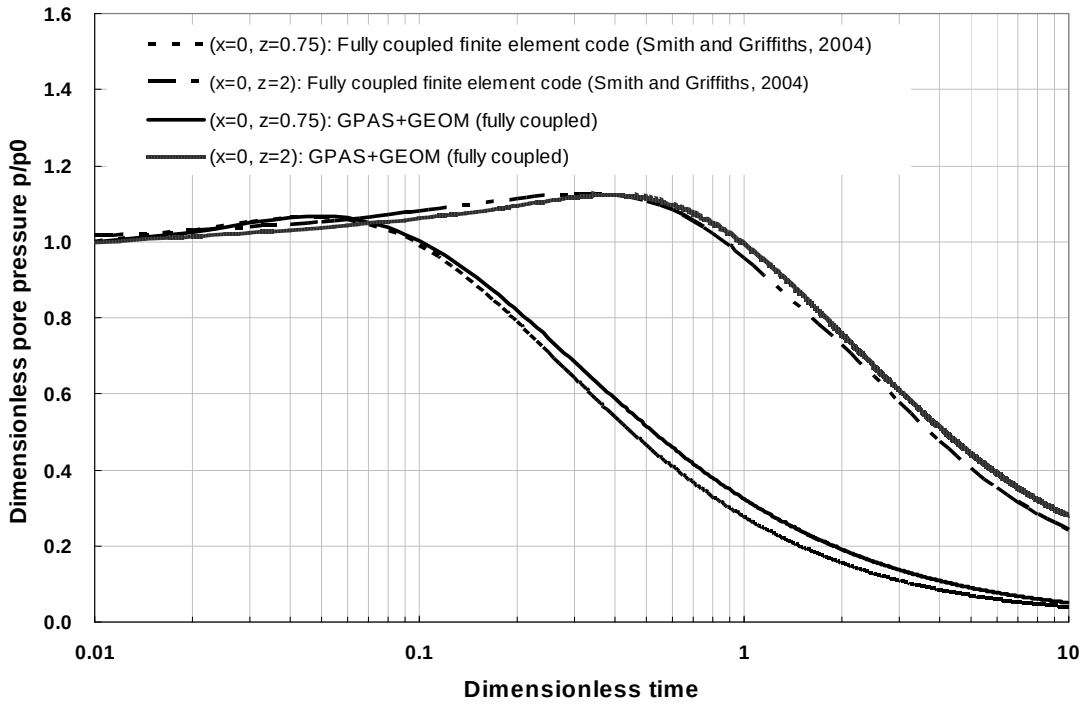

Figure 6-11: The Mandel-Cryer effects are predicted by the numerical solutions at (x=0, z=0.75) and (x=0, z=2) for Case 6.1.6.1.2.

6.1.6.2 2D Primary Depletion with Twelve-Component Fluid Mixture

This is a two-dimensional, primary depletion case with a 12-component fluid to show the capability of GPAS fully coupled with geomechanics. Table 6-3 gives the reservoir, fluid, and rock properties for this case.

The critical properties of component are shown in Table 6-4. The simulation run has a $12 \times 1 \times 4$ grid mesh as shown in Figure 6-12, an initial porosity of 0.35, a permeability of 10 md, an initial water saturation of 0.17, and an initial uniform pressure of 6000 psi. The time-step and convergence check was controlled by GPAS automatically. In total, four producers located along the z direction at the 1st, 13th, 25th, and 37th gridblocks were operating under a constant bottomhole pressure of 500 psi.

The simulation period was 120 days. The geomechanics model uses an 8-node rectangular quadrilateral element. A constant overburden stress of 4.1370×10^4 kN/m^2 (6000 psi) is applied at the top of the reservoir.

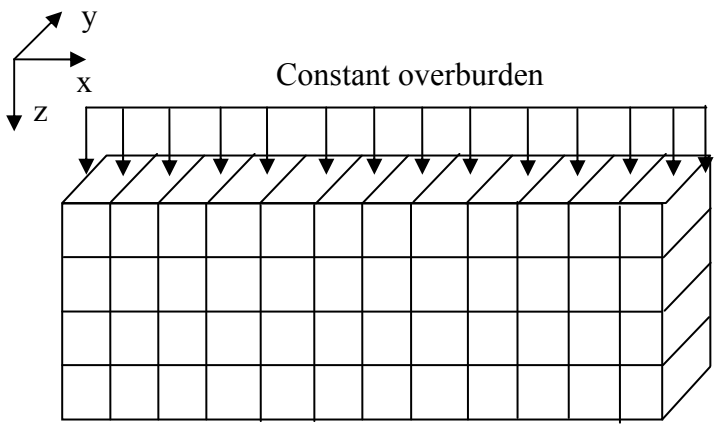

Figure 6-12: Schematic reservoir geometry for Case 6.1.6.2.

Table 6-3: Input parameters for Case 6.1.6.2

Property	Value
Reservoir size (ft^3)	1200 x 10 x 40
Reservoir gridblock size (ft^3)	100 x 10 x 10
No. of gridblocks	12 x 1 x 4
Young's modulus (kPa)	9×10^6
Poisson's ratio	0
Matrix permeability (x,y,z) (md)	10
Matrix porosity	0.35
Initial water saturation	0.17
Water viscosity (cp)	1.0
Water/oil compressibility (1/psi)	0.000003
Initial reservoir pressure (psi)	6000
Production constraint (BHP) (psi)	500

Table 6-4: Component critical properties used in Case 6.1.6.2

Component	T_c (^oR)	P_c (psi)	V_c (ft^3/lb-mole)	MW_i (lbm/lb-mole)
CO_2	547.5	1071.6	0.416	44.0
C_1	343.0	667.8	1.599	16.0
C_2	549.7	707.8	2.451	30.0
C_3	665.7	616.3	3.211	44.1
N-C_4	765.3	550.7	4.088	58.1
N-C_5	845.3	488.6	4.946	72.1
C_6	913.4	436.9	5.923	86.2
C_{7-9}	1040.2	415.4	8.553	145.1
C_{10}	1111.8	304.0	10.087	142.3
C_{10-13}	1199.6	225.3	13.110	223.2
C_{15}	1270.0	200.0	16.696	206.0
C_{14-19}	1346.5	203.9	23.070	353.5
C_{20}	1380.0	162.0	21.484	282.0
C_{20-35}	1532.7	158.0	33.253	554.5
C_{36+}	1667.0	94.8	83.571	1052.0

The reservoir fluid-flows from the left side (x = 0 ft) during the production period. Figure 6-13 shows the change of pressure distribution of the top reservoir layer during the production. Note that the initially reservoir pressure is uniformly distributed at 6000 psi which is equilibrated with the overburden stress 6000 psi. However, after production, fluid pressures of a part of the reservoir are increased above 6000 psi in the early time (<

40 days). This phenomenon is caused by the coupling effect of fluid-flow and reservoir compaction. This so-called the Noordbergum effect was also obtained by other investigators (Verruijt 1969; Kim and Parizek 1977; Gutierrez and Lewis 2002) and is also observed in the pressure-driven production. Figure 6-13 shows that the Noordbergum effect remains till to about 40 days. The pressure is reduced to about 500 psi at the end of the simulation.

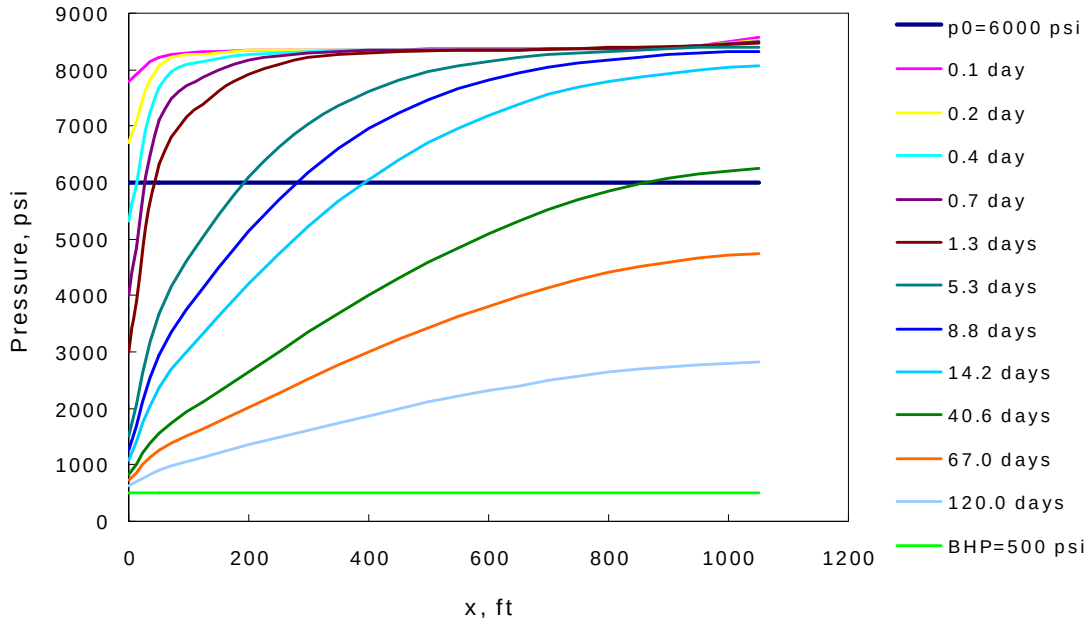

Figure 6-13: Pressure distribution of the top reservoir layer for Case 6.1.6.2.

Figure 6-14 shows that compaction along the z axis not only depends on a constant overburden stress (6000 psi) on the top the reservoir, but also varies with the change of gridblock pressure. With time, the increase in displacement is more gradual, which follows the more gradual change of pressure. Finally, the pressure drop at well locations between two consecutive time-steps becomes almost zero, and then the

associated displacements also tended towards a stable state (about 0.34 ft compaction at x = 0 ft), which can be seen in Figure 6-13 and Figure 6-14.

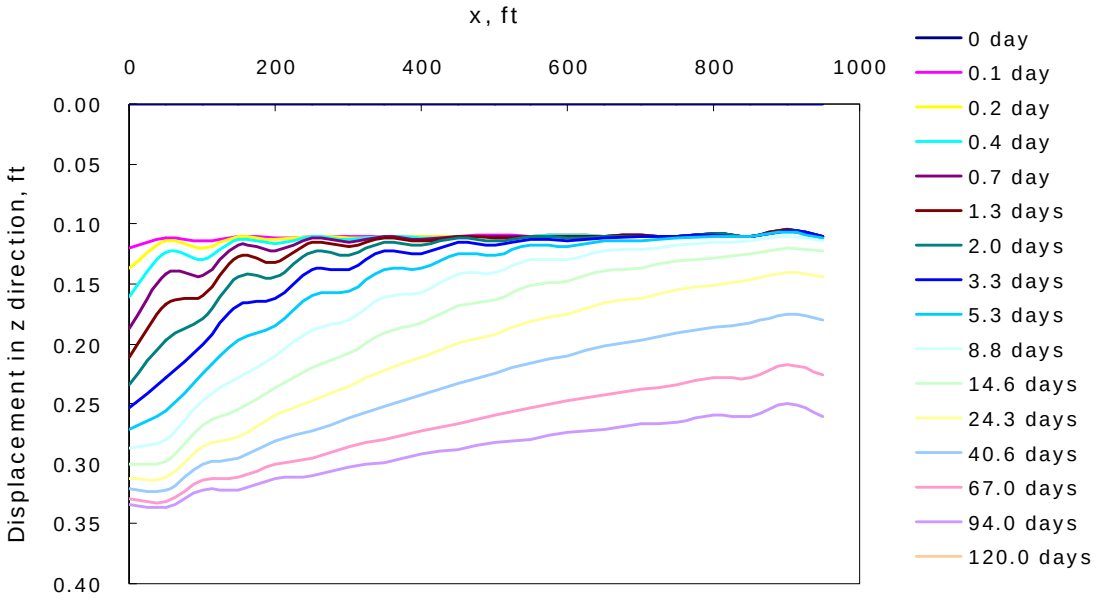

Figure 6-14: Displacements in z direction of the top reservoir layer for Case 6.1.6.2.

6.1.6.3 3D Primary Depletion with Three-Component Fluid Mixture

A three-dimensional, primary depletion case simulates a reservoir with three components, C_{10}, C_{15}, and C_{20} with the initial compositions, 0.5, 0.25, and 0.25, respectively. There is a constant overburden stress (6000 psi) on the top the reservoir, which has the dimensions, 200 ft x 200 ft x 200 ft. Again, the solid and fluid properties are shown in Table 6-3 and Table 6-4. A $2\times20\times20$ grid is used, as shown in Figure 6-15. The boundary conditions of the fluid-flow model and the solid model are also described in the figure.

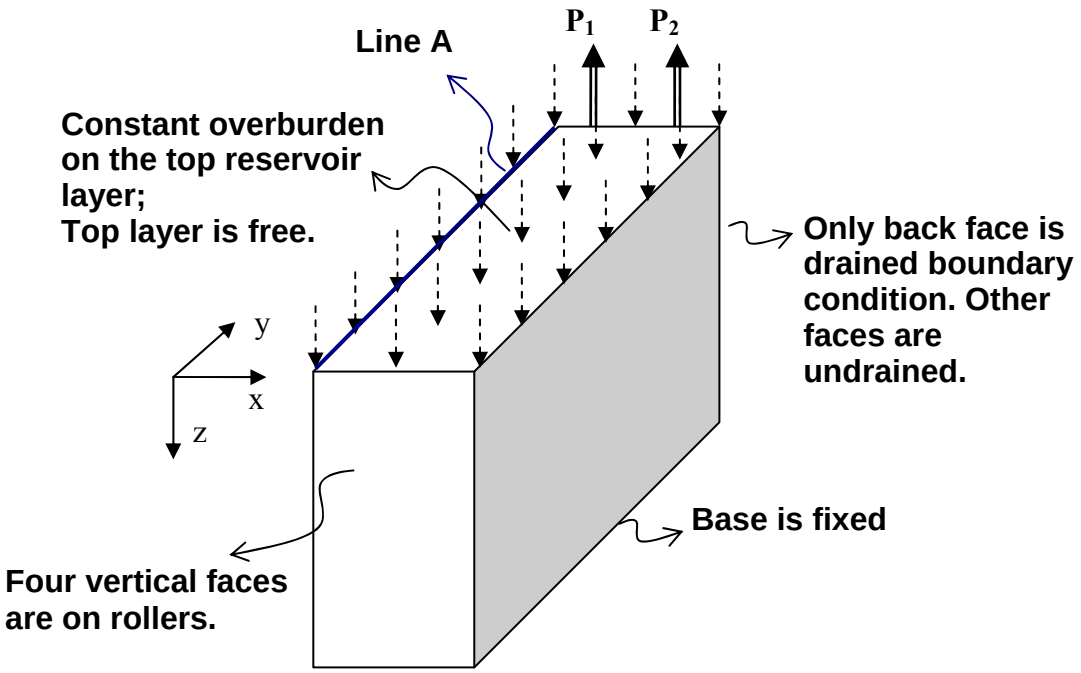

Figure 6-15: Schematic reservoir geometry for Case 6.1.6.3.

For the geomechanics model, there are a total 800 20-node brick (hexahedral) elements. The total number of equations of geomechanics model is about 13,000, while the total number of equations of fluid-flow is 6,400. Hence, the total number of unknowns for this case is close to 20,000.

Figure 6-16 through Figure 6-18 show the displacements in the z direction and the y direction, and pressure distribution, along the line at x = 0 ft, z = 0 ft, and y from 0 ft to 200 ft (designated as **Line A**), respectively. The compaction profile varying with time (day) is shown in Figure 6-16. Figure 6-16 indicates the final compaction is about 1.3 ft. Note that during the early-time simulation, the displacement in the z direction is increasing along Line A because of the drained (flow) boundary condition at y = 200 ft. The fluid-flows to the back face (y = 200 ft), where two producers P_1 and P_2 are located.

Figure 6-18 illustrates the decrease of pressures from y = 0 ft to 200 ft. For this case, the Noordbergum effect also appears at 0.04 day as shown in Figure 6-18.

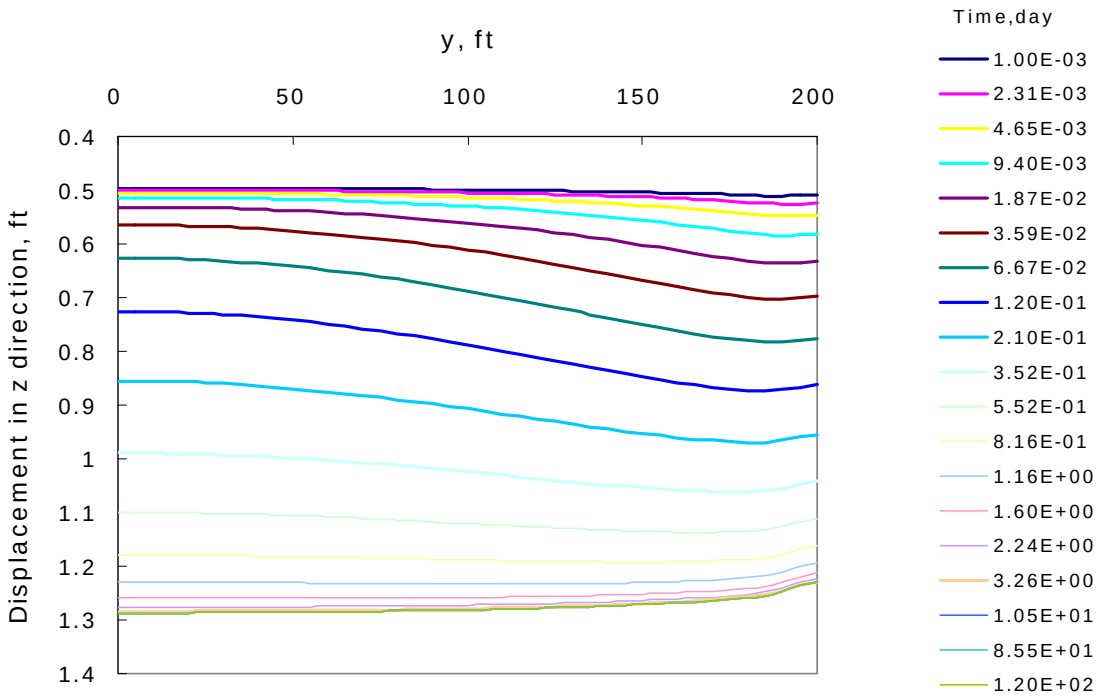

Figure 6-16: Displacements in z direction along Line A for Case 6.1.6.3.

Figure 6-17 shows that the displacement in y direction is increasing with time (day) elapsing; at 0.07 day it achieves at the maximum level and begins to decrease because an elastic constitutive model is used in this case. Meanwhile, the compaction in z direction along the producer locations makes the displacement in y direction increase negatively (tension) and finally achieves a stable status as shown in Figure 6-17. Pressure distribution as shown in Figure 6-18 demonstrates a nonmonotonic increase with time because of the coupling effects between solid and fluid at the early simulation time.

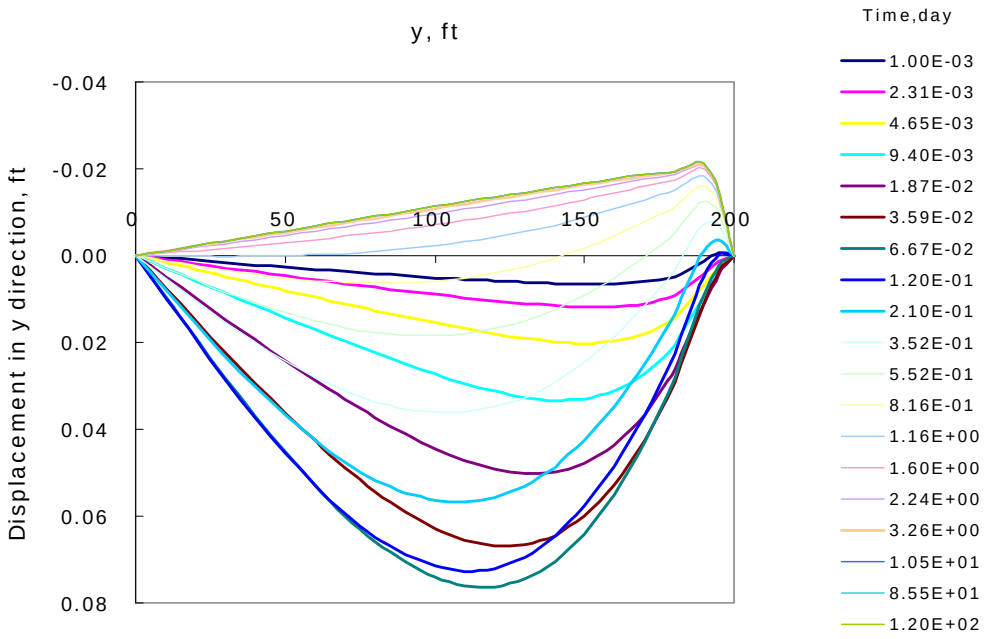

Figure 6-17: Displacements in y direction along Line A for Case 6.1.6.3.

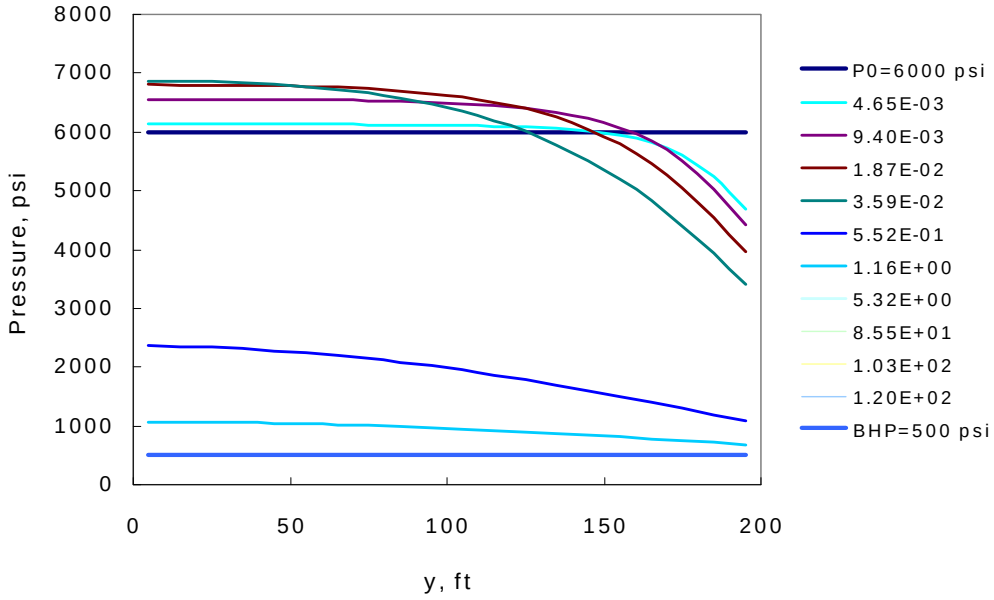

Figure 6-18: Pressure distribution along Line A for Case 6.1.6.3.

6.1.6.4 3D Primary Depletion with Different Fluid Mixtures

The following cases are designed to evaluate the effects of components of fluid on the compaction during the production. One case uses the 3-component fluid and another one uses the 6-component fluid. The initial compositions for both cases are shown in Table 6-5. The 6-component case adds three light components, C_1, C_3, and C_6, and decreases the initial composition of the heavy components C_{10}, C_{15}, and C_{20+}. Other input data values are same as Case 6.1.6.3. As shown in Figure 6-19, the light components weaken the compaction within the reservoir because of the lower pressure drops (as shown in Figure 6-20) during production periods due to their large compressibilities.

Table 6-5: Input parameters for Case 6.1.6.4

Initial composition	**3-component**	**6-component**
C_1	0.0	0.05
C_3	0.0	0.05
C_6	0.0	0.15
C_{10}	0.5	0.45
C_{15}	0.25	0.15
C_{20+}	0.25	0.15

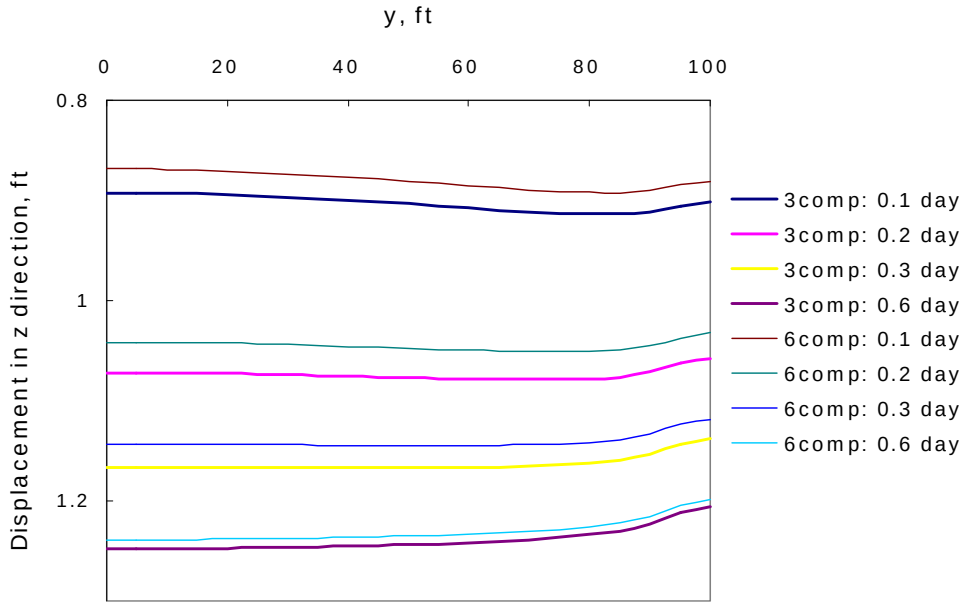

Figure 6-19: Displacements in z direction along Line A for Case 6.1.6.4.

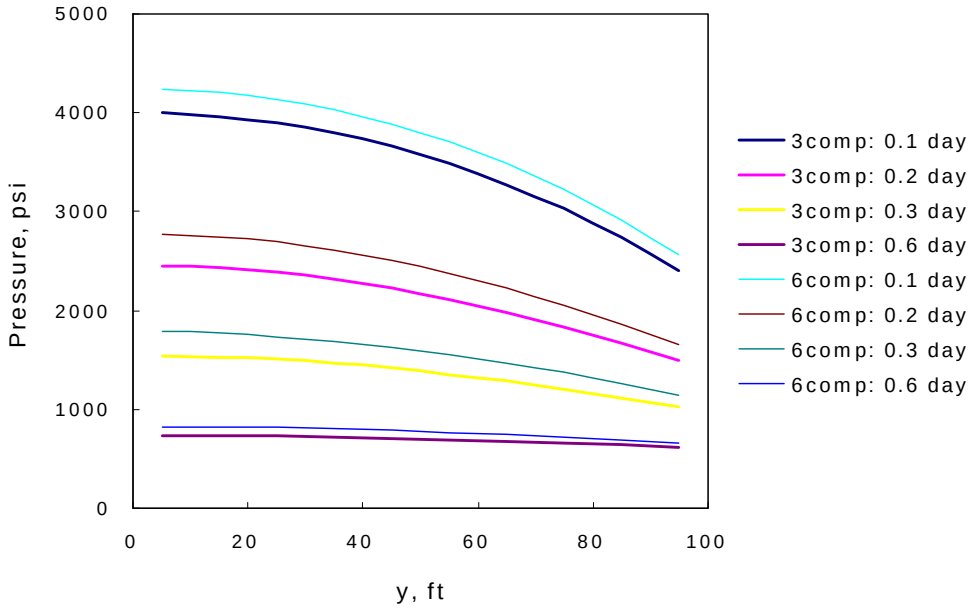

Figure 6-20: Pressure distribution along Line A for Case 6.1.6.4.

6.1.6.5 Water Flooding with Two-Component Fluid Mixture

In this section, a quarter of a five-spot simulation for a reservoir is modeled using the developed code. The input date is summized in Table 6-6. The average pressure distribution can be seen in Figure 6-21, which is increasing gradually because of water injection at (1, 1, 1) grid block. The associated oil production rate is shown in Figure 6-22. The displacement in z direction on the top layer along x = 1, as shown in Figure 6-23, demonstrates an increase as time elapses, and negative sign means that the rock compaction is tensed with increasing pore pressure. Because the producer is located at gridblocks (7, 7, 1) through (7, 7, 3), a decreasing curve of each time-step decrease along the y direction is shown in Figure 6-23.

Table 6-6: Input parameters for Case 6.1.6.5

Property	Value
Reservoir size (ft^3)	350 x 350 x 60
Reservoir gridblock size (ft^3)	50 x 50 x 20
No. of gridblocks	7 x 7 x 3
Young's modulus (kPa)	9×10^6
Poisson's ratio	0.3
Matrix permeability (x,y,z) (md)	100
Matrix porosity	0.3
Initial water saturation	0.2
Water viscosity (cp)	1.0
Water/oil compressibility (1/psi)	0.000003
Initial reservoir pressure (psi)	600
Injector injection rate, (STB/day)	400
Production constraint (BHP, psi)	600
Initial composition of C_{10} and C_{15}	0.6, 0.4

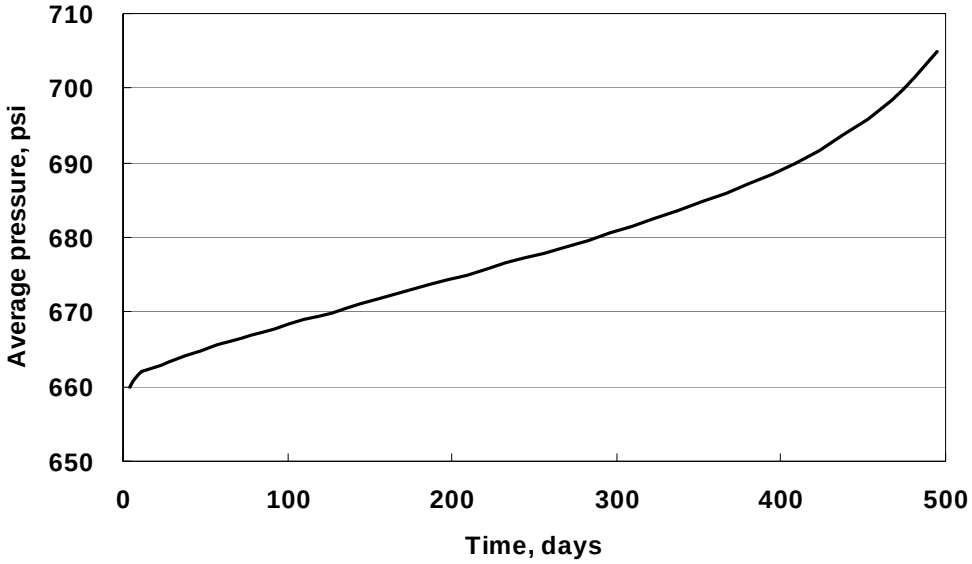

Figure 6-21: The average pressure for Case 6.1.6.5.

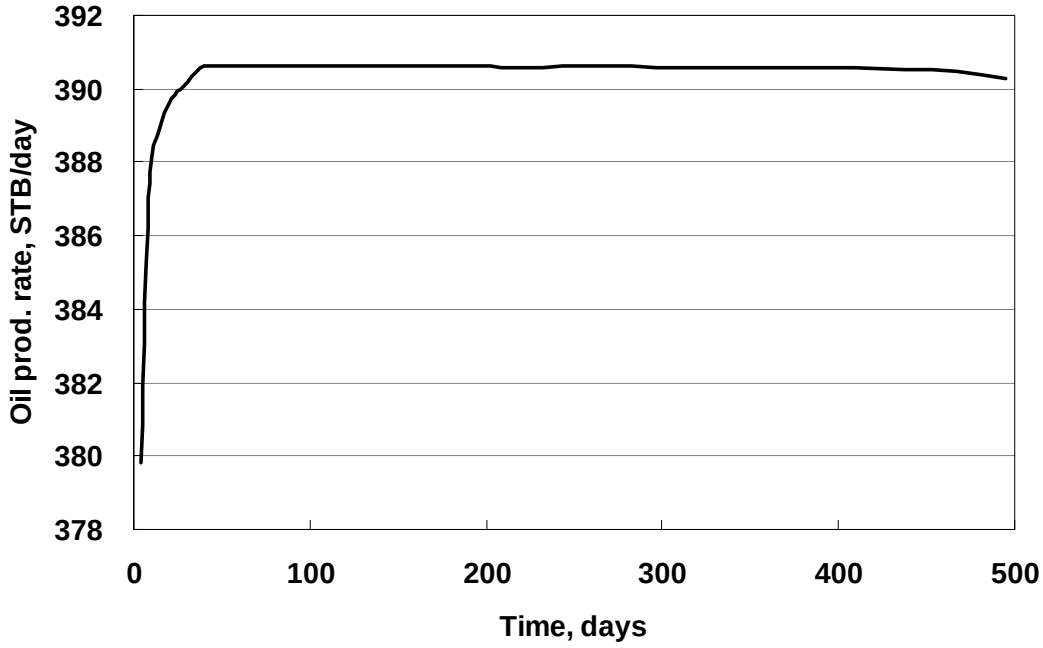

Figure 6-22: The oil production rate for Case 6.1.6.5.

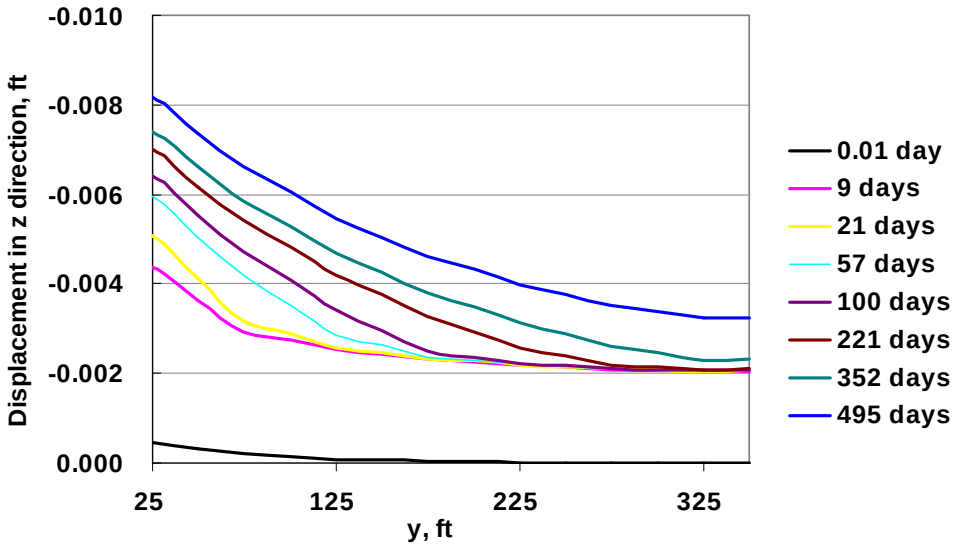

Figure 6-23: The displacement in z direction along gridblocks (1, 1, 1) through (1, 7, 1) for Case 6.1.6.5.

6.1.6.6 CO_2 Flooding with Seven-Component Fluid Mixture

A three-dimensional reservoir of 300×300×60 ft^3 and a seven-component fluid mixture is used to simulate the CO_2 injection process during the production. The initial pressure and temperature of the reservoir are 900 psia and 100˚F. Initial water saturation is 0.2, porosity is 0.25, and both horizontal and vertical permeabilities are 100 md. The reservoir is divided into 6×6×3 gridblocks. The well conditions for the injector and the producer are 300 Mscf/day and bottomhole pressure is 850 psi, respectively. Table 6-7 gives the reservoir input data. Table 6-8 presents component properties, initial reservoir and injected fluid compositions. The CO_2 injection increases the pressure of the reservoir; however, some of incremental pressure is used to compress rocks to enlarge the pore volume near injector location in the coupled geomechanics and

GPAS simulation and results in a smaller increase of fluid pressure comparing to the increase of fluid pressure from GPAS without geomechanics, as shown in Figure 6-24. Meanwhile, GPAS with geomechanics considers the variation of permeability during the production period. After 10-day CO_2 injection, the distribution of permeability in x direction at the top layer shows increase near the injector (x=1, y=1; x and y are the index of blocks in x and y directions, respectively) and decrease near the producer (x=6, y=6), as shown in Figure 6-25. Figure 6-26 represents the distributions of oil saturation from GPAS with and without geomechanics. It can be seen that GPAS without geomechanics gives a higher oil saturation around the producer (x=6, y=6, z=1), which means a higher oil production and a higher sweep speed. After 50-day operation, the average pressure begins decrease as shown in Figure 6-27. GPAS without geomechanics predicts a faster pressure-drop rate than GAPS with geomechanics. At time=152 days, GPAS with and without geomechanics predict almost the same average pressure. After this time, GPAS with geomechanics gives a higher oil production rate (Figure 6-28). Accordingly, the oil recovery difference between GPAS with and without geomechanics becomes smaller, as seen in Figure 6-29. However, the additional oil production from the coupled geomechanics and GPAS after 152-day production cannot match the loss of oil production from the lower fluid pressure. Hence, Figure 6-29 indicates a higher oil recovery from GPAS without geomechanics than GPAS with geomechanics.

Table 6-7: Input parameters for Case 6.1.6.6

Property	**Value**
Reservoir size (ft^3)	300 x 300 x 60
Reservoir gridblock size (ft^3)	50 x 50 x 20
No. of gridblocks	6 x 6 x 3
Young's modulus (kPa)	1×10^5
Poisson's ratio	0.3
Matrix permeability (x,y,z) (md)	100
Matrix porosity	0.25
Initial water saturation	0.2
Water viscosity (cp)	1.0
Water/oil compressibility (1/psi)	0.000003
Initial reservoir pressure (psi)	900
Injector injection rate, (Mscf/day)	300
Production constraint (BHP, psi)	850

Table 6-8: Properties of the components and initial composition for Case 6.1.6.6

Properties	CO_2	C_1	C_{2-3}	C_{4-6}	C_{7-15}	C_{16-27}	C_{28+}
Tc (°R)	547.5	343.0	619.5	833.8	1090.3	1351.8	1696.4
Pc (psia)	1071.6	667.8	652.6	493.0	315.4	239.9	238.1
Vc(ft^3/Lb-mol)	0.416	1.586	2.902	4.914	9.000	17.100	32.500
MW	44.0	16.0	37.0	69.5	140.9	280.9	519.6
Initial composition	0.001	0.150	0.216	0.234	0.267	0.061	0.071
Injected gas comp.	0.85	0.15	0.0	0.0	0.0	0.0	0.0

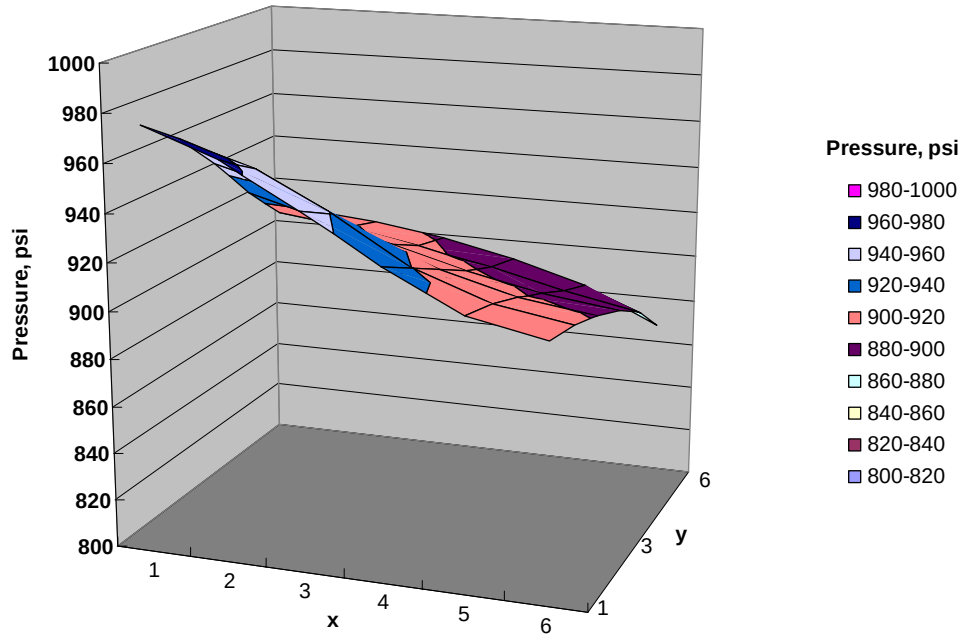

(a) GPAS with geomechanics.

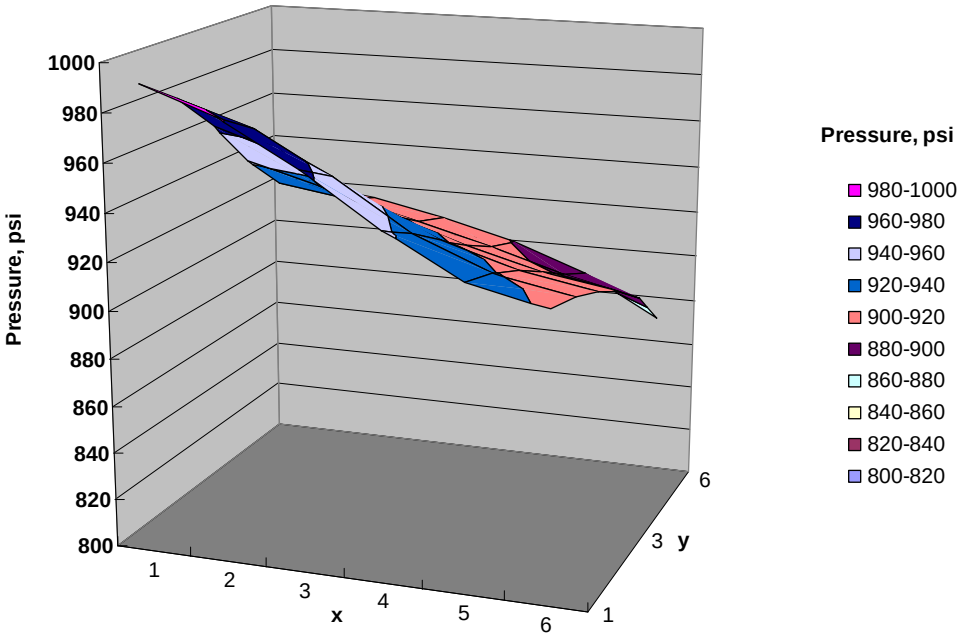

(b) GPAS without geomechanics.

Figure 6-24: The pressure distribution at 10 days for Case 6.1.6.6.

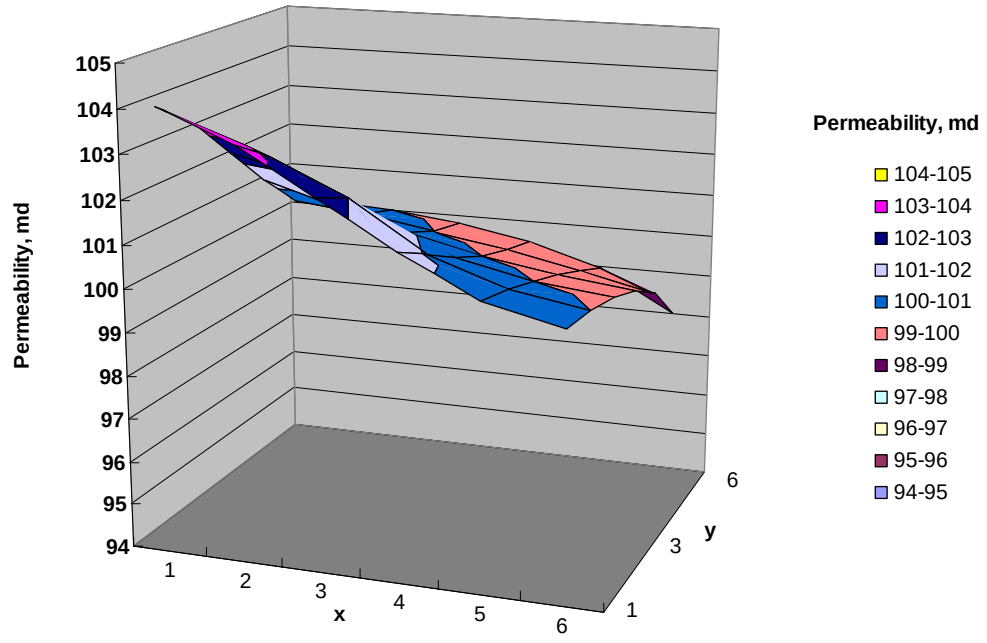

(a) GPAS with geomechanics.

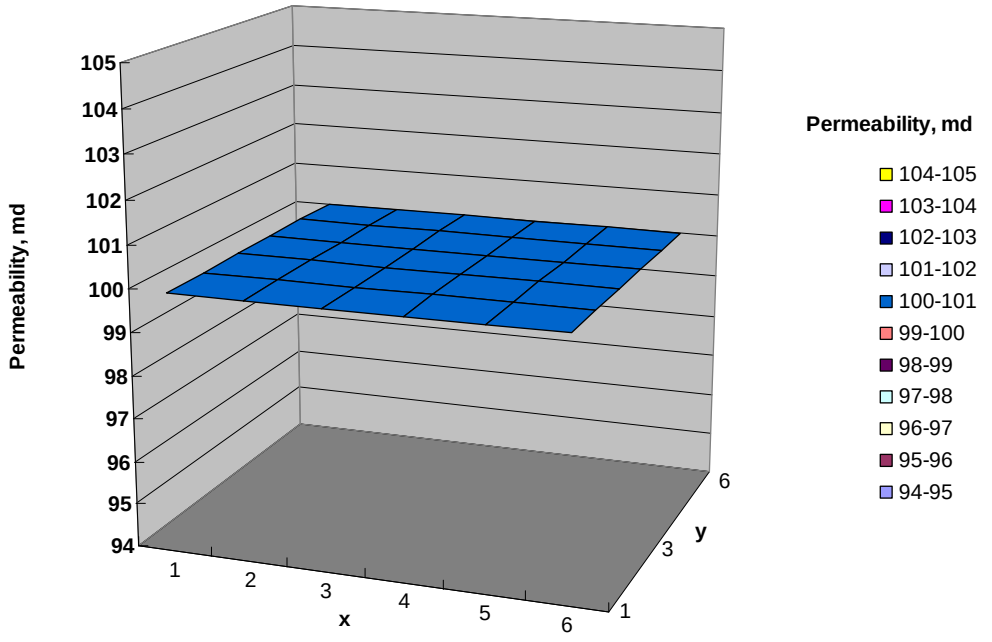

(b) GPAS without geomechanics.

Figure 6-25: The permeability (x-) distribution at 10 days for Case 6.1.6.6.

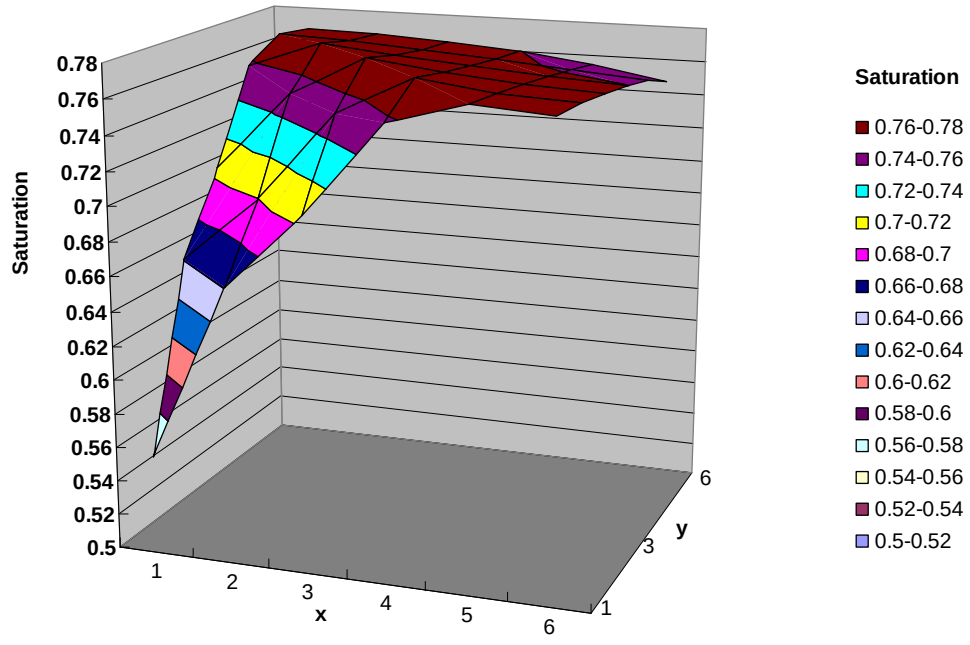

(a) GPAS with geomechanics.

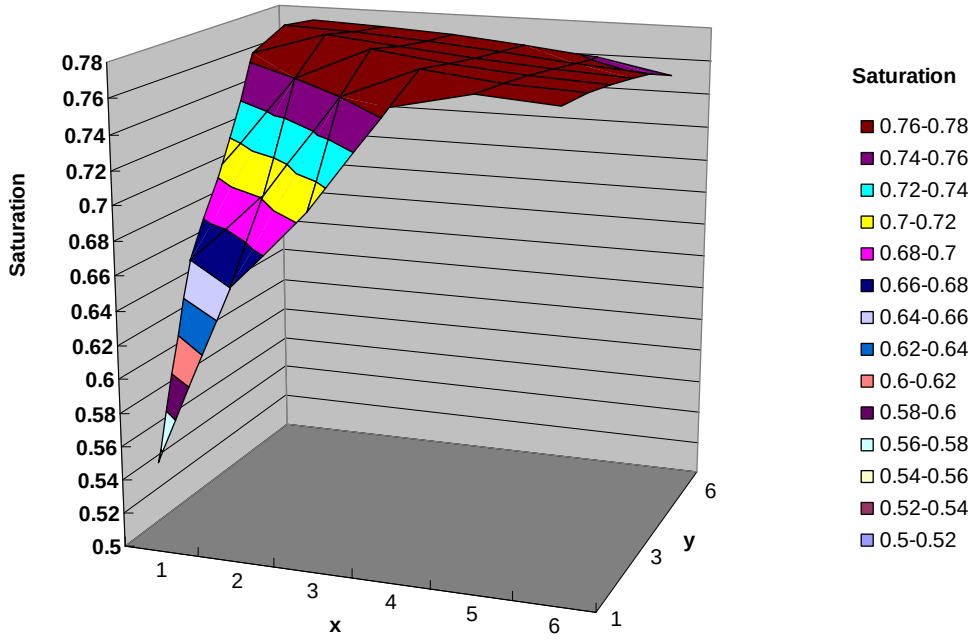

(b) GPAS without geomechanics.

Figure 6-26: The oil saturation distribution at time = 10 days for Case 6.1.6.6.

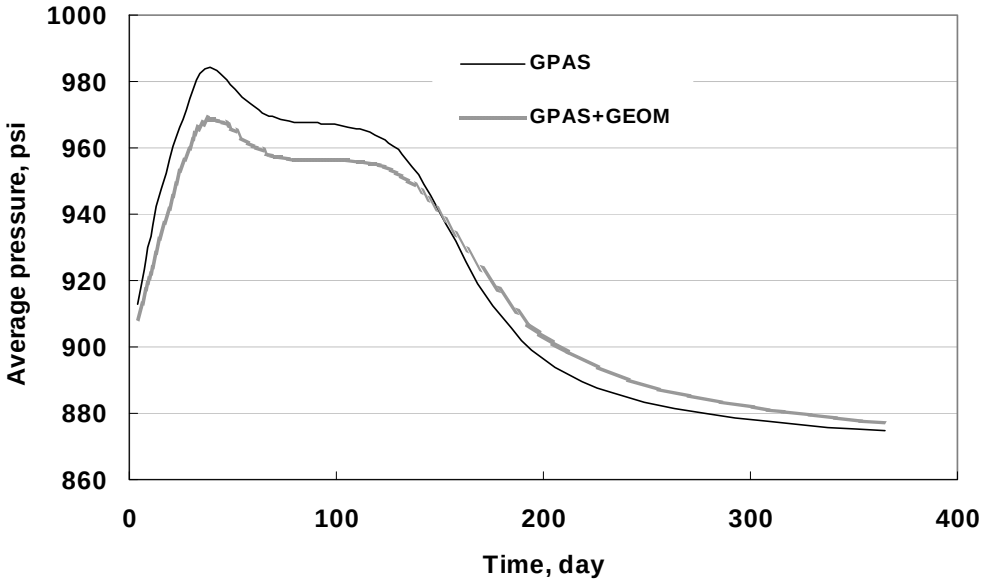

Figure 6-27: The average pressure for Case 6.1.6.6.

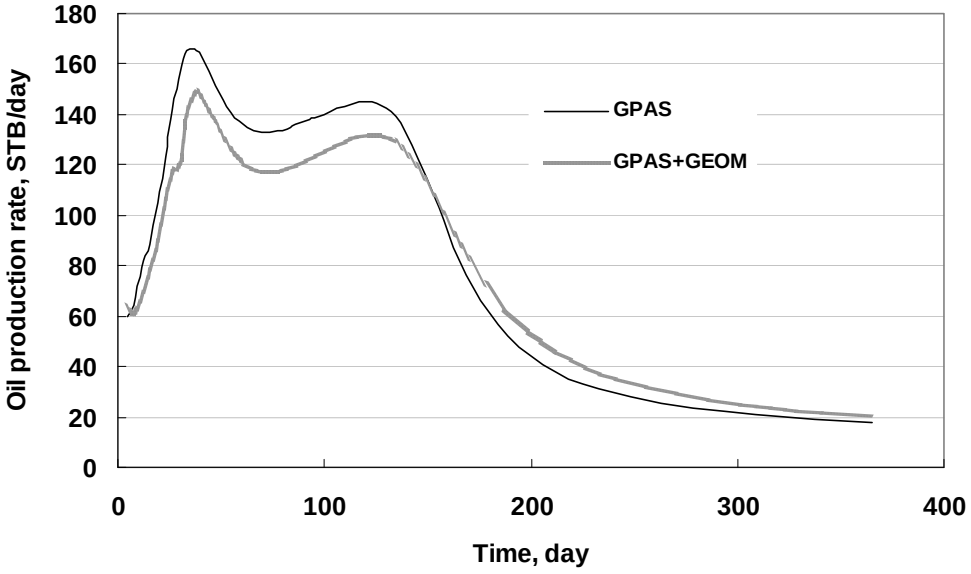

Figure 6-28: The oil production rate for Case 6.1.6.6.

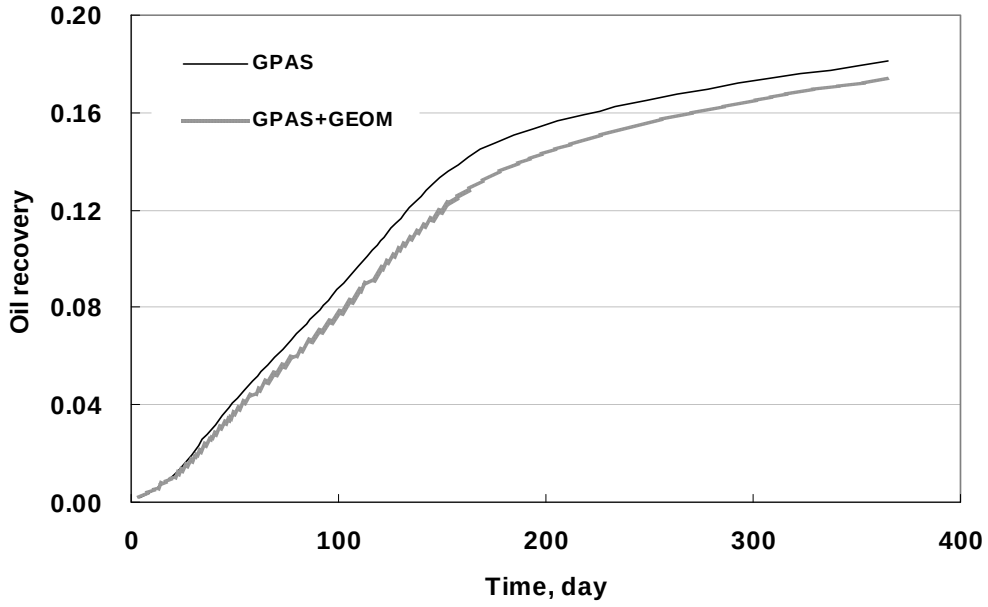

Figure 6-29: The oil recovery for Case 6.1.6.6.

6.2 ITERATIVELY COUPLED SOLUTION PROCEDURE

In general, a standalone reservoir simulator is developed with or without a simplification of the rock properties during the simulation. For example, the rock porosity is assumed to obey a linear relationship with pressure variation only; similarly, the absolute permeability is assumed constant during the production period. The above are the limitations of the current reservoir simulators: the fluids' containers, the porous media is static or idealized. The traditional stress analysis package for the porous media also dismisses the change of pore pressures. In other words, there is the existing software to cope with each scenario, fluid-flows or solid deformations. When a coupled simulation is necessary to solve problems in the hydrocarbon recovery processes, how does one reuse the existing simulators to complete more complicated modeling without

much modification? The iteratively coupled procedure is one way to answer this question.

6.2.1 Introduction

Iterative coupling solution procedure is alternative to solve Equations (3-38) approximately, not exactly. In some sense, it is a kind of an approximation of Equations (3-38). In petroleum engineering, Settari and Mourits (1994) first proposed the iteratively coupling idea and described one implementation for the poroelasticity model. Thereafter, a more general implementation was proposed by Chin et al. (2002), which is featured as a general formulation for porosity dealing with linear or nonlinear deformable solid and a complete independence between the existent reservoir simulator and the developed geomechanics module. The reservoir simulator can be coupled with a geomechanics module without any modifications to its source code except an equivalent compressibility array replacing the original constant pore compressibility scalar. Through reading and writing files, the necessary coupling information - for example, reservoir porosity, equivalent compressibility array, and pore pressure at each Newton iteration of one time-step - is exchanged between the reservoir model and the geomechanics model. Gai (2004) completed the coupling geomechanics procedure with the black-oil model using Settari and Mourits' strategy. Pan et al. (Pan et al. 2007) implemented Chin's algorithm to couple the geomechanics and a EOS-based compositional reservoir simulator (GPAS). Settari and his co-workers performed further research on the iteratively coupled process (Settari and Mourits 1995; 1997; Settari and Walters 1999; Tran et al. 2004; Tran et al. 2005).

Both above implementations are focusing on:

1. How to deal with the coupling terms to keep accuracy as high as possible in the fluid-flow governing equations and hence fully considering the coupling effects between the two models during the simulation.
2. At the same time, the robustness and the convergence of the solver are another key technology. Of course, based on the block Gauss-Seidel iteration, an implementation of iterative coupling, the simple iterative coupling procedure (**SICP**) between fluid and solid models, can be utilized; however, it will not always converge for a problem during the simulation.
3. On the other hand, for the solid model, the difficulty is how to represent the skeleton's deformation behavior accurately using appropriate linear or linear constitutive relationships.

The above three kinds of implementations of the iteratively coupled solution procedure, (1) the simple iterative coupling procedure (**SICP**), (2) Settari and Mourits (1994) and Gai (2004), and (3) Chin et al. (2002) and Pan et al. (Pan et al. 2007), will be studied in the following sections.

6.2.2 The Simple Iteratively Coupled Procedure (SICP)

The first method is the simple iteratively coupling procedure (**SICP**), which is , in fact, a block Gauss-Seidel type solver for a 2 by 2 block Jacobian system. It is based on the true Biot's consolidation theory: if it converges, its solution is the same as the one from the fully coupled solution procedure in Section 6.1 without any loss of accuracy.

Recast Equation (6-1) ignoring the superscripts, GEOM, GPAS, GEOM←GPAS, and GPAS←GEOM,

$$\begin{bmatrix} A_{11} & A_{12} \\ A_{21} & A_{22} \end{bmatrix} \begin{bmatrix} x_1 \\ x_2 \end{bmatrix} = \begin{bmatrix} b_1 \\ b_2 \end{bmatrix}. \tag{6-23}$$

SICP for the above equation is described as the following (after Saad 2000):

For k = 0,1,2,… until convergence

(1) Solve $A_{11}x_1^k = b_1 - A_{12}x_2^{k-1}$ for x_1^k;

(2) Solve $A_{22}x_2^k = b_2 - A_{21}x_1^k$ for x_2^k;

(3) Check convergence.

It is well-known that the iterative matrix of this procedure is

$$G = \begin{bmatrix} A_{11} & 0 \\ A_{21} & A_{22} \end{bmatrix}^{-1} \begin{bmatrix} 0 & -A_{12} \\ 0 & 0 \end{bmatrix}, \tag{6-24}$$

SICP converges for an arbitrary initial guess if and only if the spectral radius of the iterative matrix G is less than 1, namely,

$$\rho\left(\begin{bmatrix} A_{11} & 0 \\ A_{21} & A_{22} \end{bmatrix}^{-1} \begin{bmatrix} 0 & -A_{12} \\ 0 & 0 \end{bmatrix} \right) < 1. \tag{6-25}$$

A simple case is designed to verify this theorem numerically.

Firstly, the coupled Jacobian matrix is output as shown in Table 6-9 for the Young modulus E = 1 kPa. By checking the value of the matrix, we can find that the matrix is not a diagonal dominant one, which means that the coupling matrices can affect the solution procedure strongly and may result in divergence during iterations.

Table 6-9: The Jacobian matrix of a simple case with the Young modulus E=1 kPa.

0.833	-0.056	-0.333	0.333	-0.833	-0.500	0.417	0.056	-0.333	0.417	0.000	0.000	0.000	0.000	0.000	0.000	0.000	0.000	0.000	0.000	0.000	0.000	0.000	0.000	-0.007	-0.014	0.000	0.000	0.000	0.000	0.000	0.000
-0.056	2.000	0.000	0.056	-0.222	0.222	-0.056	0.667	0.000	0.056	0.000	0.000	0.000	0.000	0.000	0.000	0.000	0.000	0.000	0.000	0.000	0.000	0.000	0.000	0.028	-0.028	0.000	0.000	0.000	0.000	0.000	0.000
-0.333	0.000	1.333	-0.333	0.000	0.000	-0.333	0.000	0.000	-0.333	0.000	0.000	0.000	0.000	0.000	0.000	0.000	0.000	0.000	0.000	0.000	0.000	0.000	0.000	0.042	0.042	0.000	0.000	0.000	0.000	0.000	0.000
0.333	0.056	-0.333	0.833	-0.500	-0.833	0.417	-0.056	-0.333	0.417	0.000	0.000	0.000	0.000	0.000	0.000	0.000	0.000	0.000	0.000	0.000	0.000	0.000	0.000	-0.014	-0.007	0.000	0.000	0.000	0.000	0.000	0.000
-0.833	-0.222	0.000	-0.500	2.000	0.667	-0.833	0.222	0.000	-0.500	0.000	0.000	0.000	0.000	0.000	0.000	0.000	0.000	0.000	0.000	0.000	0.000	0.000	0.000	0.056	0.028	0.000	0.000	0.000	0.000	0.000	0.000
-0.500	0.222	0.000	-0.833	0.667	2.000	-0.500	-0.222	0.000	-0.833	0.000	0.000	0.000	0.000	0.000	0.000	0.000	0.000	0.000	0.000	0.000	0.000	0.000	0.000	0.028	0.056	0.000	0.000	0.000	0.000	0.000	0.000
0.417	-0.056	-0.333	0.417	-0.833	-0.500	1.667	0.000	-0.667	0.667	-0.833	-0.500	0.417	0.056	-0.333	0.417	0.000	0.000	0.000	0.000	0.000	0.000	0.000	0.000	0.000	0.000	-0.007	-0.014	0.000	0.000	0.000	0.000
0.056	0.667	0.000	-0.056	0.222	-0.222	0.000	4.000	0.000	0.000	-0.222	0.222	-0.056	0.667	0.000	0.056	0.000	0.000	0.000	0.000	0.000	0.000	0.000	0.000	0.111	-0.111	0.028	-0.028	0.000	0.000	0.000	0.000
-0.333	0.000	0.000	-0.333	0.000	0.000	-0.667	0.000	2.667	-0.667	0.000	0.000	-0.333	0.000	0.000	-0.333	0.000	0.000	0.000	0.000	0.000	0.000	0.000	0.000	0.000	0.000	0.042	0.042	0.000	0.000	0.000	0.000
0.417	0.056	-0.333	0.417	-0.500	-0.833	0.667	0.000	-0.667	1.667	-0.500	-0.833	0.417	-0.056	-0.333	0.417	0.000	0.000	0.000	0.000	0.000	0.000	0.000	0.000	0.000	0.000	-0.014	-0.007	0.000	0.000	0.000	0.000
0.000	0.000	0.000	0.000	0.000	0.000	-0.833	-0.222	0.000	-0.500	2.000	0.667	-0.833	0.222	0.000	-0.500	0.000	0.000	0.000	0.000	0.000	0.000	0.000	0.000	-0.056	-0.028	0.056	0.028	0.000	0.000	0.000	0.000
0.000	0.000	0.000	0.000	0.000	0.000	-0.500	0.222	0.000	-0.833	0.667	2.000	-0.500	-0.222	0.000	-0.833	0.000	0.000	0.000	0.000	0.000	0.000	0.000	0.000	-0.028	-0.056	0.028	0.056	0.000	0.000	0.000	0.000
0.000	0.000	0.000	0.000	0.000	0.000	0.417	-0.056	-0.333	0.417	-0.833	-0.500	1.667	0.000	-0.667	0.667	-0.833	-0.500	0.417	0.056	-0.333	0.417	0.000	0.000	0.007	0.014	0.000	0.000	-0.007	-0.014	0.000	0.000
0.000	0.000	0.000	0.000	0.000	0.000	0.056	0.667	0.000	-0.056	0.222	-0.222	0.000	4.000	0.000	0.000	-0.222	0.222	-0.056	0.667	0.000	0.056	0.000	0.000	0.028	-0.028	0.111	-0.111	0.028	-0.028	0.000	0.000
0.000	0.000	0.000	0.000	0.000	0.000	-0.333	0.000	0.000	-0.333	0.000	0.000	-0.667	0.000	2.667	-0.667	0.000	0.000	-0.333	0.000	0.000	-0.333	0.000	0.000	-0.042	-0.042	0.000	0.000	0.042	0.042	0.000	0.000
0.000	0.000	0.000	0.000	0.000	0.000	0.417	0.056	-0.333	0.417	-0.500	-0.833	0.667	0.000	-0.667	1.667	-0.500	-0.833	0.417	-0.056	-0.333	0.417	0.000	0.000	0.014	0.007	0.000	0.000	-0.014	-0.007	0.000	0.000
0.000	0.000	0.000	0.000	0.000	0.000	0.000	0.000	0.000	0.000	0.000	0.000	-0.833	-0.222	0.000	-0.500	2.000	0.667	-0.833	0.222	0.000	-0.500	0.000	0.000	0.000	0.000	-0.056	-0.028	0.056	0.028	0.000	0.000
0.000	0.000	0.000	0.000	0.000	0.000	0.000	0.000	0.000	0.000	0.000	0.000	-0.500	0.222	0.000	-0.833	0.667	2.000	-0.500	-0.222	0.000	-0.833	0.000	0.000	0.000	0.000	-0.028	-0.056	0.028	0.056	0.000	0.000
0.000	0.000	0.000	0.000	0.000	0.000	0.000	0.000	0.000	0.000	0.000	0.000	0.417	-0.056	-0.333	0.417	-0.833	-0.500	1.667	0.000	-0.667	0.667	-0.833	-0.500	0.000	0.000	0.007	0.014	0.000	0.000	-0.007	-0.014
0.000	0.000	0.000	0.000	0.000	0.000	0.000	0.000	0.000	0.000	0.000	0.000	0.056	0.667	0.000	-0.056	0.222	-0.222	0.000	4.000	0.000	0.000	-0.222	0.222	0.000	0.000	0.028	-0.028	0.111	-0.111	0.028	-0.028
0.000	0.000	0.000	0.000	0.000	0.000	0.000	0.000	0.000	0.000	0.000	0.000	-0.333	0.000	0.000	-0.333	0.000	0.000	-0.667	0.000	2.667	-0.667	0.000	0.000	0.000	0.000	-0.042	-0.042	0.000	0.000	0.042	0.042
0.000	0.000	0.000	0.000	0.000	0.000	0.000	0.000	0.000	0.000	0.000	0.000	0.417	0.056	-0.333	0.417	-0.500	-0.833	0.667	0.000	-0.667	1.667	-0.500	-0.833	0.000	0.000	0.014	0.007	0.000	0.000	-0.014	-0.007
0.000	0.000	0.000	0.000	0.000	0.000	0.000	0.000	0.000	0.000	0.000	0.000	0.000	0.000	0.000	0.000	0.000	0.000	-0.833	-0.222	0.000	-0.500	2.000	0.667	0.000	0.000	0.000	0.000	-0.056	-0.028	0.056	0.028
0.000	0.000	0.000	0.000	0.000	0.000	0.000	0.000	0.000	0.000	0.000	0.000	0.000	0.000	0.000	0.000	0.000	0.000	-0.500	0.222	0.000	-0.833	0.667	2.000	0.000	0.000	0.000	0.000	-0.028	-0.056	0.028	0.056
-0.007	0.028	0.042	-0.014	0.056	0.028	0.000	0.111	0.000	0.000	-0.056	-0.028	0.007	0.028	-0.042	0.014	0.000	0.000	0.000	0.000	0.000	0.000	0.000	0.000	-0.013	0.003	0.002	0.003	0.000	0.000	0.000	0.000
-0.014	-0.028	0.042	-0.007	0.028	0.056	0.000	-0.111	0.000	0.000	-0.028	-0.056	0.014	-0.028	-0.042	0.007	0.000	0.000	0.000	0.000	0.000	0.000	0.000	0.000	0.003	-0.013	0.003	0.002	0.000	0.000	0.000	0.000
0.000	0.000	0.000	0.000	0.000	0.000	-0.007	0.028	0.042	-0.014	0.056	0.028	0.000	0.111	0.000	0.000	-0.056	-0.028	0.007	0.028	-0.042	0.014	0.000	0.000	0.002	0.003	-0.013	0.003	0.002	0.003	0.000	0.000
0.000	0.000	0.000	0.000	0.000	0.000	-0.014	-0.028	0.042	-0.007	0.028	0.056	0.000	-0.111	0.000	0.000	-0.028	-0.056	0.014	-0.028	-0.042	0.007	0.000	0.000	0.003	0.002	0.003	-0.013	0.003	0.002	0.000	0.000
0.000	0.000	0.000	0.000	0.000	0.000	0.000	0.000	0.000	0.000	0.000	0.000	-0.007	0.028	0.042	-0.014	0.056	0.028	0.000	0.111	0.000	0.000	-0.056	-0.028	0.000	0.000	0.002	0.003	-0.013	0.003	0.002	0.003
0.000	0.000	0.000	0.000	0.000	0.000	0.000	0.000	0.000	0.000	0.000	0.000	-0.014	-0.028	0.042	-0.007	0.028	0.056	0.000	-0.111	0.000	0.000	-0.028	-0.056	0.000	0.000	0.003	0.002	0.003	-0.013	0.003	0.002
0.000	0.000	0.000	0.000	0.000	0.000	0.000	0.000	0.000	0.000	0.000	0.000	0.000	0.000	0.000	0.000	0.000	0.000	-0.007	0.028	0.042	-0.014	0.056	0.028	0.000	0.000	0.000	0.000	0.002	0.003	-0.007	0.002
0.000	0.000	0.000	0.000	0.000	0.000	0.000	0.000	0.000	0.000	0.000	0.000	0.000	0.000	0.000	0.000	0.000	0.000	-0.014	-0.028	0.042	-0.007	0.028	0.056	0.000	0.000	0.000	0.000	0.003	0.002	0.002	-0.007

Using Matlab®, the spectral radius of the iterative matrix G can be evaluated as shown in Table 6-10. Hence, for the Young modulus E = 1.0 kPa and 10 kPa, their associated spectral radii are larger than 1 and the related SICP will not converge; while for the bigger Young modulus 45 kPa, 50 kPa, 100 kPa, their associated spectral radii are less than 1 and the SICP will converge based on Equation (6-25). The numerical tests also verify these comments, as shown in Figure 6-30 and Figure 6-31.

Table 6-10: The spectral radius of the iterative matrix versus the Young modulus

The Young modulus E (kPa)	**The spectral radius of the iterative matrix**
1.0	38.5825
10.0	3.85825
45.0	0.85738
50.0	0.77165
100.0	0.38582

Hence, the convergence issue is the limitation of SICP; the alternative iterative coupling solution procedure, which improves the convergence behavior of the iteration process, is needed to be studied in the following sections. In the coupled physical processes through the porous media, one process is often dominant within the whole simulation. For example, in the coupled geomechanics and fluid-flow modeling, the fluid-flow phenomenon dominates the fluid-flow through the porous media. This is presented by the change of pressures is more rapidly and largely than the deformation of solid skeleton, of course, when the small strain theory / infinitesimal strain theory is assumed as Equation (3-1).

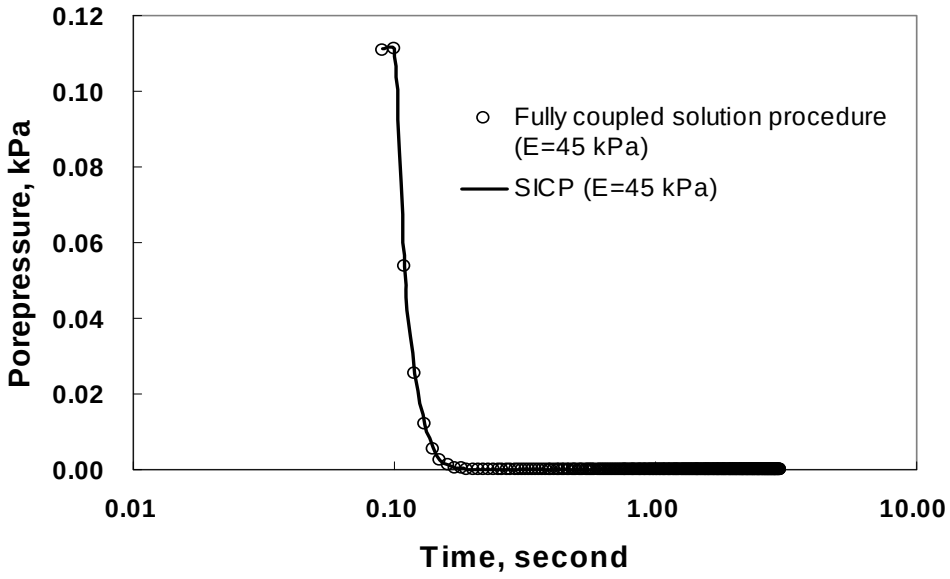

Figure 6-30: The comparison of the fully coupled solution procedure with SICP with E= 45 kPa.

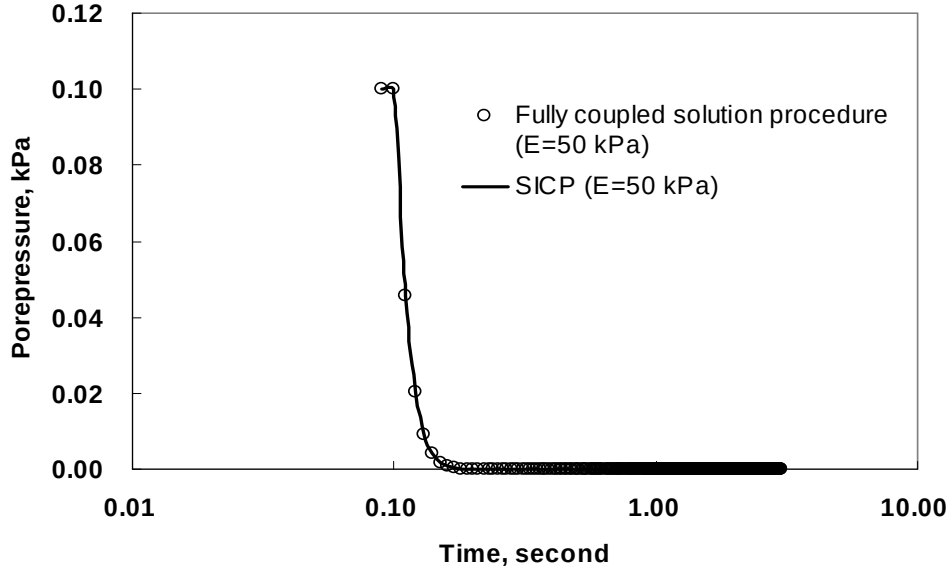

Figure 6-31: The comparison of the fully coupled solution procedure with SICP with E= 50 kPa.

6.2.3 Settari's Iteratively Coupled Solution Procedure

The second implementation of the iteratively coupled solution procedure was proposed by Settari and Mourits (1994). Its prototype could date back to Terzaghi's pseudo consolidation theory (Terzaghi 1936) which is different from the true Biot's consolidation theory. Settari and Mourits (1994) gave the complete description regarding the iteratively coupled solution procedure. For simplicity, temperature in the thermal module is discarded from the original description. Their implementation is based on the poroelasticity theory and the following two relationships are true:

$$\varepsilon_v = c_b \Delta I_1 - \left(c_b - c_s\right)\Delta p, \tag{6-26}$$

$$\phi^* = \phi^{*(0)} + \left[c_b\left(1-\phi^*\right) - c_s\right]\left(\Delta p - \Delta I_1\right), \tag{6-27}$$

where $I_1 = \left(\sigma_x + \sigma_y + \sigma_z\right)/3$. Equation (6-27) belongs to Geertsma's work in 1957. They differentiate two kinds of porosities: the true porosity and the reservoir porosity, ϕ and ϕ^* as shown in Equations (6-28) and (6-29), respectively, in their context. They followed the similar treatment as in the traditional reservoir simulator and added an extra term, $\Delta\phi_I^*$ as seen in Equation (6-30), related to the change of the total stress with the time. Their iterative coupling solution procedure (after Settari and Mourits 1994) are the following:

Within a time-step, its associated Newton iteration (k denotes the iteration counter number) is

For $k = 0,1,2,\ldots$ until convergence

(1) Calculate the residuals for the reservoir simulator using $p^{(k)}$ and other related parameters;

(2) Form the Jacobian matrix for the reservoir simulator using the $c_p^{(k)}$ coefficients;

(3) Obtain the new pressure $p^{(k+1)}$ through solving the Jacobian system in the reservoir simulator;

(4) Transfer $p^{(k+1)}$ to the geomechanics simulator and solve the new stresses $\left(\sigma_x, \sigma_y, \sigma_z\right)^{(k+1)}$ and volumetric strain $\varepsilon_v^{(k+1)}$;

(5) Calculate the true porosity $\phi^{*(k+1)}$ as follows:

$$\phi^{*(k+1)} = \phi^{*(0)} + \left[c_b \left(1 - \phi^{*(0)}\right) - c_s \right] \left[\left(p^{(k+1)} - p^{(0)} \right) - \left(I_1^{(k+1)} - I_1^{(0)} \right) \right]; \quad (6\text{-}28)$$

where c_b and c_s are called the bulk compressibility and the solid compressibility, respectively;

(6) Calculate $c_p^{(k+1)}$ and $\Delta\phi_I^{*(k+1)}$ using $\phi^{*(k+1)}$ and $\left(\sigma_x, \sigma_y, \sigma_z\right)^{(k+1)}$;

(7) Update the reservoir porosity $\phi^{(k+1)}$ using $\phi^{*(k+1)}$ and $\varepsilon_v^{(k+1)}$ as follows:

$$\phi^{(k+1)} = \phi^{*(k+1)} \left(1 - \varepsilon_v^{(k+1)}\right) \quad (6\text{-}29)$$

(8) Update another reservoir porosity $\tilde{\phi}^{(k+1)}$ as follows:

$$\tilde{\phi}^{(k+1)} - \phi^{(0)} = \phi^{(0)} \left[c_p^{(k+1)} \left(p^{(k+1)} - p^{(0)} \right) \right] + \Delta\phi_I^{*(k+1)} \quad (6\text{-}30)$$

where $\Delta\phi_I^{*(k+1)} = -\left(c_b - c_s\right)\Delta I_1$;

(9) Check convergence by taking the norm of $\left(p^{(k+1)} - p^{(k)} \right)$ and if not converged, return to (1).

Substituting Equations (6-26) and (6-27) into Equation (6-29) and comparing with Equation (6-30) gives the coefficients c_p and $\Delta\phi_I^*$:

$$c_p = \frac{\left[c_b - \left(1 - \phi^*\right) c_s \right]}{\phi^{*(0)}}, \quad (6\text{-}31)$$

$$\Delta\phi_I^* = -\left(c_b - c_s\right)\Delta I_1. \quad (6\text{-}32)$$

Also, Settari and Mourits (1994) proposed two kinds of pore compressibilities as follows, ignoring the change of the total stress $\left(\Delta I_1 = 0\right)$ with time and the grain compressibility $\left(c_s = 0\right)$.

$$c_R^I = c_p = c_b / \phi^0 = \left[\frac{3\left(1 - 2\nu\right)}{E} \right] / \phi^0, \quad (6\text{-}33)$$

and

$$c_R^{II} = c_p = c_b\left[1-\frac{2(1-2\nu)}{3(1-\nu)}\right]/\phi^0 = \left[\frac{(1-2\nu)(1+\nu)}{E(1-\nu)}\right]/\phi^0. \tag{6-34}$$

In fact, as we can see in the later section, the above compressibilities are the equivalent compressibilities describing three-dimensional and one-dimensional consolidation in the terms of soil mechanics with the assumption of the constant total stress during the settlement (Viggiani et al. 1970). Furthermore, the formulations, (6-27) or (6-28), are valid only for the poroelastics process.

6.2.4 Chin's Iteratively Coupled Solution Procedure

The third implementation of the iteratively coupled solution procedure was proposed by Chin et al. (2002), which is based on the true Biot's consolidation theory. Compared to Settari and Mourits' implementation, Chin's implement is easily extended and coupled with the nonlinear constitutive relationship. An equivalent compressibility is used to decouple the fluid-flow equations.

There are two kinds of porosities in this research, the symbol ϕ denotes "reservoir porosity" used in the reservoir fluid-flow model, while ϕ^* is true porosity calculated from the stress analysis model. The relationship between them was given by Chin et al. (2002) as follows:

$$\begin{cases} \phi^* = 1-(1-\phi_0)e^{-\varepsilon_v} \\ \phi = \left(\dfrac{1-\phi_0}{1-\phi^*}\right)\phi^* = e^{-\varepsilon_v}\phi^* \approx \phi^*(1-\varepsilon_v) \end{cases} \tag{6-35}$$

or

$$\begin{cases} \phi^* = 1-(1-\phi_0)e^{-\varepsilon_v}, \\ \phi = \left(\dfrac{1-\phi_0}{1-\phi^*}\right)\phi^* = \left(\dfrac{1-\phi_0}{(1-\phi_0)e^{-\varepsilon_v}}\right)\left[1-(1-\phi_0)e^{-\varepsilon_v}\right] = e^{\varepsilon_v}-(1-\phi_0) \approx \phi_0+\varepsilon_v. \end{cases} \tag{6-36}$$

Recast the mass balance equation, Equation (3-60),

$$V_b \frac{D\left[\left(1+\varepsilon_v\right)\phi^* N_i\right]}{Dt} - V_b \nabla \cdot \sum_{j=1}^{n_p} \left[\xi_j x_{ij} \frac{\bar{\bar{K}} k_{rj}}{\mu_j} \left(\nabla P_j - \gamma_j \nabla D \right) \right] - V_b \varepsilon_v \frac{D\left(\phi^* N_i\right)}{Dt} - q_i = 0, \quad i = 1, 2, ..., n_c + 1. \tag{6-37}$$

Using Equation (6-35) and discarding $V_b \varepsilon_v \frac{D\left(\phi^* N_i\right)}{Dt}$ (the small strain assumption), Equation (6-37) can be approximated as

$$V_b \frac{D\left(\phi N_i\right)}{Dt} - V_b \nabla \cdot \sum_{j=1}^{n_p} \left[\xi_j x_{ij} \frac{\bar{\bar{K}} k_{rj}}{\mu_j} \left(\nabla P_j - \gamma_j \nabla D \right) \right] - q_i = 0, \quad i = 1, 2, ..., n_c + 1, \tag{6-38}$$

where the reservoir porosity ϕ is evaluated using Equations (6-35) or (6-36) of the true porosity ϕ^* and the volumetric strain ε_v, which are all computed in the geomechanics model.

This implementation has the following advantages:

1. The formulation of the true porosity ϕ^* in Equation (6-35) are directly derived from the mass balance equation of solid, which can be applied to any kind of deformable porous media. The deformation behavior of solid maybe linear or nonlinear. The derivation of Equation (6-35) is the following:

Mass Balance for Solid

$$\frac{D\phi^*}{Dt} = \left(1 - \phi^*\right) \nabla \cdot v^s, \tag{6-39}$$

where the material derivative with respect to the moving solid is defined as

$$\frac{D}{Dt}(*) \equiv \frac{\partial}{\partial t}(*) + v^s \cdot \nabla (*). \tag{6-40}$$

Because the identity,

$$\nabla \cdot v^s = \nabla \cdot \frac{\partial u^s}{\partial t} = \frac{\partial \left(\nabla \cdot u^s \right)}{\partial t} = \frac{\partial \varepsilon_v}{\partial t}. \tag{6-41}$$

Hence,

$$\frac{\partial \phi^*}{\partial t} \approx \frac{D\phi^*}{Dt} = \left(1 - \phi^*\right) \nabla \cdot v^s = \left(1 - \phi^*\right) \frac{\partial \varepsilon_v}{\partial t}, \tag{6-42}$$

and the following is derived

$$\frac{\partial \phi^*}{\partial t} = \left(1-\phi^*\right)\frac{\partial \varepsilon_v}{\partial t} \quad \Leftrightarrow \quad \frac{1}{\left(1-\phi^*\right)}\cdot\frac{\partial \phi^*}{\partial t} = \frac{\partial \varepsilon_v}{\partial t}$$

$$\Rightarrow \int_0^t \frac{1}{\left(1-\phi^*\right)}\cdot\frac{\partial \phi^*}{\partial t}dt = \int_0^t \frac{\partial \varepsilon_v}{\partial t}dt \quad \Rightarrow \quad -\int_0^t \frac{\partial\left[\ln\left(1-\phi^*\right)\right]}{\partial t}dt = \varepsilon_v - 0$$

$$\Rightarrow \ln\left(\frac{1-\phi_0}{1-\phi^*}\right) = \varepsilon_v \quad \Rightarrow \quad 1-\phi_0 = \left(1-\phi^*\right)e^{\varepsilon_v}$$

$$\Rightarrow \phi^* = 1-\left(1-\phi_0\right)e^{-\varepsilon_v}.$$

2. After careful review of Equation (6-38), it can been seen that Equation (6-38) has the same terms as the one (Equation (2-1)) used in GPAS without considering geomechanics effect. This characteristic makes us link the traditional reservoir simulator and the stress analysis simulator using a few modifications. Namely, the two sets of source codes can be kept independently at most. The reservoir simulator does not need any modifications only if the reservoir simulator can read the so-called equivalent compressibility array to replace the traditional constant pore compressibility scalar. The computational procedure is: through reading and writing files, the necessary coupling information, the reservoir porosity (ϕ), the equivalent compressibility array ($\tilde{c}_p \equiv \partial\phi/\partial p$), and the pore pressure at each Newton iteration of one time-step, is exchanged between the reservoir model and the geomechanics model. The flow chart is shown as the follows:

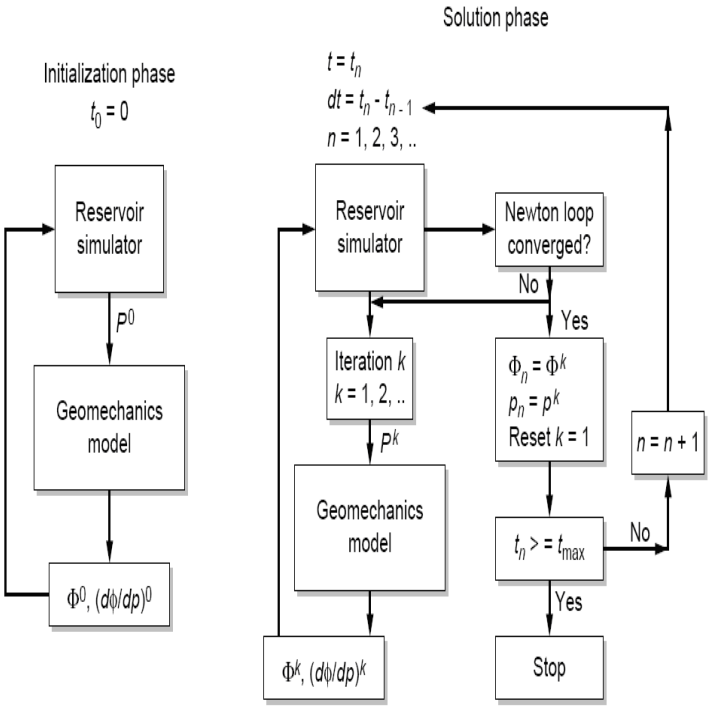

Figure 6-32: Flow Chart of Iteratively coupled Analysis (after Chin et al. 2002).

6.2.5 Terzaghi's Decoupled Solution Procedure

For the second implementation of the iteratively coupled solution procedure proposed by Settari and Mourits (1994) in Section 6.2.3, its origin could date back to Terzaghi's pseudo consolidation theory which is different from the true Biot's consolidation theory. The difference between them is whether the variation of total stresses with time is assumed or not. Terzaghi's pseudo consolidation theory ignores the variation of total stresses with time, while Biot's true consolidation theory does not assume the constant total stresses during the consolidation (Lambe and Whitman 1979). Hence, Biot's true consolidation can capture the increase in pore pressure during the early period of consolidation, which is the so-called Mandel-Cryer effect. For Terzaghi's

pseudo consolidation theory, a compressibility coefficient is derived from the assumption of a constant total stress for the linear elasticity theory and the fluid-flow equation is decoupled. However, because of the simplicity of implementation, many solutions from Terzaghi's pseudo consolidation theory have proved accurate enough and useful in practice (Viggiani et al. 1970).

6.2.5.1 The Coefficient of Consolidation

The poroelasticity equations between strains and effective stresses are the following:

$$\begin{cases} \varepsilon_x = \dfrac{1}{E}\left[\sigma_x^{'} - \nu\left(\sigma_y^{'} + \sigma_z^{'}\right)\right], \\ \varepsilon_y = \dfrac{1}{E}\left[\sigma_y^{'} - \nu\left(\sigma_z^{'} + \sigma_x^{'}\right)\right], \\ \varepsilon_z = \dfrac{1}{E}\left[\sigma_z^{'} - \nu\left(\sigma_x^{'} + \sigma_y^{'}\right)\right]; \end{cases} \tag{6-43}$$

and the effective stress law is as follows:

$$\begin{cases} \sigma_x = \sigma_x^{'} + p, \\ \sigma_y = \sigma_y^{'} + p, \\ \sigma_z = \sigma_z^{'} + p; \end{cases} \tag{6-44}$$

Adding all the three equations of (6-43) and using Equation (6-44)results in

$$\varepsilon_v = \varepsilon_x + \varepsilon_y + \varepsilon_z = \frac{1}{E}\left[(1-2\nu)\left(\sigma_x^{'} + \sigma_y^{'} + \sigma_z^{'}\right)\right]$$

$$= \frac{(1-2\nu)}{E}\left[\left(\sigma_x + \sigma_y + \sigma_z\right) - 3p\right] = \frac{(1-2\nu)}{E}\left(\theta_3 - 3p\right),$$

where $\theta_3 = \sigma_x + \sigma_y + \sigma_z$.

Hence,

$$\frac{\partial \varepsilon_v}{\partial t} = \frac{(1-2\nu)}{E}\frac{\partial \theta_3}{\partial t} - \frac{3(1-2\nu)}{E}\frac{\partial p}{\partial t}. \tag{6-45}$$

Similarly, for two-dimensional and one-dimensional consolidation, the derivations can be performed as shown in the following:

Two-dimensional consolidation

The poroelasticity equations between strains and effective stresses are the following:

$$\begin{cases} \varepsilon_x = \dfrac{1}{E}\left[\sigma_x^{'} - \nu\left(\sigma_y^{'} + \sigma_z^{'}\right)\right], \\ 0 = \dfrac{1}{E}\left[\sigma_y^{'} - \nu\left(\sigma_z^{'} + \sigma_x^{'}\right)\right], \\ \varepsilon_z = \dfrac{1}{E}\left[\sigma_z^{'} - \nu\left(\sigma_x^{'} + \sigma_y^{'}\right)\right]; \end{cases} \tag{6-46}$$

$$\varepsilon_v = \varepsilon_x + \varepsilon_y + \varepsilon_z = \frac{1}{E}\left[\left(1-2\nu\right)\left(\sigma_x^{'} + \sigma_y^{'} + \sigma_z^{'}\right)\right]$$

$$= \frac{\left(1-2\nu\right)}{E}\left[\sigma_x^{'} + \nu\left(\sigma_z^{'} + \sigma_x^{'}\right) + \sigma_z^{'}\right] = \frac{\left(1-2\nu\right)\left(1+\nu\right)}{E}\left(\sigma_z^{'} + \sigma_x^{'}\right)$$

$$= \frac{\left(1-2\nu\right)\left(1+\nu\right)}{E}\left[\left(\sigma_x + \sigma_z\right) - 2p\right] = \frac{\left(1-2\nu\right)\left(1+\nu\right)}{E}\left(\theta_2 - 2p\right),$$

where $\theta_2 = \sigma_x + \sigma_z$.

Hence,

$$\frac{\partial \varepsilon_v}{\partial t} = \frac{\left(1-2\nu\right)\left(1+\nu\right)}{E}\frac{\partial \theta_2}{\partial t} - \frac{2\left(1-2\nu\right)\left(1+\nu\right)}{E}\frac{\partial p}{\partial t}. \tag{6-47}$$

One-dimensional consolidation

The poroelasticity equations between strains and effective stresses are the following:

$$\begin{cases} 0 = \dfrac{1}{E}\left[\sigma_x^{'} - \nu\left(\sigma_y^{'} + \sigma_z^{'}\right)\right], \\ 0 = \dfrac{1}{E}\left[\sigma_y^{'} - \nu\left(\sigma_z^{'} + \sigma_x^{'}\right)\right], \\ \varepsilon_z = \dfrac{1}{E}\left[\sigma_z^{'} - \nu\left(\sigma_x^{'} + \sigma_y^{'}\right)\right]; \end{cases} \tag{6-48}$$

$$\varepsilon_v = \varepsilon_x + \varepsilon_y + \varepsilon_z = \frac{1}{E}\left[(1-2\nu)\left(\sigma_x^{'} + \sigma_y^{'} + \sigma_z^{'}\right)\right]$$

$$= \frac{(1-2\nu)}{E}\left[\nu\left(\sigma_y^{'} + \sigma_z^{'}\right) + \nu\left(\sigma_z^{'} + \sigma_x^{'}\right) + \sigma_z^{'}\right]$$

$$= \frac{(1-2\nu)}{E}\left[\nu\left(\sigma_y^{'} + \sigma_x^{'}\right) + (1+2\nu)\sigma_z^{'}\right] = \frac{(1-2\nu)}{E}\left[\sigma_z^{'} - E\varepsilon_z + (1+2\nu)\sigma_z^{'}\right]$$

$$= \frac{(1-2\nu)}{E}\left[\sigma_z^{'} - E\varepsilon_v + (1+2\nu)\sigma_z^{'}\right] = \frac{(1-2\nu)}{E}\left[2(1+\nu)\sigma_z^{'} - E\varepsilon_v\right]$$

$$= \frac{2(1-2\nu)(1+\nu)}{E}\sigma_z^{'} - (1-2\nu)\varepsilon_v$$

$$2(1-\nu)\varepsilon_v = \frac{2(1-2\nu)(1+\nu)}{E}\sigma_z^{'} = \frac{2(1-2\nu)(1+\nu)}{E}(\sigma_z - p)$$

$$\varepsilon_v = \frac{(1-2\nu)(1+\nu)}{E(1-\nu)}(\sigma_z - p) = \frac{(1-2\nu)(1+\nu)}{E(1-\nu)}(\theta_1 - p),$$

where $\theta_1 = \sigma_z$.

Hence,

$$\frac{\partial \varepsilon_v}{\partial t} = \frac{(1-2\nu)(1+\nu)}{E(1-\nu)}\left(\frac{\partial \theta_1}{\partial t} - \frac{\partial p}{\partial t}\right). \tag{6-49}$$

The key point of Terzaghi's decoupling solution procedure is that $\frac{\partial \varepsilon_v}{\partial t}$ can be approximated as the product of a coefficient of consolidation and $\frac{\partial p}{\partial t}$ as shown in Table 6-11 if the total stress is constant during the consolidation process.

Table 6-11: The coefficient of consolidation

Dimension (n)	**Terzaghi-Rendulic pseudo consolidation theory**	**Biot true consolidation theory**	**Coefficient of consolidation** ($\frac{\partial \varepsilon_v}{\partial p} = m_{v,n}, n = 1,2,3$)
1	$\frac{\partial \varepsilon_v}{\partial t} = \frac{(1-2v)(1+v)}{E(1-v)}\left(-\frac{\partial p}{\partial t}\right),$ $\frac{\partial \theta_1}{\partial t} = 0.$	$\frac{\partial \varepsilon_v}{\partial t} = \frac{(1-2v)(1+v)}{E(1-v)}\left(\frac{\partial \theta_1}{\partial t} - \frac{\partial p}{\partial t}\right).$	$\frac{(1-2v)(1+v)}{E(1-v)}$
2	$\frac{\partial \varepsilon_v}{\partial t} = \frac{2(1-2v)(1+v)}{E}\left(-\frac{\partial p}{\partial t}\right),$ $\frac{\partial \theta_2}{\partial t} = 0.$	$\frac{\partial \varepsilon_v}{\partial t} = \frac{(1-2v)(1+v)}{E}\frac{\partial \theta_2}{\partial t} - \frac{2(1-2v)(1+v)}{E}\frac{\partial p}{\partial t}.$	$\frac{2(1-2v)(1+v)}{E}$
3	$\frac{\partial \varepsilon_v}{\partial t} = \frac{3(1-2v)}{E}\left(-\frac{\partial p}{\partial t}\right),$ $\frac{\partial \theta_3}{\partial t} = 0.$	$\frac{\partial \varepsilon_v}{\partial t} = \frac{(1-2v)}{E}\frac{\partial \theta_3}{\partial t} - \frac{3(1-2v)}{E}\frac{\partial p}{\partial t}.$	$\frac{3(1-2v)}{E}$

6.2.6 The Equivalent Compressibility

From the traditional treatment of the porosity, Equation (1-6),

$$\phi = \phi_0 \left[1 + c_p \left(p - p_0 \right) \right], \tag{6-50}$$

the derivative of the porosity respect to the pressure is

$$\frac{\partial \phi}{\partial p} = \phi_0 c_p. \tag{6-51}$$

In addition, from Equation (6-36), the following is true,

$$\frac{\partial \phi}{\partial p} = \frac{\partial \varepsilon_v}{\partial p}. \tag{6-52}$$

Following the logic of traditional treatment as shown in Equation (6-51), an equivalent compressibility ($\tilde{c}_p$) is defined as follows:

$$\frac{\partial \varepsilon_v}{\partial p} \equiv \phi_0 \tilde{c}_p. \tag{6-53}$$

Considering the coefficient of consolidation as shown in Table 6-11 in Section 6.2.5.1, the equivalent compressibility ($\tilde{c}_p$) is summarized in Table 6-12.

Table 6-12: The equivalent compressibility ($\tilde{c}_p$)

Dimension **(n)**	**Coefficient of consolidation** ($\frac{\partial \varepsilon_v}{\partial p} = m_{v,n}, n = 1,2,3$)	**Equivalent compressibility** ($\tilde{c}_{p,n}, n = 1,2,3$)
1	$\frac{(1-2v)(1+v)}{E(1-v)}$	$\frac{m_{v,1}}{\phi_0} = \frac{(1-2v)(1+v)}{E(1-v)\phi_0}$
2	$\frac{2(1-2v)(1+v)}{E}$	$\frac{m_{v,2}}{\phi_0} = \frac{2(1-2v)(1+v)}{E\phi_0}$
3	$\frac{3(1-2v)}{E}$	$\frac{m_{v,3}}{\phi_0} = \frac{3(1-2v)}{E\phi_0}$

After reviewing two kinds of pore compressibilities, Equations (6-33) and (6-34), proposed by Settari and Mourits (1994), it is clear that

$$c_R^I = \tilde{c}_{p,3}, \tag{6-54}$$

$$c_R^{II} = \tilde{c}_{p,1}, \tag{6-55}$$

which are, in fact, the equivalent compressibilities for a three-dimensional consolidation and one-dimensional consolidation, respectively.

6.2.7 Convergence Evaluation

The convergence analysis of the iteratively coupled solution procedure is discussed in this section.

For SIP implementation, it convergences if and only if the spectral radius of the iterative matrix G less than 1, as shown in Equation (6-25) in Section 6.2.2. When the coupling effect between the fluid-flow and the solid deformation is not as strong, namely, when one of above physical process dominates the coupling process, SIP implementation will be one alternative solution procedure.

For Settari's implementation and Chin's implementation, the theoretical analysis for the convergence is not simple. Its convergence behavior depends on the selection of the equivalent compressibility $\tilde{c}_p$. If $\tilde{c}_p$ or each element is positive, the associated iteratively coupled solution procedure will have the same convergence characteristics with the traditional reservoir simulator with the pore compressibility c_p. When the entries of $\tilde{c}_p$ at one Newton iteration of one time-step are not always positive for all grid blocks, which means that the value at some grid blocks are negative and the ones at elsewhere are positive, the solver may have some difficulties to convergence to the physical solution. Gutierrez and Lewis (1998) also commented the following: "For instance, it is not clear whether the approach can be used in the case when the rock tends to increase in volume with a reduction in pore pressure (e.g., due to dilation during shearing). Such a volume increase would require negative pore compressibility in the

reservoir simulation and may cause numerical instability." Minkoff et al. (2003) in their loose coupling solution procedure also mentioned that the solver sometimes have difficulty converging and the user has to provide an approximate compressibility to use in the calculation of Jacobian matrix to improve the convergence of the fluid-flow solver.

A simple numerical experiment is conducted to investigate the behavior of the equivalent compressibility $\tilde{c}_p$ during the coupled simulation as shown in Table 6-13. The table shows the equivalent compressibility $\tilde{c}_p$ distributions at the second Newton iteration at two time-steps, 0.01 and 0.1 (the dimensionless time). The values are positive or negative at the different grid blocks, which result the difficulty of convergence for the solver.

How to select a good approximation of the equivalent compressibility $\tilde{c}_p$ during the simulation is an open research issue. In other words, from the mathematic point view, how to find a good preconditioner for Jacobian matrix of the fluid-flow model in the coupling modeling, is not resolved now. Of course, the approximations as shown in Table 6-12 used in Terzaghi-Rendulic pseudo consolidation theory are one of preconditioners.

6.2.8 Implementation of Iteratively Coupled Solution Procedure in GPAS

In this work, a modified Chin's implementation (Chin et al. 2002) of the iteratively coupled solution procedure is coded in GPAS. This implementation is based on the two key points:

1. Use the formulation of the true porosity ϕ^* in Equation (6-35), which are directly derived from the mass balance equation of solid and can be applied to any kind of deformable porous media. The formulation assures the accuracy of calculating the residuals.

2. Use the approximate equivalent compressibility $\tilde{c}_p$ as shown in Table 6-12 used in Terzaghi-Rendulic pseudo consolidation theory, and improve the stability and robustness of the solver of the fluid-flow's Jacobian system.
3. Use the following formulation to update the absolute permeabilities based on the variation of porosity:

$$k / k_i = \left(\phi^* / \phi_i^* \right)^n \tag{6-56}$$

where k and k_i are the current permeability and the initial permeability in x / y / z direction, ϕ^* and ϕ_i^* are the current porosity and the initial porosity, n is the power-law exponent.

Table 6-13: The equivalent compressibility $\tilde{c}_p$ during the coupled simulation

Time, ,iters = 1.000000000000000E-002 2

vms (volumetric strain) =

-0.539093	-0.544312	-0.568301	-0.548229	0.032515	0.051124	0.022454	0.010755	0.006789	0.003855	0.002451	0.001596
0.007367	0.010985	0.011446	0.005526	-0.000539	-0.008229	-0.003310	-0.002315	-0.000497	-0.000421	-0.000118	-0.000116
0.004488	0.004099	-0.002313	-0.003573	0.006136	0.003216	0.002219	-0.002308	-0.000564	-0.000576	-0.000185	-0.000177
-0.002031	-0.003485	-0.004866	-0.003063	0.001071	0.001742	0.004936	-0.001041	-0.000303	-0.000639	-0.000246	-0.000252
0.001745	0.000832	-0.000064	0.000326	0.001550	0.001397	0.003581	-0.000425	-0.000099	-0.000770	-0.000358	-0.000374
-0.000614	-0.000634	-0.000455	0.000113	0.000813	0.001007	0.002940	0.001049	0.000932	-0.000385	-0.000199	-0.000343
-0.000813	-0.000677	-0.000369	0.000106	0.000598	0.000858	0.001934	0.001064	0.001114	-0.000228	-0.000153	-0.000393
-0.001042	-0.000895	-0.000618	-0.000251	0.000132	0.000427	0.001107	0.001045	0.001432	0.000339	0.000247	-0.000138
-0.000551	-0.000447	-0.000255	-0.000012	0.000245	0.000456	0.000764	0.000871	0.001118	0.000334	0.000235	-0.000182
-0.000839	-0.000766	-0.000630	-0.000451	-0.000244	-0.000047	0.000146	0.000453	0.000819	0.000576	0.000651	0.000319
-0.000358	-0.000323	-0.000256	-0.000169	-0.000066	0.000044	0.000102	0.000309	0.000501	0.000390	0.000458	0.000207
-0.001070	-0.001034	-0.000964	-0.000866	-0.000749	-0.000602	-0.000485	-0.000142	0.000244	0.000564	0.001025	0.001116
0.001617	0.001596	0.001553	0.001486	0.001396	0.001354	0.001046	0.000786	0.000234	-0.000440	-0.001041	-0.001593

dp (change of pressure)=

-0.459201	-0.453243	-0.429124	-0.324981	-0.155177	-0.049929	-0.021055	-0.010279	-0.006624	-0.004740	-0.004103	-0.003881
-0.847400	-0.827619	-0.766064	-0.592405	-0.336456	-0.158955	-0.079999	-0.041334	-0.026347	-0.018175	-0.014777	-0.013319
-0.707522	-0.679468	-0.612082	-0.497680	-0.359313	-0.238727	-0.142391	-0.079975	-0.051463	-0.035216	-0.027748	-0.024332
-0.592124	-0.566471	-0.514106	-0.437833	-0.349762	-0.266391	-0.180826	-0.111866	-0.074075	-0.051399	-0.040318	-0.035123
-0.493603	-0.474864	-0.438511	-0.388082	-0.330314	-0.272719	-0.204290	-0.140053	-0.097527	-0.069757	-0.055176	-0.048146
-0.405287	-0.393407	-0.370783	-0.339785	-0.303805	-0.266256	-0.215993	-0.162170	-0.119780	-0.089174	-0.071717	-0.063015
-0.338083	-0.330930	-0.317284	-0.298406	-0.275993	-0.251771	-0.216523	-0.174974	-0.137399	-0.107349	-0.088543	-0.078775
-0.287170	-0.283011	-0.275021	-0.263809	-0.250177	-0.234981	-0.211306	-0.181171	-0.150539	-0.123513	-0.104925	-0.094813
-0.248423	-0.246057	-0.241472	-0.234940	-0.226833	-0.217584	-0.202436	-0.182011	-0.159180	-0.137180	-0.120602	-0.111108
-0.219102	-0.217838	-0.215367	-0.211794	-0.207268	-0.201987	-0.192916	-0.180036	-0.164354	-0.147975	-0.134516	-0.126389
-0.200934	-0.200206	-0.198774	-0.196686	-0.194010	-0.190850	-0.185262	-0.177069	-0.166502	-0.154794	-0.144502	-0.138009
-0.188776	-0.188358	-0.187533	-0.186320	-0.184747	-0.182861	-0.179460	-0.174316	-0.167364	-0.159260	-0.151721	-0.146787
-0.190598	-0.190171	-0.189326	-0.188079	-0.186456	-0.184527	-0.180936	-0.175497	-0.167896	-0.158844	-0.150141	-0.144305

$\tilde{c}_p$ (equivalent compressibility)=vms/dp

1.173980	1.200927	1.324328	1.686958	-0.209536	-1.023930	-1.066417	-1.046363	-1.024936	-0.813186	-0.597476	-0.411154
-0.008694	-0.013273	-0.014941	-0.009328	0.001602	0.051771	0.041374	0.056014	0.018865	0.023176	0.007957	0.008736
-0.006343	-0.006032	0.003778	0.007179	-0.017076	-0.013473	-0.015580	0.028859	0.010963	0.016357	0.006668	0.007279
0.003430	0.006152	0.009465	0.006996	-0.003062	-0.006541	-0.027298	0.009305	0.004085	0.012425	0.006095	0.007179
-0.003536	-0.001752	0.000147	-0.000840	-0.004694	-0.005124	-0.017528	0.003032	0.001010	0.011039	0.006489	0.007765
0.001515	0.001611	0.001227	-0.000333	-0.002678	-0.003782	-0.013612	-0.006469	-0.007784	0.004314	0.002771	0.005436
0.002404	0.002044	0.001162	-0.000357	-0.002167	-0.003409	-0.008934	-0.006079	-0.008111	0.002124	0.001731	0.004989
0.003630	0.003163	0.002246	0.000951	-0.000526	-0.001818	-0.005237	-0.005768	-0.009513	-0.002742	-0.002351	0.001461
0.002217	0.001815	0.001057	0.000052	-0.001080	-0.002097	-0.003772	-0.004783	-0.007023	-0.002438	-0.001946	0.001639
0.003829	0.003516	0.002923	0.002127	0.001177	0.000234	-0.000756	-0.002513	-0.004982	-0.003891	-0.004840	-0.002521
0.001783	0.001614	0.001290	0.000857	0.000342	-0.000233	-0.000552	-0.001742	-0.003007	-0.002519	-0.003171	-0.001499
0.005668	0.005488	0.005138	0.004649	0.004053	0.003295	0.002703	0.000813	-0.001459	-0.003540	-0.006757	-0.007603
-0.008486	-0.008394	-0.008204	-0.007898	-0.007485	-0.007339	-0.005781	-0.004477	-0.001394	0.002769	0.006931	0.011040

Table 6-13 continued

Time, ,iters = 1.000000000000000E-001 2; vms (volumetric strain) =

-0.024170	-0.023376	-0.019943	-0.012686	-0.003537	0.003540	0.006086	0.004018	0.001971	0.001248	0.000890	0.000734
-0.033329	-0.032129	-0.027832	-0.019263	-0.008581	-0.000034	0.003956	0.002993	0.001428	0.000911	0.000636	0.000510
-0.026068	-0.024965	-0.021624	-0.015440	-0.007875	-0.001650	0.001758	0.001671	0.000770	0.000485	0.000336	0.000264
-0.013167	-0.012529	-0.010824	-0.007882	-0.004349	-0.001364	0.000502	0.000684	0.000301	0.000181	0.000129	0.000101
-0.003770	-0.003563	-0.003074	-0.002293	-0.001370	-0.000561	0.000039	0.000156	0.000065	0.000030	0.000027	0.000024
-0.000221	-0.000205	-0.000178	-0.000147	-0.000109	-0.000065	-0.000002	0.000009	0.000002	-0.000015	-0.000007	-0.000002
0.000043	0.000040	0.000033	0.000022	0.000010	0.000003	0.000006	-0.000001	0.000003	-0.000013	-0.000009	-0.000005
-0.000009	-0.000008	-0.000005	-0.000002	0.000001	0.000003	0.000009	0.000010	0.000014	-0.000005	-0.000007	-0.000008
0.000006	0.000007	0.000008	0.000010	0.000010	0.000009	0.000007	0.000006	0.000006	-0.000006	-0.000007	-0.000009
0.000001	0.000002	0.000003	0.000005	0.000006	0.000006	0.000005	0.000006	0.000007	0.000000	-0.000002	-0.000007
-0.000015	-0.000014	-0.000012	-0.000010	-0.000009	-0.000007	-0.000006	-0.000001	0.000003	0.000005	0.000009	0.000009
0.000013	0.000013	0.000013	0.000013	0.000012	0.000011	0.000008	0.000007	0.000003	-0.000003	-0.000007	-0.000015
-0.000063	-0.000062	-0.000059	-0.000054	-0.000049	-0.000044	-0.000036	-0.000021	-0.000001	0.000021	0.000044	0.000056

dp (change of pressure)=

0.011320	0.011156	0.009973	0.007149	0.003459	0.000573	-0.000427	-0.000119	0.000129	0.000097	0.000088	0.000085
0.023597	0.023133	0.020612	0.014925	0.007587	0.001772	-0.000439	0.000022	0.000497	0.000389	0.000329	0.000304
0.018742	0.018275	0.016246	0.011948	0.006482	0.002074	0.000259	0.000550	0.000908	0.000734	0.000600	0.000538
0.007643	0.007494	0.006721	0.005023	0.002845	0.001093	0.000510	0.000882	0.001107	0.000932	0.000765	0.000680
-0.000170	-0.000052	0.000050	0.000030	-0.000066	-0.000084	0.000259	0.000800	0.001017	0.000934	0.000798	0.000718
-0.002502	-0.002330	-0.002012	-0.001593	-0.001129	-0.000671	-0.000085	0.000484	0.000757	0.000803	0.000738	0.000687
-0.001890	-0.001784	-0.001583	-0.001312	-0.001003	-0.000684	-0.000254	0.000194	0.000483	0.000619	0.000629	0.000615
-0.001234	-0.001179	-0.001074	-0.000929	-0.000757	-0.000571	-0.000297	0.000017	0.000274	0.000447	0.000510	0.000529
-0.000800	-0.000771	-0.000717	-0.000639	-0.000544	-0.000436	-0.000267	-0.000061	0.000139	0.000300	0.000386	0.000425
-0.000491	-0.000477	-0.000450	-0.000411	-0.000362	-0.000304	-0.000209	-0.000084	0.000054	0.000184	0.000271	0.000318
-0.000283	-0.000277	-0.000263	-0.000244	-0.000219	-0.000189	-0.000138	-0.000068	0.000017	0.000104	0.000171	0.000211
-0.000189	-0.000185	-0.000178	-0.000167	-0.000152	-0.000135	-0.000103	-0.000059	0.000000	0.000065	0.000123	0.000161
-0.000066	-0.000065	-0.000063	-0.000060	-0.000056	-0.000050	-0.000039	-0.000023	-0.000002	0.000023	0.000045	0.000060

$\tilde{C}_p$ (equivalent compressibility)=vms/dp

-2.135122	-2.095413	-1.999675	-1.774359	-1.022583	6.181841	-14.269339	-33.623042	15.312093	12.848720	10.093105	8.631736
-1.412407	-1.388889	-1.350302	-1.290610	-1.130971	-0.019395	-9.010519	134.570243	2.871936	2.340255	1.930119	1.680401
-1.390907	-1.366057	-1.331036	-1.292228	-1.214968	-0.795285	6.794553	3.040271	0.847358	0.661129	0.560371	0.490886
-1.722767	-1.671877	-1.610644	-1.569172	-1.528752	-1.248499	0.984694	0.775337	0.272176	0.193863	0.168250	0.148235
22.174494	67.935863	-61.017145	-76.197515	20.647831	6.639084	0.152116	0.195438	0.064026	0.031979	0.033494	0.033293
0.088267	0.087800	0.088413	0.092041	0.096241	0.096396	0.024136	0.017671	0.003080	-0.018626	-0.009935	-0.002760
-0.022960	-0.022503	-0.020664	-0.016420	-0.010411	-0.004752	-0.022893	-0.007155	0.006734	-0.021466	-0.014623	-0.008646
0.007594	0.006729	0.004913	0.002093	-0.001426	-0.005925	-0.028980	0.582810	0.050059	-0.011300	-0.013223	-0.014308
-0.006912	-0.008483	-0.011392	-0.015079	-0.018115	-0.019738	-0.024663	-0.092834	0.045373	-0.021613	-0.017230	-0.021435
-0.002057	-0.003720	-0.007101	-0.011853	-0.016346	-0.019155	-0.023204	-0.073481	0.132104	-0.001903	-0.007818	-0.021964
0.051466	0.050061	0.047066	0.042845	0.039360	0.039036	0.042851	0.016741	0.196956	0.047307	0.054703	0.040329
-0.068459	-0.069620	-0.072306	-0.076369	-0.080170	-0.081547	-0.080855	-0.110699	14.717348	-0.041625	-0.061201	-0.091534
0.954039	0.944180	0.925552	0.903928	0.890306	0.895173	0.924728	0.906661	0.912483	0.909667	0.984087	0.936934

6.2.9 Coupling with Fracture Module

A large number of petroleum reservoirs are classified as naturally fractured reservoirs (NFR). The behavior of naturally fractured reservoirs is different from that of the conventional reservoirs because of the discontinuity in porous media of fractured reservoirs due to tectonic activities. Hence, it is difficult to describe the fluid-flow in the fractured reservoirs.

It is well-known that there are two kinds of methods to simulate naturally fractured reservoirs, the continuum approach and the discrete approach. Dual porosity model (Barenblatt *et al.* 1960, Warren and Root 1963) is one of the continuum approaches. The media of a whole fractured reservoir is idealized into two parts: one representing a fracture network with low storage capacity but high flowing capacity and the other a continuum porous matrix with high storage capacity and low flowing capacity. Also, there are two sets of governing equations to describe the fluid-flow within the reservoir. The two continuity equations are coupled together through the transfer functions.

Tarahhom (2008) developed a dual porosity module in GPAS to simulate the naturally fractured reservoirs, in which the transfer functions are defined

For hydrocarbon components:

$$\tau_{mfi} = NM \cdot V_b \sum_{l=1}^{N_b} \frac{\partial}{\partial t}\left(\phi_m N_{mi}\right)_l, \ i = 1, \cdots n_c. \tag{6-57}$$

For water component:

$$\tau_{mfi} = NM \cdot V_b \sum_{l=1}^{N_b} \frac{\partial}{\partial t}\left(\phi_m N_{mw}\right)_l. \tag{6-58}$$

where NM is the total number of matrix blocks in a fracture gridblock and N_b is the number of matrix subgrids. At the same time, it is also assumed that the injection and production of fluids are treated as source or sink terms and wells are connected only to

the fracture system, which means that the fluid-flow between the matrix domain and the fracture domain is due to the pressure gradient between them. The exchange process is represented by the transfer functions, Equations (6-57) and (6-58). For a detailed discussion of the subject, refer to the dissertation of Tarahhom (2008).

In this research, the developed geomechanics module is iteratively coupled with the dual porosity module (Tarahhom 2008) in GPAS to study the fluid-flow through the deformed fractured porous media. It is assumed that the volume of the fracture is small enough compared to the total void volume. Hence, the body forces are carried only by the porous matrix part, which is considered a deforming medium; namely, the fracture part does not deformed and is considered a rigid medium. With the production of hydrocarbons in reservoirs, the changes of pressure result in the deformation of the matrix, the changes of the porosity and permeability of the matrix. Hence, the transfer functions vary as well, and deformation finally effects the production or injection in the fracture part. The above is the strategy of the coupling geomechanics and dual porosity modules in GPAS to model the naturally fractured reservoirs. In the following Case Studies section, further discussion will continue.

The work by Chin (2006) is an important step forward in considering the fracture as a deforming medium as well. Hence, a part of body forces or external loads are also carried by the fracture part. The changes of the fracture porosity and the fracture permeability with the changes of stress and strain distributions are modeled through the Barton-Bandis model (Barton et al. 1985).

6.2.10 Case Studies

The problems in Section 6.1.6 will be simulated using the iteratively coupled solution procedure in GPAS to verify the coupled code.

6.2.10.1 One-Dimensional Consolidation Case

In this section, Case 6.1.6.1.1 in Section 6.1.6 is simulated again, and the numerical result is plotted in Figure 1-1 and is compared with the close form solution of Schiffmann (1960). From the beginning of the dimensionless time T = 0, the load is increasing until T = 0.1, and the pore pressure within the reservoir is also increasing accordingly. After T = 0.1, the pore pressure is decreasing as the fluid is flowing out the reservoir. A good match is found between the numerical solution and the analytical solution as shown in Figure 6-33. The little discrepancy possibly results from the approximation of the equivalent compressibility used in the simulation. In other words, the interactions between the two models are not fully represented during the simulation.

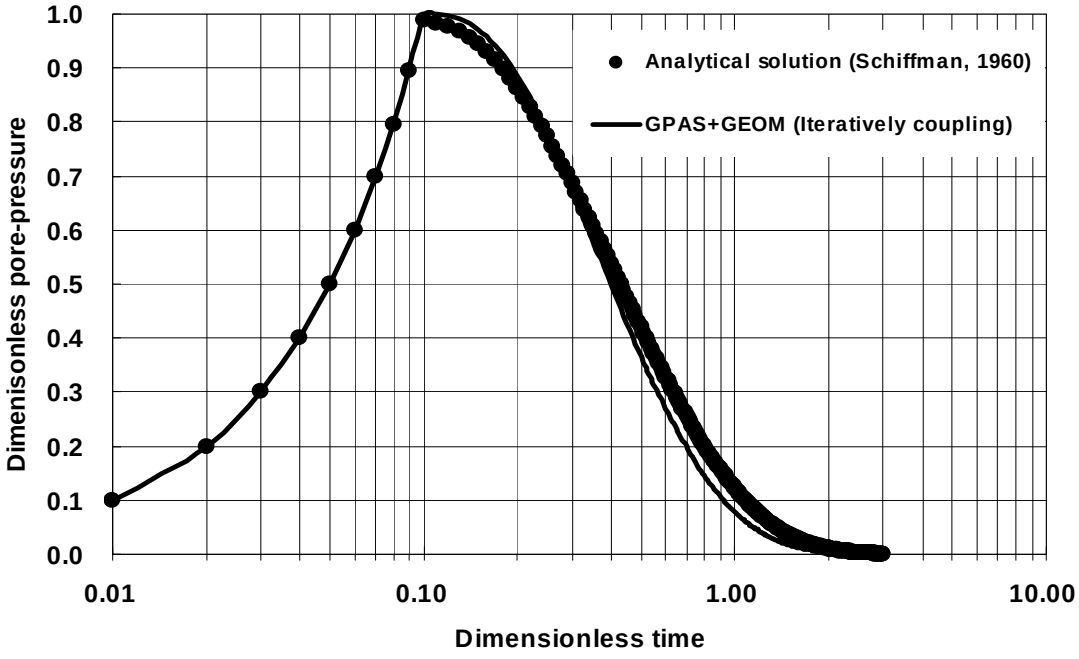

Figure 6-33: Comparison of the iteratively coupled geomechanics and GPAS with the analytical solution from Schiffmann (1960) for Case 6.1.6.1.1.

6.2.10.2 Two-Dimensional Consolidation Case

Case 6.1.6.1.2 in Section 6.1.6 is solved using the iteratively coupled geomechanics and GPAS. It is a problem of a plane stress analysis coupling with the fluid-flow, and the detailed input parameters refer to Table 6-2. A uniform strip load is utilized on the top at t = 0 and remains constant thereafter. The pore pressure profile beneath the center of the loaded strip (x/a = 0, z) is given in Figure 6-34 at the dimensionless time T = 0.1. The numerical solution from the iteratively coupled solution procedure predicts that maximum pore pressure slightly less than in the analytical solution. Again, the equivalent compressibility improves the stable of the solver for Jacobian systems; however, the coupling effect cannot capture as precisely as the fully coupled solution procedure.

Figure 6-35 compares the numerical results with the close form solution (Schiffmann et al. 1969) at one special location (x = 0, z = 2). Here, the numerical solutions include those from the fully coupled finite element code (Smith and Griffiths 2004), the Terzaghi's decoupling solution procedure, and the iteratively coupled solution procedure in GPAS. Clearly, the Terzaghi's decoupling solution procedure cannot predict the occurrence of the coupling Mandel-Cryer effect in the early time of simulation; however, during the subsequent dissipation period, the decoupling solution has a great consistency with the analytical solution as seen in the figure. As expected, the fully coupled finite element code (Smith and Griffiths 2004) can capture the coupling Mandel-Cryer effect in the early simulation time. A good match can be found between the numerical solution and the close form solution. Also, the iterative coupling solution procedure can give a good numerical solution, which matches the analytical solution; of course, the Mandel-Cryer effect is also captured in the early simulation time.

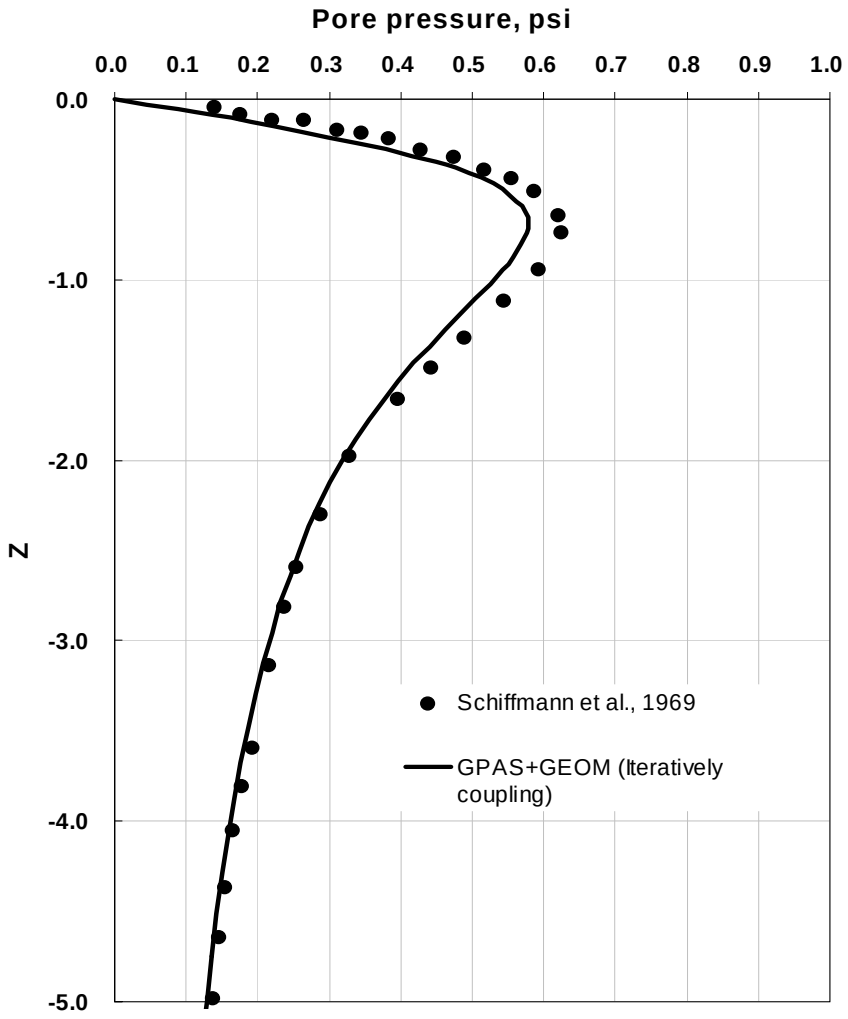

Figure 6-34: Comparison of the pore pressure profile with the analytical solution (after Schiffmann et al. 1969): beneath the center of the loaded area at dimensionless time T = 0.1 for Case 6.1.6.1.2.

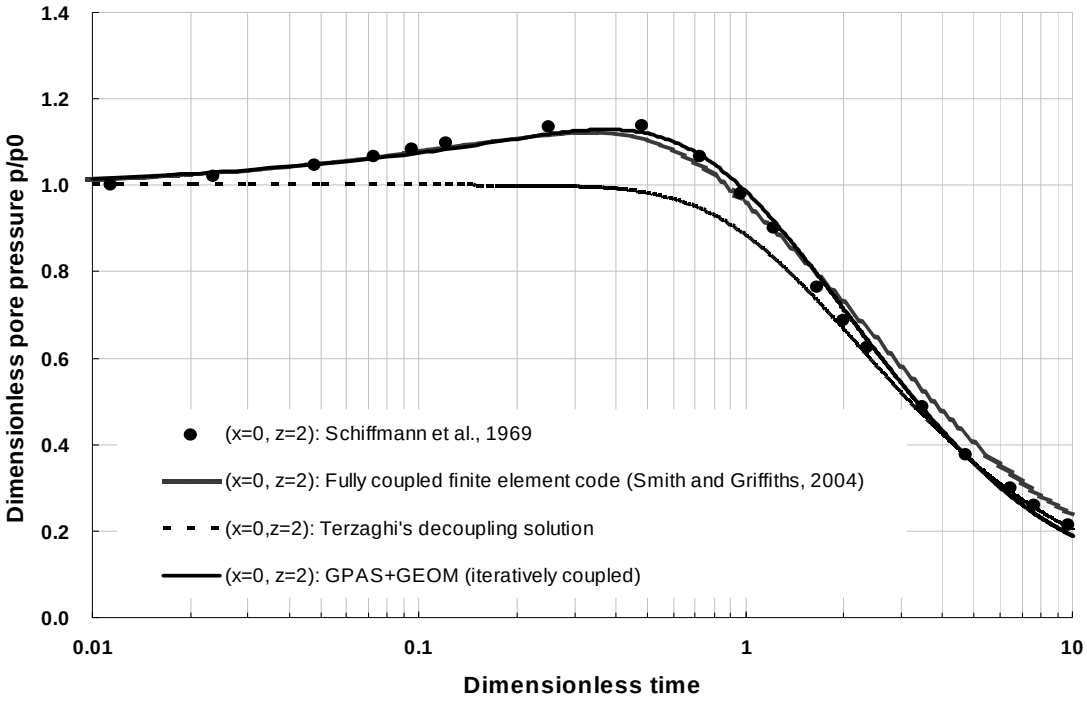

Figure 6-35: Comparison of the variation of pore pressure and time with the analytical solution (after Schiffmann et al. 1969); The Mandel-Cryer effect is predicted by the numerical solutions at (x=0, z=2) for Case 6.1.6.1.2.

The discussion for this problem is similar to that in Section 6.1.6.1.2, because the top surface is free drain (the flow boundary condition). Studies (Schiffmann et al. 1969) show that the peaks of the Mandel-Cryer effects will advance in time with increasing depth. Hence, a pair of locations, (x/a=0, z/a=0.75) and (x/a=0, z/a=2), is chosen to verify the above claim.

The numerical solutions from the fully coupled finite element code (Smith and Griffiths 2004), the Terzaghi's decoupling solution procedure, and the iteratively coupled solution procedure in GPAS are plotted in Figure 6-36. Again, the results from the Terzaghi's decoupling solution procedure do not represent the Mandel-Cryer effects. The results from the fully coupled finite element code (Smith and Griffiths 2004) and the

iteratively coupled solution procedure in GPAS are in good agreement; however, they are different from the result of the Terzaghi's decoupling solution procedure. As the depth increases, the pressure increases with time, as shown in Figure 6-37.

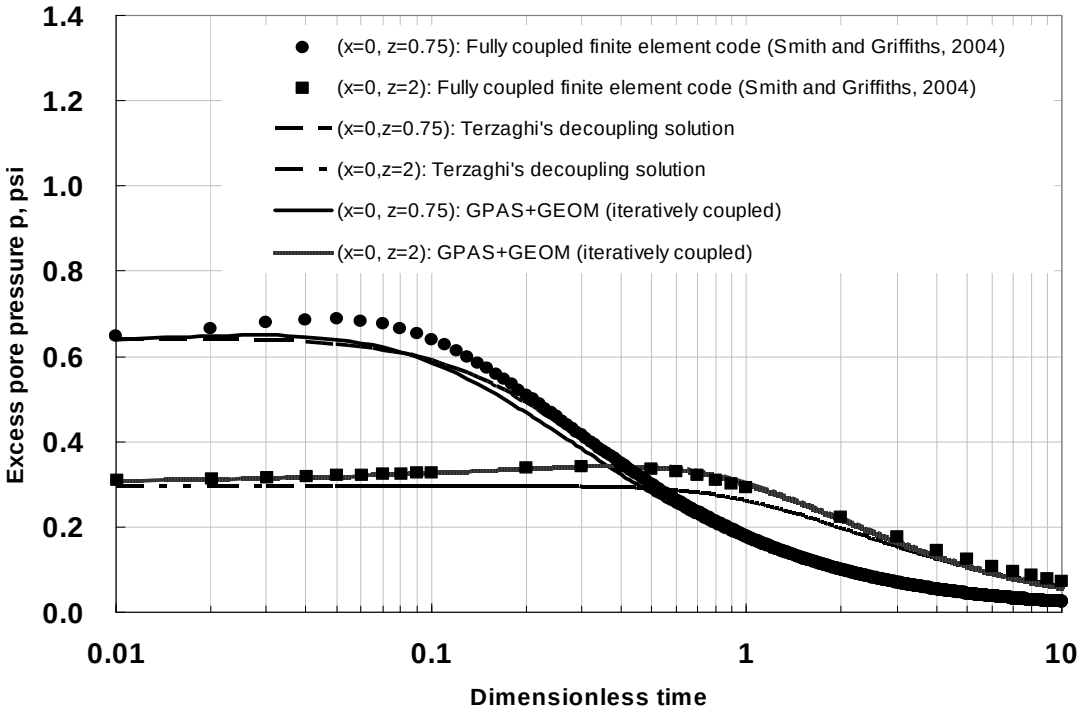

Figure 6-36: The Mandel-Cryer effects are predicted by the numerical solutions at (x=0, z=0.75) and (x=0, z=2) for Case 6.1.6.1.2.

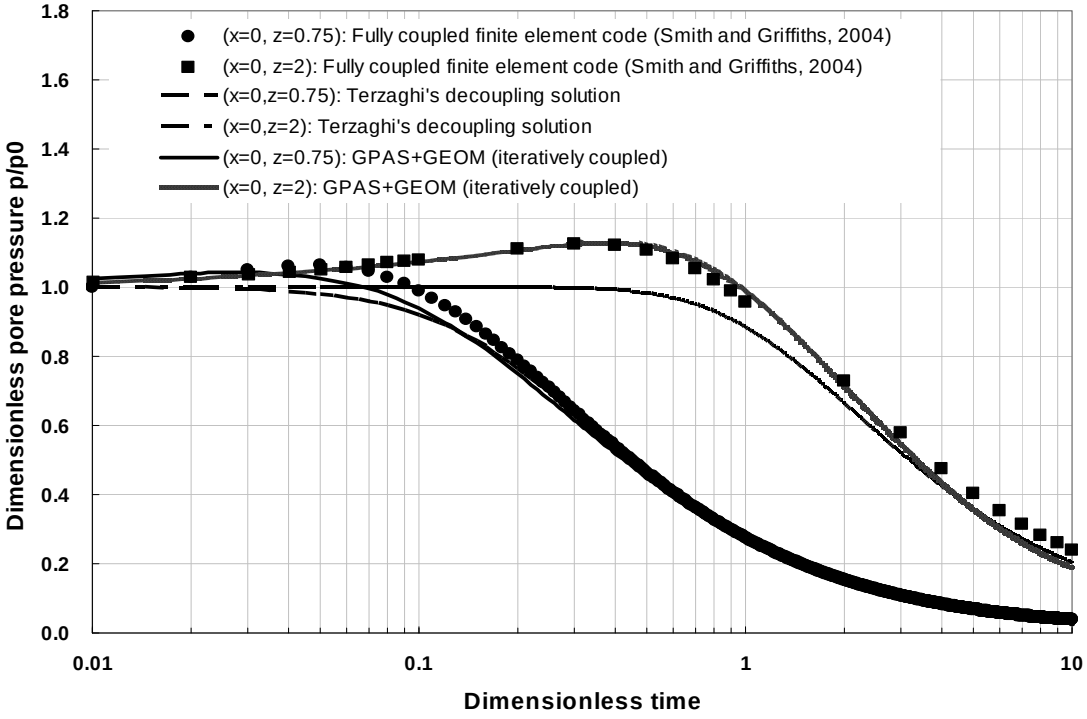

Figure 6-37: The Mandel-Cryer effects are predicted by the numerical solutions at (x=0, z=0.75) and (x=0, z=2) for Case 6.1.6.1.2.

6.2.10.3 Water Flooding with Two-Component Fluid Mixture

In this example, a quarter of a five-spot simulation for a reservoir with the size $350 \times 350 \times 50$ ft^3 using the properties listed in Table 6-14 is performed and the relative permeability data are given in Table 6-15. The mixture compositions are 0.6 for C_{10} and 0.4 for C_{15}. The number of gridblocks is 7×7×3. The permeabilities in x, y, and z directions are 100 md. The injected fluid is water at a rate of 200 STB/day. Both wells are perforated across all layers.

Figure 6-38 and Figure 6-39 investigate the effects of geomechanics on the hydrocarbon recovery. Figure 6-38 clearly shows that the coupled geomechanics can maintain a higher pressure in the early production period. The higher pressure results

from the compaction within the reservoir. Finally, the compaction significantly improves the oil recovery as shown in Figure 6-39.

Table 6-14: Summary of input data for Case 6.2.10.3

	Parameter	Value
Reservoir model	Length (ft) x Width (ft) x Thickness (ft)	350 x 350 x 60
	Number of gridblocks	7 x 7 x 3
	Gridblock size (ft^3)	50 x 50 x 20
	Porosity	0.3
	Permeability (x,y,z) (md)	100
	Rock compressibility (psi^{-1})	0
	Fluid compressibility (psi^{-1})	0
	Initial water saturation	0.2
	Water viscosity (cp)	1
	Water density (lb/ft^3)	62.343
	Initial pressure (psi)	800
	Producer (BHP)	400
	Injector (STB/day)	200
	Initial composition of C_{10} and C_{15}	0.6, 0.4
Geomechanics model	Number of elements	7 x 7 x 3
	Element type	20-node brick
	Element size (m^3)	15.2 x 15.2 x 6.0
	Young's modulus (kPa)	5.0×10^5
	Poisson's ratio	0.3

Table 6-15: Relative permeability data for Case 6.2.10.3

	Water	Oil	Gas
Endpoint	0.5	0.7	0.85
Residual saturation	0.25	0.15	0.06
Exponent800	2.5	2.0	1.5

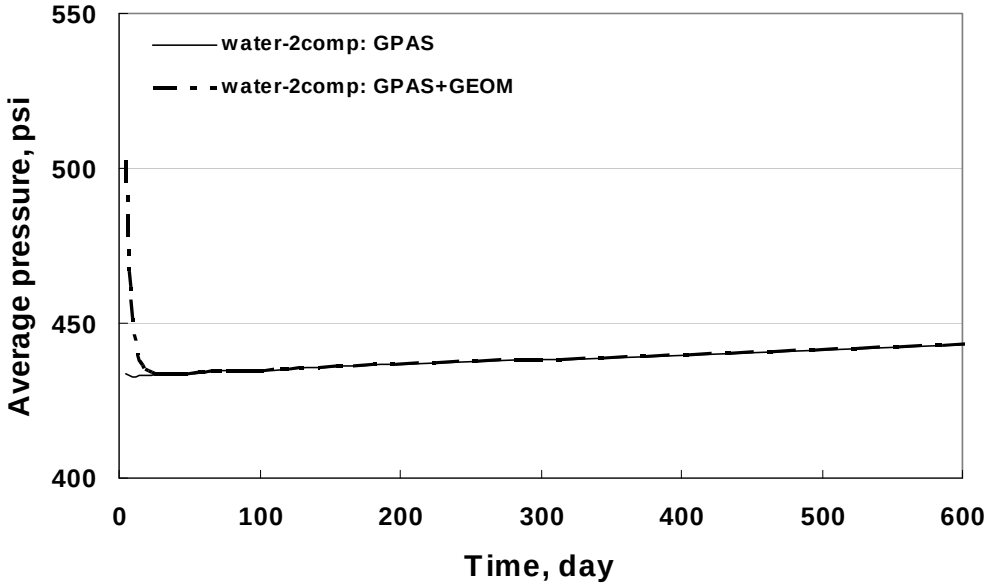

Figure 6-38: The average pressure from GPAS with and without geomechanics for Case 6.2.10.3.

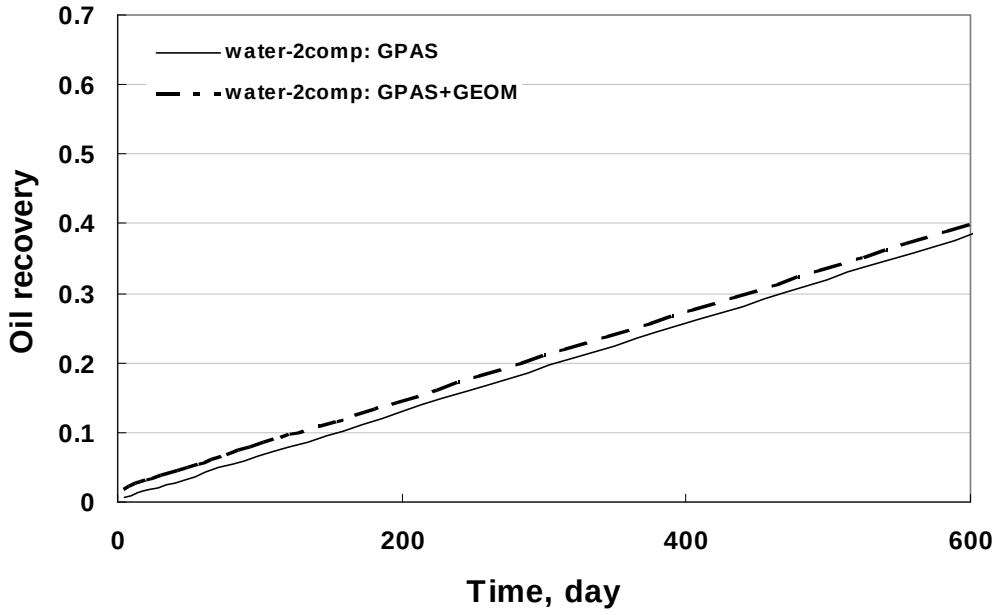

Figure 6-39: The oil recovery from GPAS with geomechanics for different Young modules for Case 6.2.10.3.

The effects of the Young's modulus on the oil recovery are then investigated. Two Young's modulus, 5.0 x 10^4 kPa (soft rock) and 5.0 x 10^5 kPa (stiff rock), are selected in the numerical experiences. Under the same production scenario, the reservoir with the soft rock gives a higher oil recovery than the reservoir with the stiff rock as expected (Figure 6-40). Meanwhile, the reservoir with the soft rock makes a slow decrease of the average pressure because of the more compaction happened during the production period, which is clearly shown in Figure 6-41.

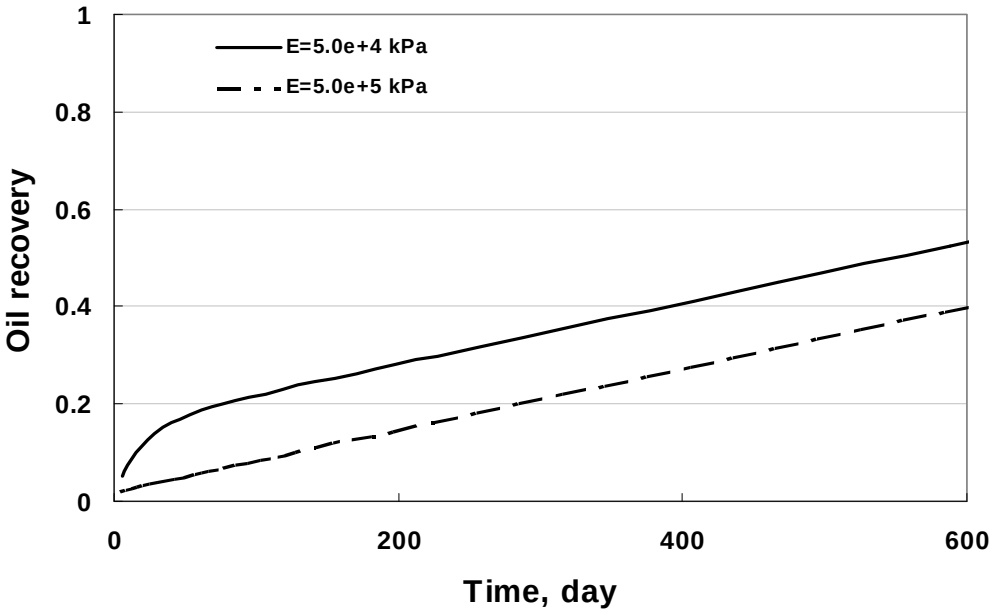

Figure 6-40: The oil recovery from GPAS with geomechanics for different Young modules for Case 6.2.10.3.

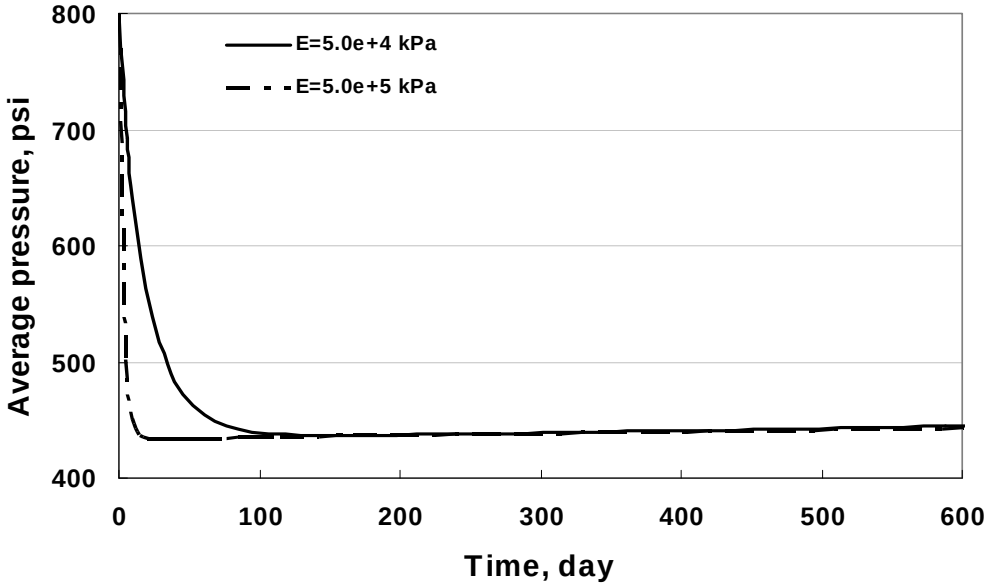

Figure 6-41: The average pressure from GPAS with geomechanics for different Young modules for Case 6.2.10.3.

The difference between GPAS with the equivalent compressibility and GPAS coupled geomechanics is investigated in the following simulations. In the following runs, the initial pressure is set to 600 psi. The injected rate of water is 400 STB/day and the BHP of the producer is 550 psi. All other input data values are kept the same, as shown in Table 6-14. For a reservoir with $E=4.0x10^4$ kPa, an equivalent compressibility can be calculated as $6.73x10^{-4}$ 1/psi. Two different runs are performed to simulate the same problem. The comparison is shown in Figure 6-42 through Figure 6-45. It is can be found that the traditional update formulation for porosity based on the equivalent compressibility under-estimates the oil recovery (Figure 6-42 and Figure 6-43) and the average pressure (Figure 6-44); meanwhile, it delays the time of water breakthrough a little bit (Figure 6-45).

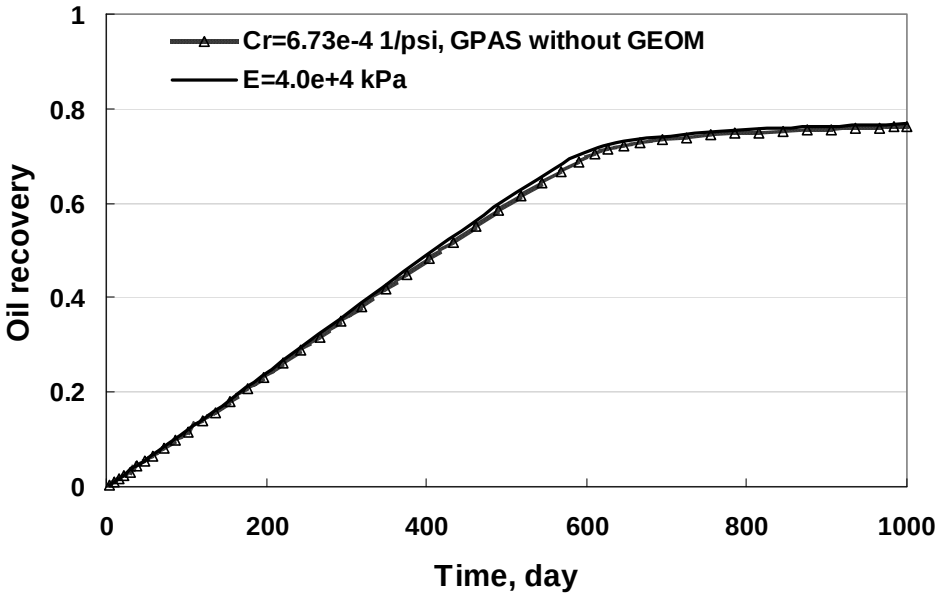

Figure 6-42: The oil recovery from GPAS with and without geomechanics for Case 6.2.10.3.

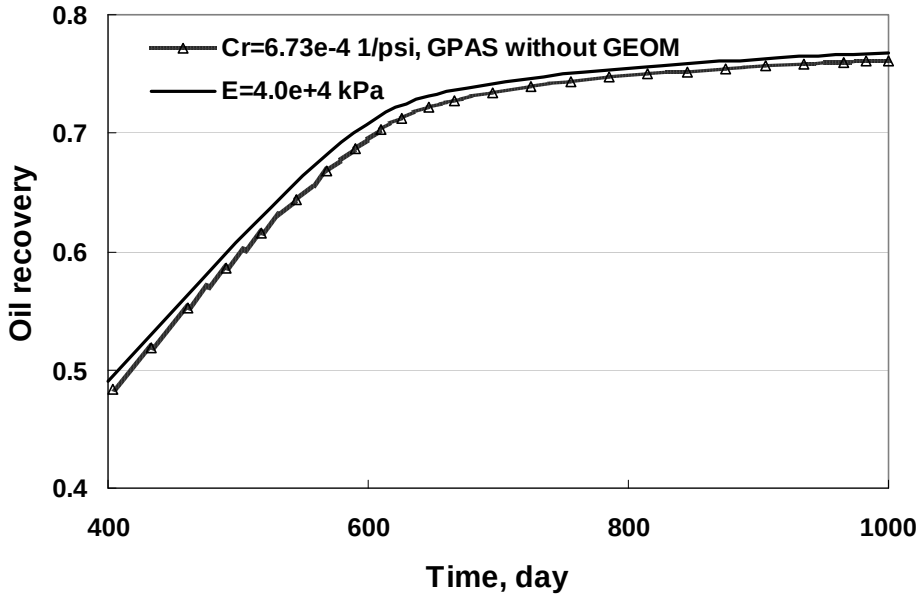

Figure 6-43: The oil recovery from GPAS with and without geomechanics for Case 6.2.10.3.

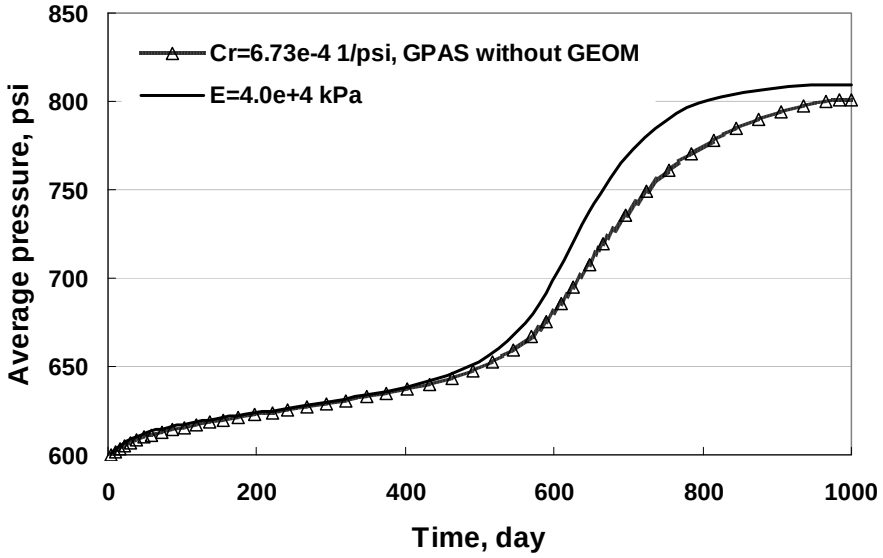

Figure 6-44: The average pressure from GPAS with and without geomechanics for Case 6.2.10.3.

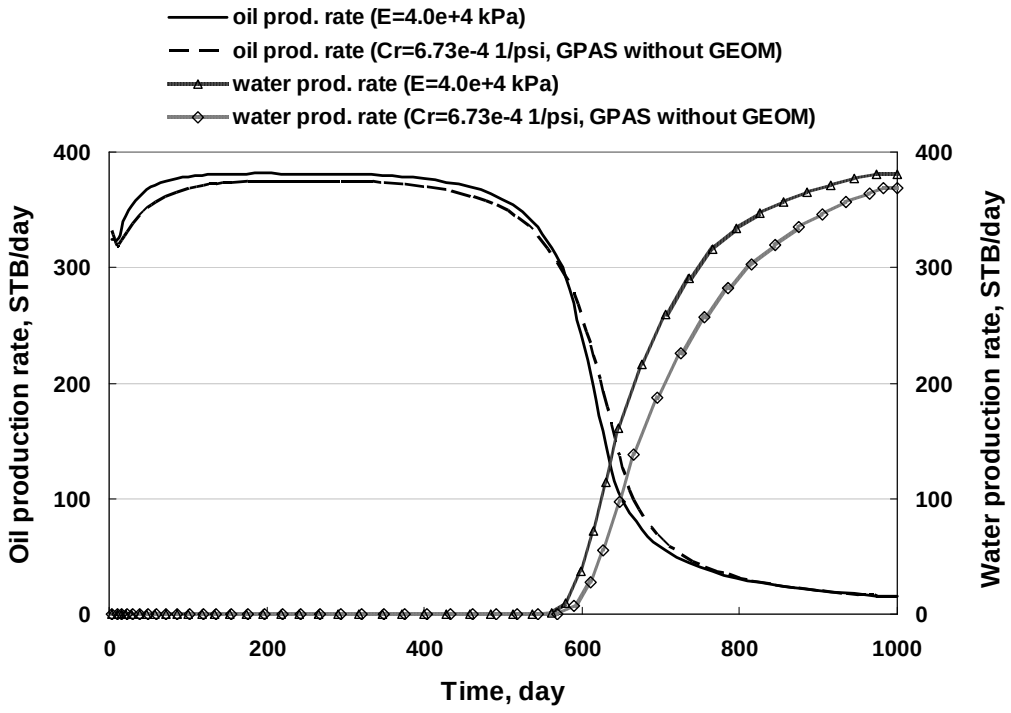

Figure 6-45: The oil /water production rate from GPAS with and without geomechanics for Case 6.2.10.3.

Now, another numerical experiment is designed to evaluate the effect of the coupling permeability on the production. In this case, BHP of the producer is changed to 600 psi and all other input data values are kept the same, as shown in Table 6-14. Figure 6-46 compares the oil recovery during production. The simulation with the coupling both porosity and permeability gives a higher oil recovery. A lower average pressure is predicted by the run of the coupling both porosity and permeability model, as shown in Figure 6-47, because the water injection process increase the permeabilities as shown in Figure 6-49. A little early water breakthrough is predicted when considering the permeability changes during the production as shown in Figure 6-48. The above early water breakthrough also means a fast sweeping of the water and a little higher oil recovery. Figure 6-49 compares the permeability in x direction at the initial time (t = 0) and the time after a 1000-day water flooding. The permeability at the injector increases above 200 md.

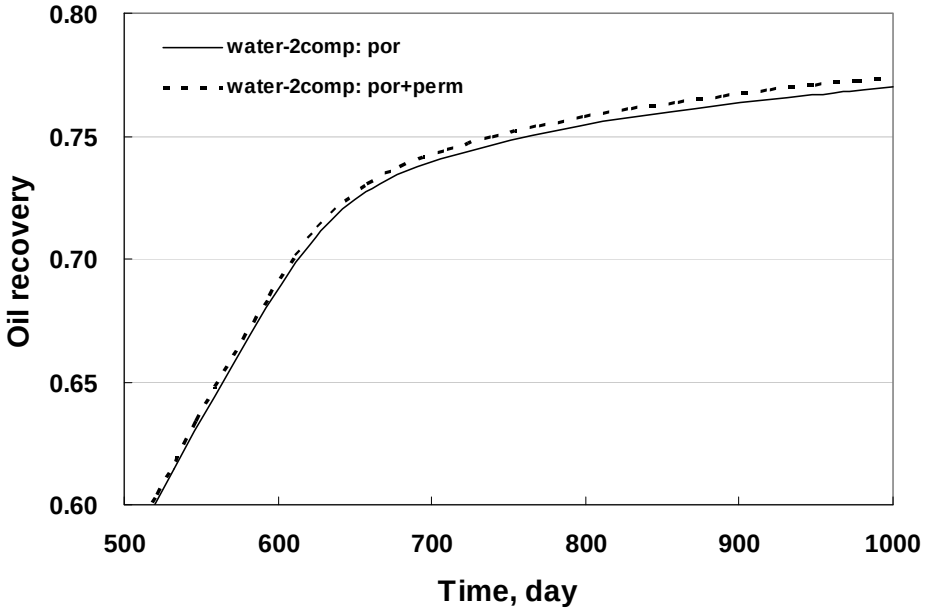

Figure 6-46: The oil recovery from GPAS with geomechanics for Case 6.2.10.3.

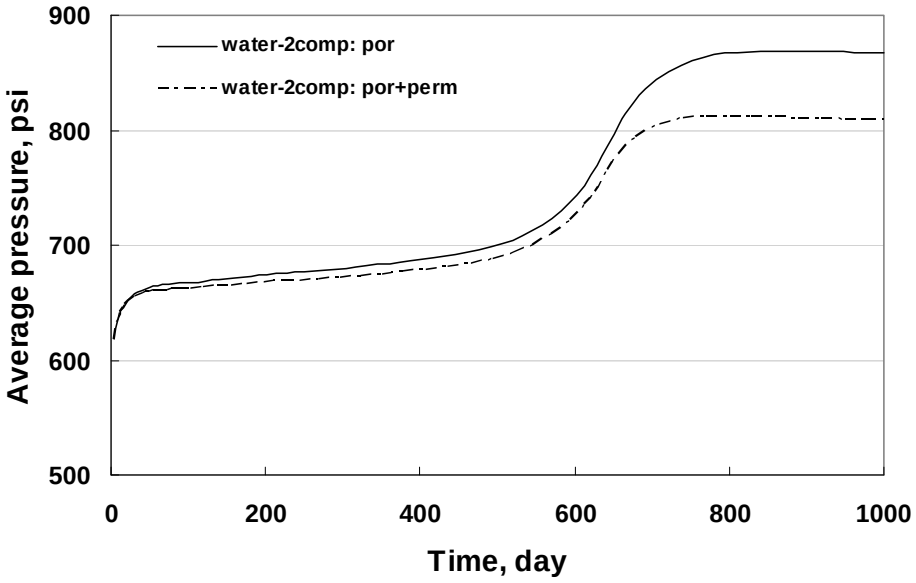

Figure 6-47: The average pressure from GPAS with geomechanics for Case 6.2.10.3.

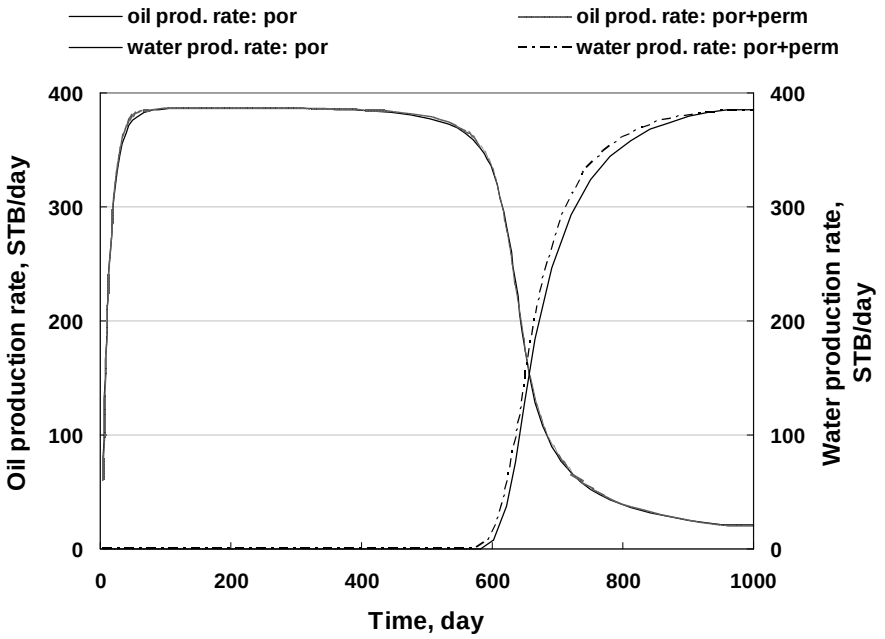

Figure 6-48: The oil / water production rate from GPAS with geomechanics for Case 6.2.10.3.

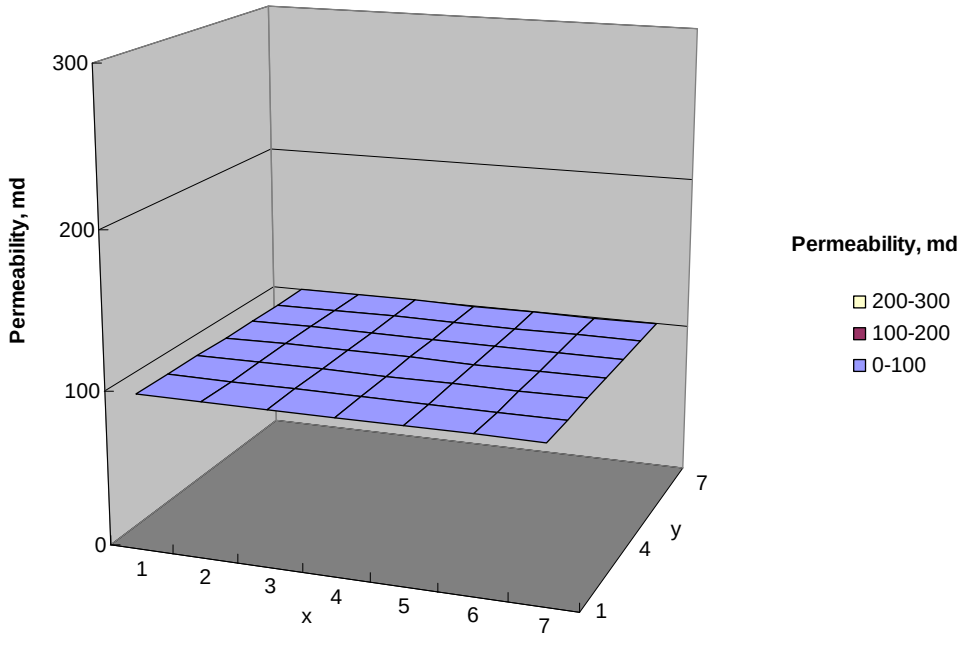

(a) Initial distribution.

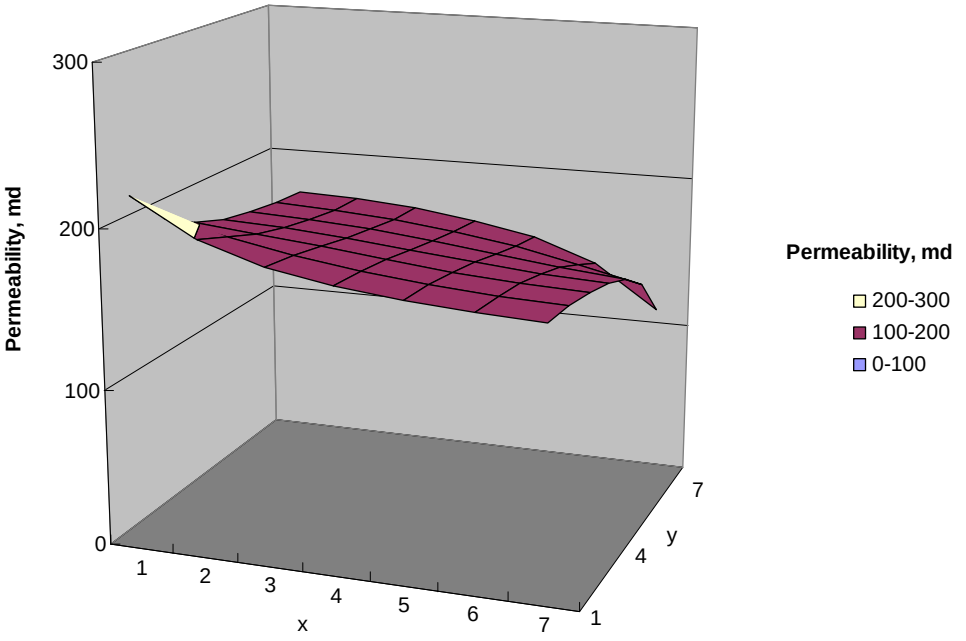

(b) Final distribution at 1000 days.

Figure 6-49: The permeability (x-) distribution from GPAS with geomechanics for Case 6.2.10.3.

6.2.10.4 CO_2 Flooding with Three-Component Fluid Mixture

A three-dimensional reservoir of 400×400×45 ft^3 and a three-component fluid mixture is used to simulate the CO_2 injection process during the production. The initial pressure and temperature of the reservoir are 500 psia and 130˚F. Initial water saturation is 0.17, porosity is 0.3, and both horizontal and vertical permeabilities are 10 md. The reservoir is divided into 10×10×3 gridblocks. The well condition for the injection well is 400 Mscf/day and production bottomhole pressure is 500 psia. Table 6-16 gives the reservoir input data. Table 6-17 presents component properties, initial reservoir and injected fluid compositions.

The oil recovery, average pressure, oil production rate, and gas production rate are presented in Figure 6-50 through Figure 6-53 to compare the difference between GPAS simulations with and without geomechanics. The coupled simulation gives a lower oil recovery than GPAS (Figure 6-50). Figure 6-50 (b) specially shows the oil recovery difference after the 800-day production between GPAS with or without geomechanics module. Similarly, a lower average pressure (Figure 6-51) and a lower oil production rate (Figure 6-52) are predicted by the coupled geomechanics and GPAS simulation. However, for the gas production rate, the coupled model gives a higher prediction, as shown in Figure 6-53, because of the predicted lower pressure. The above differences result from the fact that one part of increase of fluid pressure from the injection of CO_2 is consumed to compress the reservoir rock, enlarges the pore volume within the reservoir, slows the sweeping speed of CO_2, and reduces the effective stress. The coupling effects between the solid and the fluid in the reservoir changes the distributions of porosity and permeability during the production.

Table 6-16: Input parameters for Case 6.2.10.4

Property	Value
Reservoir size (ft^3)	400 x 400 x 45
Reservoir gridblock size (ft^3)	40 x 40 x 15
No. of gridblocks	10 x 10 x 3
Young's modulus (kPa)	9×10^5
Poisson's ratio	0.3
Matrix permeability (x,y,z) (md)	10
Matrix porosity	0.3
Initial water saturation	0.17
Water viscosity (cp)	0.8
Water/oil compressibility (1/psi)	0.000003
Initial reservoir pressure (psi)	500
Injector injection rate, (Mscf/day)	400
Production constraint (BHP, psi)	500

Table 6-17: Properties of the components and initial composition for Case 6.2.10.4

Properties	CO_2	C_1	NC_{16}
Tc (°R)	547.5	343.0	1322.4
Pc (psia)	1071.6	667.8	252.1
Vc(ft^3/Lb-mol)	0.416	1.586	13.376
MW	44.0	16.0	222.0
Initial composition	0.01	0.29	0.70
Injected gas comp.	0.85	0.15	

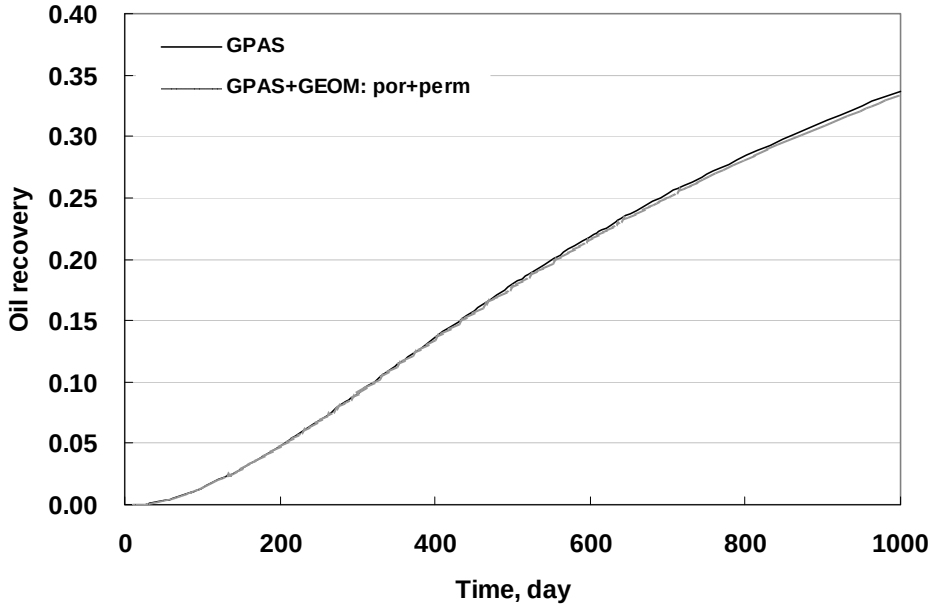

(a)

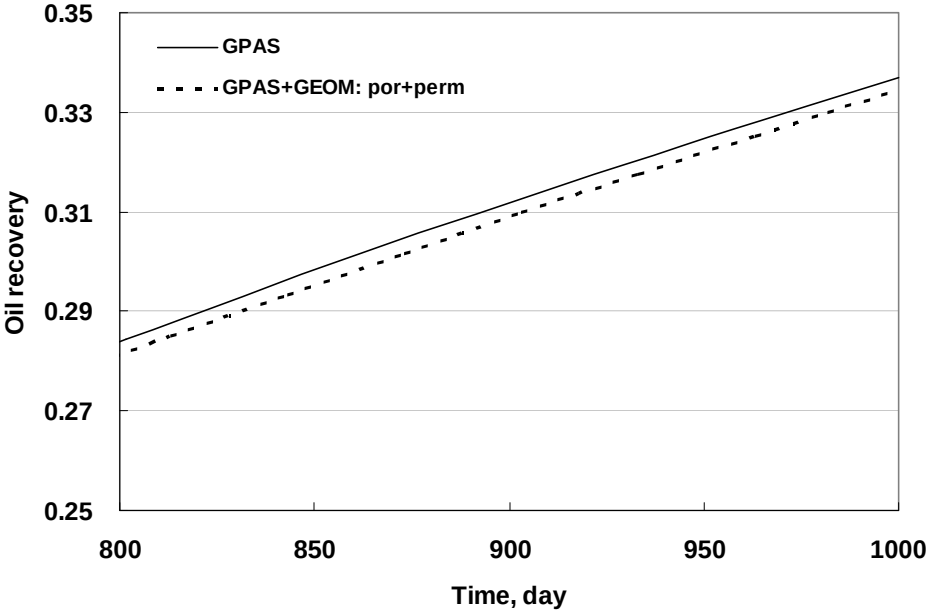

(b)

Figure 6-50: The oil recovery from GPAS with and without geomechanics for Case 6.2.10.4.

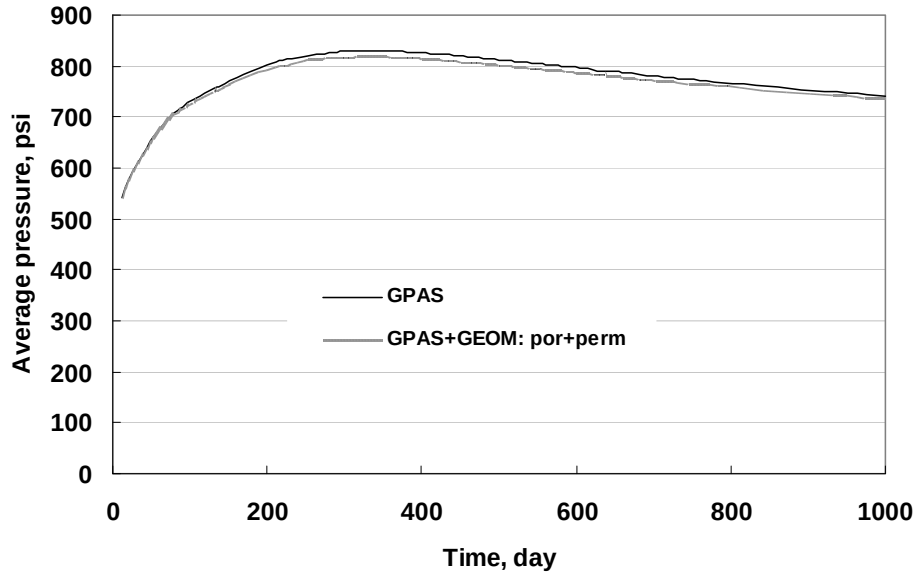

Figure 6-51: The average pressure from GPAS with and without geomechanics for Case 6.2.10.4.

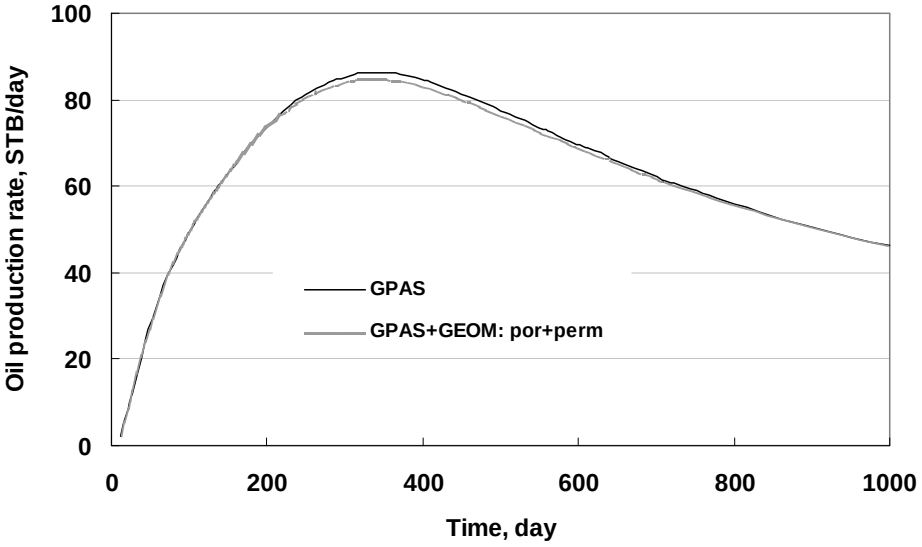

Figure 6-52: The oil production rate from GPAS with and without geomechanics for Case 6.2.10.4.

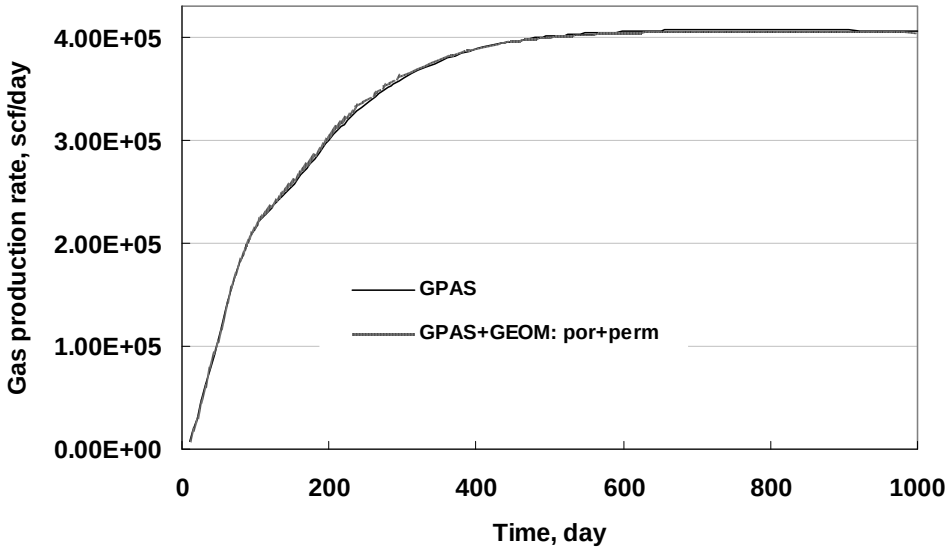

(a)

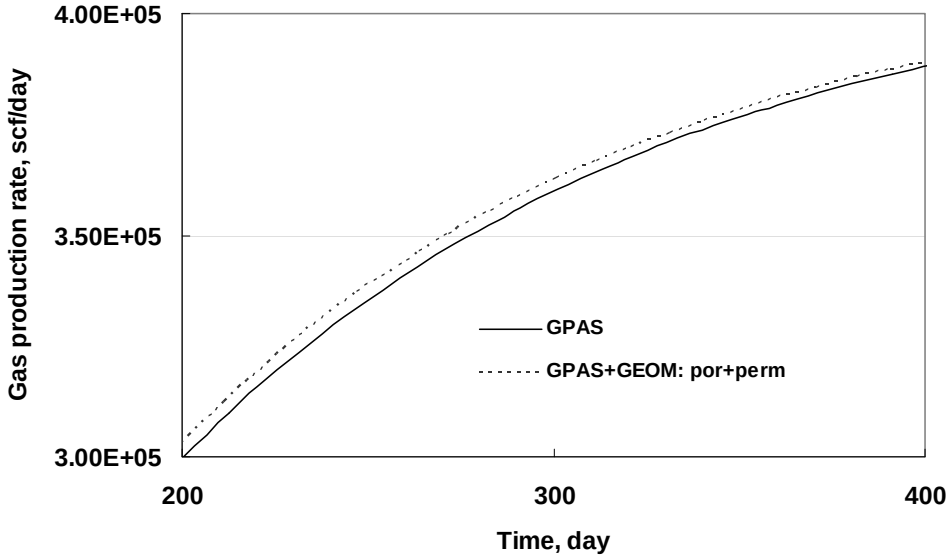

(b)

Figure 6-53: The gas production rate from GPAS with and without geomechanics for Case 6.2.10.4.

6.2.10.5 Gas Flooding with Six-Component Fluid Mixture

The SPE fifth comparative solution problem (Killough and Kossack, 1987) was simulated in this section. The three-dimensional reservoir of 560×560×100 ft^3 and a six-component fluid mixture is used to simulate the gas injection process during the production. The initial pressure and temperature of the reservoir are 1500 psia and 60˚F, respectively. Initial water saturation is 0.17, porosity is 0.35, and both horizontal and vertical permeabilities are 10 md. The reservoir is divided into 7×7×3 gridblocks. The thicknesses of three layers are 20 ft, 30 ft, and 50 ft, respectively. The well condition for the injection well is 1000 Mscf/day and production bottomhole pressure is 1300 psia. Table 6-18 gives the reservoir input data. Table 6-19 presents component properties, initial reservoir and injected fluid compositions. The oil recovery, average pressure, oil production rate, and gas production rate are presented in Figure 6-54 through Figure 6-57. The compaction within the reservoir maintains a higher average pressure from the coupled code comparing to the pressure from GPAS without geomechanics, as shown in Figure 6-55. The compaction enhances the oil recovery as well (Figure 6-54).

Table 6-18: Input parameters for Case 6.2.10.5

Property	Value
Reservoir size (ft^3)	560 x 560 x 100
Reservoir gridblock size (ft^3)	80 x 80 x 20 / 30 / 50
No. of gridblocks	7 x 7 x 3
Young's modulus (kPa)	8×10^4
Poisson's ratio	0.3
Matrix permeability (x,y,z) (md)	10
Matrix porosity	0.35
Initial water saturation	0.17
Water viscosity (cp)	1.0
Water/oil compressibility (1/psi)	0.000003
Initial reservoir pressure (psi)	1500
Injector injection rate, (Mscf/day)	1000
Production constraint (BHP, psi)	1300

Table 6-19: Properties of the components and initial composition for Case 6.2.10.5

Properties	C_1	C_3	C_6	C_{10}	C_{15}	C_{20}
Tc (°R)	343.0	665.7	913.4	1111.8	1270.0	1380.0
Pc (psia)	667.8	616.3	436.9	304.0	200.0	162.0
Vc(ft^3/Lb-mol)	1.586	3.211	5.923	10.087	16.696	21.484
MW	16.0	44.1	86.2	142.3	206.0	282.0
Initial composition	0.50	0.03	0.07	0.20	0.15	0.05
Injected gas comp.	0.77	0.20	0.01	0.01	0.005	0.005

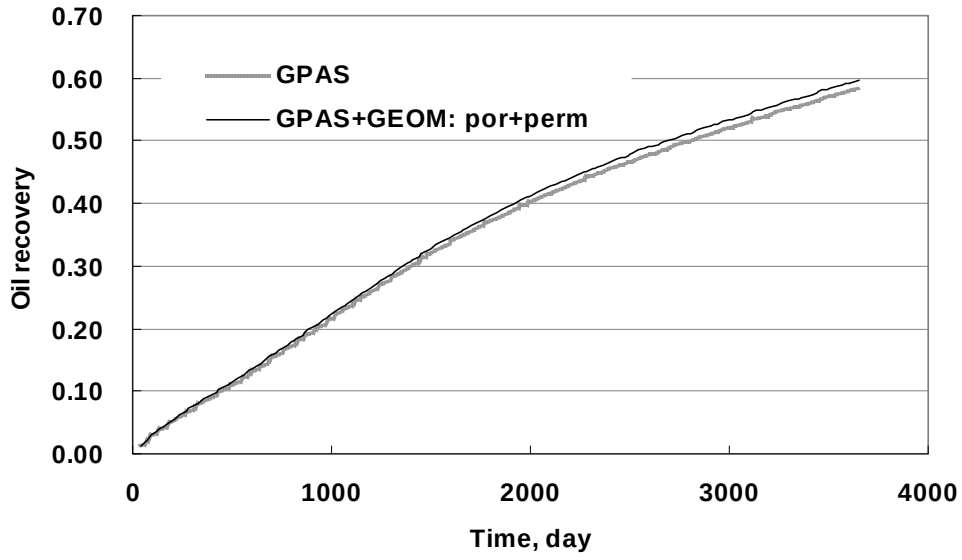

Figure 6-54: The oil recovery from GPAS with geomechanics for Case 6.2.10.5.

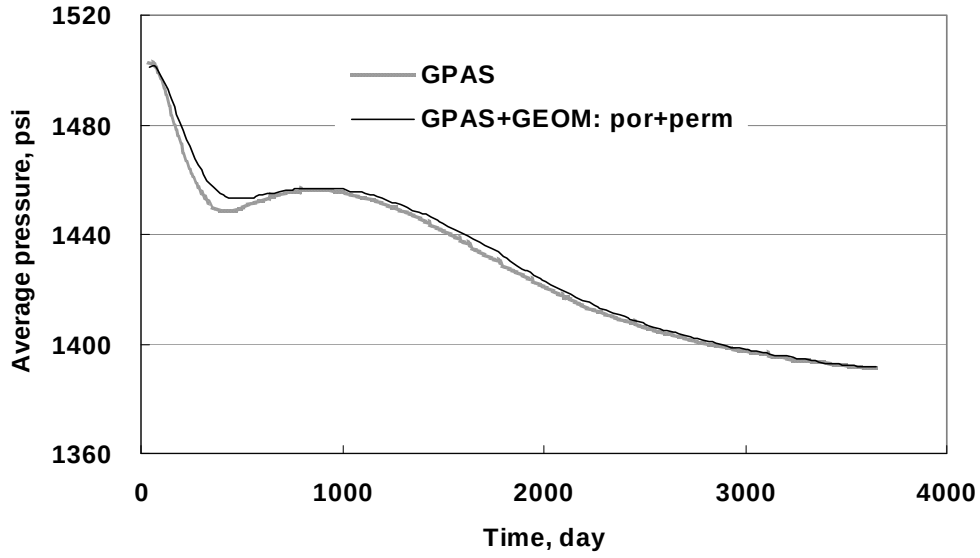

Figure 6-55: The average pressure from GPAS with geomechanics for Case 6.2.10.5.

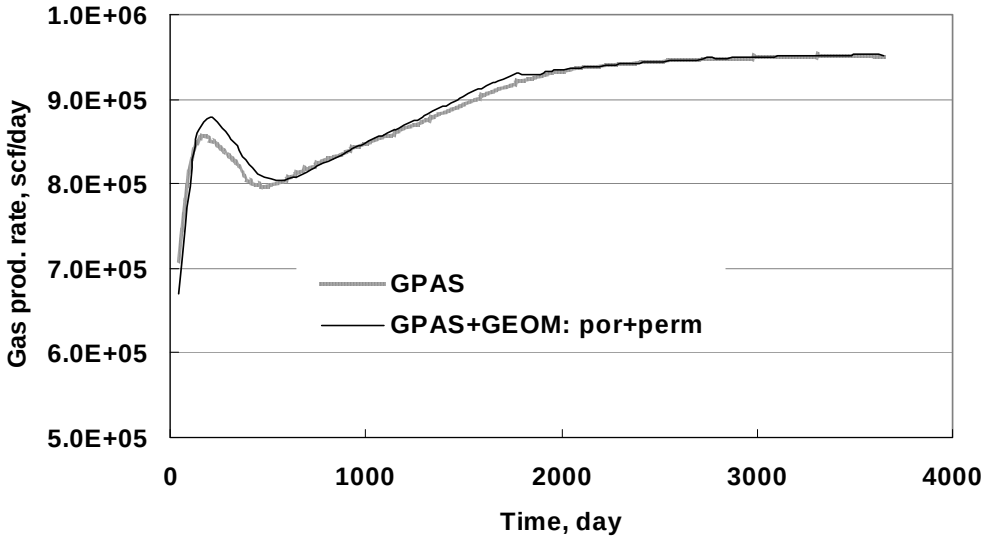

Figure 6-56: The gas production rate from GPAS with geomechanics for Case 6.2.10.5.

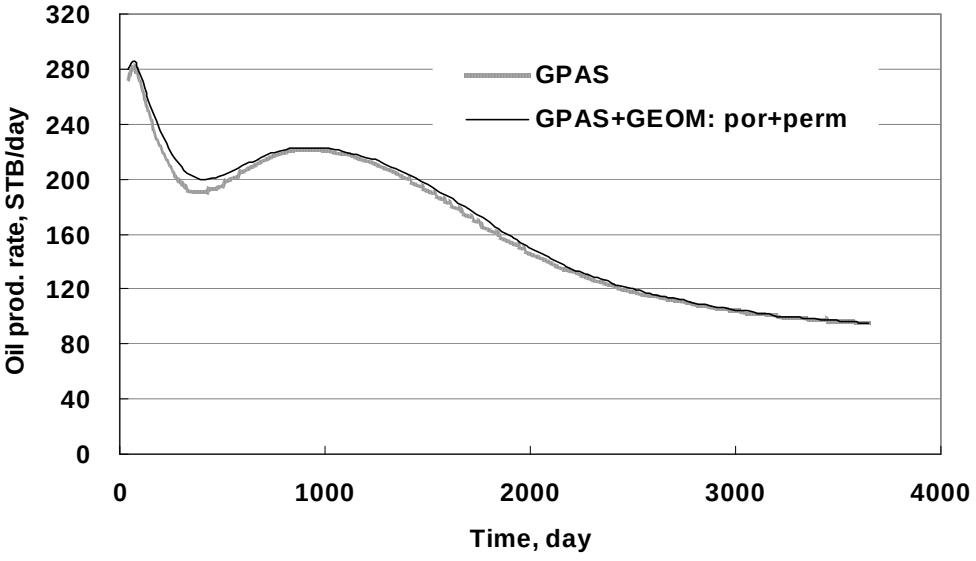

Figure 6-57: The oil production rate from GPAS with geomechanics for Case 6.2.10.5.

6.2.10.6 Water Flooding for Natural Fracture Reservoir

A modified version of Kazemi et al. (1976) quarter-five spot water flood was modeled by Tarahhom (2008). In this case, a deforming matrix with Young's module, $5.0x10^5$ kPa, and Poisson ratio, 0.3, is assumed to test the capability the coupled geomechanics dual porosity model in GPAS.

A water injector is operated at the rate of 200 stb/day and liquids are produced at a constant bottomhole pressure of 500 psi. The simulation domain is a block with the length of 600 ft, the width of 600 ft, and the depth of 30 ft. The fracture system is discretized into an 8x8x3 grid mesh. The matrix system consists of matrix subgrids of $10x10x10$ ft^3. The relative permeability data is shown in Table 6-20. All other properties of input data are given in Table 6-21.

Table 6-20: Relative permeability data for Case 6.2.10.6

		Water	**Oil**	**Gas**
Fracture model	Endpoint	1.0	1.0	0.0
	Residual saturation	0.001	0.001	0.0
	Exponent	1.46	2.15	0.0
Matrix model	Endpoint	0.2	0.92	0.0
	Residual saturation	0.25	0.3	0.0
	Exponent	1.18	1.8	0.0

Table 6-21: Input parameters for Case 6.2.10.6

	Parameter	Value
Fracture model	Length (ft) x Width (ft) x Thickness (ft)	600 x 600 x 30
	Number of gridblocks	8 x 8 x 3
	Gridblock size (ft^3)	75 x 75 x 10
	Porosity	0.02
	Permeability (md)	500
	Initial water saturation	0.001
	Water viscosity (cp)	1
	Water density (lb/ft^3)	62.343
	Initial pressure (psi)	4000
	Production pressure (psi)	3500
Matrix model	Number of matrix subgrids	2 x 2
	Subgrid size (ft^3)	10 x 10 x 10
	Porosity	0.19
	Permeability (md)	1
	Initial water saturation	0.25
	Initial pressure (psi)	4000
Geomechanics model	Number of elements	8 x 8 x 3
	Element type	20-node brick
	Element size (m^3)	22.8 x 22.8 x 3.0
	Young's modulus (kPa)	5.0×10^5
	Poisson's ratio	0.3

The simulation results are shown in Figure 6-58 through Figure 6-61 to compare the differences between GPAS and GPAS coupled with geomechanics simulators. "(por+perm)_m" means the coupling of porosity and permeability of the matrix system; "por_m" means the coupling of only porosity of the matrix system; "(por+perm)_m+perm_f" means the coupling of porosity and permeability of the matrix system and permeability of the fracture system; Figure 6-58 shows the comparison of the oil recovery versus time. The result obtained from the coupled model shows an improvement for the oil recovery because of the compaction within the matrix system of the reservoir. Because of large pressure drops during the early time-steps, the compaction production mechanism effects the oil production largely. With production, the change of pressure between two continuous time-steps is decreasing gradually; hence, the oil recovery curve tends to the one with a stable slope, which is similar to the slope of the curve without geomechanics module as shown in Figure 6-58.

In order to investigate the pressure change during the production, the average pressure versus time is plotted in Figure 6-59. The GPAS without geomechanics predicts a rapid pressure decrease from the initial uniform pressure, 4000 psi, to the constant BHP, 3500 psi, whereas the coupled geomechanics GPAS model gives a significantly slower pressure decrease because of the decreasing pore volume within the reservoir. This confirms that the deformation of the reservoir can considerably maintain the initial reservoir pressure for a long period. The maintaining high pressure contributes to the improvement of oil productivity as shown in Figure 6-58. The above improvement from the coupling effects between solid and fluids cannot be predicted by the traditional reservoir simulators, which does not consider the geomechanics effect on production.

The water production rate and the oil production rate versus time are illustrated in Figure 6-60 and Figure 6-61, respectively. A sharp water production at the beginning is predicted by the coupled model as shown in Figure 6-60, which results from the water production from the matrix domain close to the producer because of the deformation of reservoir; while the traditional reservoir simulator without geomechanics cannot capture this coupled effects. As variation in pressure profile slows down, the water production rate from the matrix compaction becomes lower as well. When the compaction of the matrix medium tends to be small enough to be ignored, the injector will dominantly contribute to the water production of the reservoir. To verify the conjecture, another case is designed with a smaller initial water saturation of the matrix system, 0.001, comparing to the original one, 0.25. The results are shown in Figure 6-62 and Figure 6-63. With the smaller initial water saturation of matrix system, there is almost no water production at the beginning. This shows that the water production at the beginning in Figure 6-60 is from the matrix system due to its compaction rather than the injector after water breakthrough.

Figure 6-64 through Figure 6-67 are shown to investigate the effects of the matrix-permeability changes on the hydrocarbon production. The following parameters, the oil recovery, the average pressure, and the water and oil production rates, are plotted to compare the coupled porosity and permeability of matrix with the coupled porosity of matrix only in the coupled simulations. The results of this case show that the change of porosity of matrix system is dominating the deformation process rather than the change of permeability of matrix system.

Another case is set up to investigate the effect of the coupling fracture permeability on the production. The simulation considers the variations of fracture permeability during production period. Figure 6-68 presents the oil recovery vs. time,

which shows that the coupling of fracture permeability reduces the oil recovery a little bit. Accordingly, the average fracture pressure (Figure 6-69) is a little higher because of the lower fracture permeability. The coupling of fracture permeability decreases the water / oil production rates, as shown in Figure 6-70 and Figure 6-71, because of the bigger pore volume inside the matrix system (Figure 6-73) and the decreased permeability of the fracture system. Figure 6-72 through Figure 6-75 give the pressure, matrix porosity and permeability, and fracture permeability distribution after 30 days production.

Figure 6-76 through Figure 6-79 compares the results of after 1200-day production between the coupled porosity and permeability of matrix system and permeability of fracture system and GPAS without geomechanics. In the later production time, the pressure drop gradients of these two run are almost same, hence, the plots show a similar trends with time for the oil recovery, the water and oil production rates.

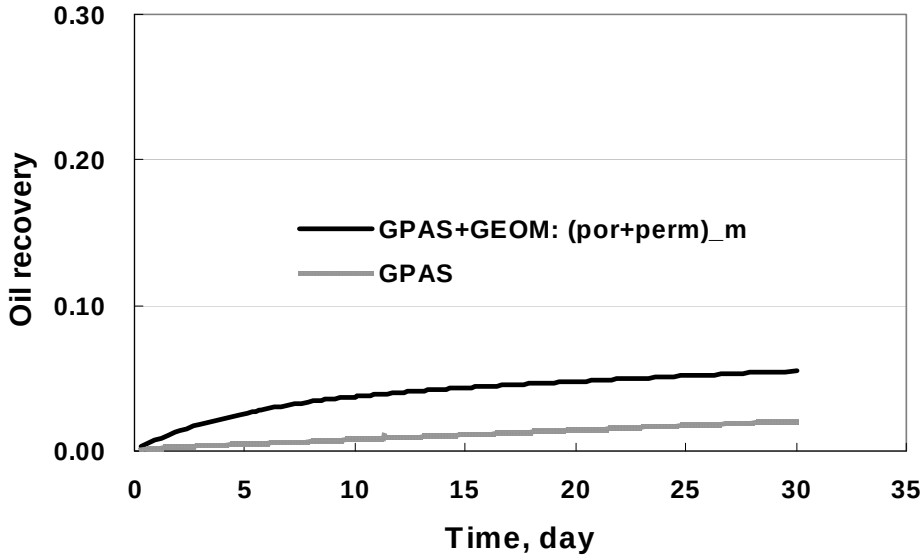

Figure 6-58: The oil recovery from GPAS with and without geomechanics for Case 6.2.10.6.

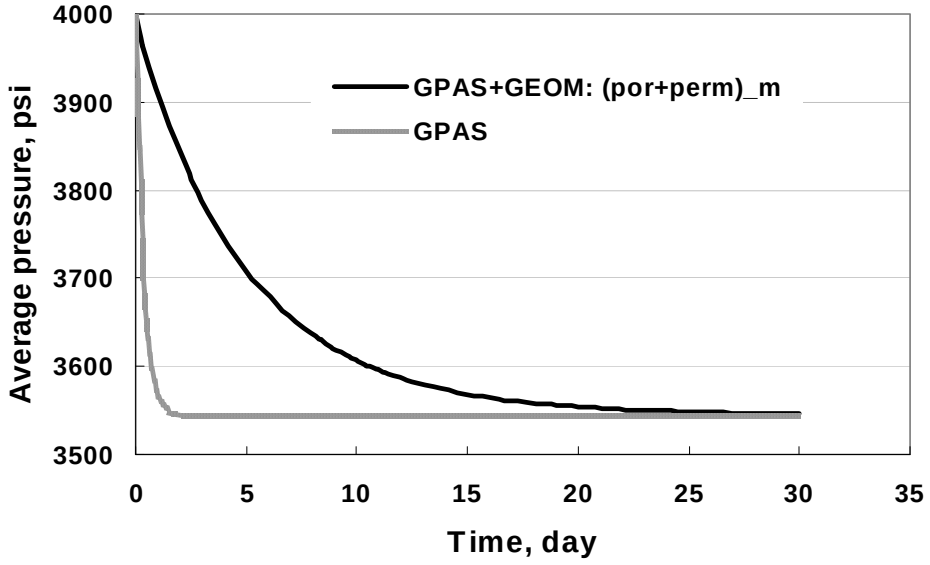

Figure 6-59: The average pressure from GPAS with and without geomechanics for Case 6.2.10.6.

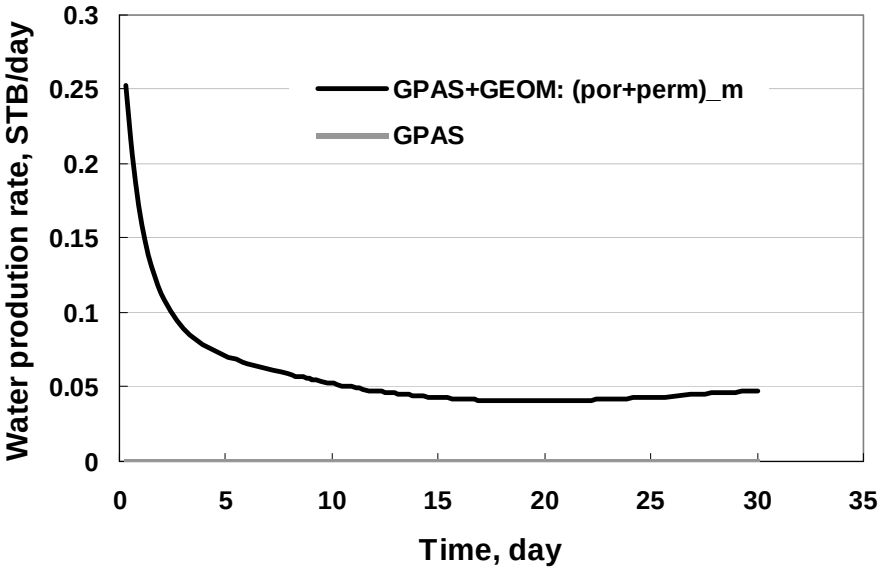

Figure 6-60: The water production rate from GPAS with and without geomechanics for Case 6.2.10.6.

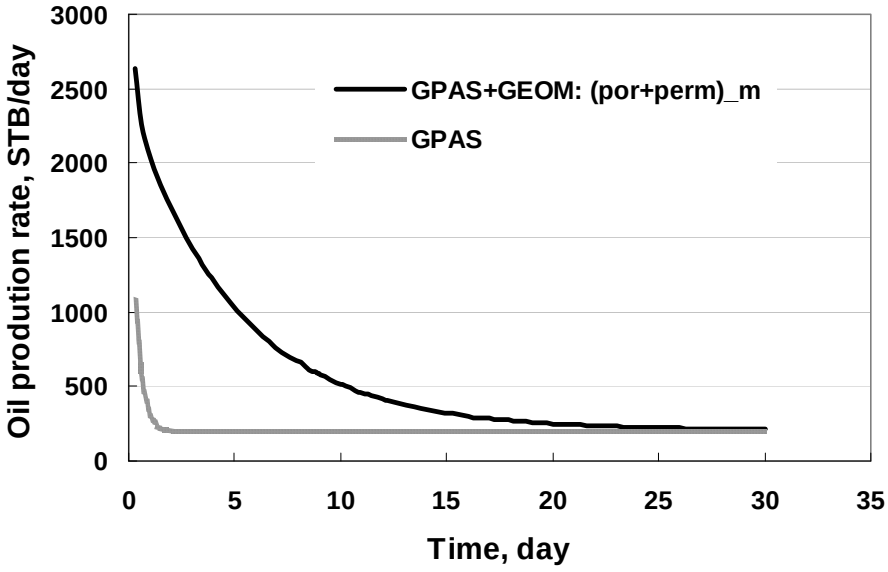

Figure 6-61: The oil production rate from GPAS with and without geomechanics for Case 6.2.10.6.

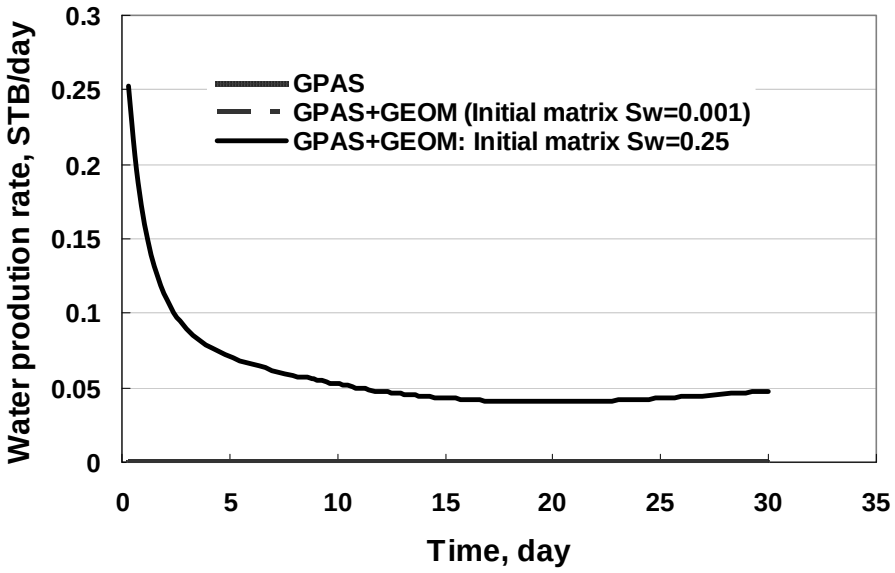

Figure 6-62: The water production rate from GPAS with and without geomechanics for Case 6.2.10.6.

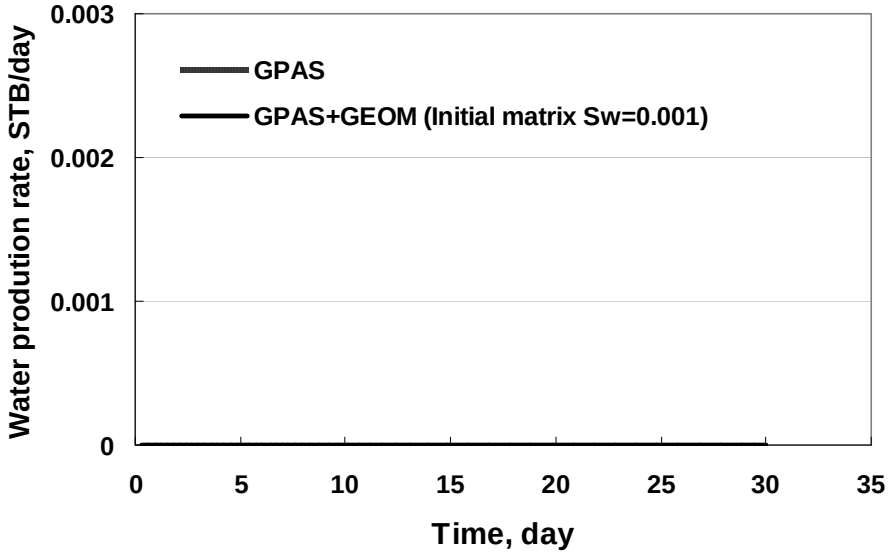

Figure 6-63: The water production rate from GPAS with and without geomechanics for Case 6.2.10.6.

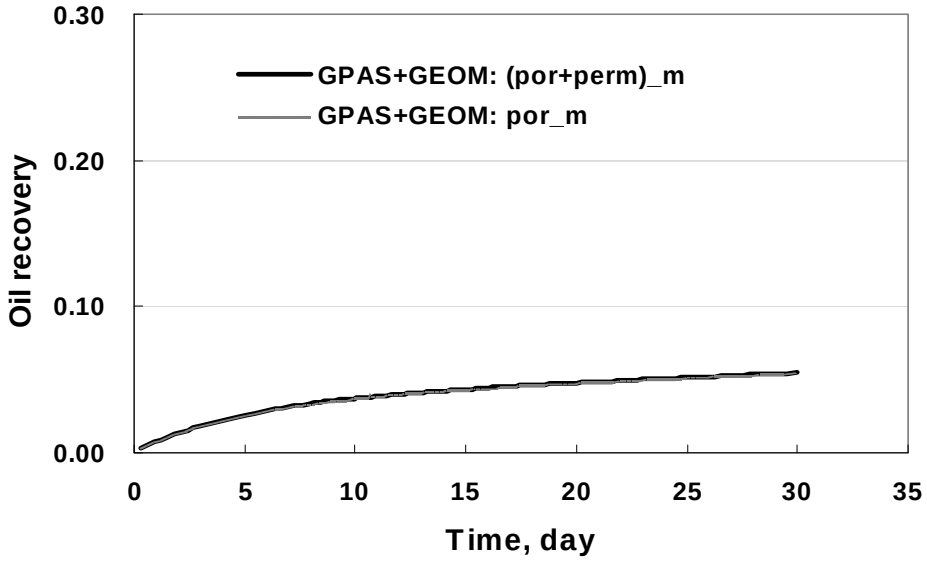

Figure 6-64: The oil recovery from GPAS with geomechanics for Case 6.2.10.6.

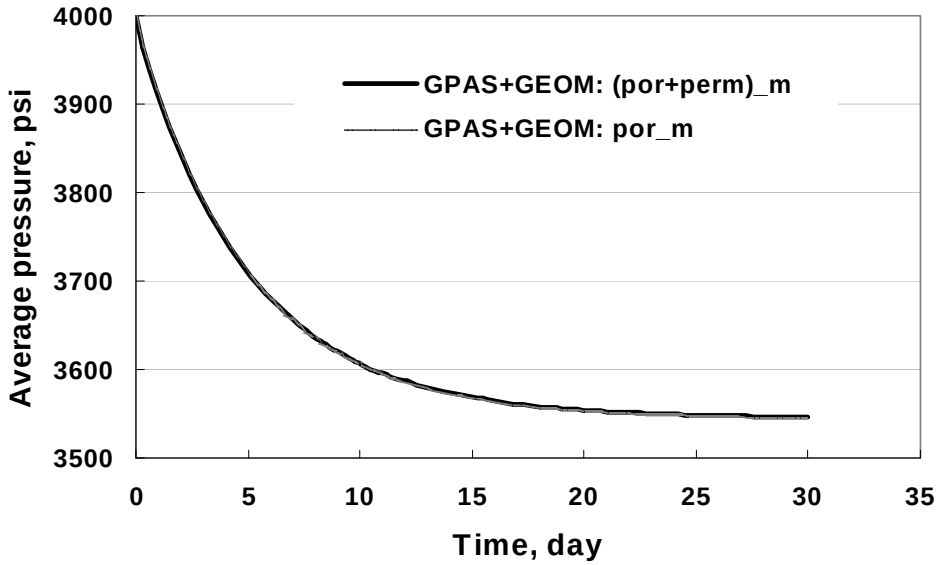

Figure 6-65: The average pressure from GPAS with geomechanics for Case 6.2.10.6.

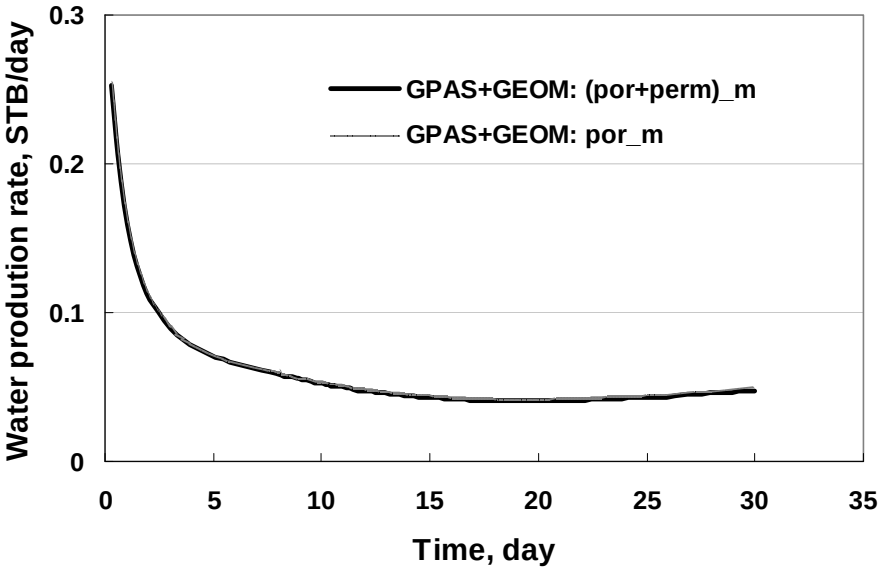

Figure 6-66: The water production rate from GPAS with geomechanics for Case 6.2.10.6.

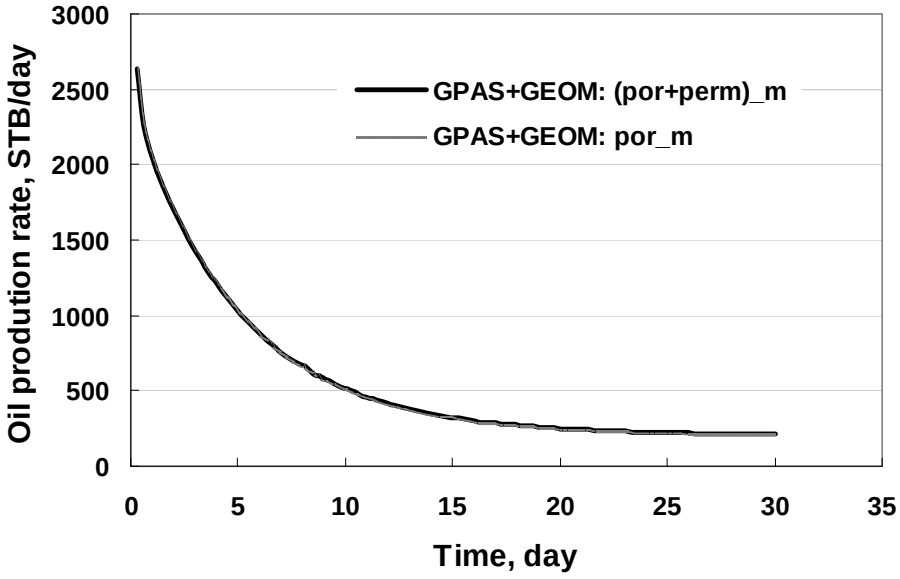

Figure 6-67: The oil production rate from GPAS with geomechanics for Case 6.2.10.6.

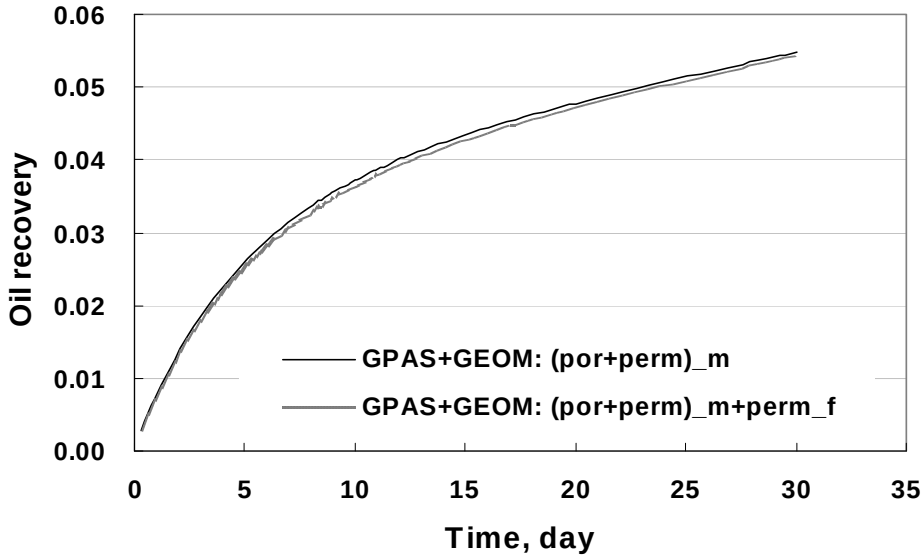

Figure 6-68: The oil recovery from GPAS with geomechanics for Case 6.2.10.6.

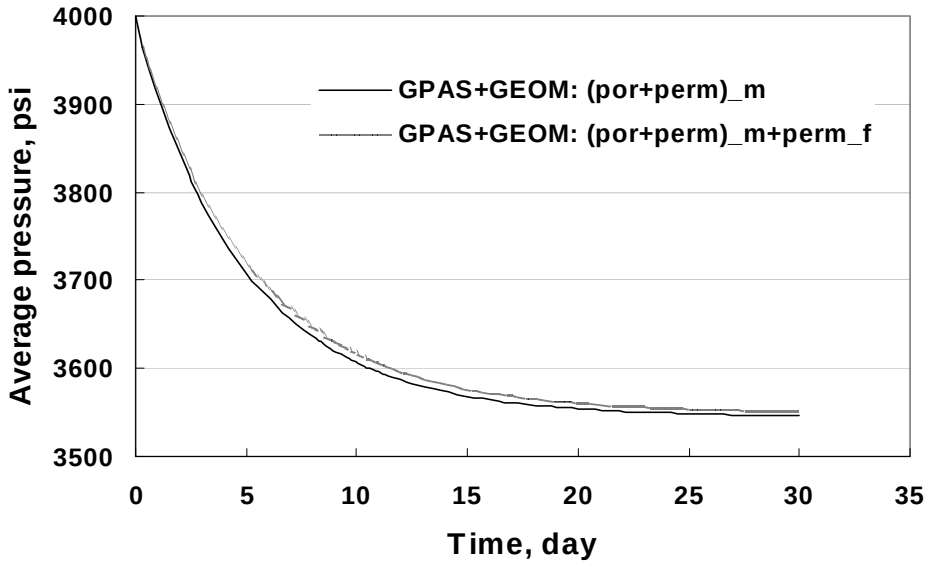

Figure 6-69: The average pressure from GPAS with geomechanics for Case 6.2.10.6.

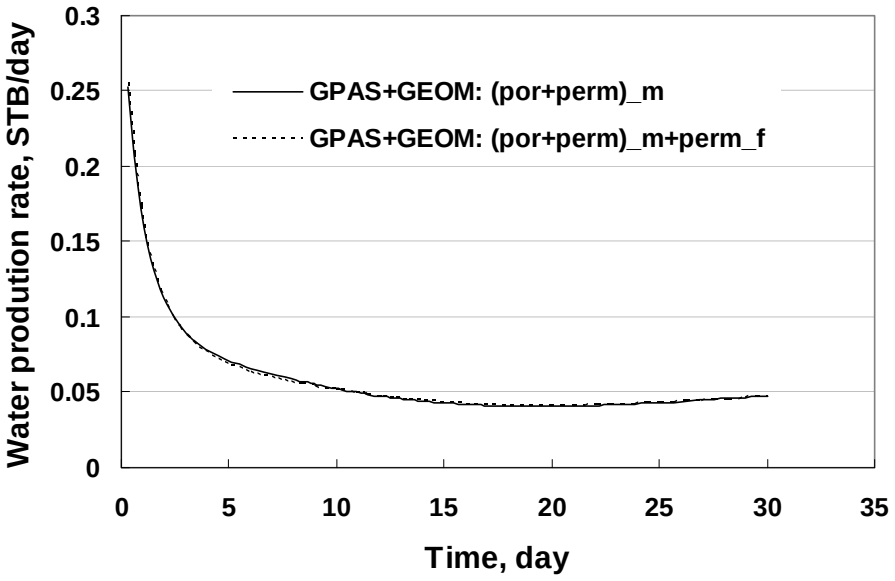

Figure 6-70: The water production rate from GPAS with geomechanics for Case 6.2.10.6.

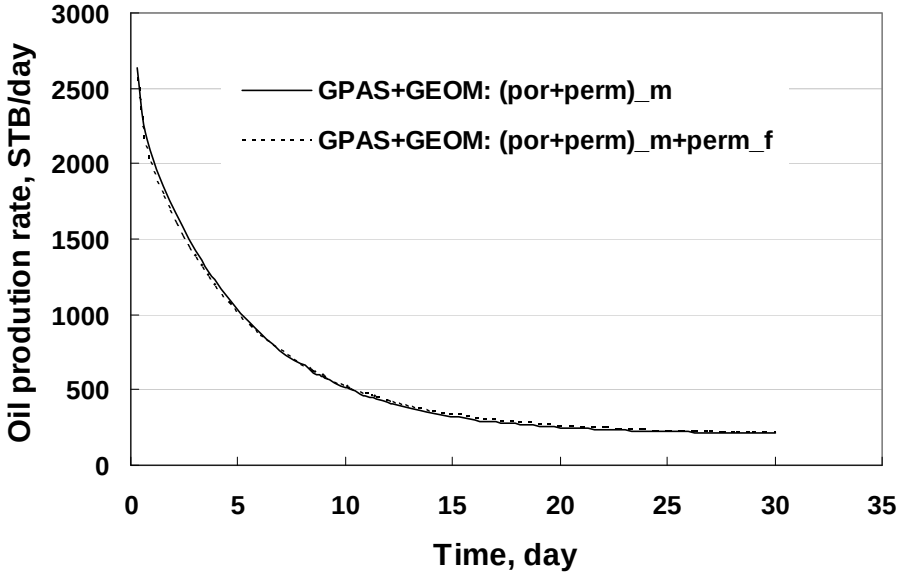

Figure 6-71: The oil production rate from GPAS with geomechanics for Case 6.2.10.6.

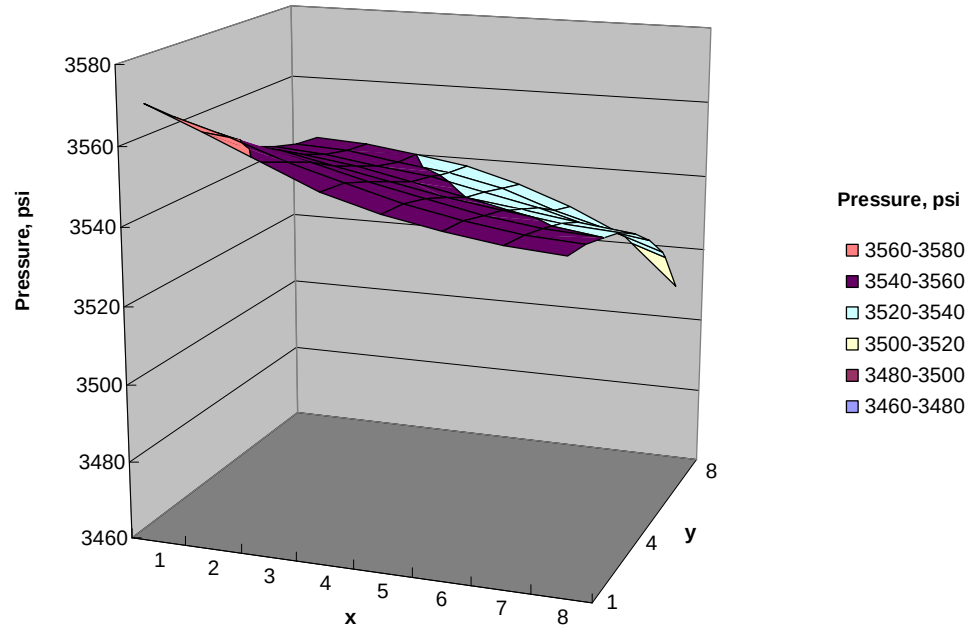

(a) The coupling of porosity and permeability of the matrix system.

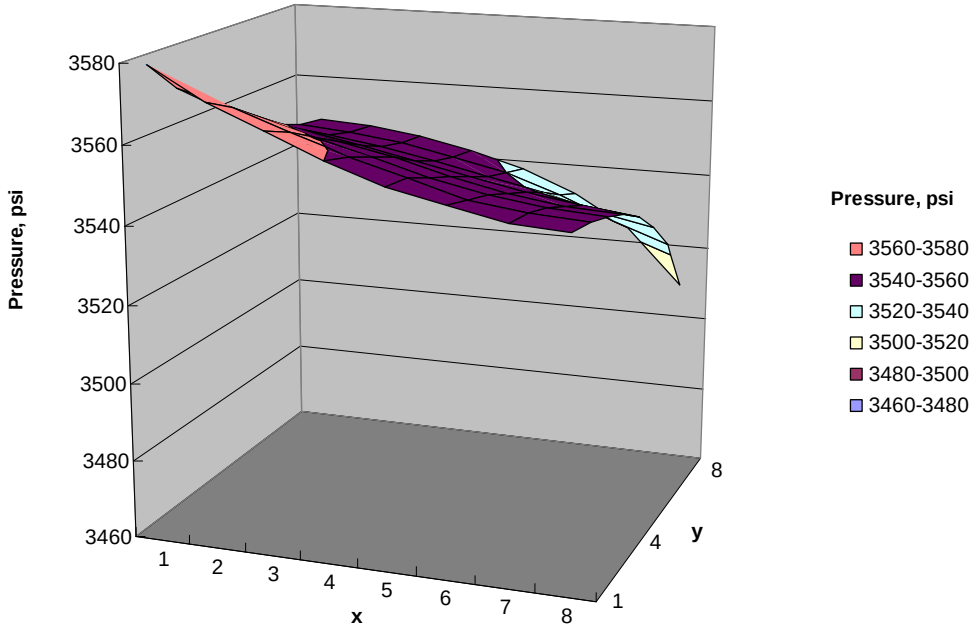

(b) The coupling of porosity and permeability of the matrix system and permeability of the fracture system.

Figure 6-72: The pressure distribution from GPAS with geomechanics for Case 6.2.10.6.

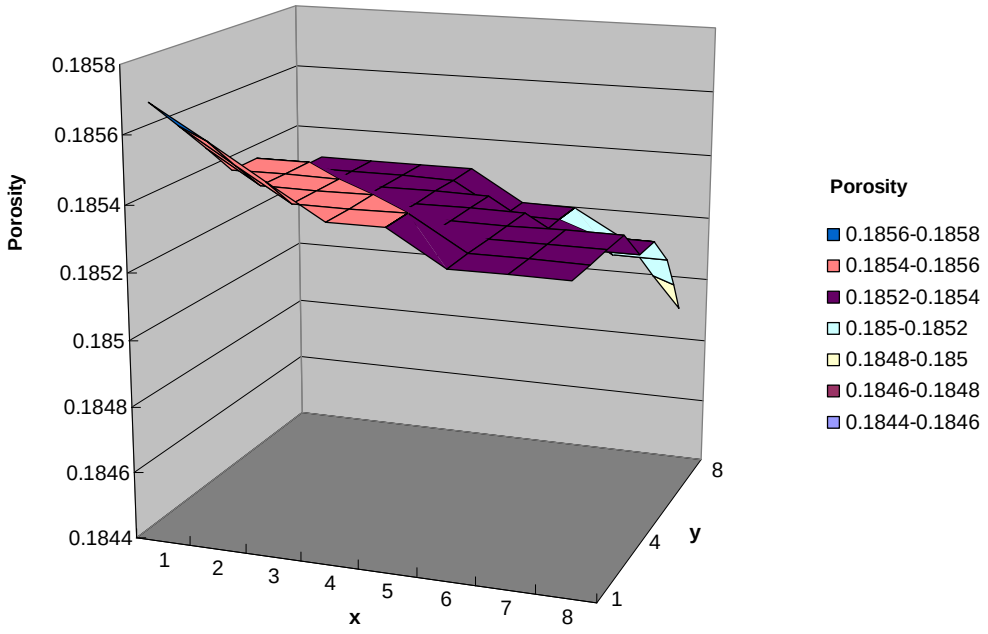

(a) The coupling of porosity and permeability of the matrix system.

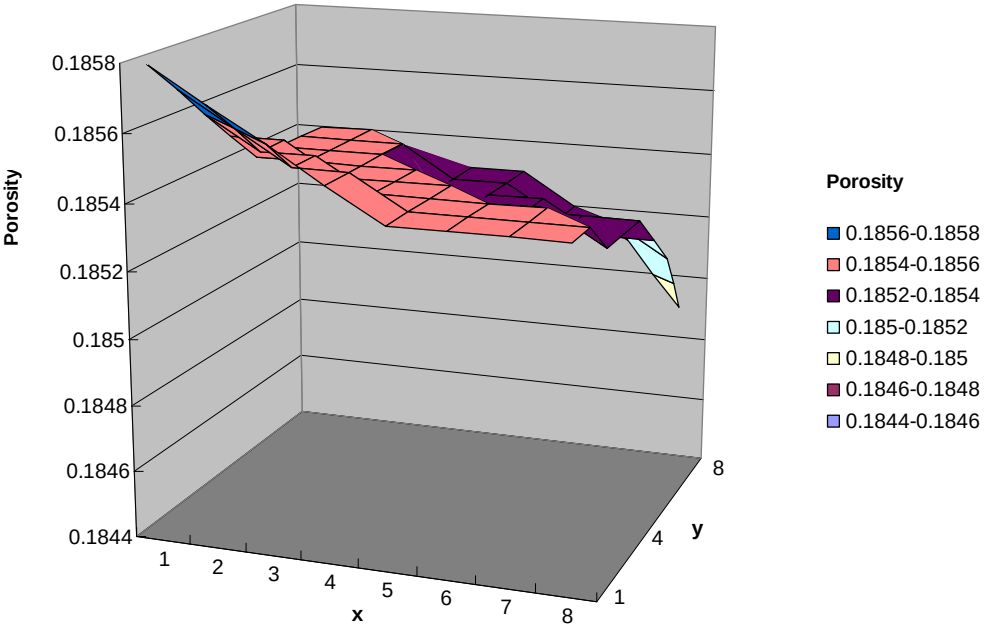

(b) The coupling of porosity and permeability of the matrix system and permeability of the fracture system.

Figure 6-73: The matrix porosity distribution of the top layer from GPAS with geomechanics for Case 6.2.10.6.

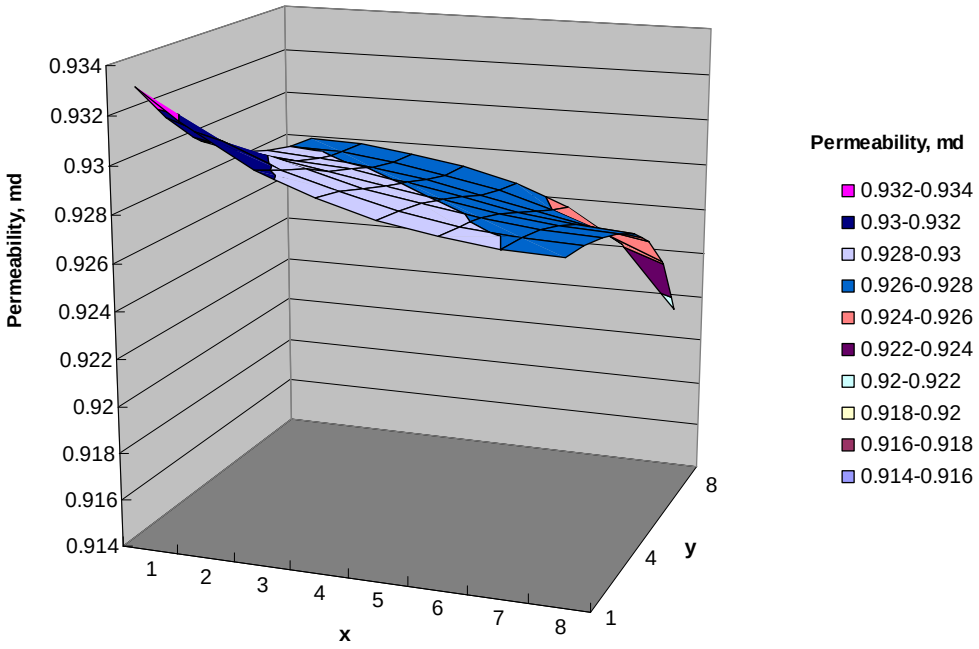

(a) The coupling of porosity and permeability of the matrix system.

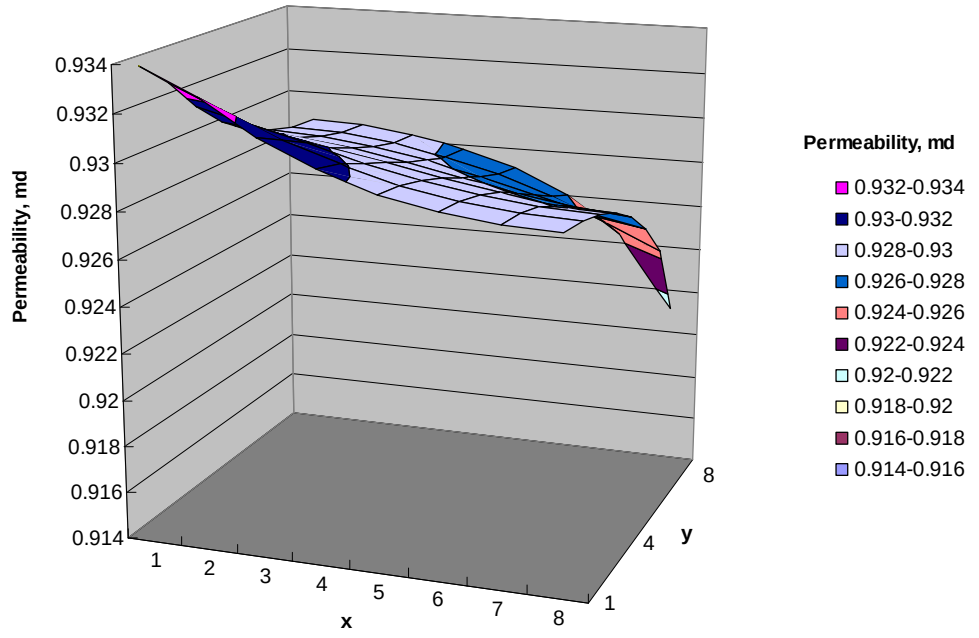

(b) The coupling of porosity and permeability of the matrix system and permeability of the fracture system.

Figure 6-74: The matrix permeability (x-) distribution of the top layer from GPAS with geomechanics for Case 6.2.10.6.

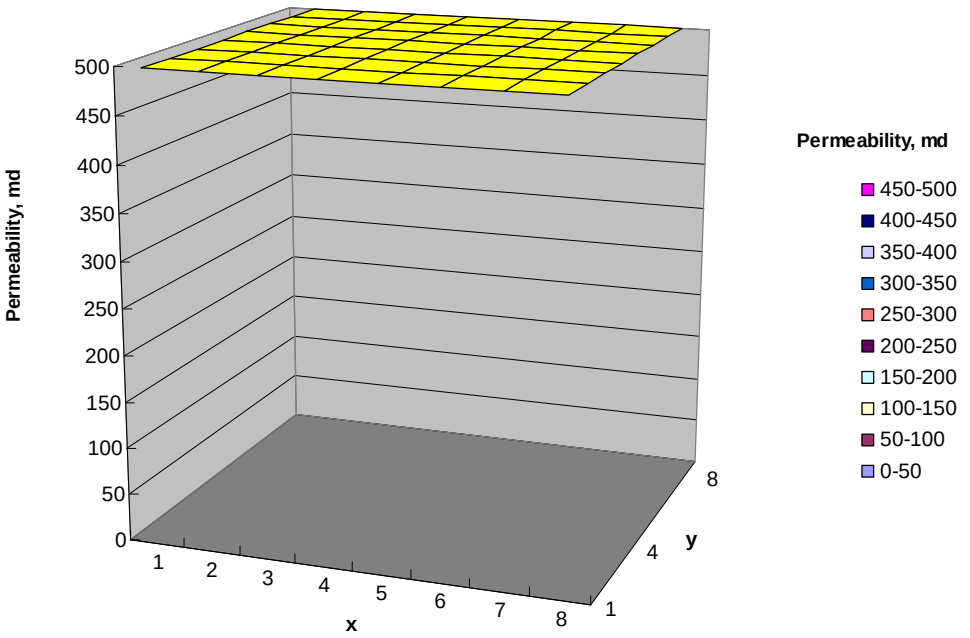

(a) The coupling of porosity and permeability of the matrix system.

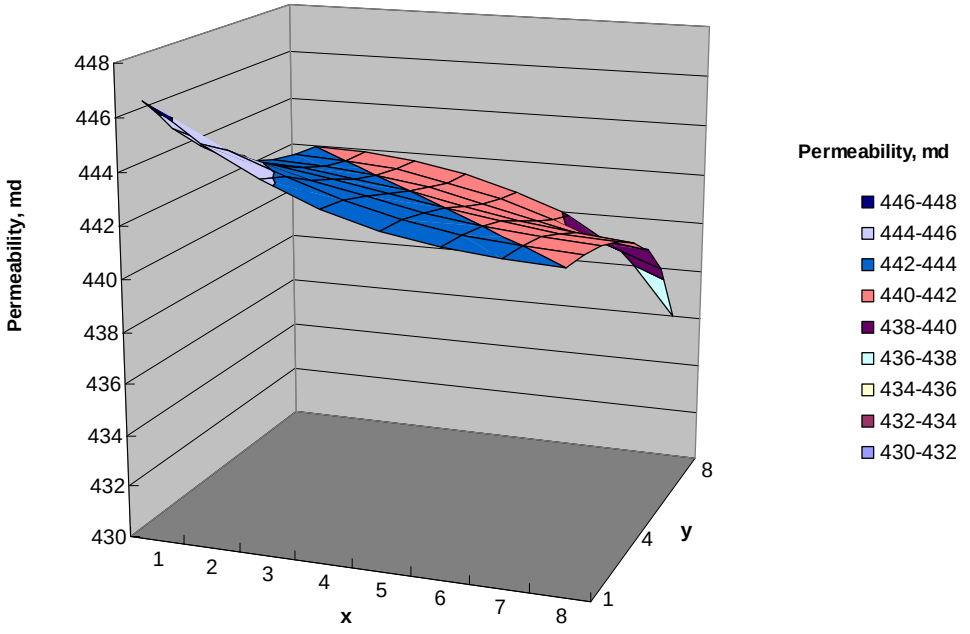

(b) The coupling of porosity and permeability of the matrix system and permeability of the fracture system.

Figure 6-75: The fracture permeability (x-) distribution of the top layer from GPAS with geomechanics for Case 6.2.10.6.

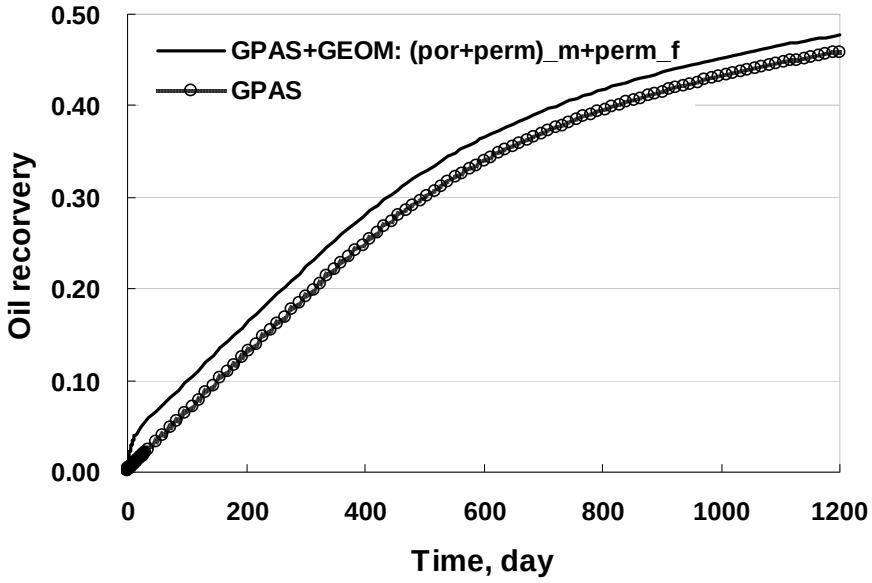

Figure 6-76: The oil recovery from GPAS with geomechanics for Case 6.2.10.6.

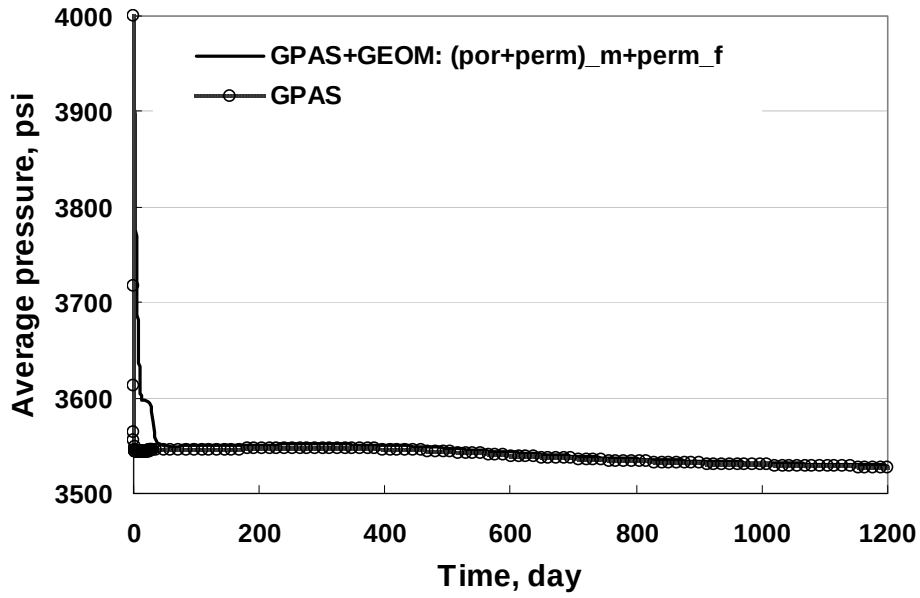

Figure 6-77: The average pressure from GPAS with geomechanics for Case 6.2.10.6.

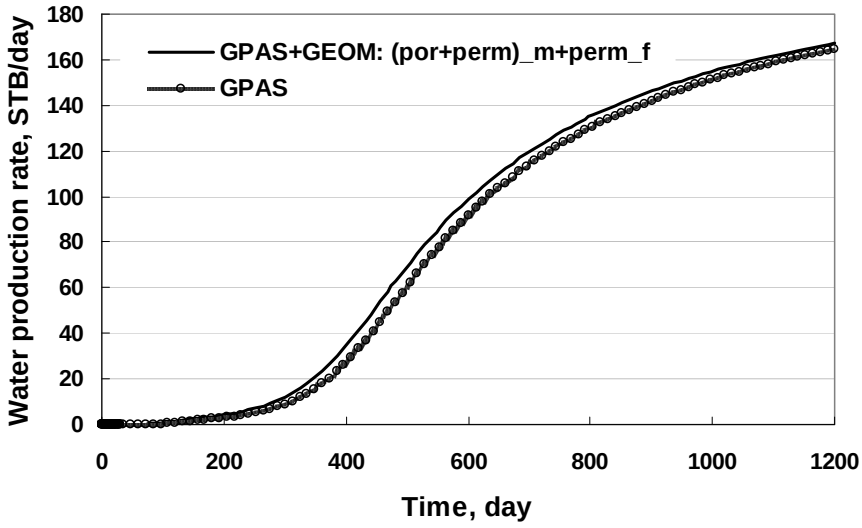

Figure 6-78: The water production rate from GPAS with geomechanics for Case 6.2.10.6.

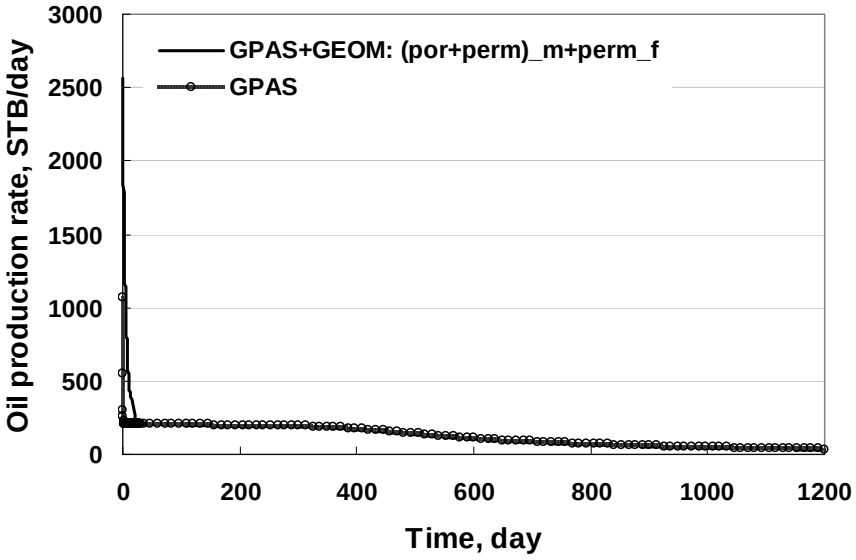

Figure 6-79: The oil production rate from GPAS with geomechanics for Case 6.2.10.6.

6.3 IMPLEMENTATION OF NONLINEAR CONSTITUTIVE MODEL IN GPAS

This section discusses poro-elastoplastic problems. A perfect plasticity as shown in Figure 6-80 is assumed during this part. The Mohr-Coulomb yield criterion is implemented in the code to define the stress conditions under which plastic deformations will occur. A comparison to the published solution is performed to verify our implementation.

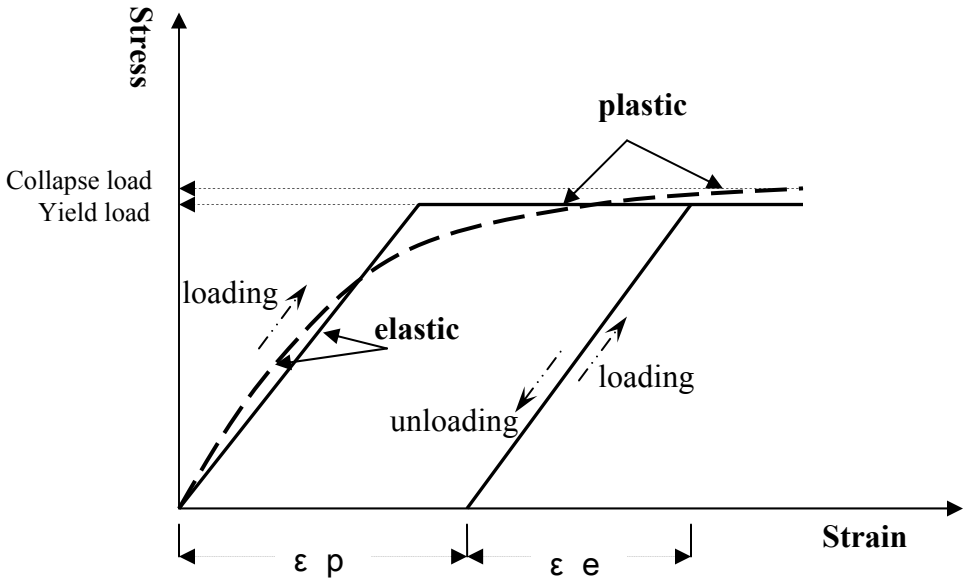

Figure 6-80: An elastic-perfectly plastic material.

6.3.1 The Mohr-Coulomb Constitutive Model

Let us recast the Mohr-Coulomb constitutive model in Section 5.2.1:

$$F_{MC} = \sigma_m \sin\phi + \bar{\sigma}\left(\frac{\cos\theta}{\sqrt{3}} - \frac{\sin\theta\sin\phi}{3}\right) - c\cos\phi, \tag{6-59}$$

where ϕ is the friction angle and c is the cohesion of the material. Both ϕ and c are the material constants determined by conducting experiments.

The Mohr Coulomb failure criterion is dependent of all the three stress invariants $(\sigma_m, \bar{\sigma}, \theta)$ defined in Section 5.1. In the principal stress space, this criterion describes an irregular hexagonal cone as shown in Figure 5-2. In a special case, when $\phi = 0^o$ (frictionless material), the Mohr-Coulomb criterion reduces to the Tresca criterion.

In this research, the Mohr-Coulomb constitutive model is implemented; while other nonlinear constitutive models presented in Section 5.2 can be coded in a similar way.

6.3.2 Incremental Formulation

When the governing equations of the solid is discretized using FEM, the following PDE will be obtained:

$$[k_m]\{\boldsymbol{u}\} + [c]\{\boldsymbol{p}\} = \{\boldsymbol{f}\}, \tag{6-60}$$

where $[k_m]$ and $[c]$ are the solid stiffness matrix and the conductivity matrix, respectively; $\{\boldsymbol{u}\}$ and $\{\boldsymbol{p}\}$ are the unknown vectors of the displacements and the pressure; $\{\boldsymbol{f}\}$ is the external loading vector which may be depend on time.

There are two types of approaches to solve Equation (6-60). The first type is the so-called "absolute load version," which considers the full external load at each time-step and is only suitable for linear elastic problems. However, when we try to solve nonlinear solid deformation problems, the second type, the "incremental load version," has to be utilized. Similar to Equation (4-66) in Section 4.2.3.4, Equation (6-60) can be rewritten as

$$[k_m]\{\Delta\boldsymbol{u}\} + [c]\{\Delta\boldsymbol{p}\} = \{\Delta\boldsymbol{f}\}, \tag{6-61}$$

where $\{\Delta\boldsymbol{u}\}$ and $\{\Delta\boldsymbol{p}\}$ are the variations of the displacement vector and the pressure vector between two continuous time-steps; $\{\Delta\boldsymbol{f}\}$ is the change of the external load between two successive time-steps.

6.3.3 Viscoplasticity Algorithm

Let us review the linear stress-strain relationship, Equation (4-43) in Section 4.2.3.3.

$$\{\boldsymbol{\sigma}\}_{(x,y,z)} = [\mathbf{D}]\{(\boldsymbol{\varepsilon} - \boldsymbol{\varepsilon}_0)\}_{(x,y,z)} + \{\boldsymbol{\sigma}_0\}_{(x,y,z)}, \tag{6-62}$$

where $\{\boldsymbol{\sigma}\}$ and $\{\boldsymbol{\varepsilon}\}$ are the stress vector and the strain vector, respectively; the subscript "0" denotes the initial values; $[\mathbf{D}]$ is the elasticity matrix related to material parameters, such as the Young's modulus and the Poisson's ratios.

In many practical problems in geomechanics, the stress-strain relationship is not always linear as shown in Equation (6-62), such as plasticity and creep. Hence, more complex constitutive models are required to represent the nonlinear deformation behavior of the solid rather than the linear elasticity (Equation (6-62)). In general, a nonlinear relationship can be written as

$$J\left(\{\boldsymbol{\sigma}\}_{(x,y,z)}, \{\boldsymbol{\varepsilon}\}_{(x,y,z)}\right) = 0, \tag{6-63}$$

where J represents a nonlinear function of the stress and strain. The above nonlinearity is called the material nonlinearity.

Based on the insight into problems, Equation (6-63) can be solved approximately using an iteration process with adjusted strains or stresses. For obtaining physical solutions, the iteration process has to be combined with small time-steps and incremental algorithm. The logic of the iteration process is to solve the nonlinearity through a series of linearity problems with adjusted strains (the initial strain method) or stresses (the initial stress method). In this research, a constant stiffness method with adjusted strains is utilized to solve Equation (6-63), as shown in Figure 6-81. The above method is also named as the viscoplasticity method (Zienkiewicz and Cormeau 1974). The algorithm can be described as

(1) Solve PDEs of solid for displacements and check for convergence. If convergence achived, go to next time-step; otherwise, continue.

For all the elements:

(2) Calculate effective stresses.

(3) If yield, then go to (4); otherwise, go to the next element.

$$F \geq 0. \tag{6-64}$$

(4) Calculate the rate of viscoplastic strain:

$$\left\{\dot{\varepsilon}^{vp}\right\} = F\left\{\frac{\partial Q}{\partial \sigma}\right\}, \tag{6-65}$$

where F and Q are the yield function and the plastic potential function, respectively.

(5) Calculate the incremental viscoplasticity strain and the accumulative viscoplasticity strain.

(6) Calculate the unbalanced body forces.

(7) Redistribute the above unbalanced body forces. Return to (1) for next plasticity iteration.

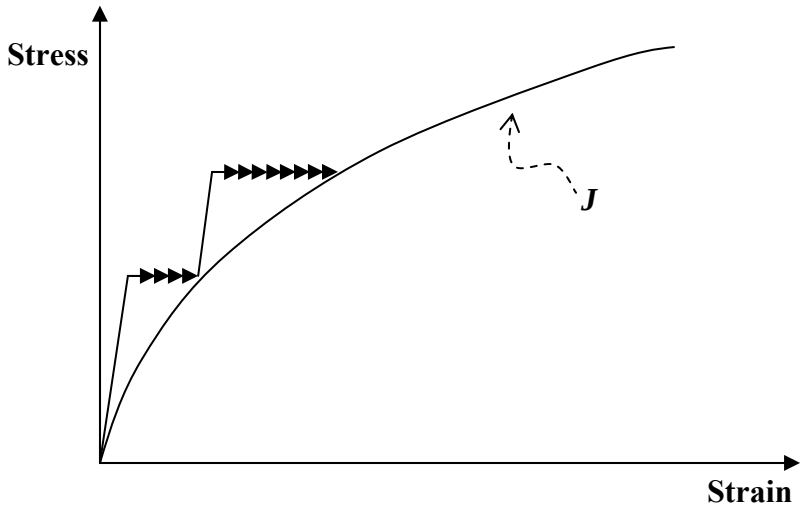

Figure 6-81: Constant stiffness method.

6.3.4 Implementation of Nonlinear Constitutive Model in GPAS

The following describes the implementation of nonlinear constitutive model in GPAS. For each Newton iteration at each time-step in GPAS,

(1) Transfer the change of pressure Δp from GPAS to GEOM.

(2) Solve PDEs of solid for displacements considering Δp as the body force. Check for convergence using displacements. If convergence achieved, return to GPAS for next Newton iteration; otherwise, continue.

For all the elements:

(3) Calculate effective stresses.

(4) If yield, then go to (5); otherwise, go to the next element.

(5) Calculate the rate of viscoplastic strain.

(6) Calculate the incremental viscoplasticity strain and the accumulative viscoplasticity strain.

(7) Calculate the unbalanced body forces among all the elements.

(8) Redistribute the above unbalanced body forces.

(9) Return to (2) for next plasticity iteration.

6.3.5 A Uni-axial Compaction Case

This section will verify the developed coupled nonlinear Mohr-Coulomb geomechanics and GPAS using results from the fully coupled finite element code (Smith and Griffiths 2004). The case is a one-block uni-axial compaction problem. Its input values are given in Table 6-22. The domain is a cube with the dimensions 200 x 200 x 200 ft^3. The initial pressure is 6000 psi, which is equal to the total stress of the solid. The Young's modulus and the Poisson's ratio of rock are 9.0×10^6 kPa and 0.35, respectively. The cohesion coefficient is 3000 kPa.

Table 6-22: Summary of input data for Case 6.3.1

	Parameter	Value
Reservoir model	Length (ft) x Width (ft) x Thickness (ft)	200 x 200 x 200
	Number of gridblocks	1 x 1 x 1
	Gridblock size (ft^3)	200 x 200 x 200
	Porosity	0.35
	Permeability (md)	10, 10, 10
	Rock compressibility (psi^{-1})	0
	Fluid compressibility (psi^{-1})	0.000003
	Initial water saturation	0.17
	Water viscosity (cp)	1
	Water density (lb/ft^3)	62.343
	Initial pressure (psi)	6000
	Producer (BHP)	500
Geomechanics model	Number of elements	1 x 1 x 1
	Element type	20-node brick (20/8)
	Element size (m^3)	61 x 61 x 61
	Young's modulus (kPa)	$9.0x10^6$
	Poisson's ratio	0.3
	Cohesion (kPa)	3000
	Dilation angle (deg.)	0
	Initial effective stress (kPa)	0

The different friction angles, 4 deg., 10 deg., 15 deg., and 30 deg., are selected to simulate the plastic deformation behaviors of rock. The results are shown in Figure 6-82. On the one hand, a good match is shown in the figure between our coupled geomechanics and GPAS code and the fully coupled finite element code (Smith and Griffiths 2004) for the friction angles of 4 deg., 10 deg., 15 deg., and 30 deg.

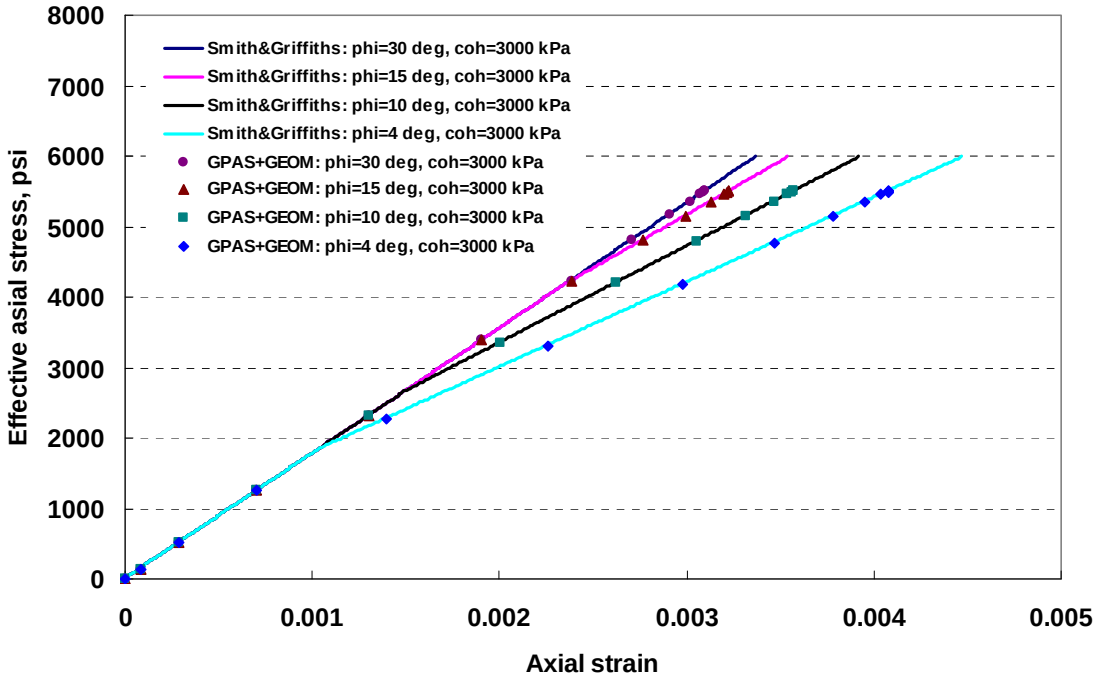

Figure 6-82: The stress-strain relationship using Mohr-Coulomb yield criteria from the coupled geomechanics GPAS and Smith and Griffiths 2004 for Case 6.3.1.

Figure 6-82 also represents the different start time of yield for the solid with the different friction angles. For a 30 deg. friction angle, the deformation of the solid behaves linear-elastically, which means a straight line of the stress-strain as shown in Figure 6-82. When the friction angle decreases to 15 deg., the solid deforms nonlinearly

and yield at the effective stress of 4200 psi. Thereafter, the solid behaves plastically. The curve of the stress-strain begins to deviate from the straight line of linear elasticity (30 deg. friction angle). For the friction angle of 10 deg., the solid begins to deform plastically at the effective stress of 2500 psi, because the less friction angle is related to a smaller stable region. As expected, a 4 deg. friction angle gives an earlier start time of plasticity deformations when the related effective stress is less than 2000 psi, as shown in Figure 6-82. With the decrease of the friction angles, the relationships of the stress-strain curve toward the positive direction of the strain. These inward curves represent plastical strains as shown in Figure 6-80.

6.3.6 3D Primary Depletion

A 3D problem with one-component (C_{10}) reservoir fluids is designed to test the developed Mohr-Coulomb constitutive model. The reservoir size has a volume of 200 x 200 x200 ft^3, which is discretized into a 2 x 8 x 4 grid mesh. For the fluid-flow model, the no-flow boundaries are applied to all the sides and two producers are drilled at (x=50 ft, y=175 ft) and (x=150 ft, y=175 ft) through all the layers. For the solid deformation model, a constant overburden stress (6000 psi) is applied on the top the reservoir, which is discretized into 64 20-node brick (hexahedral) elements. The Young module is 9 x 10^6 kPa, and Poisson ratio is 0.3. Other input data values are listed in Table 6-23.

Runs with different combinations of the friction angle (phi) and the cohesion coefficient (coh) are performed. Figure 6-83 through Figure 6-85 show the variations of the oil recovery, the average pressure, and the displacement in z direction of the point (0, 0, 0) with time. For the run with phi=10 deg. and coh=3000 kPa, the deformation of solid behaves as a linear elasticity. When a smaller coh=300 kPa is used, the deformation behavior of solid changes to nonlinear plasticity. Figure 6-83 clearly shows that the deformation of the nonlinear plasticity enhances the oil recovery compared

to that from the linear elasticity. The run with phi=15 deg. and coh=300 kPa gives an oil recovery in between results from the previous two runs. As expected, the higher nonlinear plasticity deformations maintain the higher average pressures, as shown in Figure 6-84. Figure 6-85 represents the compaction of the first gridblock of the reservoir. The displacements increase with the more plasticity evolved. The above numerical results indicate that the developed coupled geomechanics and GPAS with the nonlinear constitutive model can properly capture the primary physics of compaction production mechanism.

Table 6-23: Summary of input data for Case 6.3.6

	Parameter	Value
Reservoir model	Length (ft) x Width (ft) x Thickness (ft)	200 x 200 x 200
	Number of gridblocks	2 x 8 x 4
	Gridblock size (ft^3)	100 x 25 x 50
	Porosity	0.35
	Permeability (x,y,z) (md)	10, 10, 10
	Rock compressibility (psi^{-1})	0
	Fluid compressibility (psi^{-1})	$3.0x10^{-6}$
	Initial water saturation	0.17
	Water viscosity (cp)	1
	Water density (lb/ft^3)	62.343
	Initial pressure (psi)	6000
	Producer (BHP)	5000
Geomechanics model	Number of elements	2 x 8 x 4
	Element type	20-node brick
	Element size (m^3)	30.47 x 7.61 x 15.23
	Young's modulus (kPa)	$9.09x10^6$
	Poisson's ratio	0.3

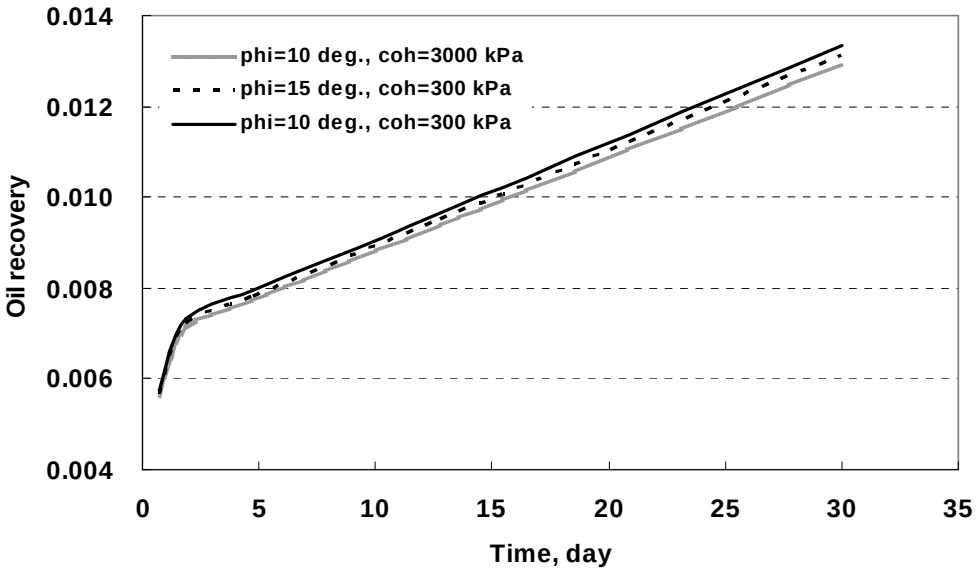

Figure 6-83: The oil recovery from GPAS with geomechanics for Case 6.3.6.

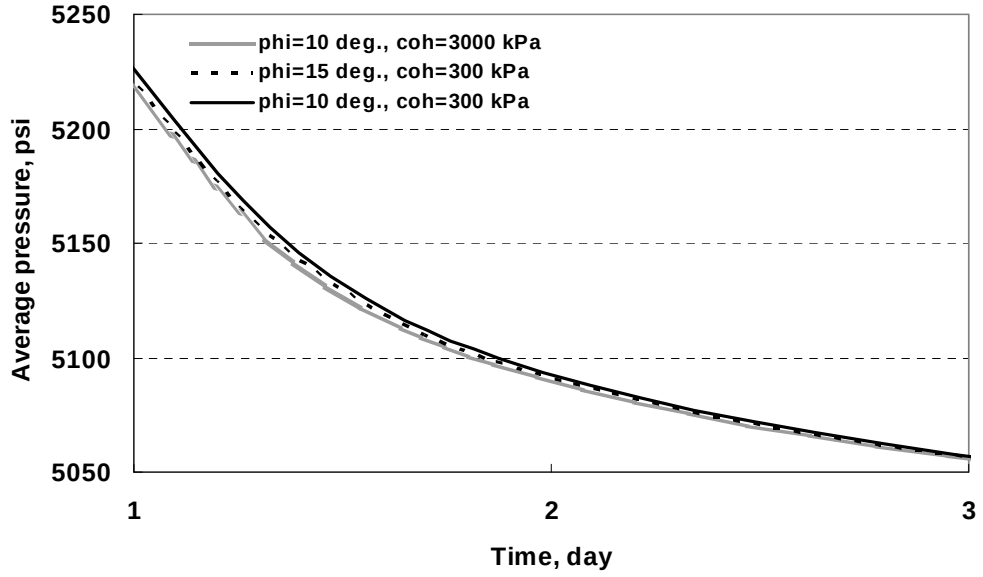

Figure 6-84: The average pressure from GPAS with geomechanics for Case 6.3.6.

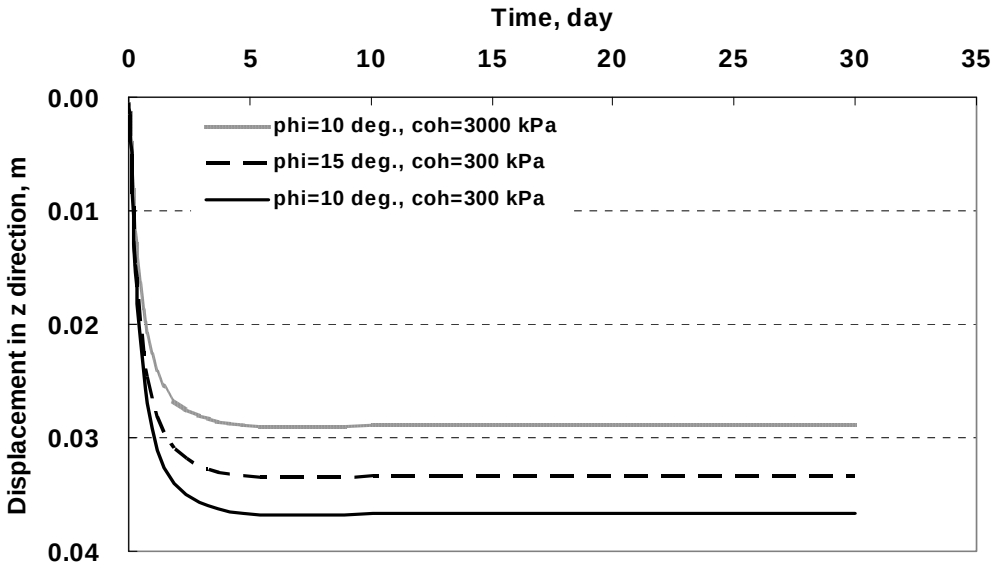

Figure 6-85: The displacement in z direction of the point (0, 0, 0) from GPAS with geomechanics for Case 6.3.6.

6.3.7 Water Flooding with Two-Component Fluid Mixture

This case is similar to Case 6.2.10.3. The initial pressure is set to 1000 psi in the following simulations. A pair of friction angle (2 deg.) and cohesion coefficient (80 kPa) is selected to model the nonlinear plasticity deformation of solids. Meanwhile, the case is used to verify the proposed coupling procedure in this research has a capability to simulate the fluid-flow problems coupled with nonlinear constitutive models. Figure 6-86 indicates that the nonlinear deformation of solid can enhance the oil recovery, because higher compaction occurs (Figure 6-87) within the reservoir with the same production scenario. Figure 6-87 presents the compaction in z direction of the point (0, $8 \leqq y \leqq 108$, 0) at 100 days. The Mohr-Coulomb model predicts 60% more compaction than the linear elasticity model. The plasticity effect decreases the magnitude of depletion of fluid pressure for early 25-day period. Therefore, the predicted average

pressure from plasticity model is higher than that from linear elasticity simulation (Figure 6-88). The higher oil production rate (Figure 6-89) is also given than the result predicted from linear elasticity simulation (Figure 6-89).

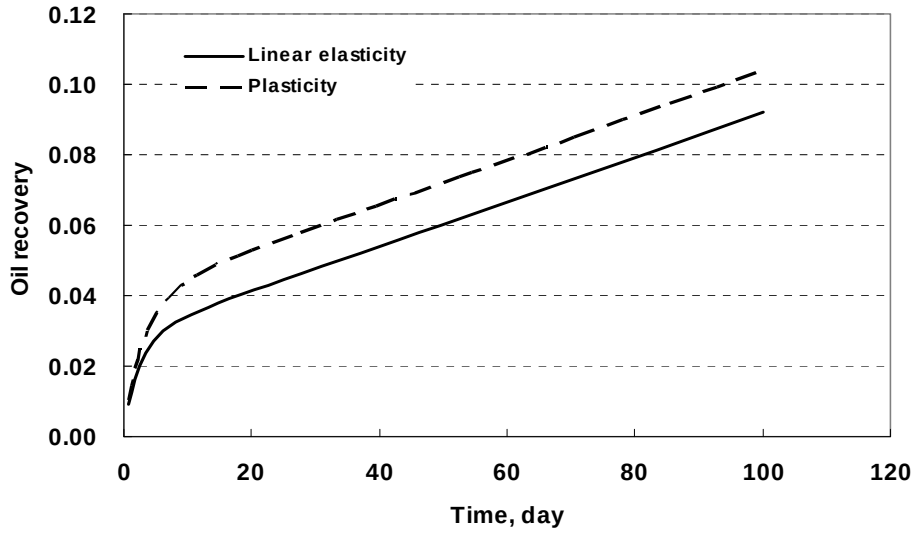

Figure 6-86: The oil recovery from GPAS with geomechanics for Case 6.3.7.

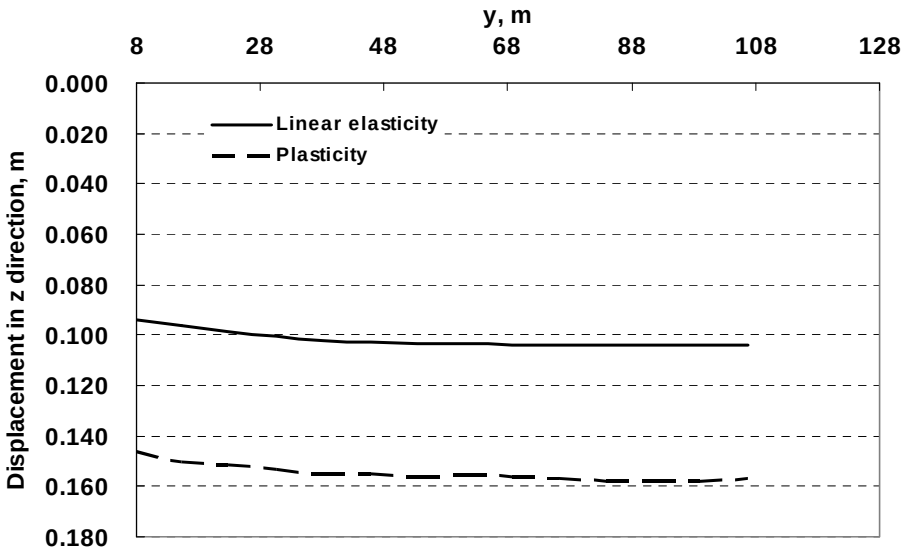

Figure 6-87: The displacement in z direction of the point (0, y, 0) at time=100 days from GPAS with geomechanics for Case 6.3.7.

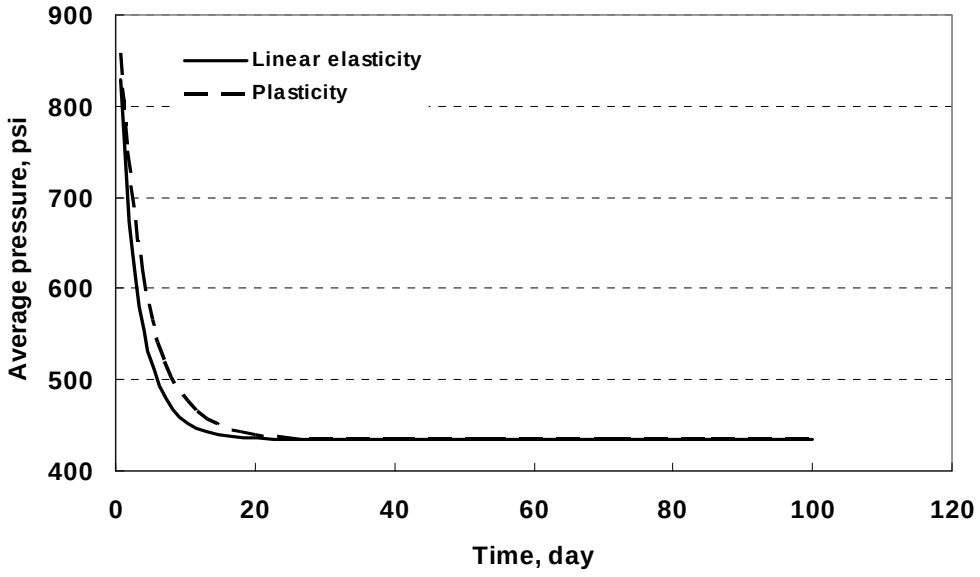

Figure 6-88: The average pressure from GPAS with geomechanics for Case 6.3.7.

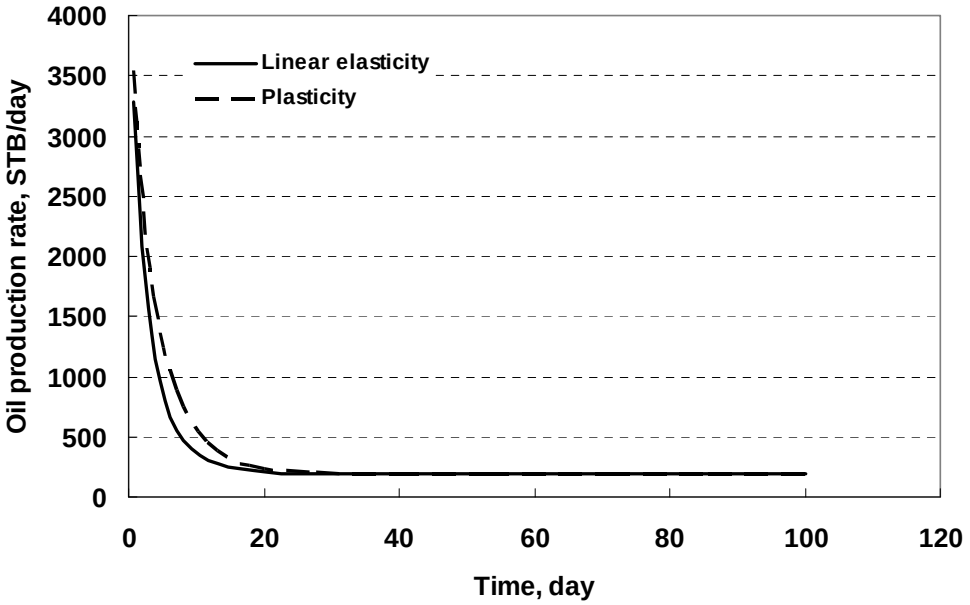

Figure 6-89: The oil production rate from GPAS with geomechanics for Case 6.3.7.

6.3.8 Gas Flooding with Six-Component Fluid Mixture

The SPE fifth comparative solution problem (Killough and Kossack, 1987) was simulated again in this section. All input data values are the same as Case 6.2.10.5, except 1000 psi BHP of the produce.

Figure 6-90 shows the strain versus the time curve. In the same production scenario, the nonlinear constitutive model with the friction angel (1 deg.) and the cohesion coefficient (20 kPa) gives more strain in z direction at first grid block (1, 1, 1). More compaction occurs within the reservoir, which defers the decrease of pressure and therefore results in a higher average pressure (Figure 6-91), an additional oil recovery (Figure 6-92), a higher oil production rate (Figure 6-93), and a little lower gas production rate (Figure 6-94).

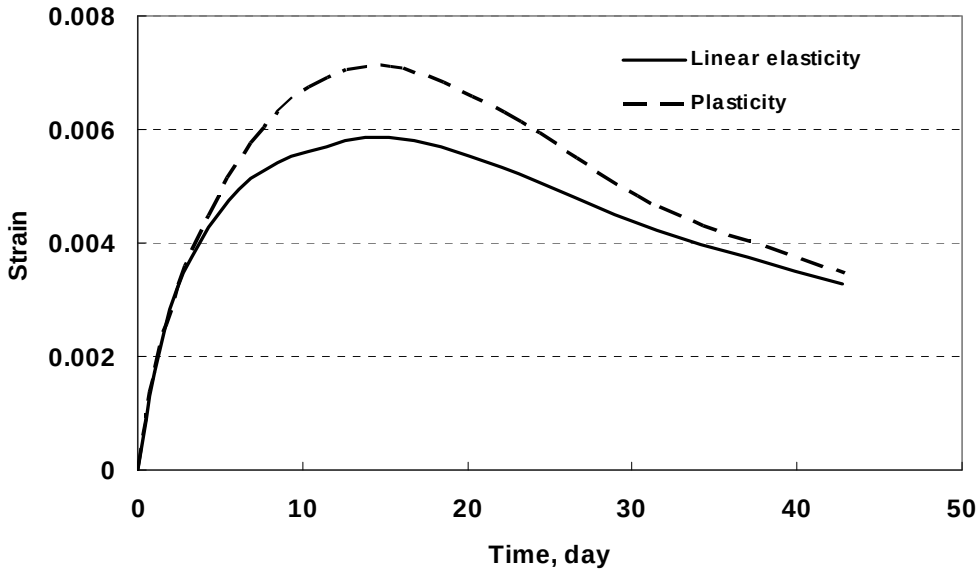

Figure 6-90: The strain in z direction of the first grid block (1, 1, 1) from GPAS with geomechanics for Case 6.3.8.

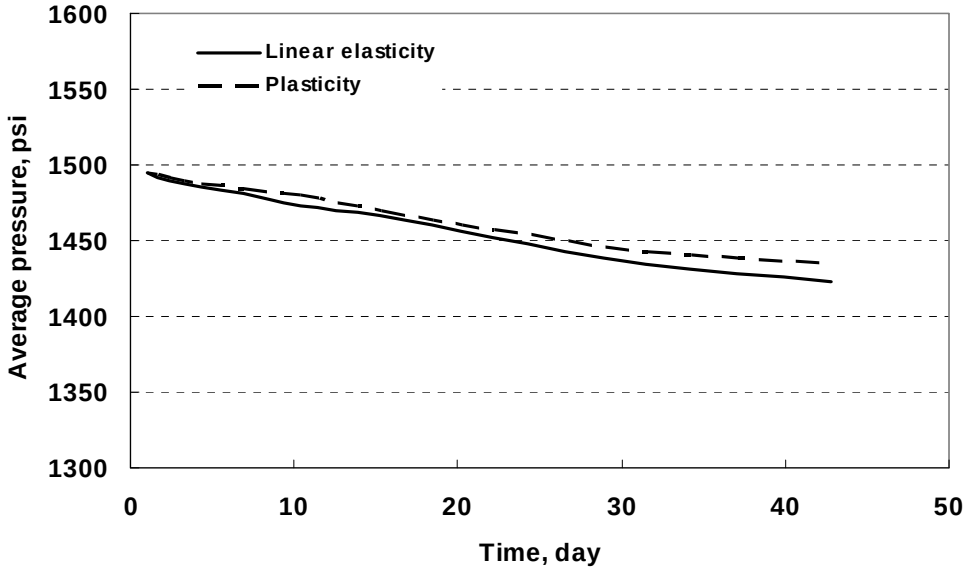

Figure 6-91: The average pressure from GPAS with geomechanics for Case 6.3.8.

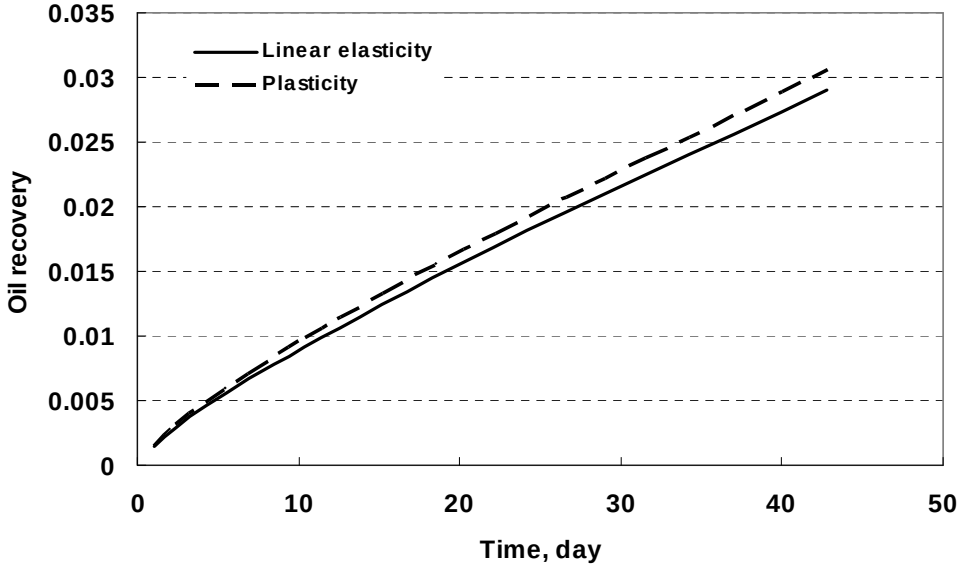

Figure 6-92: The oil recovery from GPAS with geomechanics for Case 6.3.8.

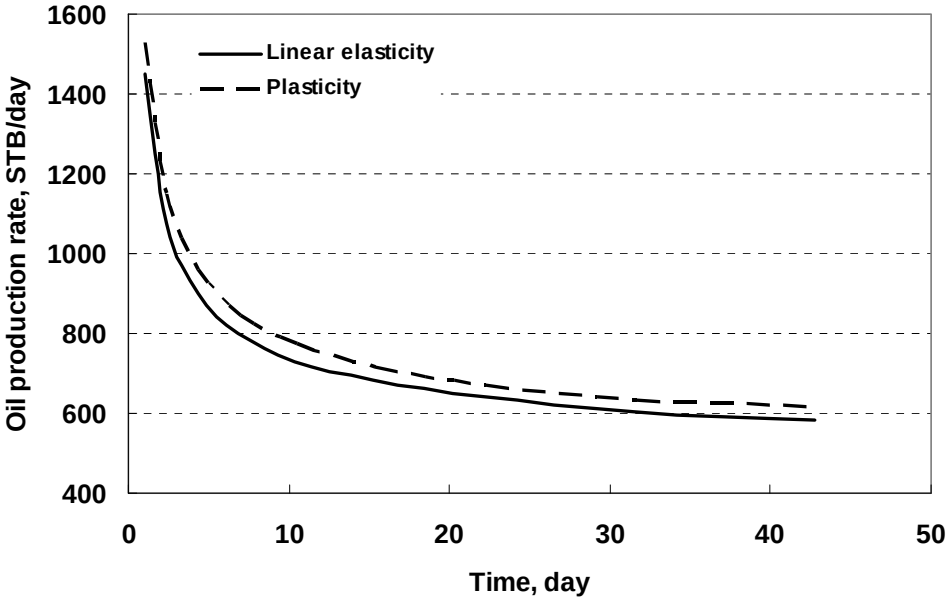

Figure 6-93: The oil production rate from GPAS with geomechanics for Case 6.3.8.

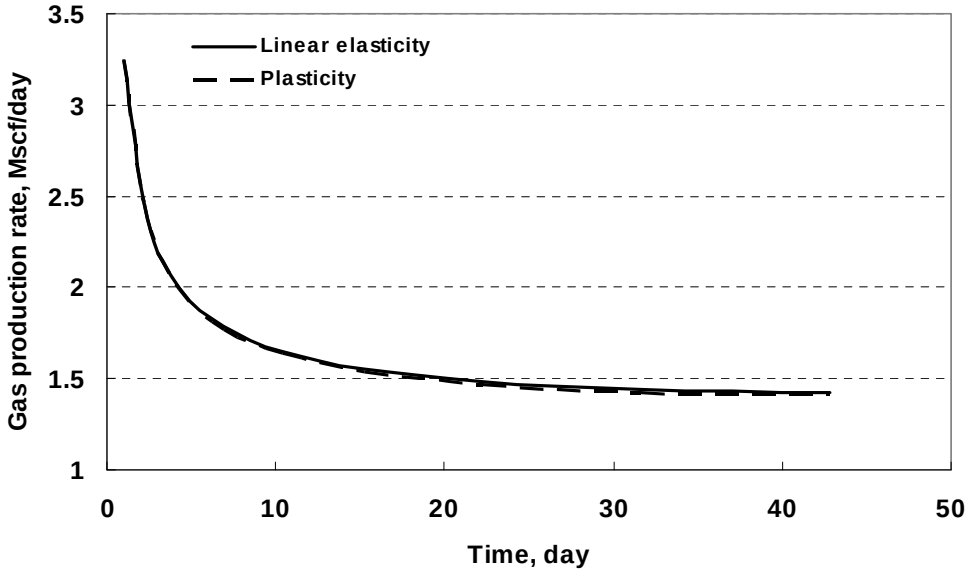

Figure 6-94: The gas production rate from GPAS with geomechanics for Case 6.3.8.

6.3.9 Water Flooding for Natural Fracture Reservoir

A modified version of Kazemi et al. (1976) quarter-five spot water flood was discussed in Case 6.2.10.6 of Section 6.2.10.6 using the linear elasticity constitutive model. This case will be remodeled using the Mohr-Coulomb constitutive model in the coupled geomechanics and GPAS. The material parameters are selected as the following: the friction angle = 3 deg. and the cohesion coefficient = 15 kPa.

Figure 6-95 and Figure 6-96 give the pressure distributions of the top layer at 0.1 day and 30 days. At 0.1 day, the two runs, the linear elasticity and the nonlinear plasticity predict the same pressure distributions. Accordingly, the two curves have the same start average pressure as shown in Figure 6-97. As the production continues and the plasticity deformation evolves, Figure 6-96 shows that the corresponding pressure distributions appear to be different. The plasticity model predicts a higher pressure than the linear elasticity model. For example, around the injector, the pressures from the plasticity model maintain above 3580 psi (Figure 6-96 (b)); while the pressures from elasticity model are below 3580 psi (Figure 6-96 (a)). Considering the grid pressure distribution at 30 days, the result from the plasticity model predicts more grids with the pressure between 3560 psi and 3580 psi. Therefore, the resulting average pressure from the linear elasticity model is lower than the pressure from plasticity model (Figure 6-97). The figure clearly shows that the inclusion of the plasticity compaction slows down the pressure depletion as expected. A higher oil recovery is obtained by the plasticity model, as shown in Figure 6-98.

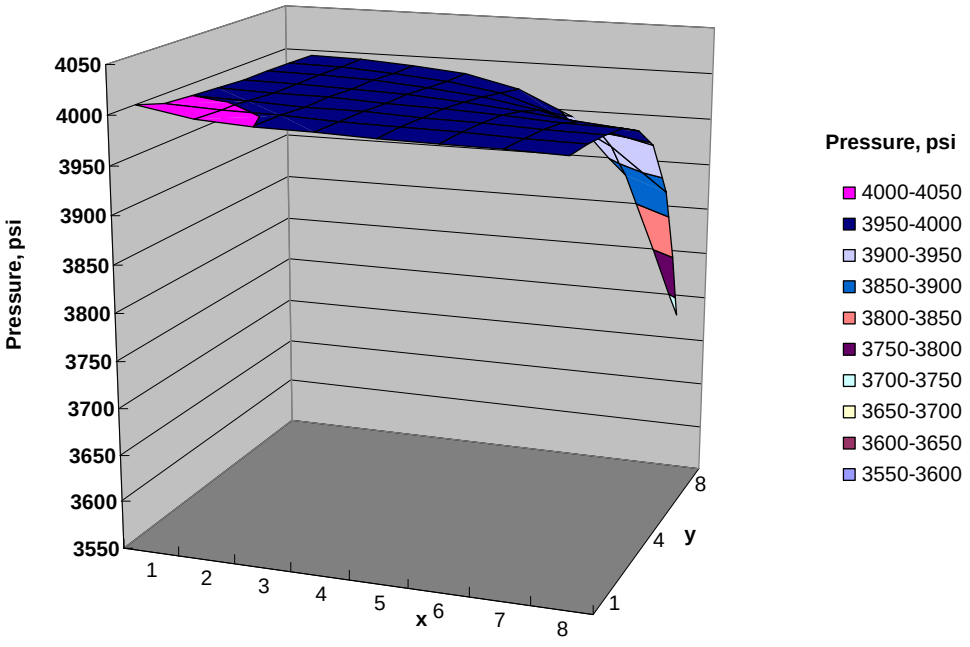

(a) Linear elasticity.

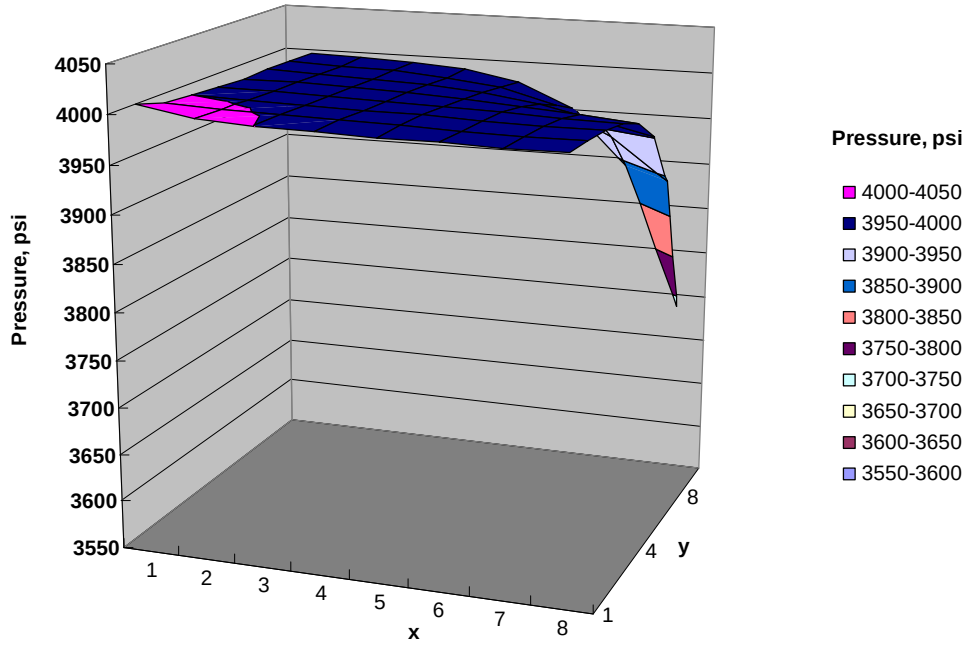

(b) Plasticity.

Figure 6-95: The pressure distribution (0.1 day) from GPAS with geomechanics for Case 6.3.9.

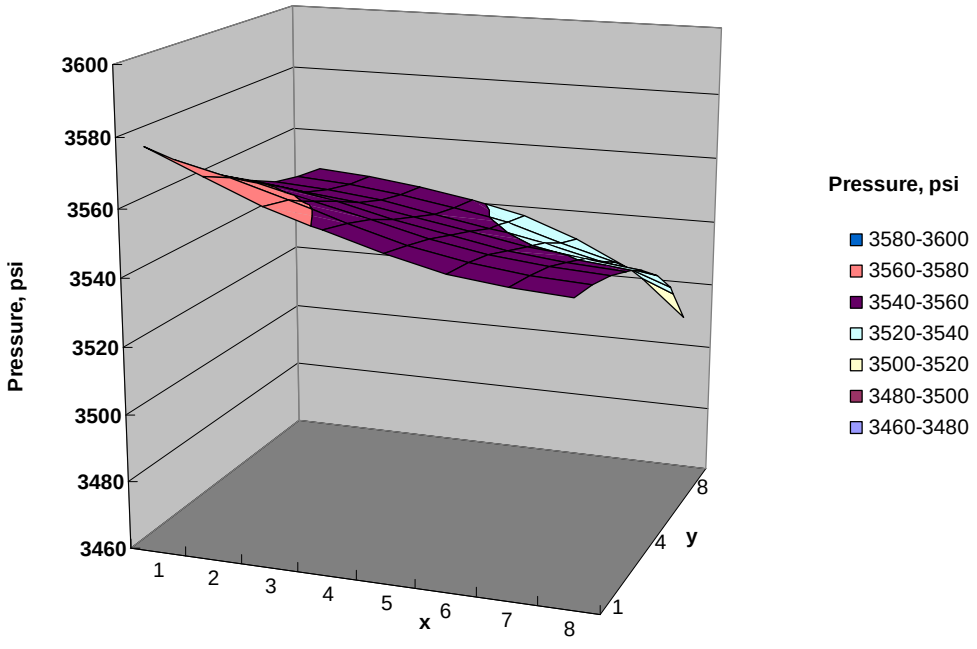

(a) Linear elasticity.

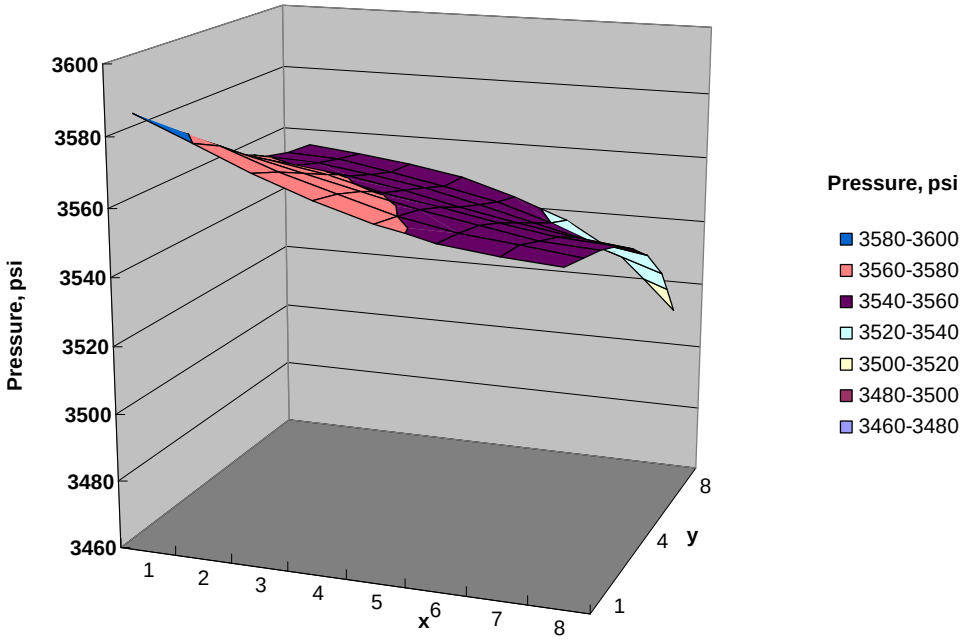

(b) Plasticity.

Figure 6-96: The pressure distribution (30 days) from GPAS with geomechanics for Case 6.3.9.

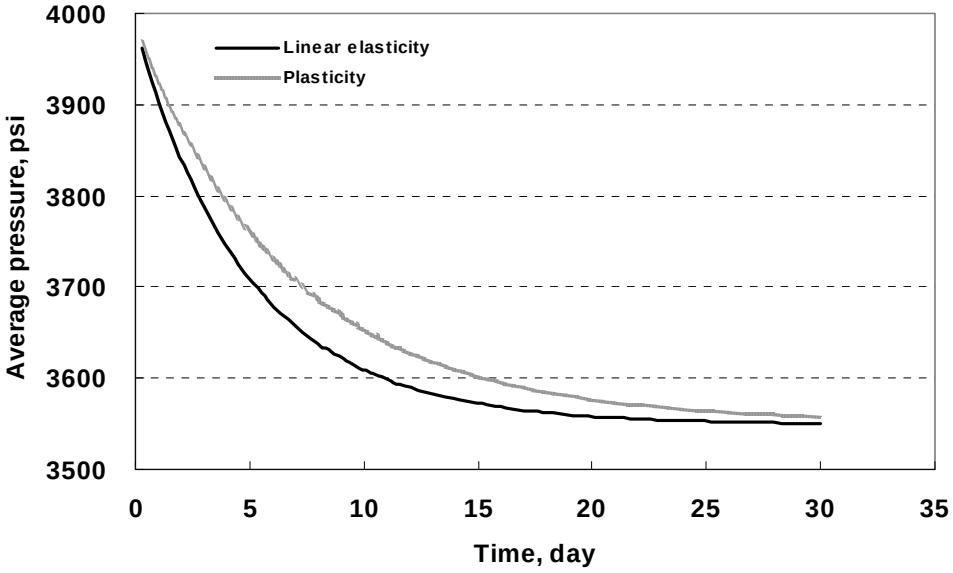

Figure 6-97: The average pressure from GPAS with geomechanics for Case 6.3.9.

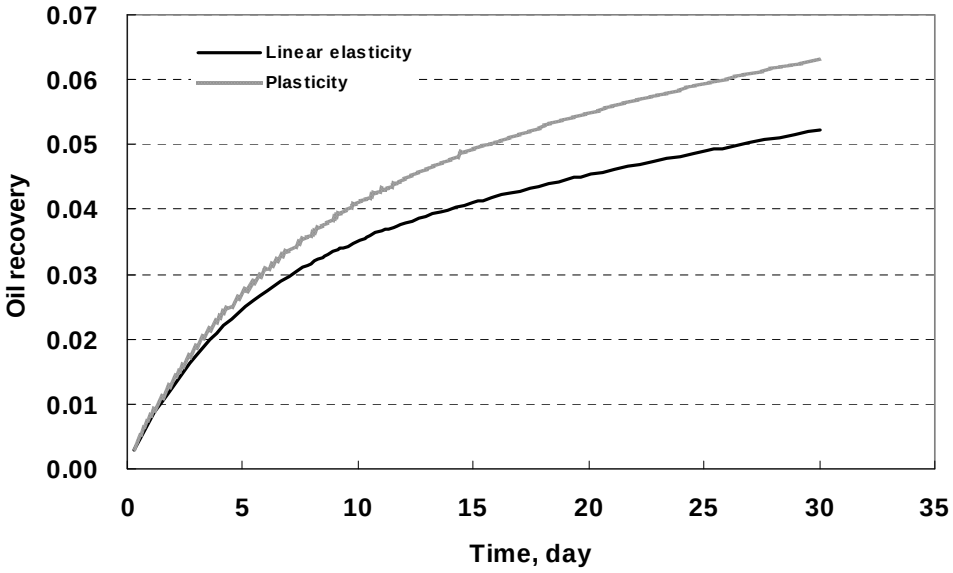

Figure 6-98: The oil recovery from GPAS with geomechanics for Case 6.3.9.

7 Comparisons of Fully and Iteratively Coupled Solution Procedures

In the last chapter, the fully coupled solution procedure and the iteratively coupled solution procedure in GPAS were verified using the cases with analytical solutions and the methods are also used to solve the coupled geomechanics and fluid-flow problems. Now, we are ready to compare the differences in detail of these two kinds for solution procedures for solving coupled geomechanics and reservoir problems.

7.1 DIFFERENCES OF IMPLEMENTATIONS

From the previous discussions and descriptions regarding the implementations of the fully coupled solution procedure and the iteratively coupled solution procedure in GPAS, it is clear that they are totally different implementations.

Figure 7-1 gives the whole idea for the associated flow charts. The differences of these two implementations are as the follows:

1. The fully coupled solution procedure based on Schur complement of geomechanics and GPAS is based on Newton iterations for each time-step. After calling the linear solver, the primary unknowns of the geomechanics model and the fluid-flow model are obtained simultaneously; this means that a 2×2 block Jacobian system is solved as one linear system. However, for the iteratively coupled solution procedure of geomechanics and GPAS, there is one Newton iteration lag between the primary unknowns of the geomechanics model and the fluid-flow model, because the two separate Jacobian systems, one for the geomechanics model and another for the fluid-flow model. The iteratively coupled solution procedure solves the two

Jacobian systems one by one and obtains the approximation of the original whole 2×2 block Jacobian system.

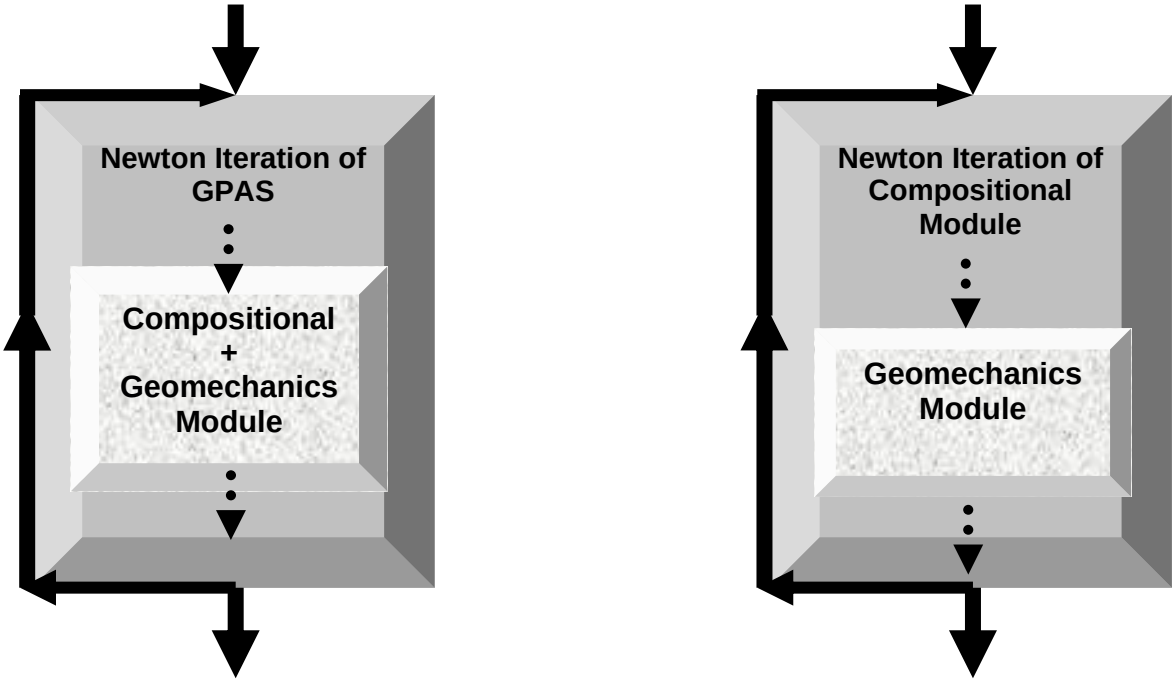

(a) Fully coupled geomechanics in GPAS

(b) Iteratively coupled geomechanics in GPAS

Figure 7-1: Comparison of the implementations of the fully coupled solution procedure and the iteratively coupled solution procedure.

2. From the mathematics point of view, the fully coupled solution procedure is equivalent to a block Gaussian elimination method with a similar convergence behavoir; however, there is not a unified convergence theory for the different implementations of the iteratively coupled solution procedure.
3. The implementation of the fully coupled solution procedure is more complicated comparing to the iteratively coupled solution procedure. The simplicity of the implementation is the main advantage of the iteratively

coupled solution procedure. Also, it can be integrated more easily with other physical models.

On the other hand, there are some common areas between these two solution procedures. Both methods

1. can be used with the current simulators in each field;
2. allow to utilize different numerical methods in each model: reservoir model (finite difference method), geomechanics model (finite element method);
3. adopt two-way communication coupling parameters, porosity and permeability;
4. can integrate with linear and nonlinear constitutive models.

7.2 COMPUTATIONAL COST ANALYSIS

The following 2×2 block Jacobian system (Equation (7-1)) can be solved using the iteratively and fully coupled solution procedures.

$$\begin{bmatrix} A_{11} & A_{12} \\ A_{21} & A_{22} \end{bmatrix} \begin{bmatrix} x_1 \\ x_2 \end{bmatrix} = \begin{bmatrix} b_1 \\ b_2 \end{bmatrix}, \tag{7-1}$$

where A_{11}, A_{12}, x_1 and b_1 are from the discretization of the geomechanics model, while A_{22}, A_{21}, x_2 and b_2 are from the discretization of the fluid-flow model; A_{12} and A_{21} are from the discretizations of the coupling terms.

First consider the iteratively coupled solution procedure, for each Newton iteration, A_{11}^{-1} and A_{22}^{-1}, will be solved alternatively. Of course, two matrix-by-vector products related to the matrixes A_{12} or A_{21} are required as well. The total elapsed time of all operations will be as follows:

$$Time_{iterative} = Time\left(A_{11}^{-1}\right) + Time\left(A_{22}^{-1}\right) + Time\left(A_{12}z\right) + Time\left(A_{21}z\right), \tag{7-2}$$

where $Time(*)$ is the estimated elapsed time for the algebraic operation $*$, and z refers to any vector whose size is compatible with associated matrix.

Now consider the fully coupled solution procedure through the Schur complement to solve Equation (7-1), the difference is that a Schur complement matrix associated with the y variable,

$$S = A_{22} - A_{21}A_{11}^{-1}A_{12}, \tag{7-3}$$

is solved instead of A_{22}. When a preconditioner, A_{22}^{-1}, is used for the Schur complement S, the total elapsed time of all operation will be estimated as the follows:

$$Time_{full} = Time\left(A_{11}^{-1}\right) + 2Time\left(A_{22}^{-1}\right) + 2Time\left(A_{11}^{-1}\right) + Time\left(A_{12}z\right) + Time\left(A_{21}z\right), \tag{7-4}$$

where 2 appears in Equation (7-4) because Bi-CGstab (l) solver is used for solving the above Schur complement and two matrix-by-vector products are required.

Hence, the ratio (RT) of the time of the iteratively coupled solution procedure and the fully coupled solution procedure can be estimated ignoring the coupling-matrix (A_{12} or A_{21})-vector products as

$$RT \equiv \frac{Time_{full}}{Time_{iterative}} \approx \frac{Time\left(A_{11}^{-1}\right) + 2Time\left(A_{22}^{-1}\right) + 2Time\left(A_{11}^{-1}\right)}{Time\left(A_{11}^{-1}\right) + Time\left(A_{22}^{-1}\right)}; \tag{7-5}$$

when $Time\left(A_{11}^{-1}\right)$ and $Time\left(A_{22}^{-1}\right)$ are assumed to be approximately equal, the following estimation can be obtained:

$$RT \equiv \frac{Time_{full}}{Time_{iterative}} \approx 2.5 \tag{7-6}$$

In fact, the above estimate is a lower one because the Schur complement matrix is a full matrix and is generally difficult to be solved even though $\boldsymbol{A_{11}}$ and $\boldsymbol{A_{22}}$ are all sparse matrixes. Hence, for individual cases, the ratio (RT) maybe a little bigger than 2.5, as shown in Table 7-7.

7.3 COMPARISON CRITERIA

For a fairness of comparison between the iteratively coupled solution procedure and the fully coupled solution procedure, the simulation results from the two solution procedures are checked in order to make sure that the following quantities are in agreement using both procedures:

1. size of time-steps;
2. for each time-step,
    a) oil recovery,
    b) average pressure of whole reservoir,
    c) pressure distribution,
    d) displacement distribution.

7.4 CASE STUDIES

Two cases are designed and simulated using both the fully coupled solution procedure and the iteratively coupled solution procedure in GPAS.

The first case is designed to test the coupled code for 3D problems with one-component (C_{10}) reservoir fluids. The reservoir size has a volume of 200 x 200 x200 ft^3, which is discretized into a 2 x 8 x 4 grid mesh. For the fluid-flow model, the no-flow boundaries are applied to all the sides and two producers are drilled at (x=50 ft, y=175 ft) and (x=150 ft, y=175 ft) through all the layers. For the solid deformation model, a constant overburden stress (6000 psi) is applied on the top the reservoir, which is discretized into 64 20-node brick (hexahedral) elements. Young module is 9.09 x 10^6 kPa, and Poisson ratio is 0.3. Other input data values are listed in Table 7-1.

The second case simulates a reservoir with three components, C_{10}, C_{15}, and C_{20} with the initial compositions, 0.5, 0.25, and 0.25, respectively. A 2 x 20 x 20 grid is used to discretize the reservoir domain. It has the same boundary condition and

producer locations as the first case. Again, for the solid deformation model, a constant overburden stress (6000 psi) is applied on the top the reservoir. Other input data values are shown in Table 7-2. The critical properties of the 3-component fluid are presented in Table 7-3; and the relative permeability data values are given in Table 6-20. For the geomechanics model, there are a total of 800 20-node brick (hexahedral) elements. The total number of equations of geomechanics model is about 13,000, while the total number of equations of fluid-flow is 6,400. Hence, the total number of unknowns for this case is close to 20,000.

Table 7-1: Summary of input data for Case 7.4.1

	Parameter	Value
Reservoir model	Length (ft) x Width (ft) x Thickness (ft)	200 x 200 x 200
	Number of gridblocks	2 x 8 x 4
	Gridblock size (ft^3)	100 x 25 x 50
	Porosity	0.35
	Permeability (x,y,z) (md)	10, 10, 10
	Rock compressibility (psi^{-1})	0
	Fluid compressibility (psi^{-1})	$3.0x10^{-6}$
	Initial water saturation	0.17
	Water viscosity (cp)	1
	Water density (lb/ft^3)	62.343
	Initial pressure (psi)	6000
	Producer (BHP)	500
Geomechanics model	Number of elements	2 x 8 x 4
	Element type	20-node brick
	Element size (m^3)	30.47 x 3.04 x 3.04
	Young's modulus (kPa)	$9.09x10^6$
	Poisson's ratio	0.3

Table 7-2: Summary of input data for Case 7.4.2

	Parameter	Value
Reservoir model	Length (ft) x Width (ft) x Thickness (ft)	200 x 200 x 200
	Number of gridblocks	2 x 20 x 20
	Gridblock size (ft^3)	100 x 10 x 10
	Porosity	0.35
	Permeability (x,y,z) (md)	10, 10, 10
	Rock compressibility (psi^{-1})	0
	Fluid compressibility (psi^{-1})	$3.0x10^{-6}$
	Initial water saturation	0.17
	Water viscosity (cp)	1
	Water density (lb/ft^3)	62.343
	Initial pressure (psi)	6000
	Producer (BHP)	500
Geomechanics model	Number of elements	2 x 20 x 20
	Element type	20-node brick
	Element size (m^3)	30.47 x 3.04 x 3.04
	Young's modulus (kPa)	$9.09x10^6$
	Poisson's ratio	0.3

Table 7-3: Initial composition and associated critical properties

Component	T_c (^oR)	P_c (psi)	V_c (ft^3/lb-mole)	MW_i (lbm/lb-mole)	Mole percent
C_{10}	1111.8	304.0	10.087	142.3	0.5
C_{15}	1270.0	200.0	16.696	206.0	0.25
C_{20}	1380.0	162.0	21.484	282.0	0.25

Table 7-4: Relative permeability data

	Water	Oil	Gas
Endpoint	0.4	0.9	0.9
Residual saturation	0.3	0.1	0.0
Exponent	3.0	2.0	2.0

7.4.1 Fully Coupled Solution Procedure

For the fully coupled solution procedure, there are two loops; one is for the Schur complement system corresponding to the convergence tolerance TOLA, anther is for the A_{11} local system corresponding to the convergence tolerance TOLB. The combination of TOLA and TOLB critically affects the converge behavior of the solution of Jacobian systems and the computational time of the code.

The sensitivity tests are performed for both cases, as shown in Table 7-5. As expected, the computational time is decreasing as the looser tolerances are used. When TOLA and TOLB is set to 10^{-3} and 10^{-6}, the residuals of the iteration process become oscillatory and cannot convergence to the solution within the limit of iteration. In other words, for this case, a good combination of TOLA and TOLB is 10^{-3} and 10^{-8}, which gives a 176-second computational time.

For Case 7.4.2, a similar numerical experiment is conducted to find a good combination of TOLA and TOLB is 10^{-4} and 10^{-14} which gives a 19123-second computational time.

Note that adjustments of TOLA and TOLB in the above numerical experiments do not affect the final converged solutions, which means that the criteria in Section 7.3 are all satisfied. The results of experiments show that the different combination of TOLA and TOLB does effect the execution time of the code of the fully coupled solution

procedure in GPAS, up to 3~4 times as seen in Table 7-5. During the numerical tests, a rule of thumb is used that the outer loop tolerance (TOLA) is always looser than the inner loop tolerance (TOLB) to avoid the divergence or non-physical solutions.

Table 7-5: Summary of CPU time of the fully coupled solution procedure

	TOLA	TOLB	CPU time (sec.)
Case 7.4.1	10^{-10}	10^{-16}	770
	10^{-6}	10^{-10}	357
	10^{-5}	10^{-7}	275
	10^{-4}	10^{-8}	179
	10^{-3}	10^{-10}	241
	10^{-3}	10^{-8}	176
	10^{-3}	10^{-6}	oscillatory sol.
Case 7.4.2	10^{-10}	10^{-16}	72223
	10^{-4}	10^{-14}	19123
	10^{-4}	10^{-10}	oscillatory sol.
	10^{-4}	10^{-8}	oscillatory sol.

7.4.2 Iteratively Coupled Solution Procedure

For the iteratively coupled solution procedure in GPAS, there is one converge tolerance for geomechanics module, noted as TOLD. The adjustment of TOLD is performed to optimize the elapsed CPU time of the coupled code. Because the iteratively coupled procedure is not as strongly coupled as the fully coupled solution procedure, the tolerance TOLD is tighter than the ones for TOLB of the fully coupled solution procedure. The loose TOLD will result the variations in time-steps, the

maximum Newton iterations or different pressure distributions, which do not satisfy the criteria in Section 7.3. The associated results are not considered as a candidate to be compared with results from the fully coupled solution procedure.

Table 7-6: Summary of CPU time of the iteratively coupled solution procedure

	TOLD	CPU time (sec.)
Case 7.4.1	10^{-16}	110
	10^{-8}	52
	10^{-6}	Time-steps changed and the max Newton iteration limit arrived.
Case 7.4.2	10^{-16}	5515
	10^{-14}	Pressure distribution is different.
	10^{-8}	The max Newton iteration limit reached; Pressure distribution is different.

7.4.3 Comparison Results

Based on the results in Sections 7.4.1 and 7.4.2, a summary of the elapsed CPU time for the two coupling solution procedures is listed in Table 7-7.

Table 7-7: Comparison of CPU time of the fully coupled solution procedure and the iteratively coupled solution procedure

	CPU time (sec.)		Ratio (*RT*)
	Iteratively coupling	Fully coupling	Fully / Iteratively
Case 7.4.1	52	176	3.3
Case 7.4.2	5515	19123	3.4

For Case 7.4.2, the results corresponding to the tests in Table 7-7 are analyzed according the criteria of comparison in Section 7.3. "Fully coupling (A)" refers to the numerical test of the fully coupled code, which uses the combination of TOLA = 10^{-10} and TOLB = 10^{-16} and gives a 72,223-second elapsed CPU time. "Fully coupling (B)" refers to the numerical test of the fully coupled code, which uses the combination of TOLA = 10^{-4} and TOLB = 10^{-14} and gives a 19,123-second elapsed CPU time. "Iteratively coupling (A)" refers to the numerical test of the iteratively coupling code, which uses the combination of TOLD = 10^{-16} and gives a 5,515-second elapsed CPU time. The variations of time-steps are shown in Figure 7-2. Figure 7-3 and Figure 7-4 compares the oil recovery and the average pressure of the reservoir with time. The pressure distributions as a function time are shown in Figure 7-5, Figure 7-6, and Figure 7-7, from which similar trend can be found. The pressure difference between two solution procedures is two psi at most for the case. The displacement distributions in y and z directions are compared for two time-steps, as given in Figure 7-8. All the above figures show that the comparison criteria in Section 7.3 are satisfied; hence the associated comparison results as shown in Table 7-7 are justified.

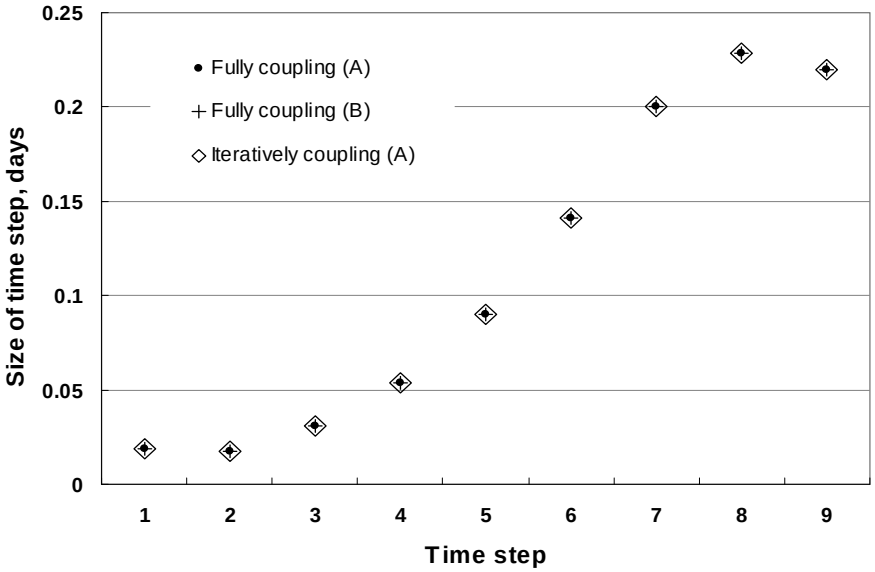

Figure 7-2: Comparison of time-step sizes for the fully coupled solution procedure and the iteratively coupled solution procedure.

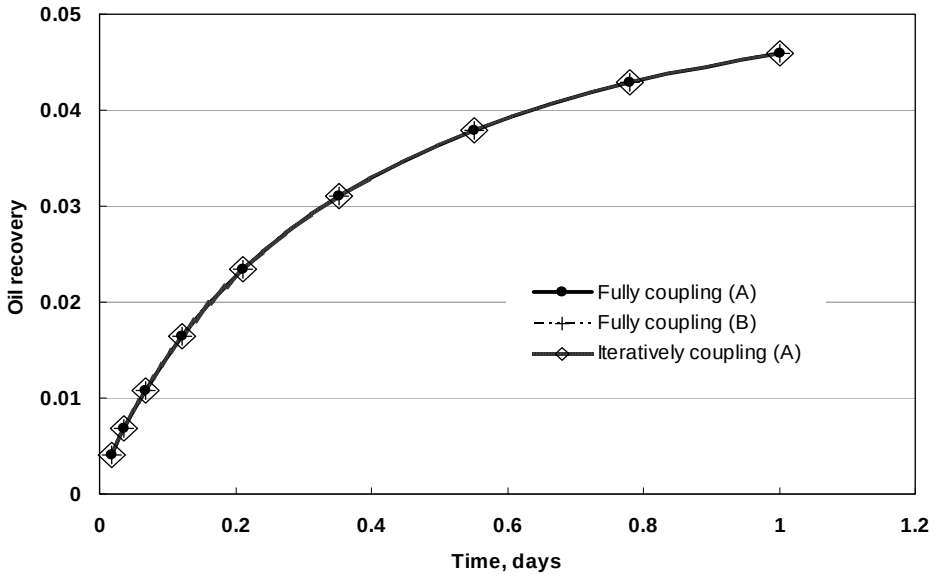

Figure 7-3: Comparison of oil recovery for the fully coupled solution procedure and the iteratively coupled solution procedure.

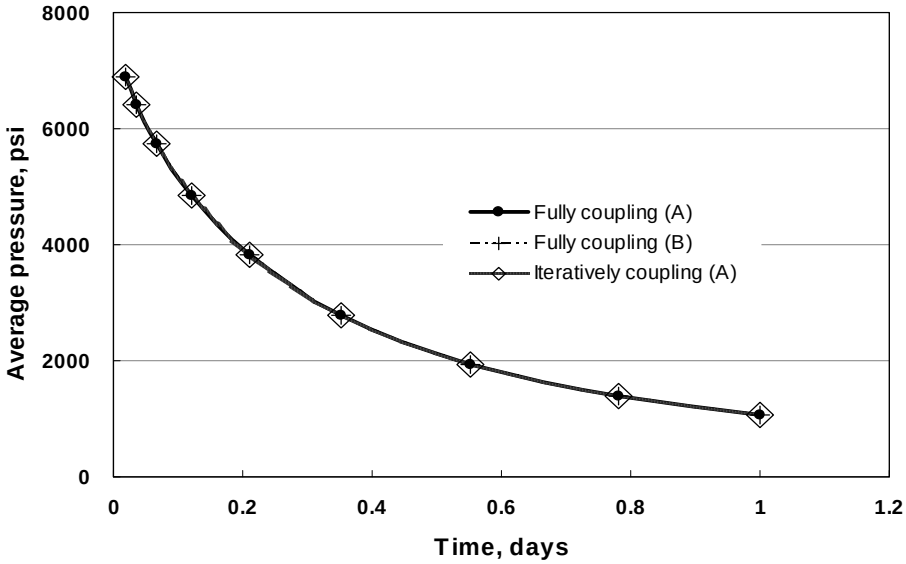

Figure 7-4: Comparison of average pressure for the fully coupled solution procedure and the iteratively coupled solution procedure.

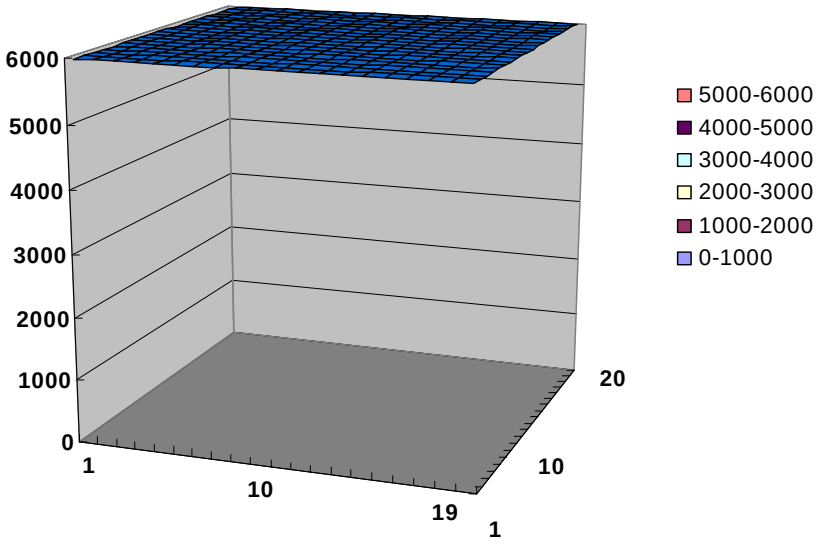

(a) The fully coupled solution procedure.

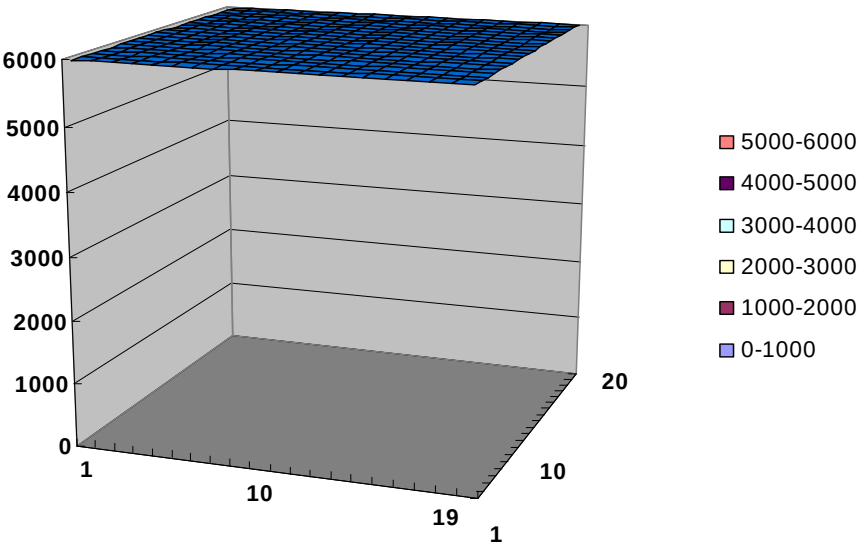

(b) The iteratively coupled solution procedure.

Figure 7-5: Comparison of pressure (psi) distributions at (x = 50 ft, y, z) and at time = 0 day.

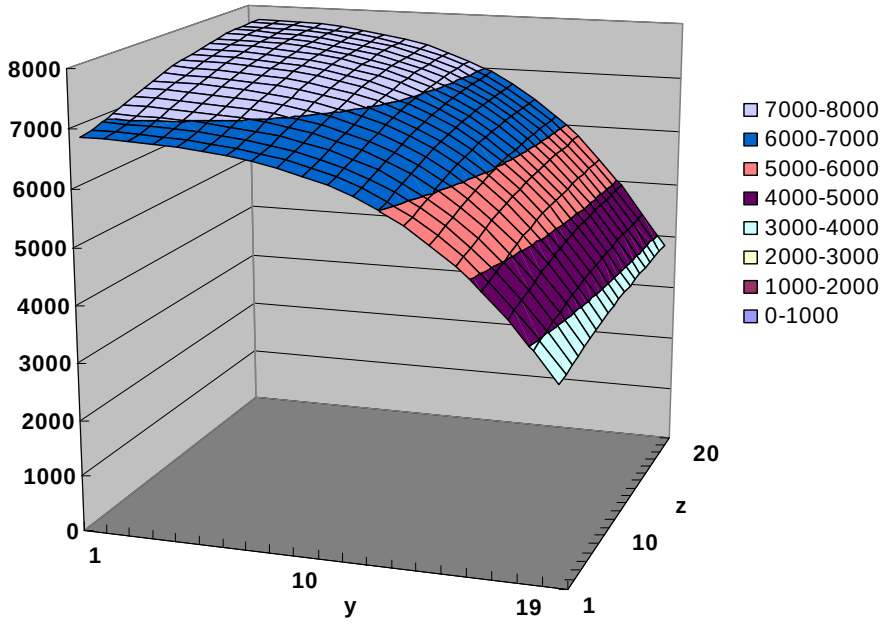

(a) The fully coupled solution procedure.

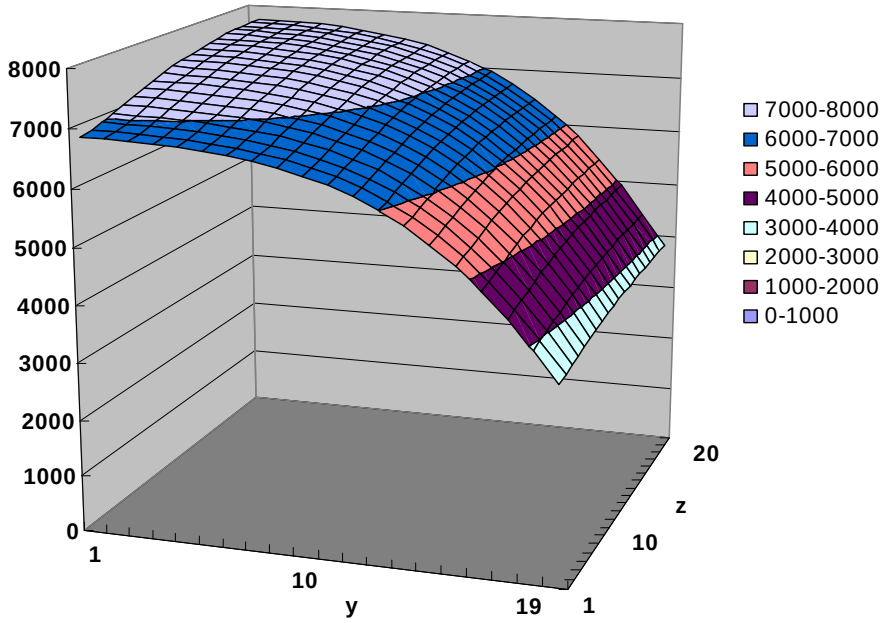

(b) The iteratively coupled solution procedure.

Figure 7-6: Comparison of pressure (psi) distributions at (x = 50 ft, y, z) and at time = 0.036 day.

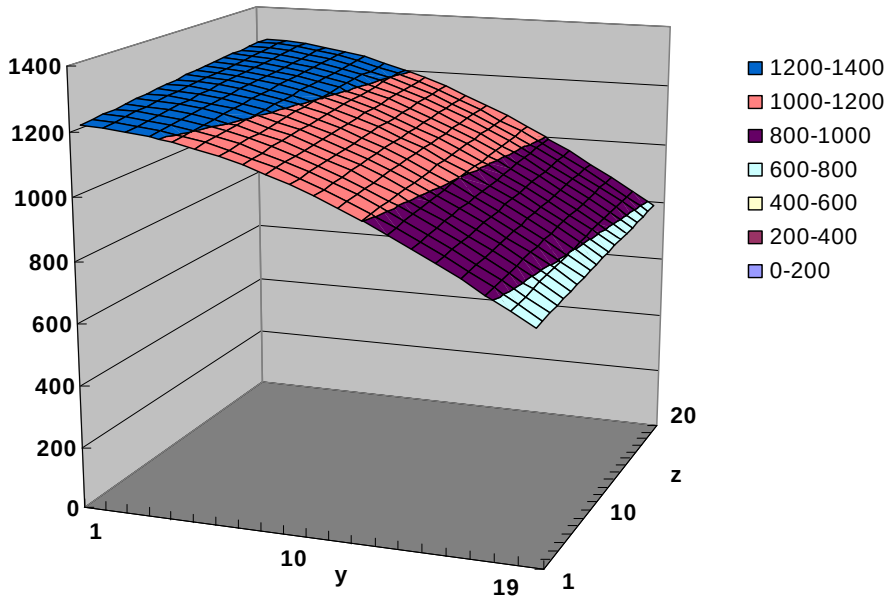

(a) The fully coupled solution procedure.

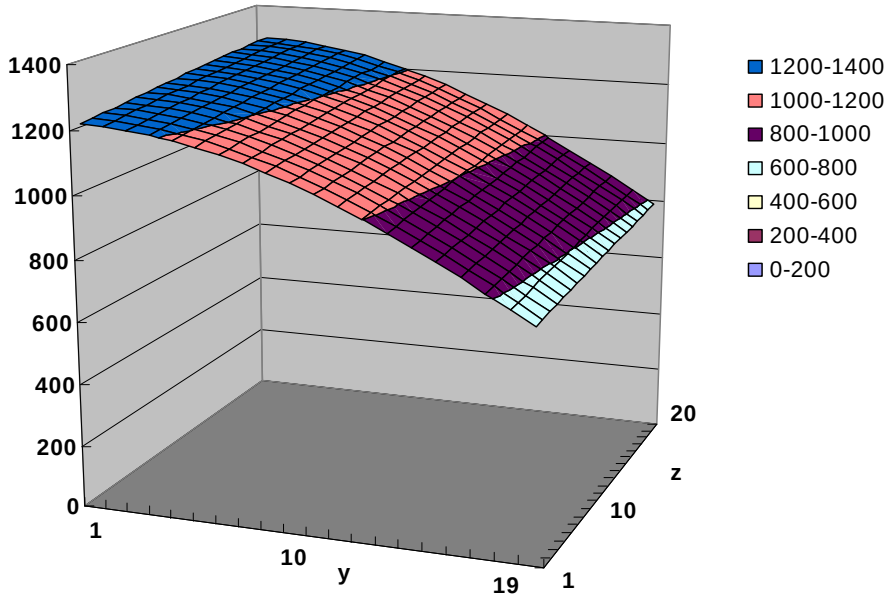

(b) The iteratively coupled solution procedure.

Figure 7-7: Comparison of pressure (psi) distributions at (x = 50 ft, y, z) and at time = 1.0 day.

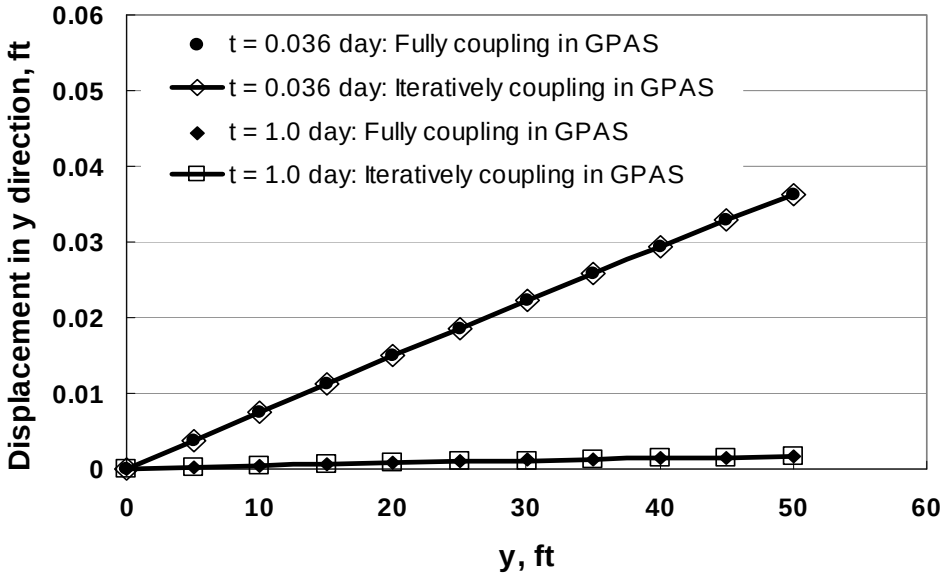

(a) The displacements in y direction.

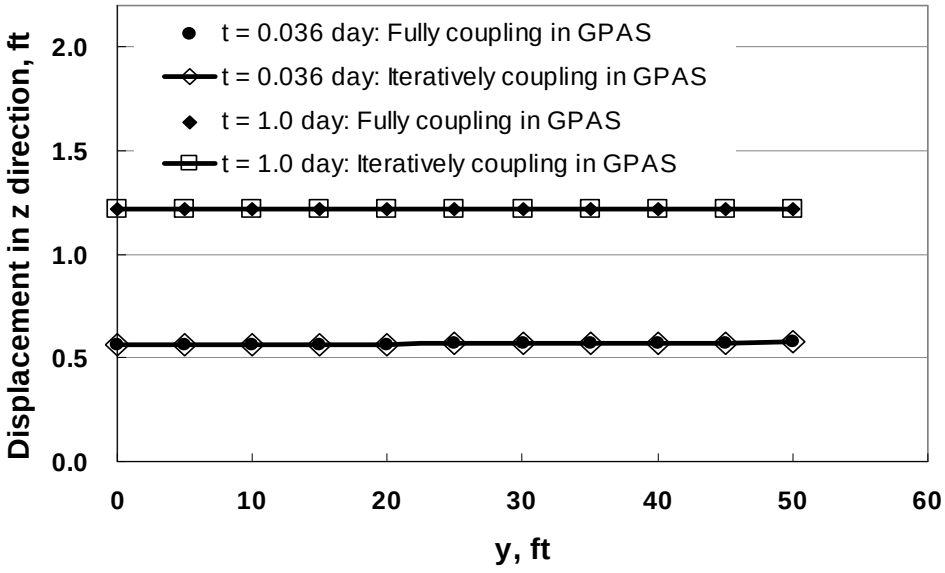

(b) The displacements in z direction.

Figure 7-8: Comparison of displacements at $(x = 0, 0 \le y \le 50, z = 0)$ and at time = 0.036 day and 1.0 day.

8 Parallelization of the Geomechanics Module

The parallelization of a finite element code is more complicated than that of a finite volume / difference method or a control volume code. One reason is that, for the former, more than one kind of the global arrays are defined and used in its implementation. However, for the later, only one kind of the global array regarding grid blocks is used in its computation. Hence, the associated partition algorithm for a finite volume / difference method or a control volume method is simpler than one for a finite element method.

In this chapter, a general parallel framework for the finite element method is presented and the geomechanics module is parallelized using this parallel framework.

8.1 Review of Parallelization for a Finite Element Method

In general, a finite element application can be divided into three modules: (1) preprocessing (mesh generation); (2) solution process; (3) post-processing. The solution processing can be subdivided into two kinds: (1) the one in which a global stiffness matrix is assembled; (2) the one in which a global system matrix is never formed, i.e., the element by element method.

8.1.1 Element-By-Element (EBE) Implementation

The element-by-element concept was firstly proposed by Hughes et al. (1983). The concept is designed to avoid the large-scale storage related to an assembled global stiffness matrix. In other words, the coefficient matrix will not be formed explicitly but implicitly. There are two kinds of applications using this EBE concept: (1) to construct the approximation of the global stiffness matrix through a series of full, element-based

local stiffness matrixes; (2) to employ the EBE concept in the Krylov subspace iterative solver, such as, CG, GMRES, BiCGstab(l) with or without preconditioners. The major operation in these kinds of solvers is the matrix-by-vector product, which can be evaluated through the dense, small matrices at the element level. In the following sections, the second approach will be employed in the general parallel framework for the finite element geomechanics code.

Hughes (2003) also pointed out that if elements are divided into noncontiguous subsets, the above matrix-by-vector product is parallelizable in nature, as shown in Figure 8-1. If the order of computations does not affect the final result, the same value will be obtained for both the sequential code and the parallel code based on EBE concept. Of course, there is no free lunch, and one of shortcomings of EBE implementation is that it is more difficult than the assembled FEM implementation to find a parallel, effective preconditioner for the Krylov subspace iterative solver.

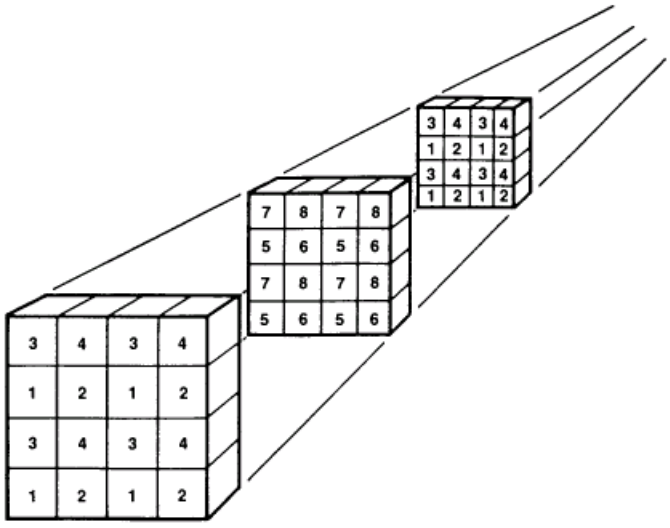

Figure 8-1: Decomposition of three-dimensional domain into three groups of brick elements for parallel processing (after Hughes 2003).

In other words, the key point of EBE implementation is the following:

$$Ap_m = \sum_{iele=1}^{nele} \left(A^{iele} \tilde{p}_m \right) \tag{8-1}$$

where A and p_m denotes as the global stiffness matrix and the associated global vector respectively, A^{iele} is the element stiffness matrix and $\tilde{p}_m$ is the local element vector mapped from p_m.

8.1.2 A General Parallelization Strategy: DDM

It is well-known that the Domain Decomposition Method (DDM), (Smith et al. 1996) is a general solution to the parallelization of a serial code. There are two kinds of algorithms using the domain decomposition method. One is a serial implementation in nature; for example, a matrix-vector product can be performed in parallel. Another is a parallel algorithm developed to a parallel computer platform, for instance, parallel non-overlapping or overlapping Schwartz type linear solvers. In other words, the parallel algorithm is totally different from the associated serial one. Some researchers, for example, Margetts (2002), have discussed this difference.

8.1.3 A Parallel Framework of FEM

Smith and his group investigated the general strategy of parallelization of a sequential finite element code. They highlighted the strategy using the EBE concept with the combination of MPI (Pettipher and Smith 1997; Smith 2000). And their in-house parallel finite element program has been employed for different applications, such as elastoplastic geomechanics material behaviors (Pettipher and Smith 1997), the coupled magnethohydrodynamic fluid-flow (Margetts 2002), the nuclear reaction pressure vessels (Margetts et al. 2006), and solution to the incompressible Navier Stokes equations. Hence, Smith and Pettipher's parallelization strategy is adopted to parallelize the coupled geomechanics and fluid-flow code in GPAS.

8.2 PARALLELIZING AN EBE IMPLEMENTATION

In this dissertation, the element by element (EBE) finite element implementation is coded and parallelized. Some parallel subroutines are directly reused from the parallel library of Smith's group (Margetts 2002). Other additional subroutines related to coupled the geomechanics and GPAS are coded by the author.

8.2.1 Partition the Global Arrays

The parallelization in this work is achieved by SPMD (Single Program, Multiple Data) programming mode using MPI, which means that each processor has its own copy of program and private memory. The SPMD using MPI is related to the distributed memory high-performance computers, which consist of independent computing nodes except the I/O server. When SPMD is selected to parallelize a serial code, its global arrays have to be distributed among the processors as evenly as possible to keep a good load balance among processors. During the computing process, necessary synchronizations have to be done for these global arrays. Note that the above synchronizations should be optimized to minimize the communication among the processors.

After reviewing the serial EBE finite element code, three kinds of global arrays have to be distributed among the processors: (1) Element-based arrays, (2) Equation-based arrays, and (3) node-based arrays. The following subsections will present how to distribute these three kinds of arrays as equally as possible.

8.2.1.1 Partition Elements

In a serial code of the finite element method, one of typical structures is the element-based loop. Within the loop, the element-based arrays involve to perform some calculations, for instance, to evaluate element stiffness matrixes. In order to parallelize

theses element-based loops, the associated element-based global arrays have to be partitioned among the processors.

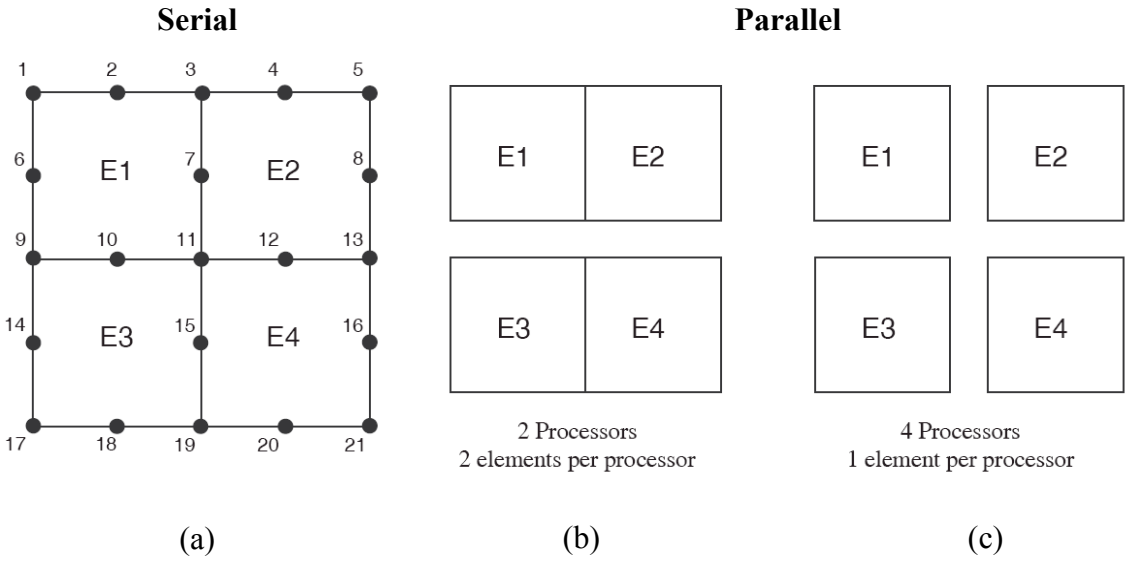

Figure 8-2: An example of distributing elements among processors (after Margetts 2003).

Figure 8-2(a) shows that a simple problem with a four-element domain which can be solved using a serial program; also it is possible to solve the same problem using two processors or four processors in parallel. Hence, the original domain with four elements can be divided into two subdomains, each of which has two elements, as shown in Figure 8-2(b); of course, the problem also can be solved using four processors and each of four subdomains has only one element as seen in Figure 8-2(c). As a result, all element stiffness matrixes have been divided among the processor and the associated matrix-by-vector can be performed in parallel, which is the key feature of EBE.

8.2.1.2 Partition Equations / Freedoms

There is another kind of global arrays in a finite element program, which length is related to the total number of freedoms or equations. The heart of the code is to obtain the approximation of primary unknown physical parameter at these discretized locations. Figure 8-3 gives an example with four element and totally 24 equations / freedoms. These 24 equations will be solved for primary unknowns, the displacements (u,v) at nodes. "0" in Figure 8-3 is noted as the knowns from the boundary conditions.

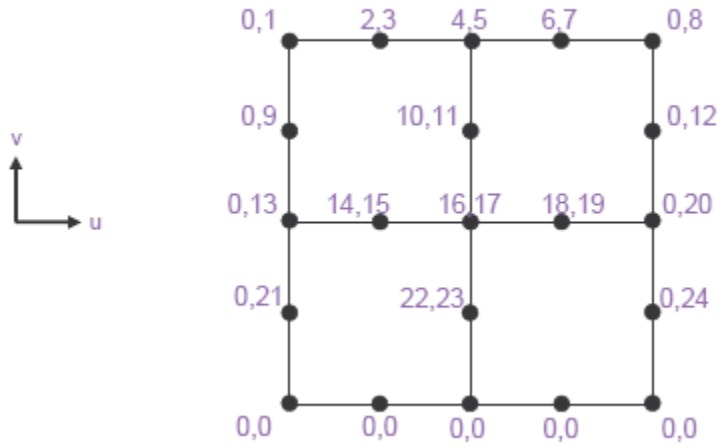

Figure 8-3: Equations ordering of a two-dimensional example (after Margetts et al. 2006).

In the current implementation, the equations are divided among processor without overlapping. There are no duplicated pseudo boundaries among the processors, which guarantee that the global equation-based arrays can be evenly distributed for a good memory balance.

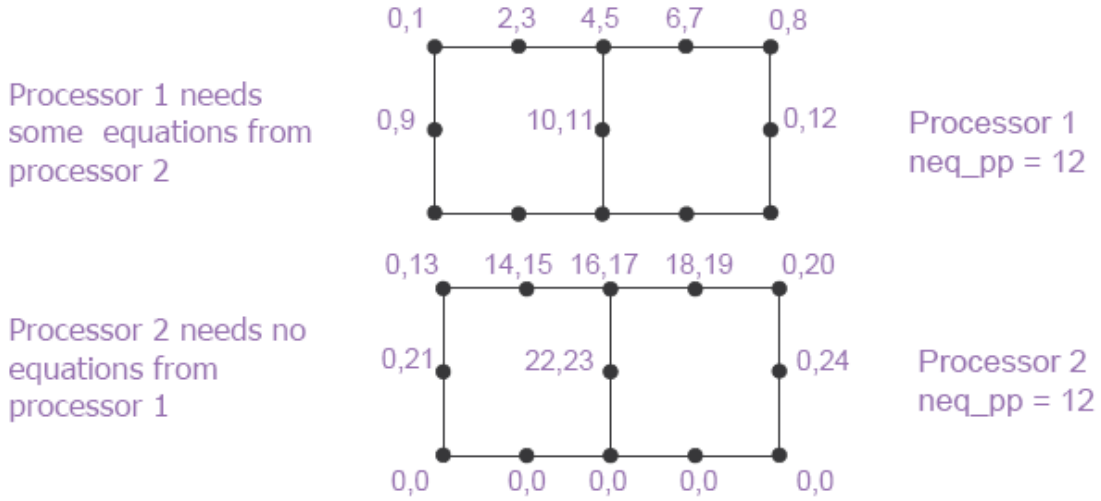

Figure 8-4: Evenly distributing equations between two processors (after Margetts et al. 2006).

As shown in Figure 8-4, for a two-processor case, after partitioning, each of them owns 12 equations equally. Note that Processor 1 sometimes needs the information at freedoms (13, 14, 15, 16, 17, 18, 19, 20) to complete the calculations related to Elements 1 and 2; so communication between Processors 1 and 2 is needed.

8.2.1.3 Adjust Nodes-based Array

Sometimes, a kind of node-based arrays is used in the finite element code. For example, the coordinate array of the nodes, the steering array of the nodes, etc. All the above arrays are modified to add another dimension, element index. Therefore, they are divided with the elements among processors. The freedom array of the nodes (which stores the boundary conditions) only focuses on boundary nodes, which length is far smaller than the total number of nodes. It is not an issue for a large-scale simulation.

Hence, after partitioning the elements, equations, and nodes among the processors, the following changes will be completed:

1. Memory localization: The large memory storage of an element-based, global array is divided by the number of the processors. The decreased memory requirement of each processor can be satisfied by the local memory at a computing node of a high performance computer. In other words, the total memory requirement in a serial code can be distributed among all the processors as evenly as possible. Hence, it is possible to simulate a large-scale problem using a parallel code.
2. Computation localization: this is the main reason why a parallel code can save CPU elapsed time comparing to the serial code and obtain a speedup.
3. I/O localization: a parallel I/O can be performed by each processor based on the local disk storage or the parallel file system.

8.3 BASIC OPERATIONS

An important observation is that there are two kinds of basic operations in an implementation of Krylov subspace solver, for example, BiCGstab(l). One is the dot-product; another is the matrix-by-vector product. Now, the parallelization of these two operations will be discussed in the following sections.

8.3.1 Dot-Product

It is very easy to perform a dot-product for two sets of distributed vectors using the intrinsic MPI procedure, MPI_ALLREDUCE with SUM option. The local dot-product is conducted for each processor, a sum operation is done by the master processor, and then the sum is broadcasted to all other processors.

8.3.2 Matrix-by-Vector Product

The parallelization of the matrix-by-vector is highly related to the divisions of the elements, the equations and the nodes.

A typical module is shown in Table 8-1 to complete $y = Ax$, where the vector x is distributed as x_pp among the processors, $xmul\_pp$ stores all the equation information for the elements of each processor after "CALL gather(x_pp,xmul_pp)", $a\_pp(:,:,iel)$ stores the element iel stiffness matrix, A denotes as the global stiffness matrix, xtemp_pp(:,iel) stores the local matrix-local vector-product for the element iel using the intrinsic function MATMUL(*) of Fortran 90. The element loop is performing the EBE operation, Equation (8-1). The distributed vector (result), y_pp, is broadcasted to all the processor after "CALL scatter(y_pp,xtemp_pp)". The matrix-by-vector $y = Ax$ is done.

Table 8-1: Parallelization of the matrix-by-vector product $y = Ax$ in an EBE code

```
xmul_pp=zero; xtemp_pp=zero; y_pp=zero;
CALL gather(x_pp,xmul_pp)
DO iel=1,nels_pp
        xtemp_pp(:,iel) = MATMUL(a_pp(:,:,iel),xmul_pp(:,iel))
END DO ;
CALL scatter(y_pp,xtemp_pp)
```

8.4 INTEGRATION WITH GPAS PARALLEL FRAMEWORK

GPAS is a parallel compositional reservoir simulator using Domain Decomposition Method (DDM). The partition and related communication functions are

managed by its framework, called IPARS. The subroutines of IPARS are all associated with the finite difference or control volume methods used in discretizing the fluid-flow equations. However, for the geomechanics module, a finite element method is implemented and also is parallelized using the EBE strategy (Pettipher and Smith 1997; Smith 2000; Margetts 2002). The balance of the two sets of parallel frameworks is an issue in the parallel coupled simulator.

It is observed that the linkage between two coupled models is the coupling parameters, the pressure or pressure change and the volumetric strain. These coupling parameters are all grid block-based or element based; hence for this reason, the coordination of two parallel frameworks is easier than expected. In addition, the partition information regarding to the equations and the nodes are limited to the finite element code of the geomechanics module, so it is totally independent of IPARS.

Hence, the framework in GPAS takes charge of the coupled geomechanics and fluid-flow simulator; while the framework in geomechanics EBE code is in a subordinate position. In Figure 8-5, GPAS framework initializes the code, including setting up the parallel environment (the number of processors, the rank of each processor, the communicator of all processors, etc.), dividing the original domain (gridblocks or elements) into subdomains (subsets of gridblocks or elements), and so on. And then the above information will be transferred to the geomechanics (EBE-FEM) framework through the dummies of subroutines. However, the two frameworks use their own parallel library, Parallel library 1 for GPAS and Parallel library 2 for Geomechanics, to complete communications among processors. When the simulation period is complete, GPAS framework finalizes all the processors of the coupled program.

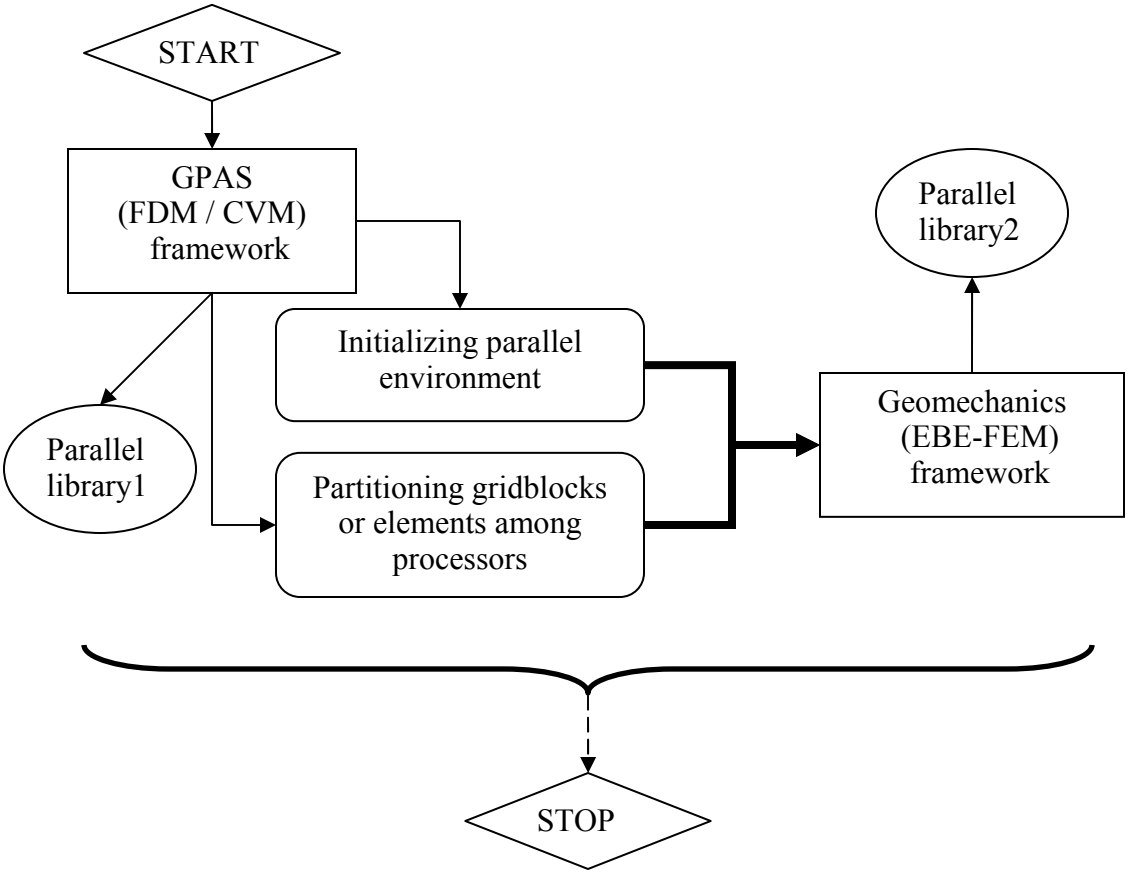

Figure 8-5: Integration of GPAS and geomechanics framework.

8.5 PARALLEL COMPUTER ENVIRONMENT

Let us define the speedup of a parallel code as the followings:

$$S = \text{speedup} = \frac{T_s}{T_p}, \tag{8-2}$$

where T_s is the execution time of serial run using a single processor; specifically, it often refers to the execution time using the one-processor version of the parallel code described above. T_p is the execution time of parallel run using the p processors. Ideally, a linear speedup using the p processors can be obtained, which means $S = p$;

however, in practice, some parts of the code is sequential in nature and the communication time increases with the number of processors, the sub-linear speedup often appears. In terms of parallel computing disciplines, a good scalability of a parallel application depends on (1) inter-processor communication, (2) load balance, and (3) I/O operations, etc.

For testing the parallel performance of the coupled geomechanics and GPAS, a set of cases were simulated on the two parallel PC clusters. One is The Lonestar Linux Cluster at The Texas Advanced Computing Center (TACC) of The University of Texas at Austin, which consists of 1300 nodes with 2 Xeon Intel Dual-Core processors per node (2.66 GHz x 4 64-bit processors, InfiniBand switch with 1 GB/s point-to-point bandwidth, a Linux OS managed by the Rocks 4.1 cluster toolkit) and has the peak performance rated is 55 TFLOPS. Another PC cluster is called Petros at The Center for Petroleum and Geosystems Engineering (CPGE) at The University of Texas at Austin, which consists of eight computing nodes (1 GHz dual processors, Gigabit Ethernet interconnect).

8.6 CASE STUDIES

For testing the consistency of the parallel coupled code, Case 7.4.2 is simulated using the different number of processors (np = 1, 2, 4, 5, 10).

For evaluating the speed-up and the scalability of the developed parallel coupled code, two cases are studied in this section.

8.6.1 Verification of the Coupled Code

Recast Case 7.4.2, a primary depletion reservoir with three components, C_{10}, C_{15}, and C_{20} with the initial compositions, 0.5, 0.25, and 0.25, respectively. A 2 x 20 x 20 grid is used to discretize the reservoir domain. The total number of unknowns for this

case is close to 20,000. For detail description of the data, refer to Section 7.4. Figure 8-6 and Figure 8-7 show the changes of the average pressure and total oil production with time, respectively, from the fully coupled geomechanics and GPAS. These results are identical regardless of the number of processor and verify the consistency of the developed code among the parallel runs. Similar results are shown in Figure 8-8 and Figure 8-9. Hence, the consistency of the developed parallel code has been verified by these runs.

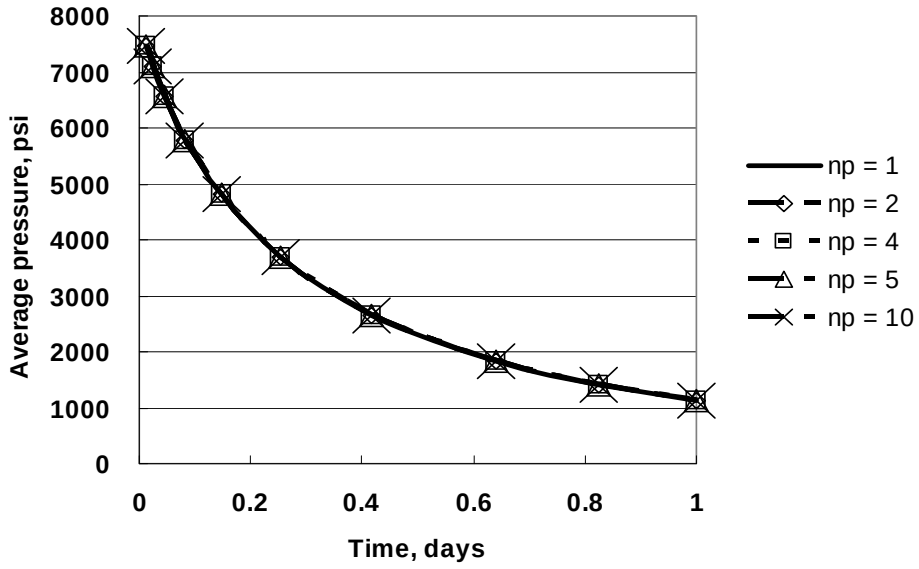

Figure 8-6: Average pressure from parallel runs of the fully coupled geomechanics in GPAS.

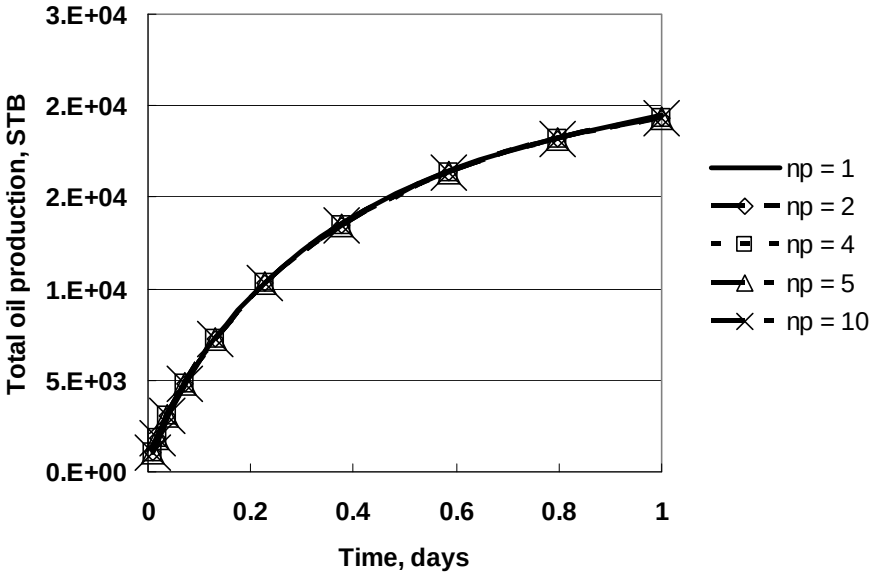

Figure 8-7: Total oil production from parallel runs of the fully coupled geomechanics in GPAS.

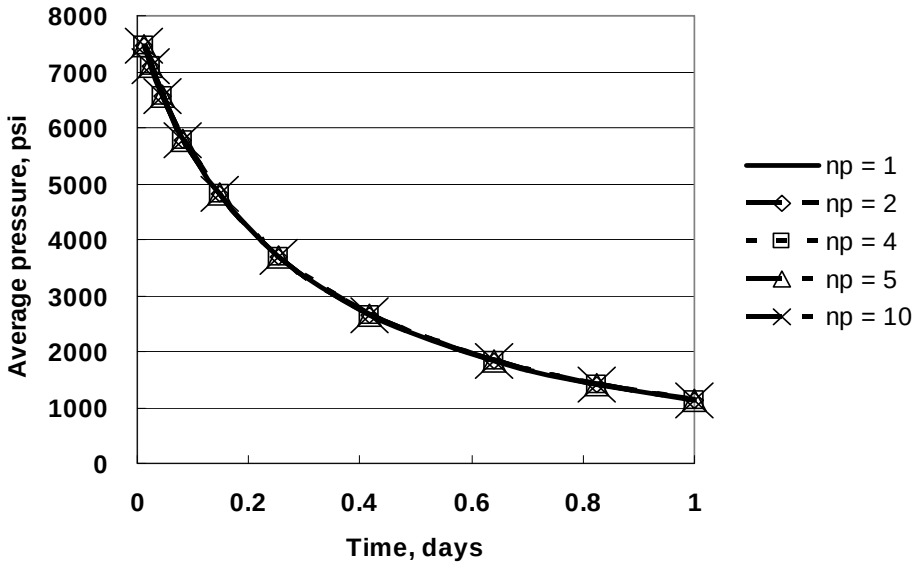

Figure 8-8: Average pressure from parallel runs of the iteratively coupled geomechanics in GPAS.

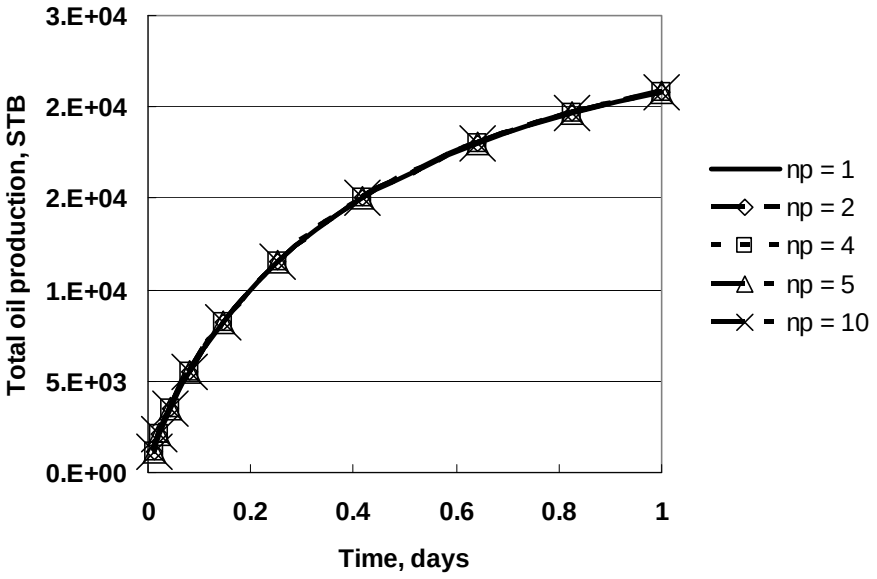

Figure 8-9: Total oil production from parallel runs of the iteratively coupled geomechanics in GPAS.

8.6.2 Speedup Evaluation

Two cases are simulated with different number of processors using Lonestar Linux Cluster at TACC to evaluate the speedup and the scalability of the developed code.

Case 8.6.2.1 considers a reservoir with 560 ft in length, 560 ft in width, and 100 ft in thickness. A 7x128x10 grid is used to discretize the reservoir. The reservoir fluid is characterized by six hydrocarbon components, C_1, C_3, C_6, C_{10}, C_{15} and C_{20}, with the initial composition, 0.5, 0.03, 0.07, 0.2, 0.15 and 0.05, respectively. The properties of components are given in Table 6-4. An injector is located at grid cells (1,1,1) through (1,1,10) operating with a constant rate injection of 1000 Mscf/day and a producer is located at grid cell (7,128,1) through (7,128,10) operating with a constant bottomhole pressure of 1000 psi. Other input data values are shown in Table 8-2.

Table 8-2: Summary of input data for Case 8.6.2.1

	Parameter	Value
Reservoir model	Length (ft) x Width (ft) x Thickness (ft)	560 x 560 x 100
	Number of gridblocks	7 x 128 x 10
	Gridblock size (ft^3)	80 x 4.4 x 10
	Porosity	0.35
	Rock compressibility (psi^{-1})	0
	Fluid compressibility (psi^{-1})	0
	Initial water saturation	0.17
	Water viscosity (cp)	1
	Water density (lb/ft^3)	62.343
	Initial pressure (psi)	1500
	Producer (BHP, psi)	1300
	Injector (STB/day)	1000
Geomechanics model	Number of elements	7 x 128 x 10
	Element type	20-node brick
	Element size (m^3)	15.2 x 15.2 x 6.0
	Young's modulus (kPa)	$9.0x10^5$
	Poisson's ratio	0.3
	Constant load (kPa)	10,342

For this case, the execution time and speed-up are shown in Figure 8-10 and Figure 8-11 for the iteratively coupled solution procedure and in Figure 8-12 and Figure 8-13 for the fully coupled solution procedure. Using the iteratively coupled solution procedure, a speed-up of 13.3 is obtained for 16 processors and a speed-up of 20.8 is achieved for 32 processors. While the fully coupled solution procedure, a speed-up of

15.2 is obtained for 16 processors and a speed-up of 28 is achieved for 32 processors. The better speed-up for the fully coupled solution procedure is because its solver is not optimized as much as the one in the iteratively coupled solution procedure. It is well-known that the computation time of each processor decreases with the increased number of processors used; however, time for parallel output and communication among processors increase at the same time. For a fixed case, there will be a critical number of processors at which the additional execution time used for the communication and output is equal to the saved time of the computation execution time. It can be expected that the total execution time with a large number of processors than the critical one will increase.

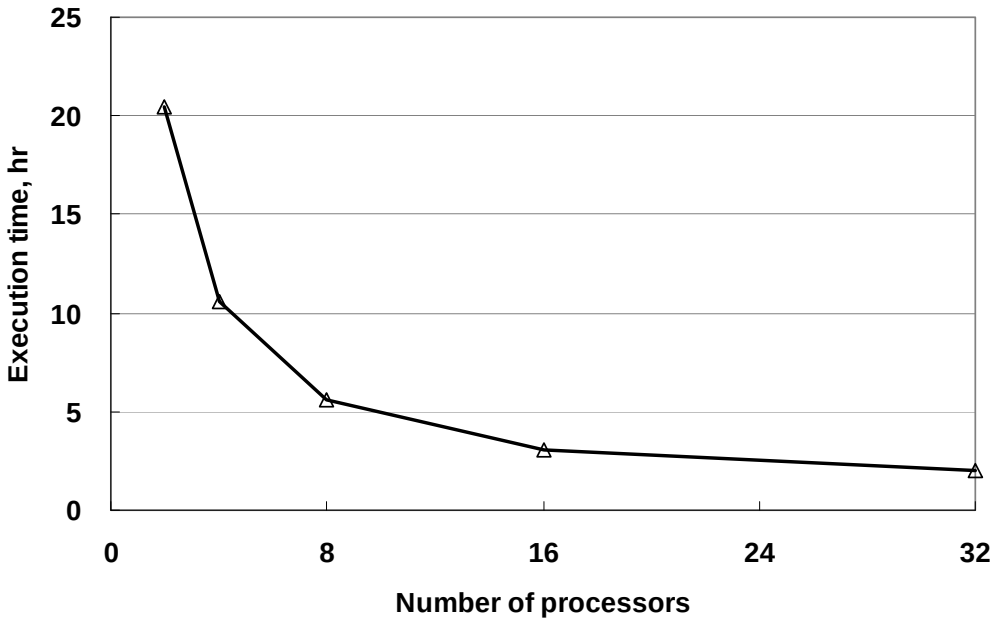

Figure 8-10: Execution time for Case 8.6.2.1 using the iteratively coupled solution procedure.

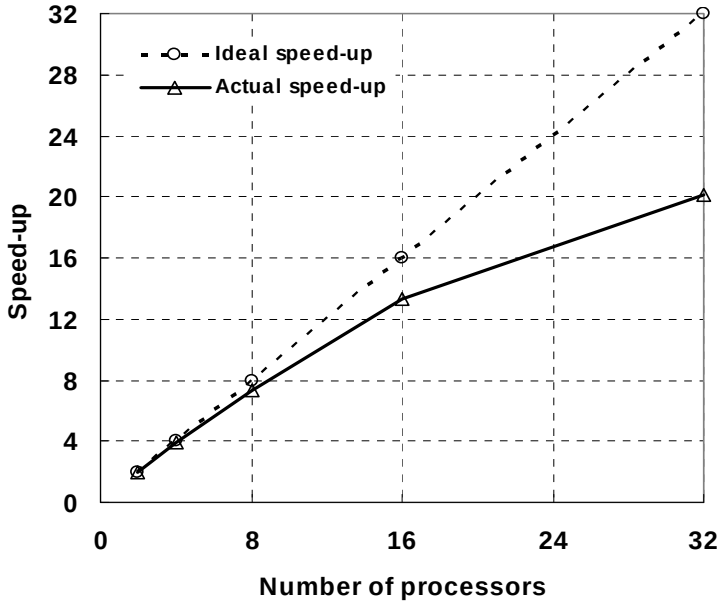

Figure 8-11: Speed-up for Case 8.6.2.1 using the iteratively coupled solution procedure.

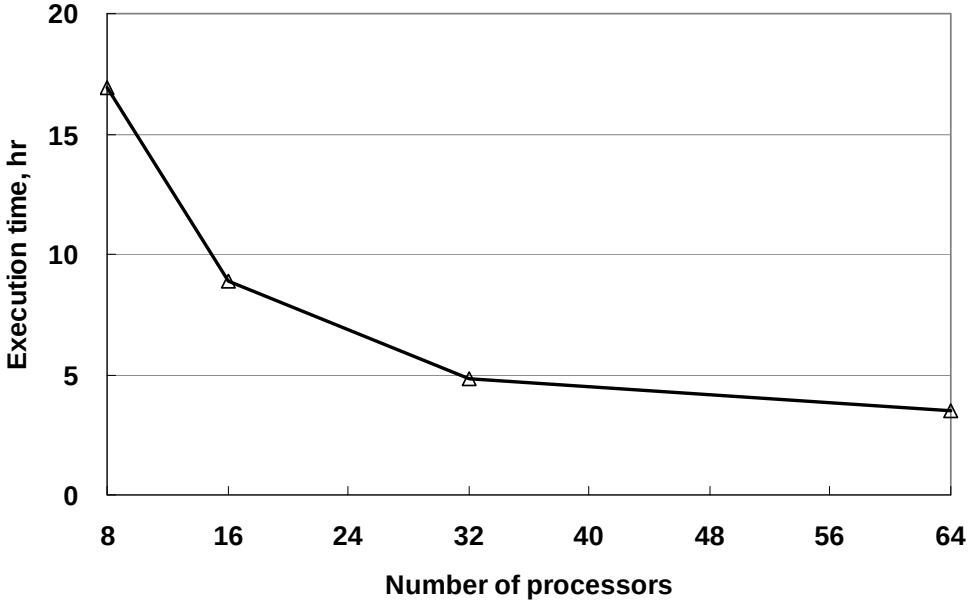

Figure 8-12: Execution time for Case 8.6.2.1 using the fully coupled solution procedure.

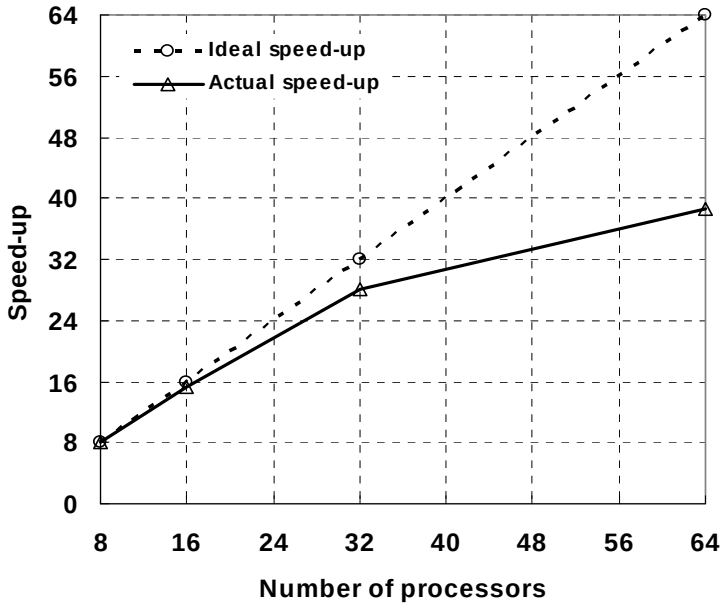

Figure 8-13: Speed-up for Case 8.6.2.1 using the fully coupled solution procedure.

Case 8.6.2.2 considers the same reservoir as described in Case 8.6.2.1. A 7x128x15 grid is used to discretize the reservoir. The reservoir fluid is characterized by ten hydrocarbon components, C_1, C_3, C_6, C_{10}, $C_{11\text{-}13}$, C_{15}, $C_{16\text{-}19}$, C_{20}, $C_{21\text{-}35}$, and C_{36+}, with the initial composition, 0.48, 0.03, 0.06, 0.2, 0.005, 0.15, 0.005, 0.05, 0.01 and 0.01, respectively. Other input values are the same as Case 8.6.2.1. The speed-up and the execution time are shown in Figure 8-14 through Figure 8-17. The total number of unknowns in this case is up to 1,102,080, and a speed-up of 23 for 32 processors using the iteratively coupled solution procedure is obtained as shown in Figure 8-14. A similar improvement can be found for the fully coupled solution procedure in Figure 8-17.

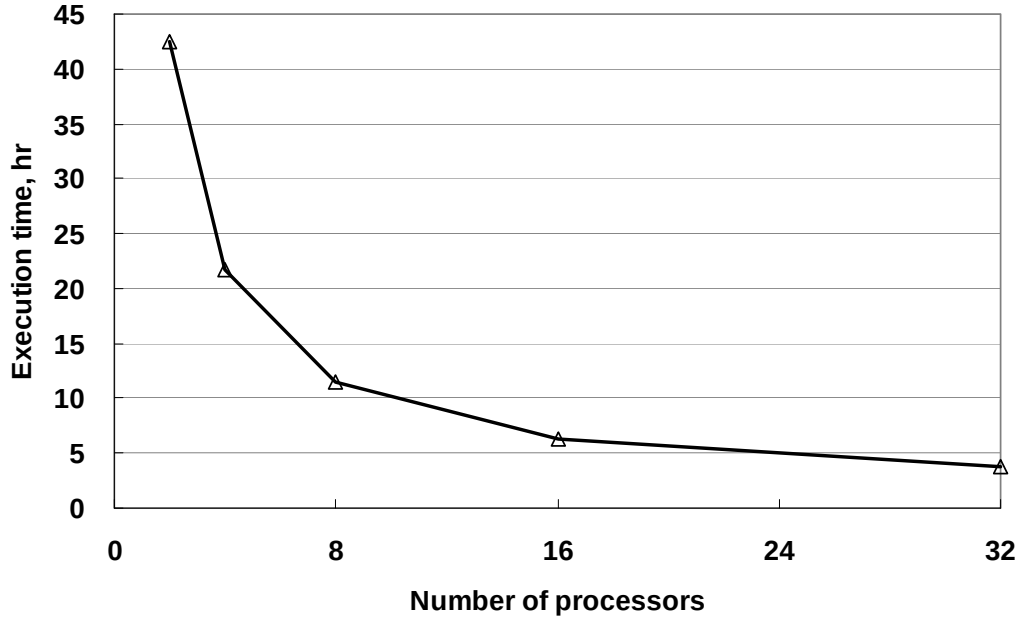

Figure 8-14: Execution time for Case 8.6.2.2 using the iteratively coupled solution procedure.

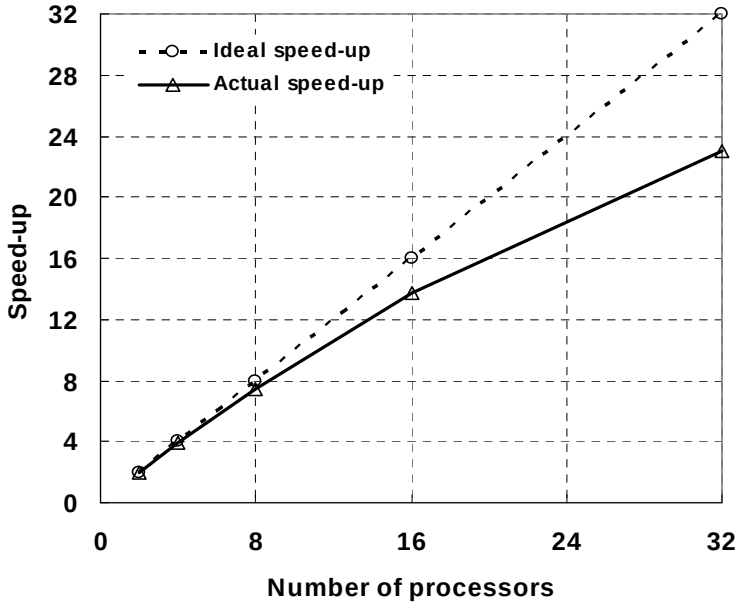

Figure 8-15: Speed-up for Case 8.6.2.2 using the iteratively coupled solution procedure.

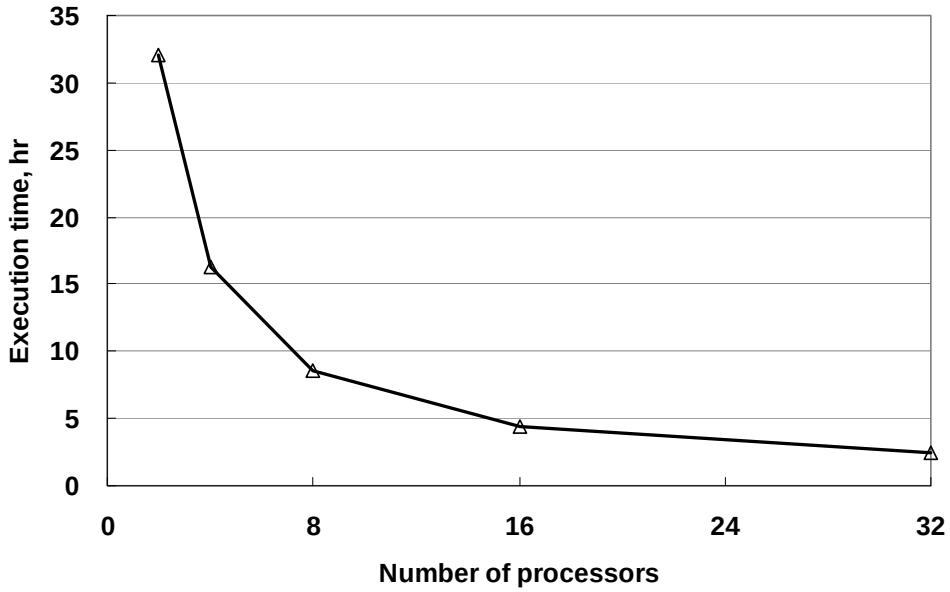

Figure 8-16: Execution time for Case 8.6.2.2 using the fully coupled solution procedure.

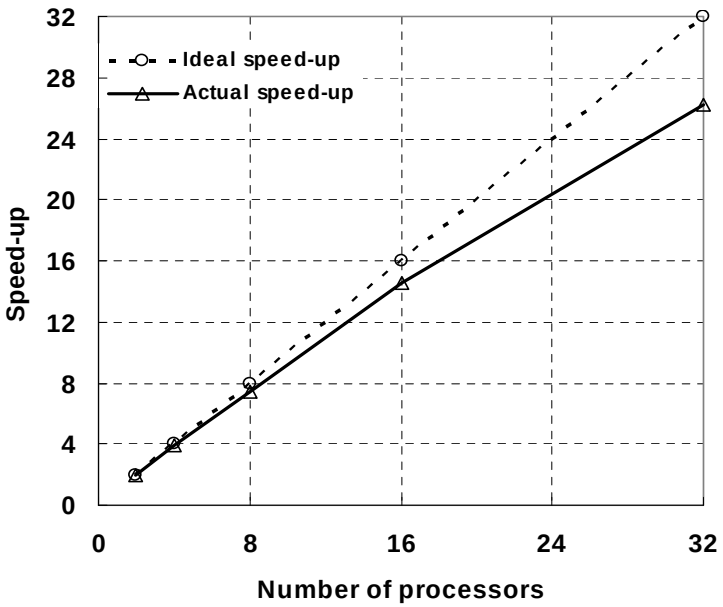

Figure 8-17: Speed-up for Case 8.6.2.2 using the fully coupled solution procedure.

8.6.3 Water Flooding for Natural Fracture Reservoir

A water flooding case for the natural fracture reservoir is simulated to verify the capability of the coupled geomechanics and GPAS with the parallel option.

The reservoir with the dimension of 1920ft×1920ft×100ft, was partition to 64×64×10 grid mesh. The total number of grid block is 163,840 and the total number of unknowns is 2,785,280. Table 8-3 describes other input vaules of this case. The simulation results using 32 processors are shown in Figure 8-18 and Figure 8-19.

Table 8-3: Summary of input data for Case 8.6.3

	Parameter	Value
Fracture model	Length (ft) x Width (ft) x Thickness (ft)	1920 x 1920 x 100
	Number of gridblocks	64 x 64 x 10
	Gridblock size (ft^3)	30 x 30 x 10
	Number of matrix subgrids	2 x 2
	Fracture porosity	0.02
	Fracture permeability (md)	500
	Matrix porosity	0.19
	Matrix permeability (md)	1
	Initial water saturation for matrix	0.25
	Water viscosity (cp)	1
	Water density (lb/ft^3)	62.343
	Initial pressure (psi)	4000
	Production BHP (psi)	3700
Geomechanics model	Number of elements	64 x 64 x 10
	Element type	20-node brick
	Young's modulus (kPa)	5.0×10^5
	Poisson's ratio	0.25

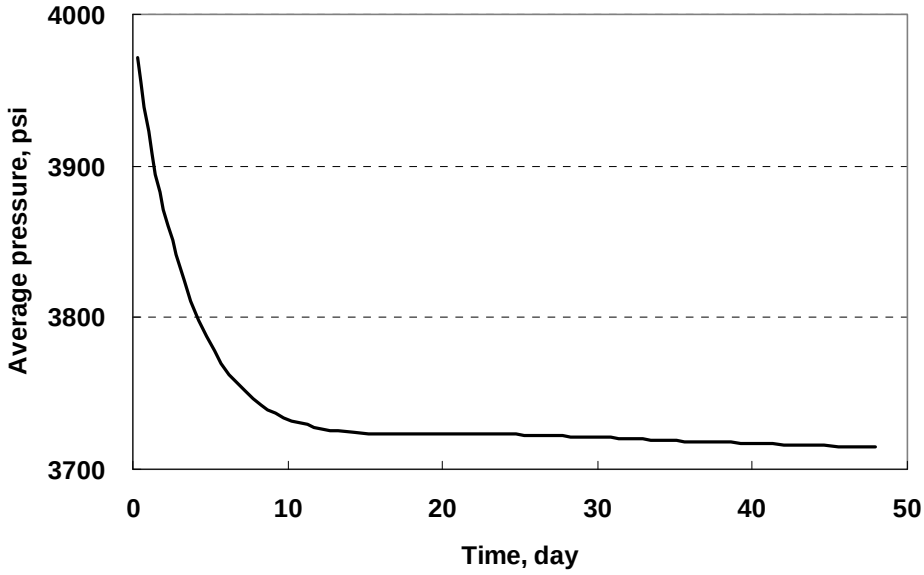

Figure 8-18: Average pressure for Case 8.6.3.

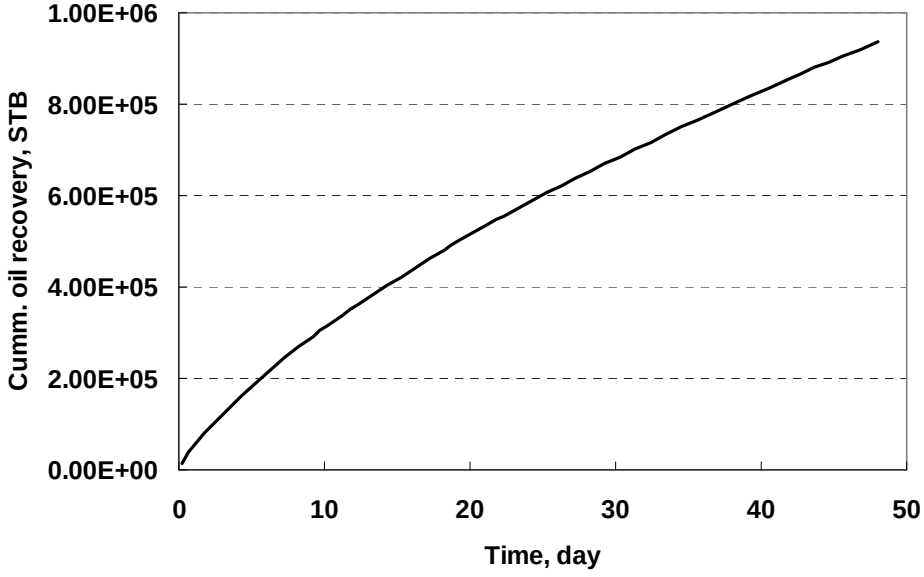

Figure 8-19: Total oil production for Case 8.6.3.

According to the above runs, a good speed-up was achieved for the parallel simulations both for iteratively coupled and fully coupled solution procedures. For example, for the second case with more than one million unknowns, the iteratively coupled solution procedure obtained a speedup of 23 for 32 processors; the fully coupled solution procedure obtained a speedup of 26 for 32 processors. This means that the developed coupled code has a capability to solve large scale problems using parallel processing. On the other hand, the good speed-up as shown in the above runs verified that the partition algorithm used in EBE for the elements, nodes, and equations can keep a good load balance among processors. The associated parallel framework for FEM has a potential to be used by other physical modules, which adopts FEM for the numerical method.

9 Summary, Conclusions and Recommendations

9.1 SUMMARY

A geomechanics model was developed and integrated into a parallel compositional reservoir simulator called General Purpose Adaptive Simulator (GPAS). The following tasks were accomplished to support the objectives:

1. A literature review was carried out for the coupled geomechanics reservoir modeling, the coupled mathematical model, the associated numerical model, the solution procedures and their implementations. The review provided solid background for the research.
2. A coupled geomechanics and compositional reservoir model was derived. In addition, the errors of different approximations for coupling terms in the formulation were analyzed.
3. A geomechanics module was developed using FEM and was used to describe the deformation behaviors of the solid phase.
4. The developed geomechanics module was parallelized for execution on massively parallel computers. A general parallel FEM framework based on Domain Decomposition Method (DDM) was incorporated into GPAS.
5. The geomechanics module was integrated into GPAS using two kinds of coupling solution procedures: the iteratively coupling and the fully coupling.
6. The two kinds of coupling parameters, porosity and permeability, were selected in this research.
7. The coupled geomechanics and GPAS was verified using analytical solutions.

8. The coupled geomechanics and GPAS was used to simulated different cases for compositional reservoir simulations, including primary depletions, water floods, gas floods, CO_2 floods, etc.
9. The coupled geomechanics module was also integrated with dual-porosity module in GPAS to perform simulations of naturally fractured reservoirs (NFR).
10. The coupled geomechanics and GPAS was used to solve large-scale problems using the developed parallel option.
11. The linear elasticity and nonlinear plasticity constitutive model was implemented to describe the rock deformation.

9.2 CONCLUSIONS

This study has shown that geomechanics has a big effect on the hydrocarbon production in some scenarios. The following conclusions can be drawn from this investigation.

1. When the reservoir rock is soft, or a big pressure drop occurs during production period, the stress-displacement modeling is necessary to be performed to guide the production. The pressure drop between two time-steps or two nonlinear iterations in the fluid-flow model is the input parameter for the solid deformation model. Hence, the geomechanics effects become important for reservoirs with large pressure variations.
2. The selection of implementations for different solution procedures has to be considered in order to reuse the existing packages and modify them (if necessary). It is well-known that the fully coupled solution procedure and the iteratively solution procedure can be used to solve the coupled geomechanics problems; however, there are many different implementations

for each method in the literature. In this research, a novel implementation of the fully coupled solution was proposed based on the Schur complement; a robust, modified implementation of the iteratively coupled solution procedure based on Terzaghi's consolidation theory was proposed to resolve the associated convergence issue.

3. The iteratively coupled solution procedure in this research can capture the Mandel-Cryer effect, which was verified by the study of a two-dimensional consolidation problem.
4. The variation of permeability with the porosity maybe affects the result of coupled simulations as shown in this research. Therefore, a porosity coupling or a porosity coupling with variable permeability was carefully used to model the coupled geomechanics and fluid-flow problems.
5. For NFR problems, the case studies in this research showed that the coupled geomechanics and GPAS can maintain higher reservoir pressure than GPAS without geomechanics. The coupled model predicted higher oil recovery than the model without geomechanics. The coupling fracture permeability has large effects on the production than the coupling matrix permeability.
6. From the case-studies, the plasticity model enhanced the geomechanics effects, maintained a higher pressure, and enhanced oil recovery.

9.3 RECOMMENDATIONS FOR FUTURE WORK

The following recommendations should be considered for future research.

1. Development of a coupled geomechanics module and GPAS for the discrete fracture model.

2. Integration of the developed geomechanics module with thermal module in GPAS to consider thermal effects for the constitutive relations for the reservoir rocks.
3. Incorporation of the developed geomechanics module with the unstructured grid option in GPAS to deal with complex reservoir geometries.
4. Investigation of effective and efficient solvers for the geomechanics module.
5. Investigation of robust preconditioners for the Schur complement used in the fully coupled solution procedure.
6. Investigation of a robust and efficient equivalent compressibility for Jacobian system used in the iteratively coupled solution procedure.
7. Implementation of lower-order element types to decrease the number of equations and the memory usage for geomechanics module.

Nomenclatures

a	Parameter
b	Parameter
$\vec{b}$	Body force per unit mass (kPa/m^3)
D	Depth from a reference datum plane (ft)
$\vec{E}$,F,G,H	Nonlinear functions used in the mathematical model
F_α	Nonlinear functions used in the mathematical model
s1	The dimension of primary unknowns of gemechanics, x_1
f1	The dimension of primary unknowns of fluid-flow, x_2
f_i^α	Fugacity of component i in the aqueous phase α (psi)
g	Gravitational acceleration constant (ft/sq sec)
K_i	Equilibrium ratio for component i, $K_i = y_i / x_i$
k	Absolute permeability (md)
k_i	Initial permeability (md)
$\overrightarrow{\overrightarrow{K}}$	Permeability tensor or a set of history dependent tensorial quantities (md)
k_{rj}	Relative permeability for phase j (dimensionless)
k_z	Kozeny constant
Lj	Ratio of moles in phase j to the total number of moles in the mixture
N_i	Moles of component i per unit pore volume (lb-mole/cu ft)
n	Time-step
n_c	Number of hydrocarbon components
n_p	Number of phases
p	Pore fluid pressure (psi)
P_i	Initial pressure (psi)
P_j	Pressure of phase j (psi)

q_i	Molar injection (positive) or production (negative) rate for component i (lb-moles/D)
S_j	Saturation of phase j
S_p	Special surface area
t	Time (day)
T	Temperature (^{0}R)
$\vec{u}$	Displacement vector in geomechanics model (m)
$\vec{v}_j$	Velocity of phase j (ft/day)
$\vec{v}^s$	Velocity of solid (ft/day)
V_b	Bulk volume for a cell (ft^3)
V_p	Pore volume for a cell (ft^3)
$\bar{v}_j$	Molar volume of phase j (ft^3/ lb-mole)
x_i	Mole fraction of component i in liquid phase
y_i	Mole fraction of component i in gas phase
x_{ij}	Mole fraction of component i in j phase

Greek Symbols

α	Correlation factor in effective stress law or a factor in effective stress law
γ_j	Gravity term for phase j, defined as $\rho_j g$ (psi/ft)
Δ	Difference operator
∇	Gradient operator
$\nabla \cdot$	Divergence operator
λ_{rj}	Relative mobility of phase j (1/cp), $\left(kk_{rj}\right)/\mu_j$
μ_j	Viscosity of phase j (cp)
ξ_j	Molar density of phase j (lb-mole/ ft^3)
ρ_j	Mass density of phase j (lbm/ft^3)
ρ_f	Mass density of fluid (lbm/ft^3)
ρ_s	Mass density of solid (kg/m^3)
$\vec{\vec{\sigma}}$	Total stress tensor in geomechanics model (kPa)
σ_m	Mean total stress state (kPa)
$\vec{\vec{\sigma}}'^s$	Effective stress tensor in geomechanics model (kPa)
σ^*	Parameter
σ_n	Effective mean normal stress (kPa)
$\sigma_{n,0}$	Reference effective mean normal stress (kPa)

τ	Shear stress (kPa)
Φ	Flow potential (psi)
ϕ	Reservoir porosity
ϕ_i	Initial porosity
ϕ^*	True porosity
ω_{ij}	Mass fraction of component i in phase j
$\overline{\overline{\delta}}$	Kronecker delta
ε_v	Volumetric strain
ε_z	Axial strain
$\overline{\overline{\varepsilon}}$	Solid strain
$\dot{\overline{\overline{\varepsilon}}}$	Solid strain rate (1/day)

Superscripts and Subscripts

fluid / f	About reservoir model (compositional model)
solid / s	About geomechanics model
x,y,z	x,y,z-direction in the Cartesian coordinate
i	Species or component number
j	Phase number, 1=water, 2=oil, 3=gas (EOS model)
k	The number of nonlinear iteration
m	Power-law exponent
n	Power-law exponents
n	The number of time-step or period
0	$t = 0$ or $t = t_0$

Appendix A: User Manual

The user's guide for the coupled geomechanics and GPAS is presented in this section.

A.1 KEYWORDS

The following section gives a description of the input keywords for the coupled geomechanics and GPAS model.

GEOMG	FLAG no units Flag for utilizing the coupled geomechanics module for GPAS and specifying the coupled solution procedure used: =69, iteratively coupled solution procedure =70, simply iteratively coupled solution procedure =71, fully coupled solution procedure =73, iteratively coupled solution procedure for NFR
PCOUP	FLAG no units Flag for coupling parameters: considering the variations of porosity only, porosity and permeability, for the matrix system or the fracture system =0, variation of matrix porosity =1, variation of matrix porosity and matrix permeability =3, variation of matrix porosity, matrix permeability, and fracture permeability
GMCL	FLAG no units Counter for calling geomechanics
THF, GEOM2D	FLAGS no units Flags unused
TOLA	Tolerence of the outer-loop for fully coupled solution procedure
LIMA	Maximum iteration of the outer-loop for fully coupled solution procedure
TOLB	Tolerence of the inner-loop for fully coupled solution procedure
LIMB	Maximum iteration of the inner -loop for fully coupled solution procedure

TOLD	Tolerence for iteratively coupled solution procedure
LIMD	Maximum iteration for iteratively coupled solution procedure
NKM	Power coefficient of the permeability coupling for the matrix system
NKF	Power coefficient of the permeability coupling for the fracture system
GRAV2	FLAG no units FALSE Ignoring the gravity effect
NONL	FLAG no units FALSE Flag for nonlinear constitutive model for the geomechanics
EQC	Equivalent compressibility

A.2 INPUT DATA

```
TITLE(2)="2-D PRIMARY DEPLETION WITH 12-COMPONENT"
DESCRIPTION()=
"THICKNESS (FT) : 40"
"LENGTH (FT) : 10"
"WIDTH (FT) : 30"
"GRID BLOCKS : 12x1x4"
COMPOSITIONAL_MODEL
TIMEEND = 120

$ I/O OPTIONS
OUTLEVEL = 1
PROCOUT
OUTPUT_PRE
OUTPUT_SAT
OUTPUT_OIL
OUTPUT_GAS
OUTPUT_WEL
OUTPUT_HIS
WELLFILE = "3COMP.WEL"

HISDATA_NUM = 100
OUTPUT_TIME() =    0 0.01 0.02 0.5 1 5 10 15 30 60 80 118 120    1000 2000 3000 3650
$NO_CRASH


$OUTPUT FREQUENCY
ISTEP(,,)=1
JSTEP(,,)=1
KSTEP(,,)=1

$ FAULT BLOCK AND MESH DATA
METHOD = 2
DOWN() = 0 0 1
NX(1) = 12    NY(1) = 1    NZ(1) = 4
MES = "cart"
DX() = 100    DY() = 10    DZ() = 10

$ COMPOUND NAMES
COMPOUND(1) = "CO2"
```

```
COMPOUND(2) = "C1"
COMPOUND(3) = "C2"
COMPOUND(4) = "C3"
COMPOUND(5) = "N-C4"
COMPOUND(6) = "N-C5"
COMPOUND(7) = "C6"
COMPOUND(8) = "C7-9"
COMPOUND(9) = "C10-13"
COMPOUND(10) = "C14-19"
COMPOUND(11) = "C20-35"
COMPOUND(12) = "C36+"

$ COMPOUND CRITICAL TEMPERATURES
CRIT()    547.57 343.04    549.76    665.68    765.32    845.37
          923.0    1040.29 1199.64 1346.56 1532.74 1667
$ COMPOUND CRITICAL PRESSURES
CRIP()    1071.6 667.8 707.8 616.3 550.7 488.6
          483.77 415.41 225.39 203.91 158.03 94.80
$ COMPOUND CRITICAL VOLUMES
CRIV()    0.416 1.602 2.451 3.3 4.088 4.946
          5.294 8.553 13.11 23.07 33.253 83.571
$ COMPOUND ACEN
ACEN()    0.225    0.013    0.0986 0.1524 0.2010 0.2539
          0.2583 0.3165 0.4255 0.5768 0.7659 1.1313
$ COMPOUND MOL WEIGHTS
MOLW()    44.01    16.04    30.07    44.10    58.12      72.15
          84.00 145.16 223.26 353.51 554.55 1052.00
$ COMPOUND PARA
PARA()    125.7429 45.8286 85.9143 126.00 166.0571 206.1429
          240.0      311.8857    437.8857    638.6    1070.1429    2062.8571
$ BINARY INTERACTION COEFFICIENTS
BINC(,) = 0.00000    0.07162 0.09399    0.09759 0.09397 0.09034
0.07454 0.09191 0.09863 0.11636 0.11636 0.16348
                0.07162    0.00000 0.00519    0.01677 0.03675 0.04421
0.00000 0.00001 0.00001 0.16940 0.17835 0.18222
                0.09399    0.00519 0.00000    0.00394 0.01226 0.02316
0.03071 0.05030 0.00497 0.04511 0.06547 0.13363
                0.09759    0.01677 0.00394    0.00000 0.00000 0.00001
0.01065 0.02209 0.00259 0.02952 0.05574 0.12456
                0.09397    0.03675 0.01226    0.00000 0.00000 0.00000
0.00026 0.00083 0.00205 0.01012 0.02093 0.05379
                0.09034    0.04421 0.02316    0.00001 0.00000 0.00000
0.00003 0.00045 0.00122 0.01001 0.01921 0.04953
                0.07454    0.00000 0.03071    0.01065 0.00026 0.00003
0.00000 0.00001 0.00001 0.00001 0.00002 0.00004
                0.09191    0.00001 0.05030    0.02209 0.00083 0.00045
0.00001 0.00000 0.00001 0.00001 0.00002 0.00002
                0.09863    0.00001 0.00497    0.00259 0.00205 0.00122
0.00001 0.00001 0.0000    0.00000 0.00000 0.00001
                0.11636    0.16940 0.04511    0.02952 0.01012 0.01001
0.00001 0.00001 0.0000    0.0000    0.00000 0.00001
                0.11636    0.17835 0.06547    0.05574 0.02093 0.01921
0.00002 0.00002 0.0000    0.0000    0.00000 0.00002
                0.16348    0.18222 0.13363    0.12456 0.05379 0.04953
0.00004 0.00002 0.00001 0.00001 0.00002 0.0000

$ MAX NUMBER OF PHASES
NPHASE = 3
$ MAXNEWT MAX NUMBER OF NEWTON ITERATION
MAXNEWT = 20

$ Initial rock & water properties
ROCKZ = 0.000000    ROCKP = 1500
H2OZ = 0.000003    H2OP = 14.696    H2OD = 3.468
SURTF = 60.0    SURPS = 14.696
RESTF = 160.0

$ TOLERANCE
```

```
CVGOPT = 2
TOL_FLASH = 0.0001
TOL_VOLUME = 0.0001
TOL_MASS = 0.0001
TOL_WATER = 0.0001
$ POROSITY
POROSITY1() = 0.35
$ PERMEABILITIES
XPERM1() = 10
YPERM1() = 10
ZPERM1() = 10
XYPERM1() = 0
XZPERM1() = 0
YZPERM1() = 0
$ INITIAL WATER SATURATION
SWINI1() = 0.17
$ INITIAL WATER CELL PRESSURE
PINI1() = 6000.0

$ INITIAL PHASE VISCOSITIES AT EACH CELL
VIS1() = 1.0

$ INITIAL COMPOSITIONS
ZXY1(,,,1) = 0.01
ZXY1(,,,2) = 0.005
ZXY1(,,,3) = 0.01
ZXY1(,,,4) = 0.01
ZXY1(,,,5) = 0.005
ZXY1(,,,6) = 0.01
ZXY1(,,,7) = 0.01
ZXY1(,,,8) = 0.01
ZXY1(,,,9) = 0.43
ZXY1(,,,10) = 0.25
ZXY1(,,,11) = 0.24
ZXY1(,,,12) = 0.01

$ RELPERM DATA
$ RELP 1 for table lookup, 2 for function based
RELP 2
$MODREL(1) = 3

$ NRELFUN 1 for corey, more to be added later
NRELFUN    1
$ data for each phase : water, phase 2 and phase 3
ENDPT() = 0.4 0.9 0.9
SR() = 0.3 0.1 0.0
EXPN() = 3.0 2.0 2.0


$--B feng pan 11/23/2006    -------- GEOMECHanics options
GEOMG =    71
GEOM2D    = 98
PCOUP = 97
THF = 0
GMCL=0
$--E feng pan 11/23/2006    -------- GEOMECHanics options

$ ============== WELL SPECIFICATIONS ==============
NUMWELL =    4
WELLNAME(1) = "PRODUCER_1"
KINDWELL(1) = 3
WELLTOP(1 TO 3,1,1) =0.0 5.0 5.0
WELLBOTTOM(1 TO 3,1,1) =10.0 5.0 5.0
DIAMETER(1,1) = 1.0
WELLPQ(1) Block
   Interpolation Linear
   Extrapolation Constant
   Data    0.0      500.0
```

```
EndBlock
WELLNAME(2) = "PRODUCER_2"
KINDWELL(2) = 3
WELLTOP(1 TO 3,1,2) =    0.0    5.0 15.0
WELLBOTTOM(1 TO 3,1,2) = 10.0 5.0 15.0
DIAMETER(1,2) = 1.0
WELLPQ(2) Block
   Interpolation Linear
   Extrapolation Constant
   Data    0.0      500.0
EndBlock
WELLNAME(3) = "PRODUCER_3"
KINDWELL(3) = 3
WELLTOP(1 TO 3,1,3) =    0.0 5.0 25.0
WELLBOTTOM(1 TO 3,1,3) = 10.0 5.0 25.0
DIAMETER(1,3) = 1.0
WELLPQ(3) Block
   Interpolation Linear
   Extrapolation Constant
   Data    0.0      500.0
EndBlock
WELLNAME(4) = "PRODUCER_4"
KINDWELL(4) = 3
WELLTOP(1 TO 3,1,4) =    0.0 5.0 35.0
WELLBOTTOM(1 TO 3,1,4) = 10.0 5.0 35.0
DIAMETER(1,4) = 1.0
WELLPQ(4) Block
   Interpolation Linear
   Extrapolation Constant
   Data    0.0      500.0
EndBlock

EndInitial

$ TRANSIENT DATA INPUT BLOCKS
BeginTime    0.0
TIME_CONTROL = 2
DELTIM = 0.01    DTIMMUL = 1.0    DTIMMAX = 30    DTIMMIN = 0.1
TUNE = 0.5    DCMAX = 0.5    DAQCMAX = 0.5    DPMAX = 0.5    DSMAX = 0.5
WZ() 0.7 0.1 0.05 0.05 0.05 0.05
EndTime


2
12 4    1
2.5434e-7       2.5434e-7       9.098499e+06       0.0          30.0    0.0    0.0 1
-2.85246e5
0               30.47851265             60.9570253              91.43553795             121.9140506             152.3925632
                182.8710759             213.3495885             243.8281012             274.3066138             304.7851265
                335.2636391             365.7421518
0.0 -3.047851265       -6.09570253             -9.143553795            -12.19140506
103680    100          0.5       1      87
177
1     0     1     0     2     1     1     0     3     1     1     1     4     1     1     0     5     1     1     1     6     1     1     0     7     1     1
1     8     1     1     0     9     1     1     1    10     1     1     0    11     1     1     1    12     1     1     0    13     1     1     1    14     1
1     0    15     1     1     1    16     1     1     0    17     1     1     1    18     1     1     0    19     1     1     1    20     1     1     0    21
1     1     1    22     1     1     0    23     1     1     1    24     1     1     0    25     0     0     1     26     0     1     0     27     1     1
0     28     1     1     0     29     1     1     0     30     1     1     0     31     1     1     0     32     1     1     0     33     1     1
0     34     1     1     0     35     1     1     0     36     1     1     0     37     1     1     0     38     0     0     0     39     0     1
0    40     1     1     0    41     1     1     1    42     1     1     0    43     1     1     1    44     1     1     0    45     1     1     1    46     1
1     0    47     1     1     1    48     1     1     0    49     1     1     1    50     1     1     0    51     1     1     1    52     1     1     0    53
1     1     1    54     1     1     0    55     1     1     1    56     1     1     0    57     1     1     1    58     1     1     0    59     1     1     1
60     1     1     0    61     1     1     1    62     1     1     0    63     0     0     1    64     0     1     0     65     1     1     0     66     1
1     0     67     1     1     0     68     1     1     0     69     1     1     0     70     1     1     0     71     1     1     0     72     1
1     0     73     1     1     0     74     1     1     0     75     1     1     0     76     0     0     0     77     0     1     0    78     1     1
0    79     1     1     1    80     1     1     0    81     1     1     1    82     1     1     0    83     1     1     1    84     1     1     0    85     1
1     1    86     1     1     0    87     1     1     1    88     1     1     0    89     1     1     1    90     1     1     0    91     1     1     1    92
1     1     0    93     1     1     1    94     1     1     0    95     1     1     1    96     1     1     0    97     1     1     1    98     1     1     0
```

```
99    1    1    1 100    1    1    0 101    0    0    1 102    0    1    0 103    1    1    0 104    1    1    0 105
1    1    0 106    1    1    0 107    1    1    0 108    1    1    0 109    1    1    0 110    1    1    0
111    1    1    0 112    1    1    0 113    1    1    0 114    0    0    0 115    0    1    0 116    1    1    0 117
1    1    1 118    1    1    0 119    1    1    1 120    1    1    0 121    1    1    1 122    1    1    0 123    1    1    1 124
1    1    0 125    1    1    1 126    1    1    0 127    1    1    1 128    1    1    0 129    1    1    1 130    1    1    0 131
1    1    1 132    1    1    0 133    1    1    1 134    1    1    0 135    1    1    1 136    1    1    0 137    1    1    1 138
1    1    0 139    0    0    1 140    0    1    0 141    1    1    0 142    1    1    0 143    1    1    0 144    1
1    0 145    1    1    0 146    1    1    0 147    1    1    0 148    1    1    0 149    1    1    0 150
1    1    0 151    1    1    0 152    0    0    0 153    0    0    0 154    0    0    0 155    0    0    1 156    0    0
0 157    0    0    1 158    0    0    0 159    0    0    1 160    0    0    0 161    0    0    1 162    0    0    0 163    0    0
1 164    0    0    0 165    0    0    1 166    0    0    0 167    0    0    1 168    0    0    0 169    0    0    1 170    0    0
0 171    0    0    1 172    0    0    0 173    0    0    1 174    0    0    0 175    0    0    1 176    0    0    0 177    0    0
1
25
1   0.0   -5.07975   2   0.0   -20.3190      3   0.0   -10.15950   4   0.0   -20.3190      5   0.0   -10.15950   6   0.0   -20.3190
7   0.0   -10.15950   8   0.0   -20.3190      9   0.0   -10.15950   10  0.0   -20.3190      11   0.0   -10.15950   12  0.0   -20.3190
13   0.0   -10.15950   14  0.0   -20.3190      15   0.0   -10.15950   16  0.0   -20.3190      17   0.0   -10.15950   18  0.0   -20.3190
19   0.0   -10.15950   20  0.0   -20.3190      21   0.0   -10.15950   22  0.0   -20.3190      23   0.0   -10.15950   24  0.0   -20.3190
25   0.0   -5.07975
0.001   250
3
0.0 0.0 1 4.13700e4 10368000 4.13700e4



TITLE(2)="3-D 3-COMPONENT PRIMARY DEPLETION"

DESCRIPTION()=
"THICKNESS (FT) : 200"
"LENGTH (FT) : 200"
"WIDTH (FT) : 200"
"GRID BLOCKS : 2x20x20"

COMPOSITIONAL_MODEL

TIMEEND = 120

$ I/O OPTIONS
OUTLEVEL = 1
PROCOUT
OUTPUT_PRE
OUTPUT_SAT
OUTPUT_OIL
OUTPUT_GAS
OUTPUT_WEL
OUTPUT_HIS

HISDATA_NUM = 100
OUTPUT_TIME() =    0 0.0001 0.0002 0.0003 0.01 0.02 0.5 1 5 10 15 30 60 80 118 120    1000 2000 3000 3650
$NO_CRASH


$OUTPUT FREQUENCY
ISTEP(,,)=1
JSTEP(,,)=1
KSTEP(,,)=1

$ FAULT BLOCK AND MESH DATA
METHOD = 2
DOWN() = 0 0 1
NX(1) = 2    NY(1) = 20 NZ(1) = 20
MES = "cart"
DX() = 100    DY() = 10    DZ() = 10

$ COMPOUND NAMES
COMPOUND(1) = "C10"
COMPOUND(2) = "C15"
COMPOUND(3) = "C20"
```

```
$ COMPOUND CRITICAL TEMPERATURES
CRIT() 1111.8 1270.0 1380.0

$ COMPOUND CRITICAL PRESSURES
CRIP()    304.0 200.0 162.0

$ COMPOUND CRITICAL VOLUMES
CRIV() 10.087 16.696 21.484

$ COMPOUND ACEN
ACEN() 0.488 0.650 0.850

$ COMPOUND MOL WEIGHTS
MOLW()    142.3 206.0 282.0

$ COMPOUND PARA
PARA()    431.0 631.0 831.0

$ BINARY INTERACTION COEFFICIENTS
BINC(,) = 0.0      0.0      0.0
          0.0      0.0      0.0
          0.0      0.0      0.0

$ MAX NUMBER OF PHASES
NPHASE = 3

$ MAXNEWT MAX NUMBER OF NEWTON ITERATION
MAXNEWT = 50

$ Initial rock & water properties
ROCKZ = 0.000000    ROCKP = 1500
H2OZ = 0.000003    H2OP = 14.696    H2OD = 3.468
SURTF = 60.0    SURPS = 14.696
RESTF = 160.0

$ TOLERANCE
CVGOPT = 2
TOL_FLASH = 0.0001
TOL_VOLUME = 0.0001
TOL_MASS = 0.0001
TOL_WATER = 0.0001

$ POROSITY
POROSITY1() = 0.35

$ PERMEABILITIES
XPERM1() = 10
YPERM1() = 10
ZPERM1() = 10
XYPERM1() = 0
XZPERM1() = 0
YZPERM1() = 0

$ INITIAL WATER SATURATION
SWINI1() = 0.17

$ INITIAL WATER CELL PRESSURE
$PINI1() = 1950.0
PINI1() = 6000.0

$ INITIAL PHASE VISCOSITIES AT EACH CELL
VIS1() = 1.0

$ INITIAL COMPOSITIONS
ZXY1(,,,1) = 0.5
ZXY1(,,,2) = 0.25
ZXY1(,,,3) = 0.25
```

```
$ RELPERM DATA
$ RELP 1 for table lookup, 2 for function based

RELP 2
$MODREL(1) = 3

$ NRELFUN 1 for corey, more to be added later
NRELFUN    1
$ data for each phase : water, phase 2 and phase 3
ENDPT() = 0.4 0.9 0.9
SR() = 0.3 0.1 0.0
EXPN() = 3.0 2.0 2.0


$--B feng pan 11/23/2006    -------- GEOMECHanics options
GEOMG =    71
GEOM2D    = 98
PCOUP = 97
THF = 0
GMCL=0
TOLA=0.0001
TOLB=0.00000000000001
$--E feng pan 11/23/2006    -------- GEOMECHanics options

$ ============== WELL SPECIFICATIONS ==============
NUMWELL =    2
WELLNAME(1) = "PRODUCER_1"
KINDWELL(1) = 3
WELLTOP(1 TO 3,1,1) =50 198.0 0.0
WELLBOTTOM(1 TO 3,1,1) =50 198.0 200.0
DIAMETER(1,1) = 1.0
WELLPQ(1) Block
   Interpolation Linear
   Extrapolation Constant
   Data    0.0      500.0
EndBlock
WELLNAME(2) = "PRODUCER_2"
KINDWELL(2) = 3
WELLTOP(1 TO 3,1,2) =150 198.0 0.0
WELLBOTTOM(1 TO 3,1,2) =150 198.0 200.0
DIAMETER(1,2) = 1.0
WELLPQ(2) Block
   Interpolation Linear
   Extrapolation Constant
   Data    0.0      500.0
EndBlock
EndInitial

$ TRANSIENT DATA INPUT BLOCKS
BeginTime    0.0
TIME_CONTROL = 2
DELTIM = 0.001    DTIMMUL = 1.0    DTIMMAX = 30    DTIMMIN = 0.001
TUNE = 0.5    DCMAX = 0.5    DAQCMAX = 0.5    DPMAX = 0.5    DSMAX = 0.5
WZ() 0.7 0.1 0.05 0.05 0.05 0.05
EndTime

3
2    20    20    1
1.0e-46    1.0e-46    9.098499e+06    0.3    30.0    0.0    0.0    1
-100
0            30.47851265          60.9570253
0            3.047851265          6.09570253          9.143553795          12.19140506          15.23925632
             18.28710759          21.33495885          24.38281012          27.43066138          30.47851265
             33.52636391          36.57421518          39.62206644          42.66991771          45.71776897
             48.76562024          51.8134715           54.86132277          57.90917403          60.9570253
0            3.047851265          6.09570253          9.143553795          12.19140506          15.23925632
             18.28710759          21.33495885          24.38281012          27.43066138          30.47851265
```

33.52636391 36.57421518 39.62206644 42.66991771 45.71776897
48.76562024 51.8134715 54.86132277 57.90917403 60.9570253
86400 10 0.5 1 1
4364
1 0 0 1 1 2 1 0 1 0 3 1 0 1 1 4 1 0 1 0 5 0 0 1 1 6 0 0 1 0
7 1 0 1 0 8 0 0 1 0 9 0 0 1 1 10 1 0 1 0 11 1 0 1 1 12 1 0 1 0
13 0 0 1 1 14 0 0 1 0 15 1 0 1 0 16 0 0 1 0 17 0 0 1 1 18 1 0 1 0
19 1 0 1 1 20 1 0 1 0 21 0 0 1 1 22 0 0 1 0 23 1 0 1 0 24 0 0 1 0
25 0 0 1 1 26 1 0 1 0 27 1 0 1 1 28 1 0 1 0 29 0 0 1 1 30 0 0 1 0
31 1 0 1 0 32 0 0 1 0 33 0 0 1 1 34 1 0 1 0 35 1 0 1 1 36 1 0 1 0
37 0 0 1 1 38 0 0 1 0 39 1 0 1 0 40 0 0 1 0 41 0 0 1 1 42 1 0 1 0
43 1 0 1 1 44 1 0 1 0 45 0 0 1 1 46 0 0 1 0 47 1 0 1 0 48 0 0 1 0
49 0 0 1 1 50 1 0 1 0 51 1 0 1 1 52 1 0 1 0 53 0 0 1 1 54 0 0 1 0
55 1 0 1 0 56 0 0 1 0 57 0 0 1 1 58 1 0 1 0 59 1 0 1 1 60 1 0 1 0
61 0 0 1 1 62 0 0 1 0 63 1 0 1 0 64 0 0 1 0 65 0 0 1 1 66 1 0 1 0
67 1 0 1 1 68 1 0 1 0 69 0 0 1 1 70 0 0 1 0 71 1 0 1 0 72 0 0 1 0
73 0 0 1 1 74 1 0 1 0 75 1 0 1 1 76 1 0 1 0 77 0 0 1 1 78 0 0 1 0
79 1 0 1 0 80 0 0 1 0 81 0 0 1 1 82 1 0 1 0 83 1 0 1 1 84 1 0 1 0
85 0 0 1 1 86 0 0 1 0 87 1 0 1 0 88 0 0 1 0 89 0 0 1 1 90 1 0 1 0
91 1 0 1 1 92 1 0 1 0 93 0 0 1 1 94 0 0 1 0 95 1 0 1 0 96 0 0 1 0
97 0 0 1 1 98 1 0 1 0 99 1 0 1 1 100 1 0 1 0 101 0 0 1 1 102 0 0 1 0
103 1 0 1 0 104 0 0 1 0 105 0 0 1 1 106 1 0 1 0 107 1 0 1 1 108 1 0 1 0
109 0 0 1 1 110 0 0 1 0 111 1 0 1 0 112 0 0 1 0 113 0 0 1 1 114 1 0 1 0
115 1 0 1 1 116 1 0 1 0 117 0 0 1 1 118 0 0 1 0 119 1 0 1 0 120 0 0 1 0
121 0 0 1 1 122 1 0 1 0 123 1 0 1 1 124 1 0 1 0 125 0 0 1 1 126 0 0 1 0
127 1 0 1 0 128 0 0 1 0 129 0 0 1 1 130 1 0 1 0 131 1 0 1 1 132 1 0 1 0
133 0 0 1 1 134 0 0 1 0 135 1 0 1 0 136 0 0 1 0 137 0 0 1 1 138 1 0 1 0
139 1 0 1 1 140 1 0 1 0 141 0 0 1 1 142 0 0 1 0 143 1 0 1 0 144 0 0 1 0
145 0 0 1 1 146 1 0 1 0 147 1 0 1 1 148 1 0 1 0 149 0 0 1 1 150 0 0 1 0
151 1 0 1 0 152 0 0 1 0 153 0 0 1 1 154 1 0 1 0 155 1 0 1 1 156 1 0 1 0
157 0 0 1 1 158 0 0 1 0 159 1 0 1 0 160 0 0 1 0 161 0 0 0 1 162 0 0 0 0
163 0 0 0 1 164 0 0 0 0 165 0 0 0 1 166 0 1 1 0 167 1 1 1 0 168 0 1 1 0
169 0 1 1 0 170 1 1 1 0 171 0 1 1 0 172 0 1 1 0 173 1 1 1 0 174 0 1 1 0
175 0 1 1 0 176 1 1 1 0 177 0 1 1 0 178 0 1 1 0 179 1 1 1 0 180 0 1 1 0
181 0 1 1 0 182 1 1 1 0 183 0 1 1 0 184 0 1 1 0 185 1 1 1 0 186 0 1 1 0
187 0 1 1 0 188 1 1 1 0 189 0 1 1 0 190 0 1 1 0 191 1 1 1 0 192 0 1 1 0
193 0 1 1 0 194 1 1 1 0 195 0 1 1 0 196 0 1 1 0 197 1 1 1 0 198 0 1 1 0
199 0 1 1 0 200 1 1 1 0 201 0 1 1 0 202 0 1 1 0 203 1 1 1 0 204 0 1 1 0
205 0 1 1 0 206 1 1 1 0 207 0 1 1 0 208 0 1 1 0 209 1 1 1 0 210 0 1 1 0
211 0 1 1 0 212 1 1 1 0 213 0 1 1 0 214 0 1 1 0 215 1 1 1 0 216 0 1 1 0
217 0 1 1 0 218 1 1 1 0 219 0 1 1 0 220 0 1 1 0 221 1 1 1 0 222 0 1 1 0
223 0 1 1 0 224 1 1 1 0 225 0 1 1 0 226 0 0 0 0 227 0 0 0 0 228 0 0 0 0
229 0 1 1 1 230 1 1 1 0 231 1 1 1 1 232 1 1 1 0 233 0 1 1 1 234 0 1 1 0
235 1 1 1 0 236 0 1 1 0 237 0 1 1 1 238 1 1 1 0 240 1 1 1 0 241 0 1 1 1
242 0 1 1 0 243 1 1 1 0 244 0 1 1 0 245 0 1 1 1 246 1 1 1 0 248 1 1 1 0
249 0 1 1 1 250 0 1 1 0 251 1 1 1 0 252 0 1 1 0 253 0 1 1 1 254 1 1 1 0
256 1 1 1 0 257 0 1 1 1 258 0 1 1 0 259 1 1 1 0 260 0 1 1 0 261 0 1 1 1
262 1 1 1 0 264 1 1 1 0 265 0 1 1 1 266 0 1 1 0 267 1 1 1 0 268 0 1 1 0
269 0 1 1 1 270 1 1 1 0 272 1 1 1 0 273 0 1 1 1 274 0 1 1 0 275 1 1 1 0
276 0 1 1 0 277 0 1 1 1 278 1 1 1 0 280 1 1 1 0 281 0 1 1 1 282 0 1 1 0
283 1 1 1 0 284 0 1 1 0 285 0 1 1 1 286 1 1 1 0 288 1 1 1 0 289 0 1 1 1
290 0 1 1 0 291 1 1 1 0 292 0 1 1 0 293 0 1 1 1 294 1 1 1 0 296 1 1 1 0
297 0 1 1 1 298 0 1 1 0 299 1 1 1 0 300 0 1 1 0 301 0 1 1 1 302 1 1 1 0
304 1 1 1 0 305 0 1 1 1 306 0 1 1 0 307 1 1 1 0 308 0 1 1 0 309 0 1 1 1
310 1 1 1 0 312 1 1 1 0 313 0 1 1 1 314 0 1 1 0 315 1 1 1 0 316 0 1 1 0
317 0 1 1 1 318 1 1 1 0 320 1 1 1 0 321 0 1 1 1 322 0 1 1 0 323 1 1 1 0
324 0 1 1 0 325 0 1 1 1 326 1 1 1 0 328 1 1 1 0 329 0 1 1 1 330 0 1 1 0
331 1 1 1 0 332 0 1 1 0 333 0 1 1 1 334 1 1 1 0 336 1 1 1 0 337 0 1 1 1
338 0 1 1 0 339 1 1 1 0 340 0 1 1 0 341 0 1 1 1 342 1 1 1 0 344 1 1 1 0
345 0 1 1 1 346 0 1 1 0 347 1 1 1 0 348 0 1 1 0 349 0 1 1 1 350 1 1 1 0
352 1 1 1 0 353 0 1 1 1 354 0 1 1 0 355 1 1 1 0 356 0 1 1 0 357 0 1 1 1
358 1 1 1 0 360 1 1 1 0 361 0 1 1 1 362 0 1 1 0 363 1 1 1 0 364 0 1 1 0
365 0 1 1 1 366 1 1 1 0 368 1 1 1 0 369 0 1 1 1 370 0 1 1 0 371 1 1 1 0
372 0 1 1 0 373 0 1 1 1 374 1 1 1 0 376 1 1 1 0 377 0 1 1 1 378 0 1 1 0
379 1 1 1 0 380 0 1 1 0 381 0 1 1 1 382 1 1 1 0 384 1 1 1 0 385 0 1 1 1
386 0 1 1 0 387 1 1 1 0 388 0 1 1 0 389 0 0 0 1 390 0 0 0 0 391 0 0 0 1
392 0 0 0 0 393 0 0 0 1 394 0 1 1 0 395 1 1 1 0 396 0 1 1 0 397 0 1 1 0
398 1 1 1 0 399 0 1 1 0 400 0 1 1 0 401 1 1 1 0 402 0 1 1 0 403 0 1 1 0

404	1	1	1	0	405	0	1	1	0	406	0	1	1	0	407	1	1	1	0	408	0	1	1	0	409	0	1	1	0
410	1	1	1	0	411	0	1	1	0	412	0	1	1	0	413	1	1	1	0	414	0	1	1	0	415	0	1	1	0
416	1	1	1	0	417	0	1	1	0	418	0	1	1	0	419	1	1	1	0	420	0	1	1	0	421	0	1	1	0
422	1	1	1	0	423	0	1	1	0	424	0	1	1	0	425	1	1	1	0	426	0	1	1	0	427	0	1	1	0
428	1	1	1	0	429	0	1	1	0	430	0	1	1	0	431	1	1	1	0	432	0	1	1	0	433	0	1	1	0
434	1	1	1	0	435	0	1	1	0	436	0	1	1	0	437	1	1	1	0	438	0	1	1	0	439	0	1	1	0
440	1	1	1	0	441	0	1	1	0	442	0	1	1	0	443	1	1	1	0	444	0	1	1	0	445	0	1	1	0
446	1	1	1	0	447	0	1	1	0	448	0	1	1	0	449	1	1	1	0	450	0	1	1	0	451	0	1	1	0
452	1	1	1	0	453	0	1	1	0	454	0	0	0	0	455	0	0	0	0	456	0	0	0	0	457	0	1	1	1
458	1	1	1	0	459	1	1	1	1	460	1	1	1	0	461	0	1	1	1	462	0	1	1	0	463	1	1	1	0
464	0	1	1	0	465	0	1	1	1	466	1	1	1	0	468	1	1	1	0	469	0	1	1	1	470	0	1	1	0
471	1	1	1	0	472	0	1	1	0	473	0	1	1	1	474	1	1	1	0	476	1	1	1	0	477	0	1	1	1
478	0	1	1	0	479	1	1	1	0	480	0	1	1	0	481	0	1	1	1	482	1	1	1	0	484	1	1	1	0
485	0	1	1	1	486	0	1	1	0	487	1	1	1	0	488	0	1	1	0	489	0	1	1	1	490	1	1	1	0
492	1	1	1	0	493	0	1	1	1	494	0	1	1	0	495	1	1	1	0	496	0	1	1	0	497	0	1	1	1
498	1	1	1	0	500	1	1	1	0	501	0	1	1	1	502	0	1	1	0	503	1	1	1	0	504	0	1	1	0
505	0	1	1	1	506	1	1	1	0	508	1	1	1	0	509	0	1	1	1	510	0	1	1	0	511	1	1	1	0
512	0	1	1	0	513	0	1	1	1	514	1	1	1	0	516	1	1	1	0	517	0	1	1	1	518	0	1	1	0
519	1	1	1	0	520	0	1	1	0	521	0	1	1	1	522	1	1	1	0	524	1	1	1	0	525	0	1	1	1
526	0	1	1	0	527	1	1	1	0	528	0	1	1	0	529	0	1	1	1	530	1	1	1	0	532	1	1	1	0
533	0	1	1	1	534	0	1	1	0	535	1	1	1	0	536	0	1	1	0	537	0	1	1	1	538	1	1	1	0
540	1	1	1	0	541	0	1	1	1	542	0	1	1	0	543	1	1	1	0	544	0	1	1	0	545	0	1	1	1
546	1	1	1	0	548	1	1	1	0	549	0	1	1	1	550	0	1	1	0	551	1	1	1	0	552	0	1	1	0
553	0	1	1	1	554	1	1	1	0	556	1	1	1	0	557	0	1	1	1	558	0	1	1	0	559	1	1	1	0
560	0	1	1	0	561	0	1	1	1	562	1	1	1	0	564	1	1	1	0	565	0	1	1	1	566	0	1	1	0
567	1	1	1	0	568	0	1	1	0	569	0	1	1	1	570	1	1	1	0	572	1	1	1	0	573	0	1	1	1
574	0	1	1	0	575	1	1	1	0	576	0	1	1	0	577	0	1	1	1	578	1	1	1	0	580	1	1	1	0
581	0	1	1	1	582	0	1	1	0	583	1	1	1	0	584	0	1	1	0	585	0	1	1	1	586	1	1	1	0
588	1	1	1	0	589	0	1	1	1	590	0	1	1	0	591	1	1	1	0	592	0	1	1	0	593	0	1	1	1
594	1	1	1	0	596	1	1	1	0	597	0	1	1	1	598	0	1	1	0	599	1	1	1	0	600	0	1	1	0
601	0	1	1	1	602	1	1	1	0	604	1	1	1	0	605	0	1	1	1	606	0	1	1	0	607	1	1	1	0
608	0	1	1	0	609	0	1	1	1	610	1	1	1	0	612	1	1	1	0	613	0	1	1	1	614	0	1	1	0
615	1	1	1	0	616	0	1	1	0	617	0	0	0	1	618	0	0	0	0	619	0	0	0	1	620	0	0	0	0
621	0	0	0	1	622	0	1	1	0	623	1	1	1	0	624	0	1	1	0	625	0	1	1	0	626	1	1	1	0
627	0	1	1	0	628	0	1	1	0	629	1	1	1	0	630	0	1	1	0	631	0	1	1	0	632	1	1	1	0
633	0	1	1	0	634	0	1	1	0	635	1	1	1	0	636	0	1	1	0	637	0	1	1	0	638	1	1	1	0
639	0	1	1	0	640	0	1	1	0	641	1	1	1	0	642	0	1	1	0	643	0	1	1	0	644	1	1	1	0
645	0	1	1	0	646	0	1	1	0	647	1	1	1	0	648	0	1	1	0	649	0	1	1	0	650	1	1	1	0
651	0	1	1	0	652	0	1	1	0	653	1	1	1	0	654	0	1	1	0	655	0	1	1	0	656	1	1	1	0
657	0	1	1	0	658	0	1	1	0	659	1	1	1	0	660	0	1	1	0	661	0	1	1	0	662	1	1	1	0
663	0	1	1	0	664	0	1	1	0	665	1	1	1	0	666	0	1	1	0	667	0	1	1	0	668	1	1	1	0
669	0	1	1	0	670	0	1	1	0	671	1	1	1	0	672	0	1	1	0	673	0	1	1	0	674	1	1	1	0
675	0	1	1	0	676	0	1	1	0	677	1	1	1	0	678	0	1	1	0	679	0	1	1	0	680	1	1	1	0
681	0	1	1	0	682	0	0	0	0	683	0	0	0	0	684	0	0	0	0	685	0	1	1	1	686	1	1	1	0
687	1	1	1	1	688	1	1	1	0	689	0	1	1	1	690	0	1	1	0	691	1	1	1	0	692	0	1	1	0
693	0	1	1	1	694	1	1	1	0	696	1	1	1	0	697	0	1	1	1	698	0	1	1	0	699	1	1	1	0
700	0	1	1	0	701	0	1	1	1	702	1	1	1	0	704	1	1	1	0	705	0	1	1	1	706	0	1	1	0
707	1	1	1	0	708	0	1	1	0	709	0	1	1	1	710	1	1	1	0	712	1	1	1	0	713	0	1	1	1
714	0	1	1	0	715	1	1	1	0	716	0	1	1	0	717	0	1	1	1	718	1	1	1	0	720	1	1	1	0
721	0	1	1	1	722	0	1	1	0	723	1	1	1	0	724	0	1	1	0	725	0	1	1	1	726	1	1	1	0
728	1	1	1	0	729	0	1	1	1	730	0	1	1	0	731	1	1	1	0	732	0	1	1	0	733	0	1	1	1
734	1	1	1	0	736	1	1	1	0	737	0	1	1	1	738	0	1	1	0	739	1	1	1	0	740	0	1	1	0
741	0	1	1	1	742	1	1	1	0	744	1	1	1	0	745	0	1	1	1	746	0	1	1	0	747	1	1	1	0
748	0	1	1	0	749	0	1	1	1	750	1	1	1	0	752	1	1	1	0	753	0	1	1	1	754	0	1	1	0
755	1	1	1	0	756	0	1	1	0	757	0	1	1	1	758	1	1	1	0	760	1	1	1	0	761	0	1	1	1
762	0	1	1	0	763	1	1	1	0	764	0	1	1	0	765	0	1	1	1	766	1	1	1	0	768	1	1	1	0
769	0	1	1	1	770	0	1	1	0	771	1	1	1	0	772	0	1	1	0	773	0	1	1	1	774	1	1	1	0
776	1	1	1	0	777	0	1	1	1	778	0	1	1	0	779	1	1	1	0	780	0	1	1	0	781	0	1	1	1
782	1	1	1	0	784	1	1	1	0	785	0	1	1	1	786	0	1	1	0	787	1	1	1	0	788	0	1	1	0
789	0	1	1	1	790	1	1	1	0	792	1	1	1	0	793	0	1	1	1	794	0	1	1	0	795	1	1	1	0
796	0	1	1	0	797	0	1	1	1	798	1	1	1	0	800	1	1	1	0	801	0	1	1	1	802	0	1	1	0
803	1	1	1	0	804	0	1	1	0	805	0	1	1	1	806	1	1	1	0	808	1	1	1	0	809	0	1	1	1
810	0	1	1	0	811	1	1	1	0	812	0	1	1	0	813	0	1	1	1	814	1	1	1	0	816	1	1	1	0
817	0	1	1	1	818	0	1	1	0	819	1	1	1	0	820	0	1	1	0	821	0	1	1	1	822	1	1	1	0
824	1	1	1	0	825	0	1	1	1	826	0	1	1	0	827	1	1	1	0	828	0	1	1	0	829	0	1	1	1
830	1	1	1	0	832	1	1	1	0	833	0	1	1	1	834	0	1	1	0	835	1	1	1	0	836	0	1	1	0
837	0	1	1	1	838	1	1	1	0	840	1	1	1	0	841	0	1	1	1	842	0	1	1	0	843	1	1	1	0
844	0	1	1	0	845	0	0	0	1	846	0	0	0	0	847	0	0	0	1	848	0	0	0	0	849	0	0	0	1

850	0	1	1	0	851	1	1	1	0	852	0	1	1	0	853	0	1	1	0	854	1	1	1	0	855	0	1	1	0
856	0	1	1	0	857	1	1	1	0	858	0	1	1	0	859	0	1	1	0	860	1	1	1	0	861	0	1	1	0
862	0	1	1	0	863	1	1	1	0	864	0	1	1	0	865	0	1	1	0	866	1	1	1	0	867	0	1	1	0
868	0	1	1	0	869	1	1	1	0	870	0	1	1	0	871	0	1	1	0	872	1	1	1	0	873	0	1	1	0
874	0	1	1	0	875	1	1	1	0	876	0	1	1	0	877	0	1	1	0	878	1	1	1	0	879	0	1	1	0
880	0	1	1	0	881	1	1	1	0	882	0	1	1	0	883	0	1	1	0	884	1	1	1	0	885	0	1	1	0
886	0	1	1	0	887	1	1	1	0	888	0	1	1	0	889	0	1	1	0	890	1	1	1	0	891	0	1	1	0
892	0	1	1	0	893	1	1	1	0	894	0	1	1	0	895	0	1	1	0	896	1	1	1	0	897	0	1	1	0
898	0	1	1	0	899	1	1	1	0	900	0	1	1	0	901	0	1	1	0	902	1	1	1	0	903	0	1	1	0
904	0	1	1	0	905	1	1	1	0	906	0	1	1	0	907	0	1	1	0	908	1	1	1	0	909	0	1	1	0
910	0	0	0	0	911	0	0	0	0	912	0	0	0	0	913	0	1	1	1	914	1	1	1	0	915	1	1	1	1
916	1	1	1	0	917	0	1	1	1	918	0	1	1	0	919	1	1	1	0	920	0	1	1	0	921	0	1	1	1
922	1	1	1	0	924	1	1	1	0	925	0	1	1	1	926	0	1	1	0	927	1	1	1	0	928	0	1	1	0
929	0	1	1	1	930	1	1	1	0	932	1	1	1	0	933	0	1	1	1	934	0	1	1	0	935	1	1	1	0
936	0	1	1	0	937	0	1	1	1	938	1	1	1	0	940	1	1	1	0	941	0	1	1	1	942	0	1	1	0
943	1	1	1	0	944	0	1	1	0	945	0	1	1	1	946	1	1	1	0	948	1	1	1	0	949	0	1	1	1
950	0	1	1	0	951	1	1	1	0	952	0	1	1	0	953	0	1	1	1	954	1	1	1	0	956	1	1	1	0
957	0	1	1	1	958	0	1	1	0	959	1	1	1	0	960	0	1	1	0	961	0	1	1	1	962	1	1	1	0
964	1	1	1	0	965	0	1	1	1	966	0	1	1	0	967	1	1	1	0	968	0	1	1	0	969	0	1	1	1
970	1	1	1	0	972	1	1	1	0	973	0	1	1	1	974	0	1	1	0	975	1	1	1	0	976	0	1	1	0
977	0	1	1	1	978	1	1	1	0	980	1	1	1	0	981	0	1	1	1	982	0	1	1	0	983	1	1	1	0
984	0	1	1	0	985	0	1	1	1	986	1	1	1	0	988	1	1	1	0	989	0	1	1	1	990	0	1	1	0
991	1	1	1	0	992	0	1	1	0	993	0	1	1	1	994	1	1	1	0	996	1	1	1	0	997	0	1	1	1
998	0	1	1	0	999	1	1	1	0	1000	0	1	1	0	1001	0	1	1	1	1002	1	1	1	0	1004	1	1	1	0
1005	0	1	1	1	1006	0	1	1	0	1007	1	1	1	0	1008	0	1	1	0	1009	0	1	1	1	1010	1	1	1	0
1012	1	1	1	0	1013	0	1	1	1	1014	0	1	1	0	1015	1	1	1	0	1016	0	1	1	0	1017	0	1	1	1
1018	1	1	1	0	1020	1	1	1	0	1021	0	1	1	1	1022	0	1	1	0	1023	1	1	1	0	1024	0	1	1	0
1025	0	1	1	1	1026	1	1	1	0	1028	1	1	1	0	1029	0	1	1	1	1030	0	1	1	0	1031	1	1	1	0
1032	0	1	1	0	1033	0	1	1	1	1034	1	1	1	0	1036	1	1	1	0	1037	0	1	1	1	1038	0	1	1	0
1039	1	1	1	0	1040	0	1	1	0	1041	0	1	1	1	1042	1	1	1	0	1044	1	1	1	0	1045	0	1	1	1
1046	0	1	1	0	1047	1	1	1	0	1048	0	1	1	0	1049	0	1	1	1	1050	1	1	1	0	1052	1	1	1	0
1053	0	1	1	1	1054	0	1	1	0	1055	1	1	1	0	1056	0	1	1	0	1057	0	1	1	1	1058	1	1	1	0
1060	1	1	1	0	1061	0	1	1	1	1062	0	1	1	0	1063	1	1	1	0	1064	0	1	1	0	1065	0	1	1	1
1066	1	1	1	0	1068	1	1	1	0	1069	0	1	1	1	1070	0	1	1	0	1071	1	1	1	0	1072	0	1	1	0
1073	0	0	0	1	1074	0	0	0	0	1075	0	0	0	1	1076	0	0	0	0	1077	0	0	0	1	1078	0	1	1	0
1079	1	1	1	0	1080	0	1	1	0	1081	0	1	1	0	1082	1	1	1	0	1083	0	1	1	0	1084	0	1	1	0
1085	1	1	1	0	1086	0	1	1	0	1087	0	1	1	0	1088	1	1	1	0	1089	0	1	1	0	1090	0	1	1	0
1091	1	1	1	0	1092	0	1	1	0	1093	0	1	1	0	1094	1	1	1	0	1095	0	1	1	0	1096	0	1	1	0
1097	1	1	1	0	1098	0	1	1	0	1099	0	1	1	0	1100	1	1	1	0	1101	0	1	1	0	1102	0	1	1	0
1103	1	1	1	0	1104	0	1	1	0	1105	0	1	1	0	1106	1	1	1	0	1107	0	1	1	0	1108	0	1	1	0
1109	1	1	1	0	1110	0	1	1	0	1111	0	1	1	0	1112	1	1	1	0	1113	0	1	1	0	1114	0	1	1	0
1115	1	1	1	0	1116	0	1	1	0	1117	0	1	1	0	1118	1	1	1	0	1119	0	1	1	0	1120	0	1	1	0
1121	1	1	1	0	1122	0	1	1	0	1123	0	1	1	0	1124	1	1	1	0	1125	0	1	1	0	1126	0	1	1	0
1127	1	1	1	0	1128	0	1	1	0	1129	0	1	1	0	1130	1	1	1	0	1131	0	1	1	0	1132	0	1	1	0
1133	1	1	1	0	1134	0	1	1	0	1135	0	1	1	0	1136	1	1	1	0	1137	0	1	1	0	1138	0	0	0	0
1139	0	0	0	0	1140	0	0	0	0	1141	0	1	1	1	1142	1	1	1	0	1143	1	1	1	1	1144	1	1	1	0
1145	0	1	1	1	1146	0	1	1	0	1147	1	1	1	0	1148	0	1	1	0	1149	0	1	1	1	1150	1	1	1	0
1152	1	1	1	0	1153	0	1	1	1	1154	0	1	1	0	1155	1	1	1	0	1156	0	1	1	0	1157	0	1	1	1
1158	1	1	1	0	1160	1	1	1	0	1161	0	1	1	1	1162	0	1	1	0	1163	1	1	1	0	1164	0	1	1	0
1165	0	1	1	1	1166	1	1	1	0	1168	1	1	1	0	1169	0	1	1	1	1170	0	1	1	0	1171	1	1	1	0
1172	0	1	1	0	1173	0	1	1	1	1174	1	1	1	0	1176	1	1	1	0	1177	0	1	1	1	1178	0	1	1	0
1179	1	1	1	0	1180	0	1	1	0	1181	0	1	1	1	1182	1	1	1	0	1184	1	1	1	0	1185	0	1	1	1
1186	0	1	1	0	1187	1	1	1	0	1188	0	1	1	0	1189	0	1	1	1	1190	1	1	1	0	1192	1	1	1	0
1193	0	1	1	1	1194	0	1	1	0	1195	1	1	1	0	1196	0	1	1	0	1197	0	1	1	1	1198	1	1	1	0
1200	1	1	1	0	1201	0	1	1	1	1202	0	1	1	0	1203	1	1	1	0	1204	0	1	1	0	1205	0	1	1	1
1206	1	1	1	0	1208	1	1	1	0	1209	0	1	1	1	1210	0	1	1	0	1211	1	1	1	0	1212	0	1	1	0
1213	0	1	1	1	1214	1	1	1	0	1216	1	1	1	0	1217	0	1	1	1	1218	0	1	1	0	1219	1	1	1	0
1220	0	1	1	0	1221	0	1	1	1	1222	1	1	1	0	1224	1	1	1	0	1225	0	1	1	1	1226	0	1	1	0
1227	1	1	1	0	1228	0	1	1	0	1229	0	1	1	1	1230	1	1	1	0	1232	1	1	1	0	1233	0	1	1	1
1234	0	1	1	0	1235	1	1	1	0	1236	0	1	1	0	1237	0	1	1	1	1238	1	1	1	0	1240	1	1	1	0
1241	0	1	1	1	1242	0	1	1	0	1243	1	1	1	0	1244	0	1	1	0	1245	0	1	1	1	1246	1	1	1	0
1248	1	1	1	0	1249	0	1	1	1	1250	0	1	1	0	1251	1	1	1	0	1252	0	1	1	0	1253	0	1	1	1
1254	1	1	1	0	1256	1	1	1	0	1257	0	1	1	1	1258	0	1	1	0	1259	1	1	1	0	1260	0	1	1	0
1261	0	1	1	1	1262	1	1	1	0	1264	1	1	1	0	1265	0	1	1	1	1266	0	1	1	0	1267	1	1	1	0
1268	0	1	1	0	1269	0	1	1	1	1270	1	1	1	0	1272	1	1	1	0	1273	0	1	1	1	1274	0	1	1	0
1275	1	1	1	0	1276	0	1	1	0	1277	0	1	1	1	1278	1	1	1	0	1280	1	1	1	0	1281	0	1	1	1
1282	0	1	1	0	1283	1	1	1	0	1284	0	1	1	0	1285	0	1	1	1	1286	1	1	1	0	1288	1	1	1	0
1289	0	1	1	1	1290	0	1	1	0	1291	1	1	1	0	1292	0	1	1	0	1293	0	1	1	1	1294	1	1	1	0

1296	1	1	1	0	1297	0	1	1	1	1298	0	1	1	0	1299	1	1	1	0	1300	0	1	1	0	1301	0	0	0	1
1302	0	0	0	0	1303	0	0	0	1	1304	0	0	0	0	1305	0	0	0	1	1306	0	1	1	0	1307	1	1	1	0
1308	0	1	1	0	1309	0	1	1	0	1310	1	1	1	0	1311	0	1	1	0	1312	0	1	1	0	1313	1	1	1	0
1314	0	1	1	0	1315	0	1	1	0	1316	1	1	1	0	1317	0	1	1	0	1318	0	1	1	0	1319	1	1	1	0
1320	0	1	1	0	1321	0	1	1	0	1322	1	1	1	0	1323	0	1	1	0	1324	0	1	1	0	1325	1	1	1	0
1326	0	1	1	0	1327	0	1	1	0	1328	1	1	1	0	1329	0	1	1	0	1330	0	1	1	0	1331	1	1	1	0
1332	0	1	1	0	1333	0	1	1	0	1334	1	1	1	0	1335	0	1	1	0	1336	0	1	1	0	1337	1	1	1	0
1338	0	1	1	0	1339	0	1	1	0	1340	1	1	1	0	1341	0	1	1	0	1342	0	1	1	0	1343	1	1	1	0
1344	0	1	1	0	1345	0	1	1	0	1346	1	1	1	0	1347	0	1	1	0	1348	0	1	1	0	1349	1	1	1	0
1350	0	1	1	0	1351	0	1	1	0	1352	1	1	1	0	1353	0	1	1	0	1354	0	1	1	0	1355	1	1	1	0
1356	0	1	1	0	1357	0	1	1	0	1358	1	1	1	0	1359	0	1	1	0	1360	0	1	1	0	1361	1	1	1	0
1362	0	1	1	0	1363	0	1	1	0	1364	1	1	1	0	1365	0	1	1	0	1366	0	0	0	0	1367	0	0	0	0
1368	0	0	0	0	1369	0	1	1	1	1370	1	1	1	0	1371	1	1	1	1	1372	1	1	1	0	1373	0	1	1	1
1374	0	1	1	0	1375	1	1	1	0	1376	0	1	1	0	1377	0	1	1	1	1378	1	1	1	0	1380	1	1	1	0
1381	0	1	1	1	1382	0	1	1	0	1383	1	1	1	0	1384	0	1	1	0	1385	0	1	1	1	1386	1	1	1	0
1388	1	1	1	0	1389	0	1	1	1	1390	0	1	1	0	1391	1	1	1	0	1392	0	1	1	0	1393	0	1	1	1
1394	1	1	1	0	1396	1	1	1	0	1397	0	1	1	1	1398	0	1	1	0	1399	1	1	1	0	1400	0	1	1	0
1401	0	1	1	1	1402	1	1	1	0	1404	1	1	1	0	1405	0	1	1	1	1406	0	1	1	0	1407	1	1	1	0
1408	0	1	1	0	1409	0	1	1	1	1410	1	1	1	0	1412	1	1	1	0	1413	0	1	1	1	1414	0	1	1	0
1415	1	1	1	0	1416	0	1	1	0	1417	0	1	1	1	1418	1	1	1	0	1420	1	1	1	0	1421	0	1	1	1
1422	0	1	1	0	1423	1	1	1	0	1424	0	1	1	0	1425	0	1	1	1	1426	1	1	1	0	1428	1	1	1	0
1429	0	1	1	1	1430	0	1	1	0	1431	1	1	1	0	1432	0	1	1	0	1433	0	1	1	1	1434	1	1	1	0
1436	1	1	1	0	1437	0	1	1	1	1438	0	1	1	0	1439	1	1	1	0	1440	0	1	1	0	1441	0	1	1	1
1442	1	1	1	0	1444	1	1	1	0	1445	0	1	1	1	1446	0	1	1	0	1447	1	1	1	0	1448	0	1	1	0
1449	0	1	1	1	1450	1	1	1	0	1452	1	1	1	0	1453	0	1	1	1	1454	0	1	1	0	1455	1	1	1	0
1456	0	1	1	0	1457	0	1	1	1	1458	1	1	1	0	1460	1	1	1	0	1461	0	1	1	1	1462	0	1	1	0
1463	1	1	1	0	1464	0	1	1	0	1465	0	1	1	1	1466	1	1	1	0	1468	1	1	1	0	1469	0	1	1	1
1470	0	1	1	0	1471	1	1	1	0	1472	0	1	1	0	1473	0	1	1	1	1474	1	1	1	0	1476	1	1	1	0
1477	0	1	1	1	1478	0	1	1	0	1479	1	1	1	0	1480	0	1	1	0	1481	0	1	1	1	1482	1	1	1	0
1484	1	1	1	0	1485	0	1	1	1	1486	0	1	1	0	1487	1	1	1	0	1488	0	1	1	0	1489	0	1	1	1
1490	1	1	1	0	1492	1	1	1	0	1493	0	1	1	1	1494	0	1	1	0	1495	1	1	1	0	1496	0	1	1	0
1497	0	1	1	1	1498	1	1	1	0	1500	1	1	1	0	1501	0	1	1	1	1502	0	1	1	0	1503	1	1	1	0
1504	0	1	1	0	1505	0	1	1	1	1506	1	1	1	0	1508	1	1	1	0	1509	0	1	1	1	1510	0	1	1	0
1511	1	1	1	0	1512	0	1	1	0	1513	0	1	1	1	1514	1	1	1	0	1516	1	1	1	0	1517	0	1	1	1
1518	0	1	1	0	1519	1	1	1	0	1520	0	1	1	0	1521	0	1	1	1	1522	1	1	1	0	1524	1	1	1	0
1525	0	1	1	1	1526	0	1	1	0	1527	1	1	1	0	1528	0	1	1	0	1529	0	0	0	1	1530	0	0	0	0
1531	0	0	0	1	1532	0	0	0	0	1533	0	0	0	1	1534	0	1	1	0	1535	1	1	1	0	1536	0	1	1	0
1537	0	1	1	0	1538	1	1	1	0	1539	0	1	1	0	1540	0	1	1	0	1541	1	1	1	0	1542	0	1	1	0
1543	0	1	1	0	1544	1	1	1	0	1545	0	1	1	0	1546	0	1	1	0	1547	1	1	1	0	1548	0	1	1	0
1549	0	1	1	0	1550	1	1	1	0	1551	0	1	1	0	1552	0	1	1	0	1553	1	1	1	0	1554	0	1	1	0
1555	0	1	1	0	1556	1	1	1	0	1557	0	1	1	0	1558	0	1	1	0	1559	1	1	1	0	1560	0	1	1	0
1561	0	1	1	0	1562	1	1	1	0	1563	0	1	1	0	1564	0	1	1	0	1565	1	1	1	0	1566	0	1	1	0
1567	0	1	1	0	1568	1	1	1	0	1569	0	1	1	0	1570	0	1	1	0	1571	1	1	1	0	1572	0	1	1	0
1573	0	1	1	0	1574	1	1	1	0	1575	0	1	1	0	1576	0	1	1	0	1577	1	1	1	0	1578	0	1	1	0
1579	0	1	1	0	1580	1	1	1	0	1581	0	1	1	0	1582	0	1	1	0	1583	1	1	1	0	1584	0	1	1	0
1585	0	1	1	0	1586	1	1	1	0	1587	0	1	1	0	1588	0	1	1	0	1589	1	1	1	0	1590	0	1	1	0
1591	0	1	1	0	1592	1	1	1	0	1593	0	1	1	0	1594	0	0	0	0	1595	0	0	0	0	1596	0	0	0	0
1597	0	1	1	1	1598	1	1	1	0	1599	1	1	1	1	1600	1	1	1	0	1601	0	1	1	1	1602	0	1	1	0
1603	1	1	1	0	1604	0	1	1	0	1605	0	1	1	1	1606	1	1	1	0	1608	1	1	1	0	1609	0	1	1	1
1610	0	1	1	0	1611	1	1	1	0	1612	0	1	1	0	1613	0	1	1	1	1614	1	1	1	0	1616	1	1	1	0
1617	0	1	1	1	1618	0	1	1	0	1619	1	1	1	0	1620	0	1	1	0	1621	0	1	1	1	1622	1	1	1	0
1624	1	1	1	0	1625	0	1	1	1	1626	0	1	1	0	1627	1	1	1	0	1628	0	1	1	0	1629	0	1	1	1
1630	1	1	1	0	1632	1	1	1	0	1633	0	1	1	1	1634	0	1	1	0	1635	1	1	1	0	1636	0	1	1	0
1637	0	1	1	1	1638	1	1	1	0	1640	1	1	1	0	1641	0	1	1	1	1642	0	1	1	0	1643	1	1	1	0
1644	0	1	1	0	1645	0	1	1	1	1646	1	1	1	0	1648	1	1	1	0	1649	0	1	1	1	1650	0	1	1	0
1651	1	1	1	0	1652	0	1	1	0	1653	0	1	1	1	1654	1	1	1	0	1656	1	1	1	0	1657	0	1	1	1
1658	0	1	1	0	1659	1	1	1	0	1660	0	1	1	0	1661	0	1	1	1	1662	1	1	1	0	1664	1	1	1	0
1665	0	1	1	1	1666	0	1	1	0	1667	1	1	1	0	1668	0	1	1	0	1669	0	1	1	1	1670	1	1	1	0
1672	1	1	1	0	1673	0	1	1	1	1674	0	1	1	0	1675	1	1	1	0	1676	0	1	1	0	1677	0	1	1	1
1678	1	1	1	0	1680	1	1	1	0	1681	0	1	1	1	1682	0	1	1	0	1683	1	1	1	0	1684	0	1	1	0
1685	0	1	1	1	1686	1	1	1	0	1688	1	1	1	0	1689	0	1	1	1	1690	0	1	1	0	1691	1	1	1	0
1692	0	1	1	0	1693	0	1	1	1	1694	1	1	1	0	1696	1	1	1	0	1697	0	1	1	1	1698	0	1	1	0
1699	1	1	1	0	1700	0	1	1	0	1701	0	1	1	1	1702	1	1	1	0	1704	1	1	1	0	1705	0	1	1	1
1706	0	1	1	0	1707	1	1	1	0	1708	0	1	1	0	1709	0	1	1	1	1710	1	1	1	0	1712	1	1	1	0
1713	0	1	1	1	1714	0	1	1	0	1715	1	1	1	0	1716	0	1	1	0	1717	0	1	1	1	1718	1	1	1	0
1720	1	1	1	0	1721	0	1	1	1	1722	0	1	1	0	1723	1	1	1	0	1724	0	1	1	0	1725	0	1	1	1
1726	1	1	1	0	1728	1	1	1	0	1729	0	1	1	1	1730	0	1	1	0	1731	1	1	1	0	1732	0	1	1	0
1733	0	1	1	1	1734	1	1	1	0	1736	1	1	1	0	1737	0	1	1	1	1738	0	1	1	0	1739	1	1	1	0

1740	0	1	1	0	1741	0	1	1	1	1742	1	1	1	0	1744	1	1	1	0	1745	0	1	1	1	1746	0	1	1	0
1747	1	1	1	0	1748	0	1	1	0	1749	0	1	1	1	1750	1	1	1	0	1752	1	1	1	0	1753	0	1	1	1
1754	0	1	1	0	1755	1	1	1	0	1756	0	1	1	0	1757	0	0	0	1	1758	0	0	0	0	1759	0	0	0	1
1760	0	0	0	0	1761	0	0	0	1	1762	0	1	1	0	1763	1	1	1	0	1764	0	1	1	0	1765	0	1	1	0
1766	1	1	1	0	1767	0	1	1	0	1768	0	1	1	0	1769	1	1	1	0	1770	0	1	1	0	1771	0	1	1	0
1772	1	1	1	0	1773	0	1	1	0	1774	0	1	1	0	1775	1	1	1	0	1776	0	1	1	0	1777	0	1	1	0
1778	1	1	1	0	1779	0	1	1	0	1780	0	1	1	0	1781	1	1	1	0	1782	0	1	1	0	1783	0	1	1	0
1784	1	1	1	0	1785	0	1	1	0	1786	0	1	1	0	1787	1	1	1	0	1788	0	1	1	0	1789	0	1	1	0
1790	1	1	1	0	1791	0	1	1	0	1792	0	1	1	0	1793	1	1	1	0	1794	0	1	1	0	1795	0	1	1	0
1796	1	1	1	0	1797	0	1	1	0	1798	0	1	1	0	1799	1	1	1	0	1800	0	1	1	0	1801	0	1	1	0
1802	1	1	1	0	1803	0	1	1	0	1804	0	1	1	0	1805	1	1	1	0	1806	0	1	1	0	1807	0	1	1	0
1808	1	1	1	0	1809	0	1	1	0	1810	0	1	1	0	1811	1	1	1	0	1812	0	1	1	0	1813	0	1	1	0
1814	1	1	1	0	1815	0	1	1	0	1816	0	1	1	0	1817	1	1	1	0	1818	0	1	1	0	1819	0	1	1	0
1820	1	1	1	0	1821	0	1	1	0	1822	0	0	0	0	1823	0	0	0	0	1824	0	0	0	0	1825	0	1	1	1
1826	1	1	1	0	1827	1	1	1	1	1828	1	1	1	0	1829	0	1	1	1	1830	0	1	1	0	1831	1	1	1	0
1832	0	1	1	0	1833	0	1	1	1	1834	1	1	1	0	1836	1	1	1	0	1837	0	1	1	1	1838	0	1	1	0
1839	1	1	1	0	1840	0	1	1	0	1841	0	1	1	1	1842	1	1	1	0	1844	1	1	1	0	1845	0	1	1	1
1846	0	1	1	0	1847	1	1	1	0	1848	0	1	1	0	1849	0	1	1	1	1850	1	1	1	0	1852	1	1	1	0
1853	0	1	1	1	1854	0	1	1	0	1855	1	1	1	0	1856	0	1	1	0	1857	0	1	1	1	1858	1	1	1	0
1860	1	1	1	0	1861	0	1	1	1	1862	0	1	1	0	1863	1	1	1	0	1864	0	1	1	0	1865	0	1	1	1
1866	1	1	1	0	1868	1	1	1	0	1869	0	1	1	1	1870	0	1	1	0	1871	1	1	1	0	1872	0	1	1	0
1873	0	1	1	1	1874	1	1	1	0	1876	1	1	1	0	1877	0	1	1	1	1878	0	1	1	0	1879	1	1	1	0
1880	0	1	1	0	1881	0	1	1	1	1882	1	1	1	0	1884	1	1	1	0	1885	0	1	1	1	1886	0	1	1	0
1887	1	1	1	0	1888	0	1	1	0	1889	0	1	1	1	1890	1	1	1	0	1892	1	1	1	0	1893	0	1	1	1
1894	0	1	1	0	1895	1	1	1	0	1896	0	1	1	0	1897	0	1	1	1	1898	1	1	1	0	1900	1	1	1	0
1901	0	1	1	1	1902	0	1	1	0	1903	1	1	1	0	1904	0	1	1	0	1905	0	1	1	1	1906	1	1	1	0
1908	1	1	1	0	1909	0	1	1	1	1910	0	1	1	0	1911	1	1	1	0	1912	0	1	1	0	1913	0	1	1	1
1914	1	1	1	0	1916	1	1	1	0	1917	0	1	1	1	1918	0	1	1	0	1919	1	1	1	0	1920	0	1	1	0
1921	0	1	1	1	1922	1	1	1	0	1924	1	1	1	0	1925	0	1	1	1	1926	0	1	1	0	1927	1	1	1	0
1928	0	1	1	0	1929	0	1	1	1	1930	1	1	1	0	1932	1	1	1	0	1933	0	1	1	1	1934	0	1	1	0
1935	1	1	1	0	1936	0	1	1	0	1937	0	1	1	1	1938	1	1	1	0	1940	1	1	1	0	1941	0	1	1	1
1942	0	1	1	0	1943	1	1	1	0	1944	0	1	1	0	1945	0	1	1	1	1946	1	1	1	0	1948	1	1	1	0
1949	0	1	1	1	1950	0	1	1	0	1951	1	1	1	0	1952	0	1	1	0	1953	0	1	1	1	1954	1	1	1	0
1956	1	1	1	0	1957	0	1	1	1	1958	0	1	1	0	1959	1	1	1	0	1960	0	1	1	0	1961	0	1	1	1
1962	1	1	1	0	1964	1	1	1	0	1965	0	1	1	1	1966	0	1	1	0	1967	1	1	1	0	1968	0	1	1	0
1969	0	1	1	1	1970	1	1	1	0	1972	1	1	1	0	1973	0	1	1	1	1974	0	1	1	0	1975	1	1	1	0
1976	0	1	1	0	1977	0	1	1	1	1978	1	1	1	0	1980	1	1	1	0	1981	0	1	1	1	1982	0	1	1	0
1983	1	1	1	0	1984	0	1	1	0	1985	0	0	0	1	1986	0	0	0	0	1987	0	0	0	1	1988	0	0	0	0
1989	0	0	0	1	1990	0	1	1	0	1991	1	1	1	0	1992	0	1	1	0	1993	0	1	1	0	1994	1	1	1	0
1995	0	1	1	0	1996	0	1	1	0	1997	1	1	1	0	1998	0	1	1	0	1999	0	1	1	0	2000	1	1	1	0
2001	0	1	1	0	2002	0	1	1	0	2003	1	1	1	0	2004	0	1	1	0	2005	0	1	1	0	2006	1	1	1	0
2007	0	1	1	0	2008	0	1	1	0	2009	1	1	1	0	2010	0	1	1	0	2011	0	1	1	0	2012	1	1	1	0
2013	0	1	1	0	2014	0	1	1	0	2015	1	1	1	0	2016	0	1	1	0	2017	0	1	1	0	2018	1	1	1	0
2019	0	1	1	0	2020	0	1	1	0	2021	1	1	1	0	2022	0	1	1	0	2023	0	1	1	0	2024	1	1	1	0
2025	0	1	1	0	2026	0	1	1	0	2027	1	1	1	0	2028	0	1	1	0	2029	0	1	1	0	2030	1	1	1	0
2031	0	1	1	0	2032	0	1	1	0	2033	1	1	1	0	2034	0	1	1	0	2035	0	1	1	0	2036	1	1	1	0
2037	0	1	1	0	2038	0	1	1	0	2039	1	1	1	0	2040	0	1	1	0	2041	0	1	1	0	2042	1	1	1	0
2043	0	1	1	0	2044	0	1	1	0	2045	1	1	1	0	2046	0	1	1	0	2047	0	1	1	0	2048	1	1	1	0
2049	0	1	1	0	2050	0	0	0	0	2051	0	0	0	0	2052	0	0	0	0	2053	0	1	1	1	2054	1	1	1	0
2055	1	1	1	1	2056	1	1	1	0	2057	0	1	1	1	2058	0	1	1	0	2059	1	1	1	0	2060	0	1	1	0
2061	0	1	1	1	2062	1	1	1	0	2064	1	1	1	0	2065	0	1	1	1	2066	0	1	1	0	2067	1	1	1	0
2068	0	1	1	0	2069	0	1	1	1	2070	1	1	1	0	2072	1	1	1	0	2073	0	1	1	1	2074	0	1	1	0
2075	1	1	1	0	2076	0	1	1	0	2077	0	1	1	1	2078	1	1	1	0	2080	1	1	1	0	2081	0	1	1	1
2082	0	1	1	0	2083	1	1	1	0	2084	0	1	1	0	2085	0	1	1	1	2086	1	1	1	0	2088	1	1	1	0
2089	0	1	1	1	2090	0	1	1	0	2091	1	1	1	0	2092	0	1	1	0	2093	0	1	1	1	2094	1	1	1	0
2096	1	1	1	0	2097	0	1	1	1	2098	0	1	1	0	2099	1	1	1	0	2100	0	1	1	0	2101	0	1	1	1
2102	1	1	1	0	2104	1	1	1	0	2105	0	1	1	1	2106	0	1	1	0	2107	1	1	1	0	2108	0	1	1	0
2109	0	1	1	1	2110	1	1	1	0	2112	1	1	1	0	2113	0	1	1	1	2114	0	1	1	0	2115	1	1	1	0
2116	0	1	1	0	2117	0	1	1	1	2118	1	1	1	0	2120	1	1	1	0	2121	0	1	1	1	2122	0	1	1	0
2123	1	1	1	0	2124	0	1	1	0	2125	0	1	1	1	2126	1	1	1	0	2128	1	1	1	0	2129	0	1	1	1
2130	0	1	1	0	2131	1	1	1	0	2132	0	1	1	0	2133	0	1	1	1	2134	1	1	1	0	2136	1	1	1	0
2137	0	1	1	1	2138	0	1	1	0	2139	1	1	1	0	2140	0	1	1	0	2141	0	1	1	1	2142	1	1	1	0
2144	1	1	1	0	2145	0	1	1	1	2146	0	1	1	0	2147	1	1	1	0	2148	0	1	1	0	2149	0	1	1	1
2150	1	1	1	0	2152	1	1	1	0	2153	0	1	1	1	2154	0	1	1	0	2155	1	1	1	0	2156	0	1	1	0
2157	0	1	1	1	2158	1	1	1	0	2160	1	1	1	0	2161	0	1	1	1	2162	0	1	1	0	2163	1	1	1	0
2164	0	1	1	0	2165	0	1	1	1	2166	1	1	1	0	2168	1	1	1	0	2169	0	1	1	1	2170	0	1	1	0
2171	1	1	1	0	2172	0	1	1	0	2173	0	1	1	1	2174	1	1	1	0	2176	1	1	1	0	2177	0	1	1	1
2178	0	1	1	0	2179	1	1	1	0	2180	0	1	1	0	2181	0	1	1	1	2182	1	1	1	0	2184	1	1	1	0

2185	0	1	1	1	2186	0	1	1	0	2187	1	1	1	0	2188	0	1	1	0	2189	0	1	1	1	2190	1	1	1	0
2192	1	1	1	0	2193	0	1	1	1	2194	0	1	1	0	2195	1	1	1	0	2196	0	1	1	0	2197	0	1	1	1
2198	1	1	1	0	2200	1	1	1	0	2201	0	1	1	1	2202	0	1	1	0	2203	1	1	1	0	2204	0	1	1	0
2205	0	1	1	1	2206	1	1	1	0	2208	1	1	1	0	2209	0	1	1	1	2210	0	1	1	0	2211	1	1	1	0
2212	0	1	1	0	2213	0	0	0	1	2214	0	0	0	0	2215	0	0	0	1	2216	0	0	0	0	2217	0	0	0	1
2218	0	1	1	0	2219	1	1	1	0	2220	0	1	1	0	2221	0	1	1	0	2222	1	1	1	0	2223	0	1	1	0
2224	0	1	1	0	2225	1	1	1	0	2226	0	1	1	0	2227	0	1	1	0	2228	1	1	1	0	2229	0	1	1	0
2230	0	1	1	0	2231	1	1	1	0	2232	0	1	1	0	2233	0	1	1	0	2234	1	1	1	0	2235	0	1	1	0
2236	0	1	1	0	2237	1	1	1	0	2238	0	1	1	0	2239	0	1	1	0	2240	1	1	1	0	2241	0	1	1	0
2242	0	1	1	0	2243	1	1	1	0	2244	0	1	1	0	2245	0	1	1	0	2246	1	1	1	0	2247	0	1	1	0
2248	0	1	1	0	2249	1	1	1	0	2250	0	1	1	0	2251	0	1	1	0	2252	1	1	1	0	2253	0	1	1	0
2254	0	1	1	0	2255	1	1	1	0	2256	0	1	1	0	2257	0	1	1	0	2258	1	1	1	0	2259	0	1	1	0
2260	0	1	1	0	2261	1	1	1	0	2262	0	1	1	0	2263	0	1	1	0	2264	1	1	1	0	2265	0	1	1	0
2266	0	1	1	0	2267	1	1	1	0	2268	0	1	1	0	2269	0	1	1	0	2270	1	1	1	0	2271	0	1	1	0
2272	0	1	1	0	2273	1	1	1	0	2274	0	1	1	0	2275	0	1	1	0	2276	1	1	1	0	2277	0	1	1	0
2278	0	0	0	0	2279	0	0	0	0	2280	0	0	0	0	2281	0	1	1	1	2282	1	1	1	0	2283	1	1	1	1
2284	1	1	1	0	2285	0	1	1	1	2286	0	1	1	0	2287	1	1	1	0	2288	0	1	1	0	2289	0	1	1	1
2290	1	1	1	0	2292	1	1	1	0	2293	0	1	1	1	2294	0	1	1	0	2295	1	1	1	0	2296	0	1	1	0
2297	0	1	1	1	2298	1	1	1	0	2300	1	1	1	0	2301	0	1	1	1	2302	0	1	1	0	2303	1	1	1	0
2304	0	1	1	0	2305	0	1	1	1	2306	1	1	1	0	2308	1	1	1	0	2309	0	1	1	1	2310	0	1	1	0
2311	1	1	1	0	2312	0	1	1	0	2313	0	1	1	1	2314	1	1	1	0	2316	1	1	1	0	2317	0	1	1	1
2318	0	1	1	0	2319	1	1	1	0	2320	0	1	1	0	2321	0	1	1	1	2322	1	1	1	0	2324	1	1	1	0
2325	0	1	1	1	2326	0	1	1	0	2327	1	1	1	0	2328	0	1	1	0	2329	0	1	1	1	2330	1	1	1	0
2332	1	1	1	0	2333	0	1	1	1	2334	0	1	1	0	2335	1	1	1	0	2336	0	1	1	0	2337	0	1	1	1
2338	1	1	1	0	2340	1	1	1	0	2341	0	1	1	1	2342	0	1	1	0	2343	1	1	1	0	2344	0	1	1	0
2345	0	1	1	1	2346	1	1	1	0	2348	1	1	1	0	2349	0	1	1	1	2350	0	1	1	0	2351	1	1	1	0
2352	0	1	1	0	2353	0	1	1	1	2354	1	1	1	0	2356	1	1	1	0	2357	0	1	1	1	2358	0	1	1	0
2359	1	1	1	0	2360	0	1	1	0	2361	0	1	1	1	2362	1	1	1	0	2364	1	1	1	0	2365	0	1	1	1
2366	0	1	1	0	2367	1	1	1	0	2368	0	1	1	0	2369	0	1	1	1	2370	1	1	1	0	2372	1	1	1	0
2373	0	1	1	1	2374	0	1	1	0	2375	1	1	1	0	2376	0	1	1	0	2377	0	1	1	1	2378	1	1	1	0
2380	1	1	1	0	2381	0	1	1	1	2382	0	1	1	0	2383	1	1	1	0	2384	0	1	1	0	2385	0	1	1	1
2386	1	1	1	0	2388	1	1	1	0	2389	0	1	1	1	2390	0	1	1	0	2391	1	1	1	0	2392	0	1	1	0
2393	0	1	1	1	2394	1	1	1	0	2396	1	1	1	0	2397	0	1	1	1	2398	0	1	1	0	2399	1	1	1	0
2400	0	1	1	0	2401	0	1	1	1	2402	1	1	1	0	2404	1	1	1	0	2405	0	1	1	1	2406	0	1	1	0
2407	1	1	1	0	2408	0	1	1	0	2409	0	1	1	1	2410	1	1	1	0	2412	1	1	1	0	2413	0	1	1	1
2414	0	1	1	0	2415	1	1	1	0	2416	0	1	1	0	2417	0	1	1	1	2418	1	1	1	0	2420	1	1	1	0
2421	0	1	1	1	2422	0	1	1	0	2423	1	1	1	0	2424	0	1	1	0	2425	0	1	1	1	2426	1	1	1	0
2428	1	1	1	0	2429	0	1	1	1	2430	0	1	1	0	2431	1	1	1	0	2432	0	1	1	0	2433	0	1	1	1
2434	1	1	1	0	2436	1	1	1	0	2437	0	1	1	1	2438	0	1	1	0	2439	1	1	1	0	2440	0	1	1	0
2441	0	0	0	1	2442	0	0	0	0	2443	0	0	0	1	2444	0	0	0	0	2445	0	0	0	1	2446	0	1	1	0
2447	1	1	1	0	2448	0	1	1	0	2449	0	1	1	0	2450	1	1	1	0	2451	0	1	1	0	2452	0	1	1	0
2453	1	1	1	0	2454	0	1	1	0	2455	0	1	1	0	2456	1	1	1	0	2457	0	1	1	0	2458	0	1	1	0
2459	1	1	1	0	2460	0	1	1	0	2461	0	1	1	0	2462	1	1	1	0	2463	0	1	1	0	2464	0	1	1	0
2465	1	1	1	0	2466	0	1	1	0	2467	0	1	1	0	2468	1	1	1	0	2469	0	1	1	0	2470	0	1	1	0
2471	1	1	1	0	2472	0	1	1	0	2473	0	1	1	0	2474	1	1	1	0	2475	0	1	1	0	2476	0	1	1	0
2477	1	1	1	0	2478	0	1	1	0	2479	0	1	1	0	2480	1	1	1	0	2481	0	1	1	0	2482	0	1	1	0
2483	1	1	1	0	2484	0	1	1	0	2485	0	1	1	0	2486	1	1	1	0	2487	0	1	1	0	2488	0	1	1	0
2489	1	1	1	0	2490	0	1	1	0	2491	0	1	1	0	2492	1	1	1	0	2493	0	1	1	0	2494	0	1	1	0
2495	1	1	1	0	2496	0	1	1	0	2497	0	1	1	0	2498	1	1	1	0	2499	0	1	1	0	2500	0	1	1	0
2501	1	1	1	0	2502	0	1	1	0	2503	0	1	1	0	2504	1	1	1	0	2505	0	1	1	0	2506	0	0	0	0
2507	0	0	0	0	2508	0	0	0	0	2509	0	1	1	1	2510	1	1	1	0	2511	1	1	1	1	2512	1	1	1	0
2513	0	1	1	1	2514	0	1	1	0	2515	1	1	1	0	2516	0	1	1	0	2517	0	1	1	1	2518	1	1	1	0
2520	1	1	1	0	2521	0	1	1	1	2522	0	1	1	0	2523	1	1	1	0	2524	0	1	1	0	2525	0	1	1	1
2526	1	1	1	0	2528	1	1	1	0	2529	0	1	1	1	2530	0	1	1	0	2531	1	1	1	0	2532	0	1	1	0
2533	0	1	1	1	2534	1	1	1	0	2536	1	1	1	0	2537	0	1	1	1	2538	0	1	1	0	2539	1	1	1	0
2540	0	1	1	0	2541	0	1	1	1	2542	1	1	1	0	2544	1	1	1	0	2545	0	1	1	1	2546	0	1	1	0
2547	1	1	1	0	2548	0	1	1	0	2549	0	1	1	1	2550	1	1	1	0	2552	1	1	1	0	2553	0	1	1	1
2554	0	1	1	0	2555	1	1	1	0	2556	0	1	1	0	2557	0	1	1	1	2558	1	1	1	0	2560	1	1	1	0
2561	0	1	1	1	2562	0	1	1	0	2563	1	1	1	0	2564	0	1	1	0	2565	0	1	1	1	2566	1	1	1	0
2568	1	1	1	0	2569	0	1	1	1	2570	0	1	1	0	2571	1	1	1	0	2572	0	1	1	0	2573	0	1	1	1
2574	1	1	1	0	2576	1	1	1	0	2577	0	1	1	1	2578	0	1	1	0	2579	1	1	1	0	2580	0	1	1	0
2581	0	1	1	1	2582	1	1	1	0	2584	1	1	1	0	2585	0	1	1	1	2586	0	1	1	0	2587	1	1	1	0
2588	0	1	1	0	2589	0	1	1	1	2590	1	1	1	0	2592	1	1	1	0	2593	0	1	1	1	2594	0	1	1	0
2595	1	1	1	0	2596	0	1	1	0	2597	0	1	1	1	2598	1	1	1	0	2600	1	1	1	0	2601	0	1	1	1
2602	0	1	1	0	2603	1	1	1	0	2604	0	1	1	0	2605	0	1	1	1	2606	1	1	1	0	2608	1	1	1	0
2609	0	1	1	1	2610	0	1	1	0	2611	1	1	1	0	2612	0	1	1	0	2613	0	1	1	1	2614	1	1	1	0
2616	1	1	1	0	2617	0	1	1	1	2618	0	1	1	0	2619	1	1	1	0	2620	0	1	1	0	2621	0	1	1	1
2622	1	1	1	0	2624	1	1	1	0	2625	0	1	1	1	2626	0	1	1	0	2627	1	1	1	0	2628	0	1	1	0

2629	0	1	1	1	2630	1	1	1	0	2632	1	1	1	0	2633	0	1	1	1	2634	0	1	1	0	2635	1	1	1	0
2636	0	1	1	0	2637	0	1	1	1	2638	1	1	1	0	2640	1	1	1	0	2641	0	1	1	1	2642	0	1	1	0
2643	1	1	1	0	2644	0	1	1	0	2645	0	1	1	1	2646	1	1	1	0	2648	1	1	1	0	2649	0	1	1	1
2650	0	1	1	0	2651	1	1	1	0	2652	0	1	1	0	2653	0	1	1	1	2654	1	1	1	0	2656	1	1	1	0
2657	0	1	1	1	2658	0	1	1	0	2659	1	1	1	0	2660	0	1	1	0	2661	0	1	1	1	2662	1	1	1	0
2664	1	1	1	0	2665	0	1	1	1	2666	0	1	1	0	2667	1	1	1	0	2668	0	1	1	0	2669	0	0	0	1
2670	0	0	0	0	2671	0	0	0	1	2672	0	0	0	0	2673	0	0	0	1	2674	0	1	1	0	2675	1	1	1	0
2676	0	1	1	0	2677	0	1	1	0	2678	1	1	1	0	2679	0	1	1	0	2680	0	1	1	0	2681	1	1	1	0
2682	0	1	1	0	2683	0	1	1	0	2684	1	1	1	0	2685	0	1	1	0	2686	0	1	1	0	2687	1	1	1	0
2688	0	1	1	0	2689	0	1	1	0	2690	1	1	1	0	2691	0	1	1	0	2692	0	1	1	0	2693	1	1	1	0
2694	0	1	1	0	2695	0	1	1	0	2696	1	1	1	0	2697	0	1	1	0	2698	0	1	1	0	2699	1	1	1	0
2700	0	1	1	0	2701	0	1	1	0	2702	1	1	1	0	2703	0	1	1	0	2704	0	1	1	0	2705	1	1	1	0
2706	0	1	1	0	2707	0	1	1	0	2708	1	1	1	0	2709	0	1	1	0	2710	0	1	1	0	2711	1	1	1	0
2712	0	1	1	0	2713	0	1	1	0	2714	1	1	1	0	2715	0	1	1	0	2716	0	1	1	0	2717	1	1	1	0
2718	0	1	1	0	2719	0	1	1	0	2720	1	1	1	0	2721	0	1	1	0	2722	0	1	1	0	2723	1	1	1	0
2724	0	1	1	0	2725	0	1	1	0	2726	1	1	1	0	2727	0	1	1	0	2728	0	1	1	0	2729	1	1	1	0
2730	0	1	1	0	2731	0	1	1	0	2732	1	1	1	0	2733	0	1	1	0	2734	0	0	0	0	2735	0	0	0	0
2736	0	0	0	0	2737	0	1	1	1	2738	1	1	1	0	2739	1	1	1	1	2740	1	1	1	0	2741	0	1	1	1
2742	0	1	1	0	2743	1	1	1	0	2744	0	1	1	0	2745	0	1	1	1	2746	1	1	1	0	2748	1	1	1	0
2749	0	1	1	1	2750	0	1	1	0	2751	1	1	1	0	2752	0	1	1	0	2753	0	1	1	1	2754	1	1	1	0
2756	1	1	1	0	2757	0	1	1	1	2758	0	1	1	0	2759	1	1	1	0	2760	0	1	1	0	2761	0	1	1	1
2762	1	1	1	0	2764	1	1	1	0	2765	0	1	1	1	2766	0	1	1	0	2767	1	1	1	0	2768	0	1	1	0
2769	0	1	1	1	2770	1	1	1	0	2772	1	1	1	0	2773	0	1	1	1	2774	0	1	1	0	2775	1	1	1	0
2776	0	1	1	0	2777	0	1	1	1	2778	1	1	1	0	2780	1	1	1	0	2781	0	1	1	1	2782	0	1	1	0
2783	1	1	1	0	2784	0	1	1	0	2785	0	1	1	1	2786	1	1	1	0	2788	1	1	1	0	2789	0	1	1	1
2790	0	1	1	0	2791	1	1	1	0	2792	0	1	1	0	2793	0	1	1	1	2794	1	1	1	0	2796	1	1	1	0
2797	0	1	1	1	2798	0	1	1	0	2799	1	1	1	0	2800	0	1	1	0	2801	0	1	1	1	2802	1	1	1	0
2804	1	1	1	0	2805	0	1	1	1	2806	0	1	1	0	2807	1	1	1	0	2808	0	1	1	0	2809	0	1	1	1
2810	1	1	1	0	2812	1	1	1	0	2813	0	1	1	1	2814	0	1	1	0	2815	1	1	1	0	2816	0	1	1	0
2817	0	1	1	1	2818	1	1	1	0	2820	1	1	1	0	2821	0	1	1	1	2822	0	1	1	0	2823	1	1	1	0
2824	0	1	1	0	2825	0	1	1	1	2826	1	1	1	0	2828	1	1	1	0	2829	0	1	1	1	2830	0	1	1	0
2831	1	1	1	0	2832	0	1	1	0	2833	0	1	1	1	2834	1	1	1	0	2836	1	1	1	0	2837	0	1	1	1
2838	0	1	1	0	2839	1	1	1	0	2840	0	1	1	0	2841	0	1	1	1	2842	1	1	1	0	2844	1	1	1	0
2845	0	1	1	1	2846	0	1	1	0	2847	1	1	1	0	2848	0	1	1	0	2849	0	1	1	1	2850	1	1	1	0
2852	1	1	1	0	2853	0	1	1	1	2854	0	1	1	0	2855	1	1	1	0	2856	0	1	1	0	2857	0	1	1	1
2858	1	1	1	0	2860	1	1	1	0	2861	0	1	1	1	2862	0	1	1	0	2863	1	1	1	0	2864	0	1	1	0
2865	0	1	1	1	2866	1	1	1	0	2868	1	1	1	0	2869	0	1	1	1	2870	0	1	1	0	2871	1	1	1	0
2872	0	1	1	0	2873	0	1	1	1	2874	1	1	1	0	2876	1	1	1	0	2877	0	1	1	1	2878	0	1	1	0
2879	1	1	1	0	2880	0	1	1	0	2881	0	1	1	1	2882	1	1	1	0	2884	1	1	1	0	2885	0	1	1	1
2886	0	1	1	0	2887	1	1	1	0	2888	0	1	1	0	2889	0	1	1	1	2890	1	1	1	0	2892	1	1	1	0
2893	0	1	1	1	2894	0	1	1	0	2895	1	1	1	0	2896	0	1	1	0	2897	0	0	0	1	2898	0	0	0	0
2899	0	0	0	1	2900	0	0	0	0	2901	0	0	0	1	2902	0	1	1	0	2903	1	1	1	0	2904	0	1	1	0
2905	0	1	1	0	2906	1	1	1	0	2907	0	1	1	0	2908	0	1	1	0	2909	1	1	1	0	2910	0	1	1	0
2911	0	1	1	0	2912	1	1	1	0	2913	0	1	1	0	2914	0	1	1	0	2915	1	1	1	0	2916	0	1	1	0
2917	0	1	1	0	2918	1	1	1	0	2919	0	1	1	0	2920	0	1	1	0	2921	1	1	1	0	2922	0	1	1	0
2923	0	1	1	0	2924	1	1	1	0	2925	0	1	1	0	2926	0	1	1	0	2927	1	1	1	0	2928	0	1	1	0
2929	0	1	1	0	2930	1	1	1	0	2931	0	1	1	0	2932	0	1	1	0	2933	1	1	1	0	2934	0	1	1	0
2935	0	1	1	0	2936	1	1	1	0	2937	0	1	1	0	2938	0	1	1	0	2939	1	1	1	0	2940	0	1	1	0
2941	0	1	1	0	2942	1	1	1	0	2943	0	1	1	0	2944	0	1	1	0	2945	1	1	1	0	2946	0	1	1	0
2947	0	1	1	0	2948	1	1	1	0	2949	0	1	1	0	2950	0	1	1	0	2951	1	1	1	0	2952	0	1	1	0
2953	0	1	1	0	2954	1	1	1	0	2955	0	1	1	0	2956	0	1	1	0	2957	1	1	1	0	2958	0	1	1	0
2959	0	1	1	0	2960	1	1	1	0	2961	0	1	1	0	2962	0	0	0	0	2963	0	0	0	0	2964	0	0	0	0
2965	0	1	1	1	2966	1	1	1	0	2967	1	1	1	1	2968	1	1	1	0	2969	0	1	1	1	2970	0	1	1	0
2971	1	1	1	0	2972	0	1	1	0	2973	0	1	1	1	2974	1	1	1	0	2976	1	1	1	0	2977	0	1	1	1
2978	0	1	1	0	2979	1	1	1	0	2980	0	1	1	0	2981	0	1	1	1	2982	1	1	1	0	2984	1	1	1	0
2985	0	1	1	1	2986	0	1	1	0	2987	1	1	1	0	2988	0	1	1	0	2989	0	1	1	1	2990	1	1	1	0
2992	1	1	1	0	2993	0	1	1	1	2994	0	1	1	0	2995	1	1	1	0	2996	0	1	1	0	2997	0	1	1	1
2998	1	1	1	0	3000	1	1	1	0	3001	0	1	1	1	3002	0	1	1	0	3003	1	1	1	0	3004	0	1	1	0
3005	0	1	1	1	3006	1	1	1	0	3008	1	1	1	0	3009	0	1	1	1	3010	0	1	1	0	3011	1	1	1	0
3012	0	1	1	0	3013	0	1	1	1	3014	1	1	1	0	3016	1	1	1	0	3017	0	1	1	1	3018	0	1	1	0
3019	1	1	1	0	3020	0	1	1	0	3021	0	1	1	1	3022	1	1	1	0	3024	1	1	1	0	3025	0	1	1	1
3026	0	1	1	0	3027	1	1	1	0	3028	0	1	1	0	3029	0	1	1	1	3030	1	1	1	0	3032	1	1	1	0
3033	0	1	1	1	3034	0	1	1	0	3035	1	1	1	0	3036	0	1	1	0	3037	0	1	1	1	3038	1	1	1	0
3040	1	1	1	0	3041	0	1	1	1	3042	0	1	1	0	3043	1	1	1	0	3044	0	1	1	0	3045	0	1	1	1
3046	1	1	1	0	3048	1	1	1	0	3049	0	1	1	1	3050	0	1	1	0	3051	1	1	1	0	3052	0	1	1	0
3053	0	1	1	1	3054	1	1	1	0	3056	1	1	1	0	3057	0	1	1	1	3058	0	1	1	0	3059	1	1	1	0
3060	0	1	1	0	3061	0	1	1	1	3062	1	1	1	0	3064	1	1	1	0	3065	0	1	1	1	3066	0	1	1	0
3067	1	1	1	0	3068	0	1	1	0	3069	0	1	1	1	3070	1	1	1	0	3072	1	1	1	0	3073	0	1	1	1

3074	0	1	1	0	3075	1	1	1	0	3076	0	1	1	0	3077	0	1	1	1	3078	1	1	1	0	3080	1	1	1	0
3081	0	1	1	1	3082	0	1	1	0	3083	1	1	1	0	3084	0	1	1	0	3085	0	1	1	1	3086	1	1	1	0
3088	1	1	1	0	3089	0	1	1	1	3090	0	1	1	0	3091	1	1	1	0	3092	0	1	1	0	3093	0	1	1	1
3094	1	1	1	0	3096	1	1	1	0	3097	0	1	1	1	3098	0	1	1	0	3099	1	1	1	0	3100	0	1	1	0
3101	0	1	1	1	3102	1	1	1	0	3104	1	1	1	0	3105	0	1	1	1	3106	0	1	1	0	3107	1	1	1	0
3108	0	1	1	0	3109	0	1	1	1	3110	1	1	1	0	3112	1	1	1	0	3113	0	1	1	1	3114	0	1	1	0
3115	1	1	1	0	3116	0	1	1	0	3117	0	1	1	1	3118	1	1	1	0	3120	1	1	1	0	3121	0	1	1	1
3122	0	1	1	0	3123	1	1	1	0	3124	0	1	1	0	3125	0	0	0	1	3126	0	0	0	0	3127	0	0	0	1
3128	0	0	0	0	3129	0	0	0	1	3130	0	1	1	0	3131	1	1	1	0	3132	0	1	1	0	3133	0	1	1	0
3134	1	1	1	0	3135	0	1	1	0	3136	0	1	1	0	3137	1	1	1	0	3138	0	1	1	0	3139	0	1	1	0
3140	1	1	1	0	3141	0	1	1	0	3142	0	1	1	0	3143	1	1	1	0	3144	0	1	1	0	3145	0	1	1	0
3146	1	1	1	0	3147	0	1	1	0	3148	0	1	1	0	3149	1	1	1	0	3150	0	1	1	0	3151	0	1	1	0
3152	1	1	1	0	3153	0	1	1	0	3154	0	1	1	0	3155	1	1	1	0	3156	0	1	1	0	3157	0	1	1	0
3158	1	1	1	0	3159	0	1	1	0	3160	0	1	1	0	3161	1	1	1	0	3162	0	1	1	0	3163	0	1	1	0
3164	1	1	1	0	3165	0	1	1	0	3166	0	1	1	0	3167	1	1	1	0	3168	0	1	1	0	3169	0	1	1	0
3170	1	1	1	0	3171	0	1	1	0	3172	0	1	1	0	3173	1	1	1	0	3174	0	1	1	0	3175	0	1	1	0
3176	1	1	1	0	3177	0	1	1	0	3178	0	1	1	0	3179	1	1	1	0	3180	0	1	1	0	3181	0	1	1	0
3182	1	1	1	0	3183	0	1	1	0	3184	0	1	1	0	3185	1	1	1	0	3186	0	1	1	0	3187	0	1	1	0
3188	1	1	1	0	3189	0	1	1	0	3190	0	0	0	0	3191	0	0	0	0	3192	0	0	0	0	3193	0	1	1	1
3194	1	1	1	0	3195	1	1	1	1	3196	1	1	1	0	3197	0	1	1	1	3198	0	1	1	0	3199	1	1	1	0
3200	0	1	1	0	3201	0	1	1	1	3202	1	1	1	0	3204	1	1	1	0	3205	0	1	1	1	3206	0	1	1	0
3207	1	1	1	0	3208	0	1	1	0	3209	0	1	1	1	3210	1	1	1	0	3212	1	1	1	0	3213	0	1	1	1
3214	0	1	1	0	3215	1	1	1	0	3216	0	1	1	0	3217	0	1	1	1	3218	1	1	1	0	3220	1	1	1	0
3221	0	1	1	1	3222	0	1	1	0	3223	1	1	1	0	3224	0	1	1	0	3225	0	1	1	1	3226	1	1	1	0
3228	1	1	1	0	3229	0	1	1	1	3230	0	1	1	0	3231	1	1	1	0	3232	0	1	1	0	3233	0	1	1	1
3234	1	1	1	0	3236	1	1	1	0	3237	0	1	1	1	3238	0	1	1	0	3239	1	1	1	0	3240	0	1	1	0
3241	0	1	1	1	3242	1	1	1	0	3244	1	1	1	0	3245	0	1	1	1	3246	0	1	1	0	3247	1	1	1	0
3248	0	1	1	0	3249	0	1	1	1	3250	1	1	1	0	3252	1	1	1	0	3253	0	1	1	1	3254	0	1	1	0
3255	1	1	1	0	3256	0	1	1	0	3257	0	1	1	1	3258	1	1	1	0	3260	1	1	1	0	3261	0	1	1	1
3262	0	1	1	0	3263	1	1	1	0	3264	0	1	1	0	3265	0	1	1	1	3266	1	1	1	0	3268	1	1	1	0
3269	0	1	1	1	3270	0	1	1	0	3271	1	1	1	0	3272	0	1	1	0	3273	0	1	1	1	3274	1	1	1	0
3276	1	1	1	0	3277	0	1	1	1	3278	0	1	1	0	3279	1	1	1	0	3280	0	1	1	0	3281	0	1	1	1
3282	1	1	1	0	3284	1	1	1	0	3285	0	1	1	1	3286	0	1	1	0	3287	1	1	1	0	3288	0	1	1	0
3289	0	1	1	1	3290	1	1	1	0	3292	1	1	1	0	3293	0	1	1	1	3294	0	1	1	0	3295	1	1	1	0
3296	0	1	1	0	3297	0	1	1	1	3298	1	1	1	0	3300	1	1	1	0	3301	0	1	1	1	3302	0	1	1	0
3303	1	1	1	0	3304	0	1	1	0	3305	0	1	1	1	3306	1	1	1	0	3308	1	1	1	0	3309	0	1	1	1
3310	0	1	1	0	3311	1	1	1	0	3312	0	1	1	0	3313	0	1	1	1	3314	1	1	1	0	3316	1	1	1	0
3317	0	1	1	1	3318	0	1	1	0	3319	1	1	1	0	3320	0	1	1	0	3321	0	1	1	1	3322	1	1	1	0
3324	1	1	1	0	3325	0	1	1	1	3326	0	1	1	0	3327	1	1	1	0	3328	0	1	1	0	3329	0	1	1	1
3330	1	1	1	0	3332	1	1	1	0	3333	0	1	1	1	3334	0	1	1	0	3335	1	1	1	0	3336	0	1	1	0
3337	0	1	1	1	3338	1	1	1	0	3340	1	1	1	0	3341	0	1	1	1	3342	0	1	1	0	3343	1	1	1	0
3344	0	1	1	0	3345	0	1	1	1	3346	1	1	1	0	3348	1	1	1	0	3349	0	1	1	1	3350	0	1	1	0
3351	1	1	1	0	3352	0	1	1	0	3353	0	0	0	1	3354	0	0	0	0	3355	0	0	0	1	3356	0	0	0	0
3357	0	0	0	1	3358	0	1	1	0	3359	1	1	1	0	3360	0	1	1	0	3361	0	1	1	0	3362	1	1	1	0
3363	0	1	1	0	3364	0	1	1	0	3365	1	1	1	0	3366	0	1	1	0	3367	0	1	1	0	3368	1	1	1	0
3369	0	1	1	0	3370	0	1	1	0	3371	1	1	1	0	3372	0	1	1	0	3373	0	1	1	0	3374	1	1	1	0
3375	0	1	1	0	3376	0	1	1	0	3377	1	1	1	0	3378	0	1	1	0	3379	0	1	1	0	3380	1	1	1	0
3381	0	1	1	0	3382	0	1	1	0	3383	1	1	1	0	3384	0	1	1	0	3385	0	1	1	0	3386	1	1	1	0
3387	0	1	1	0	3388	0	1	1	0	3389	1	1	1	0	3390	0	1	1	0	3391	0	1	1	0	3392	1	1	1	0
3393	0	1	1	0	3394	0	1	1	0	3395	1	1	1	0	3396	0	1	1	0	3397	0	1	1	0	3398	1	1	1	0
3399	0	1	1	0	3400	0	1	1	0	3401	1	1	1	0	3402	0	1	1	0	3403	0	1	1	0	3404	1	1	1	0
3405	0	1	1	0	3406	0	1	1	0	3407	1	1	1	0	3408	0	1	1	0	3409	0	1	1	0	3410	1	1	1	0
3411	0	1	1	0	3412	0	1	1	0	3413	1	1	1	0	3414	0	1	1	0	3415	0	1	1	0	3416	1	1	1	0
3417	0	1	1	0	3418	0	0	0	0	3419	0	0	0	0	3420	0	0	0	0	3421	0	1	1	1	3422	1	1	1	0
3423	1	1	1	1	3424	1	1	1	0	3425	0	1	1	1	3426	0	1	1	0	3427	1	1	1	0	3428	0	1	1	0
3429	0	1	1	1	3430	1	1	1	0	3432	1	1	1	0	3433	0	1	1	1	3434	0	1	1	0	3435	1	1	1	0
3436	0	1	1	0	3437	0	1	1	1	3438	1	1	1	0	3440	1	1	1	0	3441	0	1	1	1	3442	0	1	1	0
3443	1	1	1	0	3444	0	1	1	0	3445	0	1	1	1	3446	1	1	1	0	3448	1	1	1	0	3449	0	1	1	1
3450	0	1	1	0	3451	1	1	1	0	3452	0	1	1	0	3453	0	1	1	1	3454	1	1	1	0	3456	1	1	1	0
3457	0	1	1	1	3458	0	1	1	0	3459	1	1	1	0	3460	0	1	1	0	3461	0	1	1	1	3462	1	1	1	0
3464	1	1	1	0	3465	0	1	1	1	3466	0	1	1	0	3467	1	1	1	0	3468	0	1	1	0	3469	0	1	1	1
3470	1	1	1	0	3472	1	1	1	0	3473	0	1	1	1	3474	0	1	1	0	3475	1	1	1	0	3476	0	1	1	0
3477	0	1	1	1	3478	1	1	1	0	3480	1	1	1	0	3481	0	1	1	1	3482	0	1	1	0	3483	1	1	1	0
3484	0	1	1	0	3485	0	1	1	1	3486	1	1	1	0	3488	1	1	1	0	3489	0	1	1	1	3490	0	1	1	0
3491	1	1	1	0	3492	0	1	1	0	3493	0	1	1	1	3494	1	1	1	0	3496	1	1	1	0	3497	0	1	1	1
3498	0	1	1	0	3499	1	1	1	0	3500	0	1	1	0	3501	0	1	1	1	3502	1	1	1	0	3504	1	1	1	0
3505	0	1	1	1	3506	0	1	1	0	3507	1	1	1	0	3508	0	1	1	0	3509	0	1	1	1	3510	1	1	1	0
3512	1	1	1	0	3513	0	1	1	1	3514	0	1	1	0	3515	1	1	1	0	3516	0	1	1	0	3517	0	1	1	1

3518	1	1	1	0	3520	1	1	1	0	3521	0	1	1	1	3522	0	1	1	0	3523	1	1	1	0	3524	0	1	1	0
3525	0	1	1	1	3526	1	1	1	0	3528	1	1	1	0	3529	0	1	1	1	3530	0	1	1	0	3531	1	1	1	0
3532	0	1	1	0	3533	0	1	1	1	3534	1	1	1	0	3536	1	1	1	0	3537	0	1	1	1	3538	0	1	1	0
3539	1	1	1	0	3540	0	1	1	0	3541	0	1	1	1	3542	1	1	1	0	3544	1	1	1	0	3545	0	1	1	1
3546	0	1	1	0	3547	1	1	1	0	3548	0	1	1	0	3549	0	1	1	1	3550	1	1	1	0	3552	1	1	1	0
3553	0	1	1	1	3554	0	1	1	0	3555	1	1	1	0	3556	0	1	1	0	3557	0	1	1	1	3558	1	1	1	0
3560	1	1	1	0	3561	0	1	1	1	3562	0	1	1	0	3563	1	1	1	0	3564	0	1	1	0	3565	0	1	1	1
3566	1	1	1	0	3568	1	1	1	0	3569	0	1	1	1	3570	0	1	1	0	3571	1	1	1	0	3572	0	1	1	0
3573	0	1	1	1	3574	1	1	1	0	3576	1	1	1	0	3577	0	1	1	1	3578	0	1	1	0	3579	1	1	1	0
3580	0	1	1	0	3581	0	0	0	1	3582	0	0	0	0	3583	0	0	0	1	3584	0	0	0	0	3585	0	0	0	1
3586	0	1	1	0	3587	1	1	1	0	3588	0	1	1	0	3589	0	1	1	0	3590	1	1	1	0	3591	0	1	1	0
3592	0	1	1	0	3593	1	1	1	0	3594	0	1	1	0	3595	0	1	1	0	3596	1	1	1	0	3597	0	1	1	0
3598	0	1	1	0	3599	1	1	1	0	3600	0	1	1	0	3601	0	1	1	0	3602	1	1	1	0	3603	0	1	1	0
3604	0	1	1	0	3605	1	1	1	0	3606	0	1	1	0	3607	0	1	1	0	3608	1	1	1	0	3609	0	1	1	0
3610	0	1	1	0	3611	1	1	1	0	3612	0	1	1	0	3613	0	1	1	0	3614	1	1	1	0	3615	0	1	1	0
3616	0	1	1	0	3617	1	1	1	0	3618	0	1	1	0	3619	0	1	1	0	3620	1	1	1	0	3621	0	1	1	0
3622	0	1	1	0	3623	1	1	1	0	3624	0	1	1	0	3625	0	1	1	0	3626	1	1	1	0	3627	0	1	1	0
3628	0	1	1	0	3629	1	1	1	0	3630	0	1	1	0	3631	0	1	1	0	3632	1	1	1	0	3633	0	1	1	0
3634	0	1	1	0	3635	1	1	1	0	3636	0	1	1	0	3637	0	1	1	0	3638	1	1	1	0	3639	0	1	1	0
3640	0	1	1	0	3641	1	1	1	0	3642	0	1	1	0	3643	0	1	1	0	3644	1	1	1	0	3645	0	1	1	0
3646	0	0	0	0	3647	0	0	0	0	3648	0	0	0	0	3649	0	1	1	1	3650	1	1	1	0	3651	1	1	1	1
3652	1	1	1	0	3653	0	1	1	1	3654	0	1	1	0	3655	1	1	1	0	3656	0	1	1	0	3657	0	1	1	1
3658	1	1	1	0	3660	1	1	1	0	3661	0	1	1	1	3662	0	1	1	0	3663	1	1	1	0	3664	0	1	1	0
3665	0	1	1	1	3666	1	1	1	0	3668	1	1	1	0	3669	0	1	1	1	3670	0	1	1	0	3671	1	1	1	0
3672	0	1	1	0	3673	0	1	1	1	3674	1	1	1	0	3676	1	1	1	0	3677	0	1	1	1	3678	0	1	1	0
3679	1	1	1	0	3680	0	1	1	0	3681	0	1	1	1	3682	1	1	1	0	3684	1	1	1	0	3685	0	1	1	1
3686	0	1	1	0	3687	1	1	1	0	3688	0	1	1	0	3689	0	1	1	1	3690	1	1	1	0	3692	1	1	1	0
3693	0	1	1	1	3694	0	1	1	0	3695	1	1	1	0	3696	0	1	1	0	3697	0	1	1	1	3698	1	1	1	0
3700	1	1	1	0	3701	0	1	1	1	3702	0	1	1	0	3703	1	1	1	0	3704	0	1	1	0	3705	0	1	1	1
3706	1	1	1	0	3708	1	1	1	0	3709	0	1	1	1	3710	0	1	1	0	3711	1	1	1	0	3712	0	1	1	0
3713	0	1	1	1	3714	1	1	1	0	3716	1	1	1	0	3717	0	1	1	1	3718	0	1	1	0	3719	1	1	1	0
3720	0	1	1	0	3721	0	1	1	1	3722	1	1	1	0	3724	1	1	1	0	3725	0	1	1	1	3726	0	1	1	0
3727	1	1	1	0	3728	0	1	1	0	3729	0	1	1	1	3730	1	1	1	0	3732	1	1	1	0	3733	0	1	1	1
3734	0	1	1	0	3735	1	1	1	0	3736	0	1	1	0	3737	0	1	1	1	3738	1	1	1	0	3740	1	1	1	0
3741	0	1	1	1	3742	0	1	1	0	3743	1	1	1	0	3744	0	1	1	0	3745	0	1	1	1	3746	1	1	1	0
3748	1	1	1	0	3749	0	1	1	1	3750	0	1	1	0	3751	1	1	1	0	3752	0	1	1	0	3753	0	1	1	1
3754	1	1	1	0	3756	1	1	1	0	3757	0	1	1	1	3758	0	1	1	0	3759	1	1	1	0	3760	0	1	1	0
3761	0	1	1	1	3762	1	1	1	0	3764	1	1	1	0	3765	0	1	1	1	3766	0	1	1	0	3767	1	1	1	0
3768	0	1	1	0	3769	0	1	1	1	3770	1	1	1	0	3772	1	1	1	0	3773	0	1	1	1	3774	0	1	1	0
3775	1	1	1	0	3776	0	1	1	0	3777	0	1	1	1	3778	1	1	1	0	3780	1	1	1	0	3781	0	1	1	1
3782	0	1	1	0	3783	1	1	1	0	3784	0	1	1	0	3785	0	1	1	1	3786	1	1	1	0	3788	1	1	1	0
3789	0	1	1	1	3790	0	1	1	0	3791	1	1	1	0	3792	0	1	1	0	3793	0	1	1	1	3794	1	1	1	0
3796	1	1	1	0	3797	0	1	1	1	3798	0	1	1	0	3799	1	1	1	0	3800	0	1	1	0	3801	0	1	1	1
3802	1	1	1	0	3804	1	1	1	0	3805	0	1	1	1	3806	0	1	1	0	3807	1	1	1	0	3808	0	1	1	0
3809	0	0	0	1	3810	0	0	0	0	3811	0	0	0	1	3812	0	0	0	0	3813	0	0	0	1	3814	0	1	1	0
3815	1	1	1	0	3816	0	1	1	0	3817	0	1	1	0	3818	1	1	1	0	3819	0	1	1	0	3820	0	1	1	0
3821	1	1	1	0	3822	0	1	1	0	3823	0	1	1	0	3824	1	1	1	0	3825	0	1	1	0	3826	0	1	1	0
3827	1	1	1	0	3828	0	1	1	0	3829	0	1	1	0	3830	1	1	1	0	3831	0	1	1	0	3832	0	1	1	0
3833	1	1	1	0	3834	0	1	1	0	3835	0	1	1	0	3836	1	1	1	0	3837	0	1	1	0	3838	0	1	1	0
3839	1	1	1	0	3840	0	1	1	0	3841	0	1	1	0	3842	1	1	1	0	3843	0	1	1	0	3844	0	1	1	0
3845	1	1	1	0	3846	0	1	1	0	3847	0	1	1	0	3848	1	1	1	0	3849	0	1	1	0	3850	0	1	1	0
3851	1	1	1	0	3852	0	1	1	0	3853	0	1	1	0	3854	1	1	1	0	3855	0	1	1	0	3856	0	1	1	0
3857	1	1	1	0	3858	0	1	1	0	3859	0	1	1	0	3860	1	1	1	0	3861	0	1	1	0	3862	0	1	1	0
3863	1	1	1	0	3864	0	1	1	0	3865	0	1	1	0	3866	1	1	1	0	3867	0	1	1	0	3868	0	1	1	0
3869	1	1	1	0	3870	0	1	1	0	3871	0	1	1	0	3872	1	1	1	0	3873	0	1	1	0	3874	0	0	0	0
3875	0	0	0	0	3876	0	0	0	0	3877	0	1	1	1	3878	1	1	1	0	3879	1	1	1	1	3880	1	1	1	0
3881	0	1	1	1	3882	0	1	1	0	3883	1	1	1	0	3884	0	1	1	0	3885	0	1	1	1	3886	1	1	1	0
3888	1	1	1	0	3889	0	1	1	1	3890	0	1	1	0	3891	1	1	1	0	3892	0	1	1	0	3893	0	1	1	1
3894	1	1	1	0	3896	1	1	1	0	3897	0	1	1	1	3898	0	1	1	0	3899	1	1	1	0	3900	0	1	1	0
3901	0	1	1	1	3902	1	1	1	0	3904	1	1	1	0	3905	0	1	1	1	3906	0	1	1	0	3907	1	1	1	0
3908	0	1	1	0	3909	0	1	1	1	3910	1	1	1	0	3912	1	1	1	0	3913	0	1	1	1	3914	0	1	1	0
3915	1	1	1	0	3916	0	1	1	0	3917	0	1	1	1	3918	1	1	1	0	3920	1	1	1	0	3921	0	1	1	1
3922	0	1	1	0	3923	1	1	1	0	3924	0	1	1	0	3925	0	1	1	1	3926	1	1	1	0	3928	1	1	1	0
3929	0	1	1	1	3930	0	1	1	0	3931	1	1	1	0	3932	0	1	1	0	3933	0	1	1	1	3934	1	1	1	0
3936	1	1	1	0	3937	0	1	1	1	3938	0	1	1	0	3939	1	1	1	0	3940	0	1	1	0	3941	0	1	1	1
3942	1	1	1	0	3944	1	1	1	0	3945	0	1	1	1	3946	0	1	1	0	3947	1	1	1	0	3948	0	1	1	0
3949	0	1	1	1	3950	1	1	1	0	3952	1	1	1	0	3953	0	1	1	1	3954	0	1	1	0	3955	1	1	1	0
3956	0	1	1	0	3957	0	1	1	1	3958	1	1	1	0	3960	1	1	1	0	3961	0	1	1	1	3962	0	1	1	0

3963	1	1	1	0	3964	0	1	1	0	3965	0	1	1	1	3966	1	1	1	0	3968	1	1	1	0	3969	0	1	1	1
3970	0	1	1	0	3971	1	1	1	0	3972	0	1	1	0	3973	0	1	1	1	3974	1	1	1	0	3976	1	1	1	0
3977	0	1	1	1	3978	0	1	1	0	3979	1	1	1	0	3980	0	1	1	0	3981	0	1	1	1	3982	1	1	1	0
3984	1	1	1	0	3985	0	1	1	1	3986	0	1	1	0	3987	1	1	1	0	3988	0	1	1	0	3989	0	1	1	1
3990	1	1	1	0	3992	1	1	1	0	3993	0	1	1	1	3994	0	1	1	0	3995	1	1	1	0	3996	0	1	1	0
3997	0	1	1	1	3998	1	1	1	0	4000	1	1	1	0	4001	0	1	1	1	4002	0	1	1	0	4003	1	1	1	0
4004	0	1	1	0	4005	0	1	1	1	4006	1	1	1	0	4008	1	1	1	0	4009	0	1	1	1	4010	0	1	1	0
4011	1	1	1	0	4012	0	1	1	0	4013	0	1	1	1	4014	1	1	1	0	4016	1	1	1	0	4017	0	1	1	1
4018	0	1	1	0	4019	1	1	1	0	4020	0	1	1	0	4021	0	1	1	1	4022	1	1	1	0	4024	1	1	1	0
4025	0	1	1	1	4026	0	1	1	0	4027	1	1	1	0	4028	0	1	1	0	4029	0	1	1	1	4030	1	1	1	0
4032	1	1	1	0	4033	0	1	1	1	4034	0	1	1	0	4035	1	1	1	0	4036	0	1	1	0	4037	0	0	0	1
4038	0	0	0	0	4039	0	0	0	1	4040	0	0	0	0	4041	0	0	0	1	4042	0	1	1	0	4043	1	1	1	0
4044	0	1	1	0	4045	0	1	1	0	4046	1	1	1	0	4047	0	1	1	0	4048	0	1	1	0	4049	1	1	1	0
4050	0	1	1	0	4051	0	1	1	0	4052	1	1	1	0	4053	0	1	1	0	4054	0	1	1	0	4055	1	1	1	0
4056	0	1	1	0	4057	0	1	1	0	4058	1	1	1	0	4059	0	1	1	0	4060	0	1	1	0	4061	1	1	1	0
4062	0	1	1	0	4063	0	1	1	0	4064	1	1	1	0	4065	0	1	1	0	4066	0	1	1	0	4067	1	1	1	0
4068	0	1	1	0	4069	0	1	1	0	4070	1	1	1	0	4071	0	1	1	0	4072	0	1	1	0	4073	1	1	1	0
4074	0	1	1	0	4075	0	1	1	0	4076	1	1	1	0	4077	0	1	1	0	4078	0	1	1	0	4079	1	1	1	0
4080	0	1	1	0	4081	0	1	1	0	4082	1	1	1	0	4083	0	1	1	0	4084	0	1	1	0	4085	1	1	1	0
4086	0	1	1	0	4087	0	1	1	0	4088	1	1	1	0	4089	0	1	1	0	4090	0	1	1	0	4091	1	1	1	0
4092	0	1	1	0	4093	0	1	1	0	4094	1	1	1	0	4095	0	1	1	0	4096	0	1	1	0	4097	1	1	1	0
4098	0	1	1	0	4099	0	1	1	0	4100	1	1	1	0	4101	0	1	1	0	4102	0	0	0	0	4103	0	0	0	0
4104	0	0	0	0	4105	0	1	1	1	4106	1	1	1	0	4107	1	1	1	1	4108	1	1	1	0	4109	0	1	1	1
4110	0	1	1	0	4111	1	1	1	0	4112	0	1	1	0	4113	0	1	1	1	4114	1	1	1	0	4116	1	1	1	0
4117	0	1	1	1	4118	0	1	1	0	4119	1	1	1	0	4120	0	1	1	0	4121	0	1	1	1	4122	1	1	1	0
4124	1	1	1	0	4125	0	1	1	1	4126	0	1	1	0	4127	1	1	1	0	4128	0	1	1	0	4129	0	1	1	1
4130	1	1	1	0	4132	1	1	1	0	4133	0	1	1	1	4134	0	1	1	0	4135	1	1	1	0	4136	0	1	1	0
4137	0	1	1	1	4138	1	1	1	0	4140	1	1	1	0	4141	0	1	1	1	4142	0	1	1	0	4143	1	1	1	0
4144	0	1	1	0	4145	0	1	1	1	4146	1	1	1	0	4148	1	1	1	0	4149	0	1	1	1	4150	0	1	1	0
4151	1	1	1	0	4152	0	1	1	0	4153	0	1	1	1	4154	1	1	1	0	4156	1	1	1	0	4157	0	1	1	1
4158	0	1	1	0	4159	1	1	1	0	4160	0	1	1	0	4161	0	1	1	1	4162	1	1	1	0	4164	1	1	1	0
4165	0	1	1	1	4166	0	1	1	0	4167	1	1	1	0	4168	0	1	1	0	4169	0	1	1	1	4170	1	1	1	0
4172	1	1	1	0	4173	0	1	1	1	4174	0	1	1	0	4175	1	1	1	0	4176	0	1	1	0	4177	0	1	1	1
4178	1	1	1	0	4180	1	1	1	0	4181	0	1	1	1	4182	0	1	1	0	4183	1	1	1	0	4184	0	1	1	0
4185	0	1	1	1	4186	1	1	1	0	4188	1	1	1	0	4189	0	1	1	1	4190	0	1	1	0	4191	1	1	1	0
4192	0	1	1	0	4193	0	1	1	1	4194	1	1	1	0	4196	1	1	1	0	4197	0	1	1	1	4198	0	1	1	0
4199	1	1	1	0	4200	0	1	1	0	4201	0	1	1	1	4202	1	1	1	0	4204	1	1	1	0	4205	0	1	1	1
4206	0	1	1	0	4207	1	1	1	0	4208	0	1	1	0	4209	0	1	1	1	4210	1	1	1	0	4212	1	1	1	0
4213	0	1	1	1	4214	0	1	1	0	4215	1	1	1	0	4216	0	1	1	0	4217	0	1	1	1	4218	1	1	1	0
4220	1	1	1	0	4221	0	1	1	1	4222	0	1	1	0	4223	1	1	1	0	4224	0	1	1	0	4225	0	1	1	1
4226	1	1	1	0	4228	1	1	1	0	4229	0	1	1	1	4230	0	1	1	0	4231	1	1	1	0	4232	0	1	1	0
4233	0	1	1	1	4234	1	1	1	0	4236	1	1	1	0	4237	0	1	1	1	4238	0	1	1	0	4239	1	1	1	0
4240	0	1	1	0	4241	0	1	1	1	4242	1	1	1	0	4244	1	1	1	0	4245	0	1	1	1	4246	0	1	1	0
4247	1	1	1	0	4248	0	1	1	0	4249	0	1	1	1	4250	1	1	1	0	4252	1	1	1	0	4253	0	1	1	1
4254	0	1	1	0	4255	1	1	1	0	4256	0	1	1	0	4257	0	1	1	1	4258	1	1	1	0	4260	1	1	1	0
4261	0	1	1	1	4262	0	1	1	0	4263	1	1	1	0	4264	0	1	1	0	4265	0	0	0	1	4266	0	0	0	0
4267	0	0	0	1	4268	0	0	0	0	4269	0	0	0	1	4270	0	1	1	0	4271	1	1	1	0	4272	0	1	1	0
4273	0	1	1	0	4274	1	1	1	0	4275	0	1	1	0	4276	0	1	1	0	4277	1	1	1	0	4278	0	1	1	0
4279	0	1	1	0	4280	1	1	1	0	4281	0	1	1	0	4282	0	1	1	0	4283	1	1	1	0	4284	0	1	1	0
4285	0	1	1	0	4286	1	1	1	0	4287	0	1	1	0	4288	0	1	1	0	4289	1	1	1	0	4290	0	1	1	0
4291	0	1	1	0	4292	1	1	1	0	4293	0	1	1	0	4294	0	1	1	0	4295	1	1	1	0	4296	0	1	1	0
4297	0	1	1	0	4298	1	1	1	0	4299	0	1	1	0	4300	0	1	1	0	4301	1	1	1	0	4302	0	1	1	0
4303	0	1	1	0	4304	1	1	1	0	4305	0	1	1	0	4306	0	1	1	0	4307	1	1	1	0	4308	0	1	1	0
4309	0	1	1	0	4310	1	1	1	0	4311	0	1	1	0	4312	0	1	1	0	4313	1	1	1	0	4314	0	1	1	0
4315	0	1	1	0	4316	1	1	1	0	4317	0	1	1	0	4318	0	1	1	0	4319	1	1	1	0	4320	0	1	1	0
4321	0	1	1	0	4322	1	1	1	0	4323	0	1	1	0	4324	0	1	1	0	4325	1	1	1	0	4326	0	1	1	0
4327	0	1	1	0	4328	1	1	1	0	4329	0	1	1	0	4330	0	0	0	0	4331	0	0	0	0	4332	0	0	0	0
4333	0	1	1	1	4334	1	1	1	0	4335	1	1	1	1	4336	1	1	1	0	4337	0	1	1	1	4338	0	1	1	0
4339	1	1	1	0	4340	0	1	1	0	4341	0	1	1	1	4342	1	1	1	0	4344	1	1	1	0	4345	0	1	1	1
4346	0	1	1	0	4347	1	1	1	0	4348	0	1	1	0	4349	0	1	1	1	4350	1	1	1	0	4352	1	1	1	0
4353	0	1	1	1	4354	0	1	1	0	4355	1	1	1	0	4356	0	1	1	0	4357	0	1	1	1	4358	1	1	1	0
4360	1	1	1	0	4361	0	1	1	1	4362	0	1	1	0	4363	1	1	1	0	4364	0	1	1	0	4365	0	1	1	1
4366	1	1	1	0	4368	1	1	1	0	4369	0	1	1	1	4370	0	1	1	0	4371	1	1	1	0	4372	0	1	1	0
4373	0	1	1	1	4374	1	1	1	0	4376	1	1	1	0	4377	0	1	1	1	4378	0	1	1	0	4379	1	1	1	0
4380	0	1	1	0	4381	0	1	1	1	4382	1	1	1	0	4384	1	1	1	0	4385	0	1	1	1	4386	0	1	1	0
4387	1	1	1	0	4388	0	1	1	0	4389	0	1	1	1	4390	1	1	1	0	4392	1	1	1	0	4393	0	1	1	1
4394	0	1	1	0	4395	1	1	1	0	4396	0	1	1	0	4397	0	1	1	1	4398	1	1	1	0	4400	1	1	1	0
4401	0	1	1	1	4402	0	1	1	0	4403	1	1	1	0	4404	0	1	1	0	4405	0	1	1	1	4406	1	1	1	0

4408 1 1 1 0 4409 0 1 1 1 4410 0 1 1 0 4411 1 1 1 0 4412 0 1 1 0 4413 0 1 1 1
4414 1 1 1 0 4416 1 1 1 0 4417 0 1 1 1 4418 0 1 1 0 4419 1 1 1 0 4420 0 1 1 0
4421 0 1 1 1 4422 1 1 1 0 4424 1 1 1 0 4425 0 1 1 1 4426 0 1 1 0 4427 1 1 1 0
4428 0 1 1 0 4429 0 1 1 1 4430 1 1 1 0 4432 1 1 1 0 4433 0 1 1 1 4434 0 1 1 0
4435 1 1 1 0 4436 0 1 1 0 4437 0 1 1 1 4438 1 1 1 0 4440 1 1 1 0 4441 0 1 1 1
4442 0 1 1 0 4443 1 1 1 0 4444 0 1 1 0 4445 0 1 1 1 4446 1 1 1 0 4448 1 1 1 0
4449 0 1 1 1 4450 0 1 1 0 4451 1 1 1 0 4452 0 1 1 0 4453 0 1 1 1 4454 1 1 1 0
4456 1 1 1 0 4457 0 1 1 1 4458 0 1 1 0 4459 1 1 1 0 4460 0 1 1 0 4461 0 1 1 1
4462 1 1 1 0 4464 1 1 1 0 4465 0 1 1 1 4466 0 1 1 0 4467 1 1 1 0 4468 0 1 1 0
4469 0 1 1 1 4470 1 1 1 0 4472 1 1 1 0 4473 0 1 1 1 4474 0 1 1 0 4475 1 1 1 0
4476 0 1 1 0 4477 0 1 1 1 4478 1 1 1 0 4480 1 1 1 0 4481 0 1 1 1 4482 0 1 1 0
4483 1 1 1 0 4484 0 1 1 0 4485 0 1 1 1 4486 1 1 1 0 4488 1 1 1 0 4489 0 1 1 1
4490 0 1 1 0 4491 1 1 1 0 4492 0 1 1 0 4493 0 0 0 1 4494 0 0 0 0 4495 0 0 0 1
4496 0 0 0 0 4497 0 0 0 1 4498 0 1 1 0 4499 1 1 1 0 4500 0 1 1 0 4501 0 1 1 0
4502 1 1 1 0 4503 0 1 1 0 4504 0 1 1 0 4505 1 1 1 0 4506 0 1 1 0 4507 0 1 1 0
4508 1 1 1 0 4509 0 1 1 0 4510 0 1 1 0 4511 1 1 1 0 4512 0 1 1 0 4513 0 1 1 0
4514 1 1 1 0 4515 0 1 1 0 4516 0 1 1 0 4517 1 1 1 0 4518 0 1 1 0 4519 0 1 1 0
4520 1 1 1 0 4521 0 1 1 0 4522 0 1 1 0 4523 1 1 1 0 4524 0 1 1 0 4525 0 1 1 0
4526 1 1 1 0 4527 0 1 1 0 4528 0 1 1 0 4529 1 1 1 0 4530 0 1 1 0 4531 0 1 1 0
4532 1 1 1 0 4533 0 1 1 0 4534 0 1 1 0 4535 1 1 1 0 4536 0 1 1 0 4537 0 1 1 0
4538 1 1 1 0 4539 0 1 1 0 4540 0 1 1 0 4541 1 1 1 0 4542 0 1 1 0 4543 0 1 1 0
4544 1 1 1 0 4545 0 1 1 0 4546 0 1 1 0 4547 1 1 1 0 4548 0 1 1 0 4549 0 1 1 0
4550 1 1 1 0 4551 0 1 1 0 4552 0 1 1 0 4553 1 1 1 0 4554 0 1 1 0 4555 0 1 1 0
4556 1 1 1 0 4557 0 1 1 0 4558 0 0 0 0 4559 0 0 0 0 4560 0 0 0 0 4561 0 0 1 0
4562 1 0 1 0 4563 1 0 1 0 4564 1 0 1 0 4565 0 0 1 0 4566 0 0 1 0 4567 1 0 1 0 4568
0 0 1 0 4569 0 0 1 0 4570 1 0 1 0 4571 1 0 1 0 4572 1 0 1 0 4573 0 0 1 0 4574 0 0
1 0 4575 1 0 1 0 4576 0 0 1 0 4577 0 0 1 0 4578 1 0 1 0 4579 1 0 1 0 4580 1 0 1 0
4581 0 0 1 0 4582 0 0 1 0 4583 1 0 1 0 4584 0 0 1 0 4585 0 0 1 0 4586 1 0 1 0 4587
1 0 1 0 4588 1 0 1 0 4589 0 0 1 0 4590 0 0 1 0 4591 1 0 1 0 4592 0 0 1 0 4593 0 0
1 0 4594 1 0 1 0 4595 1 0 1 0 4596 1 0 1 0 4597 0 0 1 0 4598 0 0 1 0 4599 1 0 1 0
4600 0 0 1 0 4601 0 0 1 0 4602 1 0 1 0 4603 1 0 1 0 4604 1 0 1 0 4605 0 0 1 0 4606
0 0 1 0 4607 1 0 1 0 4608 0 0 1 0 4609 0 0 1 0 4610 1 0 1 0 4611 1 0 1 0 4612 1 0
1 0 4613 0 0 1 0 4614 0 0 1 0 4615 1 0 1 0 4616 0 0 1 0 4617 0 0 1 0 4618 1 0 1 0
4619 1 0 1 0 4620 1 0 1 0 4621 0 0 1 0 4622 0 0 1 0 4623 1 0 1 0 4624 0 0 1 0 4625
0 0 1 0 4626 1 0 1 0 4627 1 0 1 0 4628 1 0 1 0 4629 0 0 1 0 4630 0 0 1 0 4631 1 0
1 0 4632 0 0 1 0 4633 0 0 1 0 4634 1 0 1 0 4635 1 0 1 0 4636 1 0 1 0 4637 0 0 1 0
4638 0 0 1 0 4639 1 0 1 0 4640 0 0 1 0 4641 0 0 1 0 4642 1 0 1 0 4643 1 0 1 0 4644
1 0 1 0 4645 0 0 1 0 4646 0 0 1 0 4647 1 0 1 0 4648 0 0 1 0 4649 0 0 1 0 4650 1 0
1 0 4651 1 0 1 0 4652 1 0 1 0 4653 0 0 1 0 4654 0 0 1 0 4655 1 0 1 0 4656 0 0 1 0
4657 0 0 1 0 4658 1 0 1 0 4659 1 0 1 0 4660 1 0 1 0 4661 0 0 1 0 4662 0 0 1 0 4663 1
0 1 0 4664 0 0 1 0 4665 0 0 1 0 4666 1 0 1 0 4667 1 0 1 0 4668 1 0 1 0 4669 0 0 1 0
4670 0 0 1 0 4671 1 0 1 0 4672 0 0 1 0 4673 0 0 1 0 4674 1 0 1 0 4675 1 0 1 0 4676 1
0 1 0 4677 0 0 1 0 4678 0 0 1 0 4679 1 0 1 0 4680 0 0 1 0 4681 0 0 1 0 4682 1 0 1
0 4683 1 0 1 0 4684 1 0 1 0 4685 0 0 1 0 4686 0 0 1 0 4687 1 0 1 0 4688 0 0 1 0 4689
0 0 1 0 4690 1 0 1 0 4691 1 0 1 0 4692 1 0 1 0 4693 0 0 1 0 4694 0 0 1 0 4695 1 0 1
0 4696 0 0 1 0 4697 0 0 1 0 4698 1 0 1 0 4699 1 0 1 0 4700 1 0 1 0 4701 0 0 1 0 4702
0 0 1 0 4703 1 0 1 0 4704 0 0 1 0 4705 0 0 1 0 4706 1 0 1 0 4707 1 0 1 0 4708 1 0 1
0 4709 0 0 1 0 4710 0 0 1 0 4711 1 0 1 0 4712 0 0 1 0 4713 0 0 1 0 4714 1 0 1 0 4715
1 0 1 0 4716 1 0 1 0 4717 0 0 1 0 4718 0 0 1 0 4719 1 0 1 0 4720 0 0 1 0 4721 0 0
0 0 4722 0 0 0 0 4723 0 0 0 0 4724 0 0 0 0 4725 0 0 0 0
165
1 0.0 0.0 7.741164 2 0.0 0.0 -30.9647 3 0.0 0.0 15.48233 4 0.0 0.0 -30.9647 5 0.0 0.0 7.741164
166 0.0 0.0 -30.9647 167 0.0 0.0 -61.9293 168 0.0 0.0 -30.9647 229 0.0 0.0 15.48233 230 0.0 0.0 -
61.9293 231 0.0 0.0 30.96466 232 0.0 0.0 -61.9293 233 0.0 0.0 15.48233 394 0.0 0.0 -30.9647 395
0.0 0.0 -61.9293 396 0.0 0.0 -30.9647 457 0.0 0.0 15.48233 458 0.0 0.0 -61.9293 459 0.0 0.0 30.96466
460 0.0 0.0 -61.9293 461 0.0 0.0 15.48233 622 0.0 0.0 -30.9647 623 0.0 0.0 -61.9293 624 0.0 0.0 -
30.9647 685 0.0 0.0 15.48233 686 0.0 0.0 -61.9293 687 0.0 0.0 30.96466 688 0.0 0.0 -61.9293 689
0.0 0.0 15.48233 850 0.0 0.0 -30.9647 851 0.0 0.0 -61.9293 852 0.0 0.0 -30.9647 913 0.0 0.0 15.48233
914 0.0 0.0 -61.9293 915 0.0 0.0 30.96466 916 0.0 0.0 -61.9293 917 0.0 0.0 15.48233 1078 0.0 0.0 -
30.9647 1079 0.0 0.0 -61.9293 1080 0.0 0.0 -30.9647 1141 0.0 0.0 15.48233 1142 0.0 0.0 -61.9293 1143
0.0 0.0 30.96466 1144 0.0 0.0 -61.9293 1145 0.0 0.0 15.48233 1306 0.0 0.0 -30.9647 1307 0.0 0.0 -
61.9293 1308 0.0 0.0 -30.9647 1369 0.0 0.0 15.48233 1370 0.0 0.0 -61.9293 1371 0.0 0.0 30.96466 1372
0.0 0.0 -61.9293 1373 0.0 0.0 15.48233 1534 0.0 0.0 -30.9647 1535 0.0 0.0 -61.9293 1536 0.0 0.0 -30.9647
1597 0.0 0.0 15.48233 1598 0.0 0.0 -61.9293 1599 0.0 0.0 30.96466 1600 0.0 0.0 -61.9293 1601 0.0 0.0
15.48233 1762 0.0 0.0 -30.9647 1763 0.0 0.0 -61.9293 1764 0.0 0.0 -30.9647 1825 0.0 0.0 15.48233 1826
0.0 0.0 -61.9293 1827 0.0 0.0 30.96466 1828 0.0 0.0 -61.9293 1829 0.0 0.0 15.48233 1990 0.0 0.0 -
30.9647 1991 0.0 0.0 -61.9293 1992 0.0 0.0 -30.9647 2053 0.0 0.0 15.48233 2054 0.0 0.0 -61.9293 2055
0.0 0.0 30.96466 2056 0.0 0.0 -61.9293 2057 0.0 0.0 15.48233 2218 0.0 0.0 -30.9647 2219 0.0 0.0 -

```
61.9293  2220  0.0  0.0 -30.9647  2281  0.0  0.0  15.48233  2282  0.0  0.0 -61.9293  2283  0.0  0.0  30.96466  2284
0.0  0.0 -61.9293  2285  0.0  0.0  15.48233  2446  0.0  0.0 -30.9647  2447  0.0  0.0 -61.9293  2448  0.0  0.0 -30.9647
2509  0.0  0.0  15.48233  2510  0.0  0.0 -61.9293  2511  0.0  0.0  30.96466  2512  0.0  0.0 -61.9293  2513  0.0  0.0
15.48233  2674  0.0  0.0 -30.9647  2675  0.0  0.0 -61.9293  2676  0.0  0.0 -30.9647  2737  0.0  0.0  15.48233  2738
0.0  0.0 -61.9293  2739  0.0  0.0  30.96466  2740  0.0  0.0 -61.9293  2741  0.0  0.0  15.48233  2902  0.0  0.0 -
30.9647  2903  0.0  0.0 -61.9293  2904  0.0  0.0 -30.9647  2965  0.0  0.0  15.48233  2966  0.0  0.0 -61.9293  2967
0.0  0.0  30.96466  2968  0.0  0.0 -61.9293  2969  0.0  0.0  15.48233  3130  0.0  0.0 -30.9647  3131  0.0  0.0 -
61.9293  3132  0.0  0.0 -30.9647  3193  0.0  0.0  15.48233  3194  0.0  0.0 -61.9293  3195  0.0  0.0  30.96466  3196
0.0  0.0 -61.9293  3197  0.0  0.0  15.48233  3358  0.0  0.0 -30.9647  3359  0.0  0.0 -61.9293  3360  0.0  0.0 -30.9647
3421  0.0  0.0  15.48233  3422  0.0  0.0 -61.9293  3423  0.0  0.0  30.96466  3424  0.0  0.0 -61.9293  3425  0.0  0.0
15.48233  3586  0.0  0.0 -30.9647  3587  0.0  0.0 -61.9293  3588  0.0  0.0 -30.9647  3649  0.0  0.0  15.48233  3650
0.0  0.0 -61.9293  3651  0.0  0.0  30.96466  3652  0.0  0.0 -61.9293  3653  0.0  0.0  15.48233  3814  0.0  0.0 -
30.9647  3815  0.0  0.0 -61.9293  3816  0.0  0.0 -30.9647  3877  0.0  0.0  15.48233  3878  0.0  0.0 -61.9293  3879
0.0  0.0  30.96466  3880  0.0  0.0 -61.9293  3881  0.0  0.0  15.48233  4042  0.0  0.0 -30.9647  4043  0.0  0.0 -
61.9293  4044  0.0  0.0 -30.9647  4105  0.0  0.0  15.48233  4106  0.0  0.0 -61.9293  4107  0.0  0.0  30.96466  4108
0.0  0.0 -61.9293  4109  0.0  0.0  15.48233  4270  0.0  0.0 -30.9647  4271  0.0  0.0 -61.9293  4272  0.0  0.0 -30.9647
4333  0.0  0.0  15.48233  4334  0.0  0.0 -61.9293  4335  0.0  0.0  30.96466  4336  0.0  0.0 -61.9293  4337  0.0  0.0
15.48233  4498  0.0  0.0 -30.9647  4499  0.0  0.0 -61.9293  4500  0.0  0.0 -30.9647  4561  0.0  0.0  7.741164  4562
0.0  0.0 -30.9647  4563  0.0  0.0  15.48233  4564  0.0  0.0 -30.9647  4565  0.0  0.0  7.741164
0.001  250
3
0.0 0.0 1 4.137e4 8640000 4.137e4



TITLE(2)="3-D TWO COMPONENT WATER INJECTION"
DESCRIPTION()=
"THICKNESS (FT) : 60"
"LENGTH (FT) : 350"
"WIDTH (FT) : 350"
"GRID BLOCKS : 7x7x3"

COMPOSITIONAL_MODEL
TIMEEND = 490

$ I/O OPTIONS

OUTLEVEL = 1
PROCOUT
OUTPUT_PRE
OUTPUT_SAT
OUTPUT_OIL
OUTPUT_GAS
OUTPUT_DEN
OUTPUT_WEL
OUTPUT_HIS
WELLFILE = "3COMP.WEL"

HISDATA_NUM = 300
OUTPUT_TIME() = 0 0.1 0.2 0.3 0.4 0.5 0.6 0.7 0.8 0.9 1. 5. 10 20 30 40 50 100 200 300 500 900
$NO_CRASH

$OUTPUT FREQUENCY
ISTEP(,,)=1
JSTEP(,,)=1
KSTEP(,,)=1

$ FAULT BLOCK AND MESH DATA
METHOD = 2
DOWN() = 0 0 1
NX(1) = 7    NY(1) = 7    NZ(1) = 3
MES = "cart"
DX() = 50    DY() = 50    DZ() = 20

$ COMPOUND NAMES
COMPOUND(1) = "FC10"
COMPOUND(2) = "FC15"
$ COMPOUND CRITICAL TEMPERATURES
```

```
CRIT() 1120.11 1270.0

$ COMPOUND CRITICAL PRESSURES
CRIP() 367.647 200.0

$ COMPOUND CRITICAL VOLUMES
CRIV() 8.415 16.696

$ COMPOUND ACEN
ACEN() 0.443774 0.650

$ COMPOUND MOL WEIGHTS
MOLW() 134.0 206.0

$ COMPOUND PARA
PARA() 622.1 631.0

$ MAX NUMBER OF PHASES
NPHASE = 3

$ MAXNEWT MAX NUMBER OF NEWTON ITERATION
MAXNEWT = 20

$ Initial rock & water properties
ROCKZ = 0.0001    ROCKP = 14.7
H2OZ = 0.000003    H2OP = 14.696    H2OD = 3.468
SURTF = 60.0    SURPS = 14.696
RESTF = 140.0

$ TOLERANCE
CVGOPT = 2
TOL_FLASH = 0.001
TOL_VOLUME = 0.001
TOL_MASS = 0.001
TOL_WATER = 0.001

$ POROSITY
POROSITY1() = 0.3

$ PERMEABILITIES
XPERM1() = 100
YPERM1() = 100
ZPERM1() = 100
XYPERM1() = 0
XZPERM1() = 0
YZPERM1() = 0

$ INITIAL WATER SATURATION
SWINI1() = 0.2

$ INITIAL WATER CELL PRESSURE
PINI1() = 600.0

$ INITIAL PHASE VISCOSITIES AT EACH CELL
VIS1() = 1.0

$ INITIAL COMPOSITIONS
ZXY1(,,,1) = .6
ZXY1(,,,2) = .4
$RELPERM DATA
$ RELP 1 for table lookup, 2 for function based

RELP 2
$MODREL(1) = 3

$ NRELFUN 1 for corey, more to be added later
NRELFUN    1
$ data for each phase : water, phase 2 and phase 3
```

```
ENDPT() = 0.5 0.7 0.85
SR() = 0.25 0.15 0.06
EXPN() = 2.5 2.0 1.5
$END OF ENERGY DATA

$--B feng pan 11/23/2006    -------- GEOMECHanics options
GEOMG =    71
GEOM2D    = 98
PCOUP = 1
THF = 0
GMCL=0
TOLA=0.0000000001
LIMA=200
TOLB=0.0000000000000001
LIMB=1000
NKM=15
$--E feng pan 11/23/2006    -------- GEOMECHanics options


$ ============== WELL SPECIFICATIONS ==============
NUMWELL = 2
$ --- The first well ---
WELLNAME(1) = "INJECTOR 1"
KINDWELL(1) = 2
WELLTOP(1 TO 3,1,1) = 25 25 0
WELLBOTTOM(1 TO 3,1,1) = 25 25 60
DIAMETER(1,1) = 0.5
PRLIMIT(1) = 14695
WELLPQ(1) Block
   Interpolation Linear
   Extrapolation Constant
         Data    0.        400.0
EndBlock

$ --- The 2nd well ---
WELLNAME(2) = "PRODUCER 1"
KINDWELL(2) = 3
WELLTOP(1 TO 3,1,2) = 325 325 0
WELLBOTTOM(1 TO 3,1,2) = 325 325 60
DIAMETER(1,2) = 0.5
WELLPQ(2) Block
   Interpolation Linear
   Extrapolation Constant
   Data    0.      600.
EndBlock

EndInitial

$ TRANSIENT DATA INPUT BLOCKS
BeginTime    0.0
TIME_CONTROL = 2
DELTIM = 0.01    DTIMMUL = 1.0    DTIMMAX = 30 DTIMMIN = 0.00001
TUNE = 0.5    DCMAX = 0.5    DAQCMAX = 0.5    DPMAX = 0.5    DSMAX = 0.5
WZ()    0.0 0.0 1.0
EndTime


3
7   7   3   1
1.0e-46    1.0e-46    9.098499e+06    0.3    30.0    0.0    0.0    1
-100
0             15.24        30.48        45.72        60.96        76.2          91.44        106.68
0             15.24        30.48        45.72        60.96        76.2          91.44        106.68
0             -6.096       -12.192      -18.288
86400 10    0.5    1    1
824
1   0   0   1   1 2   1   0   1   0 3   1   0   1   1 4   1   0   1   0 5   1   0   1   1 6   1   0   1   0 7   1   0   1   1 8   1   0   1   0
9   1   0   1   1   10   1   0   1   0   11   1   0   1   1   12   1   0   1   0   13   1   0   1   1   14   1   0   1   0   15   0   0   1
```

1 16 0 0 1 0 17 1 0 1 0 18 1 0 1 0 19 1 0 1 0 20 1 0 1 0 21 1 0 1 0 22 1 0
1 0 23 0 0 1 0 24 0 0 1 1 25 1 0 1 0 26 1 0 1 1 27 1 0 1 0 28 1 0 1 1 29 1
0 1 0 30 1 0 1 1 31 1 0 1 0 32 1 0 1 1 33 1 0 1 0 34 1 0 1 1 35 1 0 1 0 36
1 0 1 1 37 1 0 1 0 38 0 0 1 1 39 0 0 1 0 40 1 0 1 0 41 1 0 1 0 42 1 0 1 0
43 1 0 1 0 44 1 0 1 0 45 1 0 1 0 46 0 0 1 0 47 0 0 1 1 48 1 0 1 0 49 1 0 1
1 50 1 0 1 0 51 1 0 1 1 52 1 0 1 0 53 1 0 1 1 54 1 0 1 0 55 1 0 1 1 56 1 0
1 0 57 1 0 1 1 58 1 0 1 0 59 1 0 1 1 60 1 0 1 0 61 0 0 1 1 62 0 0 1 0 63 1
0 1 0 64 1 0 1 0 65 1 0 1 0 66 1 0 1 0 67 1 0 1 0 68 1 0 1 0 69 0 0 1 0 70
0 0 0 1 71 0 0 0 0 72 0 0 0 1 73 0 0 0 0 74 0 0 0 1 75 0 0 0 0 76 0 0 0 1
77 0 0 0 0 78 0 0 0 1 79 0 0 0 0 80 0 0 0 1 81 0 0 0 0 82 0 0 0 1 83 0 0 0
0 84 0 0 0 1 85 0 1 1 0 86 1 1 1 0 87 1 1 1 0 88 1 1 1 0 89 1 1 1 0 90 1 1
1 0 91 1 1 1 0 92 0 1 1 0 93 0 1 1 0 94 1 1 1 0 95 1 1 1 0 96 1 1 1 0 97 1
1 1 0 98 1 1 1 0 99 1 1 1 0 100 0 1 1 0 101 0 1 1 0 102 1 1 1 0 103 1 1 1 0 104 1
1 1 0 105 1 1 1 0 106 1 1 1 0 107 1 1 1 0 108 0 1 1 0 109 0 0 0 0 110 0 0 0 0 111 0
0 0 0 112 0 0 0 0 113 0 0 0 0 114 0 0 0 0 115 0 0 0 0 116 0 0 0 0 117 0 1 1 1 118 1
1 1 0 119 1 1 1 1 120 1 1 1 0 121 1 1 1 1 122 1 1 1 0 123 1 1 1 1 124 1 1 1 0 125 1
1 1 1 126 1 1 1 0 127 1 1 1 1 128 1 1 1 0 129 1 1 1 1 130 1 1 1 0 131 0 1 1 1 132 0
1 1 0 133 1 1 1 0 134 1 1 1 0 135 1 1 1 0 136 1 1 1 0 137 1 1 1 0 138 1 1 1 0 139 0
1 1 0 140 0 1 1 1 141 1 1 1 0 143 1 1 1 0 145 1 1 1 0 147 1 1 1 0 149 1 1 1 0 151 1
1 1 0 153 1 1 1 0 154 0 1 1 1 155 0 1 1 0 156 1 1 1 0 157 1 1 1 0 158 1 1 1 0 159 1
1 1 0 160 1 1 1 0 161 1 1 1 0 162 0 1 1 0 163 0 1 1 1 164 1 1 1 0 166 1 1 1 0 168 1
1 1 0 170 1 1 1 0 172 1 1 1 0 174 1 1 1 0 176 1 1 1 0 177 0 1 1 1 178 0 1 1 0 179 1
1 1 0 180 1 1 1 0 181 1 1 1 0 182 1 1 1 0 183 1 1 1 0 184 1 1 1 0 185 0 1 1 0 186 0
0 0 1 187 0 0 0 0 188 0 0 0 1 189 0 0 0 0 190 0 0 0 1 191 0 0 0 0 192 0 0 0 1 193 0
0 0 0 194 0 0 0 1 195 0 0 0 0 196 0 0 0 1 197 0 0 0 0 198 0 0 0 1 199 0 0 0 0 200 0
0 0 1 201 0 1 1 0 202 1 1 1 0 203 1 1 1 0 204 1 1 1 0 205 1 1 1 0 206 1 1 1 0 207 1
1 1 0 208 0 1 1 0 209 0 1 1 0 210 1 1 1 0 211 1 1 1 0 212 1 1 1 0 213 1 1 1 0 214 1
1 1 0 215 1 1 1 0 216 0 1 1 0 217 0 1 1 0 218 1 1 1 0 219 1 1 1 0 220 1 1 1 0 221 1
1 1 0 222 1 1 1 0 223 1 1 1 0 224 0 1 1 0 225 0 0 0 0 226 0 0 0 0 227 0 0 0 0 228 0
0 0 0 229 0 0 0 0 230 0 0 0 0 231 0 0 0 0 232 0 0 0 0 233 0 1 1 1 234 1 1 1 0 235 1
1 1 1 236 1 1 1 0 237 1 1 1 1 238 1 1 1 0 239 1 1 1 1 240 1 1 1 0 241 1 1 1 1 242 1
1 1 0 243 1 1 1 1 244 1 1 1 0 245 1 1 1 1 246 1 1 1 0 247 0 1 1 1 248 0 1 1 0 249 1
1 1 0 250 1 1 1 0 251 1 1 1 0 252 1 1 1 0 253 1 1 1 0 254 1 1 1 0 255 0 1 1 0 256 0
1 1 1 257 1 1 1 0 259 1 1 1 0 261 1 1 1 0 263 1 1 1 0 265 1 1 1 0 267 1 1 1 0 269 1
1 1 0 270 0 1 1 1 271 0 1 1 0 272 1 1 1 0 273 1 1 1 0 274 1 1 1 0 275 1 1 1 0 276 1
1 1 0 277 1 1 1 0 278 0 1 1 0 279 0 1 1 1 280 1 1 1 0 282 1 1 1 0 284 1 1 1 0 286 1
1 1 0 288 1 1 1 0 290 1 1 1 0 292 1 1 1 0 293 0 1 1 1 294 0 1 1 0 295 1 1 1 0 296 1
1 1 0 297 1 1 1 0 298 1 1 1 0 299 1 1 1 0 300 1 1 1 0 301 0 1 1 0 302 0 0 0 1 303 0
0 0 0 304 0 0 0 1 305 0 0 0 0 306 0 0 0 1 307 0 0 0 0 308 0 0 0 1 309 0 0 0 0 310 0
0 0 1 311 0 0 0 0 312 0 0 0 1 313 0 0 0 0 314 0 0 0 1 315 0 0 0 0 316 0 0 0 1 317 0
1 1 0 318 1 1 1 0 319 1 1 1 0 320 1 1 1 0 321 1 1 1 0 322 1 1 1 0 323 1 1 1 0 324 0
1 1 0 325 0 1 1 0 326 1 1 1 0 327 1 1 1 0 328 1 1 1 0 329 1 1 1 0 330 1 1 1 0 331 1
1 1 0 332 0 1 1 0 333 0 1 1 0 334 1 1 1 0 335 1 1 1 0 336 1 1 1 0 337 1 1 1 0 338 1
1 1 0 339 1 1 1 0 340 0 1 1 0 341 0 0 0 0 342 0 0 0 0 343 0 0 0 0 344 0 0 0 0 345 0
0 0 0 346 0 0 0 0 347 0 0 0 0 348 0 0 0 0 349 0 1 1 1 350 1 1 1 0 351 1 1 1 1 352 1
1 1 0 353 1 1 1 1 354 1 1 1 0 355 1 1 1 1 356 1 1 1 0 357 1 1 1 1 358 1 1 1 0 359 1
1 1 1 360 1 1 1 0 361 1 1 1 1 362 1 1 1 0 363 0 1 1 1 364 0 1 1 0 365 1 1 1 0 366 1
1 1 0 367 1 1 1 0 368 1 1 1 0 369 1 1 1 0 370 1 1 1 0 371 0 1 1 0 372 0 1 1 1 373 1
1 1 0 375 1 1 1 0 377 1 1 1 0 379 1 1 1 0 381 1 1 1 0 383 1 1 1 0 385 1 1 1 0 386 0
1 1 1 387 0 1 1 0 388 1 1 1 0 389 1 1 1 0 390 1 1 1 0 391 1 1 1 0 392 1 1 1 0 393 1
1 1 0 394 0 1 1 0 395 0 1 1 1 396 1 1 1 0 398 1 1 1 0 400 1 1 1 0 402 1 1 1 0 404 1
1 1 0 406 1 1 1 0 408 1 1 1 0 409 0 1 1 1 410 0 1 1 0 411 1 1 1 0 412 1 1 1 0 413 1
1 1 0 414 1 1 1 0 415 1 1 1 0 416 1 1 1 0 417 0 1 1 0 418 0 0 0 1 419 0 0 0 0 420 0
0 0 1 421 0 0 0 0 422 0 0 0 1 423 0 0 0 0 424 0 0 0 1 425 0 0 0 0 426 0 0 0 1 427 0
0 0 0 428 0 0 0 1 429 0 0 0 0 430 0 0 0 1 431 0 0 0 0 432 0 0 0 1 433 0 1 1 0 434 1
1 1 0 435 1 1 1 0 436 1 1 1 0 437 1 1 1 0 438 1 1 1 0 439 1 1 1 0 440 0 1 1 0 441 0
1 1 0 442 1 1 1 0 443 1 1 1 0 444 1 1 1 0 445 1 1 1 0 446 1 1 1 0 447 1 1 1 0 448 0
1 1 0 449 0 1 1 0 450 1 1 1 0 451 1 1 1 0 452 1 1 1 0 453 1 1 1 0 454 1 1 1 0 455 1
1 1 0 456 0 1 1 0 457 0 0 0 0 458 0 0 0 0 459 0 0 0 0 460 0 0 0 0 461 0 0 0 0 462 0
0 0 0 463 0 0 0 0 464 0 0 0 0 465 0 1 1 1 466 1 1 1 0 467 1 1 1 1 468 1 1 1 0 469 1
1 1 1 470 1 1 1 0 471 1 1 1 1 472 1 1 1 0 473 1 1 1 1 474 1 1 1 0 475 1 1 1 1 476 1
1 1 0 477 1 1 1 1 478 1 1 1 0 479 0 1 1 1 480 0 1 1 0 481 1 1 1 0 482 1 1 1 0 483 1
1 1 0 484 1 1 1 0 485 1 1 1 0 486 1 1 1 0 487 0 1 1 0 488 0 1 1 1 489 1 1 1 0 491 1
1 1 0 493 1 1 1 0 495 1 1 1 0 497 1 1 1 0 499 1 1 1 0 501 1 1 1 0 502 0 1 1 1 503 0
1 1 0 504 1 1 1 0 505 1 1 1 0 506 1 1 1 0 507 1 1 1 0 508 1 1 1 0 509 1 1 1 0 510 0
1 1 0 511 0 1 1 1 512 1 1 1 0 514 1 1 1 0 516 1 1 1 0 518 1 1 1 0 520 1 1 1 0 522 1
1 1 0 524 1 1 1 0 525 0 1 1 1 526 0 1 1 0 527 1 1 1 0 528 1 1 1 0 529 1 1 1 0 530 1
1 1 0 531 1 1 1 0 532 1 1 1 0 533 0 1 1 0 534 0 0 0 1 535 0 0 0 0 536 0 0 0 1 537 0

0 0 0 538 0 0 0 1 539 0 0 0 0 540 0 0 0 1 541 0 0 0 0 542 0 0 0 1 543 0 0 0 0 544 0
0 0 1 545 0 0 0 0 546 0 0 0 1 547 0 0 0 0 548 0 0 0 1 549 0 1 1 0 550 1 1 1 0 551 1
1 1 0 552 1 1 1 0 553 1 1 1 0 554 1 1 1 0 555 1 1 1 0 556 0 1 1 0 557 0 1 1 0 558 1
1 1 0 559 1 1 1 0 560 1 1 1 0 561 1 1 1 0 562 1 1 1 0 563 1 1 1 0 564 0 1 1 0 565 0
1 1 0 566 1 1 1 0 567 1 1 1 0 568 1 1 1 0 569 1 1 1 0 570 1 1 1 0 571 1 1 1 0 572 0
1 1 0 573 0 0 0 0 574 0 0 0 0 575 0 0 0 0 576 0 0 0 0 577 0 0 0 0 578 0 0 0 0 579 0
0 0 0 580 0 0 0 0 581 0 1 1 1 582 1 1 1 0 583 1 1 1 1 584 1 1 1 0 585 1 1 1 1 586 1
1 1 0 587 1 1 1 1 588 1 1 1 0 589 1 1 1 1 590 1 1 1 0 591 1 1 1 1 592 1 1 1 0 593 1
1 1 1 594 1 1 1 0 595 0 1 1 1 596 0 1 1 0 597 1 1 1 0 598 1 1 1 0 599 1 1 1 0 600 1
1 1 0 601 1 1 1 0 602 1 1 1 0 603 0 1 1 0 604 0 1 1 1 605 1 1 1 0 607 1 1 1 0 609 1
1 1 0 611 1 1 1 0 613 1 1 1 0 615 1 1 1 0 617 1 1 1 0 618 0 1 1 1 619 0 1 1 0 620 1
1 1 0 621 1 1 1 0 622 1 1 1 0 623 1 1 1 0 624 1 1 1 0 625 1 1 1 0 626 0 1 1 0 627 0
1 1 1 628 1 1 1 0 630 1 1 1 0 632 1 1 1 0 634 1 1 1 0 636 1 1 1 0 638 1 1 1 0 640 1
1 1 0 641 0 1 1 1 642 0 1 1 0 643 1 1 1 0 644 1 1 1 0 645 1 1 1 0 646 1 1 1 0 647 1
1 1 0 648 1 1 1 0 649 0 1 1 0 650 0 0 0 1 651 0 0 0 0 652 0 0 0 1 653 0 0 0 0 654 0
0 0 1 655 0 0 0 0 656 0 0 0 1 657 0 0 0 0 658 0 0 0 1 659 0 0 0 0 660 0 0 0 1 661 0
0 0 0 662 0 0 0 1 663 0 0 0 0 664 0 0 0 1 665 0 1 1 0 666 1 1 1 0 667 1 1 1 0 668 1
1 1 0 669 1 1 1 0 670 1 1 1 0 671 1 1 1 0 672 0 1 1 0 673 0 1 1 0 674 1 1 1 0 675 1
1 1 0 676 1 1 1 0 677 1 1 1 0 678 1 1 1 0 679 1 1 1 0 680 0 1 1 0 681 0 1 1 0 682 1
1 1 0 683 1 1 1 0 684 1 1 1 0 685 1 1 1 0 686 1 1 1 0 687 1 1 1 0 688 0 1 1 0 689 0
0 0 0 690 0 0 0 0 691 0 0 0 0 692 0 0 0 0 693 0 0 0 0 694 0 0 0 0 695 0 0 0 0 696 0
0 0 0 697 0 1 1 1 698 1 1 1 0 699 1 1 1 1 700 1 1 1 0 701 1 1 1 1 702 1 1 1 0 703 1
1 1 1 704 1 1 1 0 705 1 1 1 1 706 1 1 1 0 707 1 1 1 1 708 1 1 1 0 709 1 1 1 1 710 1
1 1 0 711 0 1 1 1 712 0 1 1 0 713 1 1 1 0 714 1 1 1 0 715 1 1 1 0 716 1 1 1 0 717 1
1 1 0 718 1 1 1 0 719 0 1 1 0 720 0 1 1 1 721 1 1 1 0 723 1 1 1 0 725 1 1 1 0 727 1
1 1 0 729 1 1 1 0 731 1 1 1 0 733 1 1 1 0 734 0 1 1 1 735 0 1 1 0 736 1 1 1 0 737 1
1 1 0 738 1 1 1 0 739 1 1 1 0 740 1 1 1 0 741 1 1 1 0 742 0 1 1 0 743 0 1 1 1 744 1
1 1 0 746 1 1 1 0 748 1 1 1 0 750 1 1 1 0 752 1 1 1 0 754 1 1 1 0 756 1 1 1 0 757 0
1 1 1 758 0 1 1 0 759 1 1 1 0 760 1 1 1 0 761 1 1 1 0 762 1 1 1 0 763 1 1 1 0 764 1
1 1 0 765 0 1 1 0 766 0 0 0 1 767 0 0 0 0 768 0 0 0 1 769 0 0 0 0 770 0 0 0 1 771 0
0 0 0 772 0 0 0 1 773 0 0 0 0 774 0 0 0 1 775 0 0 0 0 776 0 0 0 1 777 0 0 0 0 778 0
0 0 1 779 0 0 0 0 780 0 0 0 1 781 0 1 1 0 782 1 1 1 0 783 1 1 1 0 784 1 1 1 0 785 1
1 1 0 786 1 1 1 0 787 1 1 1 0 788 0 1 1 0 789 0 1 1 0 790 1 1 1 0 791 1 1 1 0 792 1
1 1 0 793 1 1 1 0 794 1 1 1 0 795 1 1 1 0 796 0 1 1 0 797 0 1 1 0 798 1 1 1 0 799 1
1 1 0 800 1 1 1 0 801 1 1 1 0 802 1 1 1 0 803 1 1 1 0 804 0 1 1 0 805 0 0 0 0 806 0
0 0 0 807 0 0 0 0 808 0 0 0 0 809 0 0 0 0 810 0 0 0 0 811 0 0 0 0 812 0 0 0 0 813 0
0 1 1 814 1 0 1 0 815 1 0 1 1 816 1 0 1 0 817 1 0 1 1 818 1 0 1 0 819 1 0 1 1 820 1
0 1 0 821 1 0 1 1 822 1 0 1 0 823 1 0 1 1 824 1 0 1 0 825 1 0 1 1 826 1 0 1 0 827 0
0 1 1 828 0 0 1 0 829 1 0 1 0 830 1 0 1 0 831 1 0 1 0 832 1 0 1 0 833 1 0 1 0 834 1
0 1 0 835 0 0 1 0 836 0 0 1 1 837 1 0 1 0 838 1 0 1 1 839 1 0 1 0 840 1 0 1 1 841 1
0 1 0 842 1 0 1 1 843 1 0 1 0 844 1 0 1 1 845 1 0 1 0 846 1 0 1 1 847 1 0 1 0 848 1
0 1 1 849 1 0 1 0 850 0 0 1 1 851 0 0 1 0 852 1 0 1 0 853 1 0 1 0 854 1 0 1 0 855 1
0 1 0 856 1 0 1 0 857 1 0 1 0 858 0 0 1 0 859 0 0 1 1 860 1 0 1 0 861 1 0 1 1 862 1
0 1 0 863 1 0 1 1 864 1 0 1 0 865 1 0 1 1 866 1 0 1 0 867 1 0 1 1 868 1 0 1 0 869 1
0 1 1 870 1 0 1 0 871 1 0 1 1 872 1 0 1 0 873 0 0 1 1 874 0 0 1 0 875 1 0 1 0 876 1
0 1 0 877 1 0 1 0 878 1 0 1 0 879 1 0 1 0 880 1 0 1 0 881 0 0 1 0 882 0 0 0 1 883 0
0 0 0 884 0 0 0 1 885 0 0 0 0 886 0 0 0 1 887 0 0 0 0 888 0 0 0 1 889 0 0 0 0 890 0
0 0 1 891 0 0 0 0 892 0 0 0 1 893 0 0 0 0 894 0 0 0 1 895 0 0 0 0 896 0 0 0 1
69
1 0.0 0.0 19.35291 2 0.0 0.0 -77.4116 3 0.0 0.0 38.70582 4 0.0 0.0 -77.4116 5 0.0 0.0 19.35291 38 0.0
0.0 -77.4116 39 0.0 0.0 -154.823 40 0.0 0.0 -77.4116 53 0.0 0.0 38.70582 54 0.0 0.0 -154.823 55 0.0 0.0
77.41164 56 0.0 0.0 -154.823 57 0.0 0.0 38.70582 90 0.0 0.0 -77.4116 91 0.0 0.0 -154.823 92 0.0 0.0 -77.4116
105 0.0 0.0 38.70582 106 0.0 0.0 -154.823 107 0.0 0.0 77.41164 108 0.0 0.0 -154.823 109 0.0 0.0
38.70582 142 0.0 0.0 -77.4116 143 0.0 0.0 -154.823 144 0.0 0.0 -77.4116 157 0.0 0.0 38.70582 158 0.0
0.0 -154.823 159 0.0 0.0 77.41164 160 0.0 0.0 -154.823 161 0.0 0.0 38.70582 194 0.0 0.0 -77.4116 195
0.0 0.0 -154.823 196 0.0 0.0 -77.4116 209 0.0 0.0 38.70582 210 0.0 0.0 -154.823 211 0.0 0.0 77.41164
212 0.0 0.0 -154.823 213 0.0 0.0 38.70582 246 0.0 0.0 -77.4116 247 0.0 0.0 -154.823 248 0.0 0.0 -
77.4116 261 0.0 0.0 38.70582 262 0.0 0.0 -154.823 263 0.0 0.0 77.41164 264 0.0 0.0 -154.823 265 0.0
0.0 38.70582 298 0.0 0.0 -77.4116 299 0.0 0.0 -154.823 300 0.0 0.0 -77.4116 313 0.0 0.0 38.70582 314
0.0 0.0 -154.823 315 0.0 0.0 77.41164 316 0.0 0.0 -154.823 317 0.0 0.0 38.70582 350 0.0 0.0 -77.4116
351 0.0 0.0 -154.823 352 0.0 0.0 -77.4116 365 0.0 0.0 38.70582 366 0.0 0.0 -154.823 367 0.0 0.0
77.41164 368 0.0 0.0 -154.823 369 0.0 0.0 38.70582 402 0.0 0.0 -77.4116 403 0.0 0.0 -154.823 404 0.0
0.0 -77.4116 417 0.0 0.0 19.35291 418 0.0 0.0 -77.4116 419 0.0 0.0 38.70582 420 0.0 0.0 -77.4116 421
0.0 0.0 19.35291
0.001 250
3
0.0 0.0 1 0.0 8640000 0.0

```
TITLE(2)="3-D SEVEN COMPONENT CO2 INJECTION"

DESCRIPTION()=
"THICKNESS (FT) : 60"
"LENGTH (FT) : 300"
"WIDTH (FT) : 300"
"GRID BLOCKS : 6x6x3"

COMPOSITIONAL_MODEL
TIMEEND = 365

$ I/O OPTIONS
OUTLEVEL = 1
PROCOUT
OUTPUT_PRE
OUTPUT_SAT
OUTPUT_OIL
OUTPUT_GAS
OUTPUT_WEL
OUTPUT_HIS
WELLFILE = "7COMP.WEL"

HISDATA_NUM = 100
OUTPUT_TIME() = 0 0.1 0.2 0.3 0.4 0.5 0.6 0.7 0.8 0.9 1. 5. 10. 20.
30. 40. 50. 60 70 80 90 100 1000 2000 3000 3650


$OUTPUT FREQUENCY
ISTEP(,,)=1
JSTEP(,,)=1
KSTEP(,,)=1

$ FAULT BLOCK AND MESH DATA
METHOD = 2
DOWN() = 0 0 1
NX(1) = 6    NY(1) = 6    NZ(1) = 3
MES = "cart"
DX() = 50    DY() = 50    DZ() = 20

$ COMPOUND NAMES
COMPOUND(1) = "CO2"
COMPOUND(2) = "C1"
COMPOUND(3) = "C2-3"
COMPOUND(4) = "C4-6"
COMPOUND(5) = "C7-15"
COMPOUND(6) = "C16-27"
COMPOUND(7) = "C28+"

$ COMPOUND CRITICAL TEMPERATURES
CRIT() 547.56 288.00 619.57 833.80 1090.35 1351.83 1696.46

$ COMPOUND CRITICAL PRESSURES
CRIP() 1069.86 667.20 652.56 493.07 315.44 239.90 238.12

$ COMPOUND CRITICAL VOLUMES
CRIV() 1.506 1.586    2.902 4.914 9.000 17.100 32.500

$ COMPOUND ACEN
ACEN() 0.22500 0.00800 0.13050 0.24040 0.61770    0.95660 1.26830

$ COMPOUND MOL WEIGHTS
MOLW() 44.01 16.04 37.20    69.50 140.96 280.99 519.62

$ COMPOUND PARA
PARA() 49.0 71.0 135.1    228.6 415.4 752.5 1071.

$ BINARY INTERACTION COEFFICIENTS
```

```
BINC(,) = 0.0        0.0550 0.0550 0.0550 0.1050 0.1050 0.1050
          0.0550 0.0    0.0    0.0    0.0    0.0    0.0
          0.0550 0.0    0.0    0.0    0.0    0.0    0.0
          0.0550 0.0    0.0    0.0    0.0    0.0    0.0
          0.1050 0.0    0.0    0.0    0.0    0.0    0.0
          0.1050 0.0    0.0    0.0    0.0    0.0    0.0
          0.1050 0.0    0.0    0.0    0.0    0.0    0.0

$ MAX NUMBER OF PHASES
NPHASE = 3

$ MAXNEWT MAX NUMBER OF NEWTON ITERATION
MAXNEWT = 20

$ Initial rock & water properties
ROCKZ = 0.000003    ROCKP = 14.65
H2OZ = 0.000003    H2OP = 14.65    H2OD = 3.467
SURTF = 60.0    SURPS = 14.65
RESTF = 100.0

$ TOLERANCE
CVGOPT = 2
TOL_FLASH = 0.0001
TOL_VOLUME = 0.0001
TOL_MASS = 0.0001
TOL_WATER = 0.0001

$ POROSITY
POROSITY1() = 0.25

$ PERMEABILITIES
XPERM1() = 100
YPERM1() = 100
ZPERM1() = 100
XYPERM1() = 0
XZPERM1() = 0
YZPERM1() = 0

$ INITIAL WATER SATURATION
SWINI1() = 0.2
$ INITIAL WATER CELL PRESSURE
PINI1() = 900.0

$ INITIAL PHASE VISCOSITIES AT EACH CELL
VIS1() = 1.0

$ INITIAL COMPOSITIONS
ZXY1(,,,1) = 0.001
ZXY1(,,,2) = 0.150
ZXY1(,,,3) = 0.216
ZXY1(,,,4) = 0.234
ZXY1(,,,5) = 0.267
ZXY1(,,,6) = 0.061
ZXY1(,,,7) = 0.071

$ RELPERM DATA
$ RELP 1 for table lookup, 2 for function based

RELP 2
$MODREL(1) = 3

$ NRELFUN 1 for corey, more to be added later
NRELFUN    1
$ data for each phase : water, PHASE 2 AND PHASE 3
ENDPT() = 0.55 0.75 0.8
SR() = 0.25 0.2 0.05
EXPN() = 3.0 2.0 2.0
```

```
$--B feng pan 11/23/2006    -------- GEOMECHanics options
GEOMG =    71
GEOM2D    = 98
PCOUP = 1
THF = 0
GMCL=0
TOLA=0.0000000001
LIMA=200
TOLB=0.0000000000000001
LIMB=1000
$--E feng pan 11/23/2006    -------- GEOMECHanics options

$ ============== WELL SPECIFICATIONS ==============

NUMWELL = 2

$ --- The first well ---
WELLNAME(1) = "INJECTOR 1"
KINDWELL(1) = 2
WELLTOP(1 TO 3,1,1) = 25 25 0
WELLBOTTOM(1 TO 3,1,1) = 25 25 60
DIAMETER(1,1) = 0.5
PRLIMIT(1) = 14695
WELLPQ(1) Block
   Interpolation Linear
   Extrapolation Constant
   Data    0.          300.0
EndBlock

$ --- The 2nd well ---
WELLNAME(2) = "PRODUCER 1"
KINDWELL(2) = 3
WELLTOP(1 TO 3,1,2) = 275 275 0
WELLBOTTOM(1 TO 3,1,2) = 275 275 60
DIAMETER(1,2) = 0.5
WELLPQ(2) Block
   Interpolation Linear
   Extrapolation Constant
   Data    0.      850.0
EndBlock

EndInitial

$ TRANSIENT DATA INPUT BLOCKS
BeginTime    0.0
TIME_CONTROL = 2
DELTIM = 0.01    DTIMMUL = 1.0    DTIMMAX = 30 DTIMMIN = 0.001
TUNE = 0.5    DCMAX = 0.5    DAQCMAX = 0.5    DPMAX = 0.5    DSMAX = 0.5
WZ() 0.85 0.1499995 0.0000001 0.0000001 0.0000001 0.0000001 0.0000001    0.0
EndTime

3
6    6    3    1
1.0e-46    1.0e-46    1.098499e+05    0.3    30.0    0.0    0.0    1
-100
0              15.24        30.48        45.72        60.96        76.2          91.44
0              15.24        30.48        45.72        60.96        76.2          91.44
0              -6.096       -12.192      -18.288
86400 10    0.5    1    1
629
1    0    0    1    1    2    1    0    1    0    3    1    0    1    1    4    1    0    1    0    5    1    0    1    1    6    1    0    1    0    7    1    0    1    1    8
1    0    1    0    9    1    0    1    1 10    1    0    1    0 11    1    0    1    1 12    1    0    1    0 13    0    0    1    1 14    0    0    1    0 15    1    0
1    0 16    1    0    1    0 17    1    0    1    0 18    1    0    1    0 19    1    0    1    0 20    0    0    1    0 21    0    0    1    1 22    1    0    1    0 23
1    0    1    1 24    1    0    1    0 25    1    0    1    1 26    1    0    1    0 27    1    0    1    1 28    1    0    1    0 29    1    0    1    1 30    1    0
1    0 31    1    0    1    1 32    1    0    1    0 33    0    0    1    1 34    0    0    1    0 35    1    0    1    0 36    1    0    1    0 37    1    0    1    0 38
1    0    1    0 39    1    0    1    0 40    0    0    1    0 41    0    0    1    1 42    1    0    1    0 43    1    0    1    1 44    1    0    1    0 45    1    0
1    1 46    1    0    1    0 47    1    0    1    1 48    1    0    1    0 49    1    0    1    1 50    1    0    1    0 51    1    0    1    1 52    1    0    1    0 53
0    0    1    1 54    0    0    1    0 55    1    0    1    0 56    1    0    1    0 57    1    0    1    0 58    1    0    1    0 59    1    0    1    0 60    0    0
```

1 0 61 0 0 0 1 62 0 0 0 0 63 0 0 0 1 64 0 0 0 0 65 0 0 0 1 66 0 0 0 0 67 0 0 0 1 68
0 0 0 0 69 0 0 0 1 70 0 0 0 0 71 0 0 0 1 72 0 0 0 0 73 0 0 0 1 74 0 1 1 0 75 1 1
1 0 76 1 1 1 0 77 1 1 1 0 78 1 1 1 0 79 1 1 1 0 80 0 1 1 0 81 0 1 1 0 82 1 1 1 0 83
1 1 1 0 84 1 1 1 0 85 1 1 1 0 86 1 1 1 0 87 0 1 1 0 88 0 1 1 0 89 1 1 1 0 90 1 1
1 0 91 1 1 1 0 92 1 1 1 0 93 1 1 1 0 94 0 1 1 0 95 0 0 0 0 96 0 0 0 0 97 0 0 0 0 98
0 0 0 0 99 0 0 0 0 100 0 0 0 0 101 0 0 0 0 102 0 1 1 1 103 1 1 1 0 104 1 1 1
1 105 1 1 1 0 106 1 1 1 1 107 1 1 1 0 108 1 1 1 1 109 1 1 1 0 110 1 1 1 1 111
1 1 1 0 112 1 1 1 1 113 1 1 1 0 114 0 1 1 1 115 0 1 1 0 116 1 1 1 0 117 1 1
1 0 118 1 1 1 0 119 1 1 1 0 120 1 1 1 0 121 0 1 1 0 122 0 1 1 1 123 1 1 1 0
125 1 1 1 0 127 1 1 1 0 129 1 1 1 0 131 1 1 1 0 133 1 1 1 0 134 0 1 1 1 135 0
1 1 0 136 1 1 1 0 137 1 1 1 0 138 1 1 1 0 139 1 1 1 0 140 1 1 1 0 141 0 1 1
0 142 0 1 1 1 143 1 1 1 0 145 1 1 1 0 147 1 1 1 0 149 1 1 1 0 151 1 1 1 0 153
1 1 1 0 154 0 1 1 1 155 0 1 1 0 156 1 1 1 0 157 1 1 1 0 158 1 1 1 0 159 1 1
1 0 160 1 1 1 0 161 0 1 1 0 162 0 0 0 1 163 0 0 0 0 164 0 0 0 1 165 0 0 0 0
166 0 0 0 1 167 0 0 0 0 168 0 0 0 1 169 0 0 0 0 170 0 0 0 1 171 0 0 0 0 172 0
0 0 1 173 0 0 0 0 174 0 0 0 1 175 0 1 1 0 176 1 1 1 0 177 1 1 1 0 178 1 1 1
0 179 1 1 1 0 180 1 1 1 0 181 0 1 1 0 182 0 1 1 0 183 1 1 1 0 184 1 1 1 0 185
1 1 1 0 186 1 1 1 0 187 1 1 1 0 188 0 1 1 0 189 0 1 1 0 190 1 1 1 0 191 1 1
1 0 192 1 1 1 0 193 1 1 1 0 194 1 1 1 0 195 0 1 1 0 196 0 0 0 0 197 0 0 0 0
198 0 0 0 0 199 0 0 0 0 200 0 0 0 0 201 0 0 0 0 202 0 0 0 0 203 0 1 1 1 204 1
1 1 0 205 1 1 1 1 206 1 1 1 0 207 1 1 1 1 208 1 1 1 0 209 1 1 1 1 210 1 1 1
0 211 1 1 1 1 212 1 1 1 0 213 1 1 1 1 214 1 1 1 0 215 0 1 1 1 216 0 1 1 0 217
1 1 1 0 218 1 1 1 0 219 1 1 1 0 220 1 1 1 0 221 1 1 1 0 222 0 1 1 0 223 0 1
1 1 224 1 1 1 0 226 1 1 1 0 228 1 1 1 0 230 1 1 1 0 232 1 1 1 0 234 1 1 1 0
235 0 1 1 1 236 0 1 1 0 237 1 1 1 0 238 1 1 1 0 239 1 1 1 0 240 1 1 1 0 241 1
1 1 0 242 0 1 1 0 243 0 1 1 1 244 1 1 1 0 246 1 1 1 0 248 1 1 1 0 250 1 1 1
0 252 1 1 1 0 254 1 1 1 0 255 0 1 1 1 256 0 1 1 0 257 1 1 1 0 258 1 1 1 0 259
1 1 1 0 260 1 1 1 0 261 1 1 1 0 262 0 1 1 0 263 0 0 0 1 264 0 0 0 0 265 0 0
0 1 266 0 0 0 0 267 0 0 0 1 268 0 0 0 0 269 0 0 0 1 270 0 0 0 0 271 0 0 0 1
272 0 0 0 0 273 0 0 0 1 274 0 0 0 0 275 0 0 0 1 276 0 1 1 0 277 1 1 1 0 278 1
1 1 0 279 1 1 1 0 280 1 1 1 0 281 1 1 1 0 282 0 1 1 0 283 0 1 1 0 284 1 1 1
0 285 1 1 1 0 286 1 1 1 0 287 1 1 1 0 288 1 1 1 0 289 0 1 1 0 290 0 1 1 0 291
1 1 1 0 292 1 1 1 0 293 1 1 1 0 294 1 1 1 0 295 1 1 1 0 296 0 1 1 0 297 0 0
0 0 298 0 0 0 0 299 0 0 0 0 300 0 0 0 0 301 0 0 0 0 302 0 0 0 0 303 0 0 0 0
304 0 1 1 1 305 1 1 1 0 306 1 1 1 1 307 1 1 1 0 308 1 1 1 1 309 1 1 1 0 310 1
1 1 1 311 1 1 1 0 312 1 1 1 1 313 1 1 1 0 314 1 1 1 1 315 1 1 1 0 316 0 1 1
1 317 0 1 1 0 318 1 1 1 0 319 1 1 1 0 320 1 1 1 0 321 1 1 1 0 322 1 1 1 0 323
0 1 1 0 324 0 1 1 1 325 1 1 1 0 327 1 1 1 0 329 1 1 1 0 331 1 1 1 0 333 1 1
1 0 335 1 1 1 0 336 0 1 1 1 337 0 1 1 0 338 1 1 1 0 339 1 1 1 0 340 1 1 1 0
341 1 1 1 0 342 1 1 1 0 343 0 1 1 0 344 0 1 1 1 345 1 1 1 0 347 1 1 1 0 349 1
1 1 0 351 1 1 1 0 353 1 1 1 0 355 1 1 1 0 356 0 1 1 1 357 0 1 1 0 358 1 1 1
0 359 1 1 1 0 360 1 1 1 0 361 1 1 1 0 362 1 1 1 0 363 0 1 1 0 364 0 0 0 1 365
0 0 0 0 366 0 0 0 1 367 0 0 0 0 368 0 0 0 1 369 0 0 0 0 370 0 0 0 1 371 0 0
0 0 372 0 0 0 1 373 0 0 0 0 374 0 0 0 1 375 0 0 0 0 376 0 0 0 1 377 0 1 1 0
378 1 1 1 0 379 1 1 1 0 380 1 1 1 0 381 1 1 1 0 382 1 1 1 0 383 0 1 1 0 384 0
1 1 0 385 1 1 1 0 386 1 1 1 0 387 1 1 1 0 388 1 1 1 0 389 1 1 1 0 390 0 1 1
0 391 0 1 1 0 392 1 1 1 0 393 1 1 1 0 394 1 1 1 0 395 1 1 1 0 396 1 1 1 0 397
0 1 1 0 398 0 0 0 0 399 0 0 0 0 400 0 0 0 0 401 0 0 0 0 402 0 0 0 0 403 0 0
0 0 404 0 0 0 0 405 0 1 1 1 406 1 1 1 0 407 1 1 1 1 408 1 1 1 0 409 1 1 1 1
410 1 1 1 0 411 1 1 1 1 412 1 1 1 0 413 1 1 1 1 414 1 1 1 0 415 1 1 1 1 416 1
1 1 0 417 0 1 1 1 418 0 1 1 0 419 1 1 1 0 420 1 1 1 0 421 1 1 1 0 422 1 1 1
0 423 1 1 1 0 424 0 1 1 0 425 0 1 1 1 426 1 1 1 0 428 1 1 1 0 430 1 1 1 0 432
1 1 1 0 434 1 1 1 0 436 1 1 1 0 437 0 1 1 1 438 0 1 1 0 439 1 1 1 0 440 1 1
1 0 441 1 1 1 0 442 1 1 1 0 443 1 1 1 0 444 0 1 1 0 445 0 1 1 1 446 1 1 1 0
448 1 1 1 0 450 1 1 1 0 452 1 1 1 0 454 1 1 1 0 456 1 1 1 0 457 0 1 1 1 458 0
1 1 0 459 1 1 1 0 460 1 1 1 0 461 1 1 1 0 462 1 1 1 0 463 1 1 1 0 464 0 1 1
0 465 0 0 0 1 466 0 0 0 0 467 0 0 0 1 468 0 0 0 0 469 0 0 0 1 470 0 0 0 0 471
0 0 0 1 472 0 0 0 0 473 0 0 0 1 474 0 0 0 0 475 0 0 0 1 476 0 0 0 0 477 0 0
0 1 478 0 1 1 0 479 1 1 1 0 480 1 1 1 0 481 1 1 1 0 482 1 1 1 0 483 1 1 1 0
484 0 1 1 0 485 0 1 1 0 486 1 1 1 0 487 1 1 1 0 488 1 1 1 0 489 1 1 1 0 490 1
1 1 0 491 0 1 1 0 492 0 1 1 0 493 1 1 1 0 494 1 1 1 0 495 1 1 1 0 496 1 1 1
0 497 1 1 1 0 498 0 1 1 0 499 0 0 0 0 500 0 0 0 0 501 0 0 0 0 502 0 0 0 0 503
0 0 0 0 504 0 0 0 0 505 0 0 0 0 506 0 1 1 1 507 1 1 1 0 508 1 1 1 1 509 1 1
1 0 510 1 1 1 1 511 1 1 1 0 512 1 1 1 1 513 1 1 1 0 514 1 1 1 1 515 1 1 1 0
516 1 1 1 1 517 1 1 1 0 518 0 1 1 1 519 0 1 1 0 520 1 1 1 0 521 1 1 1 0 522 1
1 1 0 523 1 1 1 0 524 1 1 1 0 525 0 1 1 0 526 0 1 1 1 527 1 1 1 0 529 1 1 1
0 531 1 1 1 0 533 1 1 1 0 535 1 1 1 0 537 1 1 1 0 538 0 1 1 1 539 0 1 1 0 540
1 1 1 0 541 1 1 1 0 542 1 1 1 0 543 1 1 1 0 544 1 1 1 0 545 0 1 1 0 546 0 1

```
1 1 547 1 1 1 0 549 1 1 1 0 551 1 1 1 0 553 1 1 1 0 555 1 1 1 0 557 1 1 1 0
558 0 1 1 1 559 0 1 1 0 560 1 1 1 0 561 1 1 1 0 562 1 1 1 0 563 1 1 1 0 564 1
1 1 0 565 0 1 1 0 566 0 0 0 1 567 0 0 0 0 568 0 0 0 1 569 0 0 0 0 570 0 0 0
1 571 0 0 0 0 572 0 0 0 1 573 0 0 0 0 574 0 0 0 1 575 0 0 0 0 576 0 0 0 1 577
0 0 0 0 578 0 0 0 1 579 0 1 1 0 580 1 1 1 0 581 1 1 1 0 582 1 1 1 0 583 1 1
1 0 584 1 1 1 0 585 0 1 1 0 586 0 1 1 0 587 1 1 1 0 588 1 1 1 0 589 1 1 1 0
590 1 1 1 0 591 1 1 1 0 592 0 1 1 0 593 0 1 1 0 594 1 1 1 0 595 1 1 1 0 596 1
1 1 0 597 1 1 1 0 598 1 1 1 0 599 0 1 1 0 600 0 0 0 0 601 0 0 0 0 602 0 0 0
0 603 0 0 0 0 604 0 0 0 0 605 0 0 0 0 606 0 0 0 0 607 0 0 1 1 608 1 0 1 0 609
1 0 1 1 610 1 0 1 0 611 1 0 1 1 612 1 0 1 0 613 1 0 1 1 614 1 0 1 0 615 1 0
1 1 616 1 0 1 0 617 1 0 1 1 618 1 0 1 0 619 0 0 1 1 620 0 0 1 0 621 1 0 1 0
622 1 0 1 0 623 1 0 1 0 624 1 0 1 0 625 1 0 1 0 626 0 0 1 0 627 0 0 1 1 628 1
0 1 0 629 1 0 1 1 630 1 0 1 0 631 1 0 1 1 632 1 0 1 0 633 1 0 1 1 634 1 0 1
0 635 1 0 1 1 636 1 0 1 0 637 1 0 1 1 638 1 0 1 0 639 0 0 1 1 640 0 0 1 0 641
1 0 1 0 642 1 0 1 0 643 1 0 1 0 644 1 0 1 0 645 1 0 1 0 646 0 0 1 0 647 0 0
1 1 648 1 0 1 0 649 1 0 1 1 650 1 0 1 0 651 1 0 1 1 652 1 0 1 0 653 1 0 1 1
654 1 0 1 0 655 1 0 1 1 656 1 0 1 0 657 1 0 1 1 658 1 0 1 0 659 0 0 1 1 660 0
0 1 0 661 1 0 1 0 662 1 0 1 0 663 1 0 1 0 664 1 0 1 0 665 1 0 1 0 666 0 0 1
0 667 0 0 0 1 668 0 0 0 0 669 0 0 0 1 670 0 0 0 0 671 0 0 0 1 672 0 0 0 0 673
0 0 0 1 674 0 0 0 0 675 0 0 0 1 676 0 0 0 0 677 0 0 0 1 678 0 0 0 0 679 0 0
0 1
69
1 0.0 0.0 19.35291 2 0.0 0.0 -77.4116 3 0.0 0.0 38.70582 4 0.0 0.0 -77.4116 5 0.0 0.0 19.35291 38 0.0
0.0 -77.4116 39 0.0 0.0 -154.823 40 0.0 0.0 -77.4116 53 0.0 0.0 38.70582 54 0.0 0.0 -154.823 55 0.0 0.0
77.41164 56 0.0 0.0 -154.823 57 0.0 0.0 38.70582 90 0.0 0.0 -77.4116 91 0.0 0.0 -154.823 92 0.0 0.0 -77.4116
105 0.0 0.0 38.70582 106 0.0 0.0 -154.823 107 0.0 0.0 77.41164 108 0.0 0.0 -154.823 109 0.0 0.0 38.70582
142 0.0 0.0 -77.4116 143 0.0 0.0 -154.823 144 0.0 0.0 -77.4116 157 0.0 0.0 38.70582 158 0.0 0.0 -154.823
159 0.0 0.0 77.41164 160 0.0 0.0 -154.823 161 0.0 0.0 38.70582 194 0.0 0.0 -77.4116 195 0.0 0.0 -154.823
196 0.0 0.0 -77.4116 209 0.0 0.0 38.70582 210 0.0 0.0 -154.823 211 0.0 0.0 77.41164 212 0.0 0.0 -154.823
213 0.0 0.0 38.70582 246 0.0 0.0 -77.4116 247 0.0 0.0 -154.823 248 0.0 0.0 -77.4116 261 0.0 0.0
38.70582 262 0.0 0.0 -154.823 263 0.0 0.0 77.41164 264 0.0 0.0 -154.823 265 0.0 0.0 38.70582 298 0.0 0.0 -
77.4116 299 0.0 0.0 -154.823 300 0.0 0.0 -77.4116 313 0.0 0.0 38.70582 314 0.0 0.0 -154.823 315 0.0 0.0
77.41164 316 0.0 0.0 -154.823 317 0.0 0.0 38.70582 350 0.0 0.0 -77.4116 351 0.0 0.0 -154.823 352 0.0 0.0 -
77.4116 365 0.0 0.0 38.70582 366 0.0 0.0 -154.823 367 0.0 0.0 77.41164 368 0.0 0.0 -154.823 369 0.0 0.0
38.70582 402 0.0 0.0 -77.4116 403 0.0 0.0 -154.823 404 0.0 0.0 -77.4116 417 0.0 0.0 19.35291 418 0.0 0.0
-77.4116 419 0.0 0.0 38.70582 420 0.0 0.0 -77.4116 421 0.0 0.0 19.35291
0.001 250
3
0.0 0.0 1 0.0 8640000 0.0


TITLE(2)="3-D TWO COMPONENT WATER INJECTION"

DESCRIPTION()=
"THICKNESS (FT) : 60"
"LENGTH (FT) : 350"
"WIDTH (FT) : 350"
"GRID BLOCKS : 7x7x3"

COMPOSITIONAL_MODEL
$DEBUGS

TIMEEND = 1000

$ I/O OPTIONS

OUTLEVEL = 1
$SPLINEOUT
$GEOMOUT
PROCOUT
OUTPUT_PRE
$OUTPUT_NPH
OUTPUT_SAT
OUTPUT_OIL
OUTPUT_GAS
OUTPUT_DEN
OUTPUT_WEL
```

```
OUTPUT_HIS
WELLFILE = "3COMP.WEL"

HISDATA_NUM = 300
OUTPUT_TIME() =    10 20 30 40 50 100 200 300 500 900
$NO_CRASH


$OUTPUT FREQUENCY
ISTEP(,,)=1
JSTEP(,,)=1
KSTEP(,,)=1

$ FAULT BLOCK AND MESH DATA
METHOD = 2
DOWN() = 0 0 1
NX(1) = 7    NY(1) = 7    NZ(1) = 3
MES = "cart"
DX() = 50    DY() = 50    DZ() = 20

$ COMPOUND NAMES
COMPOUND(1) = "FC10"
COMPOUND(2) = "FC15"
$ COMPOUND CRITICAL TEMPERATURES
CRIT() 1120.11 1270.0

$ COMPOUND CRITICAL PRESSURES
CRIP() 367.647 200.0

$ COMPOUND CRITICAL VOLUMES
CRIV() 8.415 16.696

$ COMPOUND ACEN
ACEN() 0.443774 0.650

$ COMPOUND MOL WEIGHTS
MOLW() 134.0 206.0

$ COMPOUND PARA
PARA() 622.1 631.0

$ MAX NUMBER OF PHASES
NPHASE = 3

$ MAXNEWT MAX NUMBER OF NEWTON ITERATION
MAXNEWT = 20

$ Initial rock & water properties
ROCKZ = 0.0000    ROCKP = 14.7
H2OZ = 0.000000    H2OP = 14.696    H2OD = 3.468
SURTF = 60.0    SURPS = 14.696
RESTF = 140.0

$ TOLERANCE
CVGOPT = 2
TOL_FLASH = 0.001
TOL_VOLUME = 0.001
TOL_MASS = 0.001
TOL_WATER = 0.001

$ POROSITY
POROSITY1() = 0.3

$ PERMEABILITIES
XPERM1() = 100
YPERM1() = 100
ZPERM1() = 100
XYPERM1() = 0
```

```
XZPERM1() = 0
YZPERM1() = 0

$ INITIAL WATER SATURATION
SWINI1() = 0.2

$ INITIAL WATER CELL PRESSURE
PINI1() = 800.0

$ INITIAL PHASE VISCOSITIES AT EACH CELL
VIS1() = 1.0

$ INITIAL COMPOSITIONS
ZXY1(,,,1) = .6
ZXY1(,,,2) = .4
$RELPERM DATA
$ RELP 1 for table lookup, 2 for function based

RELP 2
$MODREL(1) = 3

$ NRELFUN 1 for corey, more to be added later
NRELFUN    1
$ data for each phase : water, phase 2 and phase 3
ENDPT() = 0.5 0.7 0.85
SR() = 0.25 0.15 0.06
EXPN() = 2.5 2.0 1.5
$END OF ENERGY DATA



$--B feng pan 11/23/2006    -------- GEOMECHanics options
GEOMG =    69
GEOM2D    = 98
PCOUP = 97
THF = 0
GMCL=0
TOLA=0.0000000001
LIMA=200
TOLB=0.0000000000000001
LIMB=1000
$ITPORM=5
EQC=3
$--E feng pan 11/23/2006    -------- GEOMECHanics options

$ ============== WELL SPECIFICATIONS ==============

NUMWELL = 2

$ --- The first well ---
WELLNAME(1) = "INJECTOR 1"
KINDWELL(1) = 2
WELLTOP(1 TO 3,1,1) = 25 25 0
WELLBOTTOM(1 TO 3,1,1) = 25 25 60
DIAMETER(1,1) = 0.5
PRLIMIT(1) = 14695
WELLPQ(1) Block
   Interpolation Linear
   Extrapolation Constant
         Data    0.        200.0
EndBlock

$ --- The 2nd well ---
WELLNAME(2) = "PRODUCER 1"
KINDWELL(2) = 3
WELLTOP(1 TO 3,1,2) = 325 325 0
WELLBOTTOM(1 TO 3,1,2) = 325 325 60
DIAMETER(1,2) = 0.5
```

```
WELLPQ(2) Block
   Interpolation Linear
   Extrapolation Constant
   Data   0.      400.
EndBlock

EndInitial

$ TRANSIENT DATA INPUT BLOCKS
BeginTime   0.0
TIME_CONTROL = 2
DELTIM = 0.01   DTIMMUL = 1.0   DTIMMAX = 30 DTIMMIN = 0.00001
TUNE = 0.5   DCMAX = 0.5   DAQCMAX = 0.5   DPMAX = 0.5   DSMAX = 0.5
WZ()   0.0 0.0 1.0
EndTime

3
7   7   3   1
1.0e-46   1.0e-46   5.098499e+05   0.3   30.0   0.0   0.0   1
-100
0            15.24       30.48       45.72       60.96       76.2        91.44       106.68
0            15.24       30.48       45.72       60.96       76.2        91.44       106.68
0            -6.096      -12.192     -18.288
86400 10   0.5   1   1
824
1   0   0   1   1   2   1   0   1   0   3   1   0   1   1   4   1   0   1   0   5   1   0   1   1   6   1   0   1   0   7   1   0   1   1   8
1   0   1   0   9   1   0   1   1   10   1   0   1   0   11   1   0   1   1   12   1   0   1   0   13   1   0   1   1   14   1   0   1   0
15   0   0   1   1   16   0   0   1   0   17   1   0   1   0   18   1   0   1   0   19   1   0   1   0   20   1   0   1   0   21   1   0   1
0   22   1   0   1   0   23   0   0   1   0   24   0   0   1   1   25   1   0   1   0   26   1   0   1   1   27   1   0   1   0   28   1   0
1   1   29   1   0   1   0   30   1   0   1   1   31   1   0   1   0   32   1   0   1   1   33   1   0   1   0   34   1   0   1   1   35   1
0   1   0   36   1   0   1   1   37   1   0   1   0   38   0   0   1   1   39   0   0   1   0   40   1   0   1   0   41   1   0   1   0   42
1   0   1   0   43   1   0   1   0   44   1   0   1   0   45   1   0   1   0   46   0   0   1   0   47   0   0   1   1   48   1   0   1   0
49   1   0   1   1   50   1   0   1   0   51   1   0   1   1   52   1   0   1   0   53   1   0   1   1   54   1   0   1   0   55   1   0   1
1   56   1   0   1   0   57   1   0   1   1   58   1   0   1   0   59   1   0   1   1   60   1   0   1   0   61   0   0   1   1   62   0   0
1   0   63   1   0   1   0   64   1   0   1   0   65   1   0   1   0   66   1   0   1   0   67   1   0   1   0   68   1   0   1   0   69   0
0   1   0   70   0   0   0   1   71   0   0   0   0   72   0   0   0   1   73   0   0   0   0   74   0   0   0   1   75   0   0   0   0   76
0   0   0   1   77   0   0   0   0   78   0   0   0   1   79   0   0   0   0   80   0   0   0   1   81   0   0   0   0   82   0   0   0   1
83   0   0   0   0   84   0   0   0   1   85   0   1   1   0   86   1   1   1   0   87   1   1   1   0   88   1   1   1   0   89   1   1   1
0   90   1   1   1   0   91   1   1   1   0   92   0   1   1   0   93   0   1   1   0   94   1   1   1   0   95   1   1   1   0   96   1   1
1   0   97   1   1   1   0   98   1   1   1   0   99   1   1   1   0   100   0   1   1   0   101   0   1   1   0   102   1   1   1   0   103
1   1   1   0   104   1   1   1   0   105   1   1   1   0   106   1   1   1   0   107   1   1   1   0   108   0   1   1   0   109   0   0
0   0   110   0   0   0   0   111   0   0   0   0   112   0   0   0   0   113   0   0   0   0   114   0   0   0   0   115   0   0   0   0
116   0   0   0   0   117   0   1   1   1   118   1   1   1   0   119   1   1   1   1   120   1   1   1   0   121   1   1   1   1   122   1
1   1   0   123   1   1   1   1   124   1   1   1   0   125   1   1   1   1   126   1   1   1   0   127   1   1   1   1   128   1   1   1
0   129   1   1   1   1   130   1   1   1   0   131   0   1   1   1   132   0   1   1   0   133   1   1   1   0   134   1   1   1   0   135
1   1   1   0   136   1   1   1   0   137   1   1   1   0   138   1   1   1   0   139   0   1   1   0   140   0   1   1   1   141   1   1
1   0   143   1   1   1   0   145   1   1   1   0   147   1   1   1   0   149   1   1   1   0   151   1   1   1   0   153   1   1   1   0
154   0   1   1   1   155   0   1   1   0   156   1   1   1   0   157   1   1   1   0   158   1   1   1   0   159   1   1   1   0   160   1
1   1   0   161   1   1   1   0   162   0   1   1   0   163   0   1   1   1   164   1   1   1   0   166   1   1   1   0   168   1   1   1
0   170   1   1   1   0   172   1   1   1   0   174   1   1   1   0   176   1   1   1   0   177   0   1   1   1   178   0   1   1   0   179
1   1   1   0   180   1   1   1   0   181   1   1   1   0   182   1   1   1   0   183   1   1   1   0   184   1   1   1   0   185   0   1
1   0   186   0   0   0   1   187   0   0   0   0   188   0   0   0   1   189   0   0   0   0   190   0   0   0   1   191   0   0   0   0
192   0   0   0   1   193   0   0   0   0   194   0   0   0   1   195   0   0   0   0   196   0   0   0   1   197   0   0   0   0   198   0
0   0   1   199   0   0   0   0   200   0   0   0   1   201   0   1   1   0   202   1   1   1   0   203   1   1   1   0   204   1   1   1
0   205   1   1   1   0   206   1   1   1   0   207   1   1   1   0   208   0   1   1   0   209   0   1   1   0   210   1   1   1   0   211
1   1   1   0   212   1   1   1   0   213   1   1   1   0   214   1   1   1   0   215   1   1   1   0   216   0   1   1   0   217   0   1
1   0   218   1   1   1   0   219   1   1   1   0   220   1   1   1   0   221   1   1   1   0   222   1   1   1   0   223   1   1   1   0
224   0   1   1   0   225   0   0   0   0   226   0   0   0   0   227   0   0   0   0   228   0   0   0   0   229   0   0   0   0   230   0
0   0   0   231   0   0   0   0   232   0   0   0   0   233   0   1   1   1   234   1   1   1   0   235   1   1   1   1   236   1   1   1
0   237   1   1   1   1   238   1   1   1   0   239   1   1   1   1   240   1   1   1   0   241   1   1   1   1   242   1   1   1   0   243
1   1   1   1   244   1   1   1   0   245   1   1   1   1   246   1   1   1   0   247   0   1   1   1   248   0   1   1   0   249   1   1
1   0   250   1   1   1   0   251   1   1   1   0   252   1   1   1   0   253   1   1   1   0   254   1   1   1   0   255   0   1   1   0
256   0   1   1   1   257   1   1   1   0   259   1   1   1   0   261   1   1   1   0   263   1   1   1   0   265   1   1   1   0   267   1
1   1   0   269   1   1   1   0   270   0   1   1   1   271   0   1   1   0   272   1   1   1   0   273   1   1   1   0   274   1   1   1
0   275   1   1   1   0   276   1   1   1   0   277   1   1   1   0   278   0   1   1   0   279   0   1   1   1   280   1   1   1   0   282
1   1   1   0   284   1   1   1   0   286   1   1   1   0   288   1   1   1   0   290   1   1   1   0   292   1   1   1   0   293   0   1
1   1   294   0   1   1   0   295   1   1   1   0   296   1   1   1   0   297   1   1   1   0   298   1   1   1   0   299   1   1   1   0
300   1   1   1   0   301   0   1   1   0   302   0   0   0   1   303   0   0   0   0   304   0   0   0   1   305   0   0   0   0   306   0
```

0 0 1 307 0 0 0 0 308 0 0 0 1 309 0 0 0 0 310 0 0 0 1 311 0 0 0 0 312 0 0 0
1 313 0 0 0 0 314 0 0 0 1 315 0 0 0 0 316 0 0 0 1 317 0 1 1 0 318 1 1 1 0 319
1 1 1 0 320 1 1 1 0 321 1 1 1 0 322 1 1 1 0 323 1 1 1 0 324 0 1 1 0 325 0 1
1 0 326 1 1 1 0 327 1 1 1 0 328 1 1 1 0 329 1 1 1 0 330 1 1 1 0 331 1 1 1 0
332 0 1 1 0 333 0 1 1 0 334 1 1 1 0 335 1 1 1 0 336 1 1 1 0 337 1 1 1 0 338 1
1 1 0 339 1 1 1 0 340 0 1 1 0 341 0 0 0 0 342 0 0 0 0 343 0 0 0 0 344 0 0 0
0 345 0 0 0 0 346 0 0 0 0 347 0 0 0 0 348 0 0 0 0 349 0 1 1 1 350 1 1 1 0 351
1 1 1 1 352 1 1 1 0 353 1 1 1 1 354 1 1 1 0 355 1 1 1 1 356 1 1 1 0 357 1 1
1 1 358 1 1 1 0 359 1 1 1 1 360 1 1 1 0 361 1 1 1 1 362 1 1 1 0 363 0 1 1 1
364 0 1 1 0 365 1 1 1 0 366 1 1 1 0 367 1 1 1 0 368 1 1 1 0 369 1 1 1 0 370 1
1 1 0 371 0 1 1 0 372 0 1 1 1 373 1 1 1 0 375 1 1 1 0 377 1 1 1 0 379 1 1 1
0 381 1 1 1 0 383 1 1 1 0 385 1 1 1 0 386 0 1 1 1 387 0 1 1 0 388 1 1 1 0 389
1 1 1 0 390 1 1 1 0 391 1 1 1 0 392 1 1 1 0 393 1 1 1 0 394 0 1 1 0 395 0 1
1 1 396 1 1 1 0 398 1 1 1 0 400 1 1 1 0 402 1 1 1 0 404 1 1 1 0 406 1 1 1 0
408 1 1 1 0 409 0 1 1 1 410 0 1 1 0 411 1 1 1 0 412 1 1 1 0 413 1 1 1 0 414 1
1 1 0 415 1 1 1 0 416 1 1 1 0 417 0 1 1 0 418 0 0 0 1 419 0 0 0 0 420 0 0 0
1 421 0 0 0 0 422 0 0 0 1 423 0 0 0 0 424 0 0 0 1 425 0 0 0 0 426 0 0 0 1 427
0 0 0 0 428 0 0 0 1 429 0 0 0 0 430 0 0 0 1 431 0 0 0 0 432 0 0 0 1 433 0 1
1 0 434 1 1 1 0 435 1 1 1 0 436 1 1 1 0 437 1 1 1 0 438 1 1 1 0 439 1 1 1 0
440 0 1 1 0 441 0 1 1 0 442 1 1 1 0 443 1 1 1 0 444 1 1 1 0 445 1 1 1 0 446 1
1 1 0 447 1 1 1 0 448 0 1 1 0 449 0 1 1 0 450 1 1 1 0 451 1 1 1 0 452 1 1 1
0 453 1 1 1 0 454 1 1 1 0 455 1 1 1 0 456 0 1 1 0 457 0 0 0 0 458 0 0 0 0 459
0 0 0 0 460 0 0 0 0 461 0 0 0 0 462 0 0 0 0 463 0 0 0 0 464 0 0 0 0 465 0 1
1 1 466 1 1 1 0 467 1 1 1 1 468 1 1 1 0 469 1 1 1 1 470 1 1 1 0 471 1 1 1 1
472 1 1 1 0 473 1 1 1 1 474 1 1 1 0 475 1 1 1 1 476 1 1 1 0 477 1 1 1 1 478 1
1 1 0 479 0 1 1 1 480 0 1 1 0 481 1 1 1 0 482 1 1 1 0 483 1 1 1 0 484 1 1 1
0 485 1 1 1 0 486 1 1 1 0 487 0 1 1 0 488 0 1 1 1 489 1 1 1 0 491 1 1 1 0 493
1 1 1 0 495 1 1 1 0 497 1 1 1 0 499 1 1 1 0 501 1 1 1 0 502 0 1 1 1 503 0 1
1 0 504 1 1 1 0 505 1 1 1 0 506 1 1 1 0 507 1 1 1 0 508 1 1 1 0 509 1 1 1 0
510 0 1 1 0 511 0 1 1 1 512 1 1 1 0 514 1 1 1 0 516 1 1 1 0 518 1 1 1 0 520 1
1 1 0 522 1 1 1 0 524 1 1 1 0 525 0 1 1 1 526 0 1 1 0 527 1 1 1 0 528 1 1 1
0 529 1 1 1 0 530 1 1 1 0 531 1 1 1 0 532 1 1 1 0 533 0 1 1 0 534 0 0 0 1 535
0 0 0 0 536 0 0 0 1 537 0 0 0 0 538 0 0 0 1 539 0 0 0 0 540 0 0 0 1 541 0 0
0 0 542 0 0 0 1 543 0 0 0 0 544 0 0 0 1 545 0 0 0 0 546 0 0 0 1 547 0 0 0 0
548 0 0 0 1 549 0 1 1 0 550 1 1 1 0 551 1 1 1 0 552 1 1 1 0 553 1 1 1 0 554 1
1 1 0 555 1 1 1 0 556 0 1 1 0 557 0 1 1 0 558 1 1 1 0 559 1 1 1 0 560 1 1 1
0 561 1 1 1 0 562 1 1 1 0 563 1 1 1 0 564 0 1 1 0 565 0 1 1 0 566 1 1 1 0 567
1 1 1 0 568 1 1 1 0 569 1 1 1 0 570 1 1 1 0 571 1 1 1 0 572 0 1 1 0 573 0 0
0 0 574 0 0 0 0 575 0 0 0 0 576 0 0 0 0 577 0 0 0 0 578 0 0 0 0 579 0 0 0 0
580 0 0 0 0 581 0 1 1 1 582 1 1 1 0 583 1 1 1 1 584 1 1 1 0 585 1 1 1 1 586 1
1 1 0 587 1 1 1 1 588 1 1 1 0 589 1 1 1 1 590 1 1 1 0 591 1 1 1 1 592 1 1 1
0 593 1 1 1 1 594 1 1 1 0 595 0 1 1 1 596 0 1 1 0 597 1 1 1 0 598 1 1 1 0 599
1 1 1 0 600 1 1 1 0 601 1 1 1 0 602 1 1 1 0 603 0 1 1 0 604 0 1 1 1 605 1 1
1 0 607 1 1 1 0 609 1 1 1 0 611 1 1 1 0 613 1 1 1 0 615 1 1 1 0 617 1 1 1 0
618 0 1 1 1 619 0 1 1 0 620 1 1 1 0 621 1 1 1 0 622 1 1 1 0 623 1 1 1 0 624 1
1 1 0 625 1 1 1 0 626 0 1 1 0 627 0 1 1 1 628 1 1 1 0 630 1 1 1 0 632 1 1 1
0 634 1 1 1 0 636 1 1 1 0 638 1 1 1 0 640 1 1 1 0 641 0 1 1 1 642 0 1 1 0 643
1 1 1 0 644 1 1 1 0 645 1 1 1 0 646 1 1 1 0 647 1 1 1 0 648 1 1 1 0 649 0 1
1 0 650 0 0 0 1 651 0 0 0 0 652 0 0 0 1 653 0 0 0 0 654 0 0 0 1 655 0 0 0 0
656 0 0 0 1 657 0 0 0 0 658 0 0 0 1 659 0 0 0 0 660 0 0 0 1 661 0 0 0 0 662 0
0 0 1 663 0 0 0 0 664 0 0 0 1 665 0 1 1 0 666 1 1 1 0 667 1 1 1 0 668 1 1 1
0 669 1 1 1 0 670 1 1 1 0 671 1 1 1 0 672 0 1 1 0 673 0 1 1 0 674 1 1 1 0 675
1 1 1 0 676 1 1 1 0 677 1 1 1 0 678 1 1 1 0 679 1 1 1 0 680 0 1 1 0 681 0 1
1 0 682 1 1 1 0 683 1 1 1 0 684 1 1 1 0 685 1 1 1 0 686 1 1 1 0 687 1 1 1 0
688 0 1 1 0 689 0 0 0 0 690 0 0 0 0 691 0 0 0 0 692 0 0 0 0 693 0 0 0 0 694 0
0 0 0 695 0 0 0 0 696 0 0 0 0 697 0 1 1 1 698 1 1 1 0 699 1 1 1 1 700 1 1 1
0 701 1 1 1 1 702 1 1 1 0 703 1 1 1 1 704 1 1 1 0 705 1 1 1 1 706 1 1 1 0 707
1 1 1 1 708 1 1 1 0 709 1 1 1 1 710 1 1 1 0 711 0 1 1 1 712 0 1 1 0 713 1 1
1 0 714 1 1 1 0 715 1 1 1 0 716 1 1 1 0 717 1 1 1 0 718 1 1 1 0 719 0 1 1 0
720 0 1 1 1 721 1 1 1 0 723 1 1 1 0 725 1 1 1 0 727 1 1 1 0 729 1 1 1 0 731 1
1 1 0 733 1 1 1 0 734 0 1 1 1 735 0 1 1 0 736 1 1 1 0 737 1 1 1 0 738 1 1 1
0 739 1 1 1 0 740 1 1 1 0 741 1 1 1 0 742 0 1 1 0 743 0 1 1 1 744 1 1 1 0 746
1 1 1 0 748 1 1 1 0 750 1 1 1 0 752 1 1 1 0 754 1 1 1 0 756 1 1 1 0 757 0 1
1 1 758 0 1 1 0 759 1 1 1 0 760 1 1 1 0 761 1 1 1 0 762 1 1 1 0 763 1 1 1 0
764 1 1 1 0 765 0 1 1 0 766 0 0 0 1 767 0 0 0 0 768 0 0 0 1 769 0 0 0 0 770 0
0 0 1 771 0 0 0 0 772 0 0 0 1 773 0 0 0 0 774 0 0 0 1 775 0 0 0 0 776 0 0 0
1 777 0 0 0 0 778 0 0 0 1 779 0 0 0 0 780 0 0 0 1 781 0 1 1 0 782 1 1 1 0 783
1 1 1 0 784 1 1 1 0 785 1 1 1 0 786 1 1 1 0 787 1 1 1 0 788 0 1 1 0 789 0 1

```
1  0  790  1  1  1  0  791  1  1  1  0  792  1  1  1  0  793  1  1  1  0  794  1  1  1  0  795  1  1  1  0
796  0  1  1  0  797  0  1  1  0  798  1  1  1  0  799  1  1  1  0  800  1  1  1  0  801  1  1  1  0  802  1
1  1  0  803  1  1  1  0  804  0  1  1  0  805  0  0  0  0  806  0  0  0  0  807  0  0  0  0  808  0  0  0
0  809  0  0  0  0  810  0  0  0  0  811  0  0  0  0  812  0  0  0  0  813  0  0  1  1  814  1  0  1  0  815
1  0  1  1  816  1  0  1  0  817  1  0  1  1  818  1  0  1  0  819  1  0  1  1  820  1  0  1  0  821  1  0
1  1  822  1  0  1  0  823  1  0  1  1  824  1  0  1  0  825  1  0  1  1  826  1  0  1  0  827  0  0  1  1
828  0  0  1  0  829  1  0  1  0  830  1  0  1  0  831  1  0  1  0  832  1  0  1  0  833  1  0  1  0  834  1
0  1  0  835  0  0  1  0  836  0  0  1  1  837  1  0  1  0  838  1  0  1  1  839  1  0  1  0  840  1  0  1
1  841  1  0  1  0  842  1  0  1  1  843  1  0  1  0  844  1  0  1  1  845  1  0  1  0  846  1  0  1  1  847
1  0  1  0  848  1  0  1  1  849  1  0  1  0  850  0  0  1  1  851  0  0  1  0  852  1  0  1  0  853  1  0
1  0  854  1  0  1  0  855  1  0  1  0  856  1  0  1  0  857  1  0  1  0  858  0  0  1  0  859  0  0  1  1
860  1  0  1  0  861  1  0  1  1  862  1  0  1  0  863  1  0  1  1  864  1  0  1  0  865  1  0  1  1  866  1
0  1  0  867  1  0  1  1  868  1  0  1  0  869  1  0  1  1  870  1  0  1  0  871  1  0  1  1  872  1  0  1
0  873  0  0  1  1  874  0  0  1  0  875  1  0  1  0  876  1  0  1  0  877  1  0  1  0  878  1  0  1  0  879
1  0  1  0  880  1  0  1  0  881  0  0  1  0  882  0  0  0  1  883  0  0  0  0  884  0  0  0  1  885  0  0
0  0  886  0  0  0  1  887  0  0  0  0  888  0  0  0  1  889  0  0  0  0  890  0  0  0  1  891  0  0  0  0
892  0  0  0  1  893  0  0  0  0  894  0  0  0  1  895  0  0  0  0  896  0  0  0  1
69
   1   0.0   0.0   19.35291   2   0.0   0.0  -77.4116   3   0.0   0.0   38.70582    4   0.0   0.0  -77.4116   5   0.0   0.0   19.35291
38   0.0   0.0  -77.4116   39   0.0   0.0  -154.823   40   0.0   0.0  -77.4116    53   0.0   0.0   38.70582    54   0.0   0.0  -154.823
55   0.0   0.0   77.41164   56   0.0   0.0  -154.823    57   0.0   0.0   38.70582   90   0.0   0.0  -77.4116   91   0.0   0.0  -154.823
92   0.0   0.0  -77.4116   105   0.0   0.0   38.70582   106   0.0   0.0  -154.823   107   0.0   0.0   77.41164   108   0.0   0.0  -
154.823   109   0.0   0.0   38.70582   142   0.0   0.0  -77.4116   143   0.0   0.0  -154.823    144   0.0   0.0  -77.4116   157   0.0
0.0   38.70582   158   0.0   0.0  -154.823   159   0.0   0.0   77.41164   160   0.0   0.0  -154.823   161   0.0   0.0   38.70582   194
0.0   0.0  -77.4116   195   0.0   0.0  -154.823    196   0.0   0.0  -77.4116   209   0.0   0.0   38.70582   210   0.0   0.0  -154.823
211   0.0   0.0   77.41164   212   0.0   0.0  -154.823   213   0.0   0.0   38.70582   246   0.0   0.0  -77.4116   247   0.0   0.0  -
154.823    248   0.0   0.0  -77.4116   261   0.0   0.0   38.70582   262   0.0   0.0  -154.823   263   0.0   0.0   77.41164   264   0.0
0.0  -154.823   265   0.0   0.0   38.70582   298   0.0   0.0  -77.4116   299   0.0   0.0  -154.823    300   0.0   0.0  -77.4116   313
0.0   0.0   38.70582   314   0.0   0.0  -154.823   315   0.0   0.0   77.41164   316   0.0   0.0  -154.823   317   0.0   0.0   38.70582
350   0.0   0.0  -77.4116   351   0.0   0.0  -154.823    352   0.0   0.0  -77.4116   365   0.0   0.0   38.70582   366   0.0   0.0  -
154.823   367   0.0   0.0   77.41164   368   0.0   0.0  -154.823   369   0.0   0.0   38.70582   402   0.0   0.0  -77.4116   403   0.0
0.0  -154.823    404   0.0   0.0  -77.4116   417   0.0   0.0   19.35291   418   0.0   0.0  -77.4116   419   0.0   0.0   38.70582   420
0.0   0.0  -77.4116   421   0.0   0.0   19.35291
0.001   250
3
0.0 0.0 1 0.0              8640000 0.0



TITLE(2)="3-D THREE COMPONENT CO2 INJECTION"

DESCRIPTION()=
"THICKNESS (FT) : 45"
"LENGTH (FT) : 750"
"WIDTH (FT) : 750"
"GRID BLOCKS : 15x15x3"

COMPOSITIONAL_MODEL
$DEBUGS

TIMEEND = 1000.0

$ I/O OPTIONS

OUTLEVEL = 1
$SPLINEOUT
$GEOMOUT
PROCOUT
OUTPUT_PRE
$OUTPUT_NPH
OUTPUT_SAT
OUTPUT_OIL
OUTPUT_GAS
$OUTPUT_DEN
OUTPUT_WEL
OUTPUT_HIS
WELLFILE = "3COMP.WEL"
```

```
HISDATA_NUM = 100
OUTPUT_TIME() =    100 1000 2000 3000 3650
$NO_CRASH


$OUTPUT FREQUENCY
ISTEP(,,)=1
JSTEP(,,)=1
KSTEP(,,)=1

$ FAULT BLOCK AND MESH DATA
METHOD = 2
DOWN() = 0 0 1
NX(1) = 10    NY(1) = 10    NZ(1) = 3
MES = "cart"
DX() = 40    DY() = 40    DZ() = 15

$ COMPOUND NAMES
COMPOUND(1) = "CO2"
COMPOUND(2) = "C1"
COMPOUND(3) = "NC16"

$ COMPOUND CRITICAL TEMPERATURES
CRIT()    547.5700 343.0800 1322.43

$ COMPOUND CRITICAL PRESSURES
CRIP() 1071.6000 667.1961 252.105

$ COMPOUND CRITICAL VOLUMES
CRIV()    1.5060 1.5860 13.3768

$ COMPOUND ACEN
ACEN()    0.2250    0.0080 0.6225

$ COMPOUND MOL WEIGHTS
MOLW()    44.0100 16.0430 222.0

$ COMPOUND PARA
PARA()    49.0000 71.0000 831.9

$ BINARY INTERACTION COEFFICIENTS
BINC(,) = 0.0        0.12    0.12
                0.12      0.0      0.0
                0.12      0.0      0.0

$ MAX NUMBER OF PHASES
NPHASE = 3

$ MAXNEWT MAX NUMBER OF NEWTON ITERATION
MAXNEWT = 20

$ Initial rock & water properties
ROCKZ = 0.000004    ROCKP = 14.65
H2OZ = 0.000003    H2OP = 14.65    H2OD = 3.467
SURTF = 60.0    SURPS = 14.65
RESTF = 130.0

$ TOLERANCE
CVGOPT = 2
TOL_FLASH = 0.0001
TOL_VOLUME = 0.0001
TOL_MASS = 0.0001
TOL_WATER = 0.0001

$ POROSITY
POROSITY1() = 0.3

$ PERMEABILITIES
```

```
XPERM1() = 10
YPERM1() = 10
ZPERM1() = 10
XYPERM1() = 0
XZPERM1() = 0
YZPERM1() = 0

$ INITIAL WATER SATURATION
SWINI1() = 0.17
$ INITIAL WATER CELL PRESSURE
PINI1() = 500.0

$ INITIAL PHASE VISCOSITIES AT EACH CELL
VIS1() = 0.8

$ INITIAL COMPOSITIONS
ZXY1(,,,1) = .01
ZXY1(,,,2) = .29
ZXY1(,,,3) = .7

$ RELPERM DATA
$ RELP 1 for table lookup, 2 for function based

RELP 2
$MODREL(1) = 3

$ NRELFUN 1 for corey, more to be added later
NRELFUN    1
$ data for each phase : water, phase 2 and phase 3
ENDPT() = 0.4 0.7 0.9
SR() = 0.2 0.1 0.0
EXPN() = 3.0 2.0 2.0



$--B feng pan 11/23/2006    -------- GEOMECHanics options
GEOMG =    69
GEOM2D    = 98
PCOUP = 1
THF = 0
GMCL=0
TOLA=0.0000000001
LIMA=200
TOLB=0.0000000000000001
LIMB=1000
NKM=6
$--E feng pan 11/23/2006    -------- GEOMECHanics options

$ ================ WELL SPECIFICATIONS ================

NUMWELL = 2

$ --- The first well ---
WELLNAME(1) = "INJECTOR 1"
KINDWELL(1) = 2
WELLTOP(1 TO 3,1,1) = 25 25 0
WELLBOTTOM(1 TO 3,1,1) = 25 25 45
DIAMETER(1,1) = 0.44
PRLIMIT(1) = 14695
WELLPQ(1) Block
   Interpolation Linear
   Extrapolation Constant
   Data    0.        400.0
EndBlock

$ --- The 2nd well ---
WELLNAME(2) = "PRODUCER 1"
```

KINDWELL(2) = 3
WELLTOP(1 TO 3,1,2) = 380 380 0
WELLBOTTOM(1 TO 3,1,2) = 380 380 45
DIAMETER(1,2) = 0.44
WELLPQ(2) Block
  Interpolation Linear
  Extrapolation Constant
  Data 0. 500.0
EndBlock

EndInitial

$ TRANSIENT DATA INPUT BLOCKS
BeginTime 0.0
TIME_CONTROL = 2
DELTIM = 0.1 DTIMMUL = 1.0 DTIMMAX = 30 DTIMMIN = 0.001
TUNE = 0.5 DCMAX = 0.5 DAQCMAX = 0.5 DPMAX = 0.5 DSMAX = 0.2
$MAXMOL = 1 MAXP = 10000 ERRLIMIT = 0.2
WZ() 0.85 0.1499999 0.0000001 0.0
EndTime

3
10 10 3 1
1.0e-46 1.0e-46 9.098499e+05 0.3 30.0 0.0 0.0 1
-100
0 12.192 24.384 36.576 48.768 60.96 73.152 85.344 97.536 109.728 121.92
0 12.192 24.384 36.576 48.768 60.96 73.152 85.344 97.536 109.728 121.92
0 -4.572 -9.144 -13.716
86400 10 0.5 1 1
1565
1 0 0 1 1 2 1 0 1 0 3 1 0 1 1 4 1 0 1 0 5 1 0 1 1 6 1 0 1 0 7 1 0 1 1 8
1 0 1 0 9 1 0 1 1 10 1 0 1 0 11 1 0 1 1 12 1 0 1 0 13 1 0 1 1 14 1 0 1 0
15 1 0 1 1 16 1 0 1 0 17 1 0 1 1 18 1 0 1 0 19 1 0 1 1 20 1 0 1 0 21 0 0 1
1 22 0 0 1 0 23 1 0 1 0 24 1 0 1 0 25 1 0 1 0 26 1 0 1 0 27 1 0 1 0 28 1 0
1 0 29 1 0 1 0 30 1 0 1 0 31 1 0 1 0 32 0 0 1 0 33 0 0 1 1 34 1 0 1 0 35 1
0 1 1 36 1 0 1 0 37 1 0 1 1 38 1 0 1 0 39 1 0 1 1 40 1 0 1 0 41 1 0 1 1 42
1 0 1 0 43 1 0 1 1 44 1 0 1 0 45 1 0 1 1 46 1 0 1 0 47 1 0 1 1 48 1 0 1 0
49 1 0 1 1 50 1 0 1 0 51 1 0 1 1 52 1 0 1 0 53 0 0 1 1 54 0 0 1 0 55 1 0 1
0 56 1 0 1 0 57 1 0 1 0 58 1 0 1 0 59 1 0 1 0 60 1 0 1 0 61 1 0 1 0 62 1 0
1 0 63 1 0 1 0 64 0 0 1 0 65 0 0 1 1 66 1 0 1 0 67 1 0 1 1 68 1 0 1 0 69 1
0 1 1 70 1 0 1 0 71 1 0 1 1 72 1 0 1 0 73 1 0 1 1 74 1 0 1 0 75 1 0 1 1 76
1 0 1 0 77 1 0 1 1 78 1 0 1 0 79 1 0 1 1 80 1 0 1 0 81 1 0 1 1 82 1 0 1 0
83 1 0 1 1 84 1 0 1 0 85 0 0 1 1 86 0 0 1 0 87 1 0 1 0 88 1 0 1 0 89 1 0 1
0 90 1 0 1 0 91 1 0 1 0 92 1 0 1 0 93 1 0 1 0 94 1 0 1 0 95 1 0 1 0 96 0 0
1 0 97 0 0 0 1 98 0 0 0 0 99 0 0 0 1 100 0 0 0 0 101 0 0 0 1 102 0 0 0 0 103
0 0 0 1 104 0 0 0 0 105 0 0 0 1 106 0 0 0 0 107 0 0 0 1 108 0 0 0 0 109 0 0
0 1 110 0 0 0 0 111 0 0 0 1 112 0 0 0 0 113 0 0 0 1 114 0 0 0 0 115 0 0 0 1
116 0 0 0 0 117 0 0 0 1 118 0 1 1 0 119 1 1 1 0 120 1 1 1 0 121 1 1 1 0 122 1
1 1 0 123 1 1 1 0 124 1 1 1 0 125 1 1 1 0 126 1 1 1 0 127 1 1 1 0 128 0 1 1
0 129 0 1 1 0 130 1 1 1 0 131 1 1 1 0 132 1 1 1 0 133 1 1 1 0 134 1 1 1 0 135
1 1 1 0 136 1 1 1 0 137 1 1 1 0 138 1 1 1 0 139 0 1 1 0 140 0 1 1 0 141 1 1
1 0 142 1 1 1 0 143 1 1 1 0 144 1 1 1 0 145 1 1 1 0 146 1 1 1 0 147 1 1 1 0
148 1 1 1 0 149 1 1 1 0 150 0 1 1 0 151 0 0 0 0 152 0 0 0 0 153 0 0 0 0 154 0
0 0 0 155 0 0 0 0 156 0 0 0 0 157 0 0 0 0 158 0 0 0 0 159 0 0 0 0 160 0 0 0
0 161 0 0 0 0 162 0 1 1 1 163 1 1 1 0 164 1 1 1 1 165 1 1 1 0 166 1 1 1 1 167
1 1 1 0 168 1 1 1 1 169 1 1 1 0 170 1 1 1 1 171 1 1 1 0 172 1 1 1 1 173 1 1
1 0 174 1 1 1 1 175 1 1 1 0 176 1 1 1 1 177 1 1 1 0 178 1 1 1 1 179 1 1 1 0
180 1 1 1 1 181 1 1 1 0 182 0 1 1 1 183 0 1 1 0 184 1 1 1 0 185 1 1 1 0 186 1
1 1 0 187 1 1 1 0 188 1 1 1 0 189 1 1 1 0 190 1 1 1 0 191 1 1 1 0 192 1 1 1
0 193 0 1 1 0 194 0 1 1 1 195 1 1 1 0 197 1 1 1 0 199 1 1 1 0 201 1 1 1 0 203
1 1 1 0 205 1 1 1 0 207 1 1 1 0 209 1 1 1 0 211 1 1 1 0 213 1 1 1 0 214 0 1
1 1 215 0 1 1 0 216 1 1 1 0 217 1 1 1 0 218 1 1 1 0 219 1 1 1 0 220 1 1 1 0
221 1 1 1 0 222 1 1 1 0 223 1 1 1 0 224 1 1 1 0 225 0 1 1 0 226 0 1 1 1 227 1
1 1 0 229 1 1 1 0 231 1 1 1 0 233 1 1 1 0 235 1 1 1 0 237 1 1 1 0 239 1 1 1
0 241 1 1 1 0 243 1 1 1 0 245 1 1 1 0 246 0 1 1 1 247 0 1 1 0 248 1 1 1 0 249
1 1 1 0 250 1 1 1 0 251 1 1 1 0 252 1 1 1 0 253 1 1 1 0 254 1 1 1 0 255 1 1
1 0 256 1 1 1 0 257 0 1 1 0 258 0 0 0 1 259 0 0 0 0 260 0 0 0 1 261 0 0 0 0
262 0 0 0 1 263 0 0 0 0 264 0 0 0 1 265 0 0 0 0 266 0 0 0 1 267 0 0 0 0 268 0

0 0 1 269 0 0 0 0 270 0 0 0 1 271 0 0 0 0 272 0 0 0 1 273 0 0 0 0 274 0 0 0
1 275 0 0 0 0 276 0 0 0 1 277 0 0 0 0 278 0 0 0 1 279 0 1 1 0 280 1 1 1 0 281
1 1 1 0 282 1 1 1 0 283 1 1 1 0 284 1 1 1 0 285 1 1 1 0 286 1 1 1 0 287 1 1
1 0 288 1 1 1 0 289 0 1 1 0 290 0 1 1 0 291 1 1 1 0 292 1 1 1 0 293 1 1 1 0
294 1 1 1 0 295 1 1 1 0 296 1 1 1 0 297 1 1 1 0 298 1 1 1 0 299 1 1 1 0 300 0
1 1 0 301 0 1 1 0 302 1 1 1 0 303 1 1 1 0 304 1 1 1 0 305 1 1 1 0 306 1 1 1
0 307 1 1 1 0 308 1 1 1 0 309 1 1 1 0 310 1 1 1 0 311 0 1 1 0 312 0 0 0 0 313
0 0 0 0 314 0 0 0 0 315 0 0 0 0 316 0 0 0 0 317 0 0 0 0 318 0 0 0 0 319 0 0
0 0 320 0 0 0 0 321 0 0 0 0 322 0 0 0 0 323 0 1 1 1 324 1 1 1 0 325 1 1 1 1
326 1 1 1 0 327 1 1 1 1 328 1 1 1 0 329 1 1 1 1 330 1 1 1 0 331 1 1 1 1 332 1
1 1 0 333 1 1 1 1 334 1 1 1 0 335 1 1 1 1 336 1 1 1 0 337 1 1 1 1 338 1 1 1
0 339 1 1 1 1 340 1 1 1 0 341 1 1 1 1 342 1 1 1 0 343 0 1 1 1 344 0 1 1 0 345
1 1 1 0 346 1 1 1 0 347 1 1 1 0 348 1 1 1 0 349 1 1 1 0 350 1 1 1 0 351 1 1
1 0 352 1 1 1 0 353 1 1 1 0 354 0 1 1 0 355 0 1 1 1 356 1 1 1 0 358 1 1 1 0
360 1 1 1 0 362 1 1 1 0 364 1 1 1 0 366 1 1 1 0 368 1 1 1 0 370 1 1 1 0 372 1
1 1 0 374 1 1 1 0 375 0 1 1 1 376 0 1 1 0 377 1 1 1 0 378 1 1 1 0 379 1 1 1
0 380 1 1 1 0 381 1 1 1 0 382 1 1 1 0 383 1 1 1 0 384 1 1 1 0 385 1 1 1 0 386
0 1 1 0 387 0 1 1 1 388 1 1 1 0 390 1 1 1 0 392 1 1 1 0 394 1 1 1 0 396 1 1
1 0 398 1 1 1 0 400 1 1 1 0 402 1 1 1 0 404 1 1 1 0 406 1 1 1 0 407 0 1 1 1
408 0 1 1 0 409 1 1 1 0 410 1 1 1 0 411 1 1 1 0 412 1 1 1 0 413 1 1 1 0 414 1
1 1 0 415 1 1 1 0 416 1 1 1 0 417 1 1 1 0 418 0 1 1 0 419 0 0 0 1 420 0 0 0
0 421 0 0 0 1 422 0 0 0 0 423 0 0 0 1 424 0 0 0 0 425 0 0 0 1 426 0 0 0 0 427
0 0 0 1 428 0 0 0 0 429 0 0 0 1 430 0 0 0 0 431 0 0 0 1 432 0 0 0 0 433 0 0
0 1 434 0 0 0 0 435 0 0 0 1 436 0 0 0 0 437 0 0 0 1 438 0 0 0 0 439 0 0 0 1
440 0 1 1 0 441 1 1 1 0 442 1 1 1 0 443 1 1 1 0 444 1 1 1 0 445 1 1 1 0 446 1
1 1 0 447 1 1 1 0 448 1 1 1 0 449 1 1 1 0 450 0 1 1 0 451 0 1 1 0 452 1 1 1
0 453 1 1 1 0 454 1 1 1 0 455 1 1 1 0 456 1 1 1 0 457 1 1 1 0 458 1 1 1 0 459
1 1 1 0 460 1 1 1 0 461 0 1 1 0 462 0 1 1 0 463 1 1 1 0 464 1 1 1 0 465 1 1
1 0 466 1 1 1 0 467 1 1 1 0 468 1 1 1 0 469 1 1 1 0 470 1 1 1 0 471 1 1 1 0
472 0 1 1 0 473 0 0 0 0 474 0 0 0 0 475 0 0 0 0 476 0 0 0 0 477 0 0 0 0 478 0
0 0 0 479 0 0 0 0 480 0 0 0 0 481 0 0 0 0 482 0 0 0 0 483 0 0 0 0 484 0 1 1
1 485 1 1 1 0 486 1 1 1 1 487 1 1 1 0 488 1 1 1 1 489 1 1 1 0 490 1 1 1 1 491
1 1 1 0 492 1 1 1 1 493 1 1 1 0 494 1 1 1 1 495 1 1 1 0 496 1 1 1 1 497 1 1
1 0 498 1 1 1 1 499 1 1 1 0 500 1 1 1 1 501 1 1 1 0 502 1 1 1 1 503 1 1 1 0
504 0 1 1 1 505 0 1 1 0 506 1 1 1 0 507 1 1 1 0 508 1 1 1 0 509 1 1 1 0 510 1
1 1 0 511 1 1 1 0 512 1 1 1 0 513 1 1 1 0 514 1 1 1 0 515 0 1 1 0 516 0 1 1
1 517 1 1 1 0 519 1 1 1 0 521 1 1 1 0 523 1 1 1 0 525 1 1 1 0 527 1 1 1 0 529
1 1 1 0 531 1 1 1 0 533 1 1 1 0 535 1 1 1 0 536 0 1 1 1 537 0 1 1 0 538 1 1
1 0 539 1 1 1 0 540 1 1 1 0 541 1 1 1 0 542 1 1 1 0 543 1 1 1 0 544 1 1 1 0
545 1 1 1 0 546 1 1 1 0 547 0 1 1 0 548 0 1 1 1 549 1 1 1 0 551 1 1 1 0 553 1
1 1 0 555 1 1 1 0 557 1 1 1 0 559 1 1 1 0 561 1 1 1 0 563 1 1 1 0 565 1 1 1
0 567 1 1 1 0 568 0 1 1 1 569 0 1 1 0 570 1 1 1 0 571 1 1 1 0 572 1 1 1 0 573
1 1 1 0 574 1 1 1 0 575 1 1 1 0 576 1 1 1 0 577 1 1 1 0 578 1 1 1 0 579 0 1
1 0 580 0 0 0 0 1 581 0 0 0 0 582 0 0 0 0 1 583 0 0 0 0 584 0 0 0 0 1 585 0 0 0 0
586 0 0 0 0 1 587 0 0 0 0 588 0 0 0 0 1 589 0 0 0 0 590 0 0 0 0 1 591 0 0 0 0 592 0
0 0 1 593 0 0 0 0 594 0 0 0 0 1 595 0 0 0 0 596 0 0 0 0 1 597 0 0 0 0 0 598 0 0 0
1 599 0 0 0 0 0 600 0 0 0 0 1 601 0 1 1 0 602 1 1 1 0 603 1 1 1 0 604 1 1 1 0 605
1 1 1 0 606 1 1 1 0 607 1 1 1 0 608 1 1 1 0 609 1 1 1 0 610 1 1 1 0 611 0 1
1 0 612 0 1 1 0 613 1 1 1 0 614 1 1 1 0 615 1 1 1 0 616 1 1 1 0 617 1 1 1 0
618 1 1 1 0 619 1 1 1 0 620 1 1 1 0 621 1 1 1 0 622 0 1 1 0 623 0 1 1 0 624 1
1 1 0 625 1 1 1 0 626 1 1 1 0 627 1 1 1 0 628 1 1 1 0 629 1 1 1 0 630 1 1 1
0 631 1 1 1 0 632 1 1 1 0 633 0 1 1 0 634 0 0 0 0 635 0 0 0 0 636 0 0 0 0 637
0 0 0 0 638 0 0 0 0 639 0 0 0 0 640 0 0 0 0 641 0 0 0 0 642 0 0 0 0 643 0 0
0 0 644 0 0 0 0 645 0 1 1 1 646 1 1 1 0 647 1 1 1 1 648 1 1 1 0 649 1 1 1 1
650 1 1 1 0 651 1 1 1 1 652 1 1 1 0 653 1 1 1 1 654 1 1 1 0 655 1 1 1 1 656 1
1 1 0 657 1 1 1 1 658 1 1 1 0 659 1 1 1 1 660 1 1 1 0 661 1 1 1 1 662 1 1 1
0 663 1 1 1 1 664 1 1 1 0 665 0 1 1 1 666 0 1 1 0 667 1 1 1 0 668 1 1 1 0 669
1 1 1 0 670 1 1 1 0 671 1 1 1 0 672 1 1 1 0 673 1 1 1 0 674 1 1 1 0 675 1 1
1 0 676 0 1 1 0 677 0 1 1 1 678 1 1 1 0 680 1 1 1 0 682 1 1 1 0 684 1 1 1 0
686 1 1 1 0 688 1 1 1 0 690 1 1 1 0 692 1 1 1 0 694 1 1 1 0 696 1 1 1 0 697 0
1 1 1 698 0 1 1 0 699 1 1 1 0 700 1 1 1 0 701 1 1 1 0 702 1 1 1 0 703 1 1 1
0 704 1 1 1 0 705 1 1 1 0 706 1 1 1 0 707 1 1 1 0 708 0 1 1 0 709 0 1 1 1 710
1 1 1 0 712 1 1 1 0 714 1 1 1 0 716 1 1 1 0 718 1 1 1 0 720 1 1 1 0 722 1 1
1 0 724 1 1 1 0 726 1 1 1 0 728 1 1 1 0 729 0 1 1 1 730 0 1 1 0 731 1 1 1 0
732 1 1 1 0 733 1 1 1 0 734 1 1 1 0 735 1 1 1 0 736 1 1 1 0 737 1 1 1 0 738 1
1 1 0 739 1 1 1 0 740 0 1 1 0 741 0 0 0 1 742 0 0 0 0 743 0 0 0 1 744 0 0 0
0 745 0 0 0 1 746 0 0 0 0 747 0 0 0 1 748 0 0 0 0 749 0 0 0 1 750 0 0 0 0 751
0 0 0 1 752 0 0 0 0 753 0 0 0 1 754 0 0 0 0 755 0 0 0 1 756 0 0 0 0 757 0 0

0 1 758 0 0 0 0 759 0 0 0 1 760 0 0 0 0 761 0 0 0 1 762 0 1 1 0 763 1 1 1 0
764 1 1 1 0 765 1 1 1 0 766 1 1 1 0 767 1 1 1 0 768 1 1 1 0 769 1 1 1 0 770 1
1 1 0 771 1 1 1 0 772 0 1 1 0 773 0 1 1 0 774 1 1 1 0 775 1 1 1 0 776 1 1 1
0 777 1 1 1 0 778 1 1 1 0 779 1 1 1 0 780 1 1 1 0 781 1 1 1 0 782 1 1 1 0 783
0 1 1 0 784 0 1 1 0 785 1 1 1 0 786 1 1 1 0 787 1 1 1 0 788 1 1 1 0 789 1 1
1 0 790 1 1 1 0 791 1 1 1 0 792 1 1 1 0 793 1 1 1 0 794 0 1 1 0 795 0 0 0 0
796 0 0 0 0 797 0 0 0 0 798 0 0 0 0 799 0 0 0 0 800 0 0 0 0 801 0 0 0 0 802 0
0 0 0 803 0 0 0 0 804 0 0 0 0 805 0 0 0 0 806 0 1 1 1 807 1 1 1 0 808 1 1 1
1 809 1 1 1 0 810 1 1 1 1 811 1 1 1 0 812 1 1 1 1 813 1 1 1 0 814 1 1 1 1 815
1 1 1 0 816 1 1 1 1 817 1 1 1 0 818 1 1 1 1 819 1 1 1 0 820 1 1 1 1 821 1 1
1 0 822 1 1 1 1 823 1 1 1 0 824 1 1 1 1 825 1 1 1 0 826 0 1 1 1 827 0 1 1 0
828 1 1 1 0 829 1 1 1 0 830 1 1 1 0 831 1 1 1 0 832 1 1 1 0 833 1 1 1 0 834 1
1 1 0 835 1 1 1 0 836 1 1 1 0 837 0 1 1 0 838 0 1 1 1 839 1 1 1 0 841 1 1 1
0 843 1 1 1 0 845 1 1 1 0 847 1 1 1 0 849 1 1 1 0 851 1 1 1 0 853 1 1 1 0 855
1 1 1 0 857 1 1 1 0 858 0 1 1 1 859 0 1 1 0 860 1 1 1 0 861 1 1 1 0 862 1 1
1 0 863 1 1 1 0 864 1 1 1 0 865 1 1 1 0 866 1 1 1 0 867 1 1 1 0 868 1 1 1 0
869 0 1 1 0 870 0 1 1 1 871 1 1 1 0 873 1 1 1 0 875 1 1 1 0 877 1 1 1 0 879 1
1 1 0 881 1 1 1 0 883 1 1 1 0 885 1 1 1 0 887 1 1 1 0 889 1 1 1 0 890 0 1 1
1 891 0 1 1 0 892 1 1 1 0 893 1 1 1 0 894 1 1 1 0 895 1 1 1 0 896 1 1 1 0 897
1 1 1 0 898 1 1 1 0 899 1 1 1 0 900 1 1 1 0 901 0 1 1 0 902 0 0 0 1 903 0 0
0 0 904 0 0 0 1 905 0 0 0 0 906 0 0 0 1 907 0 0 0 0 908 0 0 0 1 909 0 0 0 0
910 0 0 0 1 911 0 0 0 0 912 0 0 0 1 913 0 0 0 0 914 0 0 0 1 915 0 0 0 0 916 0
0 0 1 917 0 0 0 0 918 0 0 0 1 919 0 0 0 0 920 0 0 0 1 921 0 0 0 0 922 0 0 0
1 923 0 1 1 0 924 1 1 1 0 925 1 1 1 0 926 1 1 1 0 927 1 1 1 0 928 1 1 1 0 929
1 1 1 0 930 1 1 1 0 931 1 1 1 0 932 1 1 1 0 933 0 1 1 0 934 0 1 1 0 935 1 1
1 0 936 1 1 1 0 937 1 1 1 0 938 1 1 1 0 939 1 1 1 0 940 1 1 1 0 941 1 1 1 0
942 1 1 1 0 943 1 1 1 0 944 0 1 1 0 945 0 1 1 0 946 1 1 1 0 947 1 1 1 0 948 1
1 1 0 949 1 1 1 0 950 1 1 1 0 951 1 1 1 0 952 1 1 1 0 953 1 1 1 0 954 1 1 1
0 955 0 1 1 0 956 0 0 0 0 957 0 0 0 0 958 0 0 0 0 959 0 0 0 0 960 0 0 0 0 961
0 0 0 0 962 0 0 0 0 963 0 0 0 0 964 0 0 0 0 965 0 0 0 0 966 0 0 0 0 967 0 1
1 1 968 1 1 1 0 969 1 1 1 1 970 1 1 1 0 971 1 1 1 1 972 1 1 1 0 973 1 1 1 1
974 1 1 1 0 975 1 1 1 1 976 1 1 1 0 977 1 1 1 1 978 1 1 1 0 979 1 1 1 1 980 1
1 1 0 981 1 1 1 1 982 1 1 1 0 983 1 1 1 1 984 1 1 1 0 985 1 1 1 1 986 1 1 1
0 987 0 1 1 1 988 0 1 1 0 989 1 1 1 0 990 1 1 1 0 991 1 1 1 0 992 1 1 1 0 993
1 1 1 0 994 1 1 1 0 995 1 1 1 0 996 1 1 1 0 997 1 1 1 0 998 0 1 1 0 999 0 1
1 1 1000 1 1 1 0 1002 1 1 1 0 1004 1 1 1 0 1006 1 1 1 0 1008 1 1 1 0 1010 1 1
1 0 1012 1 1 1 0 1014 1 1 1 0 1016 1 1 1 0 1018 1 1 1 0 1019 0 1 1 1 1020 0 1
1 0 1021 1 1 1 0 1022 1 1 1 0 1023 1 1 1 0 1024 1 1 1 0 1025 1 1 1 0 1026 1 1
1 0 1027 1 1 1 0 1028 1 1 1 0 1029 1 1 1 0 1030 0 1 1 0 1031 0 1 1 1 1032 1 1
1 0 1034 1 1 1 0 1036 1 1 1 0 1038 1 1 1 0 1040 1 1 1 0 1042 1 1 1 0 1044 1 1
1 0 1046 1 1 1 0 1048 1 1 1 0 1050 1 1 1 0 1051 0 1 1 1 1052 0 1 1 0 1053 1 1
1 0 1054 1 1 1 0 1055 1 1 1 0 1056 1 1 1 0 1057 1 1 1 0 1058 1 1 1 0 1059 1 1
1 0 1060 1 1 1 0 1061 1 1 1 0 1062 0 1 1 0 1063 0 0 0 1 1064 0 0 0 0 1065 0 0
0 1 1066 0 0 0 0 1067 0 0 0 1 1068 0 0 0 0 1069 0 0 0 1 1070 0 0 0 0 1071 0 0
0 1 1072 0 0 0 0 1073 0 0 0 1 1074 0 0 0 0 1075 0 0 0 1 1076 0 0 0 0 1077 0 0
0 1 1078 0 0 0 0 1079 0 0 0 1 1080 0 0 0 0 1081 0 0 0 1 1082 0 0 0 0 1083 0 0
0 1 1084 0 1 1 0 1085 1 1 1 0 1086 1 1 1 0 1087 1 1 1 0 1088 1 1 1 0 1089 1 1
1 0 1090 1 1 1 0 1091 1 1 1 0 1092 1 1 1 0 1093 1 1 1 0 1094 0 1 1 0 1095 0 1
1 0 1096 1 1 1 0 1097 1 1 1 0 1098 1 1 1 0 1099 1 1 1 0 1100 1 1 1 0 1101 1 1
1 0 1102 1 1 1 0 1103 1 1 1 0 1104 1 1 1 0 1105 0 1 1 0 1106 0 1 1 0 1107 1 1
1 0 1108 1 1 1 0 1109 1 1 1 0 1110 1 1 1 0 1111 1 1 1 0 1112 1 1 1 0 1113 1 1
1 0 1114 1 1 1 0 1115 1 1 1 0 1116 0 1 1 0 1117 0 0 0 0 1118 0 0 0 0 1119 0 0
0 0 1120 0 0 0 0 1121 0 0 0 0 1122 0 0 0 0 1123 0 0 0 0 1124 0 0 0 0 1125 0 0
0 0 1126 0 0 0 0 1127 0 0 0 0 1128 0 1 1 1 1129 1 1 1 0 1130 1 1 1 1 1131 1 1
1 0 1132 1 1 1 1 1133 1 1 1 0 1134 1 1 1 1 1135 1 1 1 0 1136 1 1 1 1 1137 1 1
1 0 1138 1 1 1 1 1139 1 1 1 0 1140 1 1 1 1 1141 1 1 1 0 1142 1 1 1 1 1143 1 1
1 0 1144 1 1 1 1 1145 1 1 1 0 1146 1 1 1 1 1147 1 1 1 0 1148 0 1 1 1 1149 0 1
1 0 1150 1 1 1 0 1151 1 1 1 0 1152 1 1 1 0 1153 1 1 1 0 1154 1 1 1 0 1155 1 1
1 0 1156 1 1 1 0 1157 1 1 1 0 1158 1 1 1 0 1159 0 1 1 0 1160 0 1 1 1 1161 1 1
1 0 1163 1 1 1 0 1165 1 1 1 0 1167 1 1 1 0 1169 1 1 1 0 1171 1 1 1 0 1173 1 1
1 0 1175 1 1 1 0 1177 1 1 1 0 1179 1 1 1 0 1180 0 1 1 1 1181 0 1 1 0 1182 1 1
1 0 1183 1 1 1 0 1184 1 1 1 0 1185 1 1 1 0 1186 1 1 1 0 1187 1 1 1 0 1188 1 1
1 0 1189 1 1 1 0 1190 1 1 1 0 1191 0 1 1 0 1192 0 1 1 1 1193 1 1 1 0 1195 1 1
1 0 1197 1 1 1 0 1199 1 1 1 0 1201 1 1 1 0 1203 1 1 1 0 1205 1 1 1 0 1207 1 1
1 0 1209 1 1 1 0 1211 1 1 1 0 1212 0 1 1 1 1213 0 1 1 0 1214 1 1 1 0 1215 1 1
1 0 1216 1 1 1 0 1217 1 1 1 0 1218 1 1 1 0 1219 1 1 1 0 1220 1 1 1 0 1221 1 1
1 0 1222 1 1 1 0 1223 0 1 1 0 1224 0 0 0 1 1225 0 0 0 0 1226 0 0 0 1 1227 0 0
0 0 1228 0 0 0 1 1229 0 0 0 0 1230 0 0 0 1 1231 0 0 0 0 1232 0 0 0 1 1233 0 0

0	0	1234	0	0	0	1	1235	0	0	0	0	1236	0	0	0	1	1237	0	0	0	0	1238	0	0	0	1	1239	0	0
0	0	1240	0	0	0	1	1241	0	0	0	0	1242	0	0	0	1	1243	0	0	0	0	1244	0	0	0	1	1245	0	1
1	0	1246	1	1	1	0	1247	1	1	1	0	1248	1	1	1	0	1249	1	1	1	0	1250	1	1	1	0	1251	1	1
1	0	1252	1	1	1	0	1253	1	1	1	0	1254	1	1	1	0	1255	0	1	1	0	1256	0	1	1	0	1257	1	1
1	0	1258	1	1	1	0	1259	1	1	1	0	1260	1	1	1	0	1261	1	1	1	0	1262	1	1	1	0	1263	1	1
1	0	1264	1	1	1	0	1265	1	1	1	0	1266	0	1	1	0	1267	0	1	1	0	1268	1	1	1	0	1269	1	1
1	0	1270	1	1	1	0	1271	1	1	1	0	1272	1	1	1	0	1273	1	1	1	0	1274	1	1	1	0	1275	1	1
1	0	1276	1	1	1	0	1277	0	1	1	0	1278	0	0	0	0	1279	0	0	0	0	1280	0	0	0	0	1281	0	0
0	0	1282	0	0	0	0	1283	0	0	0	0	1284	0	0	0	0	1285	0	0	0	0	1286	0	0	0	0	1287	0	0
0	0	1288	0	0	0	0	1289	0	1	1	1	1290	1	1	1	0	1291	1	1	1	1	1292	1	1	1	0	1293	1	1
1	1	1294	1	1	1	0	1295	1	1	1	1	1296	1	1	1	0	1297	1	1	1	1	1298	1	1	1	0	1299	1	1
1	1	1300	1	1	1	0	1301	1	1	1	1	1302	1	1	1	0	1303	1	1	1	1	1304	1	1	1	0	1305	1	1
1	1	1306	1	1	1	0	1307	1	1	1	1	1308	1	1	1	0	1309	0	1	1	1	1310	0	1	1	0	1311	1	1
1	0	1312	1	1	1	0	1313	1	1	1	0	1314	1	1	1	0	1315	1	1	1	0	1316	1	1	1	0	1317	1	1
1	0	1318	1	1	1	0	1319	1	1	1	0	1320	0	1	1	0	1321	0	1	1	1	1322	1	1	1	0	1324	1	1
1	0	1326	1	1	1	0	1328	1	1	1	0	1330	1	1	1	0	1332	1	1	1	0	1334	1	1	1	0	1336	1	1
1	0	1338	1	1	1	0	1340	1	1	1	0	1341	0	1	1	1	1342	0	1	1	0	1343	1	1	1	0	1344	1	1
1	0	1345	1	1	1	0	1346	1	1	1	0	1347	1	1	1	0	1348	1	1	1	0	1349	1	1	1	0	1350	1	1
1	0	1351	1	1	1	0	1352	0	1	1	0	1353	0	1	1	1	1354	1	1	1	0	1356	1	1	1	0	1358	1	1
1	0	1360	1	1	1	0	1362	1	1	1	0	1364	1	1	1	0	1366	1	1	1	0	1368	1	1	1	0	1370	1	1
1	0	1372	1	1	1	0	1373	0	1	1	1	1374	0	1	1	0	1375	1	1	1	0	1376	1	1	1	0	1377	1	1
1	0	1378	1	1	1	0	1379	1	1	1	0	1380	1	1	1	0	1381	1	1	1	0	1382	1	1	1	0	1383	1	1
1	0	1384	0	1	1	0	1385	0	0	0	1	1386	0	0	0	0	1387	0	0	0	1	1388	0	0	0	0	1389	0	0
0	1	1390	0	0	0	0	1391	0	0	0	1	1392	0	0	0	0	1393	0	0	0	1	1394	0	0	0	0	1395	0	0
0	1	1396	0	0	0	0	1397	0	0	0	1	1398	0	0	0	0	1399	0	0	0	1	1400	0	0	0	0	1401	0	0
0	1	1402	0	0	0	0	1403	0	0	0	1	1404	0	0	0	0	1405	0	0	0	1	1406	0	1	1	0	1407	1	1
1	0	1408	1	1	1	0	1409	1	1	1	0	1410	1	1	1	0	1411	1	1	1	0	1412	1	1	1	0	1413	1	1
1	0	1414	1	1	1	0	1415	1	1	1	0	1416	0	1	1	0	1417	0	1	1	0	1418	1	1	1	0	1419	1	1
1	0	1420	1	1	1	0	1421	1	1	1	0	1422	1	1	1	0	1423	1	1	1	0	1424	1	1	1	0	1425	1	1
1	0	1426	1	1	1	0	1427	0	1	1	0	1428	0	1	1	0	1429	1	1	1	0	1430	1	1	1	0	1431	1	1
1	0	1432	1	1	1	0	1433	1	1	1	0	1434	1	1	1	0	1435	1	1	1	0	1436	1	1	1	0	1437	1	1
1	0	1438	0	1	1	0	1439	0	0	0	0	1440	0	0	0	0	1441	0	0	0	0	1442	0	0	0	0	1443	0	0
0	0	1444	0	0	0	0	1445	0	0	0	0	1446	0	0	0	0	1447	0	0	0	0	1448	0	0	0	0	1449	0	0
0	0	1450	0	1	1	1	1451	1	1	1	0	1452	1	1	1	1	1453	1	1	1	0	1454	1	1	1	1	1455	1	1
1	0	1456	1	1	1	1	1457	1	1	1	0	1458	1	1	1	1	1459	1	1	1	0	1460	1	1	1	1	1461	1	1
1	0	1462	1	1	1	1	1463	1	1	1	0	1464	1	1	1	1	1465	1	1	1	0	1466	1	1	1	1	1467	1	1
1	0	1468	1	1	1	1	1469	1	1	1	0	1470	0	1	1	1	1471	0	1	1	0	1472	1	1	1	0	1473	1	1
1	0	1474	1	1	1	0	1475	1	1	1	0	1476	1	1	1	0	1477	1	1	1	0	1478	1	1	1	0	1479	1	1
1	0	1480	1	1	1	0	1481	0	1	1	0	1482	0	1	1	1	1483	1	1	1	0	1485	1	1	1	0	1487	1	1
1	0	1489	1	1	1	0	1491	1	1	1	0	1493	1	1	1	0	1495	1	1	1	0	1497	1	1	1	0	1499	1	1
1	0	1501	1	1	1	0	1502	0	1	1	1	1503	0	1	1	0	1504	1	1	1	0	1505	1	1	1	0	1506	1	1
1	0	1507	1	1	1	0	1508	1	1	1	0	1509	1	1	1	0	1510	1	1	1	0	1511	1	1	1	0	1512	1	1
1	0	1513	0	1	1	0	1514	0	1	1	1	1515	1	1	1	0	1517	1	1	1	0	1519	1	1	1	0	1521	1	1
1	0	1523	1	1	1	0	1525	1	1	1	0	1527	1	1	1	0	1529	1	1	1	0	1531	1	1	1	0	1533	1	1
1	0	1534	0	1	1	1	1535	0	1	1	0	1536	1	1	1	0	1537	1	1	1	0	1538	1	1	1	0	1539	1	1
1	0	1540	1	1	1	0	1541	1	1	1	0	1542	1	1	1	0	1543	1	1	1	0	1544	1	1	1	0	1545	0	1
1	0	1546	0	0	0	1	1547	0	0	0	0	1548	0	0	0	1	1549	0	0	0	0	1550	0	0	0	1	1551	0	0
0	0	1552	0	0	0	1	1553	0	0	0	0	1554	0	0	0	1	1555	0	0	0	0	1556	0	0	0	1	1557	0	0
0	0	1558	0	0	0	1	1559	0	0	0	0	1560	0	0	0	1	1561	0	0	0	0	1562	0	0	0	1	1563	0	0
0	0	1564	0	0	0	1	1565	0	0	0	0	1566	0	0	0	1	1567	0	1	1	0	1568	1	1	1	0	1569	1	1
1	0	1570	1	1	1	0	1571	1	1	1	0	1572	1	1	1	0	1573	1	1	1	0	1574	1	1	1	0	1575	1	1
1	0	1576	1	1	1	0	1577	0	1	1	0	1578	0	1	1	0	1579	1	1	1	0	1580	1	1	1	0	1581	1	1
1	0	1582	1	1	1	0	1583	1	1	1	0	1584	1	1	1	0	1585	1	1	1	0	1586	1	1	1	0	1587	1	1
1	0	1588	0	1	1	0	1589	0	1	1	0	1590	1	1	1	0	1591	1	1	1	0	1592	1	1	1	0	1593	1	1
1	0	1594	1	1	1	0	1595	1	1	1	0	1596	1	1	1	0	1597	1	1	1	0	1598	1	1	1	0	1599	0	1
1	0	1600	0	0	0	0	1601	0	0	0	0	1602	0	0	0	0	1603	0	0	0	0	1604	0	0	0	0	1605	0	0
0	0	1606	0	0	0	0	1607	0	0	0	0	1608	0	0	0	0	1609	0	0	0	0	1610	0	0	0	0	1611	0	0
1	1	1612	1	0	1	0	1613	1	0	1	1	1614	1	0	1	0	1615	1	0	1	1	1616	1	0	1	0	1617	1	0
1	1	1618	1	0	1	0	1619	1	0	1	1	1620	1	0	1	0	1621	1	0	1	1	1622	1	0	1	0	1623	1	0
1	1	1624	1	0	1	0	1625	1	0	1	1	1626	1	0	1	0	1627	1	0	1	1	1628	1	0	1	0	1629	1	0
1	1	1630	1	0	1	0	1631	0	0	1	1	1632	0	0	1	0	1633	1	0	1	0	1634	1	0	1	0	1635	1	0
1	0	1636	1	0	1	0	1637	1	0	1	0	1638	1	0	1	0	1639	1	0	1	0	1640	1	0	1	0	1641	1	0
1	0	1642	0	0	1	0	1643	0	0	1	1	1644	1	0	1	0	1645	1	0	1	1	1646	1	0	1	0	1647	1	0
1	1	1648	1	0	1	0	1649	1	0	1	1	1650	1	0	1	0	1651	1	0	1	1	1652	1	0	1	0	1653	1	0
1	1	1654	1	0	1	0	1655	1	0	1	1	1656	1	0	1	0	1657	1	0	1	1	1658	1	0	1	0	1659	1	0
1	1	1660	1	0	1	0	1661	1	0	1	1	1662	1	0	1	0	1663	0	0	1	1	1664	0	0	1	0	1665	1	0
1	0	1666	1	0	1	0	1667	1	0	1	0	1668	1	0	1	0	1669	1	0	1	0	1670	1	0	1	0	1671	1	0
1	0	1672	1	0	1	0	1673	1	0	1	0	1674	0	0	1	0	1675	0	0	1	1	1676	1	0	1	0	1677	1	0

1 1 1678 1 0 1 0 1679 1 0 1 1 1680 1 0 1 0 1681 1 0 1 1 1682 1 0 1 0 1683 1 0
1 1 1684 1 0 1 0 1685 1 0 1 1 1686 1 0 1 0 1687 1 0 1 1 1688 1 0 1 0 1689 1 0
1 1 1690 1 0 1 0 1691 1 0 1 1 1692 1 0 1 0 1693 1 0 1 1 1694 1 0 1 0 1695 0 0
1 1 1696 0 0 1 0 1697 1 0 1 0 1698 1 0 1 0 1699 1 0 1 0 1700 1 0 1 0 1701 1 0
1 0 1702 1 0 1 0 1703 1 0 1 0 1704 1 0 1 0 1705 1 0 1 0 1706 0 0 1 0 1707 0 0
0 1 1708 0 0 0 0 1709 0 0 0 1 1710 0 0 0 0 1711 0 0 0 1 1712 0 0 0 0 1713 0 0
0 1 1714 0 0 0 0 1715 0 0 0 1 1716 0 0 0 0 1717 0 0 0 1 1718 0 0 0 0 1719 0 0
0 1 1720 0 0 0 0 1721 0 0 0 1 1722 0 0 0 0 1723 0 0 0 1 1724 0 0 0 0 1725 0 0
0 1 1726 0 0 0 0 1727 0 0 0
169
1 0.0 0.0 19.35291 2 0.0 0.0 -77.4116 3 0.0 0.0 38.70582 4 0.0 0.0 -77.4116 5 0.0 0.0 19.35291
38 0.0 0.0 -77.4116 39 0.0 0.0 -154.823 40 0.0 0.0 -77.4116 53 0.0 0.0 38.70582 54 0.0 0.0 -154.823 55
0.0 0.0 77.41164 56 0.0 0.0 -154.823 57 0.0 0.0 38.70582 90 0.0 0.0 -77.4116 91 0.0 0.0 -154.823 92
0.0 0.0 -77.4116 105 0.0 0.0 38.70582 106 0.0 0.0 -154.823 107 0.0 0.0 77.41164 108 0.0 0.0 -
154.823 109 0.0 0.0 38.70582 142 0.0 0.0 -77.4116 143 0.0 0.0 -154.823 144 0.0 0.0 -77.4116 157
0.0 0.0 38.70582 158 0.0 0.0 -154.823 159 0.0 0.0 77.41164 160 0.0 0.0 -154.823 161 0.0 0.0
38.70582 194 0.0 0.0 -77.4116 195 0.0 0.0 -154.823 196 0.0 0.0 -77.4116 209 0.0 0.0 38.70582 210
0.0 0.0 -154.823 211 0.0 0.0 77.41164 212 0.0 0.0 -154.823 213 0.0 0.0 38.70582 246 0.0 0.0 -
77.4116 247 0.0 0.0 -154.823 248 0.0 0.0 -77.4116 261 0.0 0.0 38.70582 262 0.0 0.0 -154.823 263
0.0 0.0 77.41164 264 0.0 0.0 -154.823 265 0.0 0.0 38.70582 298 0.0 0.0 -77.4116 299 0.0 0.0 -
154.823 300 0.0 0.0 -77.4116 313 0.0 0.0 38.70582 314 0.0 0.0 -154.823 315 0.0 0.0 77.41164 316
0.0 0.0 -154.823 317 0.0 0.0 38.70582 350 0.0 0.0 -77.4116 351 0.0 0.0 -154.823 352 0.0 0.0 -77.4116
365 0.0 0.0 38.70582 366 0.0 0.0 -154.823 367 0.0 0.0 77.41164 368 0.0 0.0 -154.823 369 0.0 0.0
38.70582 402 0.0 0.0 -77.4116 403 0.0 0.0 -154.823 404 0.0 0.0 -77.4116 417 0.0 0.0 19.35291 418
0.0 0.0 -77.4116 419 0.0 0.0 38.70582 420 0.0 0.0 -77.4116 421 0.0 0.0 19.35291
0.001 250
3
0.0 0.0 1 0.0 8640000 0.0

TITLE(2)="3-D SIX COMPONENT GAS INJECTION"

DESCRIPTION()=
"THICKNESS (FT) : 100"
"LENGTH (FT) : 560"
"WIDTH (FT) : 560"
"GRID BLOCKS : 7x7x3"

COMPOSITIONAL_MODEL
$DEBUGS

TIMEEND = 3650

$ I/O OPTIONS

OUTLEVEL = 1
PROCOUT
OUTPUT_PRE
OUTPUT_SAT
OUTPUT_OIL
OUTPUT_GAS
OUTPUT_WEL
OUTPUT_HIS
WELLFILE = "6COMP.WEL"

HISDATA_NUM = 100
OUTPUT_TIME() = 100 1000 2000 3000 3650
$NO_CRASH

$OUTPUT FREQUENCY
ISTEP(,,)=1
JSTEP(,,)=1
KSTEP(,,)=1

$ FAULT BLOCK AND MESH DATA
METHOD = 2

```
DOWN() = 0 0 1
NX(1) = 7    NY(1) = 7    NZ(1) = 3
MES = "cart"
DX() = 80    DY() = 80    DZ() = 20 30 50

$ COMPOUND NAMES
COMPOUND(1) = "C1"          COMPOUND(2) = "C3"
COMPOUND(3) = "C6"          COMPOUND(4) = "C10"
COMPOUND(5) = "C15"         COMPOUND(6) = "C20"

$ COMPOUND CRITICAL TEMPERATURES
CRIT()    343.0 665.7 913.4 1111.8 1270.0 1380.0

$ COMPOUND CRITICAL PRESSURES
CRIP()    667.8 616.3 436.9 304.0 200.0 162.0

$ COMPOUND CRITICAL VOLUMES
CRIV()    1.599 3.211 5.923 10.087 16.696 21.484

$ COMPOUND ACEN
ACEN()    0.013 0.152 0.301 0.488 0.650 0.850

$ COMPOUND MOL WEIGHTS
MOLW()    16.0 44.1 86.2 142.3 206.0 282.0

$ COMPOUND PARA
PARA()    71.00 151.0 271.0 431.0 631.0 831.0

$ BINARY INTERACTION COEFFICIENTS
BINC(,) = 0.0      0.0      0.0    0.0    0.05    0.05
                  0.0      0.0      0.0    0.0    0.005 0.005
                  0.0      0.0      0.0    0.0    0.0      0.0
                  0.0      0.0      0.0    0.0    0.0      0.0
                  0.05     0.005 0.0    0.0    0.0      0.0
                  0.05     0.005 0.0    0.0    0.0      0.0

$ MAX NUMBER OF PHASES
NPHASE = 3

$ MAXNEWT MAX NUMBER OF NEWTON ITERATION
MAXNEWT = 20

$ Initial rock & water properties
ROCKZ = 0.000001    ROCKP = 1500
H2OZ = 0.000003    H2OP = 14.696    H2OD = 3.468
SURTF = 60.0    SURPS = 14.696
RESTF = 160.0

$ TOLERANCE
CVGOPT = 2
TOL_FLASH = 0.0001
TOL_VOLUME = 0.0001
TOL_MASS = 0.0001
TOL_WATER = 0.0001

$ POROSITY
POROSITY1() = 0.35

$ PERMEABILITIES
XPERM1() = 10
YPERM1() = 10
ZPERM1() = 10
XYPERM1() = 0
XZPERM1() = 0
YZPERM1() = 0

$ INITIAL WATER SATURATION
SWINI1() = 0.17
```

```
$ INITIAL WATER CELL PRESSURE
PINI1() = 1500.0

$ INITIAL PHASE VISCOSITIES AT EACH CELL
VIS1() = 1.0

$ INITIAL COMPOSITIONS
ZXY1(,,,1) = .5
ZXY1(,,,2) = .03
ZXY1(,,,3) = .07
ZXY1(,,,4) = .2
ZXY1(,,,5) = .15
ZXY1(,,,6) = .05

$ RELPERM DATA
$ RELP 1 for table lookup, 2 for function based

RELP 2
$MODREL(1) = 3

$ NRELFUN 1 for corey, more to be added later
NRELFUN    1
$ data for each phase : water, phase 2 and phase 3
ENDPT() = 0.4 0.9 0.9
SR() = 0.3 0.1 0.0
EXPN() = 3.0 2.0 2.0


$--B feng pan 11/23/2006    -------- GEOMECHanics options
GEOMG =    70
GEOM2D    = 98
PCOUP = 1
THF = 0
GMCL=0
TOLA=0.0000000001
LIMA=200
TOLB=0.0000000000000001
LIMB=1000
$--E feng pan 11/23/2006    -------- GEOMECHanics options

$ ============== WELL SPECIFICATIONS ==============

NUMWELL = 2

$ --- The first well ---
WELLNAME(1) = "INJECTOR 1"
KINDWELL(1) = 2
WELLTOP(1 TO 3,1,1) = 40 40 0
WELLBOTTOM(1 TO 3,1,1) = 40 40 100
DIAMETER(1,1) = 1.0
PRLIMIT(1) = 14695
WELLPQ(1) Block
   Interpolation Linear
   Extrapolation Constant
   Data    0.          1000.
EndBlock

$ --- The 2nd well ---
WELLNAME(2) = "PRODUCER 1"
KINDWELL(2) = 3
WELLTOP(1 TO 3,1,2) = 520 520 0
WELLBOTTOM(1 TO 3,1,2) = 520 520 100
DIAMETER(1,2) = 1.0
WELLPQ(2) Block
   Interpolation Linear
   Extrapolation Constant
   Data    0.      1300.
```

EndBlock

EndInitial

$ TRANSIENT DATA INPUT BLOCKS
BeginTime 0.0
TIME_CONTROL = 2
DELTIM = 1 DTIMMUL = 1.0 DTIMMAX = 30 DTIMMIN = 0.1
TUNE = 0.5 DCMAX = 0.5 DAQCMAX = 0.5 DPMAX = 0.5 DSMAX = 0.5
WZ() 0.77 0.20 0.01 0.01 0.005 0.005 0.0
EndTime

3
7 7 3 1
1.0e-46 1.0e-46 8.098499e+04 0.3 30.0 0.0 0.0 1
-100
0 24.384 48.768 73.152 97.536 121.92 146.304 170.688
0 24.384 48.768 73.152 97.536 121.92 146.304 170.688
0 -6.096 -15.24 -30.48
86400 10 0.5 1 1
824
1 0 0 1 1 2 1 0 1 0 3 1 0 1 1 4 1 0 1 0 5 1 0 1 1 6 1 0 1 0 7 1 0 1 1 8
1 0 1 0 9 1 0 1 1 10 1 0 1 0 11 1 0 1 1 12 1 0 1 0 13 1 0 1 1 14 1 0 1 0
15 0 0 1 1 16 0 0 1 0 17 1 0 1 0 18 1 0 1 0 19 1 0 1 0 20 1 0 1 0 21 1 0 1
0 22 1 0 1 0 23 0 0 1 0 24 0 0 1 1 25 1 0 1 0 26 1 0 1 1 27 1 0 1 0 28 1 0
1 1 29 1 0 1 0 30 1 0 1 1 31 1 0 1 0 32 1 0 1 1 33 1 0 1 0 34 1 0 1 1 35 1
0 1 0 36 1 0 1 1 37 1 0 1 0 38 0 0 1 1 39 0 0 1 0 40 1 0 1 0 41 1 0 1 0 42
1 0 1 0 43 1 0 1 0 44 1 0 1 0 45 1 0 1 0 46 0 0 1 0 47 0 0 1 1 48 1 0 1 0
49 1 0 1 1 50 1 0 1 0 51 1 0 1 1 52 1 0 1 0 53 1 0 1 1 54 1 0 1 0 55 1 0 1
1 56 1 0 1 0 57 1 0 1 1 58 1 0 1 0 59 1 0 1 1 60 1 0 1 0 61 0 0 1 1 62 0 0
1 0 63 1 0 1 0 64 1 0 1 0 65 1 0 1 0 66 1 0 1 0 67 1 0 1 0 68 1 0 1 0 69 0
0 1 0 70 0 0 0 1 71 0 0 0 0 72 0 0 0 1 73 0 0 0 0 74 0 0 0 1 75 0 0 0 0 76
0 0 0 1 77 0 0 0 0 78 0 0 0 1 79 0 0 0 0 80 0 0 0 1 81 0 0 0 0 82 0 0 0 1
83 0 0 0 0 84 0 0 0 1 85 0 1 1 0 86 1 1 1 0 87 1 1 1 0 88 1 1 1 0 89 1 1 1
0 90 1 1 1 0 91 1 1 1 0 92 0 1 1 0 93 0 1 1 0 94 1 1 1 0 95 1 1 1 0 96 1 1
1 0 97 1 1 1 0 98 1 1 1 0 99 1 1 1 0 100 0 1 1 0 101 0 1 1 0 102 1 1 1 0 103
1 1 1 0 104 1 1 1 0 105 1 1 1 0 106 1 1 1 0 107 1 1 1 0 108 0 1 1 0 109 0 0
0 0 110 0 0 0 0 0 111 0 0 0 0 112 0 0 0 0 113 0 0 0 0 114 0 0 0 0 115 0 0 0 0
116 0 0 0 0 117 0 1 1 1 118 1 1 1 0 119 1 1 1 1 120 1 1 1 0 121 1 1 1 1 122 1
1 1 0 123 1 1 1 1 124 1 1 1 0 125 1 1 1 1 126 1 1 1 0 127 1 1 1 1 128 1 1 1
0 129 1 1 1 1 130 1 1 1 0 131 0 1 1 1 132 0 1 1 0 133 1 1 1 0 134 1 1 1 0 135
1 1 1 0 136 1 1 1 0 137 1 1 1 0 138 1 1 1 0 139 0 1 1 0 140 0 1 1 1 141 1 1
1 0 143 1 1 1 0 145 1 1 1 0 147 1 1 1 0 149 1 1 1 0 151 1 1 1 0 153 1 1 1 0
154 0 1 1 1 155 0 1 1 0 156 1 1 1 0 157 1 1 1 0 158 1 1 1 0 159 1 1 1 0 160 1
1 1 0 161 1 1 1 0 162 0 1 1 0 163 0 1 1 1 164 1 1 1 0 166 1 1 1 0 168 1 1 1
0 170 1 1 1 0 172 1 1 1 0 174 1 1 1 0 176 1 1 1 0 177 0 1 1 1 178 0 1 1 0 179
1 1 1 0 180 1 1 1 0 181 1 1 1 0 182 1 1 1 0 183 1 1 1 0 184 1 1 1 0 185 0 1
1 0 186 0 0 0 1 187 0 0 0 0 188 0 0 0 1 189 0 0 0 0 190 0 0 0 1 191 0 0 0 0
192 0 0 0 1 193 0 0 0 0 194 0 0 0 1 195 0 0 0 0 196 0 0 0 1 197 0 0 0 0 198 0
0 0 1 199 0 0 0 0 200 0 0 0 1 201 0 1 1 0 202 1 1 1 0 203 1 1 1 0 204 1 1 1
0 205 1 1 1 0 206 1 1 1 0 207 1 1 1 0 208 0 1 1 0 209 0 1 1 0 210 1 1 1 0 211
1 1 1 0 212 1 1 1 0 213 1 1 1 0 214 1 1 1 0 215 1 1 1 0 216 0 1 1 0 217 0 1
1 0 218 1 1 1 0 219 1 1 1 0 220 1 1 1 0 221 1 1 1 0 222 1 1 1 0 223 1 1 1 0
224 0 1 1 0 225 0 0 0 0 226 0 0 0 0 227 0 0 0 0 228 0 0 0 0 229 0 0 0 0 230 0
0 0 0 231 0 0 0 0 232 0 0 0 0 233 0 1 1 1 234 1 1 1 0 235 1 1 1 1 236 1 1 1
0 237 1 1 1 1 238 1 1 1 0 239 1 1 1 1 240 1 1 1 0 241 1 1 1 1 242 1 1 1 0 243
1 1 1 1 244 1 1 1 0 245 1 1 1 1 246 1 1 1 0 247 0 1 1 1 248 0 1 1 0 249 1 1
1 0 250 1 1 1 0 251 1 1 1 0 252 1 1 1 0 253 1 1 1 0 254 1 1 1 0 255 0 1 1 0
256 0 1 1 1 257 1 1 1 0 259 1 1 1 0 261 1 1 1 0 263 1 1 1 0 265 1 1 1 0 267 1
1 1 0 269 1 1 1 0 270 0 1 1 1 271 0 1 1 0 272 1 1 1 0 273 1 1 1 0 274 1 1 1
0 275 1 1 1 0 276 1 1 1 0 277 1 1 1 0 278 0 1 1 0 279 0 1 1 1 280 1 1 1 0 282
1 1 1 0 284 1 1 1 0 286 1 1 1 0 288 1 1 1 0 290 1 1 1 0 292 1 1 1 0 293 0 1
1 1 294 0 1 1 0 295 1 1 1 0 296 1 1 1 0 297 1 1 1 0 298 1 1 1 0 299 1 1 1 0
300 1 1 1 0 301 0 1 1 0 302 0 0 0 1 303 0 0 0 0 304 0 0 0 1 305 0 0 0 0 306 0
0 0 1 307 0 0 0 0 308 0 0 0 1 309 0 0 0 0 310 0 0 0 1 311 0 0 0 0 312 0 0 0
1 313 0 0 0 0 314 0 0 0 1 315 0 0 0 0 316 0 0 0 1 317 0 1 1 0 318 1 1 1 0 319
1 1 1 0 320 1 1 1 0 321 1 1 1 0 322 1 1 1 0 323 1 1 1 0 324 0 1 1 0 325 0 1
1 0 326 1 1 1 0 327 1 1 1 0 328 1 1 1 0 329 1 1 1 0 330 1 1 1 0 331 1 1 1 0

332 0 1 1 0 333 0 1 1 0 334 1 1 1 0 335 1 1 1 0 336 1 1 1 0 337 1 1 1 0 338 1
1 1 0 339 1 1 1 0 340 0 1 1 0 341 0 0 0 0 342 0 0 0 0 343 0 0 0 0 344 0 0 0
0 345 0 0 0 0 346 0 0 0 0 347 0 0 0 0 348 0 0 0 0 349 0 1 1 1 350 1 1 1 0 351
1 1 1 1 352 1 1 1 0 353 1 1 1 1 354 1 1 1 0 355 1 1 1 1 356 1 1 1 0 357 1 1
1 1 358 1 1 1 0 359 1 1 1 1 360 1 1 1 0 361 1 1 1 1 362 1 1 1 0 363 0 1 1 1
364 0 1 1 0 365 1 1 1 0 366 1 1 1 0 367 1 1 1 0 368 1 1 1 0 369 1 1 1 0 370 1
1 1 0 371 0 1 1 0 372 0 1 1 1 373 1 1 1 0 375 1 1 1 0 377 1 1 1 0 379 1 1 1
0 381 1 1 1 0 383 1 1 1 0 385 1 1 1 0 386 0 1 1 1 387 0 1 1 0 388 1 1 1 0 389
1 1 1 0 390 1 1 1 0 391 1 1 1 0 392 1 1 1 0 393 1 1 1 0 394 0 1 1 0 395 0 1
1 1 396 1 1 1 0 398 1 1 1 0 400 1 1 1 0 402 1 1 1 0 404 1 1 1 0 406 1 1 1 0
408 1 1 1 0 409 0 1 1 1 410 0 1 1 0 411 1 1 1 0 412 1 1 1 0 413 1 1 1 0 414 1
1 1 0 415 1 1 1 0 416 1 1 1 0 417 0 1 1 0 418 0 0 0 1 419 0 0 0 0 420 0 0 0
1 421 0 0 0 0 422 0 0 0 1 423 0 0 0 0 424 0 0 0 1 425 0 0 0 0 426 0 0 0 1 427
0 0 0 0 428 0 0 0 1 429 0 0 0 0 430 0 0 0 1 431 0 0 0 0 432 0 0 0 1 433 0 1
1 0 434 1 1 1 0 435 1 1 1 0 436 1 1 1 0 437 1 1 1 0 438 1 1 1 0 439 1 1 1 0
440 0 1 1 0 441 0 1 1 0 442 1 1 1 0 443 1 1 1 0 444 1 1 1 0 445 1 1 1 0 446 1
1 1 0 447 1 1 1 0 448 0 1 1 0 449 0 1 1 0 450 1 1 1 0 451 1 1 1 0 452 1 1 1
0 453 1 1 1 0 454 1 1 1 0 455 1 1 1 0 456 0 1 1 0 457 0 0 0 0 458 0 0 0 0 459
0 0 0 0 460 0 0 0 0 461 0 0 0 0 462 0 0 0 0 463 0 0 0 0 464 0 0 0 0 465 0 1
1 1 466 1 1 1 0 467 1 1 1 1 468 1 1 1 0 469 1 1 1 1 470 1 1 1 0 471 1 1 1 1
472 1 1 1 0 473 1 1 1 1 474 1 1 1 0 475 1 1 1 1 476 1 1 1 0 477 1 1 1 1 478 1
1 1 0 479 0 1 1 1 480 0 1 1 0 481 1 1 1 0 482 1 1 1 0 483 1 1 1 0 484 1 1 1
0 485 1 1 1 0 486 1 1 1 0 487 0 1 1 0 488 0 1 1 1 489 1 1 1 0 491 1 1 1 0 493
1 1 1 0 495 1 1 1 0 497 1 1 1 0 499 1 1 1 0 501 1 1 1 0 502 0 1 1 1 503 0 1
1 0 504 1 1 1 0 505 1 1 1 0 506 1 1 1 0 507 1 1 1 0 508 1 1 1 0 509 1 1 1 0
510 0 1 1 0 511 0 1 1 1 512 1 1 1 0 514 1 1 1 0 516 1 1 1 0 518 1 1 1 0 520 1
1 1 0 522 1 1 1 0 524 1 1 1 0 525 0 1 1 1 526 0 1 1 0 527 1 1 1 0 528 1 1 1
0 529 1 1 1 0 530 1 1 1 0 531 1 1 1 0 532 1 1 1 0 533 0 1 1 0 534 0 0 0 1 535
0 0 0 0 536 0 0 0 1 537 0 0 0 0 538 0 0 0 1 539 0 0 0 0 540 0 0 0 1 541 0 0
0 0 542 0 0 0 1 543 0 0 0 0 544 0 0 0 1 545 0 0 0 0 546 0 0 0 1 547 0 0 0 0
548 0 0 0 1 549 0 1 1 0 550 1 1 1 0 551 1 1 1 0 552 1 1 1 0 553 1 1 1 0 554 1
1 1 0 555 1 1 1 0 556 0 1 1 0 557 0 1 1 0 558 1 1 1 0 559 1 1 1 0 560 1 1 1
0 561 1 1 1 0 562 1 1 1 0 563 1 1 1 0 564 0 1 1 0 565 0 1 1 0 566 1 1 1 0 567
1 1 1 0 568 1 1 1 0 569 1 1 1 0 570 1 1 1 0 571 1 1 1 0 572 0 1 1 0 573 0 0
0 0 574 0 0 0 0 575 0 0 0 0 576 0 0 0 0 577 0 0 0 0 578 0 0 0 0 579 0 0 0 0
580 0 0 0 0 581 0 1 1 1 582 1 1 1 0 583 1 1 1 1 584 1 1 1 0 585 1 1 1 1 586 1
1 1 0 587 1 1 1 1 588 1 1 1 0 589 1 1 1 1 590 1 1 1 0 591 1 1 1 1 592 1 1 1
0 593 1 1 1 1 594 1 1 1 0 595 0 1 1 1 596 0 1 1 0 597 1 1 1 0 598 1 1 1 0 599
1 1 1 0 600 1 1 1 0 601 1 1 1 0 602 1 1 1 0 603 0 1 1 0 604 0 1 1 1 605 1 1
1 0 607 1 1 1 0 609 1 1 1 0 611 1 1 1 0 613 1 1 1 0 615 1 1 1 0 617 1 1 1 0
618 0 1 1 1 619 0 1 1 0 620 1 1 1 0 621 1 1 1 0 622 1 1 1 0 623 1 1 1 0 624 1
1 1 0 625 1 1 1 0 626 0 1 1 0 627 0 1 1 1 628 1 1 1 0 630 1 1 1 0 632 1 1 1
0 634 1 1 1 0 636 1 1 1 0 638 1 1 1 0 640 1 1 1 0 641 0 1 1 1 642 0 1 1 0 643
1 1 1 0 644 1 1 1 0 645 1 1 1 0 646 1 1 1 0 647 1 1 1 0 648 1 1 1 0 649 0 1
1 0 650 0 0 0 1 651 0 0 0 0 652 0 0 0 1 653 0 0 0 0 654 0 0 0 1 655 0 0 0 0
656 0 0 0 1 657 0 0 0 0 658 0 0 0 1 659 0 0 0 0 660 0 0 0 1 661 0 0 0 0 662 0
0 0 1 663 0 0 0 0 664 0 0 0 1 665 0 1 1 0 666 1 1 1 0 667 1 1 1 0 668 1 1 1
0 669 1 1 1 0 670 1 1 1 0 671 1 1 1 0 672 0 1 1 0 673 0 1 1 0 674 1 1 1 0 675
1 1 1 0 676 1 1 1 0 677 1 1 1 0 678 1 1 1 0 679 1 1 1 0 680 0 1 1 0 681 0 1
1 0 682 1 1 1 0 683 1 1 1 0 684 1 1 1 0 685 1 1 1 0 686 1 1 1 0 687 1 1 1 0
688 0 1 1 0 689 0 0 0 0 690 0 0 0 0 691 0 0 0 0 692 0 0 0 0 693 0 0 0 0 694 0
0 0 0 695 0 0 0 0 696 0 0 0 0 697 0 1 1 1 698 1 1 1 0 699 1 1 1 1 700 1 1 1
0 701 1 1 1 1 702 1 1 1 0 703 1 1 1 1 704 1 1 1 0 705 1 1 1 1 706 1 1 1 0 707
1 1 1 1 708 1 1 1 0 709 1 1 1 1 710 1 1 1 0 711 0 1 1 1 712 0 1 1 0 713 1 1
1 0 714 1 1 1 0 715 1 1 1 0 716 1 1 1 0 717 1 1 1 0 718 1 1 1 0 719 0 1 1 0
720 0 1 1 1 721 1 1 1 0 723 1 1 1 0 725 1 1 1 0 727 1 1 1 0 729 1 1 1 0 731 1
1 1 0 733 1 1 1 0 734 0 1 1 1 735 0 1 1 0 736 1 1 1 0 737 1 1 1 0 738 1 1 1
0 739 1 1 1 0 740 1 1 1 0 741 1 1 1 0 742 0 1 1 0 743 0 1 1 1 744 1 1 1 0 746
1 1 1 0 748 1 1 1 0 750 1 1 1 0 752 1 1 1 0 754 1 1 1 0 756 1 1 1 0 757 0 1
1 1 758 0 1 1 0 759 1 1 1 0 760 1 1 1 0 761 1 1 1 0 762 1 1 1 0 763 1 1 1 0
764 1 1 1 0 765 0 1 1 0 766 0 0 0 1 767 0 0 0 0 768 0 0 0 1 769 0 0 0 0 770 0
0 0 1 771 0 0 0 0 772 0 0 0 1 773 0 0 0 0 774 0 0 0 1 775 0 0 0 0 776 0 0 0
1 777 0 0 0 0 778 0 0 0 1 779 0 0 0 0 780 0 0 0 1 781 0 1 1 0 782 1 1 1 0 783
1 1 1 0 784 1 1 1 0 785 1 1 1 0 786 1 1 1 0 787 1 1 1 0 788 0 1 1 0 789 0 1
1 0 790 1 1 1 0 791 1 1 1 0 792 1 1 1 0 793 1 1 1 0 794 1 1 1 0 795 1 1 1 0
796 0 1 1 0 797 0 1 1 0 798 1 1 1 0 799 1 1 1 0 800 1 1 1 0 801 1 1 1 0 802 1
1 1 0 803 1 1 1 0 804 0 1 1 0 805 0 0 0 0 806 0 0 0 0 807 0 0 0 0 808 0 0 0
0 809 0 0 0 0 810 0 0 0 0 811 0 0 0 0 812 0 0 0 0 813 0 0 1 1 814 1 0 1 0 815

1 0 1 1 816 1 0 1 0 817 1 0 1 1 818 1 0 1 0 819 1 0 1 1 820 1 0 1 0 821 1 0
1 1 822 1 0 1 0 823 1 0 1 1 824 1 0 1 0 825 1 0 1 1 826 1 0 1 0 827 0 0 1 1
828 0 0 1 0 829 1 0 1 0 830 1 0 1 0 831 1 0 1 0 832 1 0 1 0 833 1 0 1 0 834 1
0 1 0 835 0 0 1 0 836 0 0 1 1 837 1 0 1 0 838 1 0 1 1 839 1 0 1 0 840 1 0 1
1 841 1 0 1 0 842 1 0 1 1 843 1 0 1 0 844 1 0 1 1 845 1 0 1 0 846 1 0 1 1 847
1 0 1 0 848 1 0 1 1 849 1 0 1 0 850 0 0 1 1 851 0 0 1 0 852 1 0 1 0 853 1 0
1 0 854 1 0 1 0 855 1 0 1 0 856 1 0 1 0 857 1 0 1 0 858 0 0 1 0 859 0 0 1 1
860 1 0 1 0 861 1 0 1 1 862 1 0 1 0 863 1 0 1 1 864 1 0 1 0 865 1 0 1 1 866 1
0 1 0 867 1 0 1 1 868 1 0 1 0 869 1 0 1 1 870 1 0 1 0 871 1 0 1 1 872 1 0 1
0 873 0 0 1 1 874 0 0 1 0 875 1 0 1 0 876 1 0 1 0 877 1 0 1 0 878 1 0 1 0 879
1 0 1 0 880 1 0 1 0 881 0 0 1 0 882 0 0 0 1 883 0 0 0 0 884 0 0 0 1 885 0 0
0 0 886 0 0 0 1 887 0 0 0 0 888 0 0 0 1 889 0 0 0 0 890 0 0 0 1 891 0 0 0 0
892 0 0 0 1 893 0 0 0 0 894 0 0 0 1 895 0 0 0 0 896 0 0 0 1
69
1 0.0 0.0 19.35291 2 0.0 0.0 -77.4116 3 0.0 0.0 38.70582 4 0.0 0.0 -77.4116 5 0.0 0.0
19.35291 38 0.0 0.0 -77.4116 39 0.0 0.0 -154.823 40 0.0 0.0 -77.4116 53 0.0 0.0 38.70582 54 0.0 0.0
-154.823 55 0.0 0.0 77.41164 56 0.0 0.0 -154.823 57 0.0 0.0 38.70582 90 0.0 0.0 -77.4116 91 0.0 0.0
-154.823 92 0.0 0.0 -77.4116 105 0.0 0.0 38.70582 106 0.0 0.0 -154.823 107 0.0 0.0 77.41164 108
0.0 0.0 -154.823 109 0.0 0.0 38.70582 142 0.0 0.0 -77.4116 143 0.0 0.0 -154.823 144 0.0 0.0 -77.4116
157 0.0 0.0 38.70582 158 0.0 0.0 -154.823 159 0.0 0.0 77.41164 160 0.0 0.0 -154.823 161 0.0 0.0
38.70582 194 0.0 0.0 -77.4116 195 0.0 0.0 -154.823 196 0.0 0.0 -77.4116 209 0.0 0.0 38.70582 210
0.0 0.0 -154.823 211 0.0 0.0 77.41164 212 0.0 0.0 -154.823 213 0.0 0.0 38.70582 246 0.0 0.0 -77.4116
247 0.0 0.0 -154.823 248 0.0 0.0 -77.4116 261 0.0 0.0 38.70582 262 0.0 0.0 -154.823 263 0.0 0.0
77.41164 264 0.0 0.0 -154.823 265 0.0 0.0 38.70582 298 0.0 0.0 -77.4116 299 0.0 0.0 -154.823 300
0.0 0.0 -77.4116 313 0.0 0.0 38.70582 314 0.0 0.0 -154.823 315 0.0 0.0 77.41164 316 0.0 0.0 -154.823
317 0.0 0.0 38.70582 350 0.0 0.0 -77.4116 351 0.0 0.0 -154.823 352 0.0 0.0 -77.4116 365 0.0 0.0
38.70582 366 0.0 0.0 -154.823 367 0.0 0.0 77.41164 368 0.0 0.0 -154.823 369 0.0 0.0 38.70582 402
0.0 0.0 -77.4116 403 0.0 0.0 -154.823 404 0.0 0.0 -77.4116 417 0.0 0.0 19.35291 418 0.0 0.0 -77.4116
419 0.0 0.0 38.70582 420 0.0 0.0 -77.4116 421 0.0 0.0 19.35291
0.001 250
3
0.0 0.0 1 0.0 8640000 0.0

TITLE(2)="WATER FLOOD OF NFR"

DESCRIPTION()=
"THICKNESS (FT) : 30 "
"LENGTH (FT) : 75 "
"WIDTH (FT) : 75 "
"GRID BLOCKS : 8x8x3 "

COMPOSITIONAL_MODEL
DUAL_POROSITY
TIMEEND = 30

$ I/O OPTIONS

OUTLEVEL = 1
OUTPUT_PRE
OUTPUT_SAT
OUTPUT_VIS
OUTPUT_DEN
OUTPUT_WEL
PROCOUT
OUTPUT_HIS

OUTPUT_TIME() = 0 0.1 0.2 0.3 0.4 0.5 0.6 0.7 0.8 0.9 1. 5. 10. 20.
30. 40. 50. 60 70 80 90 100. 200. 300. 400 500 500. 700. 1000. 1200

$TIME_ENLARGE
$NO_CRASH

ISTEP(,,) = 1
JSTEP(,,) = 1
KSTEP(,,) = 1

```
$ DEBUGGING OPTION
$BUGKEY(15)

$ FAULT BLOCK AND MESH DATA
METHOD = 2
DOWN() = 0 0 1
MES="cart"
NX(1) = 8 NY(1) = 8    NZ(1) = 3
DX() = 75 DY() = 75 DZ() = 10

$ CORNER OF BLOCK 1,1,1
XYZ111(1 TO 3,1) = 0 0 0

$ SUBGRID DATA
NSH = 2
NSV = 2
DXM() = 10 DYM() = 10 DZM() = 10
MCAPP=1

$ COMPOUND NAMES
COMPOUND(1) = "C10"

$ COMPOUND CRITICAL TEMPERATURES
CRIT() 1111.8

$ COMPOUND CRITICAL PRESSURES
CRIP()    304.0

$ COMPOUND CRITICAL VOLUMES
$CRIV() 12.087
CRIV() 10.087

$ COMPOUND ACEN
ACEN() 0.488

$ COMPOUND MOL WEIGHTS
MOLW() 142.3

$ COMPOUND PARA
PARA() 431.0

$ MAX NUMBER OF PHASES
NPHASE = 3

$ Initial rock & water properties
ROCKZ = 0.00000    ROCKP = 4000
H2OZ =     0.00000000    H2OP = 14.7          H2OD = 3.467
SURTF = 60.0    SURPS = 14.7
RESTF = 60.0

$ TOLERANCE
$CVGOPT = 2
TOL_FLASH = 0.0001
TOL_VOLUME = 0.0001
TOL_MASS = 0.0001
TOL_WATER = 0.0001
TOL_MAT = 0.0001
MAXNEWT = 20

$ POROSITY
POROSITY1() = 0.02
MPOROSITY1() = 0.19

$ PERMEABILITIES

XPERM1() = 500
MXPERM1() = 1
```

```
YPERM1() = 500
MYPERM1() = 1

ZPERM1() = 10
MZPERM1() = 1

$ INITIAL WATER SATURATION
SWINI1() = 0.001
MSWINI1() = 0.25

$ INITIAL WATER CELL PRESSURE
PINI1() = 4000
MPINI1() = 4000

$ INITIAL PHASE VISCOSITIES AT EACH CELL
VIS1() = 0.5
MVIS1() = 0.5

IOILVIS
OILVIS 2.0

$ INITIAL COMPOSITIONS
ZXY1(,,,1) = 1.000
ZXYM1() = 1.000


$ RELPERM DATA
$ RELP 1 for table lookup, 2 for function based
RELP    2
RELPM    2
$ NRELFUN 1 for corey, more to be added later
NRELFUN    1
NRELFUNM    1
$ data for each phase : water, phase 2 and phase 3
ENDPT() =    1.0 1.0 0.0
SR() = 0.001 0.001 0.0
EXPN() = 1.46 2.15 0.0

ENDPTM() =    0.2 0.92 0.0
SRM() = 0.25 0.3 0.0
EXPNM() = 1.18 1.8 0.0


PCGO(1) Block              $ GAS-OIL CAPILLARY PRESSURE - ROCK TYPE 1
  Interpolation Linear
  Extrapolation Same
$ Nodes    .46    .64
$ Pole     .18
$ Constraint    0 At .8222
$ Constraint    0 At .86
$ Constraint    0 At .9
  Data
  0.0      0.0,
  1.0      0.0
EndBlock

PCOW(1) Block              $ WATER-OIL CAPILLARY PRESSURE - ROCK TYPE 1
  Interpolation Linear
  Extrapolation Same
  Data
0.0010    4.0001 ,
0.0510    2.8391 ,
0.1010    1.9780 ,
0.1510    1.3498 ,
0.2010    0.9000 ,
0.2510    0.5845 ,
0.3010    0.3685 ,
```

```
0.3510    0.2244 ,
0.4010    0.1314 ,
0.4510    0.0734 ,
0.5010    0.0388 ,
0.5510    0.0191 ,
0.6010    0.0087 ,
0.6510    0.0035 ,
0.7010    0.0013 ,
0.7510    0.0004 ,
0.8010    0.0001 ,
0.8510    0.0000 ,
0.9010    0.0000 ,
0.9510    0.0000
EndBlock

PCGOM(1) Block              $ GAS-OIL CAPILLARY PRESSURE FOR ROCK MATRIX
   Interpolation Linear
   Extrapolation Same
   Data    0.0    0.0 , 1. 0.0
EndBlock

PCOWM(1) Block              $ WATER-OIL CAPILLARY PRESSURE FOR ROCK MATRIX
   Interpolation Linear
   Extrapolation Same
   Data
0.2500    4.0001 ,
0.3000    3.1606 ,
0.3500    2.4198 ,
0.4000    1.7778 ,
0.4500    1.2346 ,
0.5000    0.7901 ,
0.5500    0.4445 ,
0.6000    0.1975 ,
0.6500    0.0494 ,
0.7000    0.0000
EndBlock


$--B feng pan 11/23/2006    -------- GEOMECHanics options
GEOMG =    73
GEOM2D    = 98
PCOUP = 1
THF = 0
GMCL=0
TOLA=0.0000000001
LIMA=200
TOLB=0.0000000000000001
LIMB=1000
EQC=3
$--B feng pan 11/23/2006    -------- GEOMECHanics options


NUMWELL=2

WELLNAME(1) = "INJECTOR"
KINDWELL(1) = 2
PRLIMIT(1) = 10000
WELLTOP(1 TO 3,1,1) =        37.5 37.5 0
WELLBOTTOM(1 TO 3,1,1) = 37.5 37.5 30.
DIAMETER(1,1) = 1.
WELLPQ(1) Block
   Interpolation Linear
   Extrapolation Constant
     Data    0.    200
EndBlock

WELLNAME(2) = "PRODUCER"
KINDWELL(2) = 3
```

```
WELLTOP(1 TO 3,1,2) =        562.5 562.5 0.
WELLBOTTOM(1 TO 3,1,2) = 562.5 562.5 30.
DIAMETER(1,2) = 1.
WELLPQ(2) Block
   Interpolation Linear
   Extrapolation Constant
    Data    0.    3500.
EndBlock

EndInitial

$ TRANSIENT DATA INPUT BLOCKS

BeginTime        0.0
$ INJECTED FLUID COMPOSITION
WZ() 0.000 1.000
TIME_CONTROL = 2
DELTIM = 0.1 DTIMMUL = 1.0    DTIMMAX = 1 DTIMMIN = 0.1
DPMAX = 1 DSMAX = 0.1 DCMAX = 0.1 DAQCMAX = 1
AQCOMP_WFINJ(,1) = 0.0
EndTime

3
8   8   3   1
1.0e-46   1.0e-46   5.0e+05   0.3   30.0   0.0   0.0 1
-100
0            22.85888449          45.71776897          68.57665346          91.43553795          114.2944224
             137.1533069          160.0121914          182.8710759
0            22.85888449          45.71776897          68.57665346          91.43553795          114.2944224
             137.1533069          160.0121914          182.8710759
0            -3.047851265         -6.09570253          -9.143553795
86400 10    0.5    1    1
1045
     1   0   0   1   1    2   1   0   1   1    3   1   0   1   1    4   1   0   1   1    5   1   0   1   1    6   1   0   1   1    7   1   0
1   1    8   1   0   1   1    9   1   0   1   1   10   1   0   1   1   11   1   0   1   1   12   1   0   1   1   13   1   0   1   1   14   1
0   1   1   15   1   0   1   1   16   1   0   1   1   17   0   0   1   1   18   0   0   1   1   19   1   0   1   1   20   1   0   1   1   21
1   0   1   1   22   1   0   1   1   23   1   0   1   1   24   1   0   1   1   25   1   0   1   1   26   0   0   1   1   27   0   0   1   1
28   1   0   1   1   29   1   0   1   1   30   1   0   1   1   31   1   0   1   1   32   1   0   1   1   33   1   0   1   1   34   1   0   1
1   35   1   0   1   1   36   1   0   1   1   37   1   0   1   1   38   1   0   1   1   39   1   0   1   1   40   1   0   1   1   41   1   0
1   1   42   1   0   1   1   43   0   0   1   1   44   0   0   1   1   45   1   0   1   1   46   1   0   1   1   47   1   0   1   1   48   1
0   1   1   49   1   0   1   1   50   1   0   1   1   51   1   0   1   1   52   0   0   1   1   53   0   0   1   1   54   1   0   1   1   55
1   0   1   1   56   1   0   1   1   57   1   0   1   1   58   1   0   1   1   59   1   0   1   1   60   1   0   1   1   61   1   0   1   1
62   1   0   1   1   63   1   0   1   1   64   1   0   1   1   65   1   0   1   1   66   1   0   1   1   67   1   0   1   1   68   1   0   1
1   69   0   0   1   1   70   0   0   1   1   71   1   0   1   1   72   1   0   1   1   73   1   0   1   1   74   1   0   1   1   75   1   0
1   1   76   1   0   1   1   77   1   0   1   1   78   0   0   1   1   79   0   0   0   1   80   0   0   0   1   81   0   0   0   1   82   0
0   0   1   83   0   0   0   1   84   0   0   0   1   85   0   0   0   1   86   0   0   0   1   87   0   0   0   1   88   0   0   0   1   89
0   0   0   1   90   0   0   0   1   91   0   0   0   1   92   0   0   0   1   93   0   0   0   1   94   0   0   0   1   95   0   0   0   1
96   0   1   1   1   97   1   1   1   1   98   1   1   1   1   99   1   1   1   1  100   1   1   1   1  101   1   1   1   1  102   1   1   1
1  103   1   1   1   1  104   0   1   1   1  105   0   1   1   1  106   1   1   1   1  107   1   1   1   1  108   1   1   1   1  109   1   1   1
1  110   1   1   1   1  111   1   1   1   1  112   1   1   1   1  113   0   1   1   1  114   0   1   1   1  115   1   1   1   1  116   1   1   1
1  117   1   1   1   1  118   1   1   1   1  119   1   1   1   1  120   1   1   1   1  121   1   1   1   1  122   0   1   1   1  123   0   0   0
1  124   0   0   0   1  125   0   0   0   1  126   0   0   0   1  127   0   0   0   1  128   0   0   0   1  129   0   0   0   1  130   0   0   0
1  131   0   0   0   1  132   0   1   1   1  133   1   1   1   1  134   1   1   1   1  135   1   1   1   1  136   1   1   1   1  137   1   1   1
1  138   1   1   1   1  139   1   1   1   1  140   1   1   1   1  141   1   1   1   1  142   1   1   1   1  143   1   1   1   1  144   1   1   1
1  145   1   1   1   1  146   1   1   1   1  147   1   1   1   1  148   0   1   1   1  149   0   1   1   1  150   1   1   1   1  151   1   1   1
1  152   1   1   1   1  153   1   1   1   1  154   1   1   1   1  155   1   1   1   1  156   1   1   1   1  157   0   1   1   1  158   0   1   1
1  159   1   1   1   1  161   1   1   1   1  163   1   1   1   1  165   1   1   1   1  167   1   1   1   1  169   1   1   1   1  171   1   1   1
1  173   1   1   1   1  174   0   1   1   1  175   0   1   1   1  176   1   1   1   1  177   1   1   1   1  178   1   1   1   1  179   1   1   1
1  180   1   1   1   1  181   1   1   1   1  182   1   1   1   1  183   0   1   1   1  184   0   1   1   1  185   1   1   1   1  187   1   1   1
1  189   1   1   1   1  191   1   1   1   1  193   1   1   1   1  195   1   1   1   1  197   1   1   1   1  199   1   1   1   1  200   0   1   1
1  201   0   1   1   1  202   1   1   1   1  203   1   1   1   1  204   1   1   1   1  205   1   1   1   1  206   1   1   1   1  207   1   1   1
1  208   1   1   1   1  209   0   1   1   1  210   0   0   0   1  211   0   0   0   1  212   0   0   0   1  213   0   0   0   1  214   0   0   0
1  215   0   0   0   1  216   0   0   0   1  217   0   0   0   1  218   0   0   0   1  219   0   0   0   1  220   0   0   0   1  221   0   0   0
1  222   0   0   0   1  223   0   0   0   1  224   0   0   0   1  225   0   0   0   1  226   0   0   0   1  227   0   1   1   1  228   1   1   1
1  229   1   1   1   1  230   1   1   1   1  231   1   1   1   1  232   1   1   1   1  233   1   1   1   1  234   1   1   1   1  235   0   1   1
1  236   0   1   1   1  237   1   1   1   1  238   1   1   1   1  239   1   1   1   1  240   1   1   1   1  241   1   1   1   1  242   1   1   1
1  243   1   1   1   1  244   0   1   1   1  245   0   1   1   1  246   1   1   1   1  247   1   1   1   1  248   1   1   1   1  249   1   1   1
1  250   1   1   1   1  251   1   1   1   1  252   1   1   1   1  253   0   1   1   1  254   0   0   0   1  255   0   0   0   1  256   0   0   0
```

1 257	0	0	0	1 258	0	0	0	1 259	0	0	0	1 260	0	0	0	1 261	0	0	0	1 262	0	0	0	1 263	0	1	1
1 264	1	1	1	1 265	1	1	1	1 266	1	1	1	1 267	1	1	1	1 268	1	1	1	1 269	1	1	1	1 270	1	1	1
1 271	1	1	1	1 272	1	1	1	1 273	1	1	1	1 274	1	1	1	1 275	1	1	1	1 276	1	1	1	1 277	1	1	1
1 278	1	1	1	1 279	0	1	1	1 280	0	1	1	1 281	1	1	1	1 282	1	1	1	1 283	1	1	1	1 284	1	1	1
1 285	1	1	1	1 286	1	1	1	1 287	1	1	1	1 288	0	1	1	1 289	0	1	1	1 290	1	1	1	1 292	1	1	1
1 294	1	1	1	1 296	1	1	1	1 298	1	1	1	1 300	1	1	1	1 302	1	1	1	1 304	1	1	1	1 305	0	1	1
1 306	0	1	1	1 307	1	1	1	1 308	1	1	1	1 309	1	1	1	1 310	1	1	1	1 311	1	1	1	1 312	1	1	1
1 313	1	1	1	1 314	0	1	1	1 315	0	1	1	1 316	1	1	1	1 318	1	1	1	1 320	1	1	1	1 322	1	1	1
1 324	1	1	1	1 326	1	1	1	1 328	1	1	1	1 330	1	1	1	1 331	0	1	1	1 332	0	1	1	1 333	1	1	1
1 334	1	1	1	1 335	1	1	1	1 336	1	1	1	1 337	1	1	1	1 338	1	1	1	1 339	1	1	1	1 340	0	1	1
1 341	0	0	0	1 342	0	0	0	1 343	0	0	0	1 344	0	0	0	1 345	0	0	0	1 346	0	0	0	1 347	0	0	0
1 348	0	0	0	1 349	0	0	0	1 350	0	0	0	1 351	0	0	0	1 352	0	0	0	1 353	0	0	0	1 354	0	0	0
1 355	0	0	0	1 356	0	0	0	1 357	0	0	0	1 358	0	1	1	1 359	1	1	1	1 360	1	1	1	1 361	1	1	1
1 362	1	1	1	1 363	1	1	1	1 364	1	1	1	1 365	1	1	1	1 366	0	1	1	1 367	0	1	1	1 368	1	1	1
1 369	1	1	1	1 370	1	1	1	1 371	1	1	1	1 372	1	1	1	1 373	1	1	1	1 374	1	1	1	1 375	0	1	1
1 376	0	1	1	1 377	1	1	1	1 378	1	1	1	1 379	1	1	1	1 380	1	1	1	1 381	1	1	1	1 382	1	1	1
1 383	1	1	1	1 384	0	1	1	1 385	0	0	0	1 386	0	0	0	1 387	0	0	0	1 388	0	0	0	1 389	0	0	0
1 390	0	0	0	1 391	0	0	0	1 392	0	0	0	1 393	0	0	0	1 394	0	1	1	1 395	1	1	1	1 396	1	1	1
1 397	1	1	1	1 398	1	1	1	1 399	1	1	1	1 400	1	1	1	1 401	1	1	1	1 402	1	1	1	1 403	1	1	1
1 404	1	1	1	1 405	1	1	1	1 406	1	1	1	1 407	1	1	1	1 408	1	1	1	1 409	1	1	1	1 410	0	1	1
1 411	0	1	1	1 412	1	1	1	1 413	1	1	1	1 414	1	1	1	1 415	1	1	1	1 416	1	1	1	1 417	1	1	1
1 418	1	1	1	1 419	0	1	1	1 420	0	1	1	1 421	1	1	1	1 423	1	1	1	1 425	1	1	1	1 427	1	1	1
1 429	1	1	1	1 431	1	1	1	1 433	1	1	1	1 435	1	1	1	1 436	0	1	1	1 437	0	1	1	1 438	1	1	1
1 439	1	1	1	1 440	1	1	1	1 441	1	1	1	1 442	1	1	1	1 443	1	1	1	1 444	1	1	1	1 445	0	1	1
1 446	0	1	1	1 447	1	1	1	1 449	1	1	1	1 451	1	1	1	1 453	1	1	1	1 455	1	1	1	1 457	1	1	1
1 459	1	1	1	1 461	1	1	1	1 462	0	1	1	1 463	0	1	1	1 464	1	1	1	1 465	1	1	1	1 466	1	1	1
1 467	1	1	1	1 468	1	1	1	1 469	1	1	1	1 470	1	1	1	1 471	0	1	1	1 472	0	0	0	1 473	0	0	0
1 474	0	0	0	1 475	0	0	0	1 476	0	0	0	1 477	0	0	0	1 478	0	0	0	1 479	0	0	0	1 480	0	0	0
1 481	0	0	0	1 482	0	0	0	1 483	0	0	0	1 484	0	0	0	1 485	0	0	0	1 486	0	0	0	1 487	0	0	0
1 488	0	0	0	1 489	0	1	1	1 490	1	1	1	1 491	1	1	1	1 492	1	1	1	1 493	1	1	1	1 494	1	1	1
1 495	1	1	1	1 496	1	1	1	1 497	0	1	1	1 498	0	1	1	1 499	1	1	1	1 500	1	1	1	1 501	1	1	1
1 502	1	1	1	1 503	1	1	1	1 504	1	1	1	1 505	1	1	1	1 506	0	1	1	1 507	0	1	1	1 508	1	1	1
1 509	1	1	1	1 510	1	1	1	1 511	1	1	1	1 512	1	1	1	1 513	1	1	1	1 514	1	1	1	1 515	0	1	1
1 516	0	0	0	1 517	0	0	0	1 518	0	0	0	1 519	0	0	0	1 520	0	0	0	1 521	0	0	0	1 522	0	0	0
1 523	0	0	0	1 524	0	0	0	1 525	0	1	1	1 526	1	1	1	1 527	1	1	1	1 528	1	1	1	1 529	1	1	1
1 530	1	1	1	1 531	1	1	1	1 532	1	1	1	1 533	1	1	1	1 534	1	1	1	1 535	1	1	1	1 536	1	1	1
1 537	1	1	1	1 538	1	1	1	1 539	1	1	1	1 540	1	1	1	1 541	0	1	1	1 542	0	1	1	1 543	1	1	1
1 544	1	1	1	1 545	1	1	1	1 546	1	1	1	1 547	1	1	1	1 548	1	1	1	1 549	1	1	1	1 550	0	1	1
1 551	0	1	1	1 552	1	1	1	1 554	1	1	1	1 556	1	1	1	1 558	1	1	1	1 560	1	1	1	1 562	1	1	1
1 564	1	1	1	1 566	1	1	1	1 567	0	1	1	1 568	0	1	1	1 569	1	1	1	1 570	1	1	1	1 571	1	1	1
1 572	1	1	1	1 573	1	1	1	1 574	1	1	1	1 575	1	1	1	1 576	0	1	1	1 577	0	1	1	1 578	1	1	1
1 580	1	1	1	1 582	1	1	1	1 584	1	1	1	1 586	1	1	1	1 588	1	1	1	1 590	1	1	1	1 592	1	1	1
1 593	0	1	1	1 594	0	1	1	1 595	1	1	1	1 596	1	1	1	1 597	1	1	1	1 598	1	1	1	1 599	1	1	1
1 600	1	1	1	1 601	1	1	1	1 602	0	1	1	1 603	0	0	0	1 604	0	0	0	1 605	0	0	0	1 606	0	0	0
1 607	0	0	0	1 608	0	0	0	1 609	0	0	0	1 610	0	0	0	1 611	0	0	0	1 612	0	0	0	1 613	0	0	0
1 614	0	0	0	1 615	0	0	0	1 616	0	0	0	1 617	0	0	0	1 618	0	0	0	1 619	0	0	0	1 620	0	1	1
1 621	1	1	1	1 622	1	1	1	1 623	1	1	1	1 624	1	1	1	1 625	1	1	1	1 626	1	1	1	1 627	1	1	1
1 628	0	1	1	1 629	0	1	1	1 630	1	1	1	1 631	1	1	1	1 632	1	1	1	1 633	1	1	1	1 634	1	1	1
1 635	1	1	1	1 636	1	1	1	1 637	0	1	1	1 638	0	1	1	1 639	1	1	1	1 640	1	1	1	1 641	1	1	1
1 642	1	1	1	1 643	1	1	1	1 644	1	1	1	1 645	1	1	1	1 646	0	1	1	1 647	0	0	0	1 648	0	0	0
1 649	0	0	0	1 650	0	0	0	1 651	0	0	0	1 652	0	0	0	1 653	0	0	0	1 654	0	0	0	1 655	0	0	0
1 656	0	1	1	1 657	1	1	1	1 658	1	1	1	1 659	1	1	1	1 660	1	1	1	1 661	1	1	1	1 662	1	1	1
1 663	1	1	1	1 664	1	1	1	1 665	1	1	1	1 666	1	1	1	1 667	1	1	1	1 668	1	1	1	1 669	1	1	1
1 670	1	1	1	1 671	1	1	1	1 672	0	1	1	1 673	0	1	1	1 674	1	1	1	1 675	1	1	1	1 676	1	1	1
1 677	1	1	1	1 678	1	1	1	1 679	1	1	1	1 680	1	1	1	1 681	0	1	1	1 682	0	1	1	1 683	1	1	1
1 685	1	1	1	1 687	1	1	1	1 689	1	1	1	1 691	1	1	1	1 693	1	1	1	1 695	1	1	1	1 697	1	1	1
1 698	0	1	1	1 699	0	1	1	1 700	1	1	1	1 701	1	1	1	1 702	1	1	1	1 703	1	1	1	1 704	1	1	1
1 705	1	1	1	1 706	1	1	1	1 707	0	1	1	1 708	0	1	1	1 709	1	1	1	1 711	1	1	1	1 713	1	1	1
1 715	1	1	1	1 717	1	1	1	1 719	1	1	1	1 721	1	1	1	1 723	1	1	1	1 724	0	1	1	1 725	0	1	1
1 726	1	1	1	1 727	1	1	1	1 728	1	1	1	1 729	1	1	1	1 730	1	1	1	1 731	1	1	1	1 732	1	1	1
1 733	0	1	1	1 734	0	0	0	1 735	0	0	0	1 736	0	0	0	1 737	0	0	0	1 738	0	0	0	1 739	0	0	0
1 740	0	0	0	1 741	0	0	0	1 742	0	0	0	1 743	0	0	0	1 744	0	0	0	1 745	0	0	0	1 746	0	0	0
1 747	0	0	0	1 748	0	0	0	1 749	0	0	0	1 750	0	0	0	1 751	0	1	1	1 752	1	1	1	1 753	1	1	1
1 754	1	1	1	1 755	1	1	1	1 756	1	1	1	1 757	1	1	1	1 758	1	1	1	1 759	0	1	1	1 760	0	1	1
1 761	1	1	1	1 762	1	1	1	1 763	1	1	1	1 764	1	1	1	1 765	1	1	1	1 766	1	1	1	1 767	1	1	1
1 768	0	1	1	1 769	0	1	1	1 770	1	1	1	1 771	1	1	1	1 772	1	1	1	1 773	1	1	1	1 774	1	1	1
1 775	1	1	1	1 776	1	1	1	1 777	0	1	1	1 778	0	0	0	1 779	0	0	0	1 780	0	0	0	1 781	0	0	0
1 782	0	0	0	1 783	0	0	0	1 784	0	0	0	1 785	0	0	0	1 786	0	0	0	1 787	0	1	1	1 788	1	1	1

1 789 1 1 1 1 790 1 1 1 1 791 1 1 1 1 792 1 1 1 1 793 1 1 1 1 794 1 1 1 1 795 1 1 1
1 796 1 1 1 1 797 1 1 1 1 798 1 1 1 1 799 1 1 1 1 800 1 1 1 1 801 1 1 1 1 802 1 1 1
1 803 0 1 1 1 804 0 1 1 1 805 1 1 1 1 806 1 1 1 1 807 1 1 1 1 808 1 1 1 1 809 1 1 1
1 810 1 1 1 1 811 1 1 1 1 812 0 1 1 1 813 0 1 1 1 814 1 1 1 1 816 1 1 1 1 818 1 1 1
1 820 1 1 1 1 822 1 1 1 1 824 1 1 1 1 826 1 1 1 1 828 1 1 1 1 829 0 1 1 1 830 0 1 1
1 831 1 1 1 1 832 1 1 1 1 833 1 1 1 1 834 1 1 1 1 835 1 1 1 1 836 1 1 1 1 837 1 1 1
1 838 0 1 1 1 839 0 1 1 1 840 1 1 1 1 842 1 1 1 1 844 1 1 1 1 846 1 1 1 1 848 1 1 1
1 850 1 1 1 1 852 1 1 1 1 854 1 1 1 1 855 0 1 1 1 856 0 1 1 1 857 1 1 1 1 858 1 1 1
1 859 1 1 1 1 860 1 1 1 1 861 1 1 1 1 862 1 1 1 1 863 1 1 1 1 864 0 1 1 1 865 0 0 0
1 866 0 0 0 1 867 0 0 0 1 868 0 0 0 1 869 0 0 0 1 870 0 0 0 1 871 0 0 0 1 872 0 0 0
1 873 0 0 0 1 874 0 0 0 1 875 0 0 0 1 876 0 0 0 1 877 0 0 0 1 878 0 0 0 1 879 0 0 0
1 880 0 0 0 1 881 0 0 0 1 882 0 1 1 1 883 1 1 1 1 884 1 1 1 1 885 1 1 1 1 886 1 1 1
1 887 1 1 1 1 888 1 1 1 1 889 1 1 1 1 890 0 1 1 1 891 0 1 1 1 892 1 1 1 1 893 1 1 1
1 894 1 1 1 1 895 1 1 1 1 896 1 1 1 1 897 1 1 1 1 898 1 1 1 1 899 0 1 1 1 900 0 1 1
1 901 1 1 1 1 902 1 1 1 1 903 1 1 1 1 904 1 1 1 1 905 1 1 1 1 906 1 1 1 1 907 1 1 1
1 908 0 1 1 1 909 0 0 0 1 910 0 0 0 1 911 0 0 0 1 912 0 0 0 1 913 0 0 0 1 914 0 0 0
1 915 0 0 0 1 916 0 0 0 1 917 0 0 0 1 918 0 1 1 1 919 1 1 1 1 920 1 1 1 1 921 1 1 1
1 922 1 1 1 1 923 1 1 1 1 924 1 1 1 1 925 1 1 1 1 926 1 1 1 1 927 1 1 1 1 928 1 1 1
1 929 1 1 1 1 930 1 1 1 1 931 1 1 1 1 932 1 1 1 1 933 1 1 1 1 934 0 1 1 1 935 0 1 1
1 936 1 1 1 1 937 1 1 1 1 938 1 1 1 1 939 1 1 1 1 940 1 1 1 1 941 1 1 1 1 942 1 1 1
1 943 0 1 1 1 944 0 1 1 1 945 1 1 1 1 947 1 1 1 1 949 1 1 1 1 951 1 1 1 1 953 1 1 1
1 955 1 1 1 1 957 1 1 1 1 959 1 1 1 1 960 0 1 1 1 961 0 1 1 1 962 1 1 1 1 963 1 1 1
1 964 1 1 1 1 965 1 1 1 1 966 1 1 1 1 967 1 1 1 1 968 1 1 1 1 969 0 1 1 1 970 0 1 1
1 971 1 1 1 1 973 1 1 1 1 975 1 1 1 1 977 1 1 1 1 979 1 1 1 1 981 1 1 1 1 983 1 1 1
1 985 1 1 1 1 986 0 1 1 1 987 0 1 1 1 988 1 1 1 1 989 1 1 1 1 990 1 1 1 1 991 1 1 1
1 992 1 1 1 1 993 1 1 1 1 994 1 1 1 1 995 0 1 1 1 996 0 0 0 1 997 0 0 0 1 998 0 0 0
1 999 0 0 0 1 1000 0 0 0 1 1001 0 0 0 1 1002 0 0 0 1 1003 0 0 0 1 1004 0 0 0 1
1005 0 0 0 1 1006 0 0 0 1 1007 0 0 0 1 1008 0 0 0 1 1009 0 0 0 1 1010 0 0 0 1
1011 0 0 0 1 1012 0 0 0 1 1013 0 1 1 1 1014 1 1 1 1 1015 1 1 1 1 1016 1 1 1 1
1017 1 1 1 1 1018 1 1 1 1 1019 1 1 1 1 1020 1 1 1 1 1021 0 1 1 1 1022 0 1 1 1
1023 1 1 1 1 1024 1 1 1 1 1025 1 1 1 1 1026 1 1 1 1 1027 1 1 1 1 1028 1 1 1 1
1029 1 1 1 1 1030 0 1 1 1 1031 0 1 1 1 1032 1 1 1 1 1033 1 1 1 1 1034 1 1 1 1
1035 1 1 1 1 1036 1 1 1 1 1037 1 1 1 1 1038 1 1 1 1 1039 0 1 1 1 1040 0 0 0 1
1041 0 0 0 1 1042 0 0 0 1 1043 0 0 0 1 1044 0 0 0 1 1045 0 0 0 1 1046 0 0 0 1
1047 0 0 0 1 1048 0 0 0 1 1049 0 0 1 1 1050 1 0 1 1 1051 1 0 1 1 1052 1 0 1 1
1053 1 0 1 1 1054 1 0 1 1 1055 1 0 1 1 1056 1 0 1 1 1057 1 0 1 1 1058 1 0 1 1
1059 1 0 1 1 1060 1 0 1 1 1061 1 0 1 1 1062 1 0 1 1 1063 1 0 1 1 1064 1 0 1 1
1065 0 0 1 1 1066 0 0 1 1 1067 1 0 1 1 1068 1 0 1 1 1069 1 0 1 1 1070 1 0 1 1
1071 1 0 1 1 1072 1 0 1 1 1073 1 0 1 1 1074 0 0 1 1 1075 0 0 1 1 1076 1 0 1 1
1077 1 0 1 1 1078 1 0 1 1 1079 1 0 1 1 1080 1 0 1 1 1081 1 0 1 1 1082 1 0 1 1
1083 1 0 1 1 1084 1 0 1 1 1085 1 0 1 1 1086 1 0 1 1 1087 1 0 1 1 1088 1 0 1 1
1089 1 0 1 1 1090 1 0 1 1 1091 0 0 1 1 1092 0 0 1 1 1093 1 0 1 1 1094 1 0 1 1
1095 1 0 1 1 1096 1 0 1 1 1097 1 0 1 1 1098 1 0 1 1 1099 1 0 1 1 1100 0 0 1 1
1101 0 0 1 1 1102 1 0 1 1 1103 1 0 1 1 1104 1 0 1 1 1105 1 0 1 1 1106 1 0 1 1
1107 1 0 1 1 1108 1 0 1 1 1109 1 0 1 1 1110 1 0 1 1 1111 1 0 1 1 1112 1 0 1 1
1113 1 0 1 1 1114 1 0 1 1 1115 1 0 1 1 1116 1 0 1 1 1117 0 0 1 1 1118 0 0 1 1
1119 1 0 1 1 1120 1 0 1 1 1121 1 0 1 1 1122 1 0 1 1 1123 1 0 1 1 1124 1 0 1 1
1125 1 0 1 1 1126 0 0 1 1 1127 0 0 0 1 1128 0 0 0 1 1129 0 0 0 1 1130 0 0 0 1
1131 0 0 0 1 1132 0 0 0 1 1133 0 0 0 1 1134 0 0 0 1 1135 0 0 0 1 1136 0 0 0 1
1137 0 0 0 1 1138 0 0 0 1 1139 0 0 0 1 1140 0 0 0 1 1141 0 0 0 1 1142 0 0 0 1
1143 0 0 0 1
225
1 0.0 0.0 43.544 2 0.0 0.0 -174.176 3 0.0 0.0 87.088 4 0.0 0.0 -174.176 5 0.0 0.0 87.088 6 0.0
0.0 -174.176 7 0.0 0.0 87.088 8 0.0 0.0 -174.176 9 0.0 0.0 87.088 10 0.0 0.0 -174.176 11 0.0 0.0
87.088 12 0.0 0.0 -174.176 13 0.0 0.0 87.088 14 0.0 0.0 -174.176 15 0.0 0.0 87.088 16 0.0 0.0 -
174.176 17 0.0 0.0 43.544 96 0.0 0.0 -174.176 97 0.0 0.0 -348.352 98 0.0 0.0 -348.352 99 0.0 0.0 -
348.352 100 0.0 0.0 -348.352 101 0.0 0.0 -348.352 102 0.0 0.0 -348.352 103 0.0 0.0 -348.352 104
0.0 0.0 -174.176 132 0.0 0.0 87.088 133 0.0 0.0 -348.352 134 0.0 0.0 174.176 135 0.0 0.0 -348.352
136 0.0 0.0 174.176 137 0.0 0.0 -348.352 138 0.0 0.0 174.176 139 0.0 0.0 -348.352 140 0.0 0.0
174.176 141 0.0 0.0 -348.352 142 0.0 0.0 174.176 143 0.0 0.0 -348.352 144 0.0 0.0 174.176 145 0.0
0.0 -348.352 146 0.0 0.0 174.176 147 0.0 0.0 -348.352 148 0.0 0.0 87.088 227 0.0 0.0 -174.176 228
0.0 0.0 -348.352 229 0.0 0.0 -348.352 230 0.0 0.0 -348.352 231 0.0 0.0 -348.352 232 0.0 0.0 -
348.352 233 0.0 0.0 -348.352 234 0.0 0.0 -348.352 235 0.0 0.0 -174.176 263 0.0 0.0 87.088 264 0.0
0.0 -348.352 265 0.0 0.0 174.176 266 0.0 0.0 -348.352 267 0.0 0.0 174.176 268 0.0 0.0 -348.352 269
0.0 0.0 174.176 270 0.0 0.0 -348.352 271 0.0 0.0 174.176 272 0.0 0.0 -348.352 273 0.0 0.0 174.176
274 0.0 0.0 -348.352 275 0.0 0.0 174.176 276 0.0 0.0 -348.352 277 0.0 0.0 174.176 278 0.0 0.0 -
348.352 279 0.0 0.0 87.088 358 0.0 0.0 -174.176 359 0.0 0.0 -348.352 360 0.0 0.0 -348.352 361 0.0
0.0 -348.352 362 0.0 0.0 -348.352 363 0.0 0.0 -348.352 364 0.0 0.0 -348.352 365 0.0 0.0 -348.352

366 0.0 0.0 -174.176 394 0.0 0.0 87.088 395 0.0 0.0 -348.352 396 0.0 0.0 174.176 397 0.0 0.0 -348.352 398 0.0 0.0 174.176 399 0.0 0.0 -348.352 400 0.0 0.0 174.176 401 0.0 0.0 -348.352 402 0.0 0.0 174.176 403 0.0 0.0 -348.352 404 0.0 0.0 174.176 405 0.0 0.0 -348.352 406 0.0 0.0 174.176 407 0.0 0.0 -348.352 408 0.0 0.0 174.176 409 0.0 0.0 -348.352 410 0.0 0.0 87.088 489 0.0 0.0 -174.176 490 0.0 0.0 -348.352 491 0.0 0.0 -348.352 492 0.0 0.0 -348.352 493 0.0 0.0 -348.352 494 0.0 0.0 -348.352 495 0.0 0.0 -348.352 496 0.0 0.0 -348.352 497 0.0 0.0 -174.176 525 0.0 0.0 87.088 526 0.0 0.0 -348.352 527 0.0 0.0 174.176 528 0.0 0.0 -348.352 529 0.0 0.0 174.176 530 0.0 0.0 -348.352 531 0.0 0.0 174.176 532 0.0 0.0 -348.352 533 0.0 0.0 174.176 534 0.0 0.0 -348.352 535 0.0 0.0 174.176 536 0.0 0.0 -348.352 537 0.0 0.0 174.176 538 0.0 0.0 -348.352 539 0.0 0.0 174.176 540 0.0 0.0 -348.352 541 0.0 0.0 87.088 620 0.0 0.0 -174.176 621 0.0 0.0 -348.352 622 0.0 0.0 -348.352 623 0.0 0.0 -348.352 624 0.0 0.0 -348.352 625 0.0 0.0 -348.352 626 0.0 0.0 -348.352 627 0.0 0.0 -348.352 628 0.0 0.0 -174.176 656 0.0 0.0 87.088 657 0.0 0.0 -348.352 658 0.0 0.0 174.176 659 0.0 0.0 -348.352 660 0.0 0.0 174.176 661 0.0 0.0 -348.352 662 0.0 0.0 174.176 663 0.0 0.0 -348.352 664 0.0 0.0 174.176 665 0.0 0.0 -348.352 666 0.0 0.0 174.176 667 0.0 0.0 -348.352 668 0.0 0.0 174.176 669 0.0 0.0 -348.352 670 0.0 0.0 174.176 671 0.0 0.0 -348.352 672 0.0 0.0 87.088 751 0.0 0.0 -174.176 752 0.0 0.0 -348.352 753 0.0 0.0 -348.352 754 0.0 0.0 -348.352 755 0.0 0.0 -348.352 756 0.0 0.0 -348.352 757 0.0 0.0 -348.352 758 0.0 0.0 -348.352 759 0.0 0.0 -174.176 787 0.0 0.0 87.088 788 0.0 0.0 -348.352 789 0.0 0.0 174.176 790 0.0 0.0 -348.352 791 0.0 0.0 174.176 792 0.0 0.0 -348.352 793 0.0 0.0 174.176 794 0.0 0.0 -348.352 795 0.0 0.0 174.176 796 0.0 0.0 -348.352 797 0.0 0.0 174.176 798 0.0 0.0 -348.352 799 0.0 0.0 174.176 800 0.0 0.0 -348.352 801 0.0 0.0 174.176 802 0.0 0.0 -348.352 803 0.0 0.0 87.088 882 0.0 0.0 -174.176 883 0.0 0.0 -348.352 884 0.0 0.0 -348.352 885 0.0 0.0 -348.352 886 0.0 0.0 -348.352 887 0.0 0.0 -348.352 888 0.0 0.0 -348.352 889 0.0 0.0 -348.352 890 0.0 0.0 -174.176 918 0.0 0.0 87.088 919 0.0 0.0 -348.352 920 0.0 0.0 174.176 921 0.0 0.0 -348.352 922 0.0 0.0 174.176 923 0.0 0.0 -348.352 924 0.0 0.0 174.176 925 0.0 0.0 -348.352 926 0.0 0.0 174.176 927 0.0 0.0 -348.352 928 0.0 0.0 174.176 929 0.0 0.0 -348.352 930 0.0 0.0 174.176 931 0.0 0.0 -348.352 932 0.0 0.0 174.176 933 0.0 0.0 -348.352 934 0.0 0.0 87.088 1013 0.0 0.0 -174.176 1014 0.0 0.0 -348.352 1015 0.0 0.0 -348.352 1016 0.0 0.0 -348.352 1017 0.0 0.0 -348.352 1018 0.0 0.0 -348.352 1019 0.0 0.0 -348.352 1020 0.0 0.0 -348.352 1021 0.0 0.0 -174.176 1049 0.0 0.0 43.544 1050 0.0 0.0 -174.176 1051 0.0 0.0 87.088 1052 0.0 0.0 -174.176 1053 0.0 0.0 87.088 1054 0.0 0.0 -174.176 1055 0.0 0.0 87.088 1056 0.0 0.0 -174.176 1057 0.0 0.0 87.088 1058 0.0 0.0 -174.176 1059 0.0 0.0 87.088 1060 0.0 0.0 -174.176 1061 0.0 0.0 87.088 1062 0.0 0.0 -174.176 1063 0.0 0.0 87.088 1064 0.0 0.0 -174.176 1065 0.0 0.0 43.544
0.001 250
3
0.0 0.0 1 0.0 8640000 0.0

TITLE(2)="3-D PRIMARY DEPLETION (NONLINEAR CONST)"

DESCRIPTION()=
"THICKNESS (FT) : 200"
"LENGTH (FT) : 200"
"WIDTH (FT) : 200"
"GRID BLOCKS : 2x8x4"

COMPOSITIONAL_MODEL
$DEBUGS

TIMEEND = 30

$ I/O OPTIONS

OUTLEVEL = 1
PROCOUT
OUTPUT_PRE
OUTPUT_SAT
OUTPUT_OIL
OUTPUT_GAS
OUTPUT_WEL
OUTPUT_HIS

HISDATA_NUM = 100
OUTPUT_TIME() = 0 0.0001 0.0002 0.0003 0.01 0.02 0.5 1 5 10 15 30 60 80 118 120 1000 2000 3000 3650
$NO_CRASH

$OUTPUT FREQUENCY

```
ISTEP(,,)=1
JSTEP(,,)=1
KSTEP(,,)=1

$ FAULT BLOCK AND MESH DATA
METHOD = 2
DOWN() = 0 0 1
$$$$NX(1) = 2    NY(1) = 8 NZ(1) = 2
NX(1) = 2    NY(1) = 8 NZ(1) = 4
MES = "cart"
DX() = 100    DY() = 25    DZ() =    50.

$ COMPOUND NAMES
COMPOUND(1) = "C10"

$ COMPOUND CRITICAL TEMPERATURES
CRIT() 1111.8

$ COMPOUND CRITICAL PRESSURES
CRIP()    304.0

$ COMPOUND CRITICAL VOLUMES
CRIV() 10.087

$ COMPOUND ACEN
ACEN() 0.488

$ COMPOUND MOL WEIGHTS
MOLW()    142.3

$ COMPOUND PARA
PARA()    431.0

$ MAX NUMBER OF PHASES
NPHASE = 3

$ MAXNEWT MAX NUMBER OF NEWTON ITERATION
MAXNEWT = 20

$ Initial rock & water properties
ROCKZ = 0.000000    ROCKP = 1500
H2OZ = 0.000003    H2OP = 14.696    H2OD = 3.468
SURTF = 60.0    SURPS = 14.696
RESTF = 160.0

$ TOLERANCE
CVGOPT = 2
TOL_FLASH = 0.001
TOL_VOLUME = 0.001
TOL_MASS = 0.001
TOL_WATER = 0.001

$ POROSITY
POROSITY1() = 0.35

$ PERMEABILITIES
XPERM1() = 10
YPERM1() = 10
ZPERM1() = 10
XYPERM1() = 0
XZPERM1() = 0
YZPERM1() = 0

$ INITIAL WATER SATURATION
SWINI1() = 0.17

$ INITIAL WATER CELL PRESSURE
$PINI1() = 1950.0
```

```
PINI1() = 6000.0

$ INITIAL PHASE VISCOSITIES AT EACH CELL
VIS1() = 1.0

$ INITIAL COMPOSITIONS
ZXY1(,,,1) = 1.0

$ RELPERM DATA
$ RELP 1 for table lookup, 2 for function based

RELP 2
$MODREL(1) = 3

$ NRELFUN 1 for corey, more to be added later
NRELFUN    1
$ data for each phase : water, phase 2 and phase 3
ENDPT() = 0.4 0.9 0.9
SR() = 0.3 0.1 0.0
EXPN() = 3.0 2.0 2.0


$--B feng pan 11/23/2006    -------- GEOMECHanics options
GEOMG =    69
GEOM2D    = 98
PCOUP = 97
THF = 0
GMCL=0
TOLD=0.0000000000000001
LIMD=1000
NONL=1
EQC=3
$--E feng pan 11/23/2006    -------- GEOMECHanics options

$ ============== WELL SPECIFICATIONS ==============

NUMWELL =    2

WELLNAME(1) = "PRODUCER_1"
KINDWELL(1) = 3
WELLTOP(1 TO 3,1,1) =50 187.5 0.0
WELLBOTTOM(1 TO 3,1,1) =50 187.5 200.0
DIAMETER(1,1) = 1.0
WELLPQ(1) Block
   Interpolation Linear
   Extrapolation Constant
   Data    0.0      5000.0
EndBlock

WELLNAME(2) = "PRODUCER_2"
KINDWELL(2) = 3
WELLTOP(1 TO 3,1,2) =150      187.5 0.0
WELLBOTTOM(1 TO 3,1,2) =150      187.5 200.0
DIAMETER(1,2) = 1.0
WELLPQ(2) Block
   Interpolation Linear
   Extrapolation Constant
   Data    0.0      5000.0
EndBlock

EndInitial

$ TRANSIENT DATA INPUT BLOCKS
BeginTime    0.0
TIME_CONTROL = 2
DELTIM = 0.01    DTIMMUL = 1.0    DTIMMAX = 30    DTIMMIN = 0.01
TUNE = 0.5    DCMAX = 0.5    DAQCMAX = 0.5    DPMAX = 0.5    DSMAX = 0.5
EndTime
```

3
2 8 4 1
1.0e-46 1.0e-46 9.098499e+06 0.3 10.0 30.0 0.0 1
-0.0
0 30.47851265 60.9570253
0 7.619628162 15.23925632 22.85888449 30.47851265 38.09814081
45.71776897 53.33739714 60.9570253
0 -15.23925632 -30.47851265 -45.71776897 -60.9570253
86400 10 0.5 1 1
432
1 0 0 1 0 2 1 0 1 0 3 1 0 1 0 4 1 0 1 0 5 0 0 1 0 6 0 0 1 0 7 1 0 1
0 8 0 0 1 0 9 0 0 1 1 10 1 0 1 0 11 1 0 1 1 12 1 0 1 0 13 0 0 1 1 14
0 0 1 0 15 1 0 1 0 16 0 0 1 0 17 0 0 1 1 18 1 0 1 0 19 1 0 1 1 20 1 0
1 0 21 0 0 1 1 22 0 0 1 0 23 1 0 1 0 24 0 0 1 0 25 0 0 1 1 26 1 0 1 0
27 1 0 1 1 28 1 0 1 0 29 0 0 1 1 30 0 0 1 0 31 1 0 1 0 32 0 0 1 0 33 0
0 0 1 34 0 0 0 0 35 0 0 0 1 36 0 0 0 0 37 0 0 0 1 38 0 1 1 0 39 1 1 1
0 40 0 1 1 0 41 0 1 1 0 42 1 1 1 0 43 0 1 1 0 44 0 1 1 0 45 1 1 1 0 46
0 1 1 0 47 0 1 1 0 48 1 1 1 0 49 0 1 1 0 50 0 0 0 0 0 51 0 0 0 0 0 52 0 0
0 0 53 0 1 1 0 54 1 1 1 0 55 1 1 1 0 56 1 1 1 0 57 0 1 1 0 58 0 1 1 0
59 1 1 1 0 60 0 1 1 0 61 0 1 1 1 62 1 1 1 0 64 1 1 1 0 65 0 1 1 1 66 0
1 1 0 67 1 1 1 0 68 0 1 1 0 69 0 1 1 1 70 1 1 1 0 72 1 1 1 0 73 0 1 1
1 74 0 1 1 0 75 1 1 1 0 76 0 1 1 0 77 0 1 1 1 78 1 1 1 0 80 1 1 1 0 81
0 1 1 1 82 0 1 1 0 83 1 1 1 0 84 0 1 1 0 85 0 0 0 1 86 0 0 0 0 0 87 0 0
0 1 88 0 0 0 0 0 89 0 0 0 0 1 90 0 1 1 0 91 1 1 1 0 92 0 1 1 0 93 0 1 1 0
94 1 1 1 0 95 0 1 1 0 96 0 1 1 0 97 1 1 1 0 98 0 1 1 0 99 0 1 1 0 100 1
1 1 0 101 0 1 1 0 102 0 0 0 0 0 103 0 0 0 0 0 104 0 0 0 0 0 105 0 1 1 0 106 1 1 1
0 107 1 1 1 0 108 1 1 1 0 109 0 1 1 0 110 0 1 1 0 111 1 1 1 0 112 0 1 1 0 113
0 1 1 1 114 1 1 1 0 116 1 1 1 0 117 0 1 1 1 118 0 1 1 0 119 1 1 1 0 120 0 1
1 0 121 0 1 1 1 122 1 1 1 0 124 1 1 1 0 125 0 1 1 1 126 0 1 1 0 127 1 1 1 0
128 0 1 1 0 129 0 1 1 1 130 1 1 1 0 132 1 1 1 0 133 0 1 1 1 134 0 1 1 0 135 1
1 1 0 136 0 1 1 0 137 0 0 0 1 138 0 0 0 0 139 0 0 0 1 140 0 0 0 0 141 0 0 0
1 142 0 1 1 0 143 1 1 1 0 144 0 1 1 0 145 0 1 1 0 146 1 1 1 0 147 0 1 1 0 148
0 1 1 0 149 1 1 1 0 150 0 1 1 0 151 0 1 1 0 152 1 1 1 0 153 0 1 1 0 154 0 0
0 0 155 0 0 0 0 156 0 0 0 0 157 0 1 1 0 158 1 1 1 0 159 1 1 1 0 160 1 1 1 0
161 0 1 1 0 162 0 1 1 0 163 1 1 1 0 164 0 1 1 0 165 0 1 1 1 166 1 1 1 0 168 1
1 1 0 169 0 1 1 1 170 0 1 1 0 171 1 1 1 0 172 0 1 1 0 173 0 1 1 1 174 1 1 1
0 176 1 1 1 0 177 0 1 1 1 178 0 1 1 0 179 1 1 1 0 180 0 1 1 0 181 0 1 1 1 182
1 1 1 0 184 1 1 1 0 185 0 1 1 1 186 0 1 1 0 187 1 1 1 0 188 0 1 1 0 189 0 0
0 1 190 0 0 0 0 191 0 0 0 1 192 0 0 0 0 193 0 0 0 1 194 0 1 1 0 195 1 1 1 0
196 0 1 1 0 197 0 1 1 0 198 1 1 1 0 199 0 1 1 0 200 0 1 1 0 201 1 1 1 0 202 0
1 1 0 203 0 1 1 0 204 1 1 1 0 205 0 1 1 0 206 0 0 0 0 207 0 0 0 0 208 0 0 0
0 209 0 1 1 0 210 1 1 1 0 211 1 1 1 0 212 1 1 1 0 213 0 1 1 0 214 0 1 1 0 215
1 1 1 0 216 0 1 1 0 217 0 1 1 1 218 1 1 1 0 220 1 1 1 0 221 0 1 1 1 222 0 1
1 0 223 1 1 1 0 224 0 1 1 0 225 0 1 1 1 226 1 1 1 0 228 1 1 1 0 229 0 1 1 1
230 0 1 1 0 231 1 1 1 0 232 0 1 1 0 233 0 1 1 1 234 1 1 1 0 236 1 1 1 0 237 0
1 1 1 238 0 1 1 0 239 1 1 1 0 240 0 1 1 0 241 0 0 0 1 242 0 0 0 0 243 0 0 0
1 244 0 0 0 0 245 0 0 0 1 246 0 1 1 0 247 1 1 1 0 248 0 1 1 0 249 0 1 1 0 250
1 1 1 0 251 0 1 1 0 252 0 1 1 0 253 1 1 1 0 254 0 1 1 0 255 0 1 1 0 256 1 1
1 0 257 0 1 1 0 258 0 0 0 0 259 0 0 0 0 260 0 0 0 0 261 0 1 1 0 262 1 1 1 0
263 1 1 1 0 264 1 1 1 0 265 0 1 1 0 266 0 1 1 0 267 1 1 1 0 268 0 1 1 0 269 0
1 1 1 270 1 1 1 0 272 1 1 1 0 273 0 1 1 1 274 0 1 1 0 275 1 1 1 0 276 0 1 1
0 277 0 1 1 1 278 1 1 1 0 280 1 1 1 0 281 0 1 1 1 282 0 1 1 0 283 1 1 1 0 284
0 1 1 0 285 0 1 1 1 286 1 1 1 0 288 1 1 1 0 289 0 1 1 1 290 0 1 1 0 291 1 1
1 0 292 0 1 1 0 293 0 0 0 1 294 0 0 0 0 295 0 0 0 1 296 0 0 0 0 297 0 0 0 1
298 0 1 1 0 299 1 1 1 0 300 0 1 1 0 301 0 1 1 0 302 1 1 1 0 303 0 1 1 0 304 0
1 1 0 305 1 1 1 0 306 0 1 1 0 307 0 1 1 0 308 1 1 1 0 309 0 1 1 0 310 0 0 0 0
0 311 0 0 0 0 312 0 0 0 0 313 0 1 1 0 314 1 1 1 0 315 1 1 1 0 316 1 1 1 0 317
0 1 1 0 318 0 1 1 0 319 1 1 1 0 320 0 1 1 0 321 0 1 1 1 322 1 1 1 0 324 1 1
1 0 325 0 1 1 1 326 0 1 1 0 327 1 1 1 0 328 0 1 1 0 329 0 1 1 1 330 1 1 1 0
332 1 1 1 0 333 0 1 1 1 334 0 1 1 0 335 1 1 1 0 336 0 1 1 0 337 0 1 1 1 338 1
1 1 0 340 1 1 1 0 341 0 1 1 1 342 0 1 1 0 343 1 1 1 0 344 0 1 1 0 345 0 0 0
1 346 0 0 0 0 347 0 0 0 1 348 0 0 0 0 349 0 0 0 1 350 0 1 1 0 351 1 1 1 0 352
0 1 1 0 353 0 1 1 0 354 1 1 1 0 355 0 1 1 0 356 0 1 1 0 357 1 1 1 0 358 0 1
1 0 359 0 1 1 0 360 1 1 1 0 361 0 1 1 0 362 0 0 0 0 363 0 0 0 0 364 0 0 0 0
365 0 1 1 0 366 1 1 1 0 367 1 1 1 0 368 1 1 1 0 369 0 1 1 0 370 0 1 1 0 371 1
1 1 0 372 0 1 1 0 373 0 1 1 1 374 1 1 1 0 376 1 1 1 0 377 0 1 1 1 378 0 1 1
0 379 1 1 1 0 380 0 1 1 0 381 0 1 1 1 382 1 1 1 0 384 1 1 1 0 385 0 1 1 1 386

0 1 1 0 387 1 1 1 0 388 0 1 1 0 389 0 1 1 1 390 1 1 1 0 392 1 1 1 0 393 0 1
1 1 394 0 1 1 0 395 1 1 1 0 396 0 1 1 0 397 0 0 0 1 398 0 0 0 0 399 0 0 0 1
400 0 0 0 0 401 0 0 0 1 402 0 1 1 0 403 1 1 1 0 404 0 1 1 0 405 0 1 1 0 406 1
1 1 0 407 0 1 1 0 408 0 1 1 0 409 1 1 1 0 410 0 1 1 0 411 0 1 1 0 412 1 1 1
0 413 0 1 1 0 414 0 0 0 0 415 0 0 0 0 416 0 0 0 0 417 0 0 1 0 418 1 0 1 0 419
1 0 1 0 420 1 0 1 0 421 0 0 1 0 422 0 0 1 0 423 1 0 1 0 424 0 0 1 0 425 0 0
1 1 426 1 0 1 0 427 1 0 1 1 428 1 0 1 0 429 0 0 1 1 430 0 0 1 0 431 1 0 1 0
432 0 0 1 0 433 0 0 1 1 434 1 0 1 0 435 1 0 1 1 436 1 0 1 0 437 0 0 1 1 438 0
0 1 0 439 1 0 1 0 440 0 0 1 0 441 0 0 1 1 442 1 0 1 0 443 1 0 1 1 444 1 0 1
0 445 0 0 1 1 446 0 0 1 0 447 1 0 1 0 448 0 0 1 0 449 0 0 0 1 450 0 0 0 0 451
0 0 0 1 452 0 0 0 0 453 0 0 0 1
69
1 0.0 0.0 19.35291 2 0.0 0.0 -77.4116 3 0.0 0.0 38.70582 4 0.0 0.0 -77.4116 5 0.0 0.0 19.35291 38
0.0 0.0 -77.4116 39 0.0 0.0 -154.823 40 0.0 0.0 -77.4116 53 0.0 0.0 38.70582 54 0.0 0.0 -154.823 55 0.0
0.0 77.41164 56 0.0 0.0 -154.823 57 0.0 0.0 38.70582 90 0.0 0.0 -77.4116 91 0.0 0.0 -154.823 92 0.0
0.0 -77.4116 105 0.0 0.0 38.70582 106 0.0 0.0 -154.823 107 0.0 0.0 77.41164 108 0.0 0.0 -154.823 109
0.0 0.0 38.70582 142 0.0 0.0 -77.4116 143 0.0 0.0 -154.823 144 0.0 0.0 -77.4116 157 0.0 0.0 38.70582
158 0.0 0.0 -154.823 159 0.0 0.0 77.41164 160 0.0 0.0 -154.823 161 0.0 0.0 38.70582 194 0.0 0.0 -
77.4116 195 0.0 0.0 -154.823 196 0.0 0.0 -77.4116 209 0.0 0.0 38.70582 210 0.0 0.0 -154.823 211 0.0
0.0 77.41164 212 0.0 0.0 -154.823 213 0.0 0.0 38.70582 246 0.0 0.0 -77.4116 247 0.0 0.0 -154.823 248
0.0 0.0 -77.4116 261 0.0 0.0 38.70582 262 0.0 0.0 -154.823 263 0.0 0.0 77.41164 264 0.0 0.0 -154.823
265 0.0 0.0 38.70582 298 0.0 0.0 -77.4116 299 0.0 0.0 -154.823 300 0.0 0.0 -77.4116 313 0.0 0.0
38.70582 314 0.0 0.0 -154.823 315 0.0 0.0 77.41164 316 0.0 0.0 -154.823 317 0.0 0.0 38.70582 350 0.0
0.0 -77.4116 351 0.0 0.0 -154.823 352 0.0 0.0 -77.4116 365 0.0 0.0 38.70582 366 0.0 0.0 -154.823 367
0.0 0.0 77.41164 368 0.0 0.0 -154.823 369 0.0 0.0 38.70582 402 0.0 0.0 -77.4116 403 0.0 0.0 -154.823
404 0.0 0.0 -77.4116 417 0.0 0.0 19.35291 418 0.0 0.0 -77.4116 419 0.0 0.0 38.70582 420 0.0 0.0 -
77.4116 421 0.0 0.0 19.35291
0.001 10
3
0.0 0.0 1 0.000 8640000 0.000

Bibliography

Ahmed, T. H. 2006. *Reservoir engineering handbook*. Burlington, MA, USA: Elsevier/Gulf Professional Publishing.

Aziz, K., and A Settari. 1979. *Petroleum reservoir simulation*. New York, USA: Elsevier Applied Science Publishers.

Bagheri, M., and A. Settari. 2005. Modeling of geomechanics in naturally fractured reservoirs. Paper SPE 93083 presented at the 2005 SPE Reservoir Symposium, Houston, Texas, USA, 31 January - 2 February.

Barton, N., S. Bandis, and K. Bakhtar. 1985. Strength, deformation and conductivity coupling of rock joints. *International Journal of Rock Mechanics and Mining Sciences & Geomechanics Abstracts*, 22, no.3:121-140.

Bear, Jacob. 1972. *Dynamics of fluids in porous media*. New York, USA: American Elsevier publishing company, Inc.

Biot, M. A. 1941. General theory of three-dimensional consolidation. *Journal Applied Physics*, v12, no.2:155-164.

Biot, M. A. 1956. Theory of deformation of a porous viscoelastic anisotropic solid. *Journal Applied Physics*, v27, no.5:459-467.

Chen, H. Y., L. E. Teufel, and R. L. Lee. 1995. Coupled fluid flow and geomechanics in reservoir study - I. Theory and governing equations. Paper SPE 30752 presented at the 1995 SPE Annual Technical Conference and Exhibition, Dallas, TX, USA, 22-25 October.

Chin, L. Y. 2006. Coupling geomechanics and multi-phase flow in fractured reservoirs. Presented at Reservoir Simulation Joint Project Meeting, The University of Texas at Austin, Feb. 24.

Chin, L. Y., and R. R. Boade. 1990. Full-field, 3-D finite element subsidence model for Ekofisk., Paper presented at the 3rd North Sea Chalk Symposium, Copenhagen, Denmark, 11-12 June.

Chin, L. Y., R. Raghavan, and L. K. Thomas. 2000. Fully coupled analysis of well responses in stress-sensitive reservoirs. *SPE Reservoir Evaluation & Engineering*, v3, no.5:435-443.

Chin, L. Y., R. Raghavan, and L. K. Thomas. 1998a. Fully coupled analysis of well responses in stress-sensitive reservoirs. Paper SPE 48967 presented at the SPE 1998 Annual Technical Conference and Exhibition, New Orleans, Louisiana, USA, 27-30 September.

Chin, L. Y., R. Raghavan, and L. K. Thomas. 1998b. Fully-coupled geomechanics and fluid-flow analysis of wells with stress-dependent permeability. Paper SPE 48857 (58968) presented at the International Conference and Exhibition, Beijing, China, 2-6 November.

Chin, L. Y., and L. K. Thomas. 1999. Fully coupled analysis of improved oil recovery by reservoir compaction. Paper SPE 56753 presented at the 1999 SPE Annual Technical Conference and Exhibition held in Houston, Texas, USA, 3-6 October.

Chin, L. Y., L. K. Thomas, J. E. Sylte, and R. G. Pierson. 2002. Iterative coupled analysis of geomechanics and fluid flow for rock compaction in reservoir simulation. *Oil & Gas Science and Technology - Rev IFP,* v57, no.5:485-497.

Chin, L. Y., L. K. Thomas, J. E. Sylte, and R. G. Pierson. 2003. Coupled geomechanics and reservoir simulation: A field-scale three-dimensional example from Ekofisk. Reservoir Simulation Joint Industry Project Meeting, University of Texas at Austin, USA, Feb. 7.

Computer Modeling Group. 2006. CMG 2006: STARS User Manual.

Daim, F., R. Eymard, M. Mainguy, and R. Masson. 2002. A preconditioned conjugated gradient based algorithm for coupling geomechanical-reservoir simulations. *Oil & Gas Science and Technology - Rev IFP,* v57, no.5:515-523.

Das, Braja M. 1998. *Principle of geotechnical engineering*. Boston, USA: PWS.

Fjaer, E., R. M. Holt, P. Horsrud, and A. M. Raaen. 1992. *Developments in petroleum science 33: petroleum related rock mechanics*. Amsterdam, Netherlands: Elsevier Science Publishers B.V.

Fredrich, J. T., J. G. Arguello, G. L. Deitrick, and E. P. de Rouffignac. 1998. Geomechanical modeling of reservoir compaction, surface subsidence, and casing damage at the belridge diatomite field. paper SPE 47284 (65354) presented at the 1998 SPE/ISRM Eurock, Trondheim, Norway, 8-10 July.

Gai, X. L. 2004. A coupled geomechanical and reservoir flow model on parallel computers. PhD dissertation, The University of Texas at Austin, Austin, Texas, USA.

Gai, X. L., R. H. Dean, M. F. Wheeler, and R. Liu. 2003. Coupled geomechanical and reservoir modeling on parallel computers. Paper SPE 79700 presented at the 2003 SPE Reservoir Simulation Symposium, Houston, USA, 3-5 February.

Geertsma, J. 1957. The effect of fluid pressure decline on volumetric change of porous media. *Transaction of American Institute of Mining, Metallurgical, and Petroleum Engineers*, v210:331-340.

Gutierrez, M., and R. W. Lewis. 1998. The role of geomechanics in reservoir simulation. Paper presented at the SPE/ISRM Eurock'98, Trondheim, Norway, 8-10 July.

Gutierrez, M., and R. W. Lewis. 2002. Coupling of fluid flow and deformation in underground formation. *Journal of Engineering Mechanics,* v128, no.7:779-787.

Hibbeler, R. C. 2004. *Mechanics of materials*. USA: Prentice Hall.

Hughes, T. J. R. 2003. *The finite element method: linear static and dynamic finite element analysis*. New York, USA: Dover Publications Inc.

Hughes, T. J. R., I. Levit, and J. Winget. 1983. An element-by-element solution algorithm for problems of structural and solid mechanics. *Computer Methods in Applied Mechanics and Engineering*, v36, no.2:241-254.

Ji, Lujun, A. Settari, and R. B. Sullivan. 2004. Methods for modeling dynamic fractures in coupled reservoir and geomechanics simulation. Paper SPE 90874 presented at the 2004 SPE Annual Technical Conference and Exhibition, Houston, Texas, USA, 26-29 September.

Kazemi, H., L. S. Merrill Jr., K. L. Porterfield, and P. R. Zeman. 1976. Numerical simulation of water-oil flow in naturally fractured reservoirs. *SPE Journal*, 16, no.6:317-326.

Kim, J. M., and R. R. Parizek. 1977. Numerical simulation of the Noordbergum effect resulting from groundwater pumping in a layered acquifer. *The Journal of Hydrology*, v202, no.1:231-243.

Koutsabeloulis, N. C., and S. A Hope. 1998. Coupled stress/fluid/thermal multi-phase reservoir simulation studies incorporating rock mechanics. SPE/ISRM Eurock'98, Trondheim, Norway, 8-10 July.

Lacy, Sara J. 1986. Numerical procedures for nonlinear transient analysis of two-phase soil systems (Geotechnical, finite-element method). PhD dissertation, Princeton University, Princeton, New Jersey, USA.

Lake, L. W. 1989. *Enhanced oil recovery*. Englewood Cliffs, New Jersey, USA: Prentice Hall.

Lambe, T. W., and R. V. Whitman. 1979. *Soil mechanics, SI version*. New York, USA: Wiley.

Lewis, R. W., and W. K. S. Pao. 2002. Numerical simulation of three-phase flow in deforming fractured reservoirs. *Oil & Gas Science and Technology Rev.IFP*, v57, no.5:499-514.

Lewis, R. W., and B. A. Schrefler. 1998. *The finite element method in the static and dynamic deformation and consolidation of porous media (2nd ed.)*. New York, USA: John Wiley & Sons.

Lewis, R. W., and Y. Sukirman. 1993. Finite element modeling of three-phase flow in deforming saturated oil reservoirs. *International Journal for Numerical and Analytical Methods in Geomechanics*, v17:577-598.

Li, Pingke. 2006. Numerical simulation of the SAGD process coupled with geomechanical behavior. PhD Dissertation, University of Alberta, Edmonton, Alberta, Australia.

Longuemare, P., M. Mainguy, P. Lemonnier, A. Onaisi, Ch. Gerard, and N. Koutsabeloulis. 2002. Geomechanics in reservoir simulation: overview of coupling methods and field case study. *Oil & Gas Science and Technology Rev IFP,* v57, no.5:471-483.

Margetts, L. 2003. Programming the parallel finite element method., Presentation at MRCCS/NSF Summer School, Manchester Computing, Sept. 1-5, 2003.

Margetts, L. 2002. Parallel finite element analysis. PhD dissertation, The University of Manchester, UK.

Margetts, L., Smith I.M., J. Leng, and R. Crouch. 2006. Parallel 3D finite element analysis of nuclear reactor pressure vessels., Paper presented in ACME, Belfat, April, 2006.

Mattax, Calvin C., and Robert L. Dalton. 1990. *Reservoir simulation*. Houston, USA: SPE Monograph Volume 13.

McNamee, J., and R. E. Gibson. 1960b. Plane strain and axially symmetric problems of the consolidation of a semi-infinite clay stratum. *Quarterly Journal of Mechanics and Applied Mathematics*, v13:210-227.

McNamee, J., and R. E. Gibson. 1960a. Displacement function and linear transform applied to diffusion through porous elastic media. *Quarterly Journal of Mechanics and Applied Mathematics*, v13:98-111.

Minkoff, S. E., C. M. Stone, J. G. Arguello, S. Bryant, J. Eaton, M. Peszynska, and M. F. Wheeler. 1999. Staggered in time coupling of reservoir flow simulation and geomechanical deformation: step 1 -- one-way coupling. Paper SPE 51920 presented at the 1999 SPE Reservoir Simulation Symposium, Houston, Texas, USA, 14-17 February.

Minkoff, S. E., C. M. Stone, S. Bryant, M. Peszynska, and M. F. Wheeler. 2003. Coupled fluid flow and geomechanical deformation modeling. *Journal of Petroleum Science and Engineering*, v38:37-56.

Osorio, J. G., H. Y. Chen, L. Teufel, and S. Schaffer. 1998. A two-domain, fully coupled fluid-flow / geomechanical simulation model for reservoirs with stress-sensitive mechanical and fluid-flow properties. SPE/ISRM Eurock'98, Trondheim, Norway, 8-10 July.

Pan, F., K. Sepehrnoori, and L. Y. Chin. 2009. A New Solution Procedure for a Fully Coupled Geomechanics and Compositional Reservoir Simulator. Paper SPE 119029 presented at the 2009 SPE Reservoir Simulation Symposium held in The Woodlands, Texas, USA, 2-4 February.

Pan, F., K. Sepehrnoori, and L. Y. Chin. 2007. Development of a coupled geomechanics model for a parallel compositional reservoir simulator. Paper SPE 109867 presented at the 2007 SPE Annual Technical Conference and Exhibition held in Anaheim,California,USA,11-14 November.

Peters, E. J. 2004. *Advanced Petrophysics*. Austin, Texas, USA: the text note of the University of Texas at Austin.

Pettipher, M. A., and I. M. Smith. 1997. The development of an MPP implementation of a suite of finite element codes. Paper presented in Proceedings of High Performance Computing and Networking 1997, Vienna; Also at Lecture Notes in Computer Science, Springer: v1225: 400-409.

Prevost, J. H. 1997. Partitioned solution procedure for simultaneous integration of coupled-field problems. *Communications in Numerical Methods in Engineering*, v13, no.4:239-247.

Ran, Q. Q., and S. L. Li. 1997. Study on Dynamic Models of Reservoir Parameters in the Coupled Simulation of Multi-phase Flow and Reservoir Deformation. *Petroleum Exploration and Development*, v24, no.2:61-65.

Rutqvist, J., L. Borgesson, M. Chijimatsu, A. Kobayashi, L. Jing, T. S. Nguyen, J. Noorishad, and C.-F. Tsang. 2001. Thermohydromechanics of partially saturated geological media: governing equations and formulation of four finite element models. *International journal of rock mechanics and mining sciences*, v38, no.1:105-127.

Saad, Y. 2000. *Iterative methods for sparse linear systems*. Philadelphia: Society for Industrial and Applied Mathematics.

Schiffmann, R. L. 1960. Field applications of soil consolidation under time-dependent loading and varying permeability. *Highway Research Board Bulletin*, no.248:1-25.

Schiffmann, R. L., T-F. Chen, and Jane C. Jordan. 1969. An analysis of consolidation theories. *ASCE Journal of the soil mechanics and foundations division*, v95, no.SM1:285-312.

Schlumberger. 2002. ECLIPSE GeoMechanics: Rock stress calculations software coupled with ECLIPSE simulator. Schlumberger Information Solutions, Houston, Texas.

Settari, A. 2000. Reservoir simulation: A powerful tool for understanding and managing reservoir complexity. A SPE Distinguished Lecturer Program (2000-2001), November.

Settari, A., and F. M. Mourits. 1995. *A Coupled Reservoir and Geomechanical Simulation System*.: paper SPE 29112 (50939) presented at the 1995 SPE Reservoir Simulation Symposium held in San Antonio, Texas, USA, 12-15 February.

Settari, A., and F. M. Mourits. 1994. Coupling of geomechanics and reservoir simulation models. *Proceedings of the Eighth International Conference on Computer Methods and Advances*, v3:2151-2158.

Settari, A., and D. A. Walters. 1999. Advances in coupled geomechanical and reservoir modeling with applications to reservoir compaction. Paper SPE 74142/51927 presented at the 1999 SPE Reservoir Simulation Symposium, Houston, Texas, USA, 14-17 February.

Sleijpen, Gerard L. G., and Diederik R. Fokkema. 1993. BiCGstab(l) for linear equations involving unsymmetric matrices with complex spectrum. *Electronic Transaction on Numerical Analysis*, v1:11-32.

Smith, B. F., P. E. Bjrstad, and W. D. Gropp. 1996. *Domain decomposition: parallel multilevel methods for elliptic partial differential equations*. Cambridge; New York: Cambridge University Press.

Smith, G. D. 1985. *Numerical solution of partial differential equations: finite difference methods*. Oxford, England: Clarendon Press.

Smith, G. N., and Ian G. N. Smith. 1998. *Elements of soil mechanics*. Malden, USA: Blackwell Science Ltd.

Smith, I. M. 2000. General purpose parallel finite element programming. *Engineering Computations*, v17, no.1:75-91.

Smith, I. M., and D. V. Griffiths. 2004. *Programming the finite element method*. Chichester, England: John Wiley & Sons Ltd.

Spencer, A. J. M. 1980. *Continuum mechanics*. New York, USA: Dover Publications, Inc.

Stone, T., B. Garfield, P. Papanastasiou, and J. Fuller. 2000. Fully coupled geomechanics in a commercial reservoir simulator. Paper SPE 65107 presented at the SPE European Petroleum Conference, Paris, France, 24-25 October.

Sulak, R. M. 1991. Ekofisk Field: The first 20 years. *Journal of Petroleum Technology*, October.

Sulak, R. M., L. K. Thomas, and R. R. Boade. 1991. 3D reservoir simulation of Ekofisk compaction drive. *SPE Journal of Petroleum Technology*, v43, no.10:1272-1278.

Tarahhom, F. 2008. Development of an implicit full-tensor dual porosity compositional reservoir simulator. PhD dissertation, The University of Texas at Austin, Austin, Texas, USA.

Terzaghi, K. 1936. *Theoretical soil mechanics*. New York, USA: Wiley.

Terzaghi, K., R. B. Peck, and G. Mesri. 1996. *Soil mechanics in engineering practice*. New York, USA: Wiley-Interscience.

Thomas, L. K., L. Y. Chin, R. G. Pierson, and J. E. Sylte. 2002. Coupled geomechanics and reservoir simulation. Paper SPE 77723 (87339) presented at the 2002 SPE Annual Technical Conference and Exhibition, San Antonio, Texas, USA, 29 September-2 October.

Tran, D., L. Nghiem, and L. Buchanan. 2005. Improved iterative coupling of geomechanics with reservoir simulation. Paper SPE 93244 presented at the 2005 SPE Reservoir Symposium held in Houston, Texas, USA, 31 January-2 February.

Tran, D., A. Settari, and L. Nghiem. 2004. New iterative coupling between a reservoir simulator and a geomechanics module. Paper SPE 78192 (88989) presented at the SPE/ISRM Rock Mechanics Conference, Irving, Texas, USA, 20-23 October.

Verruijt, A. 1995. *Computational geomechanics*. Boston, USA: Kluwer Academic Publishers.

-----. 1969. *Elastic storage of aquifers*. New York, USA: Academic.

Viggiani, C., E. H. Davis, and H. G. Poulos. 1970. Discussions of an Analysis of Consolidation Theories. *ASCE Journal of the soil mechanics and foundations division*, v96, no.SM1:331-336.

Walsh, M. P., and L. W. Lake. 2003. *A generalized approach to primary hydrocarbon recovery*. Boston, USA: Elsevier.

Wan, Jing. 2002. Stabilized finite element method for coupled geomechanics and multiphase flow. PhD dissertation, Stanford University, Stanford, California, USA.

Wang, P., S. Balay, K. Sepehrnoori, J. Wheeler, J. Abate, B. Smith, and G. A. Pope. 1999. A fully implicit parallel EOS compositional simulator for large scale reservoir simulation. Paper SPE 51885 presented at the 1999 SPE 15th Reservoir Simulation Symposium, Houston, Texas, USA, 14-17 February.

Wang, P., I. Yotov, M. F. Wheeler, T. Arbogast, C. Dawson, M. Parashar, and K. Sepehrnoori. 1997. A new generation EOS compositional reservoir simulator: Part I - formulation and discretization. Paper SPE 37979 presented at the SPE Reservoir Simulation Symposium, Dallas, Texas, USA, 8-11 June.

Zienkiewicz, O. C. 1972. *Finite element method in engineering science*. New York: McGraw-Hill Education.

Zienkiewicz, O. C., and I. C. Cormeau. 1974. Visco-plasticity and creep in elastic solids-unified numerical solution approach. *International Journal of Numerical Methods in Engineering*, v8:821-845.

Zienkiewicz, O. C., and R. L. Taylor. 2000. *The finite element method*. New York, USA: John Wiley.

Zyvoloski, G. A., O'Sullivan M.J., and D. E. Krol. 1979. Finite difference techniques for modelling geothermal reservoirs. *International Journal for Numerical and Analytical Methods in Geomechanics*, v3, no.4:355-366.

VITA

Feng Pan attended The Middle School of Heihe, Heilongjiang, China. In September, 1991, he entered The Heilongjiang University in Harbin and earned a Bachelor of Engineering degree in Computational Mathematics and Application Software Engineering in August, 1995. In September, 1995, he went to The Jilin University in Changchun and obtained a Master of Science degree in Computational Mathematics in June, 1998. From 1998 through 2004, he worked at the Institute of Software of Chinese Academy of Sciences in Beijing as a researcher. Subsequently he enrolled in the Ph.D. program at the University of Texas at Austin in August, 2004.

Permanent address: Pan, Zhenyou,
Heihe, Heilongjiang Province, 164300
People's Republic of China

This dissertation was typed by the author.